LBL-18570
UC-13 c.1

MATERIALS AND MOLECULAR RESEARCH DIVISION

Annual Report 1984

June 1985

For Reference

Not to be taken from this room

Lawrence Berkeley Laboratory
University of California
Berkeley, California 94720

Prepared for the
U.S. Department of Energy under Contract DE-AC03-76SF00098

LBL-18570
LBL-18570 c.1

DISCLAIMER

This document was prepared as an account of work sponsored by the United States Government. While this document is believed to contain correct information, neither the United States Government nor any agency thereof, nor the Regents of the University of California, nor any of their employees, makes any warranty, express or implied, or assumes any legal responsibility for the accuracy, completeness, or usefulness of any information, apparatus, product, or process disclosed, or represents that its use would not infringe privately owned rights. Reference herein to any specific commercial product, process, or service by its trade name, trademark, manufacturer, or otherwise, does not necessarily constitute or imply its endorsement, recommendation, or favoring by the United States Government or any agency thereof, or the Regents of the University of California. The views and opinions of authors expressed herein do not necessarily state or reflect those of the United States Government or any agency thereof or the Regents of the University of California.

LBL-18570

MATERIALS AND MOLECULAR RESEARCH DIVISION

Annual Report 1984

June 1985

Norman E. Phillips, Division Head
Rolf H. Muller, Asst. Division Head for Research
Conway V. Peterson, Asst. Division Head for Administration

Lawrence Berkeley Laboratory
University of California
Berkeley, California 94720

Materials Sciences

Chemical Sciences

Nuclear Sciences

Fossil Energy

Energy Storage Systems

Magnetic Fusion Energy

Health and Environmental Sciences

Work for Others

Appendices

Contents

GENERAL INTRODUCTION

Rolf H. Muller xi

MATERIALS SCIENCES

Metallurgy and Ceramics

Structure of Materials

Structure and Properties of Transformation Interfaces
Ronald Gronsky, Investigator 1

Microstructure, Properties, and Alloy Design: Inorganic Materials
Gareth Thomas, Investigator 5

Solid-State Phase-Transformation Mechanisms
Kenneth H. Westmacott, Investigator 14

National Center for Electron Microscopy
Gareth Thomas, Ronald Gronsky, and Kenneth H. Westmacott, Investigators 18

In Situ Investigations of Gas-Solid Reactions by Electron Microscopy
James W. Evans, Investigator 32

Local Atomic Configurations in Solid Solutions
Didier de Fontaine, Investigator 34

Collaborative Studies by Transmission Electron Microscopy
Norman E. Phillips, Investigator 37

Mechanical Properties

Theoretical Problems in Alloy Design
John W. Morris, Jr., Investigator 38

Mechanical Properties of Ceramics
Anthony G. Evans, Investigator 46

Environmentally Affected Crack Growth in Engineering Materials
Robert O. Ritchie, Investigator 50

Physical Properties

Interfaces and Ceramic Microstructures
Joseph A. Pask, Investigator 56

High-Temperature Reactions
Alan W. Searcy, Investigator 58

Structure-Property Relationships in Semiconductor Materials
Jack Washburn, Investigator 62

Chemical Properties and Processing of Refractory Ceramics
Lutgard C. De Jonghe, Investigator 67

Structure and Properties of Composite Materials
Robert H. Bragg, Investigator 70
Ceramic Interfaces
Andreas M. Glaeser, Investigator 73
Engineering Materials
Abrasive, Erosive, and Sliding Wear of Materials
Iain Finnie, Investigator 75
Erosion and Spalling in Brittle Solids
Anthony G. Evans, Investigator 77
Solid-State Physics
Experimental Research
Far-Infrared Spectroscopy
Paul L. Richards, Investigator 80
Experimental Solid-State Physics and Quantum Electronics
Yuan R. Shen, Investigator 84
Excitations in Solids
Carson D. Jeffries, Investigator 89
Time-Resolved Spectroscopies in Solids
Peter Y. Yu, Investigator 92
Superconductivity, Superconducting Devices, and 1/f Noise
John Clarke, Investigator 94
Theoretical Research
Theoretical Studies of the Electronic Properties of Solid Surfaces
Leo M. Falicov, Investigator 99
Theoretical Solid-State Physics
Marvin L. Cohen, Investigator 102
Surface, Chemisorption, and Theory of Solids
Steven G. Louie, Investigator 107
Materials Chemistry
Chemical Structure
Low-Temperature Properties of Materials
Norman E. Phillips, Investigator 111
Electrochemical Processes
Charles W. Tobias, Investigator 114
High-Temperature and Surface Chemistry
High-Temperature Thermodynamics
Leo Brewer, Investigator 118
Chemistry and Materials Problems in Energy Production Technologies
Donald R. Olander, Investigator 120

Plasma-Enhanced Deposition of Thin Films
Dennis W. Hess, Investigator 123

Electrochemical Phase Boundaries
Rolf H. Muller, Investigator 124

Solid-State and Surface Reactions
Gabor A. Somorjai, Investigator 127

Nuclear Magnetic Resonance
Alexander Pines, Investigator 138

CHEMICAL SCIENCES

Fundamental Interactions

Photochemical and Radiation Sciences

Photon-Assisted Surface Reactions, Materials, and Mechanisms
Gabor A. Somorjai, Investigator 155

Photochemistry of Materials in the Stratosphere
Harold S. Johnston, Investigator 158

Chemical Physics

Energy Transfer and Structural Studies of Molecules on Surfaces
Charles B. Harris, Investigator 161

Selective Photochemistry
C. Bradley Moore, Investigator 165

Physical Chemistry with Emphasis on Thermodynamic Properties
Kenneth S. Pitzer, Investigator 168

Molecular Interactions
William A. Lester, Jr., Investigator 172

Spectroscopy and Structures of Reactive Intermediates
Richard J. Saykally, Investigator 175

Theory of Atomic and Molecular Collision Processes
William H. Miller, Investigator 178

Photoelectron Spectroscopy
David A. Shirley, Investigator 182

Crossed Molecular Beams
Yuan T. Lee, Investigator 191

Potential-Energy Surfaces for Chemical Reactions
Henry F. Schaefer III, Investigator 198

Atomic Physics

Atomic Physics
Richard Marrus, Investigator 203

Processes and Techniques

Chemical Energy

Formation of Oxyacids of Sulfur from SO_2
Robert E. Connick, Investigator 208

Catalytic Hydrogenation of CO
Gabor A. Somorjai and Alexis T. Bell, Investigators 210

Organometallic Chemistry of Coal Conversion
K. Peter Vollhardt, Investigator 216

Synthetic and Physical Chemistry
William L. Jolly, Investigator 219

Chemistry and Morphology of Coal Liquefaction
Heinz Heinemann, Investigator, with Alexis T. Bell, R.H. Fish, and Gabor A. Somorjai, Investigators 222

(Joint funding; see Fossil Energy Section)

Electrochemical Systems
John Newman, Investigator 223

High-Energy Oxidizers and Delocalized-Electron Solids
Neil Bartlett, Investigator 224

Transition-Metal-Catalyzed Conversion of CO, NO, H_2, and Organic Molecules to Fuels and Petrochemicals
Robert G. Bergman, Investigator 228

Chemical Engineering Sciences

High-Pressure Phase Equilibria in Hydrocarbon-Water (Brine) Systems
John M. Prausnitz, Investigator 232

NUCLEAR SCIENCES

Low-Energy Nuclear Sciences

Heavy-Element Chemistry

Actinide Chemistry
Norman M. Edelstein, Richard A. Andersen, Neil Bartlett, John G. Conway, Kenneth N. Raymond, Glenn T. Seaborg, Andrew Streitwieser, Jr., David H. Templeton, and Allan Zalkin, Investigators 237

FOSSIL ENERGY

A Review of Unsolved Problems of Pressing Importance in Fluid Mechanics Affected Erosion
Joseph A.C. Humphrey, Investigator 253

Electrode Surface Chemistry
Philip N. Ross, Investigator 255

Studies of Materials Erosion in Coal Conversion and Utilization Systems
Alan V. Levy, Investigator 258

Chemistry and Morphology of Coal Liquefaction
Heinz Heinemann, Investigator, with Alexis T. Bell, R.H. Fish, and Gabor A. Somorjai, Investigators 260

(Joint funding with Chemical Sciences)

ENERGY STORAGE SYSTEMS

Electrochemical Energy Storage
Lutgard C. De Jonghe, James W. Evans, Rolf H. Muller, John Newman, Philip N. Ross, and Charles W. Tobias, Investigators 265

Surface Morphology of Metals in Electrodeposition
Charles W. Tobias, Investigator 265

Metal Couples in Non-Aqueous Electrolytes
Charles W. Tobias, Investigator 267

Engineering Analysis of Electrolytic Gas Evolution
Charles W. Tobias, Investigator 269

Surface Layers on Battery Materials
Rolf H. Muller, Investigator 272

Electrode Kinetics and Electrocatalysis
Philip N. Ross, Investigator 275

Electrical and Electrochemical Behavior of Particulate Electrodes
James W. Evans, Investigator 278

Electrochemical Properties of Solid Electrolytes
Lutgard C. De Jonghe, Investigator 282

Analysis and Simulation of Electrochemical Systems
John Newman, Investigator 285

MAGNETIC FUSION ENERGY

Structural Materials and Weldments for High-Field Superconducting Magnets
John W. Morris, Jr., Investigator 289

HEALTH AND ENVIRONMENTAL SCIENCES

Semiconductor Materials and Devices
Eugene E. Haller, Investigator 293

WORK FOR OTHERS

Office of Naval Research

Quantum Monte Carlo for Molecular Studies
William A. Lester, Jr., Investigator 299

Electron-Phonon Coupling and the Properties of Thin Films and Inhomogeneous Superconductors
Vladimir Z. Kresin, Investigator 300

Department of Transportation

Enhanced Fuel Capability of Marine Diesels
Alan V. Levy, Investigator 302

Los Alamos National Laboratory

Determination of the Solubilities and Complexation of Waste Radionuclides Pertinent to Geologic Disposal at the Nevada Tuff Site
Heino Nitsche and Norman Edelstein, Investigators 303

Oak Ridge National Laboratory

Tribology of Cylinder Wall-Piston Ring Pairs
Alan V. Levy, Investigator 304

Electric Power Research Institute

Reaction Mechanism of the Oxidation of Bisulfite Ion by Oxygen
Robert E. Connick, Investigator 305

Selective Catalytic Hydrogenation of Polynuclear Heteroaromatic Nitrogen Compounds
Heinz Heinemann and Richard H. Fish, Investigators 306

APPENDICES

Appendix A. Division Personnel 307

Appendix B. Division Committees 320

Appendix C. List of Divisional Seminars 321

Appendix D. List of Investigators 330

GENERAL INTRODUCTION

On September 1, 1984, Professor Norman E. Phillips became Division Head of MMRD, taking over from Professor Alan Searcy, who had served for 4-1/2 years in the position. Starting on January 1, 1985, Norman took a 6-month sabbatical leave that had been arranged before he was offered the Division Head position. In his absence, I have been serving as Acting Division Head.

In 1984 MMRD investigators continued to collect an impressive list of honors and awards. A selection of these honors appears below.

- Two MMRD researchers, Robert G. Bergman and Paul L. Richards, were elected members of the American Academy of Arts and Sciences.
- Three MMRD researchers—Eugene D. Commins, William L. Jolly, and Kenneth N. Raymond—were elected Fellows of the American Association for the Advancement of Science.
- Two MMRD researchers, Richard J. Saykally and Angelica M. Stacy, received National Science Foundation Young Investigator awards.
- Two MMRD researchers, Richard J. Saykally and K. Peter Vollhardt, were awarded Miller Professorships in 1984.
- Five MMRD researchers have been recognized as being among the 100 brightest United States scientists under 40 years old, as determined by the December 1984 *Science Digest*. They are Ronald Gronsky, Alexander Pines, Robert O. Ritchie, Henry F. Schaefer III, and K. Peter Vollhardt.
- Two MMRD researchers, Alexander Pines and Y. Ron Shen, received Humboldt Senior Scientist awards.
- Two MMRD researchers, William A. Lester, Jr., and William Miller, were elected Fellows of the American Physical Society.
- Alexis T. Bell received the Paul H. Emmet Award by the W.R. Grace Company for his contributions to the field of catalysis.
- Robert G. Bergman was elected to the National Academy of Sciences.
- Leo Brewer was honored by a special Festschrift volume (Volume 17) of *High Temperature Science*.
- Didier de Fontaine chaired the 1984 Gordon Conference on Physical Metallurgy.
- Lutgard De Jonghe was elected a Fellow of the American Ceramic Society.
- Anthony G. Evans was awarded the Clyde Professorship at the University of Utah and became the Vice President of the American Ceramic Society.
- James W. Evans received the Mathewson Gold Medal of The Metallurgical Society of the American Institute of Mining, Metallurgical, and Petroleum Engineers.
- Harold S. Johnston received the American Chemical Society's 1985 Award in the Chemistry of Contemporary Technological Problems for his environmental work.
- The late Earl L. Muetterties was posthumously awarded the 1984 Remsen Award from the American Chemical Society for distinguished service in chemistry.
- John S. Newman received the David C. Grahame Award of the Division of Physical Electrochemistry of The Electrochemical Society.
- Donald R. Olander was elected a Fellow of the American Nuclear Society.
- Alexander Pines received the AT&T Bell Laboratories Special Purpose Award.
- Kenneth S. Pitzer received the Robert A. Welch Award for his contribution to the field of theoretical chemistry and for developing analytic methods involving original combinations of quantum mechanics, statistics, and thermodynamics. Professor Pitzer also received the Berkeley Citation, the highest honor given by the University of California at Berkeley.
- John Prausnitz was elected a Fellow of the American Institute for Chemical Engineering.
- Kenneth N. Raymond received the 1984 Ernest O. Lawrence Award for his outstanding contributions to the field of nuclear chemistry.
- Paul Richards was honored by the Materials Sciences Division of the U.S. Department of Energy for outstanding scientific accomplishment in solid-state physics.

- Robert O. Ritchie received the Alcoa Foundation Fellowship.
- Henry F. Schaefer III was elected a member of the International Academy of Quantum Molecular Sciences.
- Glenn T. Seaborg was named the first recipient of the Glenn T. Seaborg Actinide Award. Professor Seaborg was also named Chairman of the Lawrence Hall of Science and an Honorary Fellow of the College of Letters and Science at the University of California at Los Angeles.
- Charles W. Tobias was awarded the William N. Lacey Memorial Lectureship at California Institute of Technology.
- Jack Washburn and his graduate student Jerzy Mazur won first place in the transmission electron microscope class for their poster at the 1984 International Metallographic Exhibit.

MMRD's staff at the end of 1984 consisted of 11 staff senior scientists, 54 University of California Berkeley faculty investigators, 11 staff scientists, 126 postdoctorals and other temporary scientific personnel, 311 graduate students (including guest students), and a support staff of 94 technical, administrative, and clerical personnel, for a total of 607. During the calendar year 531 journal articles and LBL reports were published by MMRD members. Students associated with MMRD received 13 M.S., one M.E., and 28 Ph.D. degrees in 1984.

In 1984 Professor Steven G. Louie was added to the MMRD staff as a faculty investigator. Professor Louie's area of specialization is in solid-state theory and theoretical studies of surfaces and interfaces. His research includes studies of electronic and structural properties of materials and *ab initio* studies of bulk, surface, and interface systems.

Another new staff member added in 1984 is Professor Angelica Stacy. Professor Stacy's research interests include the preparation of new materials using novel synthetic routes. Professor Stacy was supported by Director's Program Development Funds in 1984.

The Atomic Resolution Microscope (ARM) at the National Center for Electron Microscopy (NCEM) was formally made accessible to the user community in July 1984. This microscope has the finest resolution of any microscope in the world, with 1.7-Angstrom resolution proven. Users from all over the world, including a number from private industry, have already taken advantage of the instrument.

Six MMRD investigators have key positions in the Center for Advanced Materials (CAM). Anthony Evans is Acting Director of CAM; Heinz Heinemann is Industry Participation Officer; John Clarke is Project Leader of the Advanced Instrumentation for Surface Science group; Lutgard De Jonghe is Project Leader of the Advanced Structural Ceramics group; Anthony Evans is Project Leader of the Interconnection/Insulation Technologies group; Eugene Haller is Project Leader of the Electronic Materials group; and Gabor Somorjai is Project Leader of the Catalysis group. In addition. Kenneth Pitzer served as the first Acting Director of CAM, serving from CAM's founding to October 1, 1984. With the construction of the new Surface Science and Catalysis Laboratory, which began in April 1985, more space should be made available for research in Building 62. The delineation of programs between CAM and MMRD will be an important issue in the near future.

Several new initiatives are being proposed for future funding. These include:

- *The Nuclear Magnetic Resonance Laboratory (NMRL).* This laboratory, under the overall guidance of Professor Alexander Pines, has two main thrusts: the development of new techniques and concepts in order to extend the applicability of NMR, and the establishment of science and technology collaborations with researchers from MMRD, CAM, and other LBL divisions, as well as with users from private industry.
- *Raman Studies of Surface Processes.* This program, directed by Dr. Gerd Rosenblatt, has as its goal new understanding of rotational and vibrational energy levels, dynamics, and reactivity of molecules adsorbed on surfaces using unenhanced spontaneous Raman spectroscopy.
- *Structure determination at the metal-solution interface by x-ray total reflection Bragg diffraction (TRBD).* This program, directed by Dr. Philip Ross, pursues a new method of determining the *in situ* structure at metal/solution interfaces, using the phenomenon of total reflection of x-rays at glancing incidence. Initial experiments will focus on the study of electrolytic growth of copper epitaxy on gold single crystals in a copper solution, with future experiments directed at systems important for magnetic recording heads and electro-optics.

The MMRD Annual Review of 1984 programs was held on February 28 and March 1, 1985. Dr. James Phillips of AT&T Bell Laboratories served as Chair. The other reviewers were Professor William

Chupka, Department of Chemistry, Yale University; Professor Alan Ardell, Chair, Materials Science and Engineering Department, UCLA; Professor John Bercaw, Chemistry Department, California Institute of Technology; Dr. Richard Claassen, Vice President, Livermore Programs, Sandia National Laboratories (Livermore); and Dr. Adam Heller, Head, Electronic Materials Research, AT&T Bell Laboratories.

A review of 1984 programs supported by the Chemical Sciences Division of the Office of Basic Energy Sciences was held on March 4–6, 1985. The DOE Program Managers attending were Richard Kandel (Chief), Allan Laufer, and Mary Gress from the Fundamental Interactions Branch; and F. Dee Stevenson (Chief), Robert S. Marianelli, John L. Burnett, and Robert Eischens from the Processes and Techniques Branch.

The review of Materials Sciences Field Task Proposals for Fiscal Year 1987 was held in Germantown, Maryland, on March 11, 1985. DOE Program Managers attending were L.C. Ianniello, Director, Division of Materials Sciences; F.V. Nolfi, Jr. (Chief), S.M. Wolf, and R.J. Gottschall from the Metallurgy and Ceramics Branch; and M.C. Wittels (Chief), I.L. Thomas, and M.J. Weber from the Solid-State Physics and Materials Chemistry Branch.

MMRD continues to make a vital contribution to LBL's—and the nation's—scientific progress. We all look forward to the return of Professor Phillips and another productive year in 1985.

Rolf H. Muller
Acting Division Head,
Materials and Molecular Research Division

METALLURGY AND CERAMICS

STRUCTURE OF MATERIALS

Structure and Properties of Transformation Interfaces*

Ronald Gronsky, Investigator

INTRODUCTION

Transformation interfaces include homophase boundaries, heterophase boundaries, and free surfaces at which solid-state reactions are either initiated or propagated. The goal of this research program is to determine the atomic configurations of such interfaces and to establish the relationship between their detailed structure and interfacial properties (mobility, diffusivity, conductivity, and ductility), since these properties strongly influence, if not completely dominate, the overall performance of materials.

Experiments are carried out chiefly by transmission electron microscopy (TEM), including energy-dispersive x-ray and electron-energy-loss spectroscopies. Results are correlated with theoretical predictions of interfacial structure and high-spatial-resolution image simulations.

1. High-Resolution Structural Characterization of the Amorphous-Crystalline Interface in Se^+-Implanted GaAs (Publication 1)

T. Sands, D.K. Sadana, R. Gronsky, and J. Washburn

High-resolution TEM has been applied to the characterization of the amorphous-crystalline interface in (100) GaAs implanted at room temperature with Se^+ ions. The critical density of energy deposited by nuclear stopping was determined to be 11 + 2 eV per GaAs molecule. This critical-energy density appears to be most naturally defined at the 50%-amorphous/50%-crystalline transition region, which was found to possess a distinct two-phase nature, with pockets of crystalline material embedded within an amorphous matrix. However, the crystalline material itself was observed to contain channeled damage cascades (see Figure 1-1) and nuclei of stacking faults (see Figure 1-2), the latter occurring within a few atomic distances of the amorphous interface.

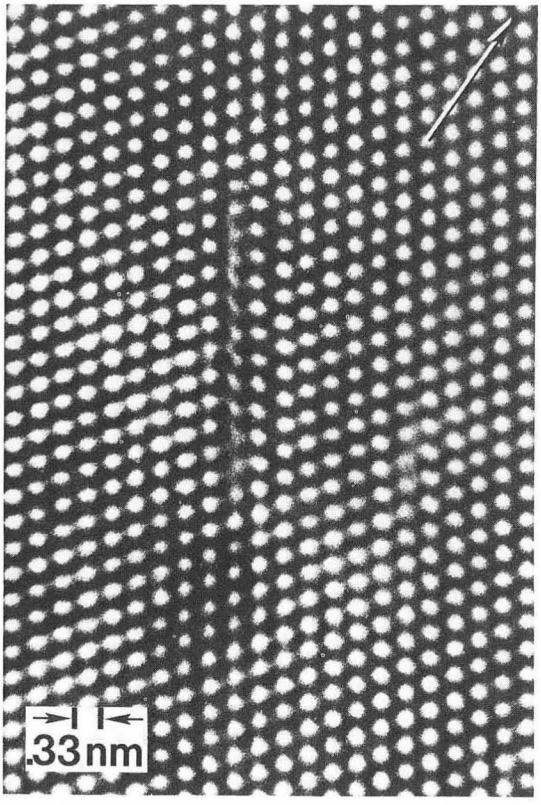

Figure 1-1. High-resolution TEM image of channeled damage cascade with 3.5-nm projected length. The cascade is 270 nm below the surface, with the arrow pointing to the sample surface. The defocus is at 90 nm. (XBB 830-9400A)

*This work was supported by the Director, Office of Energy Research, Office of Basic Energy Sciences, Materials Sciences Division of the U.S. Department of Energy under Contract No. DE-AC03-76SF00098.

Figure 1-2. High-resolution TEM image of the upper portion of the lower amorphous-crystalline transition region (~225 nm below the surface). Note the stacking-fault nucleus (A) and the channeled cascade (B). The arrow points to the sample surface; the defocus is at 90 nm. (XBB 830-9399)

2. Interface Morphology and Phase Distribution in the $Cu_{2-x}S$/CdS Heterojunction: A Transmission Electron-Microscope Investigation (Publication 5)

T. Sands, J. Washburn, and R. Gronsky

The $Cu_{2-x}S$/CdS photovoltaic device is the most thoroughly studied and developed polycrystalline thin-film solar cell. However, many of the fundamental relationships between processing, microstructure, and device performance are essentially unknown. Critical to understanding these relationships is the determination of the $Cu_{2-x}S$/CdS interface morphology and the phase distribution in the $Cu_{2-x}S$ absorber. In this study electron-optical methods have been applied to the structural characterization of single-crystal $Cu_{2-x}S$/CdS heterojunctions prepared by the aqueous ion-exchange process. Results obtained by scanning electron microscopy, TEM and diffraction, and cross-sectional high-resolution TEM (XHRTEM) are combined to develop a detailed description of the effect of surface texture on heterojunction morphology.

The XHRTEM images reveal the two-phase nature of the low-chalcocite (Cu_2S) absorber (see Figure 2-1). The tetragonal phase, a high-pressure polymorph of Cu_2S, is found to form the metallurgical junction with CdS if the local surface orientation is nearly basal. However, only low chalcocite is detected in the absorber layer if the surface is steeply inclined to the basal plane. These results are rationalized on the basis of lattice misfit, structural compatibility, and the nucleation of hcp-to-fcc transformation dislocations.

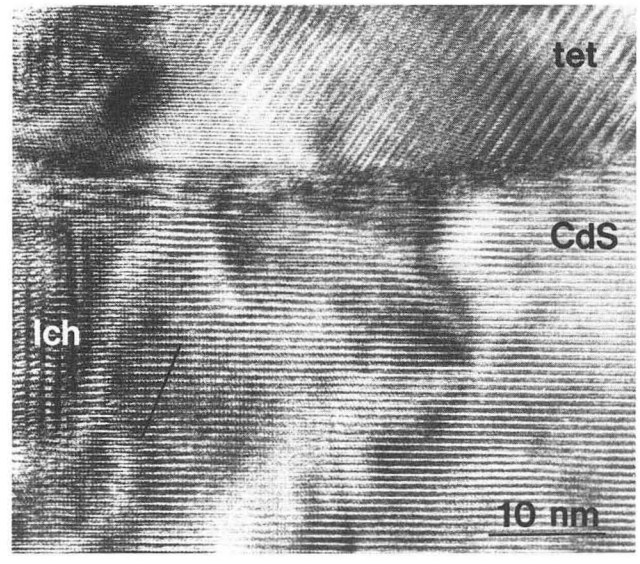

Figure 2-1. XHRTEM image of Cu_2S/CdS heterojunction formed in 5 seconds at 99°C in an etched Cd face of CdS. The line at the lower left indicates the low-chalcocite (lch)-CdS invariant line. The off-basal tetragonal-phase (tet)-CdS interface is accommodated by ledges (upper right). The low-chalcocite and tetragonal phases are in the [010] zone-axis orientation. CdS is in the [2110] zone-axis orientation. The CdS basal planes are horizontal. (XBB 830-10050)

3. Observations of Guinier-Preston (G.P.) Zones and Their Transformation to γ' in the Al-Ag System (Publication 14)

J.M. Howe, R. Gronsky, and H.I. Aaronson

Through a complex heat-treatment procedure, it was possible to induce the formation of unusually large G.P. zones (up to 800 Å diameter) in an Al-15wt% Ag alloy and to initiate their transformation to γ' platelets. The zones initially decompose across their diameter, followed by the nucleation of the γ' phase in these regions. As decomposition progresses, the spherical zones disappear completely, leaving an array of parallel γ' plates that are confined in some cases to the solute-depletion envelope of the initial zones (see Figure 3-1). These results provide conclusive evidence for the decomposition path in this system where G.P. zones indeed act as heterogeneous nucleation sites for the metastable transition phase.

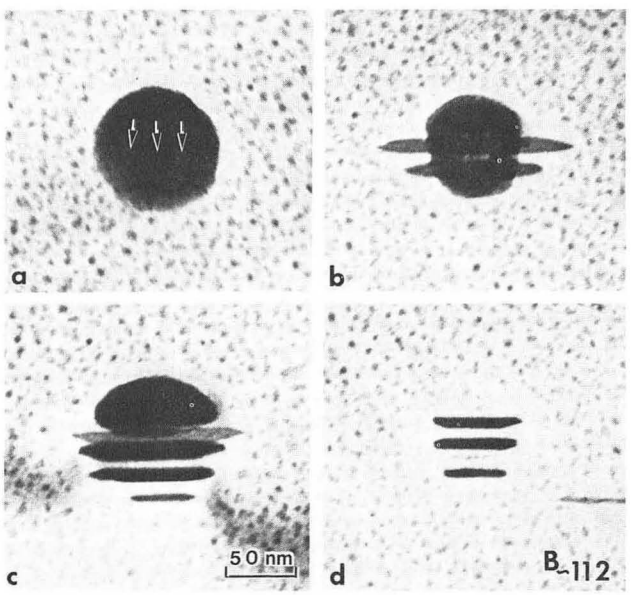

Figure 3-1. Transformation sequence of spherical G.P. zones to plate-shaped γ' precipitates in an Al-15wt% Ag alloy.
(XBB 847-5004)

4. Work in Progress

Also being studied under this project are the atomic mechanisms of oxidation of aluminum (with J.Y. Lee), employing XHRTEM of the Al/oxide interface; the atomic structure of grain boundaries in bcc metals (with E.A. Kamenetzky), incorporating computer modeling of atomic-relaxation events at the interface plane; and the atomic structure and segregation behavior of defects in Si (with J.H. Rose), encompassing both dislocations and grain boundaries in a general framework of atomistic behavior.

1984 PUBLICATIONS AND REPORTS

Refereed Journals

1. T. Sands, D. Sadana, R. Gronsky, and J. Washburn, "High Resolution Structural Characterization of the Amorphous-Crystalline Interface in Se^+-Implanted GaAs," Appl. Phys. Lett. **44**, 874 (1984); LBL-17035.
2. T. Sands, J. Washburn, and R. Gronsky, "High Resolution Study of the Relationship Between Misfit Accommodation and Growth of $Cu_{2-x}S$/CdS in CdS," Mater. Res. Soc. Symp. Proc. **31**, 241 (1984); LBL-16774.
3. T. Sands, R. Gronsky, and J. Washburn, "Characterization of Single-Crystal Cu_2S/CdS Heterojunctions by HREM," SPIE **463**, 34 (1984); LBL-17141.
4. J.H. Mazur, R. Gronsky, and J. Washburn, "Oxidation of Singular and Vicinal Surfaces of Silicon: the Structure of the Si-SiO_2 Interface," SPIE **463**, 88 (1974); LBL-17552.
5. T. Sands, J. Washburn, and R. Gronsky, "Interface Morphology and Phase Distribution in the $Cu_{2-x}S$/CdS Heterojunction: A Transmission Electron Microscope Investigation," Solar Energy Mater. **10**, 349 (1984); LBL-17677.
6. T. Sands, J. Washburn, R. Gronsky, W. Maszara, D.K. Sadana, and G.A. Rozgonyi, "Near-Surface Defects Formed During Rapid Thermal Annealing of Pre-Amorphized and BF_2^+-Implanted Silicon," Appl. Phys. Lett. **45**, 982 (1984); LBL-18000.

Other Publications

7. R. Gronsky, G. Van Tendeloo, and G. Thomas, "High Resolution Electron Microscopy Studies of the Early Stages of Decomposition in Alloys and Ceramics," in *Decomposition of Alloys: the Early Stages,* P. Haasen *et al.*, eds., Pergamon Press, New York, 1984, p. 198; LBL-17369.
8. G. Van Tendeloo, R. Gronsky, and H.R. Wenk, "Modulated Structure in Calcian Dolomites: A Study of Electron Microscopy," submitted to Acta Cryst.
9. L.E. Tanner, L.A. Jacobsen, A.R. Pelton, R. Gronsky, J.H. Perepezko, B.A. Mueller, and S.S. Brenner, "The Al-Be System: The Effects of RSP on Structure and Phase Relations," in *Proc. 5th Int. Conf. on Rapidly Quenched Metals,* September 1984.

LBL Reports

10. T.D. Sands (Ph.D. Thesis), "Formation and Degradation of $Cu_{2-x}S$/CdS Single Crystal Heterojunctions: A High Resolution Study," LBL-17684.
11. T. Sands, J. Washburn, R. Gronsky, W. Maszara, D.K. Sadana, and G.A. Rozgonyi, "Influence of the Amorphous-Crystalline Interface Morphology on Dislocation Nucleation in Pre-Amorphized Silicon," J. Elec. Mater. (in press); LBL-18172.
12. J.M. Howe, R. Gronsky, and H.I. Aaronson, "Atomic Mechanisms of Precipitate Plate Growth I. A CTEM Study of the Interfacial Structure of γ' Precipitate Plates," Acta Met. (in press); LBL-16503 Rev.
13. J.M. Howe, R. Gronsky, and H.I. Aaronson, "Atomic Mechanisms of Precipitate Plate Growth II. A HREM Study of the Interfacial Structure of γ' Precipitate Plates," Acta Met. (in press); LBL-16504 Rev.
14. J.M. Howe, R. Gronsky, and H.I. Aaronson, "Observations of G.P. Zones and Their Transformations to γ' in the Al-Ag System," submitted to Scripta Met.; LBL-18147.
15. T. Sands, J. Washburn, and R. Gronsky, "Crystallographic Relationships between GaAs, As, and Ga_2O_3 at the GaAs Thermal Oxide Interface," submitted to Mater. Lett.; LBL-18636.

Invited Talks

16. R. Gronsky, "Atomic Resolution Microscopy of Transformation Interfaces," Exxon Research and Engineering, Annandale, New Jersey, February 3, 1984.
17. E.A. Kamenetzky and R. Gronsky, "Characterization of Small Carbide and Nitride Particles Using Electron Microscopy," DOE Topical Meeting on Characterization and Behavior of Sub-Micron Nitride and Carbide Powder, Albuquerque, New Mexico, March 2, 1984.
18. R. Gronsky, "Atomic Resolution Microscopy of Interfaces in Solids," Department of Materials Science, University of Southern California, Los Angeles, April 6, 1984.
19. R. Gronsky, "Understanding Solid-Solid Interfaces," Department of Materials Science Seminar Series, University of California Berkeley, October 18, 1984.
20. R. Gronsky, "Spatially Resolved Analysis of Defect Structures by TEM/STEM," American Ceramics Society Fall Meeting, San Francisco, California, October 30, 1984.
21. R. Gronsky, "High Resolution Transmission Electron Microscopy of Technical Ceramics," American Ceramics Society Fall Meeting, San Francisco, California, October 30, 1984.
22. R. Gronsky, "Characterization of Defects in Solids at Atomic Resolution," Materials Research Society Fall Meeting, Boston, Massachusetts, November 29, 1984.
23. R. Gronsky, "Direct Imaging of Atomic Structure at Solid-Solid Interfaces," General Motors Research Laboratories, Warren, Michigan, November 30, 1984.

Microstructure, Properties, and Alloy Design: Inorganic Materials*

Gareth Thomas, Investigator

INTRODUCTION

This is a multicomponent, interdisciplinary program in physical metallurgy and ceramics designed to advance the understanding of structure-property relationships in technologically significant materials involved in energy and conservation. All tasks involve characterization of both structure and composition at the highest levels of spatial [transmission electron microscopy (TEM)] and chemical (spectroscopy) resolutions. The overall objectives are to design new materials or to more efficiently utilize existing materials with technology transfer to industrial practice without large capital investment and to realize materials and energy conservation. Specific tasks include: (1) Dual-phase ferrite-martensite steels for rod and wire: optimization of microstructure and processing, analytical studies of solute partitioning, fatigue (with Professor R.O. Ritchie), and wear. (2) Martensitic and bainitic steels: fundamental studies of phase transitions, relation to wear, grain-boundary precipitation and effect of copper, and optimization of processing to maximize toughness. (3) Electronic materials: structure of audio recording tape, piezoelectric materials, and rare-earth alloys.

ALLOY DESIGN, MICROSTRUCTURE, AND PROPERTIES: STEEL

1. The Physical Metallurgy and Alloy Design of Dual-Phase Steels (Publication 29)

Gareth Thomas

The terminology "dual phase" has become accepted to define a class of low-carbon, low-alloy steels that generally contain two phases, ferrite and martensite or ferrite and bainite, that can be obtained by relatively simple processing involving quenching from the two-phase ferrite-austenite field. If the martensite is low-carbon lath martensite, it will contain interlath austenite (see Figures 1-1 and 1-2); and if high-temperature decomposition of austenite has occurred during quenching, i.e., if bainite is present, there will be bainitic carbides. In microalloyed steels the ferrite phase may also contain the corresponding alloy carbides or nitrides. Thus, while the term "dual phase" represents the simple principle of obtaining two phases, the actual microstructures may be multiphase and quite complex. This paper discusses the general physical metallurgy of "dual-phase" steels and some potential applications.

From the standpoint of their superior properties and simplicity in composition and processing, dual-phase steels show great promise, not only for the transportation industry, but also for general structural applications, e.g., sheet, thin plate pipelines, wires, rods, and bars. Their advantages include economy of material and enormous flexibility wherein a single alloy can be manipulated to provide a wide range of products and properties.

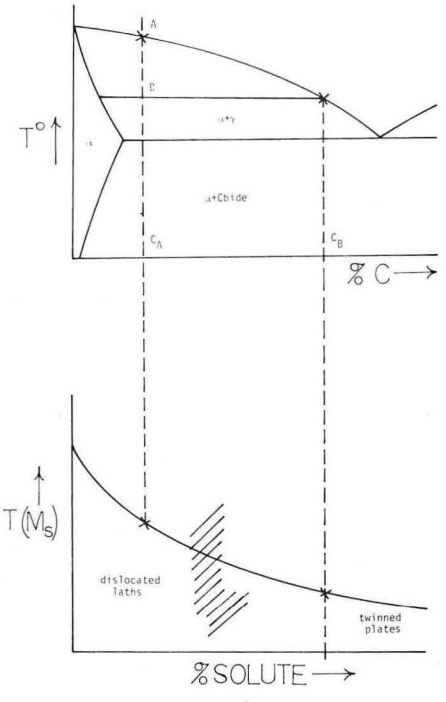

Figure 1-1. Phase diagram for a Fe-C system (above); during intercritical annealing an alloy of composition C_A will phase-separate into low-carbon ferrite and higher-carbon austenite at the intercritical annealing temperature B. If the carbon content in austenite C_B exceeds about 0.4 wt%, brittle twinned plates are formed as the Ms temperature is lowered. If the initial carbon content is much above 0.1 wt%, it will be difficult to avoid twinned martensite in dual-phase structures if the annealing temperature B is chosen to obtain 20–30% martensite.
(XBL 838-11227)

*This work was supported by the Director, Office of Energy Research, Office of Basic Energy Sciences, Materials Sciences Division of the U.S. Department of Energy under Contract No. DE-AC03-76SF00098.

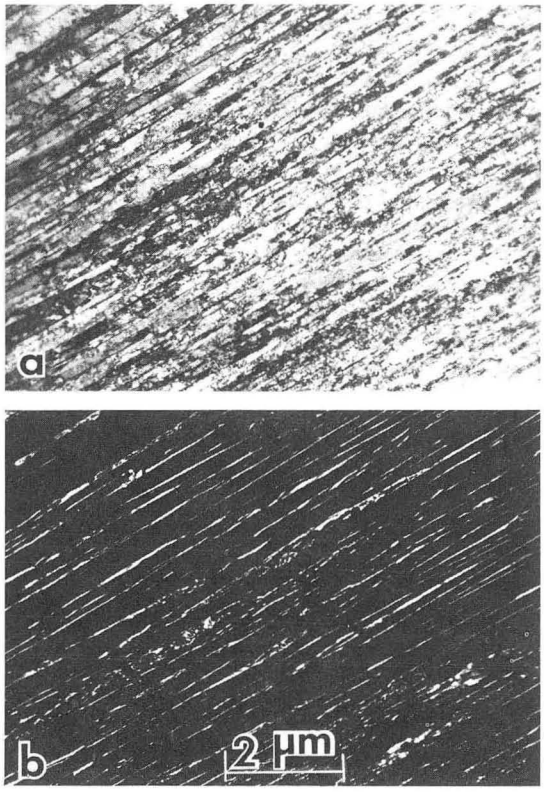

Figure 1-2. Bright-field (a) and dark-field (b) electron micrographs of lath martensite in 1010 steel. Notice the retained films between the dislocated laths. The composition corresponds to B in Figure 1-1. (XBB 800-14347)

2. Effects of Microstructure on Fatigue Crack Growth in Duplex Ferrite-Martensite Steels (Publication 1)

J.A. Wasynczuk, R.O. Ritchie, and G. Thomas

Monotonic tensile and fatigue-crack-growth tests have been performed on AISI 1018 and Fe/2Si/0.1C steels with dual-phase ferrite-martensite (DFM) microstructures. The effects of microstructure on ambient-temperature mechanical properties were examined. Two distinct martensite distributions were produced in AISI 1018 DFM. The primary differences between the two were the ferrite and martensite particle sizes. Tensile fracture was sensitive to both martensite distribution and volume fraction. For a given volume fraction of martensite, large particle sizes increased strength but drastically reduced ductility. Threshold stress-intensity ranges for fatigue crack growth in AISI 1018 DFM were found to be unaffected by the distribution or the volume fraction of martensite. However, crack-growth rates in the range $10^{-5}-10^{-3}$ mm/cycle were increased in AISI 1018 DFM when the particle sizes were large. The increased crack-growth rates were attributed to a crack-extension mechanism involving cleavage fracture in ferrite. The Fe/2Si/0.1C DFM alloy was found to have a considerably higher fatigue-threshold stress intensity than AISI 1018 DFM of comparable strength. The greater near-threshold fatigue crack propagation resistance of Fe/2Si/0.1C DFM was attributed to a meandering crack path, generated by the coarser microstructure in this steel, which promotes roughness-induced crack closure and crack-deflection effects.

3. Effect of Finish-Rolling Temperature on the Structure and Properties of Directly Quenched Nb-Containing Low-Carbon Steel (Publication 28)

N.J. Kim, A.J. Yang, and G. Thomas

The microstructure and mechanical properties of directly quenched Fe/1.49Mn/0.06C/0.05Nb steel were strongly affected by finish-rolling temperature. Finish rolling above the Ar_3 temperature produced a duplex acicular ferrite/martensite structure. Changing the finish-rolling temperature above the Ar_3 temperature did not produce any significant changes in microstructure and mechanical properties. When the alloy was further deformed in the two-phase ($\alpha + \gamma$) region, a polygonal ferrite/martensite structure was formed. The ferrite matrix had a high dislocation density due to the deformation in the ($\alpha + \gamma$) region. There was a large increase in yield and tensile strength with a small deterioration in impact toughness. Further lowering of the finish-rolling temperature decreased the volume fraction of martensite, thus decreasing the strength. These results are shown in Figure 3-1.

4. Effects of the Constituents on the Mechanical Behavior of Low-Carbon Steels (Publication 8)

N.J. Kim and G. Thomas

It is well known that the mechanical properties of steels are largely determined by their microstructures. The increasing demands for energy and materials conservation have greatly stimulated research efforts to produce high-strength steels in grades covering both structural and automotive applications. The steels should have high strength as

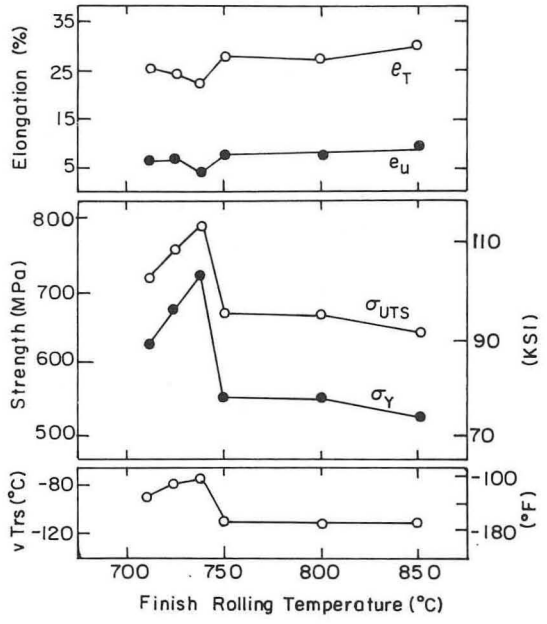

Figure 3-1. Variation of mechanical properties of directly quenched Fe/1.49Mn/0.06C/0.05Nb steel as a function of finish-rolling temperature. (XBL 822-5177)

well as good ductility and toughness simultaneously. The basic difficulty is that these properties are often incompatible in steels having conventional microstructures. The introduction of so-called dual-phase (ferrite/martensite) steel in the last decade was one of the answers to those needs with respect to the strength-ductility combinations needed for the automotive industry. The approach toward production of dual-phase structures is mostly aimed at obtaining the second phase of martensite/retained austenite within a fine-grained ferrite matrix. However, recent studies have revealed the presence of other transformation products, such as bainite and acicular ferrite.

In this paper it is shown that, although ferrite/martensite products provide excellent combinations of strength and ductility, the morphology and high strength of martensite particles result in impaired impact toughness compared to the ferrite/bainite and acicular ferrite/martensite steels, as shown in Figure 4-1.

5. Effect of Grain Size on the Mechanical Properties of Dual-Phase Fe/Si/C Steels (Publication 25)

J.H. Ahn

The present investigation is concerned with the influence of the prior austenite grain size on the mechanical properties of DFM steels. The steel used in this investigation is an Fe/2Si/0.1C alloy with an intermediate-quenching heat treatment. As the prior austenite grain size is refined, significant improvements in total elongation, reduction in area, and impact toughness can be achieved, while uniform elongation, yield, and tensile strengths are not affected. These improvements are analyzed in terms of microstructure and fracture characteristics. Careful observations of the microcracks and fracture profile show that the cleavage cracks propagate nearly straight without deviations at the ferrite/martensite interfaces within the subunits of the DFM structure, but they change their path at high-angle subunit boundaries. The crack is less likely to be deflected at the ferrite/martensite interface because the interface is coherent. In this investigation, the subunit of the DFM structure is defined as the area of aligned fibers of martensite and ferrite, having nearly the same crystallographic orientation throughout. This

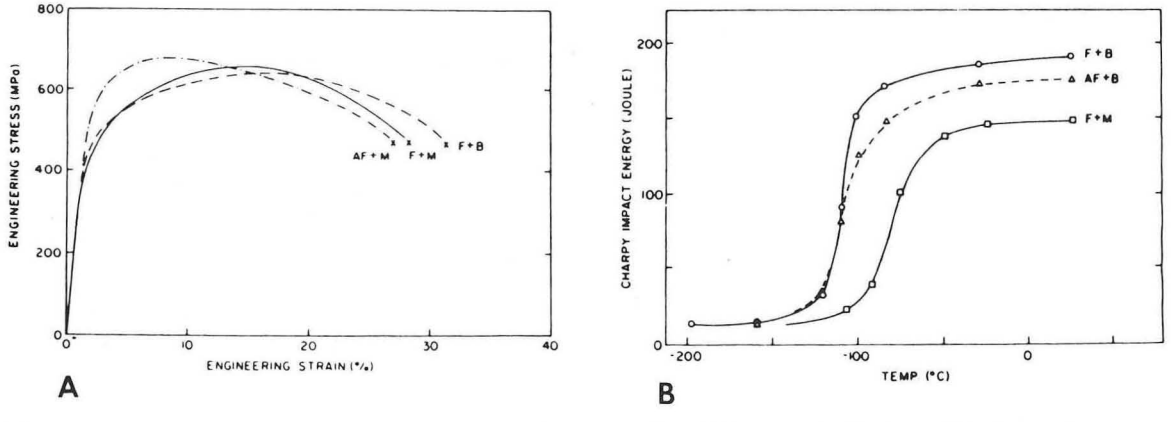

Figure 4-1. A: Effect of constituents on the stress-strain curves of multiphase steels. F: ferrite, B: bainite, M: martensite, AF: acicular ferrite. B: Charpy impact toughness transition curves of various multiphase steels. F: ferrite, B: bainite, M: martensite, AF: acicular ferrite. (XBL 851-786)

subunit is directly related to the prior martensite packets and thus is controlled by the prior austenite grain size.

6. Microstructure Formation and Solute Partitioning During Intercritical Annealing of Dual-Phase Steels (Publication 18)

M. Ohmura and G. Thomas

Microstructure formation and solute partitioning depend primarily on prior microstructure, intercritical annealing conditions, and alloy compositions. In this research, the following alloys were studied: Fe/1.5Mn/0.1C, Fe/1.5Mn/0.1Nb/0.1C, Fe/2Si/0.1C, and Fe/1.0Al/0.1C. Two types of heat treatment were used to produce dual-phase steels: (1) reheating the quenched martensitic steel to the intercritical region, and (2) controlled step cooling from austenite to the intercritical region; both cases were followed by water quenching. From these structures, compositional profiles were measured across the interface between ferrite and martensite (austenite) by scanning TEM and energy-dispersive x-ray spectroscopy, and interface motion was also measured by dilatometry and hot-stage experiments in a high-voltage electron microscope. Figure 6-1 shows one of the partitioning measurements of manganese steel, after heat treatment (1). The dotted line in Figure 6-1 is the compositional profile calculated by assuming local equilibrium at the interface. No significant partitioning has been found in the silicon and aluminum steels.

ELECTRONIC, MAGNETIC, AND PIEZOELECTRIC MATERIALS RESEARCH

An understanding of microstructure-property relationships in magnetic materials and electronic ceramics, in order to develop materials with desirable properties, is the main thrust of this program. In magnetic materials, the efforts are in the characterization and development of hard magnetic materials and magnetic recording media. There is also an effort to characterize lead-lanthanum-titanate (PLT) ceramics. Results from current research are discussed below.

7. Interaction of Magnetic Domain Walls with Microstructural Features in Spinel Ferrites (Publication 4)

I-Nan Lin, R.K. Mishra, and G. Thomas

Lorentz microscopy studies of $(Mn,Zn)Fe_2O_4$ and $LiFe_5O_8$ show that grain boundaries, pores, microcracks, stacking faults, and nonmagnetic second-phase particles act as pinning sites for moving domain walls. Second-phase particles, pores, and some grain boundaries also act as favorable sites for reverse domains to be nucleated. In addition, domain walls cannot move smoothly as they approach a grain boundary (see Figure 7-1).

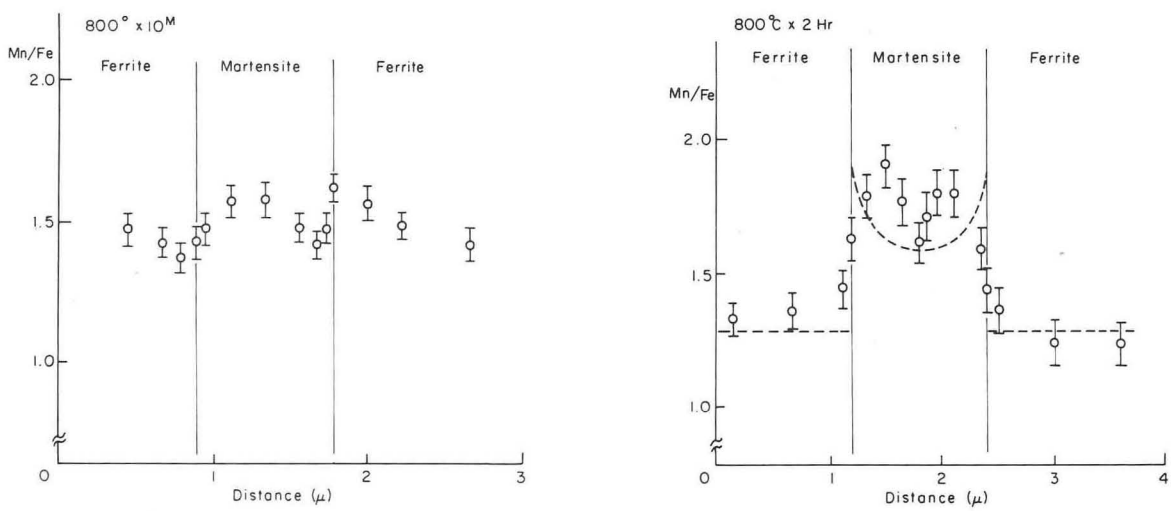

Figure 6-1. Manganese-concentration profile of Fe/1.5Mn/0.1C dual-phase steel intercritically annealed at 800°C for 10 min at 2 hr. (XBL 848-7281A)

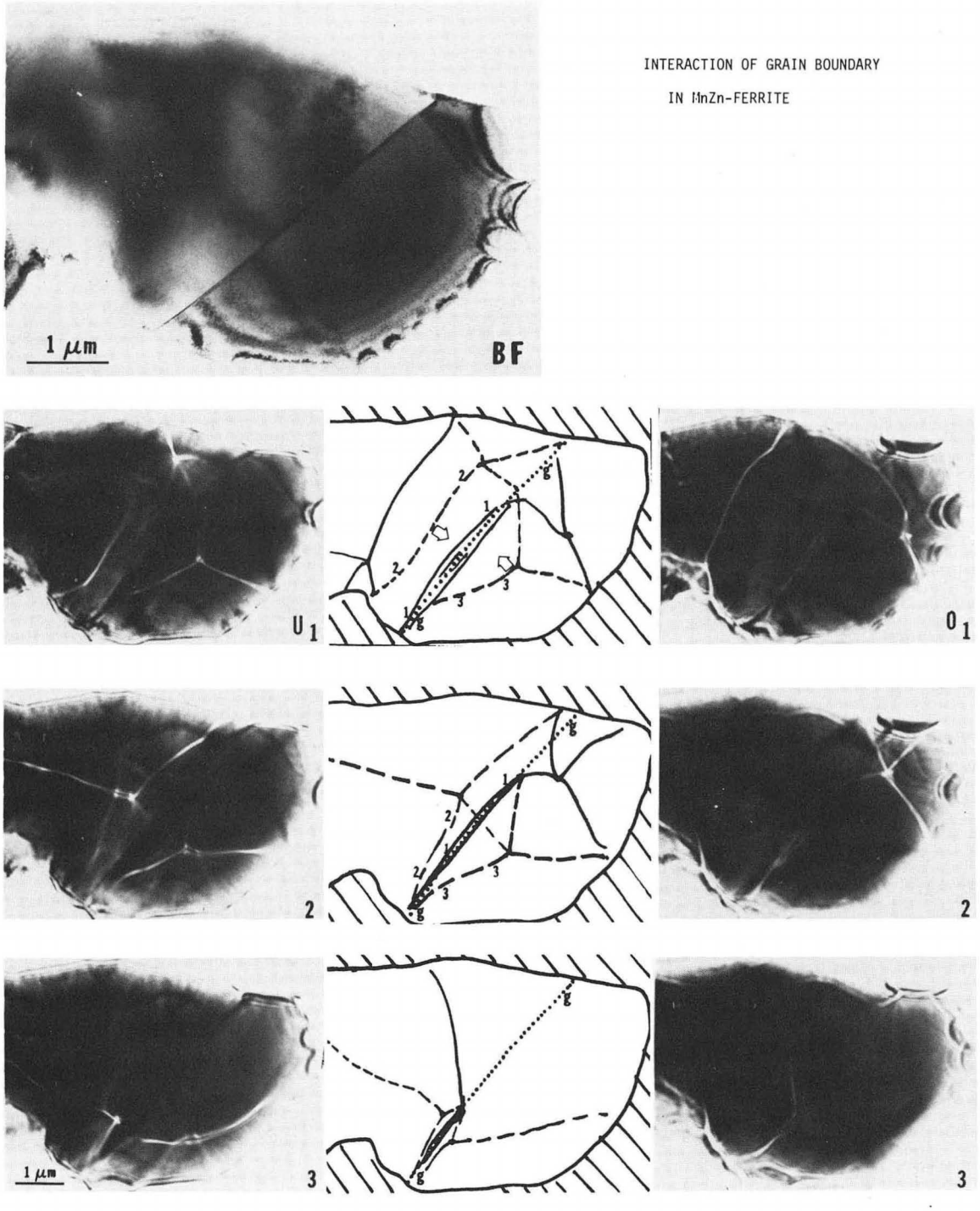

Figure 7-1. Interaction of domain wall with an edge-on grain boundary (dotted line g-g) in an $(Mn,Zn)Fe_2O_4$ sample. Domain walls parallel to grain boundary (1-1, 2-2) are stopped completely, while the domain wall normal to the grain boundary (2-3) can move up and down. The top photo is the focused image of a grain boundary. Lorentz image pairs u_1, o_1 and u_2, o_2 are taken with different applied fields. (XBB 817-7038)

8. Site Occupation of Ternary Elements in $Sm_2(CoTM)_{17}$ Compounds (Publication 10)

K.M. Krishnan, L. Rabenberg, R.K. Mishra, and G. Thomas

The crystallographic positions of Fe and Mn atoms in a $Sm_2(CoFeMn)_{17}$ permanent magnet have been investigated using electron-channeling/blocking techniques. Using the tilting and diffraction capabilites of an analytical transmission electron microscope, an electron beam was made to propagate along specific crystallographic directions in the magnet. By monitoring the characteristic x-ray spectrum as a function of incident electron-beam orientation, it was possible to determine that 88.5% of the Mn and 85.1% of the Fe atoms occupy sites in the mixed planes in this compound.

9. Determination of the Specific Site Occupation of Rare-Earth Additions in $Y_{1.7}Sm_{0.6}Lu_{0.7}Fe_5O_{12}$ Thin Films by the Orientation Dependence of Characteristic X-Ray Emissions (Publication 12)

K.M. Krishnan, Peter Rez, R. Mishra, and G. Thomas

The orientation dependence of characteristic x-ray emissions has been used to determine specific site occupations of rare-earth additions in epitaxially grown films of $Y_{1.7}Sm_{0.6}Lu_{0.7}Fe_5O_{12}$. A theoretical formulation based on the assumption of highly localized inner-shell excitations was used not only to predict specific site-sensitive orientations but also to refine experimentally observed data employing a constrained least-squares analysis to give probabilities for the occupation of the rare-earth additions in the different crystallographic sites. Thus, it has been shown that in this compound the preference for the rare-earth additions is a predominantly octahedral occupation with a probability $\gtrsim$ 95%. Some of the assumptions and limitations of the technique have also been discussed.

10. Work in Progress

An investigation has been made regarding the production of high-strength wire from low-carbon dual-phase steels. Dual-phase steel wire represents an alternative to conventional high-strength steel wire that is produced by cold-drawing a high-carbon pearlitic steel rod to large strains with several intermediate annealing or patenting heat treatments. Dual-phase steel was selected as a starting material for cold-drawing into high-strength wire because of its high strain-hardening rate and superior formability.

To produce the cold-formable dual-phase steels, the low-carbon steels ($\sim$0.1% C) were continuously hot-rolled in the austenite region and finish-rolled in the two-phase ($\alpha + \gamma$) field. The hot-rolled steel was then rapid quenched to produce dual-phase steel containing fibrous lath martensite in the fine-grained ferrite matrix.[1] The main advantages of the development of such dual-phase steels by controlled rolling over other processes are: (1) much finer ferrite grains can be obtained; (2) a more desirable martensite morphology (fine, fibrous) can be obtained; and (3) the more expensive intermediate treatment (e.g., batch heat treatment) can be deleted. Furthermore, the process can be readily used in existing steel-milling facilities.

Experimental results have shown that the dual-phase steel so produced can be continuously cold-drawn to 99.8% reduction in area for strength levels of about 400 Ksi (2760 MPa) without any intermediate or patenting heat treatments.

The effect of copper on the precipitation of proeutectoid cementite is being investigated in order to gain a better understanding of how solutes influence diffusional phase transformations in steels. Proeutectoid cementite precipitation involves a concentration of carbon atoms by diffusion through austenite and a change of crystal structure from fcc to orthorhombic. The solubility of copper in cementite is extremely low, and therefore thermodynamic considerations predict a strong tendency for the partitioning of copper away from growing cementite. However, this precipitation has been shown to occur at temperatures such that the diffusion of copper through austenite is very limited. In order to test whether this predicted partitioning of copper would affect the kinetics of proeutectoid cementite precipitation, the isothermal transformation behaviors of hypereutectoid Fe-C-Cu and Fe-C alloys were examined and compared. The time-temperature-transformation diagrams generated for these alloys showed that the kinetics of proeutectoid cementite precipitation was not significantly affected by copper. The microstructure, as seen in the optical microscope, was also substantially the same for both alloys. However, transmission electron microscopy revealed the presence of small, copper-rich fcc precipitates within the proeutectoid cementite of the

copper-containing steel. The crystallographic aspects of this precipitation are now being investigated.

The domain structure of lanthanum-modified lead titanate ferroelectric ceramics is being studied via both conventional and convergent-beam electron microscopy. Lanthanum is added to this material both to aid in the poling process and to reduce the buildup of internal bias fields, leading to aging effects. The domain structure is an important microstructural parameter relating to poling efficiency and, consequently, piezoelectric constants crucial to the operation of any number of piezoelectric devices. Important results obtained thus far have included an observed preponderance of 90° domains, the existence of 120° domains, and the evidence of a minimum grain size for domain formation. Microstructures bear striking resemblance to martensite. Future work will involve further characterization of domain-orientation relationships through convergent-beam electron microscopy, and characterization of domain wall structure using scanning transmission and high-resolution electron microscopy. Also, one may check the La distribution in the sample by x-ray energy-dispersive spectroscopy and within the lattice by x-ray channeling-enhanced microanalysis.

Gamma ferric oxide has been used for magnetic recording media for several decades, and today it still dominates the field. Because of the instability of γ-Fe_2O_3 at high temperature, it is difficult to grow single crystals of γ-Fe_2O_3; this limitation has prevented scientists from obtaining unambiguous structural results. With the high spatial resolution of convergent-beam electron diffraction, it was possible to obtain structural information directly from single-crystal acicular γ-Fe_2O_3 particles. In this way the point group of γ-Fe_2O_3 was determined to be m3m. Bright-field imaging in a conventional transmission electron microscope shows the particles with acicular shape, containing voids but no other structural defects. The microdiffraction results indicated that only a fraction of the particles have a [110] long-axis direction; most of the particles have a long-axis direction deviated from the [110] direction.

Lead-magnesium-niobate (PMN) is of commercial interest because of its low sintering temperature, which allows multilayer capacitors to be fabricated with nickel-based electrodes as opposed to the platinum-based electrodes used currently. The problem with PMN is that it has a two-phase microstructure consisting of the perovskite and pyrochlore phases. This microstructure results in poor dielectric properties, and certain sintering conditions and post-sintering heat treatments will decrease the amount of the pyrochlore phase present. We are determining the microstructure of the two-phase material and determining how the pyrochlore phase transforms to the perovskite phase.

Optical microscopy and x-ray diffraction of ZnO materials reveal the presence of what is believed to be spinel particles at the ZnO grain boundaries. A positive correlation exists between the presence of spinel particles and good current-voltage properties. A TEM investigation is being carried out to confirm the presence of spinel particles and to understand why their presence leads to good varistor properties.

A new program on lead zirconia titanate peizoelectric ceramics (PZT) has been started. PZT ceramics are used extensively in many electronic devices such as transducers, frequency filters, pyroelectric detectors, etc., due to their high planar coupling coefficient (0.6) and high Curie point (320°C). Excellent electrical properties are observed at the morphotropic-phase boundary region (MPB), which appears approximately at $PbZr_{.52}Ti_{.48}O_3$. The domain-wall configuration and the switching mechanisms under the applied field dominate their use in the devices. Thus, the research program will initially focus attention on the following: (1) the domain-wall configuration and its characteristics; (2) the number of phases present at the MPB and the extent of the region, using the convergent-beam electron-diffraction technique; and (3) the structure of the domain wall, using high-resolution electron microscopy.

Research on the microstructure-property relations of various Nd-Fe-B-based hard magnets will commence this year. One of the major problems now overcome is specimen preparation for electron microscopy and microanalysis.

---

1. Patent applied for.

1984 PUBLICATIONS AND REPORTS

Refereed Journals

1. J.A. Wasynczuk, R.O. Ritchie, and G. Thomas, "Effects of Microstructure on Fatigue Crack Growth in Duplex-Ferrite-Martensite Steels," J. Mat. Sci. Eng. **62**, 79 (1984); LBL-16118.
2. K.M. Krishnan and G. Thomas, "A Generalization of Atom Location by Channelling Enhanced Microanalysis," J. Microsc. **136**, 97 (1984); LBL-16995.

3. T.M. Shaw, G. Thomas, and R.E. Loehman, "The Formation and Microstructure of Mg-Si-O-N Glasses," J. Am. Ceram. Soc. **67**, 643 (1984); LBL-17916.†
4. I-Nan Lin, R.K. Mishra, and G. Thomas, "Interaction of Magnetic Domain Walls with Microstructural Features in Spinel Ferrites," IEEE Trans. Magn. **Mag. 20**, 134 (1984); LBL-15994.
5. G. Thomas, "Electron Microscopy of Inorganic Materials," in *Proc. 8th European Congress on Electron Microscopy,* Budapest, Hungary, August 1984, A. Csanady, P. Rohlich, and D. Szabo, eds.; Instrum. Phys. Mater. Sci. Appl. **11**, 683 (1984); LBL-17414.
6. M. Sarikaya and G. Thomas, "HREM Studies in ALN Polytypoids," in *Proc. 8th European Congress on Electron Microscopy,* Budapest, Hungary, August 1984, A. Csanady, P. Rohlich, and D. Szabo, eds.; Instrum. Phys. Mater. Sci. Appl. **11**, 227 (1984); LBL-17400abs.†
7. G. van Tendeloo and G. Thomas, "High Resolution Microscopy Investigation of the ZrO_2-ZrN System," in *Science and Technology of Zirconia II;* Adv. Ceram. **12**, 164 (1984); LBL-16240.†
8. N.J. Kim and G. Thomas, "Effects of the Constituents on the Mechanical Behavior of Low Carbon Steels," Scripta Metall. **18**, 817 (1984); LBL-18019.
9. T.R. Dinger, K.M. Krishnan, M.I. Osendi, J.S. Moya, and G. Thomas, "Investigation of ZrO_2/Mullite Solid Solution by Energy Dispersive X-Ray Spectroscopy and Electron Diffraction," Acta Metall. **32**, 1601 (1984); LBL-17970.†
10. K.M. Krishnan, L. Rabenberg, R.K. Mishra, and G. Thomas, "Site Occupation of Ternary Elements in $Sm_2(CoTM)_{17}$ Compounds," J. Appl. Phys. **55**, 2058 (1984); LBL-16874.
11. G. Thomas, "Transmission Electron Microscopy of Inorganic Materials," in *Proc. 3rd APEM Conf.,* August 29–September 2, 1984, C.M. Fatt, Ed., University of Singapore, Applied Research Corp., Singapore, 1984, p. 28; LBL-18027.
12. K.M. Krishnan, P. Rez, R. Mishra, and G. Thomas, "Determination of the Specific Site Occupation of Rare Earth Additions in $Y_{1.7}Sm_{0.6}Lu_{0.7}Fe_5O_{12}$ Thin Films by the Orientation Dependence of Characteristic X-Ray Emissions," Mat. Res. Soc. Symp. Proc. **31**, 79 (1984); LBL-16884.
13. T.R. Dinger, "AEM Investigation of ZrO_2 Solid Solution Formation in ZrO_2/Mullite Composites," in *Proc. 42nd Annual Meeting EMSA,* Detroit, Michigan, G.W. Bailey, Ed., 1984, p. 408; LBL-17403abs.†
14. R. Gronsky, G. van Tendeloo, and G. Thomas, "High Resolution Electron Microscopy Studies of the Early Stages of Decomposition in Alloys and Ceramics," in *Proc. Acta/Scripta Conf. Sonnenberg, Germany, Decomposition of Alloys: The Early Stages,* Pergamon Press, P. Haasen et al., eds., 1984, p. 198; LBL-17369.

Other Publications

15. R. Gronsky and G. Thomas, "The ARM 1000 kV Microscope at NCEM, Berkeley and Some Applications," JEOL News, **22E**, No. 2 (27), 2 (1984); LBL-17536.
16. M. Sarikaya and G, Thomas, "AEM with a Convergent Beam," in *Proc. AEM Workshop in Microbeam Analysis Society Conf.,* Lehigh University, Bethlehem, Pennsylvania, July 16–22, 1984; LBL-18340.†
17. M. Sarikaya, "Problems Related to Quantification in Analytical Electron Microscopy," in *Proc. Westec Symp.,* March 1984, Los Angeles, California, R. Kessler and J. Todd, eds., American Society for Metals; LBL-18627.†
18. M. Ohmura and G. Thomas, "Microstructure Formation and Solute Partitioning During Inter-Critical Annealing of Dual Phase Steels," J. Metals, 50 (July 1985), TMS-AIME, October 1984; LBL-18656abs.
19. Controlled Rolling Process for Dual Phase Steels and Application to Rod, Wire, Sheet, and Other Shapes, Gareth Thomas, Jae-Hwan Ahn, and Nack-Joon Kim, File No. A 41335-1/AJT/RJS, U.S. patent pending.

LBL Reports

20. Y.S. Yoon and G. Thomas, "Microstructure, Mechanical Properties and Wear of Fe-3Cr-0.4 Steels," in *Proc. 2nd Int. Conf.—Science of Hard Materials,* Rhodes, Greece, September 21–28, 1984 (in press); LBL-18623.
21. K.M. Krishnan (Ph.D. Thesis), "Determination of Specific Site Occupations in Single Crystals by Channeling Enchanced Microanalysis: Principles and Applications," LBL-17282.
22. Y.S. Yoon (M.E. Thesis), "Microstructure, Mechanical Properties and Two-Body Abrasive Wear Resistance of an Fe-3Cr-C Based Ultra-High Strength Steel," LBL-17277.
23. A.H. Nakagawa and G. Thomas, "Microstructure-Mechanical Property Relationships of Dual-Phase Steel Wire," Met. Trans. (in press); LBL-17865.
24. K.M. Krishnan, P. Rez, and G. Thomas, "Crystallographic Site Occupancy Refinements in Thin-Film Oxides by Channelling Enhanced Microanalysis," Acta Crystall. (in press); LBL-18128.
25. J. Ahn (M.S. Thesis), "Effect of Grain Size on the Mechanical Properties of Fe-2Si-0.1C Dual Phase Steels," LBL-18682.

26. J. Yan and G. Thomas, "Effect of Thermomechanical Treatments on Microstructure and Properties of Experimental Fe/3Cr/2Mn/0.5Mo/0.4C Steel," LBL-17969.
27. G. Thomas, R.K. Mishra, and J. Gau, "Study of Precipitation and Fracture in Air-Cast Mn-Al-C Magnets," J. Mat. Sci. Lett. (in press); LBL-18368.
28. N.J. Kim, A.J. Yang, and G.Thomas, "Effect of Finish Rolling Temperature on Structure Property Relations in Nb Containing Low Carbon Steels," Metall. Trans. (in press); LBL-14469.
29. G. Thomas, "The Physical Metallurgy and Alloy Design of Dual Phase Steels," Distinguished Lecture Series, Joint Center for Materials Science of New Mexico (in press); LBL-16613.
30. C.K. Kwok and G. Thomas, "Microstructure-Abrasive Wear Characteristics of Low Carbon Dual Phase Steels," Proc. Wear of Materials (in press); LBL-17632.

Invited Talks

31. G. Thomas, "Steel Futures: Some Possible Solutions," Keynote Speaker, Industrial Liaison Program, 6th Annual Conference, College of Engineering, University of California Berkeley, March 14, 1984.
32. G. Thomas, "Electron Microscopy of Magnetic Materials," Joint Seminar, American Society of Metals and Department of Physics, University of California, San Diego, April 19, 1984.
33. R.K. Mishra and G. Thomas, "Electron Microscopy and Microanalysis of Degraded ZnO Varistors," Annual Meeting, American Ceramic Society, Pittsburgh, Pennsylvania, April 29–May 3, 1983; LBL-17482abs.
34. G. Thomas, "Dual Phase Steels," invited speaker, Steel Company of Canada, Toronto, Ontario, May 17, 1984.
35. G. Thomas, "Grain Boundaries in Ceramics," invited speaker, 2nd Joint Spain-Portugal Conference on Ceramics, Lisbon, Portugal, May 24, 1984.
36. G. Thomas, "Electron Microscopy in Materials Research," series of three lectures, Chulalongkorn University, Bangkok, Thailand, August 1984.
37. G. Thomas, "Electron Microscopy and Its Applications to Metals and Ceramics," invited speaker, Physics Department, Osaka University, Japan, September 19, 1984.
38. G. Thomas, "High Resolution Electron Microscopy of Metals and Ceramics," invited lecture, Applied Physics Department, Kyushu University, Japan, September 28, 1984.
39. J.M. Rincon, J.S. Moya, M.I. Qsendi, T. Dinger, and G. Thomas, "TEM Investigation on High Toughness Materials in the System Zirconia/Mullite," 37th Pacific Coast Regional Meeting, American Ceramic Society, San Francisco, California, October 28–31, 1984; LBL-17891abs.†
40. M. Sarikaya and G. Thomas, "Nitrogen Quantification in Sialons by Electron Energy Loss Spectroscopy," 37th Pacific Coast Regional Meeting, American Ceramic Society, San Francisco, California, October 28–31, 1984; LBL-17893abs.†
41. G. Thomas, "Alloy Design of Steels," Departamento de Metalurgia e Metalomecanica, Lisbon, Portugal, October 1984.
42. G. Thomas, "Microscopy and Microanalysis of Ceramics," Departamento de Metalurgica e Metalomecanica, Lisbon, Portugal, October 1984.
43. R.K. Mishra and G. Thomas, "Electron Microscopy of Ferrites," invited keynote lecture, Fourth International Conference on Ferrites, San Francisco, California, November 1, 1984.
44. G. Thomas, "High Strength Ductile Dual Phase Wires," invited speaker, New Zealand Steel Company, New Zealand Wire and Rope, Pacific Steel, Auckland, December 3, 1984.
45. G. Thomas, "National Center for Electron Microscopy," invited speaker, BHP Central Research Laboratories, Melbourne, Australia, December 14, 1984.
46. G. Thomas, "Research on Alloy Design of Strong and Ductile Steels," invited speaker, BHP Central Research Laboratories, Melbourne, Australia, December 8, 1984.
47. G. Thomas, "The Manufacture of Dual Phase Wires," Amalgamated Steel Mills, Petaling Jaya, Malaysia, December 17, 1984.

---

†Supported by the National Science Foundation.

Solid-State Phase-Transformation Mechanisms*

Kenneth H. Westmacott, Investigator

INTRODUCTION

The purpose of this program is to obtain a detailed knowledge of the factors that govern phase changes and phase stability in order to facilitate first-principle alloy design for specific service applications. The powerful observational methods afforded by advanced electron-optical techniques, especially high-voltage electron microscopy (HVEM) and high-resolution electron microscopy, are used to study the mechanisms that cause phase transformations to occur. Since accommodation of a new phase of disparate size or structure must involve deformation, the relationship between lattice defects and precipitate phase growth is the focus of our study. This approach has been fruitful, and a developing crystallographic theory of precipitation is being tested by a parallel experimental program. Simple model systems are treated initially, followed by studies of complex alloy systems of importance in energy technology. The resulting knowledge will contribute both to understanding alloy stability in hostile environments and to designing superior materials.

1. Ledge Structure and the Mechanism of θ' Precipitate Growth in Al-Cu (Publication 1)

U. Dahmen and K.H. Westmacott

A model of precipitate plate growth developed for the Pt-C interstitial alloy system is extended to substitutional systems and compared with observations on θ' precipitation from Al/4% Cu. By analogy, simple basic units of ledge growth involving conservative and nonconservative partial-dislocation propagation on {001} planes are predicted for θ' formation directly from solid solution. In contrast to current models for Al-Cu that assume a/n[001] dislocations at ledges, single ledges (one θ' unit cell high) are necessarily associated with partial dislocations whose shear components are 1/2[100] or 1/2[010], analogous to the 1/6<112> Shockley partials in the nucleation of γ' plates on {111} planes in Al-Ag. This result is shown to be a direct outcome of a simple lattice correspondence between the face-centered cubic (fcc) matrix and the body-centered tetragonal (bct) precipitate. In general, however, double ledges (1.16 nm high) with opposite, cancelling shears form to minimize shape change. A high-resolution lattice-fringe image showing such ledges on a growing θ' precipitate is shown in Figure 1-1.

Superledges (2.03 nm high), which are frequently observed, also minimize volume change. Misfit accommodation in the broad faces of the precipitate also arises naturally in the model from epitaxial dislocations formed by combinations of growth partials. When θ' forms from θ'', the vacancy supersaturation provided by dissolving dislocation loops is thought to initiate the transformation. A commonality of behavior found for Pt-C, Al-Cu, and Al-Ag suggests a wide validity for the proposed model.

*This work was supported by the Director, Office of Energy Research, Office of Basic Energy Sciences, Materials Sciences Division of the U.S. Department of Energy under Contract No. DE-AC03-76SF00098.

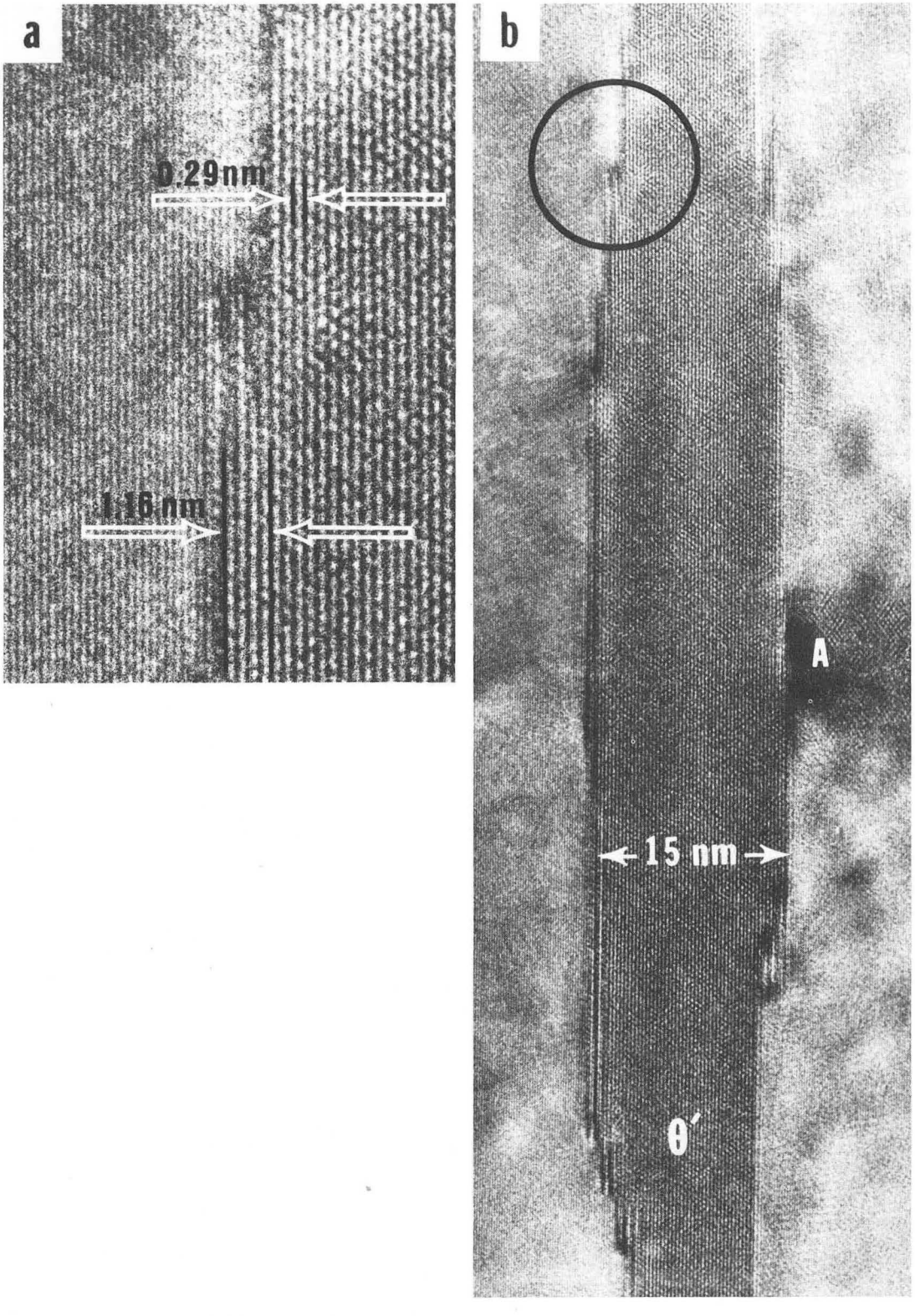

Figure 1-1. Edge-on view of (001) θ' precipitate in high-resolution axial mode; (a) is a magnified view of the ledge circled in (b). The ledges are seen nearly end-on. From (a), it is clear that these are double ledges, two θ' unit cells high. The precipitate thickness is 15 nm in the center and 8.1 nm at the ends. A precipitate of (010) variant is in direct contact with the (001) precipitate at point A in (b). (XBB 826-5060A)

2. Invariant Line Strain and Needle-Precipitate Growth Directions in Fe-Cu (Publication 3)

U. Dahmen, P. Ferguson, and K.H. Westmacott

A detailed theory of needle-precipitate growth based on the invariant-line hypothesis is presented for fcc $\rightleftarrows$ bcc (body-centered cubic) alloy systems. The basic concept, that coherent needle axes lie on cones of unextended lines, is applied to semicoherent needles. Loss of coherency and growth is shown to be possible only for those needles lying at the intersection of a cone of unextended lines with a matrix slip plane. For these needles, shear-dislocation loops can relieve the coherency stresses. Owing to the different slip geometries, <561> needle directions clustered around <110> directions are predicted for bcc Cr precipitate needles in an fcc Cu matrix, and <557> and <656> directions clustered around <111> are predicted for the inverse case of fcc Cu in bcc Fe. Precise experimental measurements on both alloy systems are in excellent agreement with the predictions. HVEM was used to examine thick foils in selected orientations where high accuracy in the measurement of needle directions could be achieved. A typical example is given in Figure 2-1. Differences observed in the incidence of <557> and <656> needles in Fe-Cu are related to the relative efficiency of the available matrix slip systems in providing transformation strain relief. The two factors that govern the precipitate crystallography are strain minimization and crystallographic strain relief.

3. Coupled Diffusion of Carbon Atoms and Vacancies in Platinum (Publication 5)

P. Ferguson, K.H. Westmacott, U. Dahmen, and R.M. Fisher

Direct evidence for the interstitial analogue of the reverse Kirkendall effect has been found in experiments of carbon diffusion through platinum membranes at 700-900°C. The carbon transport through the foil was accompanied by the formation of protrusions and depressions in the carburized and decarburized surfaces, respectively. Scanning electron micrographs illustrating these effects for membranes carburized at various temperatures are shown in Figure 3-1. The magnitude of the counterflux of platinum atoms suggests that a fraction of the carbon atoms is strongly bound to vacancies. An analysis

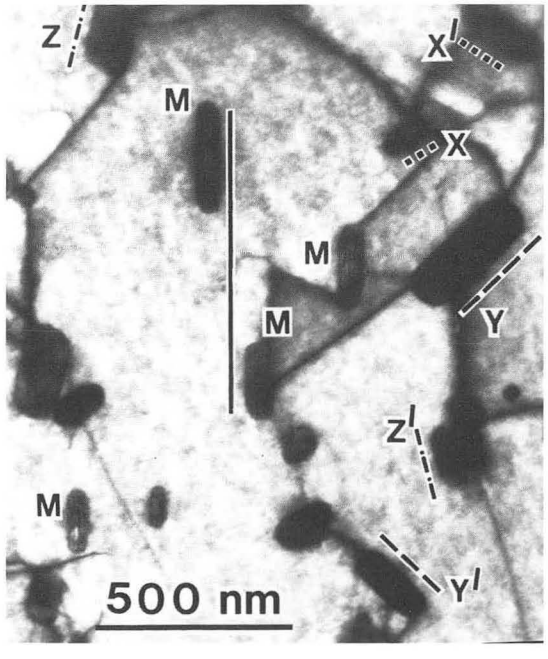

Figure 2-1. Distribution of Cu needle precipitates in a [110] zone. The needle directions can be compared directly with the predicted directions, <557> and <656>. Note the Moire fringes along precipitates marked M. The projected precipitate aspect ratio is low for Z and Z′ and high for M variants. (XBB 837-6653)

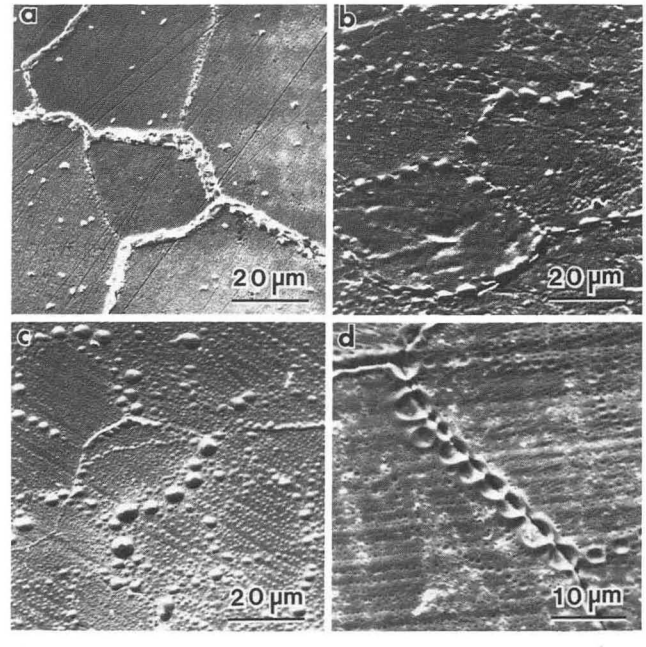

Figure 3-1. Scanning electron micrographs of the inner surface of platinum foil carburized at 700°C (a), 800°C (b), and 900°C (c), showing mounds of extruded material. The outer, decarburized foil surfaces exhibit pitting similar to that shown in (d) for the 900°C heat treatment. Note the enhanced effects at the grain boundaries. (XBB 844-2820)

based on Lomer's equation yielded a carbon-atom-vacancy binding energy $E_B \gtrsim 0.5$ eV. This value is substantially greater than the values (<0.25 ev) measured for substitutional impurity atoms in fcc metals.

4. Work in Progress

Continued progress is being made in the development of a comprehensive crystallographic theory of precipitation. The essential factors controlling the morphology and orientation of a misfitting precipitate in an elastic medium have been identified and are being incorporated in a theory that has general predictive capability.

The unusually large binding energies measured for interstitial solute-atom/vacancy complexes and the net mass transport it gives rise to have both theoretical interest and technological significance, and studies on further alloy systems are continuing. The close analogy between this phenomenon and electromigration-induced contact failure is also being examined.

1984 PUBLICATIONS AND REPORTS

Refereed Journals

1. U. Dahmen and K.H. Westmacott, "Ledge Structure and the Mechanism of θ' Precipitate Growth in Al-Cu," Phys. Stat. Sol. (a) **80**, 249 (1983); LBL-14687.
2. P. Ferguson, U. Dahmen, and K.H. Westmacott, "Morphological Aspects of α''-$Fe_{16}N_2$ Precipitation in α-Fe," Scripta Metall. **18**, 57 (1984); LBL-16661.
3. U. Dahmen, P. Ferguson, and K.H. Westmacott, "Invariant Line Strain and Needle-Precipitate Growth Directions in Fe-Cu," Acta. Metall. **32**, 803 (1984); LBL-16515.

LBL Reports

4. K.H. Westmacott and U. Dahmen, "Application of HVEM in Phase Transformation Research," LBL-17370.
5. P. Ferguson, K.H. Westmacott, R.M. Fisher, and U. Dahmen, "Coupled Diffusion of Carbon Atoms and Vacancies in Platinum," LBL-18344.
6. U. Dahmen, "Surface Relief and the Mechanism of a Phase Transformation," LBL-18405.

Invited Talks

7. K.H. Westmacott, "Application of HVEM in Phase Transformation Research," International Seminar on Phase Stability and Phase Transformation, Bombay, India, February 6–8, 1984.
8. K.H. Westmacott, "Berkeley's National Center for Electron Microscopy," Bhabha Atomic Research Center, Bombay, India, February 9, 1984.
9. U. Dahmen, "Mechanisms of Apparent Congruencies Between Diffusional and Shear Phase Transformation," Annual Meeting, American Institute of Metallurgical Engineers, Los Angeles, California, February 27–30, 1984.
10. K.H. Westmacott, "Role of Lattice Defects in Phase Transformations," 1984 Stanford Symposium, Stanford, California, February 29, 1984.
11. K.H. Westmacott, "The Role of Dislocations in Precipitation," Colloque International, Aussois, France, March 8–17, 1984.
12. K.H. Westmacott, "Transformation Tricks," Metallurgy Department seminar, Case Western Reserve University, Cleveland, Ohio, October 30, 1984.

National Center for Electron Microscopy*

Gareth Thomas, Ronald Gronsky, and Kenneth H. Westmacott, Investigators

INTRODUCTION

The National Center for Electron Microscopy (NCEM) aims to provide state-of-the-art facilities for electron-optical characterization of materials and to develop techniques of imaging, interpretation, and microanalysis.

The very high cost of modern instruments dictates time-sharing centers where facilities, support, and staff are all available. The Center, available to all qualified researchers, is built around two new microscopes, each housed in its own three-story silo. The High-Voltage Electron Microscope (HVEM), installed in 1982, accelerates electrons to energies of 1.5 million electron volts (MeV). It is the most powerful microscope of its kind in the United States. The Atomic-Resolution Microscope (ARM), installed in 1983, operates in the 0.4- to 1.0-MeV range. It offers the highest resolution in the world, with 1.6 Å already proved.

The two microscopes enable materials scientists and biologists to study samples under the most realistic conditions possible and to distinguish individual atoms even in closely packed metallic and ceramic structures.

Support facilities at the Center include 100- and 200-keV transmission electron microscopes, microanalytical instruments, equipment for preparing specimens, image-analysis devices, and computer-simulation hardware and software.

It is planned to add a 400-kV analytical microscope to take advantage of the voltage dependence of x-ray emission for research on site occupancy in complex solids as well as for general microanalytical work.

The Center is guided by a steering committee, whose present non-LBL members are Drs. J. Hren (University of Florida), Chairman; W.L. Bell (Lawrence Livermore National Laboratory); M. Gibson (Bell Laboratories); D. Howitt (University of California, Davis); F. Ponce (Xerox, Palo Alto); J.C.H. Spence (Arizona State University), and A. Taylor (Argonne National Laboratory).

*This work was supported by the Director, Office of Energy Research, Office of Basic Energy Sciences, Materials Sciences Division of the U.S. Department of Energy under Contract No. DE-AC03-76SF00098.

1. 1.5-MEV HIGH-VOLTAGE ELECTRON MICROSCOPE (HVEM)

K.H. Westmacott

Research on the HVEM covers a wide spectrum of projects, including phase-transformation studies in metals, ceramics, and minerals; semiconductor-device and amorphous-metal investigations; and biological- and medical-science applications.

Usage statistics for 1984 show an average weekly utilization of 88%. Of the outside users of the facility, about 25% are from industry, 25% are from the biological sciences, and about half are from other universities and laboratories. Abstracts of all the proposed research projects are reviewed by the Steering Committee, and copies of approved proposals are on file. A list of currently active proposals approved by the Steering Committee is given in Table 1-1.

Improvements to the instrument are continuing. The installation of a cryogenic pump on the camera chamber has reduced the pumpdown time after changing plates to 20 minutes. A further cryogenic pump will be incorporated into the system that pumps the specimen chamber. This pump will provide a better vacuum and reduced contamination, allowing longer specimen-observation times, particularly during *in situ* heating or cooling experiments.

The Birmingham double-tilt straining stage is scheduled for delivery at the beginning of 1985.

Some typical examples of HVEM work in progress are listed below.

In Situ Studies of Leaching in a Nuclear-Waste Glass (Publication 1)

D.K. McElfresh† and D.G. Howitt†

The interaction of ionizing radiation and moisture on the durability of a nuclear-waste glass was studied using *in situ* irradiation in the environmental cell. The synergistic effect of these two factors caused dramatic degradation of the glass far beyond the action of the individual effects.

An analysis of the effects of the various radiolysis products on the bulk samples revealed that the likely species causing the damage was nitric acid. This species appears to preferentially attack certain

Table 1-1
HVEM Research Proposals

Principal Investigator	Affiliation	Title
R. Ayer	Exxon	Electron-microscopic analysis of formation of surface-oxide films during high-temperature oxidation
T. Cass	Hewlett-Packard	Defect structures in semiconductor devices
C. Warble	CSIRO, Australia	Pd/MgO reaction study
R. Gronsky	LBL, MMRD	*In situ* study of the degradation of $Cu_{2-x}S/CdS$
E. Dratz	Natural Sciences Department, UC Santa Cruz	High-voltage TEM studies of ocular melanin in retinal-pigment epithelium
		Energy-dispersive spectroscopy of inclusion bodies in the thin sections of retinal-pigment epithelial cells
G. Reid	Hewlett-Packard	HVEM studies of stress-induced defect generation in CMOS-VLSI devices
J. Dash	Physics Department, Portland State University	Electrodeposition of chromium and copper in magnetic fields
		Phase transformations induced by high pressures and temperatures in a ballistic compressor
G. Thomas	LBL, MMRD	Micromechanisms of wear
		Characterization of precipitates within cemenite
		Atom location by channeling inversion voltage phenomena
		Laser surface hardening of steels
		Studies of structural defects in zeolites using HVEM
		Interface migration and solute partitioning of dual-phase steels: *in situ* studies by HVEM
G. Thomas	Sandia National Laboratory	*In situ* oxidation studies on stainless steel
M. Meyers	New Mexico Institute of Mining and Technology	Metallurgical study of dynamic fracture in metals
H. Ralston, III	UC San Francisco	Three-dimensional structure of thalamic neurons
A. Searcy	LBL, MMRD	*In situ* study of thermal decomposition of $Mg(OH)_2$
R. Wenk	Geology Department, UC Berkeley	Dislocation properties of silicate garnets

Table 1-1 (continued)

Principal Investigator	Affiliation	Title
R. Sinclair	Stanford University	Investigation of $BaTiO_3$-based dielectrics
		High-resolution multibeam lattice imaging of defects in compound semiconductors
		W-Co samples that have been deformed by microindentation
		Deformation studies of (W,Ti)C
D. Howitt	UC Davis	*In situ* studies of the kinetics of transformations in nuclear-waste glasses
		In situ environmental studies of the leaching behavior in nuclear-waste glasses
T. Budinger	LBL, Biology and Medicine Division	Blood-brain permeability studies
		Platelet architecture and responses to physical insults
		Leukemic white blood cell architecture
L. Eyring	Arizona State University	*In situ* studies of phase reactions in PrO
K. Westmacott	LBL, MMRD	Mechanism of carbon precipitation in platinum
		Dynamic hot-stage studies of precipitate development in interstitial and substitutional alloys
		Dynamic studies of changes in interface structure during the overgrowth of oxide films on metal substrates
		In situ reduction studies of NiO and related materials
		Irradiation-induced ordering in platinum-carbon alloys
A. Evans	LBL, MMRD	High-temperature deformation of ceramics
		Thin-foil studies of ceramics
		Phase-transformation toughening in 3.2% $MgO\text{-}ZrO_2$
		Studies of creep damage in Si_3N_4 and SiC
		Interfacial structure in metal-ceramic bonded systems Al_2O_3/Cu and Al_2O_3/Nb
		Crystallization and interfacial structure in SiC glass
J. Brimhall	Battelle Northwest Laboratory	Bombarding a $Mo_{50}Ni_{50}$ alloy to determine if high-energy electrons can render the material amorphous
		Bombarding $Mo_{50}Ni_{50}$ alloys made amorphous by sputter deposition by high-energy electrons at elevated temperatures to determine if the irradiation enhances the crystallization reaction
W. Stacy	Philips	Transistor pipes

Table 1-1 (continued)

Principal Investigator	Affiliation	Title
J. Porter	University of Southern California	Direct observation of the reduction of pure and doped zinc ferrite by *in situ* HVEM
		Characterization of VLS-grown ceramic whiskers
W. Owen	Biophysics Department, UC Berkeley	3-D reconstruction of extended cellular processes (axons, fibers, etc.) from serial sections of epon-embedded tissue
D. Sadana	Signetics	HVEM/ARM studies of electromigrated Al and Al-alloy films
R. Cole	UC Berkeley	Structural studies of metaphase chromosomes
J. Morris, Jr.	LBL, MMRD	Fatigue-crack propagation mechanisms of structural alloys at cryogenic temperatures
		Investigation of precipitates formed in bulk 95Pb-5Sn solder
R. Geiss	IBM	(Proprietary)
New Research		
G. Shoemaker	Mobil Research and Development Laboratory	(Proprietary)
A. Pelton	Iowa State University	Characterization of electron-induced crystalline-to-amorphous transitions in Ti-based intermetallic compounds
D. Philpott	NASA Ames Laboratory	Morphological heterogeneity of rat cardiac mitochrondria
M. Featherby	Johnson-Matthey	TEM examination of internal structure of precipitated gold spheres
L. De Jonghe	LBL, MMRD	Characterization of solid-electrolyte degradation
R. Loehman	Sandia National Laboratory	HVEM study of glass-metal reactions
A. Fox	The Polytechnic, Wolverhampton	Critical-voltage studies of alloys
		Comparative synchrotron-radiation absorption (EXAFS-XANES) and HV and electron diffraction
M. Al-Jassim	Solar Energy Research Institute	TEM investigation of GaAs/GaAsP epitaxial structures incorporating strained-layer superlattices
D. Williams	Lehigh University	Irradiation of iron-nickel alloys

phases, leading to an acceleration of damage. Work by other investigators on bulk glasses has confirmed the importance of radiolysis products on waste-glass leaching and has identified nitric acid as the most damaging component.

Future research directions in this project include investigations in specific simpler glasses to identify the influence of various components on the susceptibility to selective attack. Iron-rich silicates and certain phase-separated binary alkali silicates will be investigated using stereo microscopy to ascertain the rate of this attack into the glass and the importance of electron flux on the damage rate.

†Present address: University of California, Davis.

Screw-Dislocation Networks Generated by Stage IV Compression of Ge and Si

H.G. Brion,† P. Haasen,‡ and K.H. Westmacott

Recently stages IV and V were discovered in the work hardening of fcc and diamond-cubic crystals at high temperatures. Stage III at low temperatures is known to be due to cross-slip of screw dislocations, while steady-state creep at high temperatures is ascribed to the climb of edge dislocations. However, no direct observations of the dislocation reactions and structures responsible for stages IV and V have been made.

In the present study the dislocation configurations in Ge and Si deformed to stage IV were studied by transmission electron microscopy (TEM). Single crystals in the <123> orientation were compressed at high temperature. The HVEM was most useful for a survey of the dislocation arrangement in the main slip plane because the active slip planes at high temperature are more widely spaced than the foil thickness that is transparent at 100 kV. A typical hexagonal network on the main slip plane in Ge is shown in Figure 1-1. The mesh size is ~0.2–0.5 μm, and the misorientation across the network is ~0.1°. A detailed contrast analysis shows that these networks consist only of screw dislocations. The present study confirms the conclusion of a macroscopic analysis that dynamic recovery by climb removes the edge dislocations and forms screws in the main slip plane.

†Present address: Materials Science Department, Stanford University, Stanford, California.

‡Present address: University of Göttingen, West Germany.

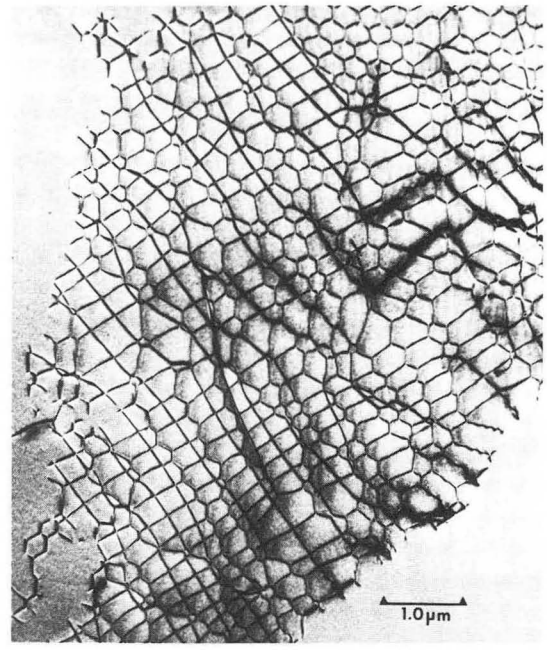

Figure 1-1. Hexagonal network of screw dislocations in the main slip plane of a Ge single crystal compressed along the <123> axis at 890°C. (XBB 853-1834)

The Use of Crystal Symmetry in the Analysis of Precipitate Morphology by TEM

U. Dahmen and K.H. Westmacott

In the characterization of microstructures, the morphology (i.e., the shape and orientation of second-phase particles) is of great importance. This type of analysis in TEM usually involves high-angle tilting and trace analysis. Sectioning by the surfaces of the thin foil can be misleading for particles 500 Å or larger. The penetrating power of 1500-keV electrons allows thick sections to be examined, extending the size range of particles whose morphology can be analyzed unambiguously. Using rod-shaped precipitates of bcc Cr in fcc Cu, a method has been developed that eliminates the need for high-angle tilting and trace analysis. Figure 1-2 shows how a micrograph recorded from a thick section of a Cu-Cr alloy in a <100> zone axis displays the symmetry elements of the cubic crystal in this projection. For every particle, another equivalent variant can be found at 90° from the first particle. Such a 2-dimensional projection of a 3-dimensional random distribution of all variants of a precipitate can give accurate and statistically significant measurements of the rod orientation by measuring angles between projected variants. The needle directions are <651>.

Figure 1-2. HVEM micrograph of a Cu-Cr alloy showing bcc Cr needles wholly contained within the foil. The <100> symmetry of the matrix is apparent in the projected angles between variants of the <651> needles. (XBB 853-1835)

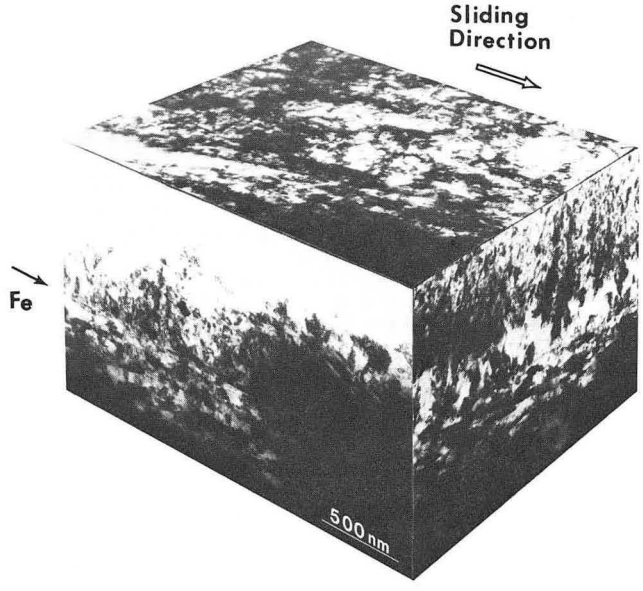

Figure 1-3. Composite micrograph showing the worn surface of a low-carbon dual-phase steel along longitudinal (left) and transverse (right) direction and also the plan view (top) parallel to the worn surface. The cross-section micrographs were obtained by cutting and ion-milling the nickel-plated worn pins in the respective directions. The top micrograph representing the worn surface was prepared by one-side jet polishing from the opposite side of the surface, with the worn surface protected by lacquer. The micrographs were obtained at 1.5 MeV. (XBB 840-9511)

Studies of Wear in Steels (Publication 5)

C.K. Kwok and G. Thomas

The advantages of the HVEM have been utilized to study subsurface structure in abraded Fe/2Si/0.1C dual-phase steel. The steel has been examined in the longitudinal direction, transverse direction, and plan view parallel to the surface. Figure 1-3 is a composite micrograph that reconstructs a microstructural model representing the worn surface. Dislocation cells, with a mean size of 20–50 nm thick and 2–3 μm long, are elongated immediately beneath the worn surface with well-defined cell boundaries aligned in the direction of abrading.

Throughout the heavily deformed subsurface region, it is not possible to distinguish the martensite phases and the ferrite matrix; thus the extensive plastic strain is distributed uniformly between the martensite phases and the ferrite phases. This strain compatibility between the two phases suppresses the likelihood of crack formation along the phase boundaries.

Application of the Critical-Voltage Effect in High-Voltage Electron Microscopy

Alan G. Fox[†] *and Robert M. Fisher*[‡]

As a result of Bloch-wave interferences, characteristic changes can be observed in both the images and the electron-diffraction patterns of pure metal or alloy specimens as the accelerating voltage of the high-voltage microscope is varied through a relatively sharp (± 2-kV) "critical voltage." This phenomenon can be used to make much more precise determinations of atomic-scattering amplitudes and Debye-Waller factors than conventional x-ray techniques. Measurements have been carried out on a number of pure metals over a range of temperatures to obtain a complete set of accurate values and comprehensive computer programs, and a data base has been developed to interpret the measurements and to predict critical-voltage values for alloys of possible interest. For example, very large changes are predicted to occur in Al-Li alloys, in keeping with the unusual properties of these alloys. Experimental studies of short-range ordering and charge redistribution in Cu-Au alloys reveal a significant increase in the {111} structure factor, corresponding

to a more spherical outer-electron distribution for Cu when alloyed with Au, in keeping with the predictions of simple band theory. In the case of Fe-Cr alloys, a small decrease in the {110} structure factor was observed, indicating a slight charge transfer (presumably from Fe to Cr). The experimental techniques and interpretative framework have been established to apply the critical-voltage effect to a wide range of alloys.

---

†Present address: The Polytechnic, Wolverhampton, England.

‡Present address: Center for Advanced Materials, Lawrence Berkeley Laboratory.

2. ATOMIC-RESOLUTION MICROSCOPE

R. Gronsky

The Atomic-Resolution Microscope (ARM) was formally made accessible to the user community in July 1984. Scientists with approved proposals are allotted one full week of instrument time to conduct their experiments. The instrument time might also include optical-diffractogram analysis of their negatives and computer simulation to aid image interpretation. A list of some of the investigations using the ARM is given in Table 2-1.

Effort has been devoted during this past year to establishing onsite computational facilities with open user work stations, improved specimen-preparation facilities for rapid cleaning or repair of specimens for high-resolution microscopy, and continued refinement of ARM operation with the recent completion of a minimum-dose exposure system for beam-sensitive materials. An example of the more recent performance of the microscope is presented in Figure 2-1.

Typical examples of ARM work in progress are listed below.

The Effect of Amorphous Surface Layers on Images of Crystals in High-Resolution Transmission Electron Microscopy (Publication 12)

R. Kilaas and R. Gronsky

The effect of a surface layer of amorphous silicon dioxide on images of crystalline silicon has been investigated for a range of crystal thicknesses varying from zero to 2.5 times that of the surface layer. Images such as the one shown in Figure 2-2 were simulated using a multislice computation routine. An amorphous surface produced fluctuations in image contrast, introducing difficulties in the interpretation of defects in very thin specimens. These difficulties are less pronounced but are still present in thicker crystals. Edges that smoothly approach zero thickness produce images that change gradually from crystalline to amorphous in character.

Image Simulation of Mullite

M.A. O'Keefe

As part of a project to characterize two-component ceramics, high-resolution images for Mullite ($2SiO_2.Al_2O_3$) in the (001) orientation were simulated by computer. A preliminary study using simplified calculations (weak phase object) showed that the Al-Si-O framework should be visible at 2.4-Å resolution, and individual Si-O and Al-O groups should be visible at 1.7-Å resolution (see Figure 2-3). A more extensive study was then conducted using a range of experimental variables (defocus and specimen thickness) that might reasonably be encountered in actual use, along with electron-optical parameters that have been measured for the ARM. Three hundred images were simulated; a random selection is shown in Figure 2-4. These images, when compared to those from the preliminary simplified images, showed that the ARM was capable of 1.7-Å resolution at the Scherzer defocus. An experimental image of unknown specimen thickness (obtained before the image simulation was performed) matched the simulated images closely at 2200–2400 Å underfocus for a specimen thickness of ~60 Å. It also matched images calculated for 1900–2200 Å defocus for specimens 200–220 Å thick. The high sensitivity of the simulated images to the experimental conditions and the difficulty in obtaining an exact match between experimental and simulated images emphasizes the need for an on-line technique to allow display of the simulated image while the experimental image is being obtained.

Research on Ceramic Glasses

R.S. Rai, R. Kilaas, and G. Thomas

One problem of critical importance in high-temperature ceramics is the formation of amorphous grain-boundary (glassy) phases in ceramics (e.g., sili-

Table 2-1
ARM Research Proposals

Principal Investigator	Affiliation	Title
G. van Tendeloo and G. Thomas	University of Antwerp, LBL	ZrO_2-ZrN alloys; ZrO_2 precipitates
		High-resolution studies of ceramics: ZrO_2-ZrN systems; new Si_3N_4 fiber materials
G. van Tenderloo	University of Antwerp	Ordered alloys
K. Merkle	Argonne National Laboratory	Tilt grain boundaries in NiO
R. Gronsky	LBL, MMRD	Structure of [001] tilt-grain boundaries in bcc materials
		Atomic mechanisms of precipitate-plate growth
		High-resolution study of the structural evolution of the $Cu_{2-x}S$/CdS interface
		Dislocations and grain boundaries in silicon—structure and segregation
		Structural and compositional characterization of $Al_xGa_{1-x}As$/GaAs interfaces by HREM
J. Washburn	LBL, MMRD	Atomic structure of the Si-SiO_2 interface
		Mechanism of gettering in elemental and compound semiconductors
		Atomic structure of III-V and II-VI compound semiconductor layers grown by molecular-beam epitaxy
G. Thomas	LBL, MMRD	High-resolution studies of glass and glass ceramics
F. Ponce	Xerox, Palo Alto	Atomic imaging of binary-compound semiconductor metals
M. Gibson	Bell Laboratories	Structure of UHV-grown epitaxial $NiSi_2$/Si interfaces and correlation with Shottky barrier height
		Studies of in-plane ordering in intercalated graphite
D. de Fontaine	LBL, MMRD	Periodic antiphase structures
K. Subramanian	Michigan State University	Determination of modulation parameters in spinodally modulated Cu-10Ni-6Sn alloy by lattice imaging
L. De Jonghe	LBL, MMRD	Characterization of Ni/ZrO_2 interface
M. Rühle	Max-Planck Institute, Stuttgart	HREM images of Nb/Al_2O_3
L. Kihlborg	University of Stockholm	Studies of structural defects and related phenomena in inorganic materials: studies of a potassium niobium oxide at atomic resolution

Table 2-1 (continued)

Principal Investigator	Affiliation	Title
R. Sinclair	Stanford University	Structural studies in tungsten carbide
D. Sadana	Signetics	HVEM/ARM studies of electromigrated Al and Al-alloy films
M. Treacy	Exxon Research and Development	Zeolite defect structures
K. Westmacott	LBL, MMRD	Ultrahigh-resolution studies of precipitate-matrix interfaces

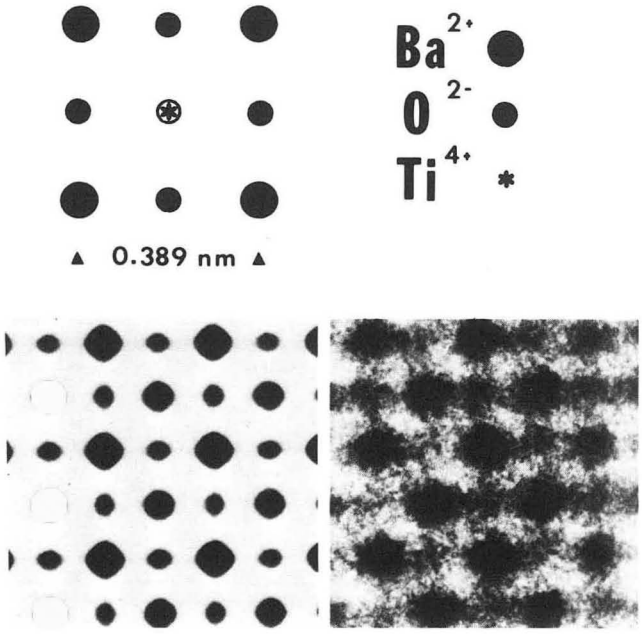

Figure 2-1. Projected structure of $BaTiO_3$ in the [001] orientation (top left). A simulated image of the structure is shown at the bottom left, and an experimental image obtained on the ARM at 1 MeV is shown at the bottom right. (XBB 843-2552)

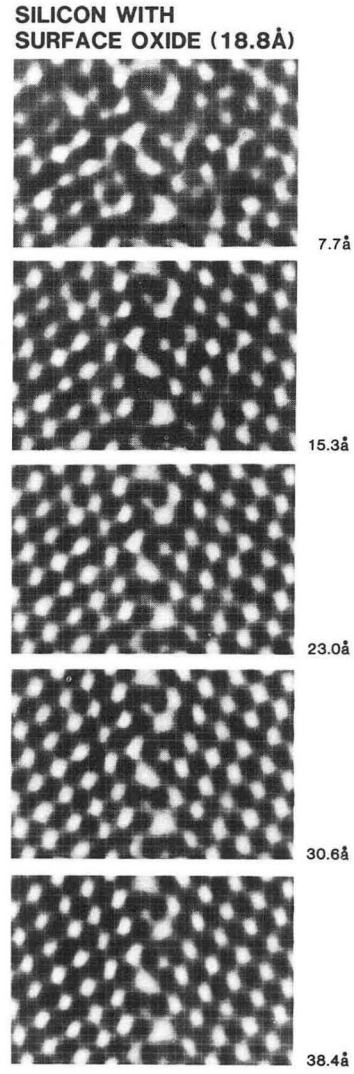

Figure 2-2. Computed electron micrographs of silicon bicrystal with native surface oxide. The total thickness of the surface layers is held constant at 18.1 Å, while the thickness of the bicrystal varies from 8 to 38 Å. (XBB 840-7593)

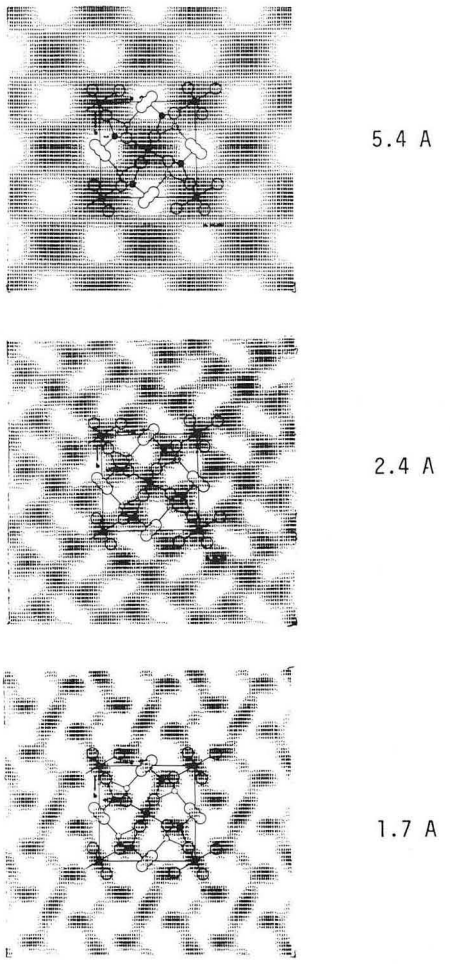

Figure 2-3. Effects of machine resolution using weak-phase object calculations. A Mullite structure is superimposed in the center of the image. Larger open circles represent oxygen; smaller solid circles represent aluminum or silicon. (XBL 853-1501)

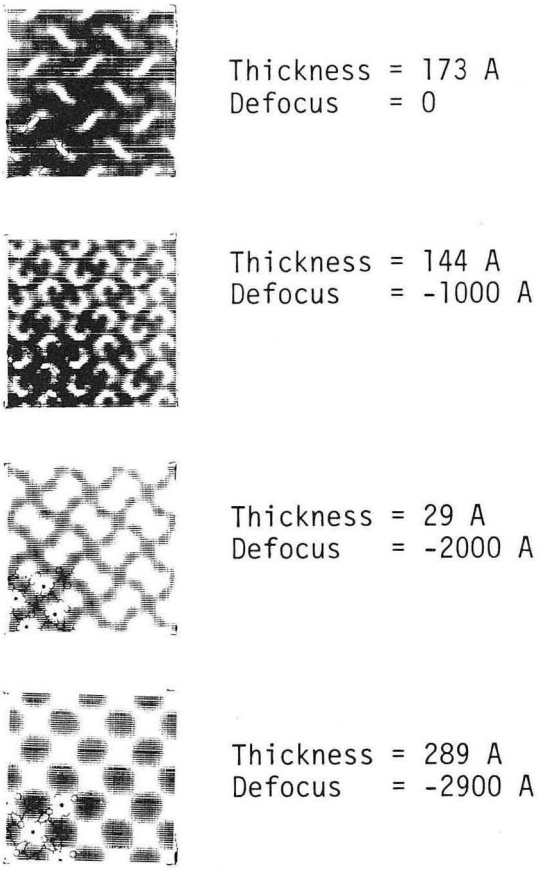

Figure 2-4. Examples of images simulating ARM operating conditions for several values of specimen thickness and machine defocus. A Mullite lattice is superimposed in the lower left corner of the images. (XBL 853-1500)

con nitride, sialons) resulting from liquid-phase sintering. Understanding the structure of such glassy phases is essential if they are to be either eliminated or crystallized to improve mechanical properties. Studies of the crystallization of glasses indicates that the process develops by a ledge mechanism similar to that observed in Gronsky's program on semiconductor oxides[1].

In an effort to try to resolve the molecular structure of glasses, computations have been performed using a simple model of SiO_2. Preliminary results are shown in Figure 2-5. The results show the critical problem of specimen thickness. The simulated image becomes almost noninterpretable when the specimen thickness exceeds about three layers.

1. R. Kilaas and R. Gronsky, LBL-18588.

Transmission Electron Microscopic Studies on Carbon-Supported Pd Catalysts

R.S. Rai, G. Thomas, and W.M. Maier[†]

An attempt has been made to characterize the suitability of Pd/C catalysts for the ROSENMUND reaction (a surface-structure-sensitive reaction) by TEM. The catalysts examined were fresh 10% Pd/C, Pd/C that had been refluxed in xylene, and catalysts annealed at 1000°C in hydrogen for 12 hours. Selected-area electron diffraction in all three cases corresponded to crystalline Pd on carbon support. High-resolution TEM studies showed that the carbon surface of the fresh Pd/C was homogeneously covered by small Pd particles (40% dispersion) of sizes in the 4–10 nm range. In the xylene-rearranged

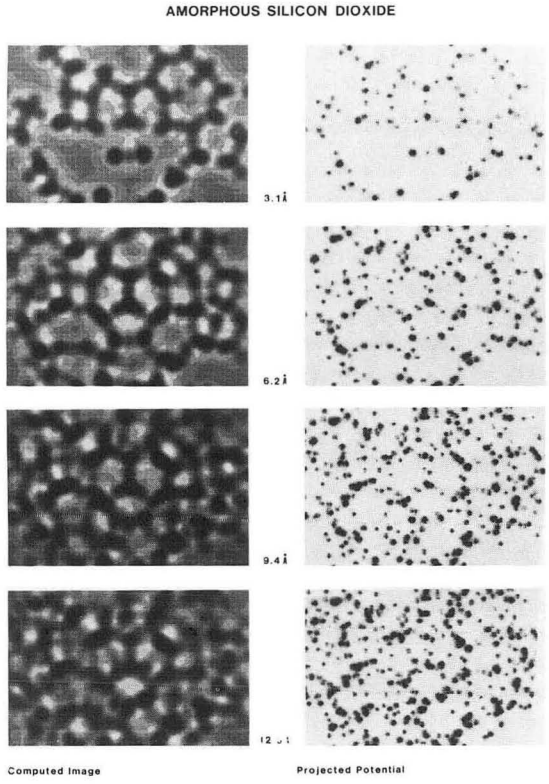

Figure 2-5. Model of SiO_2 showing random distribution of molecules. Simulated images are based on the projected potential. Notice how the images become uninterpretable in reference to the model when the film thickness exceeds about two molecular layers (⩾ 6 Å). (XBB 847-5399A)

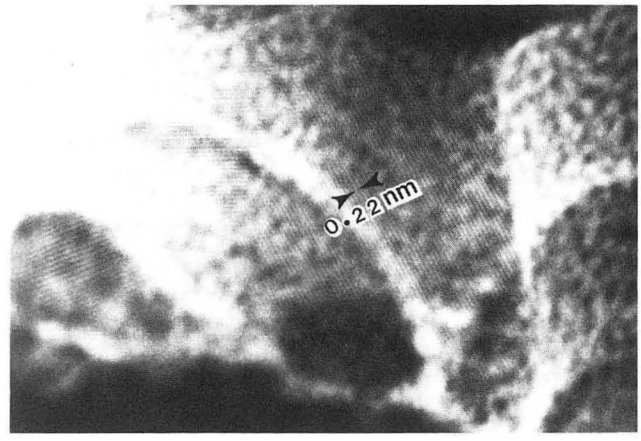

Figure 2-6. High-resolution image of a Pd/C catalyst pretreated in xylene, showing lattice fringes (d = 0.22 nm) corresponding to the periodicity of (111) planes of Pd at particle locations and the granular structure of amorphous carbon support at other places. (XBB 840-9578)

catalyst (139°C), the Pd had agglomerated in islands, leaving large areas of carbon uncovered. Three types of Pd regions were found in this case: (1) thin Pd particles on carbon support, (2) concentrated agglomerations of Pd particles, and (3) isolated Pd particles on otherwise uncovered carbon. The average particle size (~20 nm) was larger than the average particle size with the fresh catalyst, showing lower dispersion. In the Pd particles, high-resolution electron microscopy revealed lattice fringes (d ~0.22 nm) corresponding to the periodicity of (111) planes of Pd (see Figure 2-6). For the Pd/C catalyst annealed at 1000°C, the Pd particles are nearly spherical and of a wide range of sizes, but the average size (~100 nm) is larger than in the other two cases.

Knowledge of the exact orientation of Pd particles in the three cases is necessary to determine which catalyst is more active for the reaction. Microdiffraction showed that in the case of Pd/C pretreated in xylene, the thin Pd particles were frequently oriented along <110>, whereas in the other two cases the orientation appeared random. The (110) surface is a surface of high step density and corresponds to active sites for the catalyst. The chemical reaction performed with these catalysts also revealed that the catalyst pretreated in xylene was more reactive. A detailed study of Pd catalysts on

different supports such as Al_2O_3 and TiO_2 after various pretreatments is in progress.

†Present address: Department of Chemistry, University of California, Berkeley 94720.

3. ANALYTICAL ELECTRON MICROSCOPY (AEM)

U. Dahmen

A JEOL 200CX analytical microscope has been installed to provide state-of-the-art facilities for microchemical analysis to NCEM users. The 200-kV instrument, which has a side-entry double-tilt goniometer stage, can be operated in transmission or in scanning mode using primary or secondary electron detectors. A Kevex 8000 energy-dispersive x-ray analyzer with an ultrathin window and high-angle detectors allows detection and quantification of all elements from carbon to uranium in areas as small as 10 nm. The system is linked to an LSI-11/73 minicomputer with software for quantification and image analysis. The microscope is equipped with a Gatan 607 electron-energy-loss spectrometer (EELS), also linked to the minicomputer for storage and processing of EELS spectra. Both signals, electron energy loss and x ray, can be used for energy-filtered imaging or elemental mapping, respectively. The instrument allows the simultaneous acquisition and storage of energy-loss and x-ray spectra and is capable of convergent-beam electron diffraction from areas as small as 4 nm. The system is expected to be fully operational in March 1985; it will then be available to NCEM users.

An example of AEM work in progress is given below.

The Voltage and Orientation Dependence of Characteristic X-Ray Production in Thin Crystals (Publication 10)

G. Thomas, K.M. Krishnan, Y. Yokota,† and H. Hashimoto†

In preparation for the proposed addition of a 400-kV analytical microscope, a project was carried out on the Osaka 400-kV microscope involving a systematic experimental study to determine the combined effect of acceleration voltage and incident-beam orientation on the characteristic x-ray production in thin crystals (see Figure 3-1). For $MgAl_2O_4$, the voltage dependence of the orientation dependence undergoes a reversal in character above a particular voltage labeled as the "inversion" voltage. This inversion voltage has been experimentally determined to be ~270 kV for this compound, which has a spinel structure. A physical interpretation of this phenomenon in terms of the localization of the Bloch waves in the crystal has been suggested. Further detailed calculations are necessary to understand this behavior and determine its relation to the conventional critical-voltage effect. From the microanalysis point of view, it has been experimentally shown that in order to obtain an analysis independent of the incident-beam orientation or the acceleration voltage, it is essential to systematically tilt the crystal to an orientation where no lower-order Bragg-diffraction vectors are excited.

†Present address: Department of Applied Physics, Osaka University, Japan.

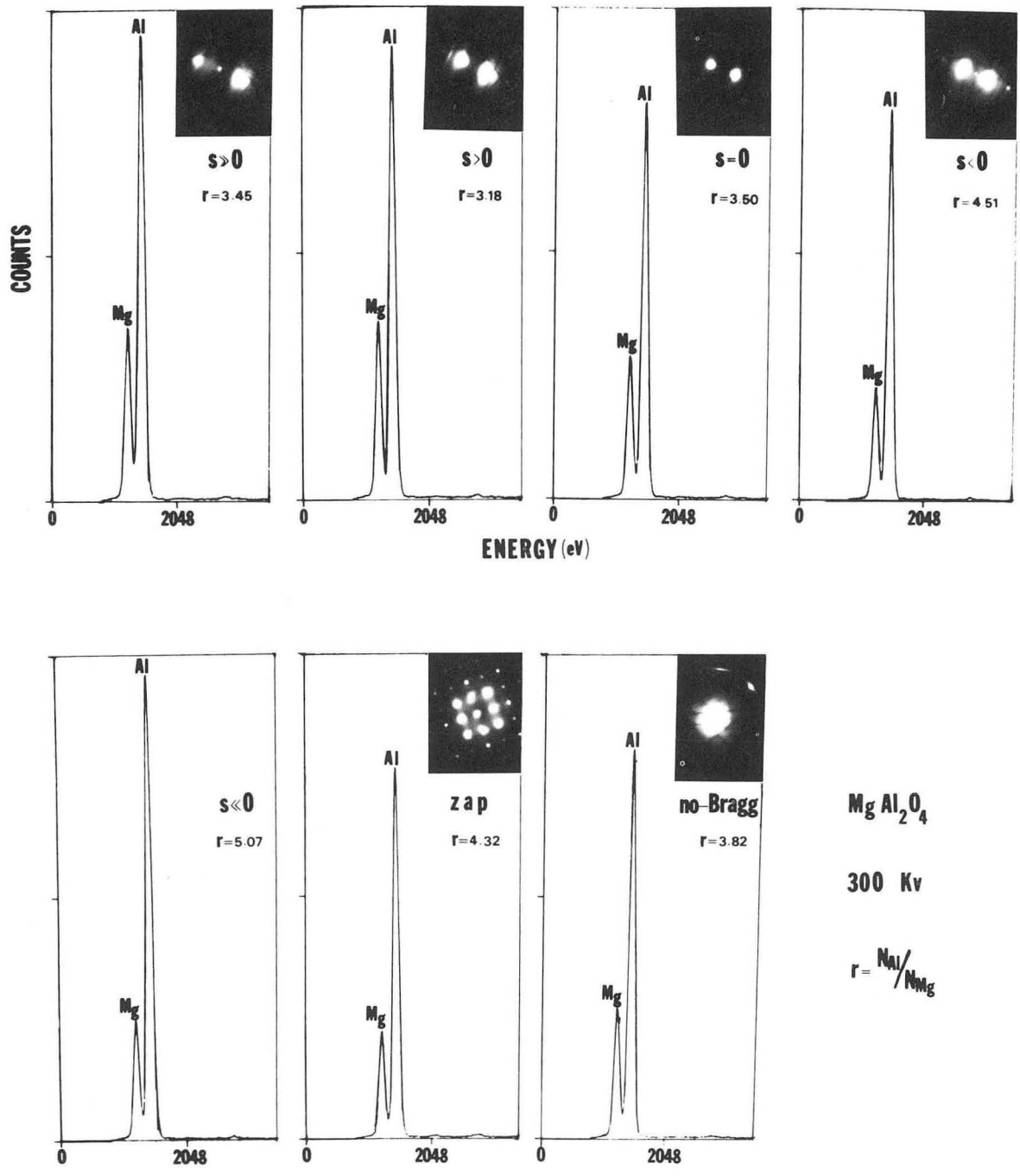

Figure 3-1. Orientation dependence of characteristic x-ray production in $MgAl_2O_4$ spinel at 300 kV for a g = 400 systematic row. (XBB 853-1739)

1984 PUBLICATIONS AND REPORTS

Refereed Journals

1. J.F. DeNatale and D.G. Howitt, "A Mechanism for Radiation Damage in Silicate Glasses," Nuc. Inst. Meth. in Phys. Res. **B1**, 489 (1984).
2. K.H. Westmacott, M. Witcomb, and U. Dahmen, "A Study of Precipitation in Interstitial Alloys, IV. The Precipitation Sequence in Pt-C," Acta Metall. **31**, 755 (1983); LBL-14777.
3. U. Dahmen, P. Ferguson, and K.H. Westmacott, "Invariant Line Strain and Needle Precipitate Growth Directions in Fe-Cu," Acta Metall. **32**, 803 (1984); LBL-16516.

4. P. Ferguson, U. Dahmen, and K.H. Westmacott, "Morphological Aspects of α'' $Fe_{16}N_2$ Precipitation in α-Fe," Scripta Metall. **18**, 57 (1984); LBL-16661.
5. K.H. Westmacott and U. Dahmen, "Application of HVEM in Phase Transformation Research," Seminar on Phase Stability and Phase Transformations, Bombay, India, Mater. Sci. Forum **3**, 325 (1985); LBL-17370.
6. R. Gronsky, "Electron Microscopy at Atomic Resolution," Mat. Res. Soc. Symp. Proc. **31**, 1 (1984); LBL-16937.
7. K.M. Krishnan and G. Thomas, "A Generalization of Atom Location by Channeling Enhanced Microanalysis," J. Microsc. **136**, 97 (1984); LBL-16995.

Other Publications

8. R. Gronsky and G. Thomas, "The ARM 1000kV Microscope at NCEM, Berkeley, and Some Applications," JEOL News **22E**, 1 (1984); LBL-17536.
9. R. Gronsky, "Resolution at its Current Limit: Applications of the Berkeley ARM," in *Proc. 42nd Ann. Meet. EMSA,* G.W. Bailey, Ed., San Francisco Press, 1984; LBL-17552.

LBL Reports

10. G. Thomas, K.M. Krishnan, Y. Yokota, and H. Hashimoto, "The Combined Effect of Acceleration Voltage and Incident Beam Orientation on the Characteristic X-Ray Production in Thin Crystals," LBL-18934.
11. K.M. Krishnan, P. Rez, and G. Thomas, "Crystallographic Site Occupancy Refinements in Thin-Film Oxides by Channeling Enhanced Microanalysis," LBL-18128.
12. R. Kilaas and R. Gronsky, "The Effect of Amorphous Surface Layers on Images of Crystals in High Resolution Transmission Electron Microscopy," LBL-18588.
13. C.K. Kwok and G. Thomas, "Microstructure-Abrasive Wear Characteristics of Low Carbon Dual Phase Steels," Proc. Wear Mater. (in press); LBL-17632.

Invited Talks

14. R. Gronsky, "The Direct Imaging of Atoms by Transmission Electron Microscopy," WESTEC '84 Symposium on Advanced Materials Characterization and Analytical Techniques, Los Angeles Convention Center, California, March 22, 1984.
15. R. Gronsky, "High Voltage Electron Microscopy for Biologists," Electron Microscopy Society of America Videotape Library Series, Life Sciences, University of California Berkeley, April 26, 1984.
16. R. Gronsky, "Atomic Resolution Microscopy," Symposium on Microstructural Characterization at Near Nanometer Resolutions, Exxon Research and Engineering, Clinton, New Jersey, July 23, 1984; LBL Summer Student Lecture Series, Lawrence Berkeley Laboratory, August 1, 1984.
17. R. Gronsky, "New Directions in Instrumentation," Workshop on Future Directions in Electron Microscopy, Electron Microscopy Society of America, Cranbrook Academy, Michigan, August 10, 1984.
18. R. Gronsky, "Microscopy for Materials Characterization," Mineral Engineering Seminar Series, Department of Materials Science and Mineral Engineering, University of California Berkeley, September 19, 1984.
19. R. Gronsky, "Analytical Technique in Electron Probe Systems," KEVEX School on Microanalysis, KEVEX Corporation, Foster City, California, November 14, 1984.
20. R. Gronsky, "Electron Microscopy for Materials Scientists," General Motors Research Laboratories, Warren, Michigan, November 30, 1984.
21. K.H. Westmacott, "Application of HVEM in Phase Transformation Research," International Seminar on Phase Stability and Phase Transformation, Bombay, India, February 6–8, 1984.
22. K.H. Westmacott, "Berkeley's National Center for Electron Microscopy," Bhabha Atomic Research Center, Bombay, India, February 9, 1984.
23. G. Thomas, "National Center for Electron Microscopy," PHB Melbourne, Australia, December 5, 1984.
24. G. Thomas, "Electron Microscopy of Magnetic Materials," Joint Seminar of the American Society for Metals and the Physics Department, University of California, San Diego, April 19, 1984.
25. G. Thomas, "Electron Microscopy in Materials Research," Chulalongkorn University, Bangkok, Thailand, August 1984.
26. G. Thomas, "Electron Microscopy and its Applications to Metals and Ceramics," Physics Department, Osaka University, Japan, September 19, 1984.
27. G. Thomas, "High Resolution Electron Microscopy of Metals and Ceramics," Applied Physics Department, Kyushu University, Japan, September 28, 1984.
28. G. Thomas, "Microscopy and Microanalysis of Ceramics," Lisbon, Portugal, October 1984.

In Situ Investigations of Gas-Solid Reactions by Electron Microscopy*

J.W. Evans, Investigator

INTRODUCTION

This work is concerned with the influence of solid microstructure on the reaction between the solid and a gas. Of particular interest is the nucleation and growth of the second solid phase when one of the products of reaction is a solid. The experimental tool used in this investigation is an environmental cell that is placed in one of the two high-voltage transmission electron microscopes at LBL. This cell enables a solid to be contacted with a gas at elevated temperatures without adversely affecting the vacuum in the microscope column. The evolution of the microstructure as the reaction proceeds can then be observed at high magnification.

Two kinds of reaction have been of interest this year: the reduction of iron oxides by hydrogen and the oxidation of doped gallium arsenide. The iron oxide study has concerned the reduction of Fe_2O_3, Fe_3O_4, and FeO. These reduction reactions are of importance in the production of steel, the major metal produced in the United States. Furthermore, these reduction reactions display features of general importance to fundamental solid-state chemistry. Gallium arsenide is used extensively in the semiconductor industry. One of the constraints limiting its wider use is the difficulty in forming an insulating film on its surface by processes such as oxidation. This behavior contrasts sharply with that of silicon, where an insulating oxide film of desirable properties forms readily. The experimental investigation on gallium arsenide at the electron microscope has produced results different from those of previous investigations using more traditional techniques.

1. *In Situ* Study of Gallium Arsenide Oxidation (Publication 3)

J.W. Evans and Mark E. Hall

Native oxide formation on GaAs was studied *in situ* using a transmission electron microscope. The GaAs was doped with silicon and oxidized at 200, 280, 320, 450, and 550°C with pure oxygen. The oxygen pressure ranged from 40 to 50 Torr. No reaction was found to occur at 200 and 280°C. An unidentified amorphous oxide was formed at 320°C. Polycrystalline β-Ga_2O_3 was formed at 450°C; oxidation at 550°C produced polycrystalline γ-Ga_2O_3.

2. Microstructural Aspects of Gas-Solid Reactions (Publication 2)

J.W. Evans and M.F. Rau

Dynamic studies of the reduction of single-crystal iron oxides have been carried out between 300 and 610°C in a high-voltage electron microscope using pure hydrogen and hydrogen/argon gas mixtures as reducing agents with pressures up to 50 Torr. The reduction of hematite by pure hydrogen below 400°C is via the following path:

Single-crystal hematite → Lath magnetite →

Porous magnetite→Porous iron.

The reduction fronts appear in hemispherical configurations, and the reduction proceeds in a topochemical manner. The transition between hematite and lath magnetite occurs rapidly, so that it may not be seen if the reaction is fast. However, the transition between porous magnetite and porous iron takes place slowly and appears to be the rate-controlling step. Directional elongated pores form at the interface of lath magnetite and porous magnetite, and spherical pores distribute randomly within the region of porous magnetite. Under the same partial pressures of hydrogen, the reduction rate of the hydrogen/argon gas mixture is at least two orders of magnitude slower than the reduction rate of pure hydrogen. The reduction takes place in an internal-reaction manner, and the product is granular magnetite. Figure 2-1 shows the nucleation and growth of iron on a reduction of magnetite by hydrogen at 2 Torr and 300°C.

When a single-crystal magnetite specimen is exposed to pure hydrogen at 350°C, pits form prior to the nucleation of porous iron. The size and shape of the pits change initially, but they are unchanged after porous iron forms. Iron nucleation takes place near or right on the pits. Iron grows isotropically when the reaction rate is fast. The reduced magnetite has a circular morphology and locates inside the specimen, implying that an edge is not necessary

*This work was supported by the Director, Office of Energy Research, Office of Basic Energy Sciences, Materials Sciences Division of the U.S. Department of Energy under Contract No. DE-AC03-76SF00098.

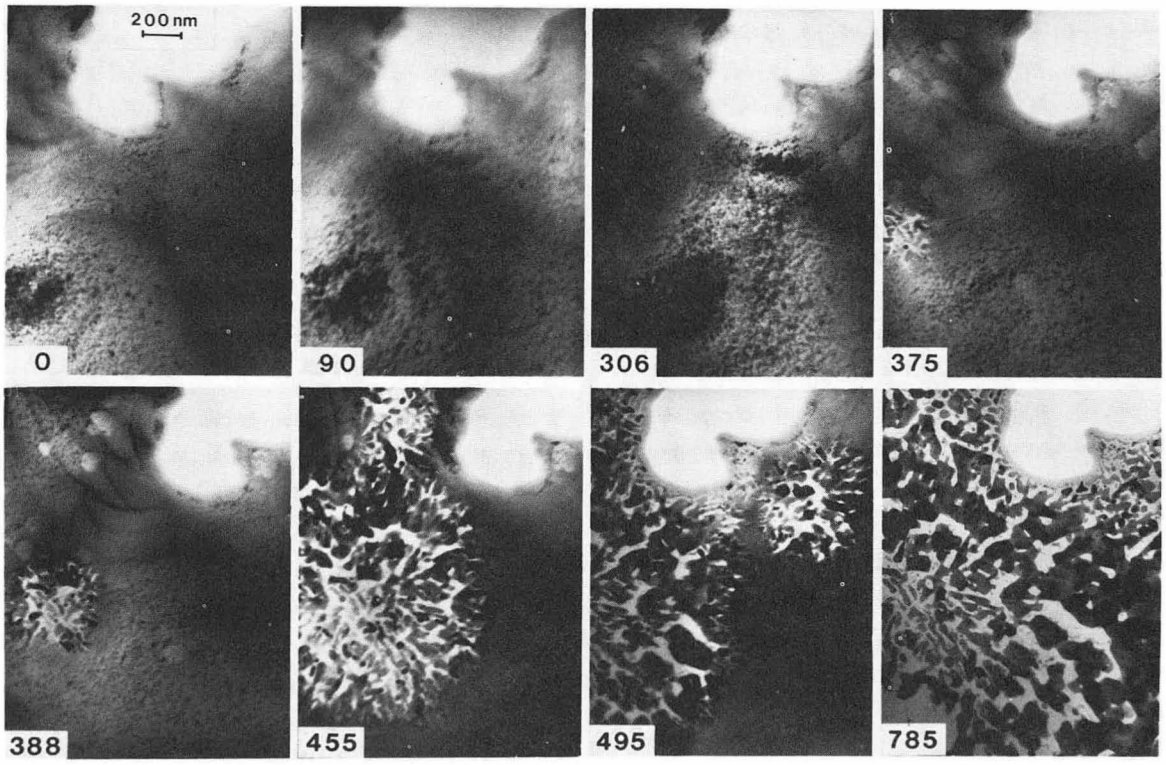

Figure 2-1. Sequence of micrographs showing the nucleation and growth of iron on a reduction of magnetite by hydrogen at 2 Torr and 300°C. The number on each micrograph is the time in seconds since the reaction temperature was reached under hydrogen. (XBB 853-1833)

for nucleation. A pronounced decrease in the reduction rate was observed when the reducing gas was replaced by hydrogen/argon gas mixtures. At a low reducing potential—e.g., conducting the reaction with a gas mixture—or during the incubation period, the reduction proceeds preferentially along certain directions. The direction with a close-packed lattice, e.g., <111>, has been shown to have a faster reaction rate.

The reduction of wustite at temperatures below 570°C occurs in a complex way. At a high reducing potential, the morphology of products is similar to the reduced magnetite. On the other hand, at a low reducing potential, disproportionation into magnetite and iron accompanies the reduction. Increasing the temperature and pressure increases the reduction rate, when pure hydrogen is used as the reducing agent. Dislocations, cracks, edges, and thin regions provide active sites for the reduction.

3. Work in Progress

Preliminary experiments are in progress on the oxidation of silicon. The oxidation of silicon is of importance in the semiconductor industry, where an oxide layer is deliberately formed in the manufacture of electronic components. Preliminary experiments are also in progress on the nucleation of a metal phase from a solid electrolyte by electrochemical reaction. By controlling the potential and coulombs passed in such experiments, it should be possible to study the nucleation and growth at different thermodynamic driving forces and readily stop and start reactions.

1984 PUBLICATIONS AND REPORTS

Other Publications

1. M.F. Rau, D. Rieck, and J.W. Evans, "The Reduction of Iron Oxide—*In Situ* Studies Using High Voltage Electron Microscopes," Annual Meeting, The Metallurgical Society of AIME, Los Angeles, California, February 1984.

LBL Reports

2. M.F. Rau (Ph.D. Thesis), "Microstructural Aspects of Gas-Solid Reactions," LBL-18901.
3. M. Hall (M.S. Thesis), "*In Situ* Study of Gallium Arsenide Oxidation," LBL-18902.

Local Atomic Configurations in Solid Solutions*

Didier de Fontaine, Investigator

INTRODUCTION

One of the most striking and baffling effects observed in alloy phases is that of long-period superstructures. Up to now, there has been no satisfactory theory to explain the temperature dependence of the period length and stability of the various ordered polytypes in generalized phase diagrams. The recently developed ANNNI (axial next-nearest-neighbor Ising) model offers, for the first time, a promising theoretical framework for understanding periodic antiphase structures. The Fisher and Selke low-temperature expansion has been extended to the ordered-alloy case, and phase-diagram calculations have been undertaken by the cluster-variation method (CVM). At first, calculations were performed for long-period superstructures in two dimensions. Such remarkable new features were discovered, however, that the two-dimensional calculations are being pursued for their own sake. Experimental work is aimed at detailed elucidation of atomic rearrangements in periodic antiphase structures in Cu_3Pd and Ag_3Mg. High-resolution transmission electron microscopy has revealed long-period polytypes in excellent agreement with theory. Another electron-microscopy study has been undertaken of short-range order in Au_4Fe, Ni_4Mo, and similar systems that exhibit predicted ⟨1½ 0⟩-type ordering stability.

1. Application of the ANNNI Model to Long-Period Superstructures (Publication 4)

Didier de Fontaine and Joseph Kulik

Existing models of long-period superstructures are reexamined in the light of the recently developed ANNNI model. In this model, long-period phases are contained in a triangular-shaped phase-diagram region bounded by a Lifshitz point on the uppermost transition-temperature line and a multiphase point at zero absolute temperature (see Figure 1-1). Periodic antiphase structures are produced by a square-wave modulation of the ordered ground state, resulting in new types of long-period superstructures, here denoted as "Fujiwara phases." The role of configurational entropy in stabilizing long-period phases is emphasized. The applicability of the ANNNI model to periodic antiphase structures in ordered alloys is examined, and the striking resemblance between predicted structures and those observed experimentally in Ag_3Mg and Au_3Zn is pointed out. The difference between "straight" and "wavy" (CuAu II) antiphase domain boundaries is discussed in the light of the model.

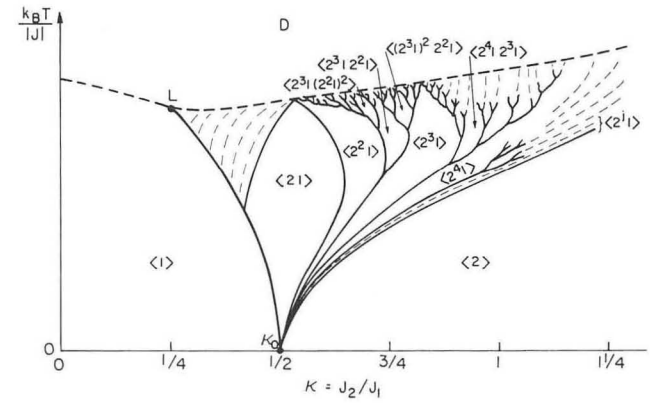

Figure 1-1. Conjectured ANNNI model phase diagram. Only a few long-period phases are shown; infinitely many others are expected, for instance in the regions covered by light dashed lines. (XBL 844-6869)

2. On the Nature of the "Short Range Order" in ⟨1½ 0⟩ Alloys (Publication 5)

G. Van Tendeloo, S. Amelinckx, and D. de Fontaine

High-resolution electron-microscope images of the ⟨1½ 0⟩ special-point short-range ordering alloys Ni_4Mo, Au_4Cr, Au_4V, and Au_4Fe are compared, and the extent to which optical diffractograms from local regions of such micrographs can be interpreted is discussed. For Au_4Cr and Ni_4Mo, the observed state of order can be interpreted as being due to the presence of microdomains of the DO_{22} structure and elements of the D1a structure, extending sometimes several unit cells along the c-direction, but being quite often only one or a small number of unit cells wide. For Au_4V and Au_4Fe, the observed diffuse intensity is probably too weak to allow decisive conclusions.

*This work was supported by the Director, Office of Energy Research, Office of Basic Energy Sciences, Materials Sciences Division of the U.S. Department of Energy under Contract No. DE-AC03-76SF00098.

3. On the Equivalence of ANNNI Model Polytypes Formed by Square-Wave Modulation and Branching Mechanisms (Publication 1)

Didier de Fontaine

Long-period structures formed by a square-wave modulation of a lattice are proved to be identical to those of stable phases found in the ANNNI model. The proof is based on a continued-fraction expansion of the modulation half-period, producing structural formulae shown to be equivalent to those obtained by a structure-combination branching process (see Figure 3-1). The same structures have been observed experimentally by high-resolution transmission electron microscopy in certain ordered alloys.

(a)

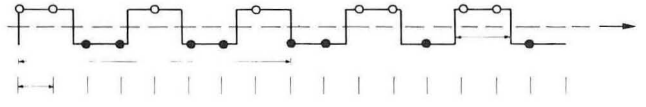

(b)

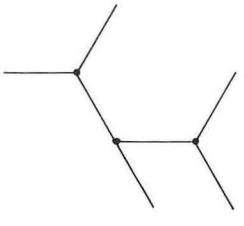

Figure 3-1. Fujiwara phase $\langle 2^2121 \rangle$: (a) square-wave modulation f(x) of period $2Ma_o$, with a polytype period $2Pa_o$, where a_o is the (unmodulated) lattice parameter; (b) equivalent graph of the corresponding structure-combination branching process, with partial domains X_i and Y_i determined by a continued-fraction expansion algorithm. (XBL 846-7074)

4. Work in Progress

Thus far, high-resolution work on Cu_3Pd has been performed on the Siemens electron microscope. Further work will be done on the JEOL 200CX, followed by detailed imaging on the atomic-resolution microscope at LBL's National Center for Electron Microscopy. The nature of antiphase boundaries will be a primary object of study, along with variation of polytype structure with temperature and composition. On the theoretical side, a two-dimensional ANNNI model is being studied by the CVM, and a modification of that model — the hexagonal network with different first-neighbor and second-neighbor interactions — is being solved exactly by a modification of the technique used for the Onsager problem. A "floating phase" has been discovered, and its phase boundaries have been calculated exactly, a result believed to be the first of its kind in theoretical statistical mechanics.

1984 PUBLICATIONS AND REPORTS

Refereed Journals

1. D. de Fontaine, "On the Equivalence of ANNNI Model Polytypes Formed by Square Wave Modulation and Branching Mechanisms," J. Phys. A: Math Gen. **17**, L713–L717 (1984); LBL-18068.

Other Publications

2. J. Kulik and D. de Fontaine, "Models of Long-Period Superstructures," in *Phase Transformations in Solids,* Maleme-Chania, Crete, June 1983, T. Tsakalakos, Ed., Mat. Res. Soc. Symp. Vol. **21**, Elsevier, 1984, pp. 225–230.

LBL Reports

3. D. de Fontaine, "On the Feasibility of *Ab Initio* Calculations of Ordering Alloy Phase Diagrams," accepted by Proc. Mat. Res. Soc.; LBL-18773.

4. D. de Fontaine and J. Kulik, "Application of the ANNNI Model to Long-Period Superstructures," Acta Metall. (in press); LBL-18067.
5. G. Van Tendeloo, S. Amelinckx, and D. de Fontaine, "On the Nature of the 'Short Range Order' in ⟨1½ 0⟩ Alloys," Acta Cryst. A (in press); LBL-18227.
6. T. Mohri, J. Sanchez, and D. de Fontaine, "Short Range Order Diffuse Intensity Calculations in the Cluster Variation Method," submitted to Acta Metall.; LBL-18774.†
7. T. Mohri, D. de Fontaine, and J.M. Sanchez, "Short Range Order Hardening with Second Neighbor Interactions in fcc Solid Solutions," submitted to Met. Trans. AIME; LBL-18775.†

Invited Talks

8. D. de Fontaine, "Application of the ANNNI Model to Long-Period Superstructures," Incommensurate Phases in Insulators Workshop, Bad Honnef, Germany, May 20–24, 1984.
9. D. de Fontaine, "(ANNNI) Long-Period Superstructures in Alloys," seminar at the University of Ghent, Belgium, May 30, 1984.
10. D. de Fontaine, "Special and Not-so-Special Points in Ordered Alloys," Materials Sciences Department Seminar, University of California Berkeley, September 27, 1984.
11. D. de Fontaine, "On the Feasibility of *Ab Initio* Calculations of Ordering Alloy Phase Diagrams," Material Research Society Conference, Boston, Massachusetts, November 27–30, 1984; LBL-18773.

†Partially funded (a postdoctoral salary) by Army Research Office, Durham, North Carolina.

Collaborative Studies by Transmission Electron Microscopy*

Norman E. Phillips, Investigator

INTRODUCTION

This program has been established to foster collaborative research between scientists with specialized skills in advanced techniques of transmission electron microscopy and scientists from other disciplines with projects requiring sophisticated microstructural characterization. Under the program, postdoctoral students or more mature visiting electron microscopists spend up to one year at LBL using the unique instrumentation available at the National Center for Electron Microscopy (NCEM) in collaborative programs with MMRD investigators recommended for support by the NCEM Steering Committee.

1. Electron Microscopy Study of the Interaction of Rhodium with Titania (Publication 1)

A.K. Singh, N.K. Pande, and A.T. Bell

Using high-resolution imaging and analysis, a study was conducted of the interaction of rhodium with titania, yielding a wealth of microstructural data on the reaction mechanisms. In Figure 1-1, a micrograph showing TiO_2-supported Rh, the Rh particles appear as flat pillbox features 20–60 Å in diameter.

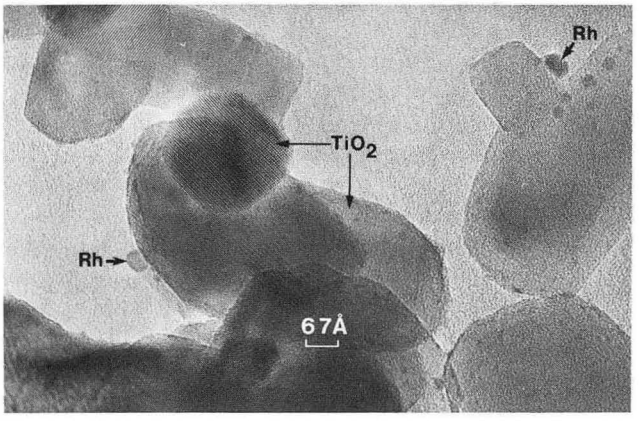

Figure 1-1. Transmission electron micrograph of TiO_2-supported Rh. Note that the Rh particles appear as flat pillbox features 20–60 Å in diameter. (XBB 840-8763)

2. Work in Progress

High-resolution results were obtained on the size, shape, and morphology of Pt particles dispersed in carbon black, and on the structural evolution of the particles as a function of heat treatment. Parallel studies of the structure of carbon black itself were also conducted at the atomic-plane level.

Structural studies of the grain boundaries in ultrapure polycrystalline lead have shown that the extent of faceting of the boundary plane is a function of impurity content. There were noticeable differences from one boundary to the next, indicating a structurally dependent oxygen-segregation process.

Analytical electron-microscopy studies of glass-metal seals have shown that there may be reaction products at the interface that induce solute partitioning on a submicron scale. The first-ever identification of a precipitate phase at such an interface was made on the S-glass/Inconel system, and the precipitate has tentatively been identified as a phosphide.

1984 PUBLICATIONS AND REPORTS

LBL Reports

1. A.K. Singh, N.K. Pande, and A.T. Bell, "Electron Microscopy Study of the Interaction of Rhodium with Titania," LBL-18583.

*This work was supported by the Director, Office of Energy Research, Office of Basic Energy Sciences, Materials Sciences Division of the U.S. Department of Energy under Contract No. DE-AC03-76SF00098.

MECHANICAL PROPERTIES

Theoretical Problems in Alloy Design*

J.W. Morris, Jr., Investigator

INTRODUCTION

This research project is concerned with the science of alloy design. It has three objectives: to develop systematic approaches to the design of new engineering materials, to build the needed scientific base, and to create new alloys that satisfy advanced engineering needs. The current research includes work on the following alloy types: (1) ferritic steels with high strength and toughness, (2) carbon steels with exceptional formability, (3) aluminum-lithium alloys with high strength, high toughness, and low density, (4) lead-tin solder contacts with outstanding fatigue resistance, and (5) high-field superconducting wire. Each of these alloy design efforts is supported by fundamental research on the relevant structure-property and structure-processing relations.

1. Advanced Metal Alloys for Energy Needs (Publication 11)

J.W. Morris, Jr.

Advanced energy technologies create a range of needs for new metal alloys that have exceptional properties that are specifically tailored to the engineering needs of particular systems. To meet these needs in a timely and economical way, it has been necessary for the metallurgical community to develop and adopt techniques for systematic alloy design. Those techniques are described and illustrated with three specific examples: (1) the development of new cryogenic structural steels for the case and support structure of high-field superconducting magnets, (2) the development of Al-Li alloys for fuel savings in aircraft, and (3) the development of formable sheet steels for use in the automotive industry.

2. The Use of Phase Transformations in the Design of Alloy Steel (Publication 8)

J.W. Morris, Jr.

This paper is intended to describe and illustrate the use of phase transformations in the design of new alloy steels. The general method of alloy design is described. Two examples are discussed: the development of new ferritic structural steels for use at cryogenic temperatures, and the development of "dual phase" steels for automotive use.

3. The Elastic Theory of the Defect Solid Solution (Publication 9)

J.W. Morris, Jr., A.G. Khatchaturyan, and Sheree H. Wen

This paper reviews the linear elastic theory of the defect solid solution. It is tutorial in nature and is primarily intended to outline the development of the theory into the mathematical form that is most suitable for the solution of practical problems. The theory treats solid solutions containing distributions of solute defects that distort the solvent lattice and interact elastically with one another. It determines the total strain of the solvent lattice and the elastic contribution to the free energy of the solution in the strong harmonic approximation. The theory is specifically developed for a binary solution of point defects in the absence of external stress. It can be extended to treat multicomponent solutions, stressed solutions, and solutions of finite defects or macroscopic inclusions. The equations governing these complex systems are also presented. The model is finally used to consider ordering and decomposition

*This work was supported by the Director, Office of Energy Research, Office of Basic Energy Sciences, Materials Sciences Division of the U.S. Department of Energy under Contract No. DE-AC03-76SF00098.

reactions in solutions whose components interact elastically.

4. Mossbauer Spectrometry Study of the Mechanical Transformation of Precipitated Austenite in 6Ni Steel (Publication 13)

B. Fultz and J.W. Morris, Jr.

A previous study suggested that precipitated austenite in in "QLT" 6Ni steel is sufficiently stable to avoid transforming to martensite in the path of a propagating crack. Impact specimens of "QLT" 6Ni steel with differing geometries were broken at 77 K and 290 K. The depth of transformation correlated with the impact energy and with the depth of the plastic zone but was mostly independent of temperature. It was concluded that the martensitic transformation of precipitated austenite occurs in the plastic deformation ahead of the crack, and in ductile fracture the precipitated austenite will not remain to interfere directly with crack propagation.

5. Characterization of Cryogenic Fe-6Ni Steel Fracture Modes: A Three-Dimensional Quantitative Analysis (Publication 15)

G.O. Fior and J.W. Morris, Jr.

Quantitative three-dimensional analyses of fracture surfaces on Fe-6Ni cryogenic steel were used to study the effect of temperature variations on the geometry of the characteristic features in different fracture modes. Stereo scanning electron-microscope (SEM) techniques combined with stereo photogrammetry provide the tools to perform such analysis on standard Charpy specimens tested with appropriate instrumentation over a 300-degree temperature range. The characteristic features of the ductile fracture mode were found to maintain a constant aspect ratio for these temperatures, while the brittle fracture modes exhibit an aspect ratio that is temperature dependent. This geometrical factor dependence of temperature in the nonductile case resembles that of the Charpy impact energy for the same temperature range. Based on these findings and on the classical stress-temperature dependence diagram, better known as the Joffee diagram, a detailed description of the ductile-to-brittle transition is discussed.

6. The Role of the Constituent Phases in Determining the Low-Temperature Toughness of 5.5Ni Cryogenic Steel (Publication 1)

J.I. Kim, H. Jae Kim, and J.W. Morris, Jr.

Ferritic Fe-Ni steels that are intended for service at low temperature are usually given an intercritical temper as the final step in their heat treatment. The temper dramatically decreases the ductile-brittle transition temperature (DBTT). Its metallurgical effect is to temper the lath martensite matrix and precipitate a distribution of fine austenite particles along the lath boundaries. Prior research suggests that the low value of DBTT is a consequence of the small effective grain size of the ferrite-austenite composite. The present research was done to test this suggestion against the counter-hypothesis that the low DBTT is due to the inherent toughness of the constituent phases. The approximate compositions of the tempered martensite and precipitated austenite phases in the composite microstructure of tempered 5.5Ni steel are known from scanning transmission electron-microscope (STEM) analysis. Bulk alloys were cast with these two compositions. Their mechanical properties were measured after heat treatment and compared to those of the parent alloy in the toughened "QLT" condition. Both of the constituent phases are brittle at low temperature. It follows that the outstanding low-temperature toughness of the tempered alloy cannot be attributed to the inherent properties of the constituent phases but must reflect their cooperative behavior in the composite microstructure. The austenitic bulk alloy was also used to investigate the stability of the precipitated austenite phase. The thermomechanical stability of the bulk alloy approximates that of the precipitated austenite within tempered 5.5Ni steel. This result is consistent with previous data and supports the conclusion that the stability of the precipitated austenite is determined mainly by its chemical composition.

7. On the Stability of Precipitated Austenite and the Toughness of 9Ni Steel (Publication 14)

B. Fultz, J.I. Kim, H.J. Kim, Y.H. Kim, G.O. Fior, and J.W. Morris, Jr.

A correlation was confirmed between the good low-temperature Charpy toughness of 9Ni steel and the stability of its precipitated austenite against the

martensitic transformation. Changes in the microstructure during isothermal tempering were studied in detail. The austenite/martensite interface is originally quite coherent over ~100 Å distances. With further tempering, however, the dislocation structure at the austenite/martensite interface changes, and this change appears to be related to the increased instability of the austenite particles. The strains inherent to the transformation of austenite particles create dislocation structures in the tempered martensite. The energy required to form these dislocation structures affects the thermodynamics of the transformation. Together with a reduction in carbon concentration during tempering, changes in these dislocation structures may also reduce the thermodynamic stability of the austenite particles as they grow larger. The large deterioration of the Charpy toughness of overtempered material is attributed, in part, to these dislocation structures, which resemble the dislocation structures found in cold-worked material.

8. The Effect of Precipitated Austenite on the Fracture of Ferritic Cryogenic Steel (Publication 16)

Darrel R. Frear

The effect of precipitated austenite on the fracture of an Fe-8Ni-2Mn-0.1Ti steel was investigated. To understand the effect an attempt was made to correlate the microstructure, mechanical properties, and the fracture-surface appearance of specimens heat treated to contain austenite or be austenite-free. The fracture surfaces were quantitatively studied using a 3D imaging technique in the SEM.

It was found that the presence of austenite had a beneficial influence on mechanical properties by lowering the DBTT. Part of this decrease was found to be due to the austenite gettering deleterious elements off the grain boundaries. Specimens that contained precipitated austenite were also found to have a smaller median facet size when fractured in a brittle transgranular mode than specimens with no austenite. The decrease in DBTT and change in fracture-surface appearance is related to the austenite transforming to martensite of a different variant than the matrix that effectively grain refines the steel and raises the cleavage stress.

9. Magnetomechanical Effects in Steels with Metastable Austenite (Publication 5)

B. Fultz

Last year we reported small effects of 8-T magnetic fields on mechanical properties of 304L stainless steel. This year we have extended these studies to tensile tests in higher magnetic fields and have found larger effects. Two distinct changes in plastic flow were observed in 18-T magnetic fields: (1) the flow stress immediately after yielding was suppressed, and (2) the work hardening in the later stages of deformation was enhanced. We argue that these two magnetically induced changes are clear evidence of two distinct effects of martensitic transformations on plastic deformation. Small magnetomechanical effects associated with martensitic transformations of retained austenite in 9Ni steel are also reported.

10. The Effects of High Magnetic Fields on the Microstructure and Toughness of Cryogenic 9Ni Steel (Publication 10)

G.O. Fior, B. Fultz, and J.W. Morris, Jr.

Commercial 9Ni cryogenic steel was heat treated to develop thermally unstable retained austenite. Some of this austenite was transformed to martensite by exposing the material to (1) cryogenic temperatures and (2) cryogenic temperatures plus 17-T magnetic fields. Those specimens exposed to the high magnetic fields consistently had the lower Charpy toughness. X-ray crystallography showed that the magnetic exposure caused additional $\gamma \rightarrow \alpha'$ transformation. Scanning electron fractography indicated that this additional $\gamma \rightarrow \alpha'$ transformation resulted in additional quasicleavage fracture and therefore a lower toughness.

It is shown that the equilibrium thermodynamics of the coexistence of magnetic phases in magnetic fields cannot account for the large increases in the amount of $\gamma \rightarrow \alpha'$ transformation caused by the magnetic field. We therefore propose that our $\gamma \rightarrow \alpha'$ transformation is a process with an activation barrier that may be overcome by magnetic exposure. The effect of the $\gamma \rightarrow \alpha'$ transformation on the Charpy energy was mostly temperature-independent, however. This suggests that the mechanism of fracture associated with the $\gamma \rightarrow \alpha'$ transformation is not thermally activated.

11. Effects of High Magnetic Fields on the Martensitic Transformation and on the Mechanical Behavior of Cryogenic Fe-9Ni Steel (Publication 19)

Gianni O. Fior

The advancement of high-field superconducting-magnet technology requires structural steel that can bear large stresses at cryogenic temperatures in the presence of high magnetic fields. One class of candidate materials is high-strength ferritic steels, such as Fe-9Ni steel, which are commonly toughened for cryogenic service by a two-phase tempering treatment that forms small austenite (γ) precipitates. A fine dispersion of submicron-sized γ is retained on cooling to cryogenic temperatures, and its presence is believed to play an important role in the suppression of the ductile-to-brittle transition of these materials. The retained γ, however, is metastable with respect to the martensitic transformation, and, since the magnetic properties of γ (paramagnetic) differ from those of the martensite (α') matrix (ferromagnetic), it is argued that a high magnetic field will influence the stability of γ.

This investigation was devoted to the study of high-magnetic-field effects on the martensitic transformation of retained γ and the corresponding effects on the mechanical properties of cryogenic Fe-9Ni steel. Thermomagnetic exposure to 16-T pulsed fields and thermomagnetomechanical exposure to 18.1-T steady fields confirmed the presence of magnetically induced $\gamma \rightarrow \alpha'$ transformation in the liquid-helium to room-temperature range. The amount of transformation exceeded that expected from equilibrium thermodynamics and resulted in a detrimental effect on the mechanical behavior of this material. The detrimental effect of the $\gamma \rightarrow \alpha'$ transformation on the mechanical properties correlated to an increase in quasicleavage fracture surface area. Microstructural characterization of the $\gamma \rightarrow \alpha'$ transformation identified the crystallographic degradation of the martensitic matrix as the source of inferior mechanical properties.

12. Welding Superalloy Sheet for Superconducting Cable Jackets (Publication 3)

L.T. Summers, M.J. Strum, and J.W. Morris, Jr.

JBK-75, an iron-based superalloy, has been selected for use as the cable-jacket material for the Westinghouse magnet of the Large Coil Project. Previous investigations of gas-tungsten-arc (GTA) welds of JBK-75 and its sister alloy A-286 have shown that age-hardened weld metal has significantly lower yield and tensile strengths than comparable heat-treated base metal. In this investigation of A-286 weldments, the undermatching properties are shown to be the result of chemical segregation during weld-pool solidification. This chemical segregation results in significant changes in the kinetics of precipitation of the γ' hardening phase.

A-286 is an iron-based precipitation-hardening stainless steel. Hardening is achieved by the precipitation of an intermetallic $Ni_3(Ti,Al)$ phase during heat treatments at temperatures usually between 650 and 800°C. The $Ni_3(Ti,Al)$ γ' phase is an ordered coherent fcc precipitate of the Ll_2-type structure. The effects of chemical composition and heat treatment on the aging response have been well characterized.

13. Critical-Current Density of Bronze-Processed Multifilamentary Nb_3Sn Wires with Magnesium Addition to the Matrix (Publication 2)

I.W. Wu, D.R. Dietderich, P.E. Johnson-Walls, J. Glazer, J.T. Holthuis, W.V. Hassenzahl, and J.W. Morris, Jr.

The effects of the addition of magnesium to the bronze of a bronze-processed multifilamentary Nb_3Sn conductor were studied. The bronze composition was varied from Cu-6.7Sn-0.0Mg to Cu-6.7Sn-0.62Mg. The magnesium was found to refine the Nb_3Sn grain size and improve the critical-current density of the superconductor. The most heavily doped wire had an optimum critical-current density three to six times better than the Mg-free control wire at all fields.

14. The Critical-Current Density and Microstructural State of an Internal Tin Multifilamentary Superconducting Wire (Publication 17)

D.R. Dietderich, J. Glazer, C. Lea, W.V. Hassenzahl, and J.W. Morris, Jr.

The critical-current density (J_c) of internal tin wires is increased when low-temperature diffusion

heat treatments are performed prior to a high-temperature reaction. To determine the variation of J with prereaction heat treatments, a copper-stabilized IGC internal-tin wire with an outside diameter of 0.267 mm was studied. The wire has filaments 2-2.5 μm in diameter, and, within the Ta barrier, the area ratio of the copper matrix and Sn core to Nb is about 2.2. Due to the character of the Cu-Sn phase diagram, heat treatments at a series of temperatures below the Nb_3Sn reaction temperature affect the local Sn concentration in the matrix about the Nb filaments. The variation in J_c resulting from these heat treatments is a consequence of the microstructural state of the conductor and the morphology of the Nb_3Sn layer produced. The results of this work show that the internal-tin and bronze-processed wires have different $J_c(H)$ characteristics. The two processes have comparable critical currents at high fields, suggesting the same H_{c2}, while at low fields the internal-tin wire is superior, suggesting a better grain morphology.

15. The Microstructural State of Nb_3Sn in a Multifilamentary Titanium-Doped Bronze-Process Wire (Publication 20)

P.E. Johnson-Walls, D. Tribula, D.R. Dietderich, W.V. Hassenzahl, and J.W. Morris, Jr.

The addition of titanium to bronze-processed Nb_3Sn wires is known to increase the upper critical field and, thus, to improve the high-field performance. High-resolution studies were done to determine the effect, if any, on the microstructure caused by Ti addition. This work used a Hitachi wire with a Nb filament diameter of 3.5 μm and a bronze-to-niobium ratio of 2.5. The bronze matrix had 7.5 at% Sn and 0.4 at% Ti. The microstructure of the Nb_3Sn layer was studied in transmission electron microscopy (TEM) on axial and longitudinal wire sections and in SEM on fractured wire surfaces. The results were compared with a previous study on a similarly processed Ti-free wire. The Ti addition caused no qualitative change in the microstructure. This result is contrasted with previous work on the beneficial effect of Mg additions that have been shown to be predominantly microstructural.

16. Cryogenic Mechanical Properties of Alloy MP35N (Publication 6)

B. Fultz, A. DuBois, H.J. Kim, and J.W. Morris, Jr.

Measurements of tensile properties, fracture toughness, and creep properties of the superalloy MP35N at 77 K and 4 K are reported. The 0.2% yield strength of MP35N at 4 K can be increased to over 2 GPa (300 ksi) after a small amount of plastic deformation. Although it is expensive and somewhat notch-sensitive, MP35N could be attractive as a structural material when extremely high strength and corrosion resistance are required.

17. Microstructure Refinement in Martensitic Fe-12Ni-0.25Ti: Thermal Mechanisms of Grain and Packet Refinement (Publication 12)

H.J. Kim and J.W. Morris, Jr.

The present work was undertaken to illustrate and clarify the three distinct metallurgical mechanisms that are used in thermal treatments to refine the effective grain size of lath martensitic steels: (1) the decomposition of austenite into distinct packets of martensite, (2) the recrystallization of the austenite on heating to above the A_f temperature, and (3) the direct refinement of martensite packets by rapid reversion to austenite. The work was also intended to identify the effective grain size in alloys having a variety of microstructures and to show that the effective grain size sometimes cannot be determined from optical or bright-field transmission electron micrographs. To accomplish this, an Fe-12Ni-0.25Ti alloy was given four types of heat treatment: (1) an anneal-and-quench treatment, (2) an intercritical anneal, (3) a single or double reversion to austenite in a furnace, and (4) a single or double rapid reversion to austenite in an induction furnace. Two effective grain sizes were identified for each heat treatment: the packet size, or dimension over which adjacent martensite laths have a common crystallographic orientation, and the prior austenite grain size. The former controls the DBTT; the latter controls intergranular embrittlement. The heat treat-

ments are shown to suppress DBTT and increase resistance to intergranular embrittlement to the extent that they decrease the relevant grain size. Rapid reversion, which causes a direct packet refinement, is the most successful of the heat treatments. It readily yields an effective grain size near 1 μm, imparting a very low DBTT and a substantial resistance to temper or hydrogen embrittlement.

18. The Influence of Precipitated Austenite on Hydrogen Embrittlement in 5.5Ni Steel (Publication 7)

Y.H. Kim, H.J. Kim, and J.W. Morris, Jr.

This work was undertaken to test the influence of precipitated austenite on transgranular hydrogen embrittlement in 5.5Ni steel. It is known from prior work that the mechanism of transgranular hydrogen embrittlement in this steel is interlath separation. Since the austenite precipitated on tempering 5.5Ni steel forms in the martensite lath boundaries, it was hypothesized that the austenite might have a beneficial effect. The experimental results show, to the contrary, that precipitated austenite decreases toughness in the presence of hydrogen. The mechanism seems straightforward. The retained austenite is transformed to martensite by the strain ahead of the crack tip. Interlath cracks appear at the periphery of the fresh martensite particles. They presumably form because of the volume change that accompanies the martensite transformation, which imposes a tension across the lath boundary and promotes interlath cracking. The interlath cracks link together to form the macroscopic fracture.

19. A Microstructural Study on the Processing and Properties of High-Field A15 Superconducting Materials (Publication 21)

I.-W.D. Wu

Superconducting properties of high-field A15 materials were studied in terms of the physical and chemical states of the A15 phases. Higher critical current is achieved through microstructural control, which is based on knowledge of the relationships between processing variables, microstructure, and the resultant properties. The A15 materials investigated include the V_3Ga and Nb_3Al phases formed by a direct-precipitation process, the multifilamentary Nb_3Sn formed by the bronze process, and bronze-processed Nb_3Sn with a Mg addition.

The direct-precipitation process has been found to have an intrinsically inferior critical current and lower stability, due to the large effective grain size, off-stoichiometric composition, and the high stability of bcc films between A15 grains. For the bronze-processed Nb_3Sn multifilamentary wire, microscopic examination reveals that the reacted layer consists of a three-shell composite structure. A mechanism to account for the formation of this structure is proposed. The critical-current density is apparently determined by the areal fraction, grain size, and composition of the central, fine-grained layer. Isothermal aging at intermediate temperatures (700-730°C) yields the best combination of microstructural features and the highest critical current. Double-aging treatments that start at 700°C and finish at 730°C improve the microstructural state of the A15 layer and enhance the critical-current density by approximately 50% at fields between 10 and 15 T. Magnesium addition to the bronze matrix increases the attainable current density (100-300%) in bronze-processed multifilamentary Nb_3Sn wires, as compared with the Mg-free wire at the nearly fully reacted heat-treatment conditions. The Mg segregates almost completely to the Nb_3Sn layer and resides predominately within the A15 matrix. The most obvious effect of the Mg addition is to retard grain coarsening during growth of the A15 layer, yielding a uniformly fine-grained A15 layer.

The theories of superconductivity, flux pinning, and the metallurgical principles of A15 conductors are critically examined. A mathematical model for calculating the free-energy increase of a superconducting body by the passage of an external current is proposed, based on the increase in kinetic energy of the electrons. A new interpretation of inductive T_c measurement and H_{c2} estimation is also discussed.

20. Pulsed-Magnetic-Field Testing of Multifilamentary Nb_3Sn Superconducting Wire (Publication 4)

J. Glazer, D.R. Dietderich, and J.W. Morris, Jr.

Critical-current density as a function of applied field $J_c(H)$ is the key design criterion for many applications of superconducting wire. Some correlations between microstructure and good properties have been made on the basis of both theory and experiment, but these relationships are not well-enough defined to obviate the need to test actual samples

frequently during the research and design process. The availability of accurate and reliable testing facilities is therefore critical to the development of practical superconductors.

This work confirms that, at a minimum, pulsed-field magnets may be used to obtain preliminary qualitative results about superconducting samples. Although the quantitative critical-current data are not as reliable as those obtained under steady fields, at high fields there is good agreement between the data. Because of the many factors that may play a role, explanation of degraded critical currents found under pulsed fields at lower applied fields is difficult. Given the present state of theory, much further investigation would be needed to clarify the precise causes of this effect and its generality to other superconductors. Nonetheless, it is apparent that pulsed-field magnets may be used effectively to direct the design process, thus allowing steady-field testing facilities to be reserved for testing the more promising materials.

1984 PUBLICATIONS AND REPORTS

Refereed Journals

1. J.I. Kim, H. Jae Kim, and J.W. Morris, Jr., "The Role of the Constituent Phases in Determining the Low Temperature Toughness of 5.5Ni Cryogenic Steel," Met. Trans. A **15A**, 2213 (1984); LBL-16231.
2. I.W. Wu, D.R. Dietderich, P.E. Johnson-Walls, J. Glazer, J.T. Holthuis, and W.V. Hassenzahl, "Critical Current Density of Bronze-Processed Multifilamentary Nb_3Sn Wires with Magnesium Addition to the Matrix," Appl. Phys. Lett. **45**, 792 (1984); LBL-16527.
3. L.T. Summers, M.J. Strum, and J.W. Morris, Jr., "Welding Superalloy Sheet for Superconducting Cable Jackets," Adv. Cryogenic Eng. **30**, 291 (1984); LBL-16530.
4. J. Glazer, D.R. Dietderich, and J.W. Morris, Jr., "Pulsed Magnetic Field Testing of Multifilamentary Nb_3Sn Superconducting Wire," Adv. Cryogenic Eng. **30**, 961 (1984); LBL-16535.
5. B. Fultz, "Magneto-Mechanical Effects in Steels with Metastable Austenite," Adv. Cryogenic Eng. **30**, 253 (1984); LBL-16536.
6. B. Fultz, A. DuBois, H.J. Kim, and J.W. Morris, Jr., "Cryogenic Mechanical Properties of Alloy MP35N," Cryogenics **24**, 687 (1984); LBL-17418.

Other Publications

7. Y.H. Kim, H.J. Kim, and J.W. Morris, Jr., "The Influence of Precipitated Austenite on Hydrogen Embrittlement in 5.5Ni Steel," U.S. Navy Report 14.
8. J.W. Morris, Jr., "The Use of Phase Transformations in the Design of Alloy Steel," in *Proc. Int. Conf. on Phase Transformations,* Vol. 21, 1984, p. 713; LBL-16550.
9. J.W. Morris, Jr., A.G. Khatchaturyan, and S.H. Wen, "The Elastic Theory of the Defect Solid Solution," in *Proc. NATO Advanced Study Inst. in Modulated Structure Materials,* T. Tsakalakos, Ed., Martinus Nijhoff, Dordrecht, Holland, 1984, p. 327; LBL-16551.

LBL Reports

10. G.O. Fior, B. Fultz, and J.W. Morris, Jr., "The Effects of High Magnetic Fields on the Microstructure and Toughness of Cryogenic 9Ni Steel," LBL-16972.
11. J.W. Morris, Jr., "Advanced Metallic Alloys for Future Energy Systems," ASM Conference on Materials for Future Energy Systems, April, 1984; LBL-17442.
12. H.J. Kim and J.W. Morris, Jr., "Microstructure Refinement in Martensitic Fe-12Ni-0.25Ti: Thermal Mechanisms of Grain and Packet Refinement," LBL-17617.
13. B. Fultz and J.W. Morris, Jr., "A Mossbauer Spectrometry Study of the Mechanical Transformation of Precipitated Austenite in 6Ni Steel," LBL-17790.
14. B. Fultz, J.I. Kim, H.J. Kim, Y.H. Kim, G.O. Fior, and J.W. Morris, Jr., "On the Stability of Precipitated Austenite and the Toughness of 9Ni Steel," LBL-17791.
15. G.O. Fior and J.W. Morris, Jr., "Characterization of Cryogenic Fe-6Ni Steel Fracture Modes: A Three Dimensional Quantitative Analysis," LBL-17792.
16. Darrel Frear (M.S. Thesis), "The Effect of Precipitated Austenite on the Fracture of Ferritic Cryogenic Steel," LBL-17910.
17. D. Dietderich, J. Glazer, C. Lea, W.V. Hassenzahl, and J.W. Morris, Jr., "The Critical Current Density and Microstructural State of an Internal Tin Multifilamentary Superconducting Wire," LBL-18654.

18. L. Summers (Ph.D. Thesis), "Effect of Chemical Segregation on the Microstructure and Properties of A-286," LBL-18655.
19. Gianni O. Fior (Ph.D. Thesis), "Effects of High Magnetic Fields on the Martensitic Transformation and on the Mechanical Behavior of Cryogenic Fe-9Ni Steel," LBL-18358.
20. P.E. Johnson-Walls, D. Tribula, D.R. Dietderich, W.V. Hassenzahl, and J.W. Morris, Jr., "The Microstructural State of Nb_3Sn in a Multifilamentary Titanium Doped Bronze-Process Wire," LBL-18704.
21. I.-W.D. Wu (Ph.D. Thesis), "A Microstructural Study on the Processing and Properties of High-Field A15 Superconducting Materials," LBL-16999.

Mechanical Properties of Ceramics*

Anthony G. Evans, Investigator

INTRODUCTION

This project is concerned with the mechanical reliability of ceramics at high temperatures. The principal research topics entail the development of predictive capabilities for the high-temperature failure of ceramics and for damage development during sintering. Elevated-temperature failure studies examine and analyze the initiation, growth, and coalescence of cracks during creep. Failure by damage accumulation within shear bands and the failure-mode transition attributed to crack blunting constitute the primary current emphases. Sintering studies are being used to examine the processes that dictate the development of damage during the sintering of inhomogeneous powder compacts. Viscoelastic stress calculations and cracking observations are subject to present investigation. In both instances, experimental measurements are correlated with theoretical models containing the dominant microstructural variables.

1. The Influence of Shear Bands on Creep Rupture in Ceramics (Publication 6)

Brian J. Dalgleish and Anthony G. Evans

The final phase of creep rupture in single-phase polycrystalline alumina consists of the formation of shear bands and subsequent crack coalescence along the bands, resulting in a serrated failure surface (see Figure 1-1). Morphological investigation of the shear bands reveals that the bands contain grain-facet-sized cavities such that the material dilates as the band propagates. The cavities within the band then coalesce and eventually induce decohesion across the band. The shear bands are invariably inclined at $\pi/3$ to the strain axis, consistent with the ratio of dilatation to shear that occurs within the band. Large-grained heterogeneities have been identified as preferred initiation sites. This preference has been attributed to shear-stress concentrations that occur at the large-grained heterogeneities because of a differential in creep viscosity. The creep-rupture strain is consequently related to the number density of large-grained heterogeneities in the material. The role of heterogeneities in creep rupture has thereby been identified.

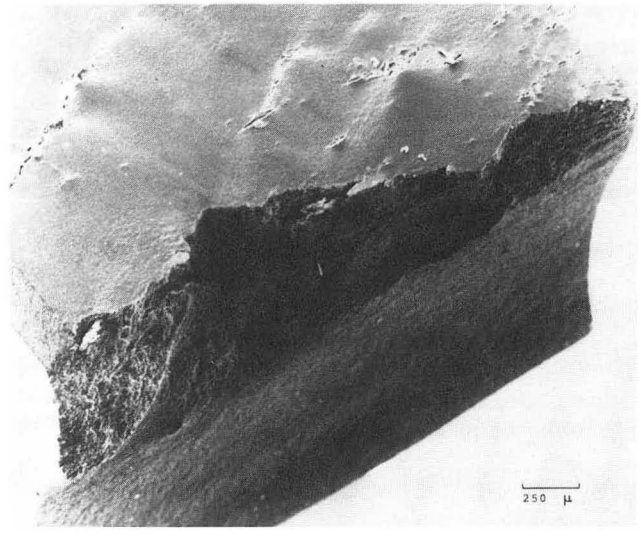

Figure 1-1. An alumina bar after failure by creep rupture. The interaction of shear bands results in a serrated fracture surface. (XBB 834-3482)

2. Creep-Crack-Growth Threshold (Publication 5)

M.D. Thouless and A.G. Evans

Prior studies have revealed that, at elevated temperatures, cracks blunt at a threshold stress-intensity factor. The blunting inhibits rupture from preexisting flaws and permits the material to exhibit enhanced rupture resistance. Eventual failure then occurs by a creep-damage process, such as shear-band formation. The blunting threshold thus emerges as an important creep-rupture parameter. An analysis of this threshold has been conducted by considering that blunting is permitted when conditions inhibit development of a creep-damage zone at the crack tip (creep-crack growth above the threshold occurs by a damage-zone mechanism). Cavity nucleation in the crack-tip zone, which is subject to creep, has thus been analyzed. A nucleation-rate-limited creep-crack-growth regime has thereby been identified (see Figure 2-1) and correlated with the threshold observed in polycrystalline Al_2O_3. This study reveals that the presence of preferred cavity

*This work was supported by the Director, Office of Energy Research, Office of Basic Energy Sciences, Materials Sciences Division of the U.S. Department of Energy under Contract No. DE-AC03-76SF00098.

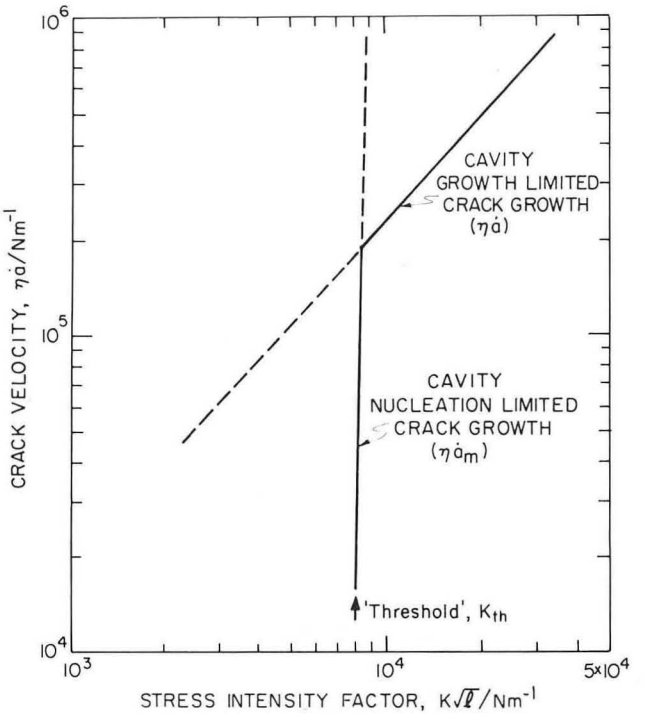

Figure 2-1. A plot of crack velocity $\eta\dot{a}$ against the stress-intensity factor $K\sqrt{\ell}$, illustrating how a threshold may arise if crack propagation is limited by cavity nucleation.
(XBL 845-6946A)

nucleation sites, such as amorphous second-phase pockets, suppresses blunting and thus encourages creep rupture from preexisting flaws. Implications for creep-rupture-resistant materials are thus manifest in the effects of microstructure on the number density of such nucleation sites.

3. Creep-Crack Growth In Liquid-Phase Sintered Ceramics (Publication 7)

M.D. Thouless and A.G. Evans

A damage-zone model of creep-crack growth, previously developed for single-phase materials, has been extended to liquid-phase sintered ceramics. In these materials, damage in the crack-tip zone is considered to consist of holes formed within the second phase, at two or three grain interfaces, as suggested by observations of creep cracks in an Al_2O_3/SiO_2 alloy. The holes then expand and coalesce by a viscous-flow mechanism. The second phase also influences creep, by acting as a preferred mass-transport path, via a solution/reprecipitation mechanism. The analysis predicts crack-growth behavior that depends strongly on the thickness of the second phase and its viscosity, as well as important effects of grain size (in agreement with results obtained for Al_2O_3). However, when normalized by the creep viscosity of the material, the crack growth rate is not much greater than that evaluated for single-phase materials. The major effects of the second phase on creep-crack growth are thus reflected in the influence of this phase on the creep viscosity and on cavity nucleation at the blunting threshold (see Publication 5). Microstructural design criteria for creep-rupture resistance are implicit in these trends.

4. Stresses and Damage in Sintering (Publication 8)

C.H. Hsueh, A.G. Evans, R.M. Cannon, and R.J. Brook

Inhomogeneities in a powder compact tend to sinter at rates different from the host material, resulting in the development of stress. The stress, in turn, may induce damage that behaves as a fracture-limiting flaw in the sintered product. A viscoelastic procedure for calculating stresses created by heterogeneities has been devised. The procedure is based on constitutive laws that describe the sintering rates, viscous relaxation rates, and elastic properties of the sintering body, as functions of density, powder size, and temperature. The laws are determined from combinations of sintering and creep models and from experimental data. Available sintering and creep data for Al_2O_3 have been used to validate the constitutive laws and subsequently to predict stresses that form around regions with initial deviations in powder size and density. Very large stresses are thereby determined to form around regions with a relatively larger initial density or particle size than the host. Important trends in stress development with temperature and powder size have also been identified. Further studies will examine the development of damage within the induced stress fields.

5. Sintering In Materials Containing a Liquid Phase (Publication 9)

J.E. Marion

An experimental and theoretical study of sintering in a model Al_2O_3 anorthite system has revealed the role of the liquid phase in the sintering process.

Transmission electron-microscopy (TEM) studies have indicated that the liquid phase rapidly establishes a steady-state thickness because of viscous flow. The steady-state channel thickness has been attributed to structural forces that develop because of ordering of the amorphous material, as determined by TEM techniques. The liquid channel then acts as a preferred mass-transport path and thereby enhances the sintering. Sintering rates predicted from models based on mass transport through the liquid phase agree closely with measurements performed on Al_2O_3/anorthite.

6. Elimination of Surface Voids (Publication 10)

M.D. Drory and A.G. Evans

Surface voids that remain after sintering have been eliminated by heat treating in a powder bed. The technique can be used to improve the resistance of surfaces to contact damage and to limit metal penetration in metal/ceramic systems. Studies conducted on MgO reveal that the elimination occurs at relatively low temperatures, without grain growth and without further densification within the interior. Models of void elimination based on surface diffusion and on evaporation/condensation from the powder bed have been developed. Comparison of the model predictions with the experimental measurements for MgO reveals that the process is surface diffusion controlled.

7. Work in Progress

Investigation of the specific influences of shear bands on creep rupture has been in progress using sequential tests to evaluate the progression of creep damage prior to rupture. These tests have revealed that a proportion of specimens ($\sim$10%) fail quite rapidly, whereas the remainder exhibit substantial rupture lives. The premature ruptures all occur without shear-band formation. Furthermore, the fracture surfaces are planar and contain a single fracture-initiating flaw. Such failures apparently occur by the growth of preexisting flaws (frequently large-grained regions), because the flaws are of sufficient size that the initial stress intensity at the flaw exceeds the crack-blunting threshold. The remaining specimens all exhibit shear-band formation and serrated failure surfaces. These specimens thus fail by a creep-damage process, at substantial creep strains (a consequence of the blunting of all preexisting flaws, due to their relatively smaller size). The predicted transition in behavior, around the crack-blunting threshold, has thus been amply demonstrated.

Sequential observations of shear bands reveal that the majority of bands nucleate at large-grained heterogeneities located either at the surfaces or in the immediate subsurface. Shear bands, once formed at heterogeneities, appear to extend to an equilibrium size and then arrest. Subsequent straining initiates additional shear bands (at heterogeneities), while cavitation damage proceeds within the previously formed bands. Eventual rupture entails the coalescence of two bands, initiated in close proximity, after the bands have experienced substantial damage. Furthermore, present data suggest that rupture occurs when the product of the stress and strain attains a critical value. The rationale for the result remains to be developed, but the result clearly constitutes a simple (if general) failure criterion for design purposes.

Further studies of crack nucleation at chemical heterogeneities are also in progress. For this purpose, small ($\sim$50-μm) SiO_2 particles are placed in arrays on the specimen surface. The specimens are then heat treated to cause the SiO_2 to penetrate into the Al_2O_3 surfaces. Thereafter, the specimens are subjected to creep. Cracks are observed to nucleate at all heterogeneities after minimal creep strains. The cracks then stop after attaining lengths 2 to 3 times the heterogeneity diameter. Final rupture involves the coalescence of arrested cracks across intervening bands. Sequential studies of the progression to failure should provide specific details regarding the influence of these heterogeneities on the rupture life. Transitions between crack-growth control and creep-damage control are also being sought.

Calculations of stresses around heterogeneities in sintering bodies are being correlated with sintering-damage observations obtained on MgO compacts. Cylindrical zones of high initial density in a low-density host develop radial cracks upon sintering. The extent of cracking is observed to depend both on the magnitude of the deviation in initial density and on the sintering temperature. The trends in cracking are attributed to the differing levels of stress generated around the heterogeneity. For purposes of stress analysis, unconstrained shrinkage rates and creep viscosities of porous compacts are measured as functions of density, grain size, and temperature. The results are then incorporated into the generalized constitutive laws for sintering and creep (developed in previous studies) needed to calculate viscoelastic stresses. For the MgO system, the analysis reveals that the stresses diminish as the tem-

perature increases, due to the larger activation energy for viscous flow than for sintering. This trend is consistent with the reduced cracking tendencies observed at the higher sintering temperatures.

The calculations of viscoelastic stresses generated during sintering have been extended to include a powder compact containing a significant volume fraction of heterogeneities. The results indicate strong effects of multiple heterogeneities. The most important trend is a reduction in stress as the heterogeneity content increases. This reduced stress is associated with the development of hydrostatic tension in the host and a related decrease in the net sintering rate of the compact. Sintering damage is thus predicted to be prevalent either around isolated heterogeneities or within an ensemble of heterogeneities. The results of these calculations are being correlated with effects of hard agglomerates on sintering rates and sintering damage. In particular, predicted effects of the spatial arrangement of agglomerates and of temperature on sintering damage are subject to present investigation.

1984 PUBLICATIONS AND REPORTS

Refereed Journals

1. M.D. Drory and A.G. Evans, "Effects of Voids at Three-Grain Junctions on Sintering and Creep Damage," J. Am. Ceram. Soc. **67** (11), 727-731 (1984); LBL-15880.
2. B.J. Dalgleish, S.M. Johnson, and A.G. Evans, "The High Temperature Failure of Polycrystalline Alumina - I. Crack Nucleation," J. Am. Ceram. Soc. **67** (11), 741-750 (1984); LBL-16167-I.
3. W. Blumenthal and A.G. Evans, "The High Temperature Failure of Polycrystalline Alumina - II. Creep Crack Growth and Blunting," J. Am. Ceram. Soc. **67** (11), 751-759 (1984); LBL-16167-II.
4. B.J. Dalgleish, S.M. Johnson, and A.G. Evans, "The High Temperature Failure of Polycrystalline Alumina - III. Failure Times," J. Am. Ceram. Soc. **67** (11), 759-763 (1984); LBL-16167-III.
5. M.D. Thouless and A.G. Evans, "Some Considerations Regarding the Creep Crack Growth Threshold," Scripta Metall. **18**, 1175-1180 (1984); LBL-17567.

LBL Reports

6. B.J. Dalgleish and A.G. Evans, "The Influence of Shear Bands on Creep Rupture in Ceramics," J. Am. Ceram. Soc. (in press); LBL-18044.
7. M.D. Thouless and A.G. Evans, "On the Phenomenon of Creep Crack Growth in Liquid Phase Sintered Materials," Acta. Metall. (in press); LBL-18789.
8. C.H. Hsueh, A.G. Evans, R.M. Cannon, and R.J. Brook, "Viscoelastic Stresses and Damage During Sintering of Heterogeneous Powder Compacts," Acta. Metall. (in press); LBL-18790.
9. J.E. Marion (Ph.D. Thesis), "Densification and Deformation in the Presence of a Liquid Phase," LBL-18140.
10. M.D. Drory and A.G. Evans, "The Elimination of Surface Voids in Ceramics," J. Am. Ceram. Soc. (in press); LBL-18373.
11. M.D. Thouless (Ph.D. Thesis), "Models of Creep Crack Growth in Ceramics," LBL-18179.

Invited Talks

12. A.G. Evans, "Creep Rupture in Ceramics," Gordon Conference, Colby College, New Hampshire, July 30, 1984.
13. A.G. Evans, "Creep Rupture in Ceramics," Cambridge University, England, February 1984.
14. A.G. Evans and W. Blumenthal, "High Temperature Failure," Creep Fracture of Engineering Materials and Structures, Swansea, England, April 1, 1984.
15. A.G. Evans, "High Temperature Failure," EEC Petten, Holland, May 1984.
16. A.G. Evans, "High Temperature Failure," Max-Planck Institute, Stuttgart, West Germany, March 1984.
17. B.J. Dalgleish, E. Slamovich, and A.G. Evans, "The Influence of Shear Bands on Creep Rupture in Ceramics," Pacific Coast Regional Meeting, American Ceramic Society, San Francisco, California, October 1984.
18. C. Ostertag and A.G. Evans, "Differential Shrinkage in Sintering," Pacific Coast Regional Meeting, American Ceramic Society, San Francisco, California, October 1984.
19. M.D. Drory and A.G. Evans, "Some Effects of Voids at Three Grain Junctions on Sintering and Creep," Pacific Coast Regional Meeting, American Ceramic Society, San Francisco, California, October 1984.
20. J. Marion and A.G. Evans, "Mechanisms of Liquid Phase Sintering," Pacific Coast Regional Meeting, American Ceramic Society, San Francisco, California, October 1984.

Environmentally Affected Crack Growth in Engineering Materials*

Robert O. Ritchie, Investigator

INTRODUCTION

The objective of this program is to examine, from combined continuum and micromechanistic points of view, the role of mechanical, microstructural, and environmental factors involved in the subcritical crack growth of flaws. Emphasis has been placed on crack growth by the following mechanisms: (1) transgranular cleavage cracking, where statistical models for brittle fracture in lower-strength steels have been developed; (2) microvoid coalescence, where models for crack-growth toughness in ductile alloys are being examined through the use of nonstationary crack analyses; and (3) fatigue crack propagation, where modeling is focused on the premature closure of cracks (crack closure) at low crack velocities approaching the threshold stress intensity ranges (ΔK_{TH}) for the dormancy of both long and short flaws. The highlight of the past year has been the utilization of the latter concept of crack closure, specifically originating from the roughness of the fracture surface due to a meandering crack path, to produce exceptionally high fatigue resistance in plain carbon steels, i.e., AISI 1008 and 1015. The approach is based on the promotion of crack deviation from the presence of certain morphologies of duplex microstructures, as developed in previous years for dual-phase Fe/0.2Si/0.1C high-purity steels.

1. Statistical Aspects of Cleavage Cracking

Tsann Lin, A.G. Evans, and R.O. Ritchie

Experimental studies on low-temperature transgranular cleavage fracture on low-carbon mild steel have been performed on microstructures where ferrite grain size and carbide size have been independently varied by heat treatment. Uniaxial tensile, single, and double-notched bend and fracture toughness (K_{Ic}) testing has been used to evaluate the flow stress, critical local-fracture stress, and crack-initiation toughness for each microstructure as a function of temperature. Results are analyzed in terms of a proposed model for cleavage fracture based on weakest-link statistics, representing a modification of that recently proposed by Evans[1] to predict the critical microstructural distance (characteristic dimension) from the crack tip, where the initial cracking event is most probable. The model, which is valid where the critical step is the propagation of grain-boundary carbide cracks into the ferrite matrix (see Figure 1-1), is discussed in terms of quantitative microstructural analyses, specifically involving the statistical distribution of cracked carbides within an active zone at the crack tip (see Figure 1-2). The prediction of macroscopic plane-strain fracture toughness in terms of the variation with microstructure and temperature is then performed using the model and confirmed using experimental measurements of yield strength, strain hardening coefficients, and the Weibull parameters describing the carbide size distribution.

1. A.G. Evans, Metall. Trans. A **14A**, 1349 (1983).

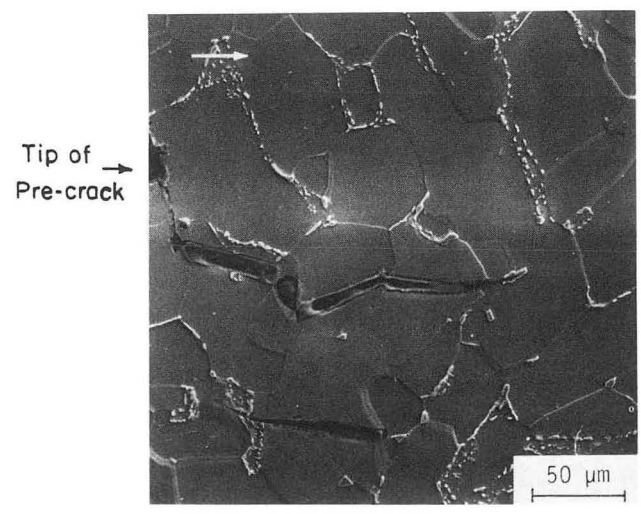

Figure 1-1. Scanning electron micrograph of cleavage cracking in AISI 1008 mild steel, showing the development of transgranular cracks initiated at cracked grain-boundary carbides ahead of the pre-crack tip. Etched in nital. (XBB 851-81)

*This work was supported by the Director, Office of Energy Research, Office of Basic Energy Sciences, Materials Sciences Division of the U.S. Department of Energy under Contract No. DE-AC03-76SF00098.

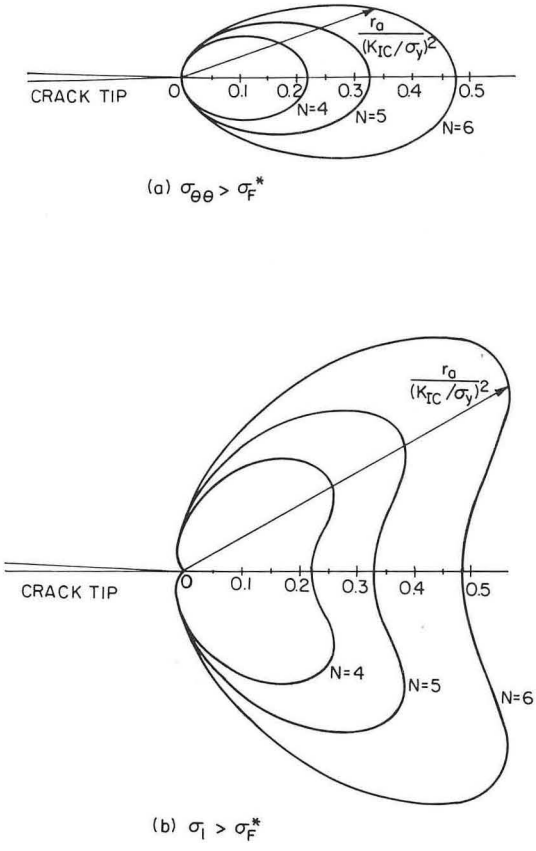

Figure 1-2. Predictions of the active zone ahead of the pre-crack tip within which eligible cracked carbides for cleavage fracture can exist. Predictions are given for various strain-hardening coefficients (N) for the cases of (a) $\sigma_{\theta\theta} > \sigma_F^*$, and (b) $\sigma_1 > \sigma_F^*$, where $\sigma_{\theta\theta}$ and σ_1 are the local $\theta\theta$ and maximum principal stress, respectively, developed at the tip of a tensile crack, and σ_F^* is the local fracture stress. (XBL 8501-5703)

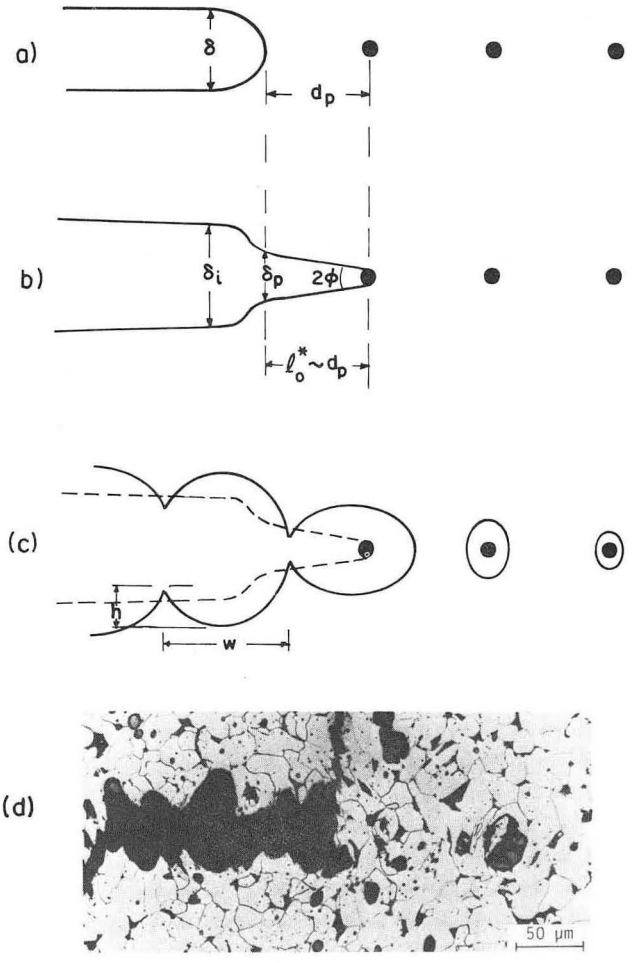

Figure 2-1. Idealization of stable crack growth via microvoid coalescence showing (a) blunted crack tip, (b) crack growth to next inclusion based on constant crack opening angle (2ϕ) or on a critical crack-opening displacement (δ_p) at distance (ℓ_o^*) behind the crack tip, (c) morphology of resulting fracture surface relevant to definition of fracture surface roughness (M = h/w), and (d) fractographic section through ductile crack growth via coalescence of voids in mild steel. (XBB 830-10794)

2. Crack Initiation and Crack-Growth Toughness

R.O. Ritchie and Tae Sung Oh

Relationships between crack initiation and crack-growth toughness have been developed using analyses of the crack-tip fields for stationary and nonstationary cracks and microscopic (local) and macroscopic (continuum) fracture criteria for the onset and continued quasistatic extension of cracks in ductile materials via microvoid coalescence (see Figure 2-1). Specifically, the local fracture parameters in such models, namely the critical fracture strains and characteristic microstructural dimensions, are described in terms of the roughness of the resulting fracture surfaces, as described in Publication 14. Currently, such models, which predict an enhanced role of microstructure in influencing crack growth as opposed to crack initiation or toughness, are evaluated in a series of very high-purity heats of Fe/1.5Ni/1Cr/0.5Mn steels, chosen to systematically vary the size, distribution, and morphology of the second-phase particles. Results are used to verify the proposed relationship between the nondimensional slope of the crack-growth resistance curve, i.e., the tearing modulus T_R and the crack-initiation fracture toughness J_{Ic}.

3. Near-Threshold Fatigue Crack Propagation (Publication 11)

R.O. Ritchie

Many studies into the propagation of fatigue cracks have focused on the near-threshold regime where growth rates per cycle approach atomic dimensions and where stress intensity ranges approach a threshold ΔK_{TH} below which cracks essentially remain dormant. In general, the many reported mechanical, microstructural, and environmental factors that can influence the fatigue threshold are shown to be effective via extrinsic mechanisms, such as crack-closure (see Figure 3-1) and crack-deflection processes, which *locally* perturb the "crack-driving force." Moreover, the predominance of such extrinsic mechanisms suggests that the validity of a threshold concept must be questioned for such situations as variable-amplitude loading or in the presence of small flaws. In the present study, current physical interpretations of near-threshold fatigue are reviewed, with reference to variable-amplitude loading effects and the apparent anomalous behavior of small cracks. Further, through comparison with classical S/N and Mode III data, the relationships between the fatigue limit and long and short crack thresholds are analyzed in terms of the many mechanisms of crack closure.

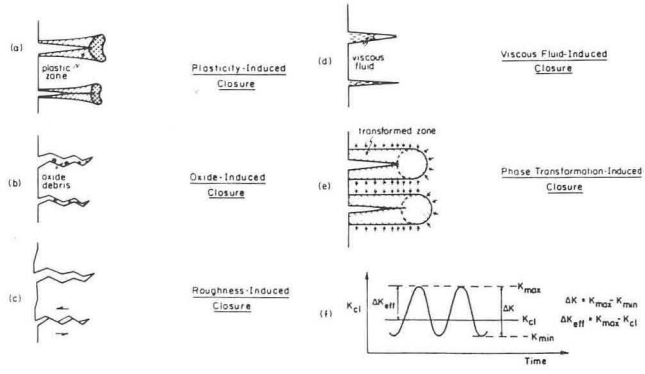

Figure 3-1. Schematic illustration of primary mechanisms of fatigue crack closure and nomenclature for defining the nominal and effective "crack driving forces." ΔK = stress intensity range. (XBL 839-6312A)

4. Optimizing Fatigue Crack Growth Resistance in Plain-Carbon Steels

J.-L. Tzou,† S. Shang, and R.O. Ritchie

Previous studies in a high-purity Fe/2Si/0.1C dual-phase steel developed by G. Thomas have indicated that the presence of specific distributions of ferrite and martensite within duplex microstructures can lead to exceptionally high resistance to fatigue crack propagation from the resultant tortuous crack-path morphology, as described in Publications 1 and 4. The effect results from a reduction in local "crack-driving force" from both crack-deflection mechanics and the production of enhanced roughness-induced closure from asperity contact across mating fracture surfaces. In the present studies, such concepts have been applied to conventional hot-rolled plain-carbon AISI 1008 and 1015 steels by intercritical annealing heat treatments to produce coarse duplex microstructures. The resulting fatigue crack propagation resistance at low load ratios is found to be extremely high, with threshold ΔK_{TH} values above 20 MPa$\sqrt{m}$ in the microstructure containing 26% martensite (see Figure 4-1). As before, such exceptionally high near-threshold fatigue crack growth resistance can be attributed to the production of a meandering crack path and the consequent crack-surface wedging from enhanced asperity contact (see Figure 4-2).

†Present address: National Semiconductor Corp., Santa Clara, California 95051.

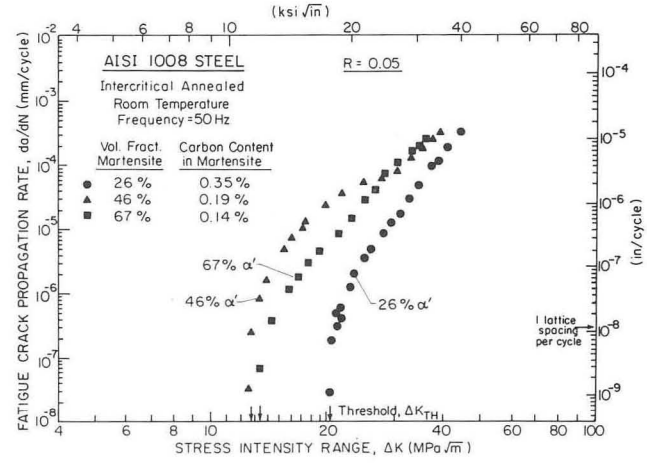

Figure 4-1. Variation in fatigue crack propagation rates (da/dN) with stress intensity range (ΔK) in an AISI 1008 plain-carbon steel, intercritically annealed to produce duplex ferritic/martensitic microstructures. (XBL 8501-5702)

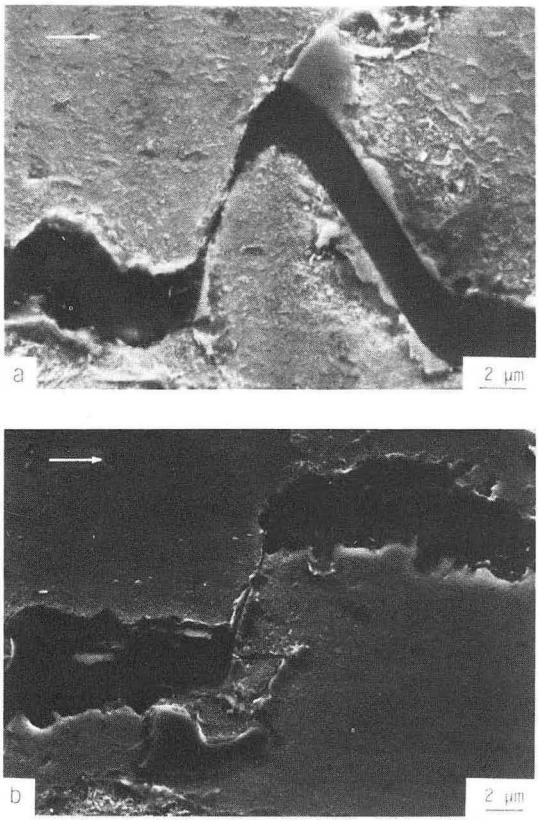

Figure 4-2. Enhanced roughness-induced crack closure from asperity contact between mating fracture surfaces in intercritically annealed AISI 1008 steel with a coarse duplex ferritic/martensitic (46%) microstructure. (a) ΔK = 13 MPa$\sqrt{m}$, (b) ΔK = 17 MPa$\sqrt{m}$. (XBB 851-82)

1984 PUBLICATIONS AND REPORTS

Refereed Journals

1. V.B. Dutta, S. Suresh, and R.O. Ritchie, "Fatigue Crack Propagation in Dual-Phase Steels: Effects of Ferritic-Martensitic Microstructures on Crack Path Morphology," Metall. Trans. A **15A**, 1193 (1984); LBL-16264.
2. J.-L. Tzou, S. Suresh, and R.O. Ritchie, "Fatigue Crack Propagation in Oil Environments - I. Crack Growth Behavior in Silicone and Paraffin Oils," Acta Metall. **33**, 105 (1985); LBL-16028.
3. J.-L. Tzou, C.H. Hsueh, A.G. Evans, and R.O. Ritchie, "Fatigue Crack Propagation in Oil Environments - II. A Model for Crack Closure Induced by Viscous Fluids," Acta Metall. **33**, 117 (1985); LBL-16842.
4. J.A. Wasynczuk, R.O. Ritchie, and G. Thomas, "Effects of Microstructure on Fatigue Crack Growth in Duplex Ferrite-Martensite Steels," Mat. Sci. Eng. **62**, 79 (1984); LBL-14891.
5. S. Suresh and R.O. Ritchie, "The Propagation of Short Fatigue Cracks," Int. Metals Rev. **29** (6), 445 (1984).†
6. E. Zaiken and R.O. Ritchie, "On the Location of Crack Closure and the Threshold Condition for Fatigue Crack Growth," Scripta Metall. **18**, 847 (1984).†
7. R.O. Ritchie, E.R. Parker, P.N. Spencer, and J.A. Todd, "A New Series of Advanced 3Cr-Mo-Ni Steels for Thick Section Pressure Vessels in High Temperature/High Pressure Hydrogen Service," J. Mat. for Energy Systems **6** (3), 151 (1984).‡

Other Publications

8. J.-L. Tzou, S. Suresh, and R.O. Ritchie, "Fatigue Crack Propagation in Viscous Environments," in *Mechanical Behavior of Materials IV, Proc. 4th Int. Conf. (ICM-4),* Stockholm, Sweden, Vol. 2, J. Carlsson and N.G. Olhsen, eds., Pergamon Press, Oxford, England, 1984, p. 711; LBL-15780.
9. S. Suresh and R.O. Ritchie, "Near-Threshold Fatigue Crack Propagation: A Perspective on the Role of Crack Closure," in *Fatigue Crack Growth Threshold Concepts,* D.L. Davidson and S. Suresh, eds., TMS-AIME, Warrendale, Pennsylvania, 1984, p. 227; LBL-16263.
10. V.B. Dutta, S. Suresh, G. Thomas, and R.O. Ritchie, "Fatigue Resistance and Microstructure of Experimental Dual Phase Fe-2Si-0.1C Steel," in *Fracture Prevention in Energy and Transport Systems,* I. Le May and S. Neves Monteiro, eds., EMAS Ltd., Warley, England, 1984, p. 457; LBL-16681.
11. R.O. Ritchie, "Thresholds for Fatigue Crack Propagation: Questions and Anomalies," in *Advances in Fracture Research '84, Proc. 6th Int. Conf. on Fracture (ICF-6),* New Delhi, India, Vol. 1, S.R. Valluri et al., eds., Pergamon Press, Oxford, England, 1984, p. 235; LBL-17646.
12. E.R. Parker, R.O. Ritchie, J.A. Todd, and P.N. Spencer, "An Advanced 3Cr-Mo-Ni Steel for Hydrogen Service," in *Research on Chrome-Moly Steel,* R.A. Swift, Ed., Vol. MPC-21, American Society for Mechanical Engineers, New York, 1984, p. 109.‡
13. R.P. Gangloff and R.O. Ritchie, "Environmental Effects Novel to the Propagation of Short Fatigue Cracks," in *Fundamentals of Deformation and Fracture,* B.A. Bilby and K.J. Miller, eds., Cambridge University Press, Cambridge, England, 1984.†

LBL Reports

14. R.O. Ritchie and A.W. Thompson, "On Macroscopic and Microscopic Analyses for Crack Initiation

and Crack Growth Toughness in Ductile Alloys," Metall. Trans. A (in press); LBL-16603.

15. R.O. Ritchie, "Near-Threshold Fatigue: An Overview of the Role of Microstructure and Environment," to be published in *Fatigue '84,* Vol. 3, C.J. Beevers, Ed., EMAS Ltd., Warley, England; LBL-18457.
16. R.O. Ritchie, "Slow Crack Growth: Macroscopic and Microscopic Aspects," to be published in *Fracture and Fracture Prevention,* G.G. Garrett, Ed., Pergamon Press, Oxford, England; LBL-18631.

Invited Talks

17. R.O. Ritchie, "Environmentally Assisted Crack Growth in Engineering Materials," Materials and Molecular Research Division, Lawrence Berkeley Laboratory, February 1984.
18. R.O. Ritchie, "Design of Low-Alloy Steels for Thick-Walled Pressure Vessels," Department of Energy, Fossil Fuel Energy Materials Program, Washington, D.C., February 1984.‡
19. R.O. Ritchie, "Mechanics and Mechanisms of Near-Threshold Fatigue Crack Growth in Metals," Royal Institute of Technology, Stockholm, Sweden, February 1984.
20. R.O. Ritchie, "Overview of Short Crack Effects in Fatigue," Symposium on Synergism of Microstructures, Mechanisms, and Mechanics in Fracture, 113th Annual Meeting, AIME, Los Angeles, California, February 1984.
21. R.O. Ritchie, "Advances in Fatigue Research at Berkeley," Industrial Liaison Conference, University of California Berkeley, March 1984.
22. R.O. Ritchie, "Crack Initiation vs. Crack Growth Toughness: An Analysis of the Micromechanisms of Stationary and Non-Stationary Cracks," Rockwell International Science Center, Thousand Oaks, California, March 1984.
23. R.O. Ritchie, "Fatigue Crack Propagation: Mode I vs. Mode III," Rocketdyne, Canoga Park, California, March 1984.
24. J.A. Todd, P.N. Spencer, R.O. Ritchie, and E.R. Parker, "Advanced Cr-Mo Steels for Pressure Vessel Applications," WESTEC '84, Los Angeles, California, March 1984.‡
25. R.P. Gangloff and R.O. Ritchie, "Environmental Aspects of the Propagation of Short Fatigue Cracks," Eshelby Memorial Symposium, Sheffield University, Sheffield, England, April 1984.
26. R.O. Ritchie, "Application of Fracture Mechanics to Fatigue Crack Propagation," University of California, Berkeley Extension College, May 1984.
27. R.O. Ritchie, "Fatigue," University of California, Berkeley Extension College, May 1984.
28. R.O. Ritchie, "Physical Basis of Fracture Toughness," University of California, Berkeley Extension College, May 1984.
29. R.O. Ritchie, "The Short Crack Problem," ASME Pressure Vessel and Piping Conference, San Antonio, Texas, June 1984.
30. R.O. Ritchie, "On the Growth of Long and Short Fatigue Cracks in Steels and Aluminum Alloys," VIII Inter-American Conference on Materials Technology, San Juan, Puerto Rico, June 1984.
31. R.O. Ritchie, "Studies of Non-Stationary Cracks," David Taylor Naval Ship Research and Development Center, Annapolis, Maryland, August 1984.
32. R.O. Ritchie and S. Suresh, "On the Role of Microstructure and Environment in Near-Threshold Fatigue," Second International Conference on Fatigue and Fatigue Thresholds, Birmingham, England, September 1984.
33. R.O. Ritchie, "The Anomalous Behavior of Small Cracks," Departmental Seminar, Materials Science and Engineering Department, University of California Berkeley, October 1984.
34. A.F. Blom and R.O.Ritchie, "Is the Concept of a Fatigue Threshold Meaningful in the Presence of Compressive Cycles?" American Society for the Testing of Materials Workshop on Fundamental Questions on Fatigue, Arlington, Texas, October 1984.†
35. R.O. Ritchie, "Local and Global 'Driving Forces' for the Growth of Fatigue Cracks in Structural Materials," Department of Chemical and Nuclear Engineering, University of California, Santa Barbara, November 1984.
36. R.O. Ritchie, "Slow Crack Growth," Second National Conference on Fracture, University of Witwatersrand, Johannesburg, South Africa, November 1984.
37. R.O. Ritchie, "New Developments in Linear and Nonlinear Elastic Fracture Mechanics," Workshop

on Recent Advances in Fracture and Fatigue, Department of Metallurgy, University of Witwatersrand, Johannesburg, South Africa, November 1984.

38. R.O. Ritchie, "New Developments in the Understanding of Fatigue: Near-Threshold Crack Growth, Variable Amplitude Loading, Small Cracks, and Closure," Workshop on Recent Advances in Fracture and Fatigue, Department of Metallurgy, University of Witwatersrand, Johannesburg, South Africa, November 1984.

†Supported by the Air Force Office of Scientific Research under Grant No. AFOSR-82-0181.

‡Supported by the Fossil Energy Materials Program, U.S. Department of Energy, through Subcontract 7843 with Oak Ridge National Laboratory under Union Carbide Contract No. W-7605-ENG-26.

PHYSICAL PROPERTIES

Interfaces and Ceramic Microstructures*

Joseph A. Pask, Investigator

INTRODUCTION

The purpose of this work is to advance the basic understanding of the nature of interfaces (primarily those between dissimilar materials, such as metals and ceramics), particularly in terms of bonding and the factors that control the development of adherence. This understanding is critical to the development of composites, protective coatings, and glass/ceramic-to-metal seals, and to the reduction of corrosion at interfaces. The work involves studies of thermodynamics and kinetics of reactions at interfaces, and wetting and spreading of liquids.

Another objective in this work is to advance the understanding of the factors that play roles in the development of desired microstructures in ceramic materials, with and without a liquid phase. This understanding depends on a knowledge of the stable and metastable phase equilibrium of interfacial phenomena from a thermodynamics point of view and of mass-transport mechanisms during sintering.

1. Liquid-Phase Sintering of TiC-Ni Composites (Publication 1)

Daniel J. Miller† and Joseph A. Pask

The sintering of TiC-Ni particle compacts was studied with specific attention to effects of processing conditions. High-temperature scanning electron microscopy was used to measure the shrinkage. Densification was progressively inhibited with increasing additions of free carbon to the system. These results were explained on the basis of changes in the eutectic reactions in the system, reduced solubility of TiC in the Ni-rich liquid, and decreased wetting of the solid by the liquid. Presintering hydrogen heat treatment reduced the carbon content of the TiC-Ni compacts and led to reduction in sintering rates and elevated temperatures of liquid-phase formation. The dynamic change in wetting angle and the increased liquid-phase formation temperature that results indicate an interfacial barrier to reaction or the formation of a compound at the Ni-carbide interface. The equilibrium ternary diagram indicates the possible formation of TiN_3. This compound would explain the observed increased temperature of liquid-phase formation. The presence of TiN_3 could not be verified with x-ray analysis, although TiN_3 could be present along interfaces. The mechanism leading to reduced liquid-phase densification in hydrogen-treated TiC-Ni systems is based on the delayed melting and reactions of Ni, permitting the formation of a framework by the TiC particles that subsequently resists penetration of the grain boundaries by the later-forming liquid.

*This work was supported by the Director, Office of Energy Research, Office of Basic Energy Sciences, Materials Sciences Division of the U.S. Department of Energy under Contract No. DE-AC03-76SF00098.

†Present address: Hewlett-Packard Microwave Technology Center, Santa Rosa, California 94501.

2. Stable and Metastable Phase Equilibria and Reactions in the SiO_2-α Al_2O_3 System (Publication 2)

Joseph A. Pask

A number of stable phase-equilibrium diagrams have been proposed for the SiO_2-α Al_2O_3 system, because procedures in the preparation of specimens are critical for several reasons. Alpha-Al_2O_3 crystals do not nucleate easily from a silicate liquid supersaturated relative to this crystal form when the silicate liquid structure is not saturated with Al_2O_3 molecules. Also, mullite precipitated and growing from an aluminosilicate melt during cooling can accommodate an excess of Al_2O_3 in its structure in comparison with mullite that is grown at a constant

temperature. As a result, metastable phase compositions and microstructures occur commonly that have been misinterpreted as being stable manifestations. Metastable phase equilibria that show a rational relationship with the extensive experimental data have thus been identified phenomenologically.

3. Work in Progress

Interpretation of published data and additional experimental studies on phase relationships in the SiO_2-α Al_2O_3 system are continuing. The effect of grain boundary and interface characters on phase equilibria are being examined and are of particular interest.

Studies on reactions between metals/alloys and glass are also continuing. The redox reactions between these materials are important, because the glass in the interfacial zone becomes saturated with oxides of the substrate metal, leading to thermodynamic equilibrium and chemical bonding at the interface. Particular attention is being addressed to systems of NiCr-based alloys and glass; this study is supported by the National Institute of Dental Research of the National Institutes of Health.

1984 PUBLICATIONS AND REPORTS

Refereed Journals

1. D.J. Miller and J.A. Pask, "Liquid-Phase Sintering of TiC-Ni Composites," J. Am. Ceram. Soc. **66**, 841 (1983); LBL-16419.
2. J.A. Pask, "Stable and Metastable Phase Equilibria and Reactions in the SiO_2-Alpha Al_2O_3 System," Ceramics International **9**, 107 (1983).

High-Temperature Reactions*

Alan W. Searcy, Investigator

INTRODUCTION

The central program objective is to deepen scientific understanding of the kinetics and thermodynamics of high-temperature reactions. A systematic study of the variables that influence the kinetics and thermodynamics of endothermic decomposition reactions (e.g., $CaCO_3 \rightarrow CaO + CO_2$) is approaching completion, and the principles established from the study will be used as a basis for studies of more complex reactions of the kind illustrated by $CaCO_3 + TiO_2 \rightarrow CaTiO_3 + CO_2$. Theoretical and experimental studies of surface thermodynamics, chemisorption, the influence of particle size on chemical and physical properties, and surface-transport processes are receiving increased emphasis. A highlight of the theoretical studies has been the quantitative evaluation of a conjecture of Gibbs that crystals will have rounded edges that are not predicted by the classical condition for equilibrium in crystalline particles (see Abstract 1). A dramatic experimental finding of collaborative experimental studies with Dario Beruto and associates at the University of Genova is that MgO, when prepared by decomposing $Mg(OH)_2$ in vacuum, can have as much as 73 kJ (17 kcal) per mole excess enthalpy content because of its very high surface area (see Abstract 4). Complementary high-resolution transmission electron-microscope (TEM) studies show that MgO produced under similar conditions is formed as porous aggregates of 2-nm cubes (see Abstract 5). Particles this small have more ions on their surface than in their "bulk."

*This work was supported by the Director, Office of Energy Research, Office of Basic Energy Sciences, Materials Sciences Division of the U.S. Department of Energy under Contract No. DE-AC03-76SF00098.

1. The Influence of Molecular Motions on the Stabilities and Shapes of Solid Particles (Publication 5)

Alan W. Searcy

A conjecture of Gibbs, that the relative weakness of bonds at crystal edges and corners would cause rounding that is not predicted by his thermodynamic expression for stable crystal shapes, is evaluated in two ways. First, the vacancy distribution necessary for dynamic equilibrium between adjacent crystal rows or layers of different bond energies is derived. Then it is shown that minimization of the total free energy of two parts of a crystal with respect to their total vacancy concentration leads to the same vacancy distribution. Generalization of these results shows that the stabilities of particles that have a fixed number of sites are greatest when vacancies are so distributed as to equalize molecular fluxes between every pair of regions of different bonding energies. Rounding will occur when the mole fractions of vacancies required at corners and edges to maintain the molecular-flux balance approach unity.

2. The Equilibrium Shapes of Small Particles (Publication 2)

Sheng-Wei Wang, L.M. Falicov, and Alan W. Searcy

The equilibrium shapes of small particles of Van der Waals face-centered-cubic solids at 0 K are studied theoretically. Calculations are presented for a variety of shapes involving {100} and {111} type faces, as well as pseudospherical particles. Second-neighbor interactions play an important role in determining particle shapes. For small enough particles there are some crossovers in the relative stability of various shapes. For this type of solid the pseudosphere is never stable (see Figure 2-1). A suitably proportioned cubooctahedron is found to be the equilibrium shape for most particles.

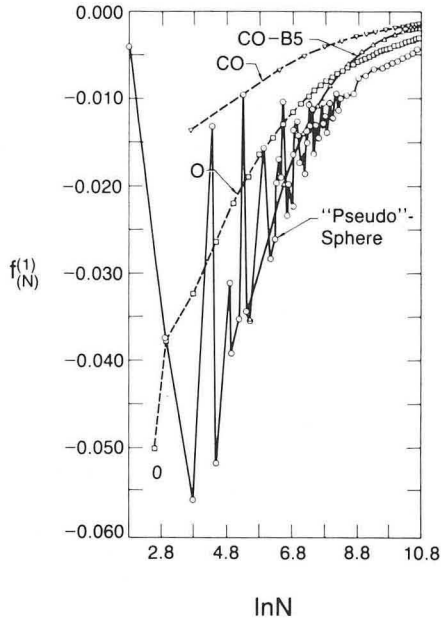

Figure 2-1. Figure of merit f(1) versus ln N plots for regular cubooctahedra CO, octahedra O, CO-B5, and pseudospheres. The lowest polyhedra considered here are for N equal to 38 for CO, 6 for O, 225 for CO-B5, and 13 for the pseudosphere. (CO-B5 particles are formed from cubooctahedra by adding an extra close-packed layer on each face.) (XBL 853-1504)

3. CO_2-Catalyzed Surface Area and Porosity Changes in High-Surface-Area CaO Aggregates (Publication 1)

Dario Beruto,† Luigi Barco,† and Alan W. Searcy

The changes in surface area and mesoporosity in aggregates of 0.01-μm cross-section CaO particles when heated in CO_2 at 686°C were determined from N_2-adsorption isotherms. Initially, the surface area decreases rapidly with little change in porosity. When the surface area has decreased below 90 m^2/g, surface-area and porosity variations become consistent with expectations for coarsening by grain-boundary or bulk diffusion. The initial rapid decrease in surface area must result from CO_2-catalyzed surface diffusion, but the data suggest that surface diffusion is not rate-limiting. The rate-limiting step may be reaction of CO_2 to form surface CO_3^{2-} ions or decomposition of these ions to O^{2-} ions and CO_2 gas.

†Permanent address: Laboratorio di Chimica, Facolta di Ingegneria, Universita di Genova, Genoa, Italy.

4. MgO of Very High Energy Content from Decomposition of $Mg(OH)_2$ (Publication 6)

Dario Beruto,† P.F. Rossi,† and Alan W. Searcy

In an effort to determine the reason that the H_2O produced by decomposition of $Mg(OH)_2$ in effusion cells approaches apparent equilibrium pressures only $\sim 10^{-4}$ times the expected equilibrium pressures, the heat of solution of MgO in HCl solutions was measured as a function of the area of the surface accessible to N_2 gas. Excess heats of formation of MgO as great as 73 kJ (17 kcal) per mole of MgO were measured for particles of N_2-accessible surface areas of $\sim$300 m^2/g, but of probable total surface areas of $\sim$600 m^2/g or more (see Figure 4-1). The activities calculated for the MgO from the excess heats are high enough to account for the low equilibrium H_2O pressures, although the H_2O pressures in an effusion cell may be in equilibrium not with all the MgO present, but only with the MgO of the surface.

†Permanent address: Istituto di Chimica, Facolta di Ingegneria, University di Genova, Genoa, Italy.

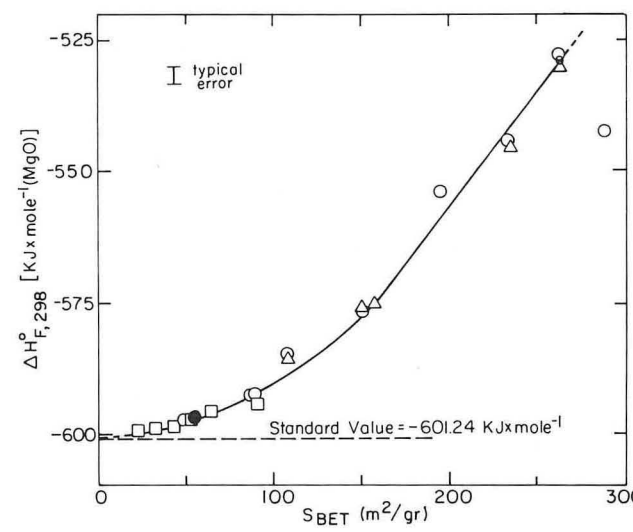

Figure 4-1. Standard heat of formation $\Delta H^o_{F,298}$ (kJ × $mole^{-1}_{(MgO)}$) derived from heat-of-solution data versus apparent surface area of MgO measured by the Brunauer-Emmett-Teller method. The squares are derived from Natarajan and coworkers.[1] The other points are derived from this study. (XBL 847-7219)

1. Natarajan et al., Trans. Far. Soc. **65**, 3088 (1969).

5. $Mg(OH)_2$ and $MgCO_3$ Decomposition Study by TEM (Publication 7)

M.G. Kim and U. Dahmen

Transmission electron microscopy was used to study $Mg(OH)_2$ and $MgCO_3$ decompositions. No intermediate phases were observed. $Mg(OH)_2$ transformed to MgO with the known orientation relationship, i.e.,

$$(0001)_{Mg(OH)_2}//(111)_{MgO} \text{ and}$$

$$[11\bar{2}0]_{Mg(OH)_2}//[1\bar{1}0]_{MgO}.$$

$MgCO_3$ transformed to MgO with the orientation relationship

$$(0001)_{MgCO_3}//(111)_{MgO} \text{ and}$$

$$[11\bar{2}0]_{MgCO_3}//[2\bar{1}\bar{1}]_{MgO}.$$

Morphological observations revealed that the external shapes of the reactant solids were maintained during the decompositions so that the product solid aggregates has porosities of about 54% and 60% from $Mg(OH)_2$ and $MgCO_3$, respectively, with the MgO particles formed in cubes (see Figure 5-1). The orientation relationships and morphological observations suggest that the oxygen octahedra in reactant solids formed semicoherent nuclei which grow to an optimum size (~2 nm) by a cooperative movement of ions from regions of lattice disrupted by the removal of gas molecules.

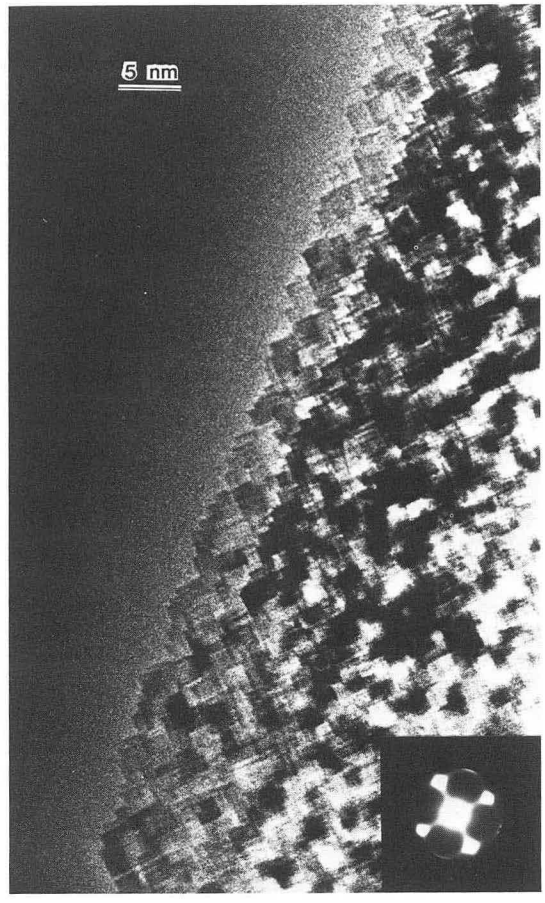

Figure 5-1. Transmission electron micrograph of the [100] orientation of MgO from $Mg(OH)_2$ decomposition. (XBB 840-8959).

6. Solid Solutions of Complex Salts: Calcite, Magnesite, and Dolomite (Publication 8)

Andreas G. Hegedus and Alan W. Searcy

The solution thermodynamics of solids with narrow solution ranges was examined, with calcite ($CaCO_3$), magnesite ($MgCO_3$), and dolomite $Mg_nCa_{(1-n)}(CO_3)_2$. Intergral and partial molal thermodynamic quantities were calculated from CO_2 pressures and compositional changes measured by means of a Tensi-Volumetric apparatus. Dolomite showed small negative heats of formation from calcite and magnesite that varied with composition from -20.9 to -27.2 kJ/mole. The entropy of formation was approximately -3.5 J-deg^{-1}-mol^{-1} for the entire compositional range. These entropies are consistent with the reaction of well-ordered reactants to form a well-ordered product. The partial molal entropies and enthalpies for CO_2 in calcite, magnesite, and the dolomites and the $CaCO_3$ and MgO partial molal entropies in the dolomites were also fairly constant.

7. The Temperature Ranges of Coexistence of High- and Low-Temperature Forms of Phases of Narrow Composition Ranges (Publication 8)

Andreas G. Hegedus and Alan W. Searcy

A subregular-solution model was applied to evaluate the temperatures and compositions of coexistence of the high- and low-temperature forms of a binary phase that is stable over a relatively narrow composition range. The temperature of congruent transition, the hyper- and hypo-stoichiometric eutectoid temperatures, and the shape of the miscibility gap were determined as a function of the thermodynamic parameters of each phase. Using the $BaCO_3$ phase transition as a case study with partial molar thermodynamic data found for CaO and CO_2 in $CaCO_3$, the difference between the congruent transition temperature and the eutectoid temperature was estimated to be $\sim$30°C, and the miscibility gap was estimated to be $\sim$0.3%.

1984 PUBLICATIONS AND REPORTS

Refereed Journals

1. D. Beruto, L. Barco, and A.W. Searcy, "CO_2-Catalyzed Surface Area and Porosity Changes in High-Surface-Area CaO Aggregates," J. Am. Ceram. Soc. **67**, 512 (1984); LBL-17191.
2. S. Wang, L.M. Falicov, and A.W. Searcy, "The Equilibrium Shapes of Small Particles," Surf. Sci. **143**, 609 (1984).
3. N.S. Jacobson, E.J. Opila, and A.W. Searcy, "The Surface Diffusion of High Temperature Vapors in Porous Alumina," High Temp. Sci. **17**, 53 (1984); LBL-16491.
4. D. Beruto, R. Botter, and A.W. Searcy, "Thermodynamics and Kinetics of Carbon Dioxide Chemisorption on Calcium Oxide," J. Phys. Chem. **88**, 4052 (1984); LBL-16589.
5. A.W. Searcy, "The Influence of Molecular Motion on the Stabilities and Shapes of Solid Particles," J. Chem. Phys. **81**, 2489 (1984); LBL-17143.

LBL Reports

6. D. Beruto, P.F. Rossi, and A.W. Searcy, "MgO of Very High Energy Content from Decomposition of $Mg(OH)_2$," LBL-18252.
7. M.G. Kim and U. Dahmen, "$Mg(OH)_2$ and $MgCO_3$ Decomposition Study by TEM," LBL-18972.
8. A.G. Hegedus (Ph.D. Thesis), "Thermodynamics of Solid Solutions of Complex Salts: Case Studies of Calcite, Magnesite and Dolomite," LBL-18879.
9. A.W. Searcy, "The Influence of Surfaces on Vapor Pressures," LBL-18351.

Invited Talks

10. A.W. Searcy, "Influence of Internal Molecular Motions on the Stabilities and Vapor Pressures of Solid Particles," Condensed Matter Physics Seminar, Department of Physics, University of California Berkeley, November 7, 1984; Materials Science and Mineral Engineering Department Seminar, University of California Berkeley, November 15, 1984.
11. A.W. Searcy, "Influence of Internal Molecular Motions of the Stabilities and Vapor Pressures of Crystalline Particles," Symposium on Catalysis by Solid, Materials Research Society, Fall Meeting, Boston, Massachusetts, November 27, 1984.

Structure-Property Relationships in Semiconductor Materials*

Jack Washburn, Investigator

INTRODUCTION

The purpose of this research program is to advance the understanding of structural defects including the structure of interfaces in semiconductor materials. Particular emphasis is placed on interfaces and defects that are formed during processing steps used for state-of-the-art solid-state device manufacture, such as ion implantation, oxidation, and contact formation. This approach has also led to several areas of basic research: for example, a continuing series of experiments aimed at a more complete understanding of the mechanism of the crystalline-to-amorphous transformation during ion damage in silicon and gallium arsenide, an investigation of the detailed mechanism of crystal growth into amorphous zones, and a study of the growth of Cu_2S layers on the surface of CdS.

High-resolution lattice-imaging electron microscopy combined with computer simulation of the images has proved to be a powerful tool for revealing and interpreting fine-scale defects and interface structures, particularly when combined with complementary observations on the same specimens, such as Rutherford-backscattering measurements, secondary-ion mass spectroscopy (SIMS), and electrical or optical measurements.

The new atomic-resolution microscope promises to extend the limits of detection to even smaller defects, perhaps making possible more direct correlations between the presence of specific structural defects and their electrical effects.

1. Interface Morphology and Phase Distribution in the $Cu_{2-x}S$/CdS Heterojunction: A Transmission Electron-Microscope Investigation (Publications 1, 7, 10, and 13)

T. Sands, J. Washburn, and R. Gronsky

The $Cu_{2-x}S$/CdS photovoltaic device is the most thoroughly studied and developed polycrystalline thin-film solar cell. However, many of the fundamental relationships between processing, microstructure, and device performance are essentially unknown. Critical to understanding these relationships is the determination of the $Cu_{2-x}S$/CdS interface morphology and the phase distribution in the $Cu_{2-x}S$ absorber. In this study electron-optical methods are applied to the structural characterization of single-crystal $Cu_{2-x}S$/CdS heterojunctions prepared by the aqueous ion-exchange process. Results obtained by scanning electron microscopy, transmission electron microscopy (TEM) and diffraction, and cross-sectional high-resolution TEM (XHRTEM) are combined to develop a detailed description of the effect of surface texture on heterojunction morphology.

The first XHRTEM images of the $Cu_{2-x}S$/CdS heterojunction show the presence of the tetragonal phase (see Figure 1-1), a high-pressure polymorph of the low-chalcocite phase. This is the first reported observation of the tetragonal phase in $Cu_{2-x}S$ layers prepared by ion exchange. Furthermore, whenever the nominal (local) surface orientation is ~60° or more from the basal orientation, the formation of low chalcocite is preferred. Conversely, when the nominal (local) surface orientation is within ~30° of the basal orientation, the tetragonal phase forms at the interface with CdS, provided nucleation sites for transformation dislocations are available. These results are explained by considering the lattice misfit, the structural compatibility of the sulfur networks, and the surface nucleation of hcp-to-fcc transformation dislocations.

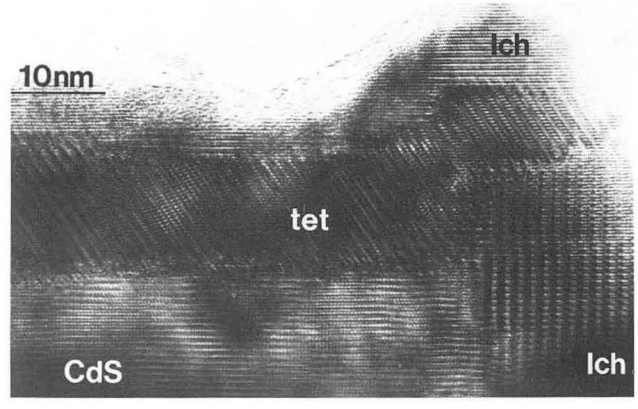

Figure 1-1. XHRTEM image of the Cu_2S/CdS heterojunction formed in 5 seconds at 99°C. The first layer to form was the thin skin of low chalcocite (lch) in the $[6\bar{4}3]$ zone-axis orientation. The tetragonal phase (tet) is in the [010] zone-axis orientation. The deep penetration of low chalcocite near the crack (lower right) is in the [010] zone-axis orientation. Note that the tet-CdS interface is parallel to the basal plane (horizontal), whereas the lch-CdS interface is steeply inclined. CdS is in the $[\bar{2}110]$ zone-axis orientation. (XBB 830-10048)

*This work was supported by the Director, Office of Energy Research, Office of Basic Energy Sciences, Materials Sciences Division of the U.S. Department of Energy under Contract No. DE-AC03-76SF00098.

2. Influence of the Amorphous-Crystalline Interface Morphology on Defect Nucleation in Preamorphized Silicon (Publications 9, 18, and 20)

T. Sands, J. Washburn, R. Gronsky, E. Myers,[†] *W. Maszara,*[†] *D.K. Sadana,*[†‡] *and G.A. Rozgonyi*[†‡]

SIMS and XHRTEM are applied to the characterization of defects formed during rapid thermal annealing of preamorphized and subsequently BF_2^+-implanted silicon (100) substrates. The nucleation of hairpin dislocations has been shown to be due to slightly misoriented crystallites present within a transition region between the amorphous layer and the crystalline substrate. The proposed mechanism of half-loop nucleation and propagation during regrowth of the amorphous layer is illustrated in Figure 2-1. By preamorphizing with Ge^+ instead of Si^+, hairpin dislocations are nearly eliminated. The absence of misoriented crystallites in the abrupt transition region of the Ge^+-preamorphized silicon is believed to be responsible for the defect-free regrowth behavior (see Figure 2-2).

[†]Present address: Materials Engineering Department, North Carolina State University, Raleigh, North Carolina 27650.

[‡]Present address: Microelectronics Center of North Carolina, Research Triangle Park, North Carolina 27709.

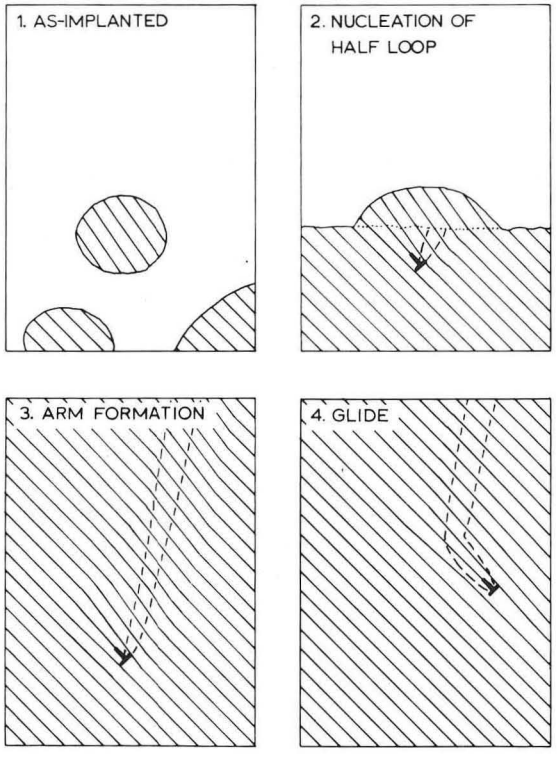

Figure 2-1. Schematic diagram illustrating the model for hairpin nucleation during rapid thermal annealing. The viewing direction is approximately [010]. The hairpin is approximately edge-on in this projection. (XBL 847-3147)

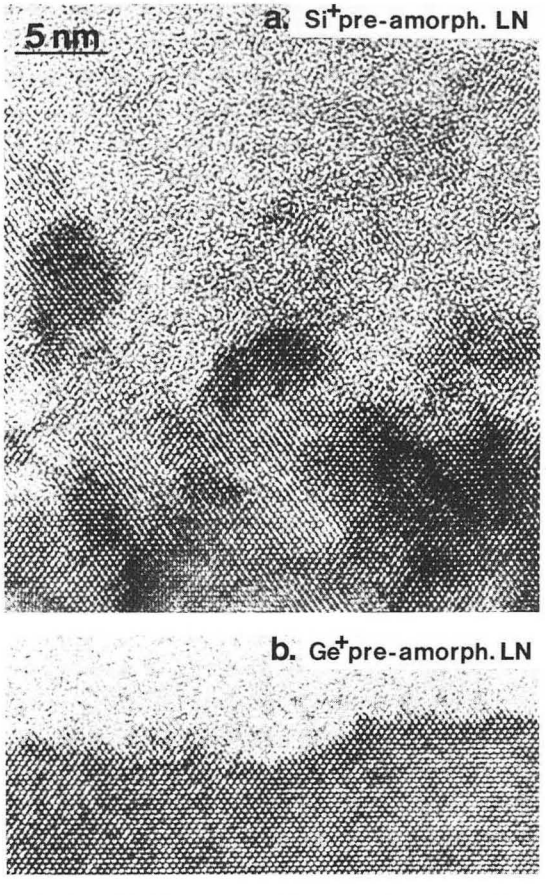

Figure 2-2. XHRTEM images of the amorphous-crystalline interface in preamorphized Si^+ (a) and Ge^+-preamorphized Si (b). Both implants were performed at liquid-nitrogen temperature with good thermal contact. (XBB 846-4778)

3. The Atomic Structure of Si-SiO_2 Interfaces Suggesting a Ledge Mechanism of Silicon Oxidation (Publication 8)

J.H. Mazur and J. Washburn

The atomic structure of Si-SiO_2 interfaces resulting from oxidation of singular {111} and vicinal (111)3°[$1\bar{1}0$] and (111)2°[$11\bar{2}$] has been studied by high-resolution electron microscopy. The following results have been shown: (1) The Si substrate terminates abruptly on atomically flat (111) terraces at the Si-SiO_2 interface (see Figure 3-1). (2) The SiO_2 appears to be amorphous right up to the interface. (3) Ledges one {111} interplanar distance (0.314 nm) high are observed on both singular and vicinal oxidized surfaces. (4) The observed structure suggests a terrace-ledge/kink model for the interface and a ledge mechanism for high-temperature oxidation similar to the evaporation mechanism of the atoms from the solid surface.

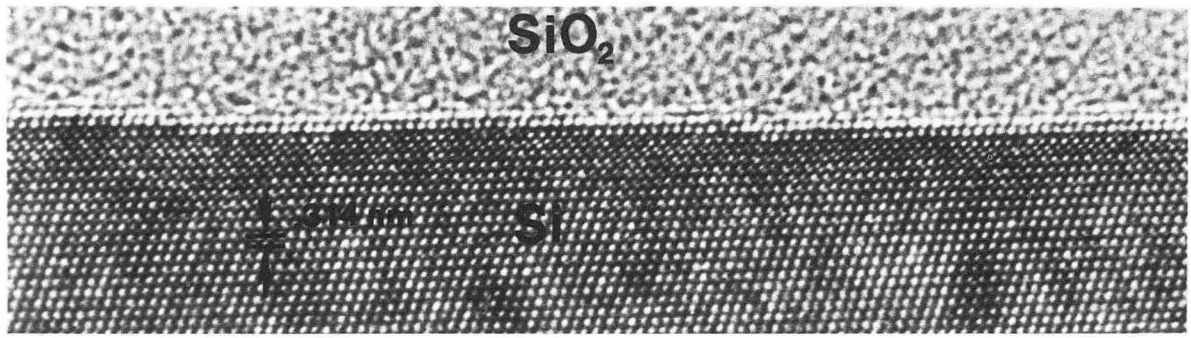

Figure 3-1. High-resolution image of a 100-nm-thick oxide film grown on a vicinal (111)2°[$11\bar{2}$] Si surface.
(XBB 846-4805)

4. High-Resolution TEM Studies of Defects Near the Si-SiO_2 Interface (Publication 4)

J.H. Mazur and J. Washburn

Using transmission electron microscopy, small defects were observed on Czochralski-grown [100] p-type boron-doped 1.5–20 Ω cm Si wafers. The wafers on which the defects were observed had oxygen concentrations of 1.4×10^{18} cm^{-3} and carbon concentrations of $4-10 \times 10^{16}$ cm^{-3}. The defects were observed after the wafers had been subjected to one-step oxidation in dry O_2 at 900°C, 1000°C, and 1150°C. All defects were observed within 100 nm of the Si-SiO_2 interface, and their habit planes were parallel to the {100} and {311} matrix planes. The defects were less than 10 nm wide and 1 nm thick. The {100} and {311} defects are interpreted tentatively as thin silica platelets and {311} stacking faults, respectively. The defect distribution near the interface was random, although the defect density appeared to be lower for higher oxidation temperatures. It is not yet clear whether the defects were formed during the oxidation treatments or were present near the surfaces of the as-received wafers.

5. High-Resolution Structural Characterization of Se^+-Implanted GaAs: Mechanisms of Amorphization and Recrystallization (Publications 2 and 3)

T. Sands, D.K. Sadana, R. Gronsky, and J. Washburn

HRTEM has been applied to the study of amorphization and recrystallization mechanisms in Se^+-implanted (100) GaAs. A selenium dose of 1×10^{14} cm^{-2} at 450 keV (projected range 1550 Å) produced an amorphous band in the depth range 250–2150 Å below the surface. The critical density of energy deposited by nuclear stopping was thus determined to be 11 ± 2 eV per Ga and As atom pair. The amorphous-crystalline transition region was found to have a distinct two-phase nature, with stacking faults at some amorphous-crystalline boundaries. On annealing at 400°C, the transition region

was observed to grow epitaxially with isolated stacking faults. These isolated faults are thought to be nucleated at the small faults in the as-implanted material. Further regrowth proceeded by nucleation and by propagation of a dense network of stacking-fault bundles. This two-stage regrowth sequence (epitaxial and faulted) explains the "incubation period" observed during many Rutherford-backscattering spectrometry studies of the annealing of ion-implanted GaAs.

6. Direct Evidence of Arsenic Clustering in High-Dose Arsenic-Implanted Silicon (Publication 6)

N.R. Wu, D.K. Sadana, and J. Washburn

High-dose ($5–7.5 \times 10^{15}$ cm^{-2}) arsenic implantation was conducted in the energy range 50–120 keV into three types of Si(100) substrates: (1) bare Si, (2) Si with a thermally grown 775-Å screen oxide, and (3) preamorphized surface-layer Si produced by self-implantation. The substrates were subsequently furnace-annealed at 600°C in N_2. Cross-section transmission electron microscopy (XTEM) revealed that in all cases discrete layers of As-related clusters and small dislocation loops occurred at depths matching the projected ranges of As into both the Si substrates and the original amorphous/crystalline interfaces, respectively. The atomic profiles of As obtained by SIMS from these samples did not show any redistribution of As. The carrier-concentration profiles from the spreading-resistance measurements indicate that only 30% of As was electrically active. Comparison of XTEM and SIMS suggests that nucleation of the clusters occurred in the regions where As was present above the solid-solubility limit in Si. The presence of recoiled oxygen has been found to stabilize the clusters.

7. Recrystallization of Amorphous Gallium Arsenide by Ion Beams (Publication 5)

D.K. Sadana, H. Choksi, J. Washburn, P.F. Byrne,† and N.W. Cheung†

An 11-MV arsenic beam was used to amorphize approximately 3.9 μm of a GaAs surface layer at liquid-nitrogen temperature. It was found that apparently amorphous GaAs can be reconverted to single-crystal GaAs by subsequent implantation at higher temperature. The recrystallization by the ion beam proceeded simultaneously from the amorphous surface and from the deep amorphous/crystalline interface. Growth of dendrites and/or microtwins occurred at the recrystallizing interfaces. By comparing the nuclear-stopping curve with the damage distribution in the cross-sectional transmission electron micrograph, the threshold value for converting crystalline GaAs into amorphous GaAs was measured to be $2–5 \times 10^{20}$ keV cm^{-3}.

---

†Present address: Department of Electrical Engineering and Computer Science, University of California, Berkeley 94720.

1984 PUBLICATIONS AND REPORTS

Refereed Journals

1. T. Sands, J. Washburn, and R. Gronsky, "High-Resolution Study of the Relationship between Misfit Accommodation and Growth of $Cu_{2-x}S$ in CdS," Mat. Res. Soc. Symp. Proc. **31**, 241 (1984); LBL-16774.
2. D.K. Sadana, T. Sands, and J. Washburn, "High-Resolution Transmission Electron Microscopy Study of Se^+-Implanted and Annealed GaAs: Mechanisms of Amorphization and Recrystallization," Appl. Phys. Lett. **44**, 623 (1984); LBL-17267.
3. T. Sands, D.K. Sadana, R. Gronsky, and J. Washburn, "High-Resolution Structural Characterization of the Amorphous-Crystalline Interface in Se^+-Implanted GaAs," Appl. Phys. Lett. **44**, 874 (1984); LBL-17035.
4. J.H. Mazur and J. Washburn, "High-Resolution TEM Studies of Defects near the Si-SiO_2 Interface," Mat. Res. Soc. Symp. Proc. **31**, 105 (1984); LBL-17114.
5. D.K. Sadana, H. Choksi, J. Washburn, P.F. Byrne, and N.W. Cheung, "Recrystallization of Amorphous Gallium Arsenide by Ion Beams," Appl. Phys. Lett. **44**, 301 (1984); LBL-17268.
6. N.R. Wu, D.K. Sadana, and J. Washburn, "Direct Evidence of Arsenic Clustering in High-Dose Arsenic-Implanted Silicon," Appl. Phys. Lett. **44**, 782 (1984); LBL-17454.
7. T. Sands, J. Washburn, and R. Gronsky, "Interface Morphology and Phase Distribution in the $Cu_{2-x}S$/CdS Heterojunction: A Transmission Electron Microscope Investigation," Solar Energy Mat. **10**, 349 (1984); LBL-17677.
8. J.H. Mazur and J. Washburn, "The Atomic Structure of Si-SiO_2 Interfaces Suggesting a Ledge Mechanism of Silicon Oxidation," in *AIP Conf. Proc., The Physics of VLSI*, J.C. Knights, Ed., American Institute of Physics, 1984, p. 52; LBL-18119.

9. T. Sands, J. Washburn, R. Gronsky, W. Maszara, D.K. Sadana, and G.A. Rozgonyi, "Near-Surface Defects Formed During Rapid Thermal Annealing of Pre-Amorphized and BF_2^+-Implanted Silicon," Appl. Phys. Lett. **45**, 982 (1984); LBL-18000.

Other Publications

10. T. Sands, R. Gronsky, and J. Washburn, "Characterization of Single-Crystal Cu_2S/CdS Heterojunctions by High-Resolution Electron Microscopy," in *Proc. Tech. Symp. SPIE*, Conf. 463, C.M. Lampert and D.K. Sadana, eds., 1984, p. 61; LBL-17141.
11. J.H. Mazur, R. Gronsky, and J. Washburn, "Oxidation of Singular and Vicinal Surfaces of Silicon: The Structure of the Si-SiO_2 Interface," in *Proc. Tech. Symp. SPIE*, Conf. 463, C.M. Lampert and D.K. Sadana, eds., 1984, p. 88; LBL-17458.
12. Y.-C. Shih, J. Washburn, and S.C. Shatas, "Effect of Heating Rate and Annealing Temperature on Twin Formation in As^+-Implanted <111> Silicon," in *Proc. Tech. Symp. SPIE*, Conf. 463, 1984, p. 93; LBL-18412.

LBL Reports

13. T. Sands (Ph.D. Thesis), "Formation and Degradation of $Cu_{2-x}S$/CdS Single-Crystal Heterojunctions: A High-Resolution Transmission Electron Microscope Study," LBL-17684.
14. D.R. Lopes (M.S. Thesis), "Further Development of a Facility for Channeling Studies: Application to Lattice Location," LBL-18185.
15. B.L. Chin (Ph.D. Thesis), "The Growth and Characterization of Single Crystal (Cd,Zn)S Thin Films Relevant to the Study of the (Cd,Zn)S/Cu_xS Photovoltaic Cell," LBL-16117.
16. H. Choksi (M.S. Thesis), "A TEM Study of Ion-Implanted Semi-Insulating Gallium Arsenide," LBL-16308.
17. T.I.S.-Y. Zee (M.S. Thesis), "The Influence of Oxygen on Segregation of Chromium at Structural Damage in Gallium Arsenide," LBL-16190.
18. T. Sands, J. Washburn, E. Myers, and D.K. Sadana, "On the Origins of Structural Defects in BF_2^+-Implanted and Rapid Thermally Annealed Silicon: Conditions for Defect-Free Regrowth," in *Proc. 1984 Ion Beam Modification of Mat. Conf.* (in press); J. Nuc. Inst. Meth.-B (in press); LBL-18045.
19. J.H. Mazur and C.M. Lampert, "High-Resolution Electron Microscopy Studies of Silica Aerogel Transparent Insulation, in *Proc. Tech. Symp. SPIE,* Conf. 502 (in press); LBL-18245.
20. T. Sands, J. Washburn, R. Gronsky, W. Maszara, D.K. Sadana, and G.A. Rozgonyi, "Influence of the Amorphous-Crystalline Interface Morphology on Dislocation Nucleation in Pre-Amorphized Silicon," in *Proc. 13th Int. Conf. on Defects in Semiconductors* (in press); J. Electron. Mat. (in press); LBL-18172.

Invited Talks

21. T. Sands, "Interface Morphology and Phase Distribution in the $Cu_{2-x}S$/CdS Heterojunction: A Transmission Electron Microscope Investigation," Hewlett-Packard Laboratories, Palo Alto, California, April 1984; Bell Communications Research, Murray Hill, New Jersey, May 1984.
22. T. Sands, "High-Resolution Imaging of Interfaces in Semiconductor Devices," Regents Oversight Committee, Lawrence Berkeley Laboratory, April 1984.
23. T. Sands, "Influence of Pre-Amorphization Parameters on Defect Generation in BF_2^+-Implanted Silicon: Implications for Shallow Junction Technology," Department of Materials Science and Engineering, Stanford University, Stanford, California, May 1984.
24. T. Sands, "Detection of Microscopic Interfacial Phases by High Resolution TEM," Department of Electrical Engineering, California Institute of Technology, Pasadena, California, October 1984.

Chemical Properties and Processing of Refractory Ceramics*

Lutgard C. De Jonghe, Investigator

INTRODUCTION

The chemical properties of ceramics are of central importance in the fabrication and application of ceramics. They define the fabrication path that permits the exploitation of the full potential of performance of ceramics and determine, for example, resistance to chemical attack at elevated temperatures and properties of metal-ceramic interface bonding. The role of the chemical properties in the behavior of ceramics is thus investigated for a number of cases of practical relevance. These cases include high-temperature reactions with a gaseous atmosphere focusing on the metal-ceramic reaction interface, metal-ceramic interface bonding, and some practical and theoretical aspects of single and multicomponent densification processes.

In a first program phase the reactions of some oxides with aggressive gases were studied. Transition-metal oxides were reacted to metal at elevated temperatures by reducing gases. A new model was developed, describing in detail the processes occurring at the gas-solid interface. The model brought together concepts in catalysis and in solid-state transport and defined how the various morphologies of the metal reaction product depended on the reaction parameters. This part of the program has been concluded.

A second study involved the examination of the role of heterocomponent additives on the densification behavior of ceramic systems containing a high-temperature eutectic. The role of such additives has been clarified in two different systems, MgF_2-CaF_2 and CaO-Al_2O_3, and the study has been concluded.

The study of some theoretical aspects of densification in model systems was started this year, but these activities were transferred later to the multidisciplinary program on Advanced Structural Ceramics in the Center for Advanced Materials.

A new effort on the role of microchemical and microstructural characteristics of a metal/ceramic interface, ZrO_2-Ni, has been initiated this year. The study seeks to investigate the relationship between the chemical interactions occurring between the substrate and the ceramic coating and its relationship to the mechanical integrity of the interface.

*This work was supported by the Director, Office of Energy Research, Office of Basic Energy Sciences, Materials Science Division of the U.S. Department of Energy under Contract No. DE-AC03-76SF00098.

1. Subeutectic Densification and Second-Phase Formation in Al_2O_3-CaO (Publication 5)

S.J. Wu and L.C. De Jonghe

The early and intermediate densification stages of calcia-containing alumina were examined at subeutectic temperatures. Up to 0.15 wt% calcia causes a decrease in the densification rates; with 0.15 to 0.7 wt% calcia an increasing densification rate was observed; more than 0.75 wt% calcia leads to a monotonically decreasing densification rate. The data, shown in Figure 1-1, may be interpreted as a competition between grain-boundary defect chemistry, enhanced subeutectic densification, and formation of calcium-aluminate phases. Initially, calcia accumulates in the grain boundaries without forming a second grain-boundary phase (see Figure 1-2). This accumulation affects the grain-boundary chemistry and may tend to decrease the grain-boundary transport rates. With increasing calcia content, the grain-boundary composition can approach the eutectic composition, thus lowering the local melting temperature and increasing the transport rates in the

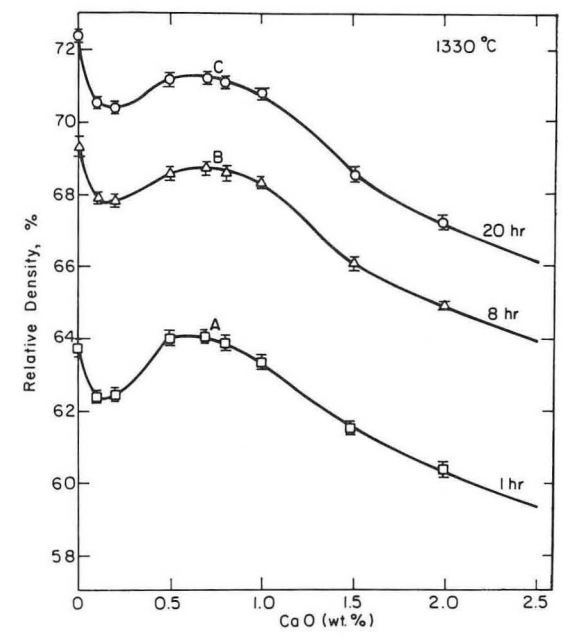

Figure 1-1. Density as a function of calcia content for isothermal and isochronal sintering of calcia-containing alumina.
(XBL 8312-6647)

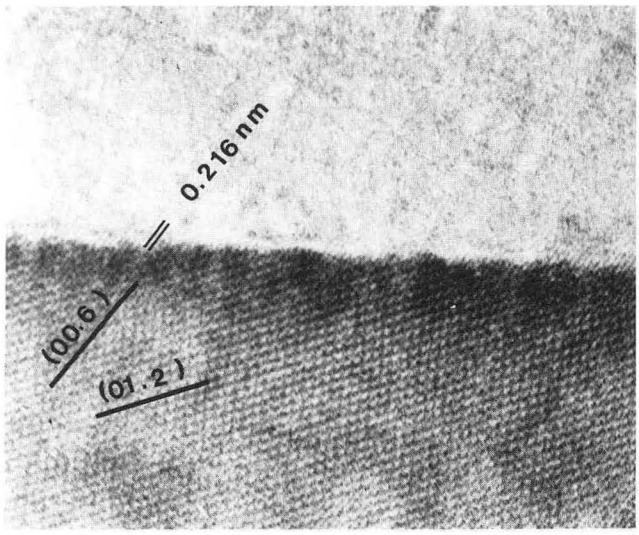

Figure 1-2. High-resolution transmission electron micrograph of alumina grain boundary in alumina with 5 wt% calcia after 20 hours at 1330°C. No grain-boundary phases are formed at the alumina-alumina grain boundaries (micrograph courtesy of R. Gronsky). (XBB 830-8848)

grain boundaries again. At still higher calcia content, formation of calcium-aluminate phases retards the densification.

2. Particle Rotation in Early Sintering (Publication 3)

C.H. Hsueh and L.C. De Jonghe

Shrinkage and rearrangement during the early stages of sintering have been considered. In such rearrangement the sintering particles can experience both additional center-to-center stresses and bending moments arising from multiparticle interactions and asymmetrical-neck formation. The response of a particle pair to the simultaneous action of these stresses has been solved analytically in a cylindrical geometry. The resulting rotation and densification rates were found to be independent of one another. An example of the normalized stress distributions on a grain boundary formed in the neck between two sintering particles is shown in Figure 2-1 for various

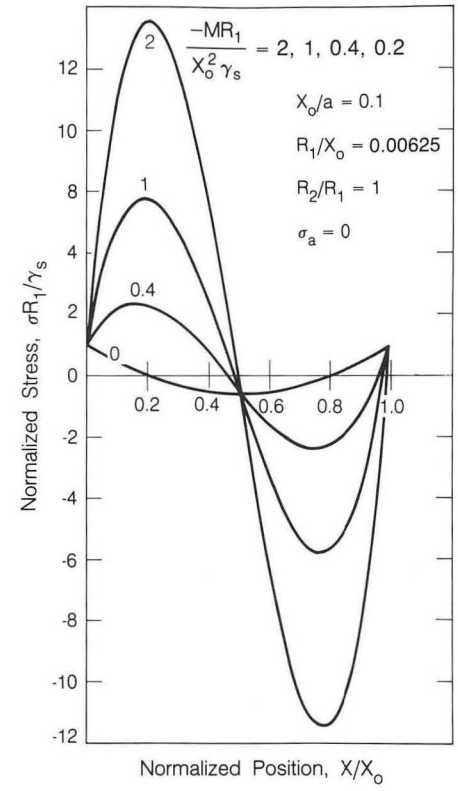

Figure 2-1. Calculated normalized stress distribution on a grain boundary (symmetrical-neck case) with applied bending moments M as indicated. (XBB 843-8360)

applied bending moments, in the absence of normal stresses, for a symmetrical neck.

3. Pore Shrinkage and Sintering Stress (Publication 4)

L.C. De Jonghe and M.N. Rahaman

The criterion for the stability of a large pore in a fine-pore matrix has been reconsidered, taking into account the pressure exerted by the densifying matrix. The results indicate that progressively larger pores can shrink, even if grain growth is minimal or

absent. The qualitative evolution of the criteria for stability of a large pore in a fine-pore matrix is shown in Figure 3-1 for the case of no grain growth. Various domains of pore stability are indicated.

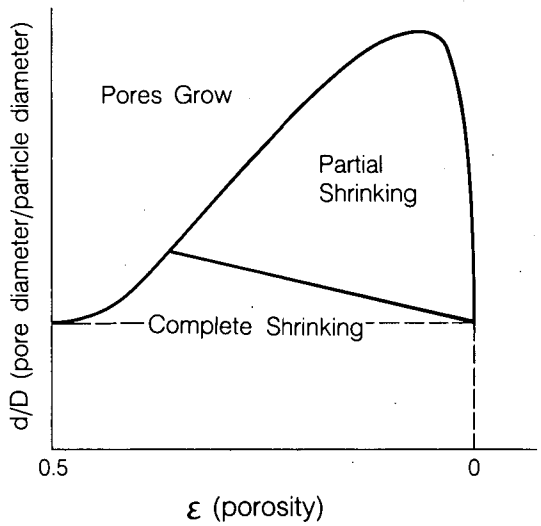

Figure 3-1. Qualitative evolution of criteria for stability of a large pore in a fine-pore matrix. (XBL 845-9802)

1984 PUBLICATIONS AND REPORTS

Refereed Journals

1. L.C. De Jonghe, H. Schmid, and M. Chang, "Interreaction between Al_2O_3 and a CaO-Al_2O_3 Melt," J. Am. Ceram. Soc. **67**, 27 (1984); LBL-15885.
2. L.C. De Jonghe and M. Chang, "Surface Oxygen Chemical Potential in a Gas-Solid Reaction," J. Electrochem. Soc. **130**, 2263 (1983); LBL-15732.
3. C.H. Hsueh and L.C. De Jonghe, "Particle Rotation in Early Sintering," J. Am. Ceram. Soc. **67**, C215 (1984); LBL-17547.
4. L.C. De Jonghe and M.N. Rahaman, "Pore Shrinkage and Sintering Stress," J. Am. Ceram. Soc. **67**, C214 (1984); LBL-17548.

LBL Reports

5. S.J. Wu and L.C. De Jonghe, "Sub-eutectic Densification and Second Phase Formation in Al_2O_3-CaO," LBL-17954.
6. J. Sasaki, N.L. Peterson, and L.C. De Jonghe, "Fast Diffusion of Iron in Single Crystal Rutile and Iron Doped Rutile," LBL-17010.
7. S.J. Wu (M.S. Thesis), "Low Temperature Sintering of Al_2O_3-CaO," LBL-16959.

Structure and Properties of Composite Materials*

Robert H. Bragg, Investigator

INTRODUCTION

The purpose of this work is to understand how the properties of hard carbons and soft carbons are related to their structure. The latter undergo a structural transformation, i.e, they graphitize and become mechanically soft when heated above about 2000°C; whereas the former do not undergo a structural transformation, even when heated above 3000°C. Soft carbons are fairly well understood, but basic knowledge concerning hard carbons has been scant. In this project, glassy carbon (GC) has been studied as a model hard carbon because it is a chemically pure (i.e, elemental carbon), monolithic solid. It has been found that the structural differences between the two classes are analogous to those between thermosetting resins (hard) and thermoplastic resins (soft). Hard carbons consist of densely interwound long laths made up of 5–10 graphite-like layers of carbon atoms, ranging from 50 to 100 Å wide, whereas soft carbons are composed of 10 to 1000 or more planar graphite-like layers of carbon atoms ranging from 50 to 10,000 Å wide. Whereas soft carbons become semimetallic electrical conductors, hard carbons resemble small band-gap amorphous semiconductors and at low temperatures display one-dimensional conduction. The major problem in carbon science now is to identify the specific mechanism(s) associated with the structural changes during graphitization. This work has led to the hypothesis that the mechanism of graphitization is the chemical decomposition of a heretofore unsuspected graphite intercalation compound, and experiments to test this hypothesis are being performed.

*This work was supported by the Director, Office of Energy Research, Office of Basic Energy Sciences, Materials Sciences Division of the U.S. Department of Energy under Contract No. DE-AC03-76SF00098.

1. Pore Size, Shape, and Growth Kinetics in Glassy Carbon (Publication 2)

Leo G. Henry† and Robert H. Bragg

Small-angle x-ray and neutron scattering and wide-range x-ray and neutron diffraction were used to characterize the structural changes in GC heat-treated in inert atmospheres in the 1000-2800°C range for up to 150 hours. Below 1800°C the pore size increased with increase in heat-treatment temperature (HTT) but was independent of heat-treatment time (HTt), and the effective crystallite size and internal strains also increased nonkinetically. Above 1800°C the radius of gyration of the pores R_g followed precipitate-coarsening kinetics (see Figure 1-1). The activation energy, $\Delta H = 76 \pm 4$ kcal/mole, is in good agreement with the accepted 71 kcal/mole for vacancy migration in the layer direction in graphite, confirming a previous result obtained from an analysis of the decrease in internal surface area during annealing.[1] The diffraction data show that most of the structural change in GC is relief of internal strain, and the lath thickness never

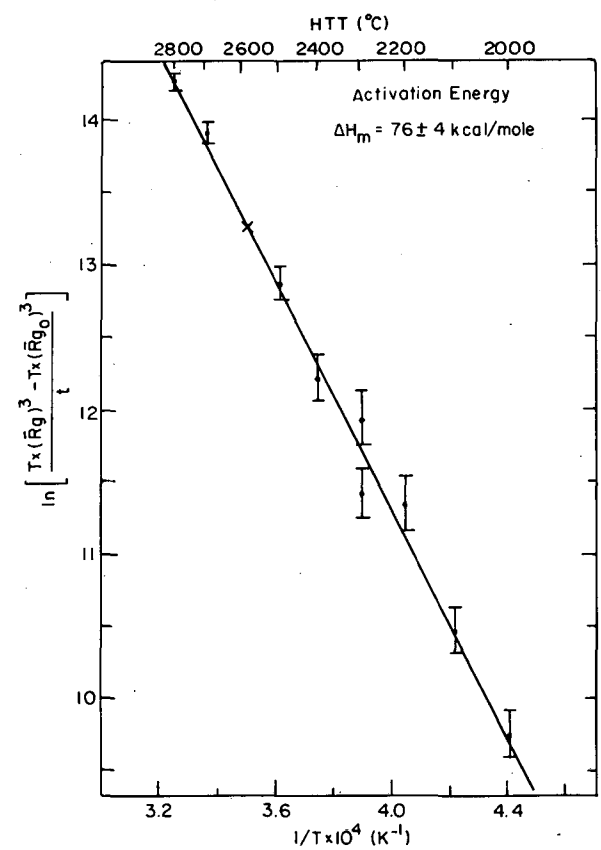

Figure 1-1. Arrhenius plots of coarsening rates of voids in glassy carbon. HTT = heat-treatment temperature. (XBL 8410-7640)

exceeds about 10 graphite-like layers. The neutron-scattering data indicate that at 1000°C GC contains about 3 mole% of hydrogen, but this decreases to less than 1 mole% after short times at 2800°C. Most of the hydrogen is evolved below about 1500°C, causing an irreversible dilatation; and at higher temperatures GC expands irreversibly because of the large anisotropy in its thermal-expansion coefficients.

†Present address: Advanced Microdevices, Sunnyvale, California.

1. S. Bose and R.H. Bragg, Carbon **19**, 289 (1981).

2. Graphitization of Pyrocarbon: Kinetics of Interlayer Spacing and Weight Loss (Publication 4)

Kazuro Kawamura† *and Robert H. Bragg*

Pyrocarbon (PyC) is a model soft carbon made by chemical vapor deposition of methane on a hot graphite substrate. Using x-ray diffraction and weight measurements, the structural changes induced by heat treatments at 2300, 2400, 2500, and 2600°C for up to 24 hours were characterized. The interlayer spacing decreased from 3.425 Å to 3.360 Å monotonically within an activation energy of 240 ± 20 kcal/mole (see Figure 2-1). The strain perpendicular to the layers first increased, then decreased sharply at about the same time that the interlayer spacing decreases most rapidly, and when the crystallite size begins to increase sharply (see Figure 2-2). Whereas the changes in these three properties were characterized by the same activation energy, the weight loss was diffusion controlled with an activation energy of about 100 ± 50 kcal/mole. The large uncertainty stems from the difficulty of measuring small weight changes. Nevertheless a graph of interlayer spacing versus weight loss reveals a precipitous decrease in interlayer spacing at a critical value of weight loss. This observation is readily explained if the initial PyC contains chemical species between the graphite-like layers, because removal of this intercalant should coincide with a decrease of the interlayer spacing to the normal value. Removal of intercalant is also consistent with changes in strain perpendicular to the layers and may possibly explain the onset of rapid crystallite growth. More definitive results should be obtained in planned experiments where the weight losses will be large enough for accurate chemical analysis.

†On leave from the Department of Chemistry, the National Defense Academy, Yokosuka, Japan.

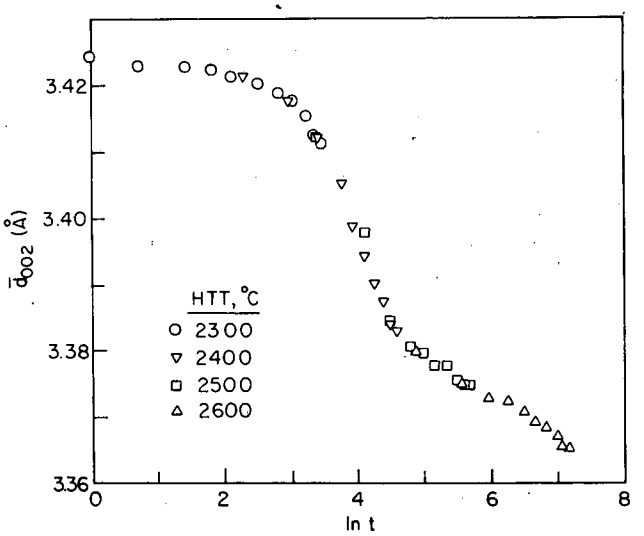

Figure 2-1. Superimposed master curve of interlayer spacing $\bar{d}_{002}$ versus ln t for several heat-treatment temperatures (HTT). (XBL 849-7342)

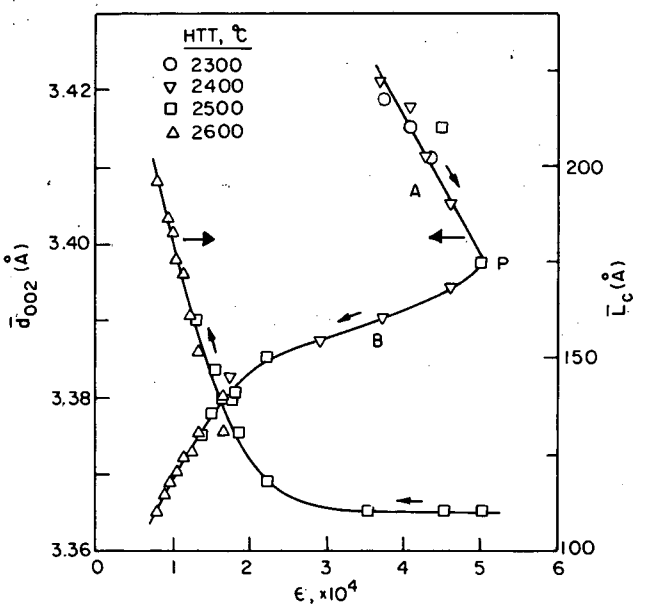

Figure 2-2. Changes in interlayer spacing $\bar{d}_{002}$ and crystallite height $\bar{L}_c$ versus lattice strain ε. The time evolution of a property is indicated by the arrows. (XBL 849-7348)

3. Carbonization and Graphitization of Coal-Tar Pitch Mixed with Trinitrophenol (Publication 5)

Kazuro Kawamura and Robert H. Bragg

It is well known that when coal-tar pitch is mixed with mono- and dinitro compounds, the formation of a mesophase during carbonization in the 200–300°C range is suppressed, and a hard honeycomb-like isotropic carbon is formed. In this work it was found that pitch coke modified with a polynitro compound also suppresses mesophase formation, and the product only partially graphitizes at 3000°C, whereas the unmodified coke graphitizes completely. X-ray-diffraction and electron-spin-resonance (ESR) measurements indicate that the 3000°C treatment produces a composite material. One of the phases is characterized by a broader reflection at 3.42 Å, and the other is characterized by a sharp reflection at 3.36 Å. It is suggested that the two-phase structure results from stress graphitization. A heretofore unreported relation between the concentration of unpaired electrons N and the shift in the g factor $\Delta g = g - 2.0023$ was found: $\ln N = A + B\Delta g$. This work demonstrates that GC can be synthesized using additions of polynitro compounds to coal-tar pitch as well as by addition of mono- and dinitro compounds.

4. Work in Progress

Work on the kinetics of structural and weight changes of PyC and pitch coke is in progress. The immediate objective is to identify the chemical species involved in weight loss during graphitization and correlate these changes with structural changes, mainly decrease of the interlayer spacing with weight loss. Pitch coke was chosen because it graphitizes readily and the weight losses can be determined far more accurately than has been possible heretofore. The results thus far are exciting: they confirm the precipitous decrease in interlayer spacing when the weight loss reaches a critical value, but it is not yet certain that the chemical species evolved is hydrogen. In one critical experiment, an attempt is being made to deliberately disorder material that is initially completely ordered. What should be observed is an increase in interlayer spacing from 3.354 Å to 3.44 Å. When this material is heat-treated, the decrease back to 3.354 Å should occur with an activation energy of about 240 kcal/mole. In another critical experiment, measurements will be made of the Hall coefficient as a function of HTT and HTt to see if there is a change of sign at a critical weight loss, as would be expected if a chemical species initially present was acting as an n-type dopant.

1984 PUBLICATIONS AND REPORTS

Refereed Journals

1. S. Flandrois, A.W. Hewat, C. Hauw, and R.H. Bragg, "Neutron Diffraction and Small Angle Scattering Investigation of Graphite-Nickel Chloride Intercalation Compounds," Syn. Met. 7, 305 (1983).

LBL Reports

2. L.G. Henry (Ph.D. Thesis), "Pore Size, Shape, and Growth Kinetics in Glassy Carbon," LBL-18021.
3. A.W. Pearson (M.S. Thesis), "Effect of Crystallite Size and Shape on the Radial Distribution Function," LBL-16604.
4. K. Kawamura and R.H. Bragg, "Graphitization of Pyrocarbon: Kinetics of Interlayer Spacing and Weight Changes," LBL-17982.
5. K. Kawamura and R.H. Bragg, "Carbonization and Graphitization of Coal Tar Pitch Mixed with Trinitrophenol," LBL-18783.
6. L.G. Henry and R.H. Bragg, "Strain Relief in Heat Treated Glassy Carbon," LBL-18510.
7. L.G. Henry and R.H. Bragg, "Kinetics of Void Growth in Glassy Carbon," LBL-18509.

Ceramic Interfaces*

Andreas M. Glaeser, Investigator

INTRODUCTION

Numerous material properties depend strongly on microstructure, necessitating control of both the microstructural characteristics (grain size, density, pore size, etc.) developed during processing and the stability of these characteristics during subsequent use. This research program focuses on improving our understanding of several processes that contribute to or control the morphological and, hence, microstructural changes occurring during both materials fabrication and utilization. Among the problems addressed are: (1) the development of thermodynamic and kinetic descriptions of the stability of continuous intergranular phases (e. g., the pore phase during intermediate stage sintering, and fibers in polycrystalline matrix composite materials), (2) a theoretical assessment of the effects of anisotropic surface and grain boundary energies on microstructural evolution during sintering, and (3) investigation of the factors that control or influence grain boundary migration behavior, and thus directly or indirectly affect the grain size and other microstructural features.

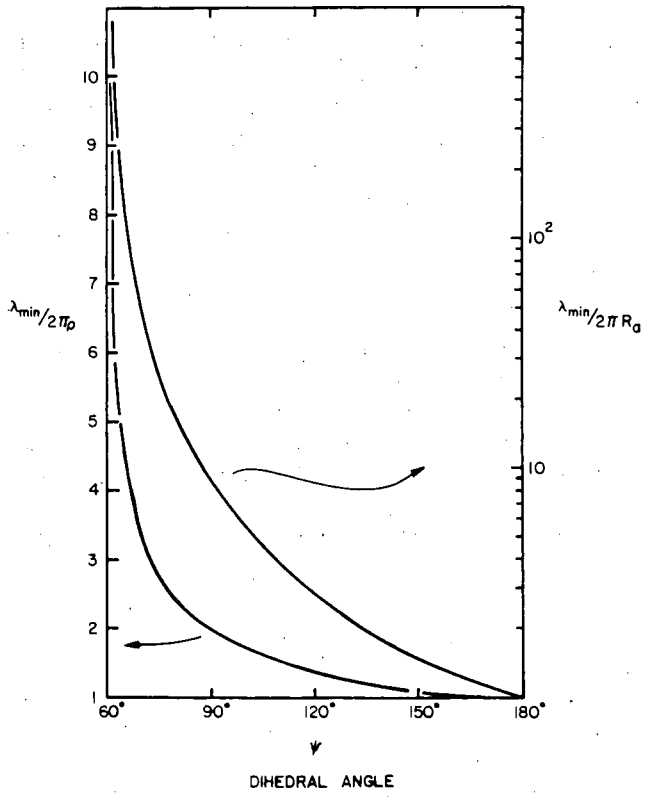

Figure 1-1. The dihedral angle dependence of λ_{min}, the minimum wavelength perturbation capable of increasing in amplitude, is presented and compared with values obtained assuming a cylindrical pore geometry. Cylindrical pores of radius R_a and ρ' have respective volumes and surface curvatures equivalent to those of a pore characterized by a dihedral angle of ψ.
(XBL 851-724)

1. Dihedral Angle Effects on the Stability of Pore Channels (Publication 1)

W. Craig Carter and Andreas M. Glaeser

Complete densification of a powder compact is accompanied by a transition from an initially continuous intergranular pore phase to a discrete pore phase. A perturbation analysis has been employed to evaluate the modifying effect of dihedral angle on the morphological stability of continuous pore channels along a three-grain junction. Channel breakdown requires perturbations having a wavelength in excess of a critical wavelength λ_{min}, which increases as the dihedral angle ψ decreases, exceeding the value predicted for cylinders at all $\psi < 180°$. The predicted behavior is presented in Figure 1-1 and compared with values obtained assuming a cylindrical pore geometry. The results have implications with respect to the uniformity of microstructure development during sintering. The theoretical analysis has recently been extended to describe the stability of continuous second phases at grain boundaries.

2. The Stability of Pore Channels: Experimental Observations (Publication 3)

Michael D. Drory and Andreas M. Glaeser

Micrographic examination of fracture surfaces of near-theoretical density compacts of MgO indicated the presence of continuous pore channels along some three-grain junctions. A spectrum of morphologies was observed, ranging from channels of nearly constant cross section to channels displaying more pronounced morphological perturbations of the type

*This work was supported by the Director, Office of Energy Research, Office of Basic Energy Sciences, Materials Sciences Division of the U.S. Department of Energy under Contract No. DE-AC03-76SF00098.

proposed to account for the breakdown of pore channels formed during wire-sintering experiments. The results suggest that at least a fraction of the isolated pores in a compact develop as a result of perturbation growth. Several difficulties in applying the thermodynamic and kinetic analyses based on cylindrical pore geometries were identified and discussed.

3. Work in Progress

Extension of the stability analysis to intergranular phases is essentially completed. Work is in progress to assess the effect of preexistant large-amplitude perturbations on the stability of continuous phases. A kinetic analysis of the breakdown of continuous intergranular phases incorporating the effect of dihedral angle is planned. Considerable changes in the magnitude of the most rapidly growing wavelength are anticipated.

High-resolution transmission electron microscopy of grain boundaries in high-purity lead is being used to determine whether there is any direct substantiating evidence for the reported grain boundary structure transformation in this material.

The effects of grain boundary and surface energy anisotropy on the nature of metastable configurations potentially resulting from interparticle neck growth, in one and two-dimensional arrays of cylinders as well as in spheres, are being assessed theoretically.

1984 PUBLICATIONS AND REPORTS

Refereed Journals

1. W.C. Carter and A.M. Glaeser, "Dihedral Angle Effects on the Stability of Pore Channels," J. Am. Ceram. Soc. **67**, C124 (1984); LBL-17079.
2. A.M. Glaeser, "Microstructure Development in Ceramics: The Role of Grain Growth," Yogyo Kyokai-Shi **92**, 537 (1984); LBL-17078.

LBL Reports

3. M.D. Drory and A.M. Glaeser, "The Stability of Pore Channels: Experimental Observations," accepted by J. Am. Ceram. Soc.; LBL-18180.

Invited Talks

4. W.C. Carter and A.M. Glaeser, "Stability of Pore Channels: Dihedral Angle Effects," 86th Annual Meeting of the American Ceramic Society, Pittsburgh, Pennsylvania, April 29–May 3, 1984.

ENGINEERING MATERIALS

Abrasive, Erosive, and Sliding Wear of Materials*

Iain Finnie, Investigator

INTRODUCTION

The purpose of this work is to explore the basic mechanisms of abrasive, erosive, and sliding wear in different types of materials. The ultimate objective of this research is quantitative predictions of wear resistance from simple materials tests. Attempts to understand the basic mechanisms follow essentially two routes. One route involves studying the role of different variables such as temperature or abrasive-particle size and uses the results to extend existing explanations of the wear process or to guide in developing new formulations. The other route involves modeling wear processes on a larger scale so that the mechanisms of removal may be observed directly.

1. The Simulation of Sliding Wear by Cyclic Plastic Deformation Under Combined Stresses (Publication 1)†

R. Glardon,‡ S. Chavez,§ and I. Finnie

A mechanical test that is believed to simulate the conditions occurring in sliding wear is described. It involves the cyclic plastic deformation of metals under combined compression and shear. The results of tests on six alloys are reported and correlated with those from wear tests. On this basis, an expression is proposed for the sliding-wear rate that is based on material behavior during cyclic plastic deformation and involves three material properties. The implications of this expression for the wear rate are discussed, and directions for future work are suggested.

*This work was supported by the Director, Office of Energy Research, Office of Basic Energy Sciences, Materials Sciences Division of the U.S. Department of Energy under Contract No. DE-AC03-76SF00098.

†Dr. Glardon was supported by the *Schweizerischer National Fonds zur Forderung der Wissenschaftlichen Forschung,* Bern, Switzerland, and the *Allgemeine Schweizerische Uhrenindustrie AG,* Biel, Switzerland.

‡Present address: Mettler Instruments AG, 8506 Greifensee, Switzerland.

§Present address: E.G.G., Idaho Falls, Idaho.

2. Some Aspects of Abrasive Wear at Elevated Temperature (Publication 2)†

S. Soemantri, A.C. McGee,‡ and I. Finnie

The abrasive wear of commercially pure aluminum and copper has been studied over a temperature range from ambient to 400°C. For two-body abrasion (fixed abrasive particles), the wear rate of copper is remarkably insensitive to temperature over the temperature range studied. Other than an increase in the region around 250°C, the wear rate of the aluminum tested was also insensitive to temperature. Three-body abrasion (loose abrasive particles) was studied using a disc-shaped specimen pressed against a rotating cup containing loose abrasive particles. Again aluminum showed very little variation of weight loss with temperature. Copper specimens showed an increase in apparent wear rate with temperature. However, this effect could be attributed largely to the oxidation occurring in these longer-term tests. A qualitative explanation for the insensitivity of wear rate to temperature in abrasion is given by referring to data in the literature on the effect of high strains and strain rates on the flow stress.

Finally, a three-body abrasive-wear tester discussed in earlier work[1] was used to study the influence of temperature. This involves a column of abrasive contained in a tube and loaded by a weight. The assembly is then placed close to the surface of a rotating-disc-shaped specimen. An analysis of this

tester shows that wear is occurring because of particles trapped between the tube and the specimen. Under these conditions aluminum shows a decrease in wear rate with increasing temperature that is attributed to embedding of abrasive in the surface, while copper shows an increase in wear rate that is attributed to oxidation. These results show that care must be taken in interpreting high-temperature abrasive-wear tests since experimental results may be influenced greatly by the choice of the tester and a corrosive environment.

†Mr. Soemantri was supported by the Indonesian State Tin Corp.

‡Present address: Lockheed Missles and Space Corp., Sunnyvale, California.

1. I. Finnie and A. Misra, Wear **85**, 57 (1983).

3. Work in Progress

A detailed analysis of the loaded-abrasive-column type of wear tester has been accepted for publication in *Wear*. A paper on the abrasive and erosive wear of composites will soon be submitted to the same journal.

Experiments in which large spherical and irregular indenters were pressed repeatedly against a surface were used to model erosive and abrasive wear. An analysis of this test, which provides insight into the mechanisms involved in wear, is now almost complete.

One of the most puzzling aspects of abrasive and erosive wear and grinding of metals has been the "size effect." This term describes the relative insensitivity of wear to abrasive-particle sizes above about 100 μm and the rapid decrease in wear rate observed as the particle size is decreased below about 100 μm. Many explanations have been offered for this phenomenon, and it has been shown in previous work[1] that none of these are generally applicable. A new approach, which invokes a surface-energy term deduced from fracture tests in addition to the energy required for plastic deformation, has been developed. This explanation of the "size effect" appears more satisfactory than any others that have been proposed.

1. I. Finnie and A. Misra, Wear **65**, 359 (1981).

1984 PUBLICATIONS AND REPORTS

Refereed Journals

1. R. Glardon, S. Chavez, and I. Finnie, "The Simulation of Sliding Wear by Cyclic Plastic Deformation Under Combined Stresses," J. Eng. Mat. Tech. **106**, 248 (1984).

Other Publications

2. S. Soemantri, A.C. McGee, and I. Finnie, "Some Aspects of Abrasive Wear at Elevated Temperature," in *Proc. 1985 Int. Conf. on Wear,* American Society of Mechanical Engineers, New York (in press).

Erosion and Spalling in Brittle Solids*

Anthony G. Evans, Investigator

INTRODUCTION

This project is concerned with the development of a fundamental understanding of the spalling, erosion, and strength degradation of brittle coatings and layers subject to thermal and mechanical (impact) loading. The principal research directions involve studies of the damage created by mechanical and thermal loads, by impacting particles, and by thermal shock. The residual stress in the coating and the adherence of the coating to the substrate are important variables in the investigation. Hence, techniques for ascertaining the magnitude of the residual stress and for characterizing the adhesion are essential study topics. Predictions of material removal by spalling constitute the primary product of this investigation. The results are applicable both to erosion/corrosion situations (wherein the corrosion product is removed by erosion) and to thermal-spalling loss in ceramic-coated systems.

1. The Thermal Spalling of Brittle Coatings (Publication 1)

R. Loh and A.G. Evans

Ceramic coatings on metal or ceramic substrates are susceptible to spalling during thermal cycling. The thermal-spalling phenomenon has been investigated using a zirconia thermal-barrier coating on a NiCrAlY substrate. Prior studies have revealed that spalling occurs in the presence of in-plane compression within the coating and thus occurs during heating. A laser heating technique has consequently been developed to investigate thermal spallation. Initial investigation of pristine coatings indicated that the coatings are spallation resistant, both on heating and cooling. However, spalling has been demonstrated to occur on heating in the presence of an initial delamination. Specifically, delaminations of varying radii have been introduced by indentation, and critical thermal loadings (power, duration, etc., of the laser pulse) for spalling have been identified as a function of delamination size. The results have been correlated with a previous spalling analysis based on post-buckling theory. Attendant implications for the spallation resistance of coatings in the presence of initial delaminations, impact-induced delaminations, and residual stress are discussed.

2. Oxidation Effects on the Adhesion of Ceramic Coatings (Publication 7)

G.C. Crumley and A.G. Evans

A systematic study of the effects of oxidation on the interfacial microstructures of a zirconia-coated nickel superalloy (NiCrAlY) has been investigated. Transmission electron-microscope (TEM) cross sections indicate that an intermediate Al_2O_3 layer forms and thickens linearly with time. In addition, Ni and Cr diffuse through the oxide layer into the ZrO_2 to form a mixed-oxide (predominantly spinel) layer. Chemical-potential gradients in the system that determine the net mass flux are discussed. Morphological changes also occur in the ZrO_2, suggestive of concurrent densification and surface diffusion. Residual stress has been demonstrated to develop in association with the microstructural changes.

The residual stress is deemed an important constituent in the oxidation-induced loss of adherence by virtue of its effect on buckling and spalling. However, it is also recognized that delaminations at or near the interface are a further prerequisite to spallation. Voids (or other sources of delamination) have not yet been systematically identified.

3. The Mechanical Properties of Ceramic/Metal Bonded Systems (Publication 5)

A.G. Evans and M. Rühle

Coating spallation and erosion/corrosion phenomena involve the propagation of cracks at or near the interface between a ceramic/metal or ceramic/ceramic interface. Fundamental studies of the mechanical properties of ceramic/metal bonded systems at elevated temperatures thus provide a basis for interpreting trends in spallation and erosion/corrosion. Preliminary investigations have been conducted on a model system, Al_2O_3/Nb. High-resolution TEM studies reveal that there is direct bonding in this system between the metal and ceramic (no intermediate metal oxide), a finding con-

*This work was supported by the Director, Office of Energy Research, Office of Basic Energy Sciences, Materials Science Division of the U.S. Department of Energy under Contract No. DE-AC03-76SF00098.

sistent with recent 'lock-in' descriptions of bonding along close-packed planes in the ceramic and metal. Fracture studies indicate the existence of stress concentrations along surfaces and edges near the interface caused by an elastic-modulus mismatch between Al_2O_3 and Nb. These stress concentrations result in edge- or surface-dominated failures, often involving subcritical crack growth. The fracture instability always occurs in the Al_2O_3, indicating that the ceramic represents the path of minimal fracture resistance in this system. In fact, cracks that extend stably to the interface tend to blunt by plastic deformation in the Nb and are thus resistant to further growth. However, rapidly growing cracks tend to be attracted to the interface and grow preferentially along the interface with no evidence of plasticity. This effect is attributed to the strong rate of dependence of the plasticity in bcc Nb and an associated ductile-to-brittle transition. Implications for rate effects in erosion and thermal shock are evident.

4. Work in Progress

Laser-induced spalling is being developed as a technique for evaluating the spallation resistance of coatings. The thermal compression developed in the coating as the laser is scanned over the surface induces spallation at locations where initial delaminations exist at the interface (or within the coating). Inferior coatings can thereby be eliminated by a laser proof test. Thermal stress-analysis techniques are used with temperature measurements to calibrate the laser system. Indentation-induced delaminations are then used with post-buckling theory to evaluate the role of delamination size and coating adherence on the spalling process. The method is being applied to zirconia coatings on NiCrAlY, Si_3N_4, and SiC, and to other oxide coatings.

Residual stresses that develop during oxidation have recently been demonstrated to constitute an important impetus for coating and layer spallation and erosion. A fundamental analysis of stress development in oxide layers is thus being developed for the spectrum of potential oxide-formation conditions, viz., control by either grain boundary or lattice diffusion of either anion or cation vacancies or interstitials. The imposition of equilibrium at grain boundaries in the oxide caused by unimpeded vacancy production or annihilation is shown to require a stress gradient as the oxide thickens, irrespective of the controlling mass-transport mechanism. However, the transport mechanism dictates the sign and magnitude of the stress. In some instances, tensile stress is predicted. Such stresses result in a porous oxide layer. In other cases, compression is expected with attendant potential for spallation. The analysis thus has basic implications for the behavior of oxide layers, as well as for the oxidation rate.

Finally, studies of the mechanical behavior of ceramic/metal bonded systems are continuing. The present emphasis is on the Al_2O_3/Cu system, as required to investigate the influence of the fcc structure, which is not subject to a ductile-to-brittle transition (as compared to bcc Nb). Initial results indicate that the plasticity in the Cu dominates the stress amplitude in the system, while the Al_2O_3 again represents the path of minimum fracture resistance.

1984 PUBLICATIONS AND REPORTS

Refereed Journals

1. A.G. Evans, G. Crumley, and E. Demeray, "The Mechanical Behavior of Brittle Coatings and Layers," Oxidation of Metals **20** (5/6), 193–216 (1983); LBL-15474.
2. A.G. Evans and J.W. Hutchinson, "On the Mechanics of Delamination and Spalling in Compressed Films," Int. J. Solids and Struc. **20** (5), 455–466 (1984); LBL-15781.
3. D.B. Marshall and A.G. Evans, "Measurement of Adherence of Resid– ually Stressed Thin Films by Indentation: I. Mechanics of Interface Delamination," J. Appl. Phys. **56** (10), 2632–2638 (1984); LBL-16841-1/2.
4. C. Rossington, D.B. Marshall, A.G. Evans, and B.T. Khuri-Yakub, "Measurement of Adherence of Residually Stressed Thin Films by Indentation: II. Experiments with ZnO/SiO," J. Appl. Phys. **56** (10), 2639-2644 (1984); LBL-16841-2/2.

LBL Reports

5. A.G. Evans and M. Rühle, "On the Mechanics of Failure in Ceramic/Metal Bonded Systems," J. de Physique (in press); LBL-18786.
6. R. Loh and A.G. Evans, "Laser Induced Thermal Shock of Ceramic Coatings," LBL-18787.
7. G. Crumley and A.G. Evans, "Effects of Oxidation on the Properties of Ceramic Coated Alloys," LBL-18788.

Invited Talks

8. A.G. Evans, "Mechanical Properties of Ceramic/Metal Bonded Systems," International Conference on the Structure and Property of Internal Interfaces, Irsee, West Germany, August 1984.
9. A.G. Evans, "Mechanical Properties of Ceramic/Metal Bonded Systems," Materials Research Society Meeting, Boston, Massachusetts, November 1984.
10. R. Loh and A.G. Evans, "Laser Induced Thermal Shock of Ceramic Coatings," Pacific Coast Regional Meeting, American Ceramic Society, San Francisco, California, October 1984.
11. A.G. Evans, "Mechanical Properties of Ceramic Coatings," Max-Planck Institute, Stuttgart, West Germany, May 1984.

SOLID-STATE PHYSICS

EXPERIMENTAL RESEARCH

Far-Infrared Spectroscopy*

Paul L. Richards, Investigator

INTRODUCTION

Improvements in infrared technology are making possible increases in the sensitivity of many types of infrared measurements. In this project, improved types of infrared detectors, mixers, and spectrometers are being developed. Improved infrared techniques are being used to do experiments in areas of fundamental and applied infrared physics where their impact is expected to be large.

Developments of infrared technology include installation and testing of a new commercial Fourier-transform infrared spectrometer, evaluation of novel concepts for ultrasensitive photoconductive detectors for the 50–1000 μm wavelength range, development of a new class of far-infrared (FIR) dichroic beam dividers, and development of a novel source of tunable far-infrared picosecond pulses.

Experiments in progress include measurements of the infrared absorption spectra of molecules chemically adsorbed on metal surfaces, measurements of the infrared spectra of one-dimensional conductors, measurements of the infrared photoconductivity of impurities in semiconductors, and measurements of picosecond far-infrared nonlinear effects.

*This work was supported by the Director, Office of Energy Research, Office of Basic Energy Sciences, Materials Sciences Division of the U.S. Department of Energy under Contract No. DE-AC03-76SF00098.

1. Infrared-Emission Spectroscopy of Adsorbate Molecules on Metal Surfaces (Publications 3, 4, and 5)

R.G. Tobin and P.L. Richards

The explanation of the observed vibrational linewidths of molecules adsorbed on metal surfaces is an active area of research in surface science. It appears that, for different systems and under different circumstances, the linewidth may be determined by inhomogeneous effects, vibrational dephasing due to coupling to other adsorbate and substrate vibrations, energy transfer into electron-hole pairs in the substrate, or energy transfer into substrate phonons. Our measurement of the C-Ni stretching-mode linewidths for CO on Ni(100) in 1983 was the first such linewidth measurement for a molecule-substrate mode on a well-characterized single-crystal metal surface. Subsequent theoretical calculations have explained the observed linewidth in terms of vibrational-energy decay into substrate phonons. For such a process, a strong dependence of the linewidth on temperature was predicted.

Our current work in this area is aimed at an experimental test of the theoretical explanations of the adsorbate-substrate mode linewidths, and particularly of the predicted temperature dependence, for the systems of CO and O on Pt(111). Because clean, well-characterized surfaces are required, and because the vibrational modes under study are very weak, the measurements are very difficult. Our infrared emission system continues to be the only apparatus capable of making such measurements.

We have measured the C-Pt stretching vibration of CO on Pt(111) and directly verified for the first time, by isotopic substitution, the accepted identification of this mode (see Figure 1-1). The observed linewidth at 302 K is 10 ± 2 cm^{-1}. Further experiments to improve the precision of that measurement and to measure the temperature dependence of the linewidth are in progress.

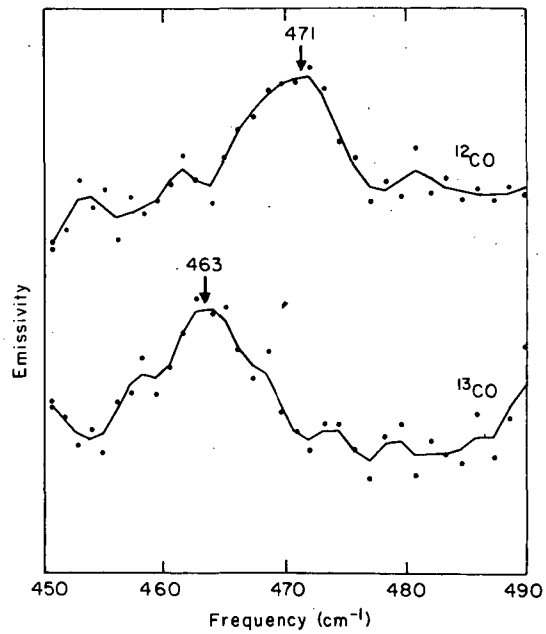

Figure 1-1. Isotope shift of C-Pt stretching mode of CO on Pt(111). The expected shift is 8.2 cm^{-1}. The instrumental resolution was ~2cm^{-1}. The solid lines were obtained by computer smoothing of the data. (XBL 851-5701)

2. Picosecond Far-Infrared Generation by Parametric Mixing (Publication 25)

T.W. Kenny and P.L. Richards

In the FIR, studies of dynamics have been restricted by the lack of intense, narrow, tunable picosecond pulses. In collaboration with M. Berg and C.B. Harris of MMRD, we have generated continuously tunable picosecond pulses from 20–200 cm^{-1} through the parametric interaction of two optical-dye laser pulses. FIR pulse energies on the order of 3 nJ were detected with a calibrated bolometer (see Figure 2-1). These energies represent a conversion efficiency from optical to FIR of 0.1 to 0.3% over the range investigated. The conversion efficiency is surprisingly constant, given the large variations in FIR absorption, diffraction, and phonon-resonance enhancement over the same range. A spectrum of the FIR pulses measured with a Fourier-transform spectrometer shows that the pulses are not significantly broadened by the generation process.

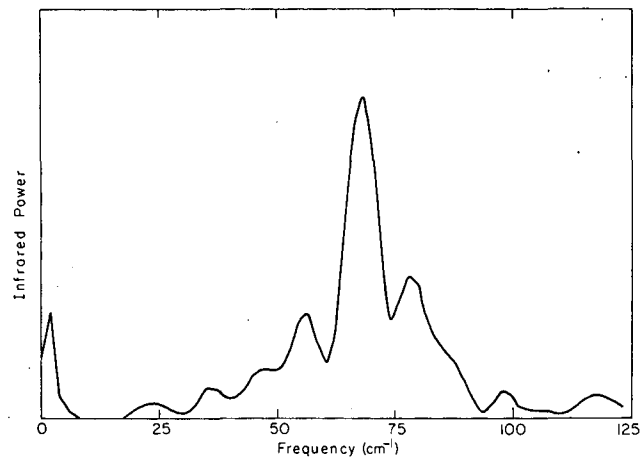

Figure 2-1. Spectrum of picosecond far-infrared pulses measured using bolometric detector and Fourier-transform spectrometer. (XBL 851-5704)

Both the relations between optical and FIR pulse power and the observed depletion of the optical pulse suggest that the process is limited by the number of optical photons available for conversion. The observation of conversion efficiencies that are constant over a large range also supports this conclusion. However, the FIR energy shows unexpectedly large pulse-to-pulse fluctuations. If the origin of these fluctuations can be understood, substantial improvements in the average efficiency may be possible.

3. Far-Infrared Dichroic Band-Pass Filters (Publication 23)

D.D. Nolte, A.E. Lange, and P.L. Richards

Filters that serve as dichroic beam dividers are useful for certain types of FIR photometers. We have used inductive cross-metal mesh as reflective coatings on solid dielectric Fabry-Perot etalons to produce dichroic filters with quality factors in the range $3 < Q < 10$. These filters reflect strongly at frequencies below the band pass and retain their well-defined band pass at angles of incidence as large as 45°. They have been used to make an efficient FIR dichroic photometer with six frequency bands between 10 and 100 cm^{-1} (see Figure 3-1).

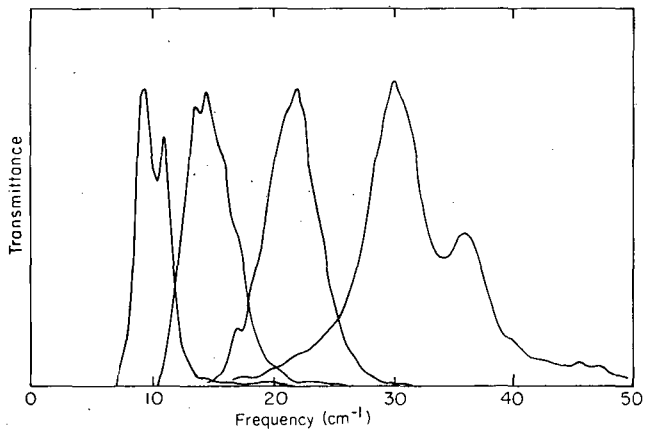

Figure 3-1. Response of four channels of a dichroic photometer using four dichroic filters plus additional low- and high-pass filters in each channel. The peak response has been normalized to the same value for each channel. (XBL 8410-8255)

4. Work in Progress

The success of our new techniques for measuring the infrared spectra of molecules chemisorbed on metal surfaces has led to a second generation of experiments involving CO on Pt to test linewidth mechanisms.

The infrared optical properties of charge-density-wave compounds $TaSe_3$, $(TaSe_4)_2I$, and $K_{0.3}MoO_3$ are being measured.

A new FIR Fourier spectrometer made by Bomem, Inc., has been acquired and is being installed and tested.

The photoconductive response of overcharged Ga sites in Ge:Ga is being measured.

Data on the nonlinear FIR response of $LiNbO_3$ on the picosecond time scale are being analyzed.

1984 PUBLICATIONS AND REPORTS

Refereed Journals

1. P.L. Richards, "Spectrum of the Microwave Background Radiation," Mitteilungen der Astronomischen Gesellschaft **60**, 175 (1983).†
2. W.A. Challener, P.L. Richards, and R.L. Greene, "Far Infrared Optical Properties of $TMTSF_2ClO_4$," J. de Phys. Colloq. **C3**, 867 (1983); LBL-15279.
3. S. Chiang, R.G. Tobin, and P.L. Richards, "Vibrational Spectroscopy of Chemisorbed Molecules by Infrared Emission," J. Vac. Sci. Technol. **A2**, 1069 (1984); LBL-15868.
4. S. Chiang, R.G. Tobin, and P.L. Richards, "The Molecule Substrate Vibration of CO on Ni(100) Studied by Infrared Emission Spectroscopy," Phys. Rev. Lett. **52**, 648 (1984); LBL-16779.
5. R.G. Tobin, S. Chiang, P.A. Thiel, and P.L. Richards, "The C=O Stretching Vibration of CO on Ni(100) by Infrared Emission Spectroscopy," Surf. Sci. **140**, 393 (1984); LBL-16780.
6. W.A. Challener and P.L. Richards, "Far Infrared Optical Properties of $NbSe_3$," Solid State Commun. **52**, 117 (1984); LBL-16855.
7. W.A. Challener, P.L. Richards, and R.L. Greene, "Far Infrared Measurements of $(TMTSF)_2ClO_4$," Solid State Commun. **51**, 765 (1984); LBL-17534.

Other Publications

8. M.R. Hueschen, E.E. Haller, and P.L. Richards, "Ge:Ga Photoconductors: Development and Ideal Performance," in *7th Int. Conf. on I-R and mm-Waves Conf. Digest,* 1983, p. L-8-4; LBL-14998.
9. W.R. McGrath, A.D. Smith, and P.L. Richards, "SIS Quasiparticle Mixing Development of a Quantum Limited Receiver," in *URSI Conf. Digest,* January 1983, p. 38.‡
10. M.R. Hueschen, P.L. Richards, and E.E. Haller, "Performance of Ge:Ga Far Infrared Detectors," in *NASA Infrared Detector Technology Workshop Proc.,* August 1983, p. 3–1.†
11. A.E. Lange and P.L. Richards, "Rocket-Borne Radiometry of the Diffuse Submillimeter Background," in *Third CalSpace Investigators Conf. Abstr.,* May 1984, p. 91.§
12. P.L. Richards, "Spectrum of the Microwave Background," in *Proc. II Bi-National Colloq. Alexander von Humboldt Foundation,* 1983, p. 65.†
13. J. B. Peterson, P.L. Richards, J.L. Bonomo, and T. Timusk, "New Measurements of the Spectrum of the Cosmic Microwave Background," in *CIRP-3 Proc.,* 1984, p. 183.†
14. W.A. Challener and P.L. Richards, "Far Infrared Optical Properties of $NbSe_3$, in *CIRP-3 Proc.,* 1984, p. 662; LBL-17293.
15. S. Chiang, R.G. Tobin, P.L. Richards, and P.A. Thiel, "Vibrational Spectra of Co on Ni(100) Studied by Infrared Emission Spectroscopy," in *CIRP-3 Proc.,* 1984, p. 675; LBL-17294.
16. W.R. McGrath, A.V. Räisänen, and P.L. Richards, "Precise Noise Measurements of Superconducting Quasiparticle Mixers," in *1984 Applied Superconducting Conf. Final Program and Abstracts,* 1984, p. 10.‡
17. W.R. McGrath, A.V. Räisänen, P.L. Richards, R.E. Harris, and F.L. Lloyd, "Accurate Noise Measure-

ments of mm-Wave SIS Mixers," in *Ninth Int. Conf. on I-R and mm-Waves Conf. Digest,* 1984, p. 421.‡

18. A.E. Lange, D. Nolte, and P.L. Richards, A Dichroic Beamsplitter for the FIR," in *Ninth Int. Conf. on I-R and mm-Waves Conf. Digest,* 1984, p. 191.
19. S. Sato, T. Matsumoto, K. Sakai, A.E. Lange, and P.L. Richards, "A New Type of Low Pass Filter Made of Glass Beads," in *Ninth Int. Conf. on I-R and mm-Waves Conf. Digest,* 1984, p. 126.§
20. H. Murakami, S. Hayakawa, T. Matsumoto, H. Matsuo, S. Sato, A.E. Lange, and P.L. Richards, "Far-Infrared and Submillimeter Antenna of Low Side Lobe," in *Ninth Int. Conf. on I-R and mm-Waves Conf. Digest,* 1984, p. 125.§
21. T. Matsumoto, S. Hayakawa, H. Murakami, S. Sato, A.E. Lange, P.L. Richards, and K. Sakai, "Instrumentation for the Observation of Far-Infrared and Submillimeter Background Radiation," in *Ninth Int. Conf. on I-R and mm-Waves Conf. Digest,* 1984, p. 119.§

LBL Reports

22. J.B. Peterson, P.L. Richards, J.L. Bonomo, and T. Timusk, "New Measurements of the Spectrum of the Cosmic Microwave Background," in *Proc. Inner-Space/Outer Space Conference* (in press); LBL-18073.
23. D.D. Nolte, A.E. Lange, and P.L. Richards, "Far-Infrared Dichroic Band-Pass Filters," Appl. Opt. (in press); LBL-18713.
24. R.G. Tobin and P.L. Richards, "Linewidths of Adsorbate-Substrate Vibrational Modes Measured by Infrared Emission Spectroscopy," Bull. Am. Phys. Soc. (in press); LBL-18780abs.
25. T.W. Kenny, P.L. Richards, M. Berg, and C.B. Harris, "Picosecond Far-Infrared Generation by Parametric Mixing," Bull. Am. Phys. Soc. (in press); LBL-18781abs.
26. M. Sherwin, A. Zettl, and P.L. Richards, "Far-Infrared Conductivity of $(TaSe_4)_2I$," Bull. Am. Phys. Soc. (in press); LBL-18782abs.

Invited Talks

27. R.G. Tobin, "Vibrational Linewidths of Adsorbates Measured by Infrared Emission Spectroscopy," seminar, University of California, Irvine, March 5, 1984.
28. P.L. Richards, "Measurements of the Cosmic Microwave Background," seminar, Department of Astrophysics, Nagoya University, Japan, March 12, 1984.
29. P.L. Richards, "Superconducting Heterodyne Receivers," seminar, Department of Physics, Osaka University, Japan, March 15, 1984.
30. R.G. Tobin, "Infrared Emission Spectroscopy of Adsorbates: CO on Ni(100)," seminar, University of California Berkeley, April 11, 1984.
31. P.L. Richards, "The Spectrum of the Microwave Background Radiation," Inner Space/Outer Space Conference, Fermilab, Batavia, Illinois, May 4, 1984.
32. P.L. Richards, "Balloon and Rocket Measurements of the Spectrum of the Cosmic Microwave Background," Observatoire de Paris-Meudon, Meudon, France, May 21, 1984; Institute d'Astrophysique, Paris, France, May 25, 1984.
33. P.L. Richards, "Superconducting Microwave Heterodyne Receivers," Meeting on Superconducting Electronics, Glasgow, Scotland, June 12, 1984.
34. P.L. Richards, "New Measurements of the Spectrum of the Cosmic Microwave Background," Third International Conference on Infrared Physics (CIRP-3), Zurich, Switzerland, July 23–27, 1984.
35. P.L. Richards, "Infrared Measurements of Molecules Chemisorbed on Metal Surfaces," Ninth International Conference on Infrared and Millimeter Waves, Takarasuka, Japan, October 22, 1984.

†Supported by the National Aeronautics and Space Administration.

‡Supported by the Office of Naval Research.

§Supported by the National Science Foundation.

Experimental Solid-State Physics and Quantum Electronics*

Y.R. Shen, Investigator

INTRODUCTION

The main objective of this program is to further the basic understanding of lasers and laser-related physics. The emphasis is on development of linear and nonlinear optical techniques for material studies and applications of these techniques to probe linear and nonlinear optical properties of gases, liquids, liquid crystals, and solids. For this purpose, both theoretical and experimental research programs on various aspects of the interaction of light with matter are being carried out. Newly developed techniques are being used to study current problems of interest: isotope separation, photochemistry, surface physics, and phase transitions. Nonlinear optical effects in matter that are not yet clearly understood are also being investigated.

Current research is largely concentrated in applying optical second-harmonic generation to surface and interface studies. Experiments in progress include the studies of adsorbed molecules on clean metal and semiconductor surfaces in ultrahigh vacuum, measurements of molecular arrangement and orientation of adsorbates at liquid/solid and air/solid interfaces, and surface enhancement on rough metal surfaces. Some effort is devoted to collaboration with G. Somorjai's group on other laser-surface studies, with Y.T. Lee's group on laser/molecular-beam interaction and molecular spectroscopy, and with theorists on calculations of current quantum-optics problems. Research on optical properties of interesting new materials is also being carried out.

*This work was supported by the Director, Office of Energy Research, Office of Basic Energy Sciences, Materials Sciences Division of the U.S. Department of Energy under Contract No. DE-AC03-76SF00098.

1. Surface Studies by Optical Second-Harmonic Generation: The Adsorption of O_2, CO, and Na on the Rh(111) Surface (Publication 1)

H.W.K. Tom, C.M. Mate, X.D. Zhu, J.E. Crowell, T.F. Heinz, G.A. Somorjai, and Y.R. Shen

Optical second-harmonic generation (SHG) was used to study the adsorption of atomic and diatomic species on a well-characterized Rh(111) crystal surface in ultrahigh vacuum (UHV). This is the first application of the SHG technique to well-defined surface systems that are also of catalytic importance. SHG was found to be sensitive to adsorption and desorption of less than 5% of a monolayer of atomic or diatomic species on Rh and could distinguish between adsorption at different sites. The results correlate very well with those obtained with conventional surface probes. This result clears the way for the successful application of SHG to other systems of interest in surface science and catalysis. The very high sensitivity, extremely fast response, and nondestructive nature of the technique make it a unique and useful surface-analysis tool. It can yield dynamic information difficult to obtain by the more standard UHV surface probes.

2. Study of the Si(111) Surface by Optical Second-Harmonic Generation: Oxidation and the Effect of Surface Phosphorus (Publication 21)

H.W.K. Tom, X.D. Zhu, Y.R. Shen, and G.A. Somorjai

Optical SHG was used to study a Si(111) 7×7 surface in a UHV chamber. The technique was shown to be sensitive to the electronic properties of the surface, and it can be used to study the growth and thermal desorption of the first layers of surface oxide, the segregation of less than 2% of a monolayer of phosphorus to the surface, and the effect of surface phosphorus on the growth of the first layer of oxide. The technique is more sensitive than Auger electron spectroscopy in detecting phosphorus. The results clear the way for further SHG studies of semiconductor interfaces and suggest that SHG diagnostics might be useful in the fabrication of well-characterized semiconductor devices. The present experiment also found for the first time a $(\sqrt{3} \times \sqrt{3})$ R30° low-energy electron-diffraction pattern that appears to be a new surface structure of

Si(111) induced by the small amount of phosphorus atoms on the surface.

3. Local-Field Enhancement on Rough Surfaces of Metals, Semimetals, and Semiconductors with the Use of Optical Second-Harmonic Generation (Publication 2)

G.T. Boyd, T. Rasing, J.R.R. Leite, and Y.R. Shen

Optical SHG was used to study the local-field enhancement caused by surface roughness on various materials ranging from the alkalis to a semiconductor. The roughness morphology was standardized by evaporating each material onto the same chemically etched glass slide, with microstructures hundreds to thousands of angstroms in size. With the laser excitation at 1.06 μm, the observed second-harmonic enhancements for different materials varied from 27 to 1×10^{-3} times that of silver. They were in fair agreement with a simple model calculation that assumed that the rough surface is composed of a distribution of noninteracting hemispheroids on a plane. The results were used to predict some rather substantial enhancements for surface Raman scattering for a number of substrate materials (see Figure 3-1).

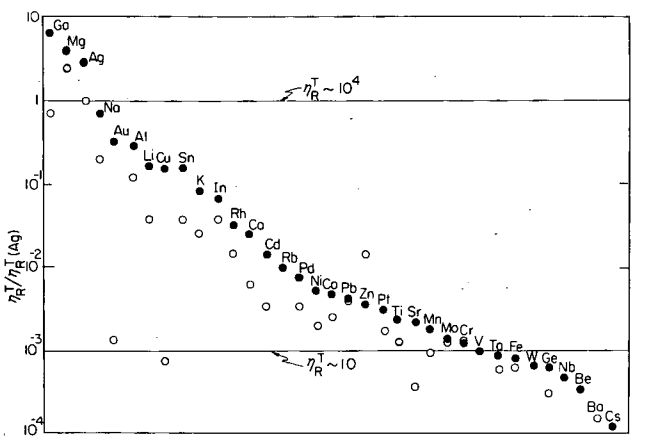

Figure 3-1. Theoretical local-field Raman enhancements relative to Ag at 0.53 μm, for excitation at λ = 0.65 μm (solid circles) and 0.53 μm (open circles). Points are displayed horizontally for clarity only. (XBL 841-6533)

4. New Electronic Levels in the Incommensurate Crystal Rb_2ZnBr_4 (Publication 7)

T. Rasing

Rb_2ZnBr_4 possesses an incommensurate phase below 355K that is characterized by an orthorhombic basic structure with space group Pcmn and a dislacive modulation with wavevector **q** = 0.3 **c**. The absence of lattice translational symmetry in incommensurate systems breaks down the usual concepts of Brillouin zones and Bloch electrons associated with periodic lattices. One consequence of the lattice modulation is a modification of the electronic energy levels. This modification was studied near the energy gap by optical-transmission measurement on Rb_2ZnBr_4. The results showed the appearance of new energy levels and were analyzed with a simple tight-binding model in which the superspace symmetry of the crystal is taken into account.

5. Spectral Broadening of Ultrashort Pulses in a Nonlinear Medium (Publication 6)

G. Yang and Y.R. Shen

High-intensity picosecond or subpicosecond pulses propagating in nonlinear condensed matter can yield an output with a nearly white continuous spectrum. This spectral superbroadening feature is a long-known phenomenon, and it has been used to create tunable ultrashort pulses in the spectral range extending from the near infrared to the near ultraviolet. Theoretical understanding of the phenomenon is, however, still rather primitive. Self-phase modulation following self-focusing and optical breakdown was believed to be the dominant mechanism for superbroadening, but the four-wave parametric process has also been proposed to explain the effect. Recent experiments show that neither mechanism seems to be responsible for the observed superbroadening.

The usual theory of self-phase modulation follows a perturbation calculation of the nonlinear wave equation. Such a calculation is no longer sufficient when the pulse intensity becomes very high. We seek a more rigorous solution for the wave equation.

By neglecting the dispersive effect and solving the wave equation directly in the space-time coordinates, the calculation automatically takes into account both the self-phase modulation due to the induced refractive-index change and the nonresonant four-wave mixing effect. In addition, the self-steepening effect of the pulse on spectral broadening can be included. Our results show a superbroadening in fair agreement with the experimental observations of Fork et al.[1]

1. Fork et al., Opt. Lett. **8**, 1 (1983).

6. Infrared Predissociation Spectra of Water Dimer in a Supersonic Molecular Beam (Publication 3)

R.H. Page, J.G. Frey, Y.R. Shen, and Y.T. Lee

The infrared absorption spectrum of the hydrogen-bonded water dimer, $(H_2O)_2$, formed in a supersonic expansion, was recorded in the region of the OH stretch by monitoring the predissociation resulting from the absorption of the radiation. The conditions were such that there was minimal contribution to the observed spectrum from higher water polymers. The observed features show considerable structure, with widths that appear to be limited by the optical resolution of 2 cm^{-1}. A combination band of the OH stretch with the water bend and an overtone of the bending vibration were also observed. The spectrum shows a rotational envelope, and it is likely that with increased resolution the rotational structure can be recorded; this would greatly enhance the feasibility of obtaining structural information on the vibrational excited states of the water dimer.

7. Work in Progress

Surface SHG is being used to study adsorption of alkali atoms on metals. The results will show how the electronic properties of the atomic adsorbates affect the optical properties of the metal surfaces. The same technique is also being used to study thermal desorption of atoms and molecules from metal surfaces; the results will be compared with those obtained from the usual thermal-desorption spectroscopy.

The possibility of using SHG to study laser-induced desorption and surface diffusion will also be considered. A tunable dye laser will be employed to perform surface spectroscopic studies with SHG. A tunable infrared laser source is being constructed to investigate vibrational spectroscopy of adsorbates by sum-frequency generation.

1984 PUBLICATIONS AND REPORTS

Refereed Journals

1. H.W.K. Tom, C.M. Mate, X.D. Zhu, J.E. Crowell, T.F. Heinz, G.A. Somorjai, and Y.R. Shen, "Surface Studies by Optical Second-Harmonic Generation: The Adsorption of O_2, CO, and Sodium on the Rh(111) Surface," Phys. Rev. Lett. **52**, 348 (1984); LBL-16798.
2. G.T. Boyd, T. Rasing, J.R.R. Leite, and Y.R. Shen, "Local-Field Enhancement on Rough Surfaces of Metals, Semimetals, and Semiconductors with the Use of Optical Second-Harmonic Generation," Phys. Rev. B **30**, 519 (1984); LBL-17507.
3. R.H. Page, J.G. Frey, Y.T. Lee, and Y.R. Shen, "Infrared Predissociation Spectra of Water Dimer in a Supersonic Molecular Beam," Chem. Phys. Lett. **106**, 373 (1984); LBL-17512.
4. S.D. Durbin and Y.R. Shen, "Two-Photon Dichroism Studies of Molecular-Orientational Distribution in a Nematic Liquid Crystal," Phys. Rev. A **30**, 1419 (1984).
5. H. Hsiung, L.P. Shi, and Y.R. Shen, "Transient Laser-Induced Molecular Reorientation and Laser Heating in a Nematic Liquid Crystal," Phys. Rev. A **30**, 1453 (1984).
6. G. Yang and Y.R. Shen, "Spectral Broadening of Ultrashort Pulses in a Nonlinear Medium," Opt. Lett. **510**, 9 (1984); LBL-17387.
7. T. Rasing, "The New Electronic Levels in the Incommensurate Crystal Rb_2ZnBr_4," Phys. Rev. Lett. **53**, 388 (1984); LBL-17821.

Other Publications

8. Y.R. Shen, *The Principles of Nonlinear Optics,* John Wiley & Sons, New York, 1984.
9. H.W.K. Tom, C.M. Mate, X.D. Zhu, J.E. Crowell, T.F. Heinz, G.A. Somorjai, and Y.R. Shen, "Surface Studies Using Optical Second-Harmonic Generation (SHG) Adsorption of CO and O_2 on Rh(111)," Bull. Am. Phys. Soc. **29**, 344 (1984); LBL-17038abs.
10. X.D. Zhu, C.M. Mate, H.W.K. Tom, J.E. Crowell, T.F. Heinz, G.A. Somorjai, and Y.R. Shen, "Surface Studies Using Optical Second-Harmonic Generation (SHG): Adsorption of Alkali Metals, Benzene, and Pyridine on Rh(111)," Bull. Am. Phys. Soc. **29**, 344 (1984); LBL-17039abs.

11. G.T. Boyd, T. Rasing, J.R.R. Leite, and Y.R. Shen, "Electromagnetic Field Enhancement at Rough Surfaces: A Study of Materials Using Second-Harmonic Generation," Bull. Am. Phys. Soc. **29**, 307 (1984); LBL-17040abs.
12. H. Hsiung, L.P. Shi, and Y.R. Shen, "Time-Dependent Laser-Induced Molecular Reorientation in a Nematic Liquid Crystal Film," Bull. Am. Phys. Soc. **29**, 394 (1984); LBL-17041abs.
13. H.W.K. Tom, T.F. Heinz, and Y.R. Shen, "Second-Harmonic Reflection from Silicon Surfaces and its Relation to Surface Symmetry," Bull. Am. Phys. Soc. **29**, 347 (1984); LBL-17042abs.
14. T. Rasing, "Experimental Observation of New Electronic Levels in an Incommensurate Crystal," Bull. Am. Phys. Soc. **29**, 236 (1984); LBL-17043abs.
15. G. Yang and Y.R. Shen, "Spectral Broadening of Picosecond Pulses in a Nonlinear Medium," J. Opt. Soc. Am. **B1**, 443 (1984); LBL-17194abs.
16. H.W.K. Tom, C.M. Mate, X.D. Zhu, J.E. Crowell, T.F. Heinz, G.A. Somorjai, and Y.R. Shen, "Studies of Atomic and Molecular Adsorption on Surfaces in Ultrahigh Vacuum," J. Opt. Soc. Am. **B1**, 446 (1984); LBL-17195abs.
17. T.F. Heinz, H.W.K. Tom, X.D. Zhu, and Y.R. Shen, "Second-Harmonic Generation in Bulk Centrosymmetric Media," J. Opt. Soc. Am. **B1**, 432 (1984).
18. T. Rasing and A. Janner, "Experimental Investigation of 4-Dimensional Superspace Crystals," Ferroelec. **53**, 301 (1984); LBL-17206.

LBL Reports

19. H.W.K. Tom (Ph.D. Thesis) "Studies of Surfaces Using Optical Second Harmonic Generation," LBL-17820.
20. T. Rasing, "Electronic Bandstructure of an Incommensurate Crystal," 17th International Conference on the Physics of Semiconductors, San Francisco, California, August 6–10, 1984; LBL-18136.
21. H.W.K. Tom, X.D. Zhu, Y.R. Shen, and G.A. Somorjai, "Investigation of the Si(111) Surface in UHV: Oxidation and Effect of Surface Phosphorus," 17th International Conference on the Physics of Semiconductors, San Francisco, California, August 6–10, 1984; LBL-18135.
22. Y.R. Shen, "Optical Second-Harmonic Generation for Surface Studies," First International Conference on the Structure of Surfaces, Berkeley, California, August 13–16, 1984; LBL-18192.
23. Y.R. Shen, "Application of Optical Second-Harmonic Generation to Surface Science," LBL-18463.
24. T. Rasing, Y.R. Shen, M.W. Kim, P. Valint, and J. Bock, "Orientation of Surfactant Molecules at a Liquid-Air Interface Measured by Optical Second-Harmonic Generation," LBL-18465.

Invited Talks

25. G. Boyd, "Surface Enhanced Optical Effects," Shell Research Laboratories, Houston, Texas, March 1, 1984; General Motors Research Laboratories, Warren, Michigan, March 30, 1984; 3M Center, St. Paul, Minnesota, April 30, 1984; Kodak Research Laboratories, Rochester, New York, June 11, 1984; Hewlett Packard, Materials Research Laboratory, Palo Alto, California, June 26, 1984; Hughes Research Laboratory, Malibu, California, June 30, 1984.
26. H.W.K. Tom, "Surface Studies Using Second-Harmonic Generation," Bell Laboratories, Murray Hill, New Jersey, March 5, 1984; IBM Research Laboratories, Yorktown Heights, New York, March 12, 1984.
27. Y.R. Shen, "Optical Second-Harmonic Generation: A Novel Method for Surface Studies," The Weitzmann Institute, Israel, March 11, 1984.
28. Y.R. Shen, "Optical Nonlinearity and Optical Bistability in Liquid Crystals," The Royal Society Meeting on Optical Bistability, Dynamical Nonlinearity, and Photonic Logic, London, England, March 23, 1984.
29. Y.R. Shen, "Surface Studies by Nonlinear Optical Techniques," Max-Planck Institute for Quantum Optics, Garching, West Germany, April 3, 1984.
30. Y.R. Shen, "Nonlinear Optical Studies of Surfaces," Laboratoire d'Optique Quantique, Ecole Polytechnique, Palaiseau, France, April 18, 1984; CNET, Paris, France, April 20, 1984.
31. Y.R. Shen, "Optical Second-Harmonic Generation for Surface Studies," Institute for Experimental Physics, University of Hamburg, West Germany, April 24, 1984.
32. Y.R. Shen, "Nonlinear Optical Effects in Liquid Crystals," Department of Physics, Fudan University, Shanghai, China, May 3, 1984.
33. Y.R. Shen, "Nonlinear Optics and Surface Science," Physics Department, Beijing University, China, May 5, 1984.
34. Y.R. Shen, "Some Applications of Nonlinear Optics to Physics," Physics Department., Yunnan University, Kunmin, China, May 10, 1984.
35. Y.R. Shen, "Interface Studies by Nonlinear Optical Techniques," Laboratory of Physical Chemistry, Technical University of Munich, Garching, West Germany, May 17, 1984.

36. Y.R. Shen, "Recent Advances in Surface Studies by Second-Harmonic Generation," Laboratory of Electrooptics, Technical University of Vienna, Austria, May 18, 1984.
37. Y.R. Shen, "Surface Studies by Optical Second-Harmonic Generation," Institute for Experimental Physics, University of Graz, Austria, May 21, 1984; Université Louis Pasteur, Laboritoire de Spectroscopie du Corps Solide, Strasbourg, France, May 25, 1984.
38. Y.R. Shen, "A Novel Surface Probe," Max-Planck-Institut für Biophysikalische Chemie, Göttingen, West Germany, May 29, 1984.
39. Y.R. Shen, "Second-Harmonic Generation as a Surface Probe," Physics Department, Technical University of Munich, West Germany, June 6, 1984.
40. Y.R. Shen, "Optical Second-Harmonic Generation: A Novel Surface Probe," Physics Department, University of Bielefeld, West Germany, June 8, 1984; Max-Planck Institute for Solid State Physics, Stuttgart, West Germany, June 12, 1984.
41. Y.R. Shen, "Optical Second-Harmonic Generation for Surface Studies," Conference on Lasers and Electrooptics 1984, Anaheim, California, June 19–22, 1984.
42. Y.R. Shen, "The Wonderful World of Nonlinear Optics," Colloquium for Munich Physicists, Munich, West Germany, June 25, 1984.
43. Y.R. Shen, "A Novel Surface Probe: Optical Second Harmonic Generation," Physics Department, University of Heidelberg, West Germany, June 29, 1984.
44. T. Rasing, "New Electronic Levels in a Crystal Exhibiting an Incommensurate Lattice Distortion," Physics Department, University of California Berkeley, September 19, 1984.
45. H.W.K. Tom, "Nonlinear Surface Spectroscopy," Fall Symposium: Interaction of Optical Radiation with Surfaces, Upstate New York Chapter of the American Vacuum Society, Troy, New York, October 22, 1984.
46. Y.R. Shen, "Nonlinear Optical Studies of Surfaces and Interfaces," Optics Center, University of Arizona, Tucson, November 8, 1984.
47. Y.R. Shen, "Studies of Surface-Enhanced Optical Effects Using Second-Harmonic Generation," Lasers '84, San Francisco, California, November 26–30, 1984.
48. T. Rasing, "New Electronic and Vibrational Levels in Incommensurate Crystals," Physics Department, Stanford University, Stanford, California, December 6, 1984.
49. T. Rasing, "Monomolecular Layers at a Liquid-Air Interface: Determination of Orientation by Optical Second-Harmonic Generation," Exxon Research Center, Annandale, New Jersey, December 12, 1984.

Excitations in Solids*

Carson D. Jeffries, Investigator

INTRODUCTION

The central objective of this program is experimental study of the onset of instabilities and pseudorandom behavior in solids, together with a detailed analysis and interpretation within the recently developed theory of chaotic dynamics. This theory displays universality and predicts that similar and recognizable modes of behavior will be observed in a very broad class of nonlinear phenomena, e.g., turbulence in fluids and plasmas as well as various instabilities in semiconducting, magnetic, ferroelectric, and piezoelectric materials. The chaotic dynamics can be viewed as a consequence of strongly driven elementary excited states. To facilitate direct comparison between observed behavior and theoretical models, specific experimental methods have been developed: bifurcation diagrams, phase-space portraits, Poincaré sections, return maps, power spectral analysis, real-time and transient analysis, and measurement of fractal dimensions. A detailed and systematic study of the chaotic dynamics of driven p-n junctions has revealed many universal patterns: period-doubling bifurcations, onset of chaos, periodic windows, and intermittency. Spin-wave instabilities in ferrite spheres display period doubling, chaos, and intermittency and can be understood by a two-dimensional quadratic map. Spatial and temporal chaotic behavior is studied in electron-hole plasma-density waves in Ge crystals, which exhibit a period-doubling route to chaos, periodic windows, and quasiperiodicity. These results have a bearing on devices of high technological interest and on a very general class of nonlinear problems of practical importance.

*This work was supported by the Director, Office of Energy Research, Office of Basic Energy Sciences, Materials Sciences Division of the U.S. Department of Energy under Contract No. DE-AC03-76SF00098.

1. Turbulence in an Electron-Hole Plasma in Ge (Publication 5)

G.A. Held, Carson Jeffries, and E.E. Haller

Helical plasma-density waves in Ge crystals at 77 K are studied in parallel electric and magnetic fields. Time records of the current I(t) through the crystal are made, with the applied voltage V as the control parameter. There is a threshold value for which I(t) develops oscillatory behavior, as shown by the Poincaré sections and power spectra in Figure 1-1(a). At higher voltages there is a Hopf bifurcation to quasiperiodicity at frequencies f_1 and f_2: the attractor is a torus (see Figure 1-1 b). Still higher voltages lead to entrainment and then to chaos via a quasiperiodic route. Figure 1-1(e) shows a section of the strange attractor. For these data Figure 1-2 is constructed, the slope yielding a fractal dimension d $\approx$2.65 for the strange attractor. This plot provides

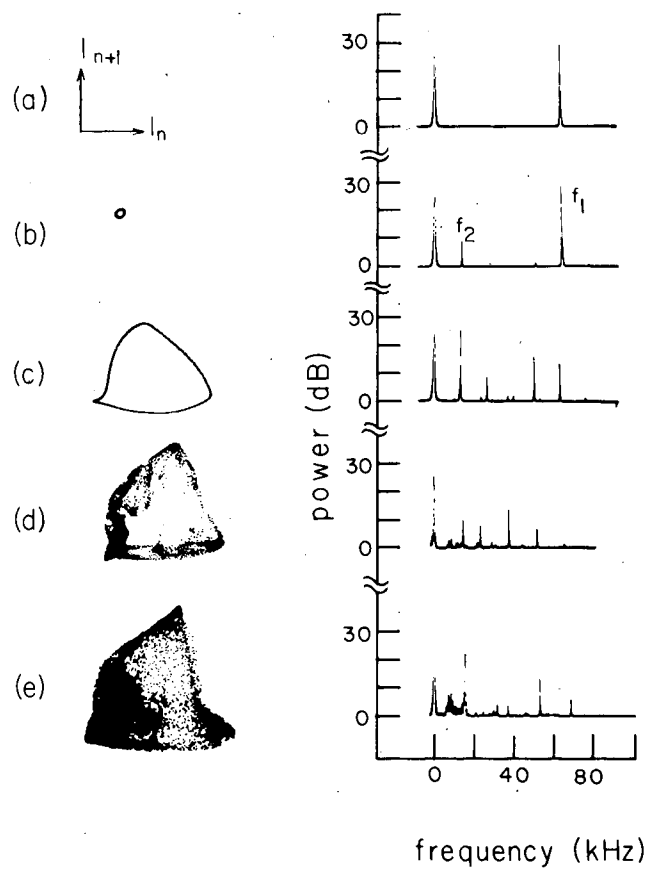

Figure 1-1. Poincaré sections, I_{n+1} vs. I_n, and power spectra P(dB) for plasma current in Ge crystal for increased values of applied voltage V: (a) 2.865, (b) 2.907, (c) 2.942, (d) 3.003, and (e) 3.058. Figures (b)-(e) show breakup of the invariant circle and a quasiperiodic route to chaos. (XBL 848-3358)

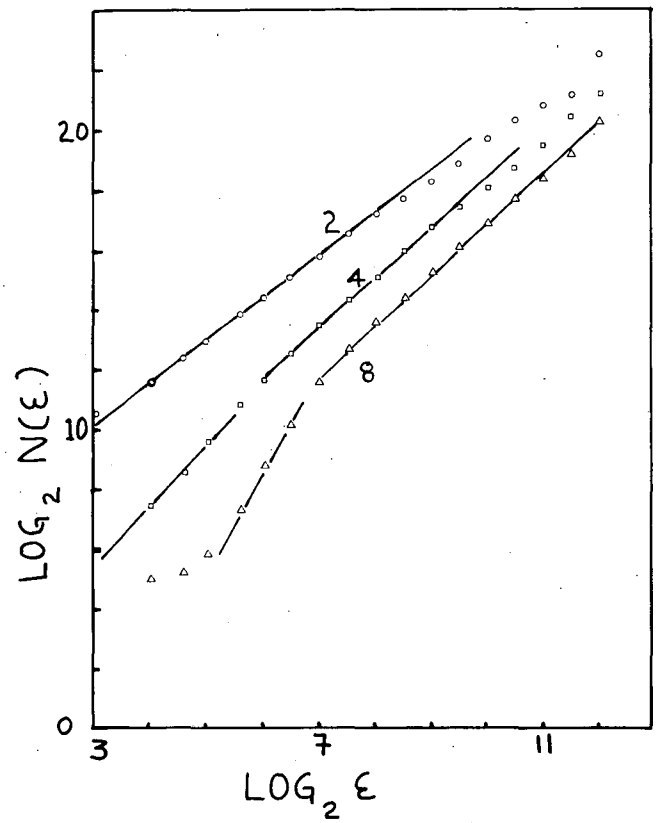

Figure 1-2. Plot to measure the fractal dimension of the attractor of Figure 1-1(e). N(ϵ) is the number of points on the attractor in a D-dimensional hypersphere of radius ϵ in a reconstructed phase space with D = 2, 4, and 8. The slope converges for D > 4; points for ϵ < 7 are due to higher dimensional random noise.
(XBL 845-1952)

an experimental method of distinguishing low-dimensional deterministic chaos from high-dimensional random noise. The plasma also exhibits a period-doubling route to chaos and intermittency. Preliminary indications are that the system can be modeled by nonlinearly coupled plasma-density waves.

2. Bifurcations of a Forced Magnetic Oscillator Near Points of Resonance (Publication 3)

Paul Bryant and Carson Jeffries

The nonlinear dynamics are explored for a forced symmetric oscillator with saturable ferromagnetic core and hysteresis. This can be modeled by a noninvertible map of the plane. An initialization technique has been developed that allows for experimental observation of both the stable and unstable manifolds of a saddle point in the Poincaré space. The system has a rich behavior dominated by a Hopf bifurcation to quasiperiodicity. The experimental dynamics near points of strong and weak resonances are studied in detail and found to be in remarkable correspondence with V.I. Arnold's theory of versal deformations of the plane. Within an Arnold entrainment horn the system displays symmetry breaking, period doubling, complimentary band merging, crises, and chaos. The symmetry breaking can be understood by use of the concept of a half-cycle map.

3. Observation of Noisy Precursors of Dynamic Instabilities (Publication 7)

Carson Jeffries and Kurt Wiesenfeld

We have measured the power spectra of a periodically driven p-n junction in the vicinity of a dynamic instability. The addition of external noise introduces new lines in the spectra, which become more prominent as a bifurcation point is approached. The scaling of the peak, width, area, and line shape of these lines is measured near the onset of two different codimension-one instabilities: the period-doubling and Hopf bifurcations. The results are in excellent agreement with recent theoretical predictions.

4. Observation of Chaotic Dynamics of Coupled Nonlinear Oscillators (Publication 8)

Robert Van Buskirk† and Carson Jeffries

The nonlinear charge-storage property of driven Si p-n-junction passive resonators gives rise to chaotic dynamics: period doubling, chaos, periodic windows, and an extended period-adding sequence corresponding to entrainment of the resonator by successive subharmonics of the driving frequency. The physical system is described; equations of motion and iterative maps are reviewed. Computed behavior is compared to data, with reasonable agreement for Poincaré sections, bifurcation diagrams, and phase diagrams in parameter space (drive voltage and drive frequency). N = 2 symmetrically coupled resonators are found to display period doubling, Hopf bifurcations, entrainment horns (Arnold tongues), breakup of the torus, and chaos. This behavior is in reasonable agreement with theoretical models based on the characteristics of single-junction

resonators. The breakup of the torus is studied in detail by Poincaré sections and power spectra. Also studied are oscillations of the torus (heteroclinic crossings) and cyclic crises. A phase diagram of the coupled resonators can be understood from the model. Poincaré sections show self-similarity and fractal structure, with measured values of fractal dimension $d = 2.03$ and $d = 2.23$ for $N = 1$ and $N = 2$ resonators, respectively. Two line-coupled resonators display a Hopf bifurcation as the drive parameter is increased, in agreement with the model. For $N = 4$ and $N = 12$ line-coupled resonators, complex quasiperiodic behavior is observed with up to 3 and 4 incommensurate frequencies, respectively.

---

†Present address: Physics Department, Harvard University, Cambridge, Massachusetts 02138.

5. Work in Progress

Experiments are in progress to study full spatiotemporal behavior in electron-hole plasmas in Ge crystals. This is being done with a set of probe contacts along the crystal; the contacts measure the plasma density as a function of space and time. These studies focus on the problems of the existence and characteristics of spatial chaos as well as temporal chaos in spatial systems. For the forced magnetic oscillator, work is in progress to construct a map that will model as accurately as possible the observed behavior in parameter space. Preliminary results show good numerical agreement for the location of the Hopf-bifurcation line and the boundaries of some entrainment horns. Other experiments in progress include measurement of a line of N coupled nonlinear oscillators comprising semiconductor junctions. Such systems with variable coupling and dissipation are expected to display high-order quasiperiodicity, spatial incoherence, and chaos. They are good models for many solid-state systems that can be viewed as a line of coupled oscillators.

1984 PUBLICATIONS AND REPORTS

Refereed Journals

1. George Gibson and Carson Jeffries, "Observation of Period Doubling and Chaos in Spin-Wave Instabilities in Yttrium Iron Garnet," Phys. Rev. A **29**, 811 (1984); LBL-15202.
2. G.A. Held, Carson Jeffries, and E.E. Haller, "Observation of Chaotic Behavior in an Electron-Hole Plasma in Ge," Phys. Rev. Lett. **52**, 1037 (1984); LBL-16948.
3. Paul Bryant and Carson Jeffries, "Bifurcations of a Forced Magnetic Oscillator Near Points of Resonance," Phys. Rev. Lett. **53**, 250 (1984); LBL-17174.

Other Publications

4. G.A. Held, Carson Jeffries, and E.E. Haller, "Observation of Spontaneous Oscillations Which Exhibit Chaotic Dynamics in an Electron-Hole Plasma in Ge," BAPS **29**, 438 (1984), American Physical Society March Meeting, Abs. HL13.
5. G.A. Held, C.D. Jeffries, and E.E. Haller, "Turbulence in Electron-Hole Plasma in Ge," abstract of paper presented at 17th International Conference on the Physics of Semiconductors, San Francisco, California, August 6–10, 1984; to appear in conference proceedings; LBL-18071.
6. C.D. Jeffries and L.V. Keldysh, *Electron-Hole Droplets in Semiconductors,* North-Holland Press, Amsterdam, 1984, Vol. **6** in series "Modern Problems in Condensed Matter Sciences."

LBL Reports

7. Carson Jeffries and Kurt Wiesenfeld, "Observation of Noisy Precursors of Dynamical Instabilities," Phys. Rev. A (in press); LBL-18145.
8. Robert Van Buskirk and Carson Jeffries, "Observation of Chaotic Dynamics of Coupled Nonlinear Oscillators," Phys. Rev. A (in press); LBL-18265.

Invited Talks

9. C.D. Jeffries, "Chaotic Dynamics of Instabilities in Solids," Nobel symposium on *The Physics of Chaos and Related Problems,* Gräftavallen, Sweden, June 11–16, 1984; to be published in Physica Scripta; LBL-17914.
10. C.D. Jeffries, "Experiments on Chaotic Dynamics," physics colloquium at Argonne National Laboratory, Argonne, Illinois, February 3, 1984.
11. C.D. Jeffries, "Patterns of Chaos," semiconductor colloquium, IBM Research Center, Yorktown Heights, New York, February 29, 1984.
12. C.D. Jeffries, "Chaotic Dynamics in Condensed Matter," conference on statistical mechanics, University of California, Davis, March 31, 1984.
13. C.D. Jeffries, "Experiments in Solid State Turbulence," colloquium at Laboratory for Plasma Fusion Studies, University of Maryland, College Park, April 26, 1984.
14. C.D. Jeffries, "Chaotic Dynamics of Instabilities in Solids," physics colloquium, University of California, Santa Cruz, May 10, 1984.

Time-Resolved Spectroscopies in Solids*

Peter Y. Yu, Investigator

INTRODUCTION

The purpose of this project is to use picosecond and subpicosecond laser pulses generated by modelocked dye lasers to study ultrafast interactions between elementary excitations in solids. These interactions include interactions between electrons and electrons or holes, between electrons and phonons, and between electrons and defects. An understanding of such interactions (such as trapping of carriers by defects) is important to electronic devices and to the processing of materials with high-power lasers (such as laser welding and annealing). By exciting materials such as GaAs with ultrafast optical pulses and probing the response of the sample with a variety of optical techniques such as photoluminescence, Raman scattering, and photoinduced absorption, it has been possible to observe and study these interactions in real time. The use of short excitation pulses also makes it possible to create transient nonequilibrium states in the material that would not normally exist under equilibrium conditions. Such possibilities include the creation of a very dense plasma of electrons and holes.

1. Free-Carrier Lifetime in Semi-insulating GaAs from Time-Resolved Band-to-Band Photoluminescence (Publication 1)

J.S. Weiner and P.Y. Yu

Deep centers are usually introduced into photodetectors to decrease the minority-carrier lifetime and hence increase the bandwidth of the detector. By monitoring the decay time of band-to-band photoluminescence in GaAs doped with deep traps such as O and Cr, the free-carrier lifetime can be measured directly without fabricating a device of the sample. The free-carrier lifetime ranges from 250 psec in GaAs:O (oxygen concentration = 6×10^{17} cm^{-3}) to less than 90 psec in GaAs:Cr (Cr concentration = 1.6×10^{17} cm^{-3}).

2. Work in Progress

The ~4-psec pulses from our synchronously pumped, modelocked dye laser have been compressed down to ~800 fsec by passing the pulses first through an optical fiber and then through a pair of gratings. These subpicosecond laser pulses will be used to monitor the expansion and relaxation of photoexcited, nonequilibrium electron-hole plasma as a function of time.

Many of the deep traps in semiconductors are associated with intrinsic defects (such as vacancies). Some of these intrinsic defects are created in devices like solar cells under operation conditions and eventually cause degradation of performance. By irradiating samples with high-energy electrons or fast neutrons, it is possible to create these intrinsic defects and then gradually anneal them out. By monitoring the free-carrier lifetime in these irradiated samples, one can determine which defects are the nonradiative recombination centers responsible for trapping the photoexcited carriers.

It has been proposed that when carriers recombine nonradiatively at deep traps, their energies are dissipated in the emission of many phonons. Since the nonradiative recombination time determined from the free-carrier time has been found to be as short as 100 psec, such nonradiative recombination can generate a large nonequilibrium population of phonons within a short time. This nonequilibrium phonon population will be measured as a function of time by Raman scattering.

1984 PUBLICATIONS AND REPORTS

Refereed Journals

1. J.S. Weiner and P.Y. Yu, "Free Carrier Lifetime in Semi-Insulating GaAs from Time-Resolved Band-to-Band Photoluminescence," J. Appl. Phys. **55**, 3889 (1984); LBL-16966.
2. C.L. Collins and P.Y. Yu, "Light Scattering from Nonequilibrium Electron-Hole Plasma Excited by Picosecond Laser Pulses in GaAs," Solid State Commun. **51**, 123 (1984); LBL-16635.
3. J.S. Weiner and P.Y. Yu, "Time-resolved Hot Luminescence and Resonant Raman Scattering: Cu_2O Revisited," Solid State Commun. **50**, 493 (1984); LBL-16156.

*This work was supported by the Director, Office of Energy Research, Office of Basic Energy Sciences, Materials Sciences Division of the U.S. Department of Energy under Contract No. DE-AC03-76SF00098.

4. C.L. Collins and P.Y. Yu, "Generation of Nonequilibrium Optical Phonons in GaAs and Their Application in Studying Intervalley Electron-Phonon Scattering," Phys. Rev. B **30**, 4501 (1984); LBL-17488.

Other Publications

5. J.S. Weiner and P.Y. Yu, "Time-Resolved Resonant Raman Scattering and Hot Luminescence at the 1S Ortho-Exciton in Cu_2O," International Conference on the Physics of Semiconductors, San Francisco, August 6–10, 1984; LBL-18275.
6. J.S. Weiner, P.Y. Yu, and N. Caswell, "Heating of Resonantly Excited Cold Excitons in Cu_2O," Bull. Am. Phys. Soc. **29**, 476 (1984).

LBL Reports

7. C.L. Collins (Ph.D. Thesis), "A Study of Hot Phonons and Hot Carriers in GaAs under Picosecond Optical Pulse Excitations," LBL-17825.
8. J.S. Weiner (Ph.D. Thesis), "A Subnanosecond Time-Resolved Emission Study of Cu_2O and GaAs," LBL-18276.

Invited Talks

9. P.Y. Yu, "Study of Photoexcited Nonequilibrium Electrons and Phonons in GaAs by Light-Scattering Techniques," IBM T.J. Watson Research Center, Yorktown Heights, New York, April 3, 1984; AT&T Bell Laboratories, Holmdel, New Jersey, April 4, 1984; Service National des Champs Intensée, CNRS, Grenoble, France, April 10, 1984.

Superconductivity, Superconducting Devices, and 1/f Noise*

John Clarke, Investigator

INTRODUCTION

Dc superconducting quantum interference devices (SQUIDs) are being used in a wide variety of applications, including geophysical measurements, noise thermometry, and nuclear and quadrupole magnetic resonance in the frequency range from a few kHz to 100 MHz. SQUIDs are being operated at temperatures down to 20 mK to study their ultimate noise limitations for such applications as transducers for gravity-wave antennas. The accuracy of measurements of the lifetime of Josephson tunnel junctions in the zero-voltage state has been greatly increased by the study of microwave-induced transitions; the results are applicable to the general problem of Brownian motion. The nonlinear dynamics of circuits containing a Josephson tunnel junction are under investigation, with particular emphasis on the noise in such systems. A detailed study is being made of the excess low-frequency noise induced in metal films by electron bombardment in an electron microscope. In addition to yielding information on the origin of the noise, these measurements may provide a new technique for investigating mobile defects in metals.

1. Flicker (1/f) Noise in Copper Films Irradiated with 500-keV Electrons: Dependence of the Noise on Induced Defects (Publication 18)

Jonathon Pelz and John Clarke

Metal films, biased with a constant current, exhibit voltage noise with a spectral density that scales approximately as 1/f, where f is the frequency. We have investigated the effects of defect density on this noise by irradiating 100-nm-thick polycrystalline copper films with 500-keV electrons. Measurements of the resistance and noise were made *in situ* at about 90 K on a cold stage in the Hitachi HU-650 electron microscope at the LBL's National Center for Electron Microscopy, with the sample, a heater, and a thermometer mounted on the optical axis.

Figure 1-1 shows several voltage power spectra $S_v(f)$ with progressively higher electron dosages: $S_v(f)$ increases by more than an order of magnitude. It is convenient to characterize the noise in terms of the parameter α, where $S_v(f) = \alpha\overline{V}^2/Nf$; here, $\overline{V}$ is the average voltage across the sample and N is the number of conduction electrons. Figure 1-2 shows the change in α, $\Delta\alpha$, vs. the change in resistivity, $\Delta\rho$, for three successive data runs. Since $\Delta\rho$ is proportional to the added defect concentration n_d, these data indicate that $\Delta\alpha$ scales as $n_d^{0.6}$. The dependence of the noise on the resistivity after the samples were annealed provides further evidence for the complicated dependence of $\Delta\alpha$ on $\Delta\rho$, as illustrated by the dotted line in Figure 1-2. The annealing process at the lower temperatures reduces the noise much more than the resistivity, producing hysteresis in the plot of $\Delta\alpha$ vs. $\Delta\rho$. This hysteresis is readily explained if one assumes that the noise arises from mobile defects that anneal out at a lower temperature than the bulk of the induced defects, which give rise to most of the increase in resistivity.

Experiments of this kind, in addition to providing an explanation for 1/f noise in metals, may prove to be a valuable new tool for studying mobile defects in metals. We are currently extending these measurements to single-crystal films and to other metals.

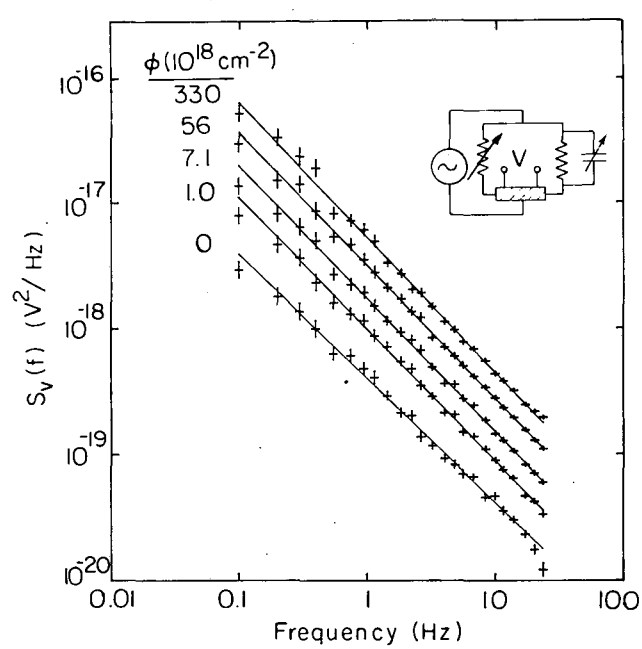

Figure 1-1. Typical excess-voltage noise-power spectra and least-square fits for different electron dosages ϕ. Inset: ac bridge configuration. (XBL 8411-6113)

*This work was supported by the Director, Office of Energy Research, Office of Basic Energy Sciences, Materials Sciences Division of the U.S. Department of Energy under Contract No. DE-AC03-76SF00098.

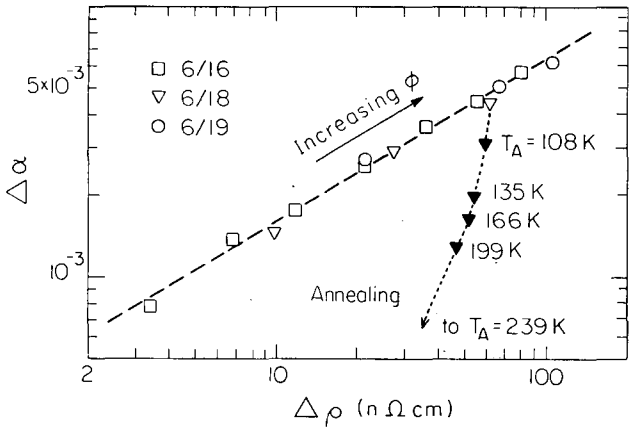

Figure 1-2. Change in 1/f noise magnitude $\Delta\alpha$ vs. change in sample resistivity $\Delta\rho$. The dashed line $\Delta\alpha \propto \Delta\rho^{0.6}$ is drawn as a guide to the eye. Points along this line correspond to increasing electron dosage ϕ, while points along the dotted line correspond to annealing to successively higher temperatures. The data point for T_A = 239 K (not shown) is $\Delta\rho \simeq 11.6$ nΩcm, $\Delta\alpha \simeq 7 \times 10^{-5}$. (XBL 8411-6114)

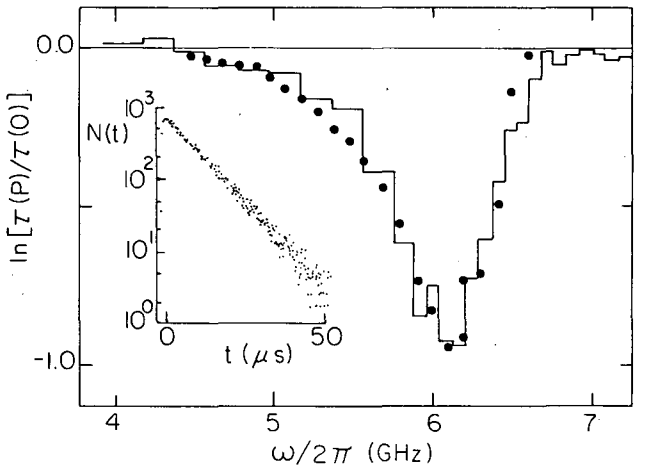

Figure 2-1. Resonance in escape time vs. microwave frequency. The dots represent measured values of $\ln[\tau(P)/\tau(O)]$ for a junction at 4.2 K with I_o = 4.64 μA, I = 3.07 μA, and $\tau(O)$ = 8.4 μs. The solid line represents the results of numerical simulation. The inset shows the exponential distribution of switching events for the same junction in the absence of microwaves. (XBL 847-7181)

2. Resonant Activation from the Zero-Voltage State of a Current-Biased Josephson Junction (Publication 7)

Michel H. Devoret, John M. Martinis, Daniel Esteve, and John Clarke

A problem of long-standing interest is the decay of the zero-voltage state of a current-biased Josephson tunnel junction by thermal activation over the potential barrier that separates it from the free-running (nonzero-voltage) regime. We have studied a new process, which we call "resonant activation," in which the escape rate is enhanced by microwaves at a frequency close to the natural frequency of the junction. This process applies to the general case of the escape from a well by Brownian motion in the presence of a weak, oscillating force.

Experiments were performed on Nb-NbOx-PbIn tunnel junctions patterned photolithographically in a 10 μm × 10 μm cross-strip geometry on Si chips. We first measured the lifetime of the zero-voltage state $\tau(0)$ in the absence of microwaves at a fixed value of the bias current. The inset in Figure 2-1 shows an example of the expected exponential behavior of the switching events. To study the effect of microwaves, we injected microwave power into the junction over the frequency range 0.1–12 GHz. In Figure 2-1 we plot $\ln[\tau(P)/\tau(O)]$ vs. microwave frequency, where P is the microwave power, and observe a significant reduction in the escape time near the natural frequency of the junction. The solid line in Figure 2-1 is from a numerical simulation of the problem and is in good agreement with the data. The non-Lorenztian nature of the response arises from the anharmonic properties of the potential. The position and width of the resonance enable us to find the resonant frequency and damping of the junction.

Apart from the inherent interest, resonant activation provides an *in situ* measurement of the junction parameters as modified by the complex impedance loading the junction. This information is essential to a quantitative investigation of thermal activation and macroscopic quantum tunneling in Josephson junctions.

3. Dynamic Input Impedance of a dc SQUID (Publication 8)

Claude Hilbert and John Clarke

The impedance of a circuit coupled to a dc SQUID is modified by the dynamic-input impedance of the SQUID, which can be characterized in terms of a dynamic inductance $\mathscr{L}$ and a dynamic resistance $\mathscr{R}$. A detailed understanding of the dependence of the quantities on the current and flux bias of the SQUID is essential for the correct design of SQUID-based amplifiers.

The apparent values of $\mathscr{L}$ and $\mathscr{R}$ for a thin-film SQUID with a tightly coupled spiral input coil were

made by connecting a capacitor across the coil to form a resonant circuit. Thus, the change in the resonant frequency and quality factor of this circuit as functions of the current and flux bias of the SQUID yielded the impedance reflected into the input circuit. The values of $\mathscr{L}$ deduced in this way were in good agreement with those calculated on an analog simulator. However, the resistance introduced into the input circuit, ΔR_i, was dominated by feedback between the output of the SQUID and the input circuit via the parastic capacitance between the SQUID and the input coil, rather than by the reflected value of $\mathscr{R}$. The experimental values of ΔR_i were satisfactorily explained in terms of a simple model.

These results were used in the design of the tuned rf amplifier described in the following abstract.

4. Dc SQUID as a Tuned Radiofrequency Amplifier (Publication 15)

Claude Hilbert and John Clarke

Dc SQUIDs have long been used in a wide variety of sensitive electrical and magnetic measurements at frequencies mostly confined to the audio range. However, there is now substantial interest in extending the response of SQUID-based amplifiers to radio frequencies: for example, for nuclear magnetic resonance (NMR) and nuclear quadrupole resonance (NQR), and as intermediate-frequency (IF) amplifiers for mixers involving superconductor-insulator-superconductor tunnel junctions. To determine whether the high sensitivity of SQUIDs can be extended to radio frequencies, we have fabricated and tested a tunnel amplifier operating at 93 MHz.

Figure 4-1 shows a dc SQUID in a tuned-amplifier configuration. The input circuit consists of a voltage source V_i, with a resistance $R_i \approx 2\Omega$, connected in series with a capacitor $C_i \approx 20$ pF and with the input coil $L_i \approx 5.6$ nH of a thin-film SQUID that has inductance L. The mutual inductance between the input coil and the SQUID is $M_i = \alpha(LL_i)^{1/2}$. The parameters of the input circuit were carefully optimized to give the lowest possible noise temperature. At a bath temperature of 4.2 K, the measured gain was 18.6 ± 0.5 dB, while the noise temperature was 1.7 ± 0.5 K. These values are in good agreement with model predictions.

The measured noise temperature represents a substantial advance in the state of the art of rf amplifiers. We are now using these amplifiers in ultrasensitive NQR and NMR measurements.

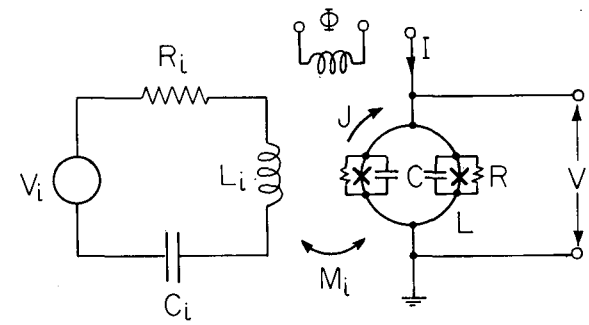

Figure 4-1. Configuration of tuned radiofrequency amplifier. (XBL 844-6880A)

5. Deterministic Hopping in a Josephson Circuit Described by a One-Dimensional Mapping (Publication 17)

Robert F. Miracky, Michel H. Devoret, and John Clarke

Analog simulations of the hopping noise of a current-biased Josephson tunnel junction shunted with an inductor in series with a resistor reveal a $1/\omega$ spectral density over two decades of frequency ω for a narrow range of bias currents. The amplitude of the low-frequency part of the spectrum decreases when white noise, representing Nyquist noise in the resistor at a few Kelvin, is added to the simulation. We explain the shape of the power spectrum and its dependence on bias current and added white noise in terms of a deterministic process, involving a one-dimensional mapping, that is analogous to that found in Pomeau-Manneville intermittency. Moreover, we are able to establish a detailed relationship between the origin of the mapping and the differential equation describing the dynamics of the system.

6. Calculation of Period Doubling in a Josephson Circuit (Publication 4)†

Kurt Wiesenfeld, Edgar Knobloch, Robert F. Miracky, and John Clarke

The method of harmonic balance is used to obtain analytic results for the differential equation describing a current-biased Josephson junction with self-capacitance that is shunted by a resistor with substantial self-inductance. This system is known to exhibit period-doubling cascades, chaos, and other

exotic nonlinear phenomena. After an accurate representation of the basic voltage oscillation is determined for high-bias currents, the value of bias current is computed for which this solution loses stability to a period-doubled mode. The predictions for moderate values of inductance agree to remarkable accuracy, typically 5%, with results obtained from both analog simulations and digital integration of the circuit equation. Moreover, the method of calculation provides a systematic scheme for achieving increasing accuracy.

†K. Wiesenfeld and E. Knobloch were supported by the California Space Institute and the Alfred P. Sloan Foundation.

7. Work in Progress

In collaboration with Professor E.L. Hahn, we are using tuned SQUID amplifiers in the radio-frequency range to study NQR and NMR in samples in the He^4 temperature range. One experiment is concerned with the detection of NQR in a sample in thermal equilibrium by noise spectroscopy. A SQUID amplifier has been fabricated to detect zero-field NMR in the frequency range up to 100 kHz and thus study molecular behavior in condensed phases; this work is in collaboration with Professor A. Pines. Our dilution refrigerator has been instrumented with a SQUID amplifier for several applications, including studies of the noise in SQUIDs at low temperatures and an investigation of noise in nonequilibrium systems. Measurements are being made of the lifetime of current-biased Josephson tunnel junctions in the quantum limit where the escape to the free-running mode is via macroscopic quantum tunneling; of particular interest is the effect of damping on the escape rate.

1984 PUBLICATIONS AND REPORTS

Refereed Journals

1. W.M. Goubau, P.M. Maxton, R.H. Koch, and J. Clarke, "Noise Correlation Lengths in Remote Reference Magnetotellurics," Geophys. **49**, 433 (1984); LBL-15484.
2. H.J. Mamin, D.J. Van Harlingen, and J. Clarke, "Charge Imbalance Induced by a Temperature Gradient in Superconducting Aluminum," Phys. Rev. B **29**, 3881 (1984); LBL-16693.
3. F. Wellstood, C. Heiden, and J. Clarke, "Integrated dc SQUID Magnetometer with a High Slew Rate," Rev. Sci. Instrum. **55**, 952 (1984); LBL-16969.
4. K. Wiesenfeld, Edgar Knobloch, R.F. Miracky, and J. Clarke, "Calculation of Period-Doubling in a Josephson Circuit, Phys. Rev. A **29**, 2102 (1984); LBL-16873.
5. R. Dalven, "Physics of the Critical Magnetic Field in Type II Superconductors," Am. J. Phys. **52**, 1043 (1984); LBL-17508.
6. Claude Hilbert and J. Clarke, "Input Impedance of an Amplifier Based on a dc Superconducting Quantum Interference Device," Appl. Phys. Lett. **45**, 799 (1984); LBL-17932.
7. M.H. Devoret, J.M. Martinis, D. Esteve, and J. Clarke, "Resonant Activation from the Zero-Voltage State of a Current-Biased Josephson Junction," Phys. Rev. Lett. **53**, 1260 (1984); LBL-18190.

Other Publications

8. C. Hilbert, J. Martinis, and J. Clarke, "Dynamic Input Impedance of a dc SQUID," Bull. Am. Phys. Soc. **29**, 523 (1984); LBL-17044abs.
9. R.F. Miracky, M.H. Devoret, and J. Clarke, "Dynamical 1/f Noise in a Josephson Junction," Bull. Am. Phys. Soc. **29**, 481 (1984); LBL-17045abs.
10. J. Martinis, M.H. Devoret, and J. Clarke, "Measurement of the Transition Rate from the Zero Voltage State of a Current-Biased Josephson Junction," Bull. Am. Phys. Soc. **29**, 363 (1984); LBL-17046abs.
11. H.J. Mamin, D.J. Van Harlingen, and J. Clarke, "Thermoelectric Generation of Charge Imbalance in Superconducting Aluminum," Bull. Am. Phys. Soc. **29**, 522 (1984); LBL-17047abs.
12. M.H. Devoret, J.M. Martinis, D. Esteve, and J. Clarke, "Resonant Activation of a Josephson Junction," Physica **126B**, 483 (1984); LBL-18195.

LBL Reports

13. R.F. Miracky (Ph.D. Thesis), "Chaos and Related Nonlinear Noise Phenomena in Josephson Tunnel Junctions," LBL-18193.
14. H.J. Mamin (Ph.D. Thesis), "Thermoelectric Charge Imbalance in Superconducing Aluminum and the Development of a Scanning Tunneling Microscope," LBL-18326.
15. C. Hilbert and John Clarke, "Dc SQUID as a Tuned Radiofrequency Amplifier," LBL-18362.
16. J. Clarke, "Experiments on Charge Imbalance in Superconductors," LBL-17388.
17. R.F. Miracky, M.H. Devoret, and J. Clarke, "Deterministic Hopping in a Josephson Circuit Described by a One-Dimensional Mapping," LBL-18680.

18. J. Pelz and J. Clarke, "Flicker (1/f) Noise in Copper Films Irradiated with 500 keV Electrons: Dependence on the Noise of Induced Defects," LBL-18893.

Invited Talks

19. J. Clarke, "Quantum Noise in Josephson Devices," Institute for Theoretical Physics, University of California, Santa Barbara, February 17, 1984.
20. J. Clarke, "Dynamic Input Impedance of the dc SQUID," Workshop on SQUIDs and Gravity Wave Detectors, Boulder, Colorado, March 15, 1984.
21. J. Clarke, "Nonlinear Dynamics of Josephson Circuits," 1984 March Meeting of the American Physical Society, Detroit, Michigan, March 26–30, 1984.
22. J. Clarke, "Chaos and Noise in Josephson Junctions," Department of Physics, University of California, Riverside, May 30, 1984.
23. J. Clarke, "Chaos and Noise in Josephson Junctions," Department of Physics, University of California, Los Angeles, May 31, 1984.
24. J. Clarke, "Recent Advances in SQUID Technology," Ross Priory Meeting on Superconducting Electronics, Ross Priory, Scotland, June 12, 1984.
25. M. Devoret, M. Martinis, and J. Clarke, "Resonant Activation and Macroscopic Quantum Tunneling from the Zero Voltage State of a Josephson Tunnel Junction," Workshop on Noise in Macroscopic Systems, University of California, Santa Barbara, June 23, 1984.
26. M. Devoret, D. Esteve, J. Martinis, and J. Clarke, "Resonant Activation in Josephson Tunnel Junctions," Workshop on Noise in Macroscopic Systems, University of California, Santa Barbara, June 23, 1984.
27. J. Clarke, "Ultrasensitive Measuring Devices," XVII International Conference on Low-Temperature Physics, Universität Karlsruhe, West Germany, August 15–22, 1984; LBL-18191.
28. J. Martinis, C. Hilbert, and J. Clarke, "Noise Calculations for the Tightly Coupled dc SQUID," Applied Superconductivity Conference, San Diego, California, September 9–13, 1984.
29. J. Clarke, "Overview of Applications of SQUIDs," SQUID Magnetometry Workshop, Coolfont '84, Berkeley Springs, West Virginia, November 12–14, 1984.
30. J.M. Martinis, M.H. Devoret, J. Clarke, and C. Urbina, "Macroscopic Quantum Tunneling in a Current Biased Josephson Junction," IV Chilean Symposium of Physics, Santiago, Chile, December 26–28, 1984; LBL-18681.

THEORETICAL RESEARCH

Theoretical Studies of the Electronic Properties of Solid Surfaces*

L.M. Falicov, Investigator

INTRODUCTION

The purpose of this program is to study properties of solid surfaces. In particular, the interest is in determining (a) structural properties of surfaces, namely the organization and arrangement of atomic constituents at equilibrium; (b) constitutional properties of the surface, in particular the segregation properties of alloys at the surface as a function of crystal structure, surface orientation, nominal chemical composition, and temperature; (c) electronic structure of surfaces, in particular electron states and electron densities in the neighborhood of the surface; (d) vibronic properties of surfaces; (e) magnetic properties of surfaces, both in magnetic solids (ferromagnetic and antiferromagnetic) and in nonmagnetic solids that may develop a magnetic surface layer; and (f) chemical properties of solids—in particular their catalytic properties—as they are related to all the basic physical properties listed above.

A variety of theoretical techniques and models have been developed to focus on the various properties (band-structure models, many-body electron physics, numerical relaxation techniques), but the emphasis is on physical aspects and their implication to experiments rather than on techniques *per se*.

Since 1978 we have worked with Dr. Eugene Haller and his group to study a set of unusual impurities in very pure semiconductors. These impurities had never been seen before and include hydrogen complexes, lithium-based complexes, carbon-nitrogen complexes, and ordinary substitutional impurities in an unusual charge state.

*This work was supported by the Director, Office of Energy Research, Office of Basic Energy Sciences, Materials Sciences Division of the U.S. Department of Energy under Contract No. DE-AC03-76SF00098.

1. Calculated Magnetization of Iron-Cobalt Disordered Alloys (Publication 6)

R.H. Victora and L.M. Falicov

The spin polarization of the disordered Fe-Co alloy was calculated using a tight-binding scheme, with single-site, full-orbital interactions treated self-consistently. Disorder is introduced by the use of the virtual-crystal approximation. Excellent agreement with the experimental spin polarization is obtained, and the unusual shape of the Fe-Co curve on the Slater-Pauling plot is explained. The magnetization of the Co-rich alloys essentially depends on the number of available d holes, while the magnetization of the Fe-rich alloys is influenced by a relatively weak electron-electron interaction. The intersection of the two effects occurs at approximately 30 at% Co and produces a maximum.

2. Calculated Surface Electronic Structure of Ferromagnetic Iron and the Ferromagnetic Order Iron-Cobalt Alloy (Publication 10)

R.H. Victora, L.M. Falicov, and Shoji Ishida[†]

The electronic and magnetic properties of the (100) and (110) surfaces of ferromagnetic iron and the ferromagnetic iron-cobalt ordered alloys were calculated self-consistently. It is found that (a) in pure bcc iron the spin polarization increases from a bulk value of 2.12 to 2.90 at the (100) surface and to 2.55 at the (110) surface; (b) the ordered FeCo alloy has a bulk spin polarization of 2.66 for the Fe constituent and 1.78 for the Co constituent, compared with 2.12 and 1.56 for the respective pure elements; (c) in the (100) surfaces of ordered FeCo, the spin polarizations are 2.95 for Fe and 2.03 for Co; (d) the (110)

surface of ordered FeCo exhibits a spin polarization of 2.75 for Fe and 1.86 for Co; (e) an atomic (110) overlayer of Fe on ordered FeCo produces a surface spin polarization of 2.63 and 2.67 for the two inequivalent Fe atoms. Agreement with available experimental data is excellent. All results can be successfully interpreted based on the saturation magnetization of Co, the relatively weak electron-electron interaction of Fe, and the surface narrowing of the electronic d band.

---

†Present address: Department of Physics, Faculty of Science, Kagoshima University, Kagoshima, Japan.

3. Dynamic Impurities in Ultrapure Semiconductors (Publication 19)

L.M. Falicov and E.E. Haller

Theoretical and experimental results are presented that shed light on a series of unusual shallow-level impurities in ultrapure germanium. These impurities, both donors and acceptors, (1) show hydrogenic spectra with signatures identical to all other shallow impurities, (2) exhibit unusual dependence in their spectra to applied uniaxial stresses, and (3) display a clear isotope effect (hydrogen to deuterium) in the electronic spectrum when the crystal-growing conditions are changed—a clear violation of the Born-Oppenheimer approximation. They are dynamic impurities consisting of a two-atom center in a fully tetrahedral environment, in which coherent nuclear motion is coupled to the electronic degrees of freedom. Experimental data, together with group-theoretical analysis, permit a complete description of these systems.

1984 PUBLICATIONS AND REPORTS

Refereed Journals

1. J. Oliva and L.M. Falicov, "Electronic Structure of Hydrogen-Based Impurity Complexes in Crystalline Germanium," Phys. Rev. B **28**, 7366 (1983).†
2. M.O. Robbins and L.M. Falicov, "Electronic Theory of Ordering and Segregation in Transitional-Metal Alloys," Phys. Rev. B **29**, 1333 (1984).†
3. Y. Wu and L.M. Falicov, "Variational Calculation of Multihole Binding Energies in Hydrogenic Impurity Centers in Semiconductors," Phys. Rev. B **29**, 3671 (1984).†
4. G.H. Vineyard and L.M. Falicov, "National Facilities for Research in the Physics of Condensed Matter," Rev. Sci. Inst. **55**, 620 (1984).
5. E.C. Sowa and L.M. Falicov, "Exactly Soluble Model of Two-Dimensional Interacting Fermions in a Uniform Magnetic Field," Phys. Rev. B **29**, 4364 (1984).†
6. R.H. Victora and L.M. Falicov, "Calculated Magnetization of Iron-Cobalt Disordered Alloys," Phys. Rev. B **30**, 259 (1984); LBL-17251.
7. L.M. Falicov and R.H. Victora, "Exact Solution of the Hubbard Model for a Four-Center Tetrahedral Cluster," Phys. Rev. B **30**, 1695 (1984).†
8. F. Aguilera-Granja, J.L. Morán-López, and L.M. Falicov, "Spatial and Magnetic Ordering of Systems Chemisorbed at the Surface of Ferromagnets," Phys. Rev. B **30**, 2666 (1984).‡
9. S. Wang, L.M. Falicov, and A.W. Searcy, "The Equilibrium Shape of Small Particles," Surf. Sci. **143**, 609 (1984); LBL-17987.
10. R.H. Victora, L.M. Falicov, and S. Ishida, "Calculated Surface Electronic Structure of Ferromagnetic Iron and the Ferromagnetic Ordered Iron-Cobalt Alloy," Phys. Rev. B **30**, 3896 (1984); LBL-17524.
11. J. Urias and L.M. Falicov, "Spectrum of an N-State Tight-Binding Hamiltonian in a Bethe Lattice," Phys. Rev. **30**, 6931 (1984).‡
12. D. Rakovic, I. Bozovic, S.A. Stepanyan, and L.A. Gribov, "Theoretical Study of the Infrared Absorption in trans-$(CH)_x$ and trans-$(CD)_x$," Phys. Rev. B **28**, 1997 (1983).†
13. D. Rakovic, I. Bozovic, L.A. Gribov, S.A. Stepanyan, and V.A. Dementiev, "Vibrational Spectra of cis-$(CH)_x$ and cis-$(CD)_x$: A Theoretical Study," Phys. Rev. B **29**, 3412 (1984).†
14. I. Bozovic and J. Delhalle, "Symmetry-Adapted Linear Combination of Atomic Orbitals Bases and Band-Structure Computation for Quasi-One-Dimensional Solids," Phys. Rev. B **29**, 4733 (1984).†
15. I. Bozovic, "Possible Band-Structure Shapes of Quasi-One-Dimensional Solids," Phys. Rev. B **29**, 6586 (1984).†
16. J. Oliva, "Mechanisms of Charge-State Determination in Hydrogen-Based Impurity Complexes in Crystalline Germanium," Phys. Rev. B **29**, 6846 (1984).†

LBL Reports

17. E.E. Haller, R.E. McMurray, Jr., N.M. Haegel, and L.M. Falicov, "Positively Charged Acceptors with $(1s)^3$ and $(1s)^4$ Configurations," LBL-17659.
18. L.M. Falicov, R.H. Victora, and J. Tersoff, "Electronic and Magnetic Properties of Transition-Metal Surfaces, Interfaces and Overlayers," LBL-18209.

19. L.M. Falicov and E.E. Haller, "Dynamic Impurities in Ultrapure Semiconductors," LBL-18210.

Invited Talks

20. L.M. Falicov, "Dynamic Impurities in Ultrapure Semiconductors," First International Conference on the Spectroscopy of Shallow Centers in Semiconductors, Berkeley, California, August, 1984; University of Paris-South, Orsay, France, March 26, 1984; Strasbourg, France, March 29, 1984;. Max-Planck-Institut für Festkorperforschung, Stuttgart, West Germany, May 15, 1984; University of Antwerp, Belgium, May 16, 1984; Nordic Institute for Theoretical Physics, Nordita, Denmark, May 28, 1984; National Center of Scientific Research, Grenoble, France, June 8, 1984.
21. L.M. Falicov, "Electronic, Magnetic, and Chemical Properties of Transition-Metal Surfaces and Interfaces," University of Paris-South, Orsay, France, April 17, 1984; l'Institut de Chimie Moleculaire d'Orsay, France, May 23, 1984; Annual Meeting of the Danish Physical Society, Elsinore, Denmark, May 30, 1984.
22. L.M. Falicov, "Magnetic States of Cobalt Overlayers on Copper (111)," University of Paris-South, Orsay, France, March 12, 1984.
23. L.M. Falicov, "Photoemission in Ce Compounds and Kondo Effects," University of Paris-South, Orsay, France, March 19, 1984.
24. L.M. Falicov, four lectures on "Electron-Electron Correlations In Molecules, Clusters, Metals, Surfaces, and Interfaces," University of Paris-South, Orsay, France, May 11 and 12, 1984; June 4 and 18, 1984.
25. L.M. Falicov, "The $\gamma-\alpha$ Phase Transition in Cerium: Partial Overview," National Center of Scientific Research, Grenoble, France, June 7, 1984.
26. L.M. Falicov, "Theoretical Studies of Short-Range Properties of Binary Alloys," Gordon Conference on Physical Metallurgy, Andover, New Hampshire, July 24, 1984.
27. L.M. Falicov, "Magnetic Properties of Transition Metal Surfaces and Overlayers," First International Conference on the Structure of Surfaces, Berkeley, California, August 16, 1984.
28. L.M. Falicov, "Physics of Materials," International Conference on Physics for Development, Trieste, Italy, October 8, 1984.

---

†Graduate student salaries, secretarial assistance, and publications costs were supported in part by the National Science Foundation through Grant No. DMR-81-06494.

‡Graduate student salaries, secretarial assistance, publication costs, and collaboration with Mexican researchers were supported in part by the National Science Foundation through grants No. DMR-81-06494 and INT-80-18688.

Theoretical Solid-State Physics*

Marvin L. Cohen, Investigator

INTRODUCTION

This research is based on applications of quantum-mechanical theory to study the properties of solids, clusters, and molecules. Much of the results obtained used the pseudopotential method and a total-energy scheme to obtain structural information. The emphasis has been on bulk, surface, and interface properties of semiconductors.

Collaborations with experimental projects here and elsewhere are frequent. The motivation for the research is the modeling properties of real materials. A new area of investigation is small clusters of alkali metals. Several reviews were written on pseudopotentials, surfaces, and the techniques involved in quantum-mechanical calculations of real-material properties.

SURFACES AND INTERFACES

1. Total Energy of the Adatom and Pyramidal-Cluster Models for Si(111) (Publication 5)

Marvin L. Cohen and John E. Northrup

The total energy is calculated for a Si(111)-(2 × 2) adatom geometry with a local bonding topology that is similar to the models of Harrison and Binning *et al.* for the structure of the Si(111)-(7 × 7) surface. This 2 × 2 model is found to be higher in energy than the Pandey chain geometry by about 0.2 eV per surface atom. The energy of a 2 × 2 pyramidal-cluster model is also calculated and is found to be higher than the chain surface by about 0.9 eV per surface atom. The activation energy for diffusion on the ideal surface is estimated.

2. Total-Energy Calculations for the 2 × 1 Antiferromagnetic and 1 × 1 Paramagnetic States of the Si(111)-(1 × 1) Surface (Publication 10)

Marvin L. Cohen and John E. Northrup

The energies of the 2 × 1 antiferromagnetic and 1 × 1 paramagnetic states of the Si(111)-(1 × 1) surface are calculated as a function of relaxation using the pseudopotential method within the local-spin-density approximation. The energy difference between these two states depends strongly on both the relaxation and the form of the local exchange-correlation-energy functional. We also find that the paramagnetic state of the π-bonded chain geometry is stable against antiferromagnetic spin ordering.

3. Ge Adsorption on the Si(111) Surface (Publication 17)

Marvin L. Cohen, S.B. Zhang, and John E. Northrup

Total-energy calculations performed for one monolayer of Ge adsorbed on Si(111) indicate that 1 × 1 models such as the atop-site and hollow-site adsorption geometries are unstable with respect to the formation of 2 × 1 Seiwatz chains of Ge adatoms. This result indicates that, for one-monolayer coverage, Ge-Ge bonds are likely to form.

STRUCTURAL AND ELECTRONIC PROPERTIES OF SEMICONDUCTORS, SEMIMETALS, AND INSULATORS

4. Structural Properties of NaCl (Publication 6)

Marvin L. Cohen and Sverre Froyen

A theoretical description of the static structural, vibrational, and solid-solid phase-transition properties of alkali halides is presented. The description is *ab initio* involving pseudopotentials and density-functional theory. Using NaCl as a prototypical example, we conclude that properties of alkali halides can be computed accurately using this first-principles approach.

*This work was supported jointly by the Director, Office of Energy Research, Office of Basic Energy Sciences, Materials Science Division of the U.S. Department of Energy under Contract No. DE-AC03-76SF00098 and by the National Science Foundation under Grant No. DMR83-19024.

5. Pressure Coefficients of Band Gaps in Semiconductors (Publication 7)

Marvin L. Cohen, K.J. Chang, and Sverre Froyen

A first-principles pseudopotential method within the local-density approximation is used to calculate the pressure coefficients for band gaps in several diamond and zincblende semiconductors. Despite the underestimation of the band gaps found in almost all local-density calculations, the predictions for the linear pressure coefficients and the critical pressures for conduction-band inversion are consistent with experiment for all cases considered.

6. Theoretical Study of BeO: Structural and Electronic Properties (Publication 9)

Marvin L. Cohen and K.J. Chang

The pseudopotential method is used to examine the static structural and electronic properties of BeO. At zero pressure, the wurtzite phase is found to be more stable in energy than the zincblende phase. At high pressure, we predict a phase transformation into an insulating rocksalt structure. The calculated charge density for the valence electrons is in good agreement with experiment.

7. Structural Theory of Graphite and Graphitic Silicon (Publication 12)

Marvin L. Cohen and M.T. Yin

The graphitic phases of C and Si are studied with the use of the pseudopotential local-density-functional approach. For graphite, good agreement with experiment is obtained for the in-plane lattice constant, interlayer spacing, isotropic bulk modulus, and graphite-diamond structural-energy difference. Graphitic Si has relatively weak bonding, and its formation is unlikely since its energy is 0.71 eV/atom higher than the diamond phase and a large negative pressure of −69 kbar is required.

8. Electron Momentum Distribution in Graphite and Lithium-Intercalated Graphite (Publication 13)

Marvin L. Cohen, M.Y. Chou, Steven G. Louie, and N.A.W. Holzwarth

Compton profiles of the first-stage graphite-intercalation compound LiC_6 have been calculated using the self-consistent pseudopotential method within the local-density-functional formalism. The difference between profiles of LiC_6 and graphite exhibits characteristic features that provide further elucidation of the electronic properties of intercalation. The change in the electron-momentum distribution in LiC_6 is qualitatively different from that predicted by the generally accepted rigid-band model.

9. High-Pressure Behavior of MgO: Structural and Electronic Properties (Publication 19)

Marvin L. Cohen and K.J. Chang

The high-pressure behavior of the structural and electronic properties of MgO is examined by the pseudopotential method within local-density theory. At zero pressure, the rocksalt phase is found to be lower in energy than a hypothetical CsCl structure. However, we predict a phase transformation into an insulating CsCl structure at a very high hydrostatic pressure of about 10 Mbar. This result predicts that the CsCl phase for MgO is unlikely to exist even in the lower mantle of the earth. The calculated ground-state properties such as lattice constant, bulk modulus, and cohesive energy for the rocksalt phase are in good agreement with experiment. The electronic-band structures at normal and high pressures are also given.

10. Structural and Electronic Properties of the High-Pressure Hexagonal Phase of Si (Publication 21)

Marvin L. Cohen and K.J. Chang

The pseudopotential method is used to examine the structural transitions of Si from β-Sn to simple

hexagonal to hexagonal close packed. The calculated transition pressures, transition volumes, and c/a ratios are in good agreement with the measured values. For the simple hexagonal phase, a soft-phonon mode and a high density of states at the Fermi level are found. These properties and the strong covalent interlayer bonding suggest the existence of superconductivity in this system. Investigation of the band structure reveals parallel bands separated by about 3 eV along the LH axis of the Brillouin zone; these are the likely origin of the main peak in the optical spectrum.

11. Compton Profile of Graphite and Lithium-Intercalated Graphite (Publication 24)

Marvin L. Cohen, M.Y. Chou, and Steven G. Louie

The momentum distribution of the valence electrons in graphite and lithium-intercalated graphite LiC_6 is studied by calculating the Compton profiles. The wavefunctions are generated from a self-consistent calculation using the pseudopotential method within the local-density-functional formalism and a mixed-basis set consisting of plane waves and linear combinations of atomic orbitals. Compton profiles along the (0001) direction are presented for both graphite and LiC_6. The difference between profiles of LiC_6 and graphite exhibits characteristic features that provide information about the change in the electronic properties resulting from intercalation.

STRUCTURAL AND ELECTRONIC PROPERTIES OF METALS

12. Dependence of Lattice Constants and Bulk Moduli on Pseudopotential Properties (Publication 4)

Marvin L. Cohen and Pui K. Lam

Using a nearly free-electron model and model pseudopotentials, an analytical relation between the Wigner-Seitz radius for a metal, r_{ws}, and the core radius of the model pseudopotential, r_c, is derived. In addition, a semiempirical formula for the bulk moduli is obtained.

13. Temperature- and Pressure-Induced Crystal Phase Transitions in Be (Publication 8)

Marvin L. Cohen, Pui K. Lam, and M.Y. Chou

Beryllium is known to undergo a hcp-bcc transition at about 1530 K and ambient pressure. This transition is studied theoretically by comparing the Gibbs free energies for the hcp, fcc, and bcc modifications of Be. The static lattice energy is calculated using the *ab initio* pseudopotential method. The phonon energy and entropy are estimated from the calculated elastic constants. A mechanism for this transition is proposed based on the results of our calculations. At high temperature, the bcc modification is found to be stabilized by the large entropy for this phase caused by the presence of soft phonon modes. Possible pressure-induced phase transitions are examined. We find that at about 1–2 Mbar both the fcc and bcc phases are more stable than the hcp phase. The regions of fcc and bcc stability lie too close to be separated in the present calculation.

14. An Angle-Resolved Photoemission Study of the Electronic Structure of Beryllium: Bulk Band Dispersions and Many-Electron Effects (Publication 23)

Marvin L. Cohen, M.Y. Chou, E. Jensen, R.A. Bartynski, T. Gustafsson, E.W. Plummer, and Gar B. Hoflund

Angle-resolved photoemission spectra from Be(0001) in the photon energy range 10–120 eV are presented and discussed. The band structure along Δ is determined and compared with our calculation using an *ab initio* self-consistent pseudopotential method in the local-density formalism. The occupied band width, characterized by the Γ_1^+ symmetry-point energy, is found to be 11.1 $\pm$ 0.1 eV, which is in excellent agreement with the calculated value of 11.16 eV. The shallowest occupied symmetry point on Δ, Γ_3^+, is found at 4.8 $\pm$ 0.1 eV; the calculated value is 4.32 eV. The lowest-energy unoccupied band is in good agreement with the calculation, with the exception of some extra structure near the plasmon threshold. This extra structure is associated with an interaction between the excited electron and plasmons. The peak widths for photon energies below 33 eV are in reasonable agreement with widths predicted for hole lifetimes in the homogeneous electron gas.

STRUCTURAL AND ELECTRONIC PROPERTIES OF MOLECULES

15. Predictions of the Bond Length and Vibrational Frequency of Ge (Publication 1)

Marvin L. Cohen and John E. Northrup

We present a pseudopotential local-spin-density calculation of the bond length, vibrational frequency, and binding energy for the state of the germanium dimer. Predictions for the equilibrium bond length and vibrational frequency are given. An overestimate of the binding energy is obtained; the estimate is consistent with other local-spin-density calculations for sp-bonded diatomic molecules.

SMALL CLUSTERS OF ALKALI METALS

16. Electronic Shell Structure and Abundances of Sodium Clusters (Publication 11)

Marvin L. Cohen, M.Y. Chou, W.D. Knight, Keith Clemenger, Walt A. de Heer, and Winston A. Saunders

Mass spectra are presented for sodium clusters of N atoms per cluster (N = 4–100) produced in a supersonic expansion with argon carrier gas. The spectra show large peaks or steps at N = 8, 20, 40, 58, and 92. These phenomena can be understood in terms of a one-electron shell model in which independent delocalized atomic 3s electrons are bound in a spherically symmetric potential well.

17. Total Energies, Abundances, and Electronic-Shell Structure of Lithium, Sodium, and Potassium Clusters (Publication 22)

Marvin L. Cohen, M.Y. Chou, and Andrew Cleland

The total energies of lithium, sodium, and potassium clusters are computed as a function of N, the number of atoms in a cluster, using a jellium local-density-functional scheme. The calculated binding-energy change shows discontinuities at certain cluster sizes because of the existence of electronic-shell structure. This result is consistent with the abundance discontinuities found in the mass spectrum for sodium. Predictions of the mass spectra are made for lithium and potassium clusters. The ionization energies for individual clusters are calculated, and these energies also show shell structure.

VIBRATIONAL PROPERTIES OF SOLIDS

18. Calculation of Phonon-Phonon Interactions and the Absence of Two-Phonon Bound States in Diamond (Publication 18)

Marvin L. Cohen, David Vanderbilt, and Steven G. Louie

We demonstrate that anharmonic phonon-phonon coupling constants can be extracted from frozen-phonon total-energy calculations. The method is applied to the optical modes of diamond. The zone-center coupling constants are completely determined through the fourth order and are used to compute an effective four-phonon vertex including virtual optical-phonon exchange. The interaction is found to have the wrong sign to allow formation of a two-phonon bound state.

1984 PUBLICATIONS AND REPORTS

Refereed Journals

1. J.E. Northrup and M.L. Cohen, "Predictions of the Bond Length and Vibrational Frequency of Ge_2," Phys. Lett. **102**, 440 (1983); LBL-17307.
2. M.L. Cohen, "Fifty Years of Pseudopotentials," Int. J. Quant. Chem: Quantum Chemistry Symposium No. 17, 583 (1983).
3. M.L. Cohen, "Semiconductor," in *Funk and Wagnalls New Encyclopedia*, Vol. 23, Funk and Wagnalls, Inc., New York, 1983, p. 295.
4. P.K. Lam and M.L. Cohen, "Dependence of Lattice Constants and Bulk Moduli on Pseudopotential Properties," Phys. Lett. **100A**, 293 (1984); LBL-17484.
5. J.E. Northrup and M.L. Cohen, "Total Energy of the Adatom and Pyramidal-Cluster Models for Si(111)," Phys. Rev. B **29**, 1966 (1984).
6. S. Froyen and M.L. Cohen, "Structural Properties of NaCl," Phys. Rev. B **29**, 3770 (1984).
7. K.J. Chang, S. Froyen, and M.L. Cohen, "Pressure Coefficients of Band Gaps in Semiconductors," Solid State Comm. **50**, 105 (1984).

8. P.K. Lam, M.Y. Chou, and M.L. Cohen, "Temperature- and Pressure-Induced Crystal Phase Transitions in Be," J. Phys. C **17**, 2065 (1984).
9. K.J. Chang and M.L. Cohen, "Theoretical Study of BeO: Structural and Electronic Properties," Solid State Comm. **50**, 487 (1984).
10. J.E. Northrup and M.L. Cohen, "Total-Energy Calculations for the 2 ×1 Antiferromagnetic and 1 × 1 Paramagnetic States of the Si(111)-(1 × 1) Surface," Phys. Rev. B **29**, 5944 (1984).
11. W.D. Knight, K. Clemenger, W.A. de Heer, W.A. Saunders, M.Y. Chou, and M.L. Cohen, "Electronic Shell Structure and Abundances of Sodium Clusters," Phys. Rev. Lett. **52**, 2141 (1984).
12. M.T. Yin and M.L. Cohen, "Structural Theory of Graphite and Graphitic Silicon," Phys. Rev. B **29**, 6996 (1984).
13. M.Y. Chou, S.G. Louie, M.L. Cohen, and N.A.W. Holzwarth, "Electron Momentum Distribution in Graphite and Lithium-Intercalated Graphite," Phys. Rev. B **30**, 1062 (1984).
14. M.L. Cohen, "Application of the Pseudopotential Model to Solids," Ann. Rev. Mat. Sci. **14**, 119 (1984).
15. M.L. Cohen, "The Fermi Atomic Pseudopotential," Am. J. Phys. **52**, 695 (1984).
16. M.L. Cohen, "Electronic Structure of Solids," Phys. Reports **110**, 293 (1984).
17. S.B. Zhang, J.E. Northrup, and M.L. Cohen, "Ge Adsorption on the Si(111) Surface," Surf. Sci. **145**, L465 (1984).
18. D. Vanderbilt, S.G. Louie, and M.L. Cohen, "Calculation of Phonon-Phonon Interaction and the Absence of Two-Phonon Bound States in Diamond," Phys. Rev. Lett. **53**, 1477 (1984).
19. K.J. Chang and M.L. Cohen, "High-Pressure Behavior of MgO: Structural and Electronic Properties," Phys. Rev. B **30**, 4774 (1984).
20. S.G. Louie and M.L. Cohen, "Electronic Properties of Surfaces," Ann. Rev. Phys. Chem. **35**, 537 (1984).
21. K.J. Chang and M.L. Cohen, "Structural and Electronic Properties of the High-Pressure Hexagonal Phases of Si," Phys. Rev. B **30**, 5376 (1984).
22. A. Cleland, M.Y. Chou, and M.L. Cohen, "Total Energies, Abundances, and Electronic Shell Structure of Lithium, Sodium, and Potassium Clusters," Solid State Comm. **52**, 645 (1984).
23. E. Jensen, R.A. Bartynski, T. Gustafsson, E.W. Plummer, M.Y. Chou, M.L. Cohen, and G.B. Hoflund, "Angle-Resolved Photoemission Study of the Electronic Structure of Beryllium: Bulk Band Dispersions and Many-Electron Effects," Phys. Rev. B **30**, 550 (1984).
24. M.L. Cohen, "Compton Profile of Graphite and Lithium-Intercalated Graphite," *Fall Proc., Materials Research Society*, Materials Research Society, Pittsburg, Pennsylvania, 1984, p. 68.

Other Publications

25. J.E. Northrup and M.L. Cohen, "Total Energy of the Adatom and Pyramidal-Cluster Models for Si(111)-(7 × 7)," Bull. Am. Phys. Soc. **29**, 264 (1984).
26. S.L. Richardson, M.Y. Chou, and M.L. Cohen, "Pseudopotential Local Density Calculation of Be_2," Bull. Am. Phys. Soc. **29**, 399 (1984).

Invited Talks

27. M.L. Cohen, "Theory of Electronic and Structural Properties of Surfaces and Interfaces," Symposium on Electron, X-ray, and Ion Spectroscopies and Their Application to Surfaces, Honolulu, Hawaii, December 28, 1983.
28. M.L. Cohen, "Computer Simulations of the Properties of Solids Using Pseudopotentials," Lawrence Livermore Laboratory, Livermore, California, February 16, 1984.
29. M.L. Cohen, Opening Address, 17th International Conference on the Physics of Semiconductors, San Francisco, August 6, 1984.
30. M.L. Cohen, Closing Address, 17th International Conference on the Physics of Semiconductors, San Francisco, California, August 10, 1984.
31. M.L. Cohen, "Theory of Surface Reconstruction," International Conference on the Structure of Surfaces, Berkeley, California, August 16, 1984.
32. M.L. Cohen, "*Ab Initio* Calculations for High-Pressure Properties of Solids," Opening Lecture at the International Conference on Physics and Physicochemistry of Highly Condensed Matter, Aussois, France, September 11, 1984.
33. M.L. Cohen, "Pseudopotential Calculations of Surface and Bulk Properties of Solids," University of Rome, Rome (Frascati), Italy, September 20, 1984.
34. M.L. Cohen, "*Ab Initio* Calculations of Structural Properties of Solids," Opening Lecture, 2nd International Conference on the Science of Hard Materials, Rhodes, Greece, September 24, 1984.
35. M.L. Cohen, "Compton Profile of Graphite and Lithium-Intercalated Graphite," Materials Research Society Meeting, Boston, Massachusetts, November 28, 1984.
36. M.L. Cohen, "Calculations of Structural and Electronic Properties of Solids," Norton-Christensen Laboratory, Salt Lake City, Utah, December 11, 1984.

Surface, Chemisorption, and Theory of Solids*

Steven G. Louie, Investigator

INTRODUCTION

The purpose of this work is to further basic understanding of the electronic and structural properties of materials and materials systems such as surfaces and interfaces. The emphasis is on carrying out quantum-mechanical calculations on realistic systems so that a microscopic understanding of material properties may be obtained from first principles. The research effort encompasses the study of bulk materials, surfaces and chemisorption systems, and defects, and the formulation and development of new theoretical techniques for calculating ground-state and excited-state properties.

The quantities obtainable from these calculations include electronic states, total energies, crystal structures, static structural properties, vibrational properties, surface electronic and geometric structures, structure and properties of defects in solids, phonon-phonon interactions, solid-solid phase transformations, and so forth. The major goals are to calculate and explain the properties of real materials and to predict properties of new systems that were formerly inaccessible to theory or experiment.

SURFACES AND CHEMISORPTION SYSTEMS

1. Hydrogen in Subsurface Sites of Pd(111): Self-Consistent Electronic Structure (Publication 8)†

C.T. Chan and Steven G. Louie

The bonding and electronic structure of hydrogen on various surface and subsurface sites of the Pd(111) surface are studied by self-consistent calculations. Results of the present calculations include the density of states, electronic character of the Pd-H bond, and analyses of surface states and surface density of states. Recent photoemission studies have suggested possible subsurface chemisorption configurations for the high-temperature "invisible" phase of H on the (111) surface of Ni, Pd, and Pt. Our results show that, for all the high-symmetry sites considered, hydrogen induces strong modifications on the surface electronic structure of Pd. The H-induced features, however, may escape detection in normal emission experiments if H occupies the subsurface octahedral sites because of symmetry constraints on the H-Pd bond wavefunctions. The theoretical results suggest two measurements for further testing of the subsurface model using photoemission spectroscopy.

*This work was supported by the Director, Office of Energy Research, Office of Basic Energy Sciences, Materials Science Division of the U.S. Department of Energy under Contract No. DE-AC03-76SF00098. Initial stages of this work were supported by a Program Development Fund from the Director of Lawrence Berkeley Laboratory.

†Supported in part (a graduate student salary) by NSF Grant No. DMR83-19024.

2. Total-Energy Minimization for Diamond (111) Surfaces: Support for an Undimerized π-Bonded Chain Reconstruction (Publications 2 and 7)†

David Vanderbilt and Steven G. Louie

A self-consistent linear-combination-of-atomic-orbitals (LCAO) approach to local-density theory is used to calculate total energies for the 1×1 and various reconstructed 2×1 models of the diamond (111) surface. Among the many models suggested, only the Pandey π-bonded chain model has a lower energy than that of the 1×1 surface. A minimum-energy structure is obtained for this model after extensive consideration of relaxations. Contrary to a previous suggestion, no dimerization of the surface chain is found to occur. The calculated surface-state band dispersion is found to be in good agreement with angle-resolved photoemission data.

†Supported in part (a postdoctoral salary) by NSF Grant No. DMR83-19024.

ELECTRONIC AND STRUCTURAL PROPERTIES OF SOLIDS

3. First-Principles LCAO Method for the Cohesive and Structural Properties of Solids: Application to Diamond (Publication 1)†

James R. Chelikowsky and Steven G. Louie

A new method for the *ab initio* calculation of the cohesive and structural properties of solids is developed. The method is based on an LCAO description of the wavefunctions, a pseudopotential construction for the ion-core potential, and a local-density treatment of exchange and correlation energies. Key elements of the method include the direct computation in real space of all the matrix elements and the flexibility in evaluating the total energy using different levels of simplifying approximations for self-consistency in the electronic charge density depending on the system under consideration. The combination of these elements allows an accurate yet less complex treatment of a wide variety of condensed-matter systems. Calculations have been performed for the prototypical covalent crystal diamond. Excellent agreement, generally within a few percent of experimental values, has been obtained for the structural properties (lattice constants, cohesive energies, bulk moduli, pressure derivatives of bulk moduli, etc.). Equally excellent results are obtained for the vibrational frequencies calculated using the frozen-phonon techniques.

†Supported in part (a graduate student salary) by NSF Grant No. DMR78-22465.

4. Nonlocal-Density Functional Theory for the Electronic and Structural Properties of Semiconductors (Publications 3 and 10)†

Mark S. Hybertsen and Steven G. Louie

Using the weighted-density approximation for the exchange-correlation energy, the band structure and bulk structural properties of the prototypical semiconductors Si and Ge have been systematically studied. The weighted-density approximation is based on an improved description of the exchange-correlation hole that explicitly accounts for the inhomogeneous charge density found in real materials. We find that the approximation as proposed is inadequate for the case of semiconductors where charge inhomogeneity is intimately connected to a gap in the excitation spectrum with consequent qualitative changes in screening. We use a simple extension of the weighted density approximation that takes account of semiconductor screening. With this functional, we find substantial improvement in the calculated minimum gap over the results of the usual local-density approximation as compared to experiment. However, the direct gaps are not significantly improved. Calculated structural properties are found to be in excellent agreement with experiment. By way of contrast, the weighted-density approximation implemented with metallic screening gives a smaller change in the band structure and, more importantly, substantially poorer calculated structural properties. A discussion of the qualitative differences between the weighted density approximation and the usual local-density approximation for covalently bonded semiconductors is presented.

†Supported in part (a graduate student salary) by NSF grants No. DMR83-19024 and DMR78-22465.

5. Electron-Momentum Distribution in Graphite and Lithium-Intercalated Graphite (Publication 4)†

M.Y. Chou, Steven G. Louie, Marvin L. Cohen, and N.A.W. Holzwarth

Compton profiles of the first-stage graphite intercalation compound LiC_6 have been calculated using the self-consistent pseudopotential method within the local-density-functional formalism. The difference between profiles of LiC_6 and graphite exhibits characteristic features that provide further elucidation of the electronic properties of intercalation. The change in the electron-momentum distribution in LiC_6 is qualitatively different from that predicted by the generally accepted rigid-band model.

†Supported in part (a graduate student salary) by NSF Grant No. DMR78-22465.

VIBRATIONAL PROPERTIES AND PHONON INTERACTIONS IN SOLIDS

6. Calculation of Phonon-Phonon Interactions and the Absence of Two-Phonon Bound States in Diamond (Publication 6)†

David Vanderbilt, Steven G. Louie, and Marvin L. Cohen

We demonstrate that anharmonic phonon-phonon coupling constants can be extracted from frozen-phonon total-energy calculations. The method is applied to the optical modes of diamond. The zone-center coupling constants are completely determined through fourth order and are used to compute an effective four-phonon vertex including virtual optical-phonon exchange. The interaction is found to have the wrong sign to allow formation of a two-phonon bound state.

†Supported in part (a postdoctoral salary) by NSF Grant No. DMR83-19024.

7. Work in Progress

The electronic and structural properties of Mo and W are being studied using the self-consistent LCAO method. The vibrational properties and the possibility of structural phase transformation to other crystal structures are being investigated.

The geometric and electronic structures of the W(100) surface for both the relaxed (1 × 1) high-temperature phase and the c(2 × 2) reconstructed low-temperature phase are being investigated. Total-energy calculations are carried out to determine the surface atomic coordinates and to determine the driving mechanism for the c(2 × 2) reconstruction.

An *ab initio* theory of the structure and properties of stacking faults in silicon is being done. The calculations, carried out for both the intrinsic and extrinsic stacking faults, give the stacking-fault energies, information on the localized electronic states associated with the faults, and the atomic rearrangements near the faults.

1984 PUBLICATIONS AND REPORTS

Refereed Journals

1. J.R. Chelikowsky and S.G. Louie, "First Principles LCAO Method for the Cohesive and Structural Properties of Solids: Application to Diamond," Phys. Rev. B **29**, 3470 (1984).†
2. D. Vanderbilt and S.G. Louie, "Total Energy Minimization for Diamond (111) Surfaces: Support for an Undimerized π-Bonded Chain Reconstruction," Phys. Rev. B **29**, 7099 (1984).‡
3. M.S. Hybertsen and S.G. Louie, "Non-Local Density Functional Theory for the Electronic and Structural Properties of Semiconductors," Solid State Comm. **51**, 451 (1984).†
4. M.Y. Chou, S.G. Louie, M.L. Cohen, and N.A.W. Holzwarth, "Electron Momentum Distribution in Graphite and Lithium-Intercalated Graphite," Phys. Rev. B **30**, 1062 (1984).†
5. N.A.W. Holzwarth, S.G. Louie, and S. Rabii, "Interlayer States in Graphite and in Alkali Metal-Graphite Intercalation Compounds," Phys. Rev. **30**, 2219 (1984).‡
6. D. Vanderbilt, S. G. Louie, and M. L. Cohen, "Calculation of Phonon-Phonon Interactions and the Absence of Two-Phonon Bound States in Diamond," Phys. Rev. Lett. **53**, 1477 (1984).‡
7. D. Vanderbilt and S. G. Louie, "Total Energies of Diamond (111) Surface Reconstructions by an LCAO Method," Phys. Rev. B **30**, 6118 (1984).‡
8. C.T. Chan and S.G. Louie, "Hydrogen in Subsurface Sites of Pd(111): Self-Consistent Electronic Structure," Phys. Rev. B **30**, 4153 (1984).‡
9. D. Vanderbilt and S. G. Louie, "A Monte Carlo Simulated Annealing Approach to Optimization over Continuous Variables," J. Comput. Phys. **56**, 259 (1984).†
10. M.S. Hybertsen and S.G. Louie, "Non-Local Density Functional Approximation for Exchange and Correlation in Semiconductors," Phys. Rev. B **30**, 5777 (1984).‡

Other Publications

11. N.A.W. Holzwarth, S.G. Louie, and S. Rabii, "Theoretical Valence Charge Densities for Graphite, Diamond, and LiC_6," in *Local Density Approximations in Quantum Chemistry and Solid State Physics*, J.P. Dahl and J. Avery, eds., Plenum Press, New York, 1984, p. 665.†

12. M.L. Cohen and S.G. Louie, "Electronic Properties of Surfaces," Ann. Rev. Phys. Chem. **35**, 537 (1984).‡
13. N.A.W. Holzwarth, S.G. Louie, and S. Rabii, "The Character of the First Unoccupied Band of Li-Intercalated Graphite," Bull. Am. Phys. Soc. **29**, 252 (1984).†
14. S.G. Louie and J.R. Chelikowsky, "First Principles LCAO Method for the Cohesive and Structural Properties of Solids," Bull. Am. Phys. Soc. **29**, 349 (1984).†
15. D. Vanderbilt and S.G. Louie, "LCAO Total Energy Calculations of Diamond (111) Surface Reconstructions," Bull. Am. Phys. Soc. **29**, 546 (1984).†

Invited Talks

16. S.G. Louie, "Non-Local Density Functional Theory for the Electronic and Structural Properties of Semiconductors," Theoretical and Mathematical Sciences Laboratory, Exxon Research and Engineering Company, Annandale, New Jersey, January 19, 1984.
17. J.R. Chelikowsky, S.G. Louie, D. Vanderbilt, and C.T. Chan, "Total Energy Method for Solids and Solid Surfaces," International Symposium on Atomic, Molecular, and Solid State Theory, Many-Body Phenomena, and Computation Methods, Palm Coast, Florida, March 8, 1984.
18. S.G. Louie, "*Ab Initio* Calculation of Anharmonic Terms and Phonon-Phonon Interactions in Solids," Theoretical and Mathematical Sciences Laboratory, Exxon Research and Engineering Company, Annandale, New Jersey, May 5, 1984.
19. S.G. Louie, "First Principles Total Energy Method for Solids and Solid Surfaces," Department of Physics, University of California, Davis, California, June 8, 1984.
20. S.G. Louie, "Pseudopotentials and Total Energy Calculations: Applications to Crystal Stability and Vibrational Properties," NATO International Advanced Study Institute on Electronic Structure, Dynamics, and Quantum Structural Properties of Condensed Matter, Corsendonk, Belgium, July 17, 1984.
21. S.G. Louie, "Pseudopotentials and Total Energy Calculations: Applications to Structural Phase Transformations," NATO International Advanced Study Institute on Electronic Structure, Dynamics, and Quantum Structural Properties of Condensed Matter, Corsendonk, Belgium, July 19, 1984.
22. S.G. Louie, "Pseudopotentials and Total Energy Calculations: Applications to Surface Structures," NATO International Advanced Study Institute on Electronic Structure, Dynamics, and Quantum Structural Properties of Condensed Matter, Corsendonk, Belgium, July 20, 1984.
23. D. Vanderbilt and S.G. Louie, "Energy Minimization Calculations for Diamond (111) Surface Reconstruction," First International Conference on the Structure of Surfaces, Berkeley, California, August 15, 1984.
24. S.G. Louie, "Total Energy Calculations and Bonding at Interfaces," International Conference on the Structure and Properties of Internal Interfaces, Irsee, West Germany, August 22, 1984.
25. S.G. Louie, "*Ab Initio* Calculations of Materials Properties," Workshop on Theory and Modeling for Materials Design, Texas A&M University, College Station, Texas, September 17, 1984.
26. S.G. Louie, "Beyond Local Density Approximation: Application to the Electronic and Structural Properties of Semiconductors," International Workshop on Total Energy Methods, Braunschweig, West Germany, December 3, 1984.

†Supported in part by NSF Grant No. DMR78-22465.
‡Supported in part by NSF Grant No. DMR83-19024.

MATERIALS CHEMISTRY

CHEMICAL STRUCTURE

Low-Temperature Properties of Materials*

Norman E. Phillips, Investigator

INTRODUCTION

Measurements of low-temperature properties of condensed-matter systems, particularly heat capacities, are used to obtain information that contributes to an understanding of the behavior of materials. There are numerous special cases in which specific-heat data provide either a test of theoretical models or values of important parameters that could not otherwise be obtained. Much of the work is in the region below 1 K, where the temperature scale is not well defined and temperature-measuring techniques are not well established. Because accurate temperature determinations are important in obtaining useful heat-capacity data, research is also conducted on methods of temperature measurement.

An accurate temperature scale has been developed to below 10 mK. Specific-heat measurements on ^{3}He in the Fermi-liquid region have established the correct values of parameters that are important to understanding the superfluid states. The specific heats of potassium, rubidium, and cesium have been measured to 0.1 K to search for predicted charge-density-wave effects. Although analysis of the data is not complete, the preliminary conclusion is that charge-density-wave effects are not present. Measurements on *Cu*Mn in high magnetic fields have mapped out the theoretically predicted phase boundary.

*This work was supported by the Director, Office of Energy Research, Office of Basic Energy Sciences, Materials Sciences Division of the U.S. Department of Energy under Contract No. DE-AC03-76SF00098.

1. Effects of Concentration and Annealing on the Specific Heat and Magnetic-Susceptibility Anomalies Associated with Spin-Glass Ordering in *Cu*Mn (Publications 1 and 2)

G.E. Brodale, R.A. Fisher, W.E. Fogle,[†] *E.W. Hornung, N.E. Phillips, and J. Van Curen*[‡]

The discovery of a small anomaly[1] in the specific heat of 0.28 at% *Cu*Mn that shifts[2] with magnetic field H in the way predicted by mean-field calculations has significant implications for the reality of thermodynamic phase transition in spin glasses. To further strengthen the identification of the anomaly with the spin-glass transition, measurements of both the specific heat C and the low-field, field-cooled magnetic susceptibility X have been made on a series of samples that cover a concentration range of almost a factor of 10 and also differ in heat treatment. The "annealed" samples show the sharp cusp in X, at a temperature approximately proportional to concentration, that is generally taken as the characteristic feature of the spin-glass transition. For the "unannealed" samples this feature is broadened and shifted in temperature, but a characteristic temperature can still be identified by analysis of X into linear and nonlinear components. The interesting result is that the anomaly in C tracks the feature in X both in temperature and, qualitatively, in magnitude. This shows conclusively that the anomaly in C is associated with the feature characteristic of the spin-glass transition, whatever its origin.

[†]Present address: National Bureau of Standards, Washington, D.C. 20234.

[‡]Present address: Rohm and Haas Co., Spring House, Pennsylvania 19477.

1. W.E. Fogle, J.D. Boyer, J. Van Curen, and N.E. Phillips, Phys. Rev. Lett. **47**, 352 (1981).

2. W.E. Fogle, J.D. Boyer, R.A. Fisher, and N.E. Phillips, Phys. Rev. Lett. **50**, 1815 (1983).

2. Curie-Weiss Parameters for *Cu*Mn (Publication 2)

R.A. Fisher, E.W. Hornung, N.E. Phillips, and J. Van Curen†

The Curie constant is an important parameter for the analysis of experimental data related to spin-glass behavior. Analyses for Mn in *Cu*Mn samples (to determine absolute entropies associated with Mn) have shown that the Mn concentration is consistently lower that the "nominal" concentration (the concentration deduced from the starting materials). Since nominal concentrations have usually been used in analyzing X data, the deduced values of the Curie constant and effective magneton number can be expected to be low. Indeed, the values obtained in this work, based on actual concentrations obtained by carefully checked analytical techniques, are significantly higher than most earlier results. The new values of the magneton numbers will be used in analyzing both C and other, high-field, X data.

†Present address: Rohm and Haas Co., Spring House, Pennsylvania 19477.

3. Low-Temperature Specific Heat of K, Rb, and Cs (Publication 3)

J. Van Curen† *and N.E. Phillips*

Accurate measurements of the specific heat of K, Rb, and Cs have been made between 0.15 and 25 K. (Measurements between 0.05 and 0.15 K are uncertain by up to 2% because of problems with long thermal-relaxation times.) The results show a number of interesting features: there is an effect of thermal cycling in Rb, possibly associated with a martensitic transition; there is an unexplained sample dependence on K; and there is no evidence requiring the assumption of spin-density wave effects.

†Present address: Rohm and Haas Co., Spring House, Pennsylvania 19477.

4. Progress in High-Pressure Calorimetry (Publication4)†

A number of refinements have been made in techniques for high-pressure, low-temperature calorimetry. They include improvements in obtaining more homogeneous pressures and in measuring pressures, and progress in extending the accessible pressure range to 20 kbar.

†Supported by the Assistant Secretary for Conservation and Renewable Energy, Office of Energy Systems Research, Energy Storage Division of the U.S. Department of Energy under Contract No. DE-AC03-76SF00098.

5. Work in Progress†

The capability of making specific-heat measurements under pressure is being exploited for measurements on "heavy Fermion" systems in which the recently discovered and dramatically different properties are very sensitive to interatomic distance. The specific heat of $CeAl_3$ shows an enormous (factor of 3 at 7 kbar) and highly nonlinear pressure dependence below 1 K. The results strongly suggest an instability near zero pressure. There is an as yet unresolved discrepancy with zero-pressure thermal-expansion data. UPt_3 is sometimes said to be a possible p-wave superconductor because of the apparent coexistence of superconductivity and spin fluctuations. The specific heat shows, in addition to the very large linear term, a large T^3 ln T term, characteristic of spin fluctuations. The spin-fluctuation contribution decreases markedly with increasing pressure, as does the critical temperature for superconductivity. This correlation is further evidence of the unusual nature of superconductivity in this system.

The unique capability of the Giauque Low-Temperature Laboratory for accurate measurements of magnetothermodynamic properties has been used to study spin glasses, both *Cu*Mn and *Ag*Mn. The fields, temperatures, and concentrations have been chosen to test the virial expansion theories of spin-glass systems in the high-field limit. These theoretical results, which are believed to be exact, can be used in combination with experimental data to test the validity of the assumed Hamiltonian. Preliminary analysis suggests that *Cu*Mn is not governed by the RKKY Hamiltonian for random spins—a result of considerable interest in evaluating its spin-glass properties.

†Work on $CeAl_3$ is done in collaboration with J. Flouquet, CRTBT-CNRS, Grenoble, France. Work on UPt_3 is done in collaboration with G.R. Stewart, Los Alamos National Laboratory, Los Alamos, New Mexico. Work on the virial-expansion theories of spin-glass systems is done in collaboration with K. Matho, CRTBT-CNRS, Grenoble, France.

1984 PUBLICATIONS AND REPORTS

Other Publications

1. G.E. Brodale, W.E. Fogle, N.E. Phillips, and J. Van Curen, "Effects of Concentration and Annealing on Specific Heat Anomaly Associated with Spin-Glass Ordering in *Cu*Mn," in *Proc. 17 Int. Conf. on Low-Temp. Phys.*, Karlsruhe, West Germany, August 15–22, 1984, U. Eckern, A. Schmid, W. Weber, and H. Wuhl, eds., North-Holland, Amsterdam, 1984, p. 621.
2. R.A. Fisher, E.W. Hornung, N.E. Phillips, and J. Van Curen, "Magnetic Susceptibility of *Cu*Mn: Curie-Weiss Parameters and the Effect of Annealing," in *Proc. 17 Int. Conf. on Low-Temp. Phys.*, Karlsruhe, West Germany, August 15–22, 1984, U. Eckern, A. Schmid, W. Weber, and H. Wuhl, eds., North-Holland, Amsterdam, 1984, p. 437.

LBL Reports

3. John Van Curen (Ph.D. Thesis), "A Calorimetric Investigation into the Possibility of Charge Density Wave Ground State in Alkali Metals," LBL-18292.
4. L. Brewer, N.E. Phillips, G.E. Brodale, R.A. Fisher, and C.M. Lisse, "Investigation of Bond-Breaking Contributions to the Specific Heat of Metals for Thermal Energy Storage Applications," LBID-975.

Electrochemical Processes*

Charles W. Tobias, Investigator

INTRODUCTION

This program is designed to advance the scientific foundations of electrochemical engineering and to broaden the range of useful applications of electrochemical transformations. Electrolysis processes have inherent advantages over thermochemical methods with respect to material yield and energy efficiency. However, in spite of their long history of economically significant applications, cell processes have not achieved their potential with respect to performance and range of applications in chemical synthesis, nor have they achieved it in energy conversion and storage. A major reason for this condition is the complex nature of transport phenomena in ionic media as they relate to charge-transfer processes at the electrode surface. The present emphasis in this program is on exploring novel methods for reducing mass-transfer resistance in high-rate applications (including electroforming of metals) and in electroorganic synthesis. The effects of fixed flow obstacles and suspended inert solid particles in flowing electrolytes on both transport rates and current distribution are measured over broad ranges of process variables; theoretical models are advanced for the interpretation of mechanisms. A major part of this effort is directed jointly with Dr. Rolf H. Muller.

Non-aqueous ionizing solvents are evaluated for potential use at ambient temperatures in electrosynthesis processes. Emphasis is placed on the thermodynamic and kinetic properties of various electrode reactions that are not feasible in aqueous media.

Applied research on the "Surface Morphology of Metals in Electrodeposition," on "Engineering Analysis of Electrolytic Gas Evolution," and on "Metal Couples in Non-Aqueous Electrolytes" is supported by the Office of Advanced Conservation Technologies, DOE, and is reported under "Electrochemical Energy Storage."

*This work was supported by the Director, Office of Energy Research, Office of Basic Energy Sciences, Materials Sciences Division of the U.S. Department of Energy under Contract No. DE-AC03-76SF00098.

1. Electrochemical Machining of Refractory Materials (Publication 10)

C.A. Coughanowr, B.A. Dissaux, R.H. Muller, and C.W. Tobias

The feasibility of electrochemical machining (ECM) of pure TiC, ZrC, TiB_2, and ZrB_2 has been established. In addition, the ECM behavior of a cemented TiC/10% Ni composite has been investigated and compared to that of its components, TiC and nickel. ECM was carried out in 2M KNO_3 and in 3M NaCl, at applied voltages of 10–30 volts and current densities of 15–115 A/cm^2, with average apparent valences of 5.7 to 9.8 eq/mol (see Table 1-1). Post-ECM surface studies on the TiC/Ni composite showed preferential dissolution of the TiC phase during machining.

Table 1-1

Average valence of dissolution (z) and IR-free cell voltage ($V-V_{IR}$) of carbides and borides at different current densities i.

Material	z (eq/gmol)	i (A/cm^2)	$V-_{VI}R$ (volts)
TiC	6.6	23–88	3–6
ZrC	5.7	19–81	3–11
TiB_2	9.3	15–103	5–8
ZrB_2	9.8	27–106	4–10

2. Mass-Transfer Enhancement by Small Flow Obstacles in Electrochemical Cells (Publication 14)

D.S. Fischl, K.J. Hanson, R.H. Muller, and C.W. Tobias

Mass-transfer enhancement by small obstacles attached to the cathode in electrolytic flow cells 5 × 5 cm in cross section and 500 mm long was investigated. Double-beam laser interferometry was used to observe the local mass-transfer boundary-layer thicknesses preceding and following the placement of rod-shaped dielectric obstacles oriented normal to the direction of electrolyte flow. Flow patterns were visualized by making dark-field photographs of suspensions of small inert particles (see Figure 2-1). In evaluating of the effectiveness of mass-transport enhancement, pressure drops and limiting currents for the reduction of ferricyanide have been measured in the 80 to 3200 Reynolds Number range. The

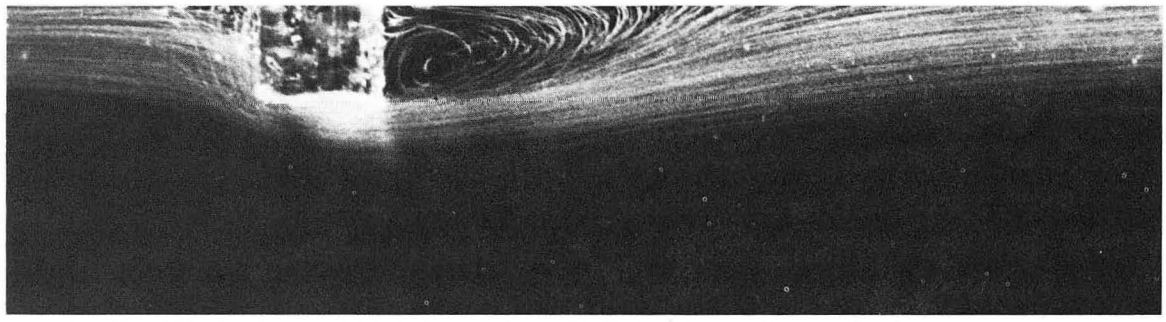

Figure 2-1. Recirculation zone downstream from a rectangular cross-section rod at Re=116; the flow is from left to right. Hydrogen bubbles tracing the flow paths were generated upstream. (XBB 832-1711A)

degree of enhancement increases with decreasing obstacle spacing until an optimal spacing of approximately 15 times the obstacle size is reached. By using these obstacles, a three- to fivefold increase in the average mass-transfer coefficient is achieved with a small fraction of the pumping power required to obtain the same limiting current by increasing the flow rate in the unobstructed channel. Small obstacles produce efficient mixing near the electrode surface, as well as corresponding improvement in uniformity and magnitude of mass-transport rates, without increasing the energy dissipation in the bulk fluid.

3. A Mathematical Model for the Periodic Electrodeposition of Multicomponent Alloys (Publication 15)

M.W. Verbrugge and C.W. Tobias

A mathematical model has been developed for the electrodeposition of multicomponent alloys by an arbitrarily specified current source. The model takes into account transient convective mass transfer to a rotating disk electrode, Butler-Volmer kinetics, and individual component activities in the electrodeposit. The model can be used to calculate current-potential relationships, ionic-concentration profiles, and electrodeposit composition. Results for the electrodeposition of a ternary alloy by a rectangular pulse are shown in Figure 3-1.

The mathematical problem couples concepts of transport and kinetic phenomena, potential theory, and thermodynamics. The method of superposition is used to solve this problem with an efficient numerical algorithm. This treatment exposes the large number of parameters that the electroplater must consider for obtaining thin alloy films with the desired properties. If an accurate model is used by the electroplater, the different plating parameters can be intelligently varied to assist in manufacturing the desired electrodeposit.

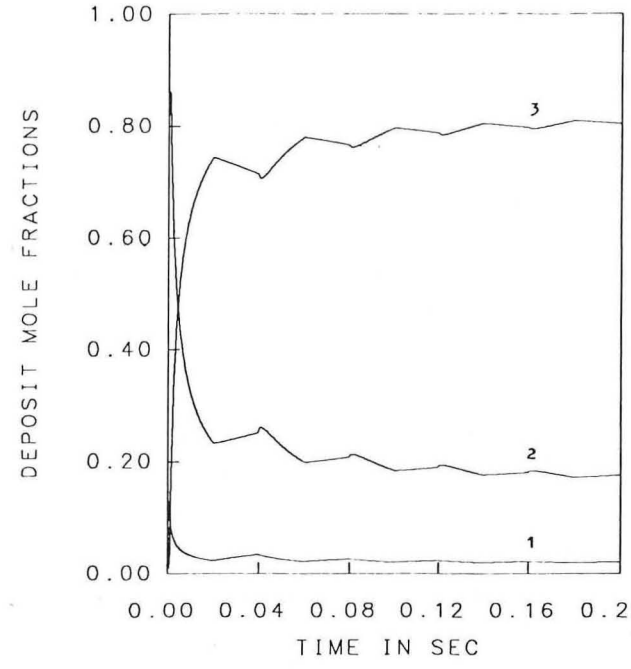

Figure 3-1. Change in composition of a ternary alloy during the initial period in pulse plating. The following values apply to the figure:

Ion	Standard potential (V)	Bulk molar concentration
1	+0.1	0.001
2	−0.1	0.010
3	−0.3	0.100

Reasonable values were chosen for other transport, thermodynamic, and kinetic constants. (XBL 853-1502)

4. Work in Progress

Mass-transport enhancement by solids suspended on a rotating disk electrode is being investigated. Theoretical models that include the rheological properties of the suspensions are under development.

The electrodeposition of metals at very high rates (on the order of 10 A/cm^2) is being investigated for possible use in electroforming complex shapes under economically attractive conditions. Copper deposits are obtained from a $CuSO_4$-H_2SO_4 solution on a rotating cylinder electrode. The dependence of surface topography, uniformity, density, and crystallinity of the deposit on deposition conditions is measured. (Paul Andersen, Dale Barkey, Rolf H. Muller, and Charles W. Tobias)

The detection limit of water in propylene carbonate (PC) has been lowered to 0.3 ppm by use of a novel nuclear magnetic-resonance (NMR) technique. Hexafluoroacetone, when added to PC, reacts quantitatively with water as well as with alcohols to form adducts that show separate peaks on the F^{19} NMR spectrum. Unlike gas chromatography, this technique can also be used in the presence of dissolved ionic solutes. (Robert C. McIntosh and Charles W. Tobias)

1984 PUBLICATIONS AND REPORTS

Other Publications

1. D.W. Dees and C.W. Tobias, "Experimental Observations of Free Convection Mass Transfer to a Horizontal Surface with a Micro-Mosaic Electrode," Electrochem. Society Meeting, Cincinnati, Ohio, May 6-11, 1984, Ext. Abstr. 84-1, pp. 535–536; based on LBL-16176.†
2. D.W. Dees and C.W. Tobias, "Mass Transfer at Gas Evolving Surfaces: A Microscopic Study," in *Proc. Int. Soc. Electrochem. Meeting,* Berkeley, California, August 5–10, 1984, Ext. Abstr., pp. 717–719; based on LBL-16176.†
3. C.A. Coughanowr, R.H. Muller, and C.W. Tobias, "Electrochemical Machining of Cemented Titanium Carbide," in *Proc. Int. Soc. Electrochem. Meeting,* Berkeley, California, August 5–10, 1984, Ext. Abstr., pp. 667–669; based on LBL-13682.
4. K.J. Hanson, M. Matlosz, J. Newman, and C.W. Tobias, "Theory of Cyclic Voltammetry for Reactions Having Complex Stoichiometry," in *Proc. Int. Soc. Electrochem. Meeting,* Berkeley, California, August 5–10, 1984, Ext. Abstr., pp. 950–952; based on LBL-18335.†
5. J. Thonstad and C.W. Tobias, "On the Coalescence of Electrolytic Gas Bubbles," in *Proc. Int. Soc. Electrochem. Meeting,* Berkeley, California, August 5–10, 1984, Ext. Abstr., pp. 950-952.†
6. K.J. Hanson and C.W. Tobias, "The Electrochemistry of the Iodide/Tri-Iodide/Iodine Redox System in Propylene Carbonate," Electrochemical Society Meeting, New Orleans, Louisiana, October 7–12, 1984, Ext. Abstr. 140, pp. 211–212; based on LBL-18335.†
7. Patents: (with P.C. Foller and M.L. Goodwin), Process for Producing Ozone, U.S. Patent No. 4,375,395 (1983); Canadian Patent No. 1,170,616 (1984).‡
8. F.R. McLarnon, R.H. Muller, and C.W. Tobias, "Interferometric Study of Combined Forced and Natural Convection" (Discussion), J. Electrochem. Soc. **120**, 1444 (1984).

LBL Reports

9. R.E. Acosta, R.H. Muller, and C.W. Tobias, "Transport Processes in Narrow Gap Channels," accepted by J. AIChE.; LBL-16067.
10. C.A. Coughanowr, B.A. Dissaux, R.H. Muller, and C.W. Tobias, "Electrochemical Machining of Refractory Materials," submitted to J. Appl. Electrochem.; LBL-18365.
11. F.R. McLarnon, R.H. Muller, and C.W. Tobias, "Interferometric Observation of Turbulent Mass Transfer in Channel Flow," submitted to J. Electrochem. Soc.; LBL-18575.
12. K.J. Hanson (Ph.D. Thesis), with C.W. Tobias, "On the Electrochemistry of Halogen Electrodes in Propylene Carbonate," LBL-18335.†
13. R.C. Anderson (M.S. Thesis), with C.W. Tobias, "Studies on Zinc Electrodes Electrodeposited from Acid Electrolytes," LBL-18646.†
14. D.S. Fischl, K.J. Hanson, R.H. Muller, and C.W. Tobias, "Mass Transfer Enhancement by Small Flow Obstacles in Electrochemical Cells," submitted to Chem. Eng. Commun.; LBL-18476.
15. M.W. Verbrugge and C.W. Tobias, "A Mathematical Model for the Periodic Electrodeposition of Multicomponent Alloys," submitted to J. Electrochem. Soc.; LBL-17739.
16. J.O. Dukovic and C.W. Tobias, "A Model for Current Distribution with Passivating Kinetics," LBL-18819.†

Invited Talks§

17. C.W. Tobias, "Introduction to the Norbert Ibl Symposium on Electrochemical Engineering," International Society of Electrochemistry Meeting, Berkeley, California, August 5–10, 1984, Ext. Abstr. B1-1.

18. C.W. Tobias (presented by J. Thonstad), "The Coalescence of Electrolytic Gas Bubbles," International Meeting on Electrolytic Bubbles, London, England, September 13–14, 1984.†
19. C.W. Tobias (presented by P.J. Sides), "Current Distribution Around, and Resistance Presented by, Gas Bubbles Adhering to an Electrode Surface," International Meeting on Electrolytic Bubbles, London, England, September 13–14, 1984.
20. C.W. Tobias (presented by J.O. Dukovic), "Current Distribution at an Electrode with an Attached Bubble," International Meeting on Electrolytic Bubbles, London, England, September 13-14, 1984.†

†Supported by the Assistant Secretary of Conservation and Renewable Energy, Office of Energy Systems Research, Energy Storage Division of the U.S. Department of Energy under Contract No. DE-AC03-76SF00098.

‡Supported entirely by University funds.

§See further list of papers presented under "Other Publications."

HIGH-TEMPERATURE AND SURFACE CHEMISTRY

High-Temperature Thermodynamics*

Leo Brewer, Investigator

INTRODUCTION

The understanding of high-temperature chemistry is not only important for processes carried out at high temperature such as those of fusion and fission reactors and fossil-fuel power generators, but it is also important for the preparation and fabrication of ceramics, metals, semiconductors, and many other materials. The understanding of high-temperature behavior is complicated by the occurrence of unusual species and phases that are often unstable at conventional temperatures. It is difficult to carry out measurements to obtain the data needed for design of high-temperature systems. Thus it is most important to develop broad predictive models that provide reliable prediction of high-temperature behavior. The experiments in progress are aimed at the testing or development of such predictive models.

Previous research of this program has led to the development of a variety of successful models of predictive capability for the behavior of gases, refractory containment materials, and many metallic systems. As an example, it has been possible to calculate binary molybdenum phase diagrams with practical engineering accuracy even for systems for which no measurements have ever been reported. At the present time the main thrust of the research is aimed at providing quantitative predictive models for the strongly interacting transition-metal alloys exhibiting generalized Lewis acid-base behavior. A variety of experimental methods are being use to characterize the thermodynamics of these systems.

1. Generalized Lewis Acid-Base Titrations of Pairs of Transition Metals (Publication 1)

John K. Gibson,[†] Leo Brewer, and Karl A. Gingerich[‡]

The presently available chemical-bonding theories of transition-metal interactions allow one to indicate qualitatively that transition metals from the left-hand side of the periodic table with vacant d orbitals, including lanthanides and actinides, will interact strongly with the nonbonding electron pairs of the platinum-group metals to form some of the most stable compounds known. However, no models are available to allow prediction of the thermodynamic properties of such compounds with sufficient accuracy for practical engineering applications. The present experiments are designed to characterize the bonding capability of the various vacant orbitals serving as acids and the electron pairs that are nonbonding in the pure metals but that interact strongly as bases with metals such as titanium or niobium.

High-temperature (1425-2750 K) thermodynamic activities of one or both components of 25 binary alloys of a group IVB-VIB element (Ti, Zr, Hf, Nb, Ta, or W) with a platinum-group element (Ru, Os, Ir, Pd, Pt, or Au) have been determined by equilibrating the alloy with the appropriate carbide and graphite, equilibrating with the nitride and nitrogen gas, or measuring the partial vapor pressure(s) thermogravimetrically or mass-spectrometrically. The extraordinary stability of this class of transition-metal alloy is attributed to a generalized Lewis acid-base interaction involving valence d electrons, and the results of these investigations are interpreted within the context of this effect. Among the conclusions made are that a nonspherically symmetrical

*This work was supported by the Director, Office of Energy Research, Office of Basic Energy Sciences, Materials Sciences Division of the U.S. Department of Energy under Contract No. DE-AC03-76SF00098.

crystal field significantly reduces the bonding effectiveness of certain valence d orbitals; the effect of the extent of delocalization of these orbitals is also considered.

---

†Present address: Chemistry Division, Oak Ridge National Laboratory, Oak Ridge, Tennessee 37830.

‡Present address: Department of Chemistry, Texas A & M University, College Station, Texas 77843.

2. Work in Progress

A temperature-gradient furnace (described in Publication 2) is being used to check the stability ranges of high-temperature phases. In most of the literature, MoC is represented as being an unstable binary phase requiring the addition of nitrogen or iron to stabilize it. The present work has established that the binary phase is stable from low temperatures up to 1100°C . Additional systems are being chosen for study where the reported stability ranges are in contradiction to expectations of predictive models.

The characterization of metallic acid-base interactions reported in publications 1 and 3 is being extended by use of high-temperature electromotive measurements using solid electrolytes, vapor-pressure measurements above 2000°C using atomic fluorescence, and phase-equilibration studies.

As illustrated in Publication 4, thermodynamic data have been compiled and extended through predictive models to provide complete thermodynamic data for all of the elements from hydrogen to lawrencium and for their oxide condensed phases and gaseous oxide species. These data are being used with calculational programs to characterize the high-temperature behavior of the elements and their oxides.

The theoretical models for prediction of the high-temperature properties of materials are being tested against available data, and improvements are being made where necessary.

1984 PUBLICATIONS AND REPORTS

Refereed Journals

1. John K. Gibson, L. Brewer, and Karl A. Gingerich, "Thermodynamics of Several Lewis-Acid-Base Stabilized Transition Metal Alloys," Met. Trans. **15A**, 2075 (1984); LBL-16815.
2. L. Brewer and D.C. Davis, "Solute Stabilization for hcp-fcc Transitions: Co-Mo," Met, Trans. **15A**, 67 (1984); LBL-16649.
3. L. Brewer, "The Generalized Lewis Acid-Base Theory: Surprising Recent Developments," J. Chem. Educ. **61**, 101 (1984); LBL-14867.
4. L. Brewer, "The Responsibility of High Temperature Scientists," High Temperature Science **17**, 1 (1984); LBL-17310.

Other Publications

5. L. Brewer, "Gases (A) Spectroscopy of Interest to High-Temperature Chemistry, and (B) Reactions Between Gases and Condensed Phases," in *Bibliography on the High-temperature Chemistry and Physics of Materials,* Vol. 28, Part 2, M.B. Hocking and V. Vasantasree, eds., IUPAC Commission on High Temperatures and Refractory Materials, London, 1984; LBL-19005.

LBL Reports

6. L. Brewer, "Methods of Evaluation," to be published in *IUPAC Handbook of Thermodynamic and Transport Properties of Alkali Metals;* LBL-19007.
7. L. Brewer, "Chemical Bonding Concepts Applied to Metals and Their Alloys," to be published as a Materials Research Society Educational Module; LBL-19006.

Invited Talks

8. L. Brewer, "Refractory Sulfide Containers," Plutonium Conference, Lawrence Livermore Laboratory, Livermore, California, January 10, 1984.
9. L. Brewer, "Unusual Intermetallic Phases," San Francisco Bay Area Chemistry Teachers Conference, Pinole, California, April 28, 1984.
10. L. Brewer, "Serious Systemic Errors in High Temperature Equilibrium Measurements," Gordon Research Conference on High Temperature Chemistry, Wolfeboro, New Hampshire, July 26, 1984.

Chemistry and Materials Problems in Energy Production Technologies*

Donald R. Olander, Investigator

INTRODUCTION

The goal of this program is to characterize the chemical and physical behavior of materials in the high-temperature radiation environment of fission and fusion reactors. The principle interest is on both the materials of the uranium-based fuels and the zirconium-based cladding in light-water nuclear reactors. The processes and properties studied include rapid transient vaporization of fuel materials by laser pulsing, high-temperature corrosion of zirconium by steam, and the release of volatile fission products from irradiated UO_2. Another aspect of the program involves molecular-beam studies of the chemical kinetics of gas-solid reactions, including hydrogen-atom reactions with silicon and its compounds and the etching of metals by halogens.

1. Oxidation of Liquid Zircaloy by Steam (Publication 1)

D.R. Olander

The oxidation kinetics of liquid Zircaloy in contact with steam is analyzed as a two-medium moving-interface diffusion problem. The course of the corrosion process is strongly influenced by the state of the metal when it melts, in particular by the thickness of the oxide skin and the fractional oxygen saturation of the metal phase at this time. If the latter is small, the oxide skin rapidly thins by dissolution into the molten metal. However, the skin never vanishes as long as exterior steam is present; after attaining a minimum thickness, the ZrO_2 layer grows until all of the metal is consumed. If the average oxygen contact of the $\alpha + \beta$ phases prior to melting is close to saturation of the liquid metal, the initial oxide layer grows monotonically with time. Calculation of the times for the skin-thinning process and for complete consumption of the metal by oxygen depend on estimates of oxygen diffusion coefficients in the high-temperature phase of ZrO_2 as well as in the liquid metal.

*This work was supported by the Director, Office of Energy Research, Office of Basic Energy Sciences, Materials Sciences Division of the U.S. Department of Energy under Contract No. DE-AC03-76SF00098.

2. Tracer Surface Diffusion on Uranium Dioxide (Publication 2)

S.Y. Zhou† and D.R. Olander

Surface diffusion on UO_2 was measured by the spreading of U-234 tracer on the surface of a duplex diffusion couple consisting of wafers of depleted and enriched UO_2 joined by a bond of uranium metal. Spurious gas-phase transport was eliminated by a masking technique. Surface-diffusion coefficients measured at temperatures between 1760 and 2110°C ranged from 0.1 to 2 cm^2/s. These results correspond to Arrhenius-type behavior with an activation energy of 72 ± 15 kcal/mol and a preexponential factor of 5×10^6 cm^2/s, with a 1–2 order-of-magnitude uncertainty range to the preexponential factor. The preexponential factor was in reasonable accord with the nonlocalized surface-diffusion model of Bonzel, although the jump distance implicit in this theory appears to be unacceptably large. No significant effect of the atomic weight of the inert species in the gaseous environment at 1-atm pressure was detected, a result that is not inconsistent with the theory.

†Present address: Institute of Atomic Energy, Beijing, People's Republic of China.

3. Reaction of Modulated-Molecular-Beam Chlorine with Polycrystalline Iron (Publication 3)

Mehdi Balooch, Donald R. Olander, and Wigbert J. Siekhaus†

The volatilization of polycrystalline iron by chlorine gas has been studied by modulated-molecular-beam/ mass-spectrometric methods. The reaction was investigated in the temperature range 300–1250 K at equivalent chlorine pressures from 2×10^{-5} to 3×10^{-4} Torr. $FeCl_2$ was the only detectable volatile reaction product; its production rate increased rapidly with surface temperature and leveled off at ~1100 K. Studies of the composition of the reacting surface by laser-stimulated desorption and by electron spectroscopy for chemical analysis (ESCA) indicated the presence of a thin scale of a

substoichiometric iron chloride at the spot struck by the molecular beam. A reaction model based on diffusion of chlorine in the scale and production of gaseous $FeCl_2$ from parallel Eley-Rideal and Langmuir-Hinshelwood processes was developed by the molecular-beam data.

†Present address: Chemistry Division, Lawrence Livermore National Laboratory, Livermore, California 94550.

4. Reaction of Chlorine with Liquid Metals: Indium and Lead (Publications 4 and 5)

M. Balooch, W.J. Siekhaus,† and D.R. Olander

The reactions of molecular chlorine with liquid and solid indium surfaces were studied by modulated-molecular-beam/ mass-spectrometric methods in the temperature range 300–650 K at equivalent chlorine pressures of 4×10^{-6} to 4×10^{-4} Torr. In a separate chamber, the surface was monitored by Auger electron spectroscopy (AES) as a function of temperature at an effective chlorine pressure of 5×10^{-4} Torr. At high temperatures InCl was the only reaction product, while at low temperatures some $InCl_2$ was observed. Near the melting point the behavior of the scattered Cl_2 signal suggested a drastic change in sticking probability: The signal changed from that of a bare indium surface to one characterizing a chloride-covered surface. The reaction probability and phase lag of the InCl product also showed rapid variations in a temperature range approximately 30°C on either side of the melting point of the metal. A reaction model based on dissociative adsorption of chlorine was developed from the molecular-beam and AES data. The model applies to both solid and liquid indium substrates and, in accord with the data, contains no discontinuity at the melting point.

The reaction of molecular chlorine with solid and liquid lead surfaces was studied by modulated-molecular-beam/mass-spectrometric methods in the temperature range 300–900 K and at equivalent chlorine pressures between 5×10^{-6} and 5×10^{-4} Torr. The only detectable volatile reaction product was $PbCl_2$. Up to the melting point of lead (601 K), the apparent reaction probability did not exceed 10^{-3}. For the liquid phase, production of $PbCl_2$ increased rapidly with increasing surface temperature, and the reaction was nonlinear with respect to chlorine equivalent pressure. A reaction model was developed that takes into account both solution-diffusion of chlorine from the surface into the liquid and production of $PbCl_2$ by parallel Eley-Rideal and Langmuir-Hinshelwood mechanisms.

†Present address: Chemistry Division, Lawrence Livermore National Laboratory, Livermore, California 94550.

5. The Surface Chemistry of the Thermal Cracking of Silane on Silicon (111) (Publication 6)

M.K. Farnaam and D.R. Olander

The kinetics of the thermal decomposition of silane gas during epitaxial growth on the (111) face of single-crystal silicon was studied by modulated-molecular-beam/mass-spectrometry methods over the temperature range 1000–1440 K and with beam intensities from 2×10^{15} to 2×10^{16} molecules/cm^2·s. An abrupt change in the apparent reaction probability was observed at ~1130 K, coinciding with a known surface-structural transformation at about the same temperature. The molecular-beam data for temperatures higher than 1130 K were used for construction of a reaction model. Additional experiments were conducted to fix certain features of the reaction mechanism. An attempt was made to measure the rate constant for desorption of unreacted silane molecules from the surface. The residence time of silane on the surface was below the sensitivity limit of the technique (<5 μs), which means that SiH_4 desorption is not rate-limiting. Applications of a simultaneous modulated beam of SiH_4 and a steady beam of SiD_4 did not produce HD molecules, thus ruling out hydrogen-atom production in the surface-reaction mechanism. According to the proposed model, silane molecules that do not reflect from the surface undergo a branched reaction with two types of sites on the surface, producing two bound SiH_2 molecules in each chemisorption event. Subsequent surface decomposition of the adsorbed SiH_2 molecules occurs with different preexponential factors, although with similar activation energies of about 17 kcal/mol for the two types of sites.

6. Heat Effects in Zircaloy Oxidation by Steam (Publication 7)

Donald R. Olander

The partitioning of the heat of combustion during Zircaloy oxidation between the gas-oxide and

oxide-metal interfaces was determined. The spatial distribution of the heat release is very sensitive to the poorly known partial molar enthalpy of oxygen dissolution in ZrO_2. This uncertainty is of minor consequence in the thermal analysis, however, because temperature gradients in the specimen due to the heat released by oxidation are very small. The temperature is mainly a function only of time. A simple lumped-capacity thermal analysis suffices to describe the temperature transient initiated by the corrosion process. A method of coupling the temperature rise caused by the heat release to the corrosion kinetics was developed.

7. Work in Progress

Two aspects of the oxidation of zirconium by steam at high temperatures (1200°C–1600°C) are under investigation. The first is the measurement of the influence of hydrogen in the steam on the kinetics of corrosion. The second is the measurement of oxygen self-diffusion in the tetragonal form of ZrO_2, and the effect of hydrogen on this property. Both experiments use microbalance techniques.

The kinetics of the reaction of zirconium by uranium dioxide, which results in liquefaction of the latter at temperatures well below the melting point, will be investigated.

The interaction of molecular iodine and HI (typical chemical forms of fission-product iodine produced in a nuclear-reactor accident) with oxidized stainless steel will be studied mass spectrometrically. The objectives are to determine (1) whether there is significant retention of iodine by the metal and what the mechanism of retention is, and (2) whether the oxidized steel serves as an effective catalyst to equilibrate the chemical species in the gas.

Laser-pulsing experiments will remeasure the rapid transient vaporization of UO_2 to rectify a calibration error found in previous work.

The molecular beam will be used to study the reactions of atomic hydrogen with silicon single crystals and with silicon carbide.

1984 PUBLICATIONS AND REPORTS

Refereed Journals

1. D.R. Olander, "Oxidation of Liquid Zircaloy by Steam," J. Nucl. Mater. **119**, 245–250 (1983); LBL-15695.
2. S.Y. Zhou and D.R. Olander, "Tracer Surface Diffusion on Uranium Dioxide," Surf. Sci. **136**, 82–102 (1984); LBL-16070.
3. M. Balooch and D.R. Olander, "Reaction of Modulated-Molecular-Beam Chlorine with Polycrystalline Iron," J. Chem. Soc., Faraday Trans. 1 **80**, 61–71 (1984); UCRL-98163.
4. M. Balooch, W.J. Siekhaus, and D.R. Olander, "Reaction of Chlorine with Liquid Metals — I. Indium," J. Phys. Chem. **88**, 3521 (1984); LBL-16357.
5. M. Balooch, W.J. Siekhaus, and D.R. Olander, "Reaction of Chlorine with Liquid Metal — II. Lead," J. Phys. Chem. **88**, 3529 (1984); LBL-16356.
6. M.K. Farnaam and D.R. Olander, "Surface Chemistry of the Thermal Cracking of Silane on Silicon (111)," Surf. Sci. **145**, 390 (1984); LBL-16921.
7. D.R. Olander, "Heat Effects in Zircaloy Oxidation by Steam," J. Electrochem. Soc. **131**, 2161 (1984); LBL-15465.

LBL Reports

8. M. Balooch, D. Olander, J. Abrefah, and W.J. Siekhaus, "Time-Resolved Auger Electron Spectroscopy Combined with Modulated Molecular Beam Techniques for Gas-Surface Reaction Kinetics Studies," LBL-18204.
9. M. Balooch, D.R. Olander, and W.J. Siekhaus, "Ion-Enhanced Chemical Reaction of XeF_2 with Silicon by Modulated Molecular Beam Mass Spectrometry," LBL-18549.

Invited Talks

10. D.R. Olander, "Heat Effect in Zircaloy Oxidation," Fourth International Conference on High-Temperature and Energy-Related Materials, Santa Fe, New Mexico, April 2, 1984.
11. D.R. Olander, "Release of Volatile Fission Products from UO_2," Topical Meeting of the American Nuclear Society on Fission Product Behavior and Source Term Research, Snowbird, Utah, July 16, 1984.
12. D.R. Olander, "Transient Vaporization of Refractory Solids by Laser Pulse Heating," Gordon Research Conference on High-Temperature Chemistry, Wolfeboro, New Hampshire, July 24, 1984.
13. M. Balooch, "Ion-Enhanced Chemical Reaction of XeF_2 with Silicon by Modulated Molecular Beam Mass Spectrometry," Meeting of the Materials Research Society, Boston, Massachusetts, November 26–30, 1984.

Plasma-Enhanced Deposition of Thin Films*

Dennis W. Hess, Investigator

INTRODUCTION

This program is designed to establish scientific foundations for the rf plasma-enhanced deposition of thin films and thereby create a unique synthetic capability for a wide spectrum of thin-film materials whose chemical, physical, and electrical properties can be controlled by varying the deposition parameters. The film structures (amorphous, polycrystalline, and crystalline), chemical composition, optical properties, magnetic properties, and conductivity (ionic and electronic) will be correlated with such plasma-deposition variables as rf power, rf frequency, substrate temperature, gas pressure, gas dynamics, source materials, and electrode spacing. Kinetic models are being developed so that increased understanding of the relationships between the deposition parameters and the resulting film properties can be obtained. Furthermore, these endeavors will assist in the elucidation of the chemistry occurring within the plasma. Results from these studies will be applied to such technologically important areas as solar-cell fabrication and structure-property relationships in catalyst-support materials.

1. Photoelectrochemical Properties of Plasma-Deposited TiO_2 Films (Publication 1)

Larry M. Williams† and Dennis W. Hess

Photoanodes were fabricated from TiO_2 films deposited onto titanium substrates by plasma-enhanced chemical-vapor deposition. The photocurrent-wavelength and photocurrent-voltage properties of the anodes were determined and compared with those of thermally grown TiO_2 photoanodes. The plasma-deposited photoanodes displayed quantum efficiencies higher than those for the thermally grown films and comparable with those reported for single-crystal rutile. The microstructure of the plasma-deposited films appeared to be primarily responsible for the high quantum efficiencies.

†Present address: Bell Laboratories, Murray Hill, New Jersey.

*This work was supported by the Director, Office of Energy Research, Office of Basic Energy Sciences, Materials Sciences Division of the U.S. Department of Energy under Contract No. DE-AC03-76SF00098.

1984 PUBLICATIONS AND REPORTS

Refereed Journals

1. L.M. Williams and D.W. Hess, "Photoelectrochemical Properties of Plasma-Deposited TiO_2 Thin Films," Thin Solid Films **115**, 13 (1984).
2. C.S. Blair and D.W. Hess, "Capacitance-Voltage Technique for the Determination of Carrier Concentrations in Thin Film Photoanodes," J. Electrochem. Soc. **131**, 932 (1984); LBL-16285.

Invited Talks

3. D.W. Hess, "The Effect of rf Glow Discharge Atmospheres on Thin Film Material Properties," Institute for Energy Conversion, University of Delaware, Newark, April 1984.

Electrochemical Phase Boundaries*

Rolf H. Muller, Investigator

INTRODUCTION

The purpose of this work is to advance the understanding of boundary layers and thin films at electrochemical interfaces. Boundary layers control the chemical environment in which electrode processes take place and are often responsible for limiting the specific rate at which reactions can be conducted. Thin films and adsorbed layers on electrodes greatly affect the kinetics of electrode reactions, such as the electrodeposition and dissolution of metals, and control the chemical properties of most metals in liquid environments. New optical techniques for the observation of electrode surfaces in liquid media are developed and used. They include spectroscopic ellipsometry combined with light-scattering measurement and Auger spectroscopy, interferometry, thin-film interference, and Doppler velocimetry. Research on electrochemical mass transfer and high-rate electrodeposition and dissolution, conducted jointly with C.W. Tobias, is described under "Electrochemical Processes," C.W. Tobias, Investigator. Another project, "Surface Layers on Battery Materials," supported by the Assistant Secretary for Conservation and Renewable Energy, Office of Energy Systems Research, Energy Storage Division of the U.S. Department of Energy, is reported under "Electrochemical Energy Storage."

1. Spectroscopic Ellipsometry of Rhodamine-B Adsorbed on Platinum, Silver, and Copper (Publication 2)

Joseph C. Farmer† and Rolf H. Muller

The use of spectroscopic ellipsometry has been investigated to determine the number and orientation of dye molecules adsorbed from solution and to find whether a specific orientation is responsible for the inhibiting effect in cathodic metal deposition. Rhodamine-B, shown schematically in Figure 1-1, was chosen as the dye because it is well characterized optically and structurally and available in high purity at low cost. Its electronic-transition moment for light adsorption lies in the plane of the aromatic rings. In solution, it absorbs light in the spectral range (370-720 nm) accessible to the spectroscopic ellipsometer.[1] Among 30 model inhibitors tested, Rhodamine-B showed the largest electrochemical effect for the electrodeposition of Pb. Substrates used were Pt, Ag, and Cu. The electrolyte was 1M $NaClO_4$, 5 mM $Pb(NO_3)_2$, 0.5-20 μM dye, acidified to a pH of 3 with $HClO_4$.

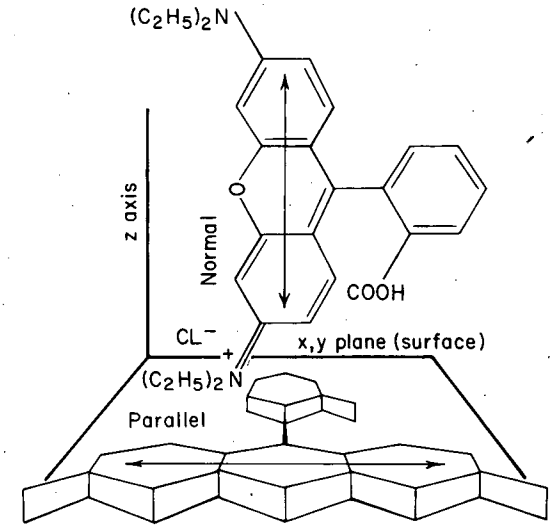

Figure 1-1. Limiting orientations of adsorbed Rhodamine-B molecules with electronic-transition moment, shown by arrows, normal or parallel to the electrode surface, represented by the x-y plane. (XBL 829-11874A)

The principal feature of the adsorbed dye layer is its large extinction coefficient at the wavelength of maximum absorption; at other wavelengths its optical constants are similar to those of the solvent, with a very small extinction coefficient. Oriented adsorbed dye molecules produce dichroism in the adsorbate layer because the electric-field vector parallel to the electronic-transition moment of the dye molecule is attenuated to a much greater extent than that normal to it. Molecular orientations and number densities were estimated from the thickness and the ordinary and extraordinary complex refractive indices of the adsorbed layer derived from the measurements. Coverages near 50% of close packing were found with primarily normal orientation on Ag and with mixed orientations on Pt and Cu. Electronic interaction of the adsorbate with the substrate

*This work was supported by the Director, Office of Energy Research, Office of Basic Energy Sciences, Materials Sciences Division of the U.S. Department of Energy under Contract No. DE-AC03-76SF00098.

can be recognized as spectral shifts in the absorption. Observations during readsorption of dye after electrochemical reduction indicate that molecules oriented normal to the surface had been reduced and are responsible for electrochemical-inhibition effects.

†Present address: Sandia Laboratory, Livermore, California 94550.

1. R.H. Muller and J.C. Farmer, *Proc. Int. Conf. Ellipsometry and other Optical Methods for Surface and Thin Film Analysis,* Paris, June 7–10, 1983; R.H. Muller and J.C. Farmer, J. de Phys. **44**, C10–57 (1983); R.H. Muller and J.C. Farmer, Rev. Sci. Instrum. **55**, 371 (1984).

2. Effects of Ion Bombardment on the Morphology of Lead Films (Publication 8)

Michael J. Armstrong and Rolf H. Muller

The effects of ion bombardment on the morphology of compact lead films were investigated with spectroscopic ellipsometry, Auger electron spectroscopy (AES), and scanning electron microscopy. The lead films studied were electrochemical and vacuum-vapor deposits under 100 nm thick. In contrast to the uniform removal of the surface by ion bombardment, assumed in the determination of composition profiles by AES, a nonuniform removal of the surface occurred upon ion bombardment, resulting in pitting or island formation. This pitting is independent of the mode of deposition of the film and the presence of an oxide overlayer. An optical model of a film distributed as islands (see Figure 2-1) was used to interpret spectroscopic ellipsometry measurements. The model was based on the coherent superposition of polarization states resulting from reflection on adjacent bare and film-covered surface elements.[1] Scanning electron micrographs confirmed the island nature of the surface morphology. The surface coverage of lead derived from spectroscopic ellipsometer measurements agreed with that derived from AES (see Figure 2-2).

1. R.H. Muller and J.C. Farmer, Surf. Sci. **135**, 525 (1983).

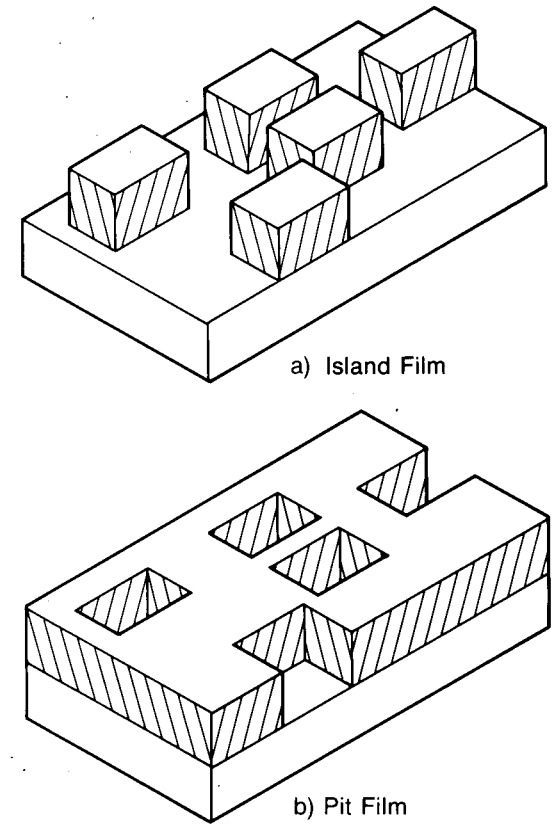

Figure 2-1. Schematic of island and pitted films formed by ion bombardment: (a) island film, continuous substrate surface; (b) pitted film, continuous film-covered surface. (XBL 847-10702)

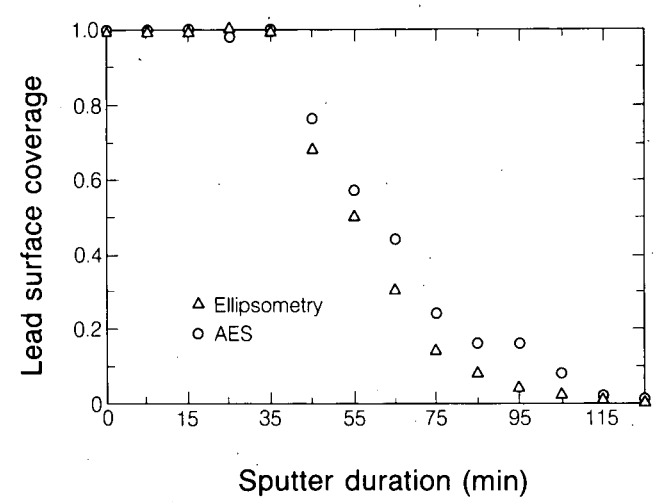

Figure 2-2. Fraction of a copper surface covered by lead as a function of sputter duration for an 0.039 C/cm^2 (369-Å compact) electrochemical deposit of lead. The coverage was determined by both Auger electron spectroscopy (circles) and spectroscopic ellipsometry (triangles). (XBL 847-9848)

3. Interferometric Observation of Turbulent Mass Transfer in Channel Flow (Publication 7)

F.R. McLarnon, R.H. Muller, and C.W. Tobias

A traveling, dual-beam laser interferometer[1] has been used to investigate mass-transfer boundary layers on planar electrodes in turbulent-channel flow. The effect of secondary flows induced near the electrode/electrolyte interface by small flow obstacles in laminar bulk flow is compared to the effect of turbulent bulk flow produced by high electrolyte flow rates in an obstacle-free flow channel (see Figure 3-1). Mass-transfer enhancement can be attained more efficiently by the use of small flow obstacles than by the use of high flow velocities.

1. K.W. Beach, R.H. Muller, and C.W. Tobias, Rev. Sci. Instrum. **40**, 1248 (1969).

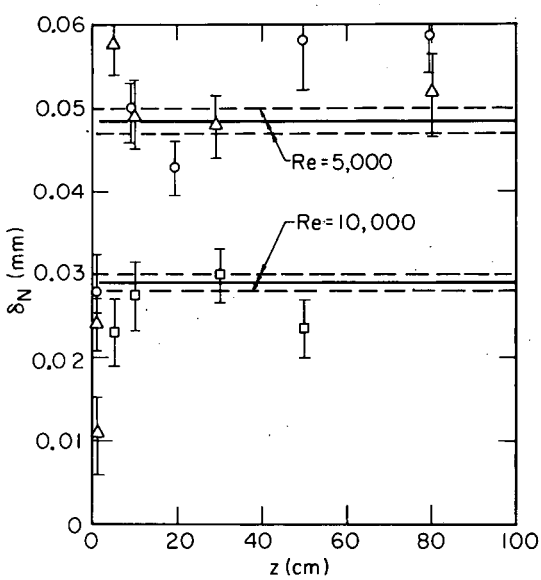

Figure 3-1. Turbulent boundary-layer thicknesses. The ordinate is the Nernst boundary-layer thickness δ_N (mm), and the abscissa is the distance z from the cathode leading edge (cm). Solid lines show the computed thickness, with the error limits, due to a 10% uncertainty in diffusion-coefficient data, indicated by dashed lines. The points were derived from experimental interferograms, with Re = 5000 and i_{avg} = 15.0 mA/cm^2 (circles), Re = 5000 and i_{avg} = 25.0 mA/cm^2 (triangles), and Re = 10,000 and i_{avg} = 25.0 mA/cm^2 (squares). (XBL 7411-8229)

4. Work in Progress

Surface forces responsible for the formation of liquid films on metal surfaces are being investigated by use of optical thin-film interference. Criteria for the stability of such films are of interest in gas evolution processes, corrosion, and fuel cells.

1984 PUBLICATIONS AND REPORTS

Refereed Journals

1. R.H. Muller and J.C. Farmer, "Fast, Self-Compensating Spectral-Scanning Ellipsometer," Rev. Sci. Instrum. **55**, 371 (1984); LBL-16703.

Other Publications

2. J.C. Farmer and R.H. Muller, "Spectroscopic Ellipsometry of Rhodamine-B Adsorbed on Platinum, Silver and Copper," in *Proc. Int. Soc. Electrochem.*, Berkeley, California, August 5–10, 1984, Ext. Abs. No. A8-8; LBL-17852.
3. Corinne A. Coughanowr, Rolf H. Muller, and Charles W. Tobias, "Electrochemical Machining of Cemented Titanium Carbide," in Proc. *Int. Soc. Electrochem.*, Berkeley, California, August 5–10, 1984, Ext. Abs. No. B3-27; LBL-18922abs.

LBL Reports

4. J.C. Farmer and R.H. Muller, "Effect of Rhodamine-B on the Electrodeposition of Lead on Copper," submitted to J. Electrochem. Soc.; LBL-17014 Rev.
5. C.A. Coughanowr, R.H. Muller, B.A. Dissaux, and C.W. Tobias, "Electrochemical Machining of Refractory Materials," submitted to J. Appl. Electrochem.; LBL-18365.
6. D.S. Fischl, K.J. Hanson, C.W. Tobias, and R.H. Muller, "Mass Transfer Enhancement by Small Flow Obstacles in Electrochemical Cells," submitted to Chem. Engr. Comm.; LBL-18476.
7. F.R. McLarnon, C.W. Tobias, and R.H. Muller, "Interferometric Observation of Turbulent Mass Transfer in Channel Flow," submitted to J. Electrochem. Soc.; LBL-18575.
8. Michael T. Armstrong (M.S. Thesis), with R.H. Muller, "Effect of Ion Bombardment on the Morphology of Lead Films," LBL-18784.

Invited Talks

9. Rolf H. Muller, Introduction to Norbert Ibl Symposium, International Society of Electrochemistry Meeting, Berkeley, California, August 5-10, 1984.

Solid-State and Surface Reactions*

Gabor A. Somorjai, Investigator

INTRODUCTION

This research program is centered on studies of catalyzed surface reactions and investigations of the atomic structure and chemical composition of solid surfaces and adsorbed monolayers. The kinetics and mechanisms of catalytic surface reactions are studied for well-characterized crystal surfaces at low and high pressures by using a combination of surface-science techniques.

The materials that are the focus of our studies are platinum, molybdenum, rhenium, rhodium, iron, vanadium, and their compounds, alkali metals, and bimetallic alloys. The adsorbates and reactants are mostly hydrocarbons, oxygen, hydrogen, and water.

Part of the investigation is directed toward atomic-scale understanding of the structure and catalytic behavior of metal surfaces. The other part is aimed at developing new catalyst materials that substitute for precious metals and exhibit high reaction rates and selectivity.

STRUCTURE AND BONDING

1. Ligand Effects for CO and H_2 Chemisorption on a Polycrystalline Pt_3Ti Surface (Publication 1)†

U. Bardi,‡ G.A. Somorjai, and P.N. Ross

We have undertaken a study of the surface chemisorption properties of the Pt_3Ti intermetallic compound. The techniques used included Auger electron spectroscopy (AES), thermal-desorption spectroscopy (TDS), and x-ray diffraction. We have found that the alloy has the bulk fcc structure of $AuCu_3$. Auger spectroscopy indicates that annealing restores the stoichiometry of the surface that is lost in the cleaning processes using Ar sputtering. CO chemisorption is found to occur with a reduced bond energy as compared to the nonalloyed Pt. H_2 chemisorption is strongly reduced in the alloy. We believe that these observations are a result of a ligand effect, i.e., a modification of the Pt chemical properties caused by charge redistribution on forming the Pt-Ti bonds.

*This work was supported by the Director, Office of Energy Research, Office of Basic Energy Sciences, Materials Sciences Division of the U.S. Department of Energy under Contract No. DE-AC03-76SF00098.

†Supported in part by the Assistant Secretary for Fossil Energy, Office of Fuel Cells, Advanced Concepts Division of the U.S. Department of Energy under Contract No. DE-AC03-76SF00098.

‡Permanent address: Institute of Physical Chemistry, University of Florence, Italy.

2. Surface Studies by Optical Second-Harmonic Generation: The Adsorption of O_2, CO, and Sodium on the Rh(111) Surface (Publication 2)

H.W.K. Tom, C.M. Mate, X.D. Zhu, J.E. Crowell,† T.F. Heinz, G.A. Somorjai, and Y.R. Shen

Optical second-harmonic generation (SHG) is used to study the adsorption of atomic and diatomic species on a well-characterized Rh(111) crystal surface in ultrahigh vacuum. The results correlate well with those obtained by other surface probes. This result clears the way for the successful application of SHG to other systems of interest in surface science and catalysis. The very high detection sensitivity, the extremely fast response, and the nondestructive nature of the technique should make it a unique and most useful surface tool.

†Present address: Department of Chemistry, University of Pittsburgh, Pittsburgh, Pennsylvania 15260.

3. Hydrogenation and H,D Exchange Studies of Ethylidyne (CCH_3) on Rh(111) Crystal Surfaces at 1 Atm Pressure Using High-Resolution Electron-Energy-Loss Spectroscopy (Publication 3)

B.E. Koel,† B.E. Bent, and G.A. Somorjai.

We have combined high-resolution electron-energy-loss spectroscopy (HREELS) with a high-pressure/low-pressure (HPLP) system to study the behavior of the monolayer structure of stable hydrocarbon species that form on single-crystal metal surfaces during catalytic reactions at atmospheric pressure. We find that a monolayer of adsorbed ethylidyne (CCH_3) on Rh(111) at 310 K does not hydrogenate to ethylene or ethane in one atmosphere

of static D_2. The methyl-group hydrogen exchange with deuterium is a slow process. The amount of exchange depends strongly on the amount of uncovered, bare-metal surface, but it depends little on the hydrogen pressure. A mechanism for H,D exchange involving ethylidene ($CHCH_3$) as an intermediate is proposed.

†Present address: Department of Chemistry, University of Colorado, Boulder 80309.

4. On the Absolute Coverage of Ethylene on Pt(111) Single-Crystal Surfaces (Publication 28)

W.T. Tysoe,† F. Zaera,‡ S.M. Davis,§ and G.A. Somorjai

The absolute saturation coverage of ethylene on Pt(111) surfaces has been determined by four independent techniques: x-ray photoelectron spectroscopy (XPS), AES, H_2 TDS, and a ^{14}C radiotracer technique. These techniques all suggest a value of one quarter at a monolayer of saturation coverage.

†Present address: Department of Chemistry, University of Wisconsin, Milwaukee 53201.

‡Present address: Brookhaven National Laboratory, Upton, New York 11973.

§Present address: Exxon Research and Development Laboratory, Baton Rouge, Louisiana 70821.

5. The Modification of Benzene and CO Adsorption on Pt(111) by the Coadsorption of Potassium or Sulfur (Publication 29)

E.L. Garfunkel,† M.H. Farias,‡ and G.A. Somorjai

The effects of potassium and sulfur on the chemisorption of CO and benzene on the Pt(111) surface have been studied by TDS. Potassium causes an increase in the desorption peak temperature of CO and a decrease in that of benzene. Sulfur, on the other hand, causes a decrease in the desorption peak temperatures for both benzene and CO. We interpret the effects of potassium on CO and benzene adsorption as electronic, while for sulfur, structural effects may dominate.

†Present address: Wright-Reiman Laboratory, Department of Chemistry, Rutgers University, New Brunswick, New Jersey 08903.

‡Present address: Instituto de Fisica, UNAM, Ensenada, Baja California, Mexico.

6. The Interaction of Oxygen with the Mo(100) and Mo(111) Single-Crystal Surfaces: Chemisorption and Oxidation at High Temperatures (Publication 30)

C. Zhang, M.A. Van Hove, and G.A. Somorjai

The interaction of oxygen with Mo(100) and Mo(111) surfaces was studied by AES, low-energy electron diffraction (LEED), and TDS over a wide range of oxygen pressure ($1 \times 10^{-8} - 5 \times 10^{-5}$ Torr), temperature (823–1200 K), and exposure (0.1–10,000 Langmuir). With increasing oxygen exposure on Mo(100), the chemisorption structures p(1 × 1), c(4 × 4), p(2 × 1), ($\sqrt{5}\times\sqrt{5}$) R26°33′, p(2 × 1), p(4 × 1), c(2 × 2), and p(2 × 1) are detected and followed by the formation of (110) and (112) facets. On Mo(111), the (4 × 4) and (1 × 3) surface structures are detected and followed by the formation of (112) facets with (2 × 1) and then (3 × 1) superlattices. For exposures exceeding ~2000 Langmuir, an oxide grows on the facets. On Mo(100), the oxide formed from 823 to 1050 K contains domains of MoO_2(110) surface parallel to the Mo(100) plane, while from 1050 to 1150 K the MoO_2(110) domains are tilted ~5° away from the Mo(100) surface. On Mo(111), the oxide contains domains of MoO_2(100) surface tilted by 19.5° away from the Mo(111) surface, i.e., parallel to Mo(112) facets. The AES results show metal oxidation states corresponding to (presumably disordered) MoO_3 and an intermediate oxide, in addition to MoO_2. The higher-valence oxide seems to be a stable compound on the oxide surface.

7. Radiotracer and Thermal-Desorption Studies of Dehydrogenation and Atmospheric Hydrogenation of Organic Fragments Obtained from ^{14}C Ethylene Chemisorbed over Pt(111) Surfaces (Publication 31)

S.M. Davis,† F. Zaera,‡ B.E. Gordon, and G.A. Somorjai

The energetics and reversibility of ethylene sequential dehydrogenation on the (111) platinum single-crystal surface have been investigated at

300–600 K using TDS and a carbon-14 radiotracer technique. Ethylidyne species produced by ^{14}C-C_2H_4 chemisorption at 300–400 K were stable with respect to hydrogenation at room temperature. However, at atmospheric hydrogen pressure and temperatures above 350 K, ethylidyne species were easily eliminated from the platinum surface by hydrogenation. For ^{14}C-C_2H_4 adsorption temperatures above 450 K, radiotracer studies revealed the presence of both "active" and "inactive" forms of partially dehydrogenated carbonaceous deposits on the platinum surface that differ greatly in their reactivity for hydrogenation and hydrogen transfer with unlabeled hydrocarbons. The inactive fraction increased with increasing adsorption temperature as the surface species became more hydrogen deficient. Removal of the active ^{14}C-containing species by hydrogen transfer occurred readily.

†Present address: Exxon Research and Development Laboratory, Baton Rouge, Louisiana 70821.

‡Present address: Brookhaven National Laboratory, Upton, New York 11973.

8. The Interpretation of Diffuse LEED Intensities (Publication 32)

D.K. Saldin,† J.B. Pendry,† M.A. Van Hove, and G.A. Somorjai

We have shown that the diffuse LEED that occurs between sharp LEED beams can be used to determine the local bonding configuration near disordered surface atoms. Two approaches to the calculation of diffuse LEED intensities are presented for the case of lattice-gas disorder of an adsorbate on a crystalline substrate. The capabilities of this technique are most similar to those of near-edge x-ray absorption fine structure (NEXAFS), but it avoids the restrictions of NEXAFS caused by the use of photons.

†Permanent address: The Blackett Laboratory, Imperial College, London SW7 2BZ, England.

9. Adsorbate-Adsorbate Interactions and the Ordering of Organic Monolayers on Metal Surfaces (Publication 33)

A. Gavezzotti,† M. Simonetta,† M.A. Van Hove, and G.A. Somorjai

To study the ordering of molecules adsorbed on single-crystal substrates, we define a molecular cross section (MCS), which measures the surface area occupied by each molecule. With this MCS, a two-dimensional packing coefficient C_{2D} can then be defined for ordered arrays of adsorbed molecules. We have analyzed values and trends for MCS and $C_{2D}$for known surface structures, especially for benzene adsorbed on metal surfaces. The packing is found to be generally less dense at surfaces than one would expect from comparison with packing in three-dimensional organic crystals. The Van der Waals packing energy and the repulsive dipole-dipole energy are also computed to study this issue. The lack of close packing is attributed to the need to respect structural coincidence with the substrate and/or coadsorption of small molecules like CO. These concepts are then applied to the prediction of the long-range order that a monolayer of adsorbed molecules may adopt; thereby possible adsorption structures can be defined, restricting the number of possibilities in a further structural determination.

†Permanent address: Dipartimento di Chimica Fisica ed Elettrochimia e, Centro CNR, 20133 Milano, Italy.

10. The Adsorbate-Induced Faceting of the Mo(111) Surface (Publication 34)

C. Zhang, A.J. Gellman, M.H. Farias,† and G.A. Somorjai

We have observed the faceting of the Mo(111) surface in the presence of adsorbed nitrogen, oxygen, sulfur, and carbon monoxide: The similarities in the surface structural rearrangements observed on going from one adsorbate to another are striking. All facet

planes produced have the form (112) × n(111) where n = O for oxygen, n = 2 for nitrogen and carbon monoxide, and n = 4 for sulfur. The resulting planes are the (112), (334), and (556) surfaces, respectively. In the cases of the atomic adsorbates, the component of the (112) plane present in the facet is seen to increase with increasing electronegativity.

†Present address: Instituto de Fisica, UNAM, Ensenada, Baja California, Mexico.

11. Potassium-Coadsorption-Induced Dissociation of CO on the Rh(111) Crystal Surface: An Isotope-Mixing Study (Publication 35)

J. Crowell,† W.T. Tysoe,‡ and G.A. Somorjai

The formation of $C^{13}O^{18}$ from a mixture of $C^{13}O^{16}$ and $C^{12}O^{18}$ proves unequivocally that molecular CO dissociates on Rh(111) when potassium is coadsorbed. The presence of a surface complex between the alkali metal and the CO is confirmed by the simultaneous desorption of potassium and CO. A minimum of 0.08 potassium atoms per surface Rh atom is necessary to induce any CO dissociation. A maximum of three CO molecules is observed to dissociate per potassium atom.

†Present address: Department of Chemistry, University of Pittsburgh, Pittsburgh, Pennsylvania 15260.

‡Present address: Department of Chemistry, University of Wisconsin, Milwaukee 53201.

12. The Chemisorption of O_2, CO, D_2, and C_2H_4 Over Epitaxially Grown Rhenium Crystalline Films (Publication 36)

F. Zaera† and G.A. Somorjai

The adsorption and desorption of oxygen, carbon monoxide, deuterium, and ethylene has been studied over rhenium films using TDS, LEED, and AES. The films, obtained by evaporating rhenium onto a platinum (111) single crystal, grow over the substrate forming (0001) basal-plane rhenium surfaces. Oxygen chemisorbs on this film, forming an ordered structure consisting of three (2 × 1) overlayer domains and giving a saturation coverage of half a monolayer of atomic oxygen. CO chemisorption is mainly molecular, although some dissociation occurs at temperatures above ~700 K. A complicated LEED pattern is obtained when saturating the surface at 150 K with CO, but it changes to a (2 × 2) or (2 × 1) structure on heating. Also, CO chemisorption can be modified by predissociated CO or preadsorbed oxygen on the rhenium surface. Deuterium desorbs in three peaks, starting at temperatures as low as 150 K. Ethylene desorbs partially intact at around 250 K, the rest decomposing and yielding hydrogen, which appears as two main peaks at 357 K and 460 K during thermal desorption. We conclude that epitaxially grown films may be an alternative to single crystals for studying chemisorption over well-ordered surfaces.

†Present address: Brookhaven National Laboratory, Upton, New York 11973.

13. An Ultraviolet Photoelectron Spectroscopy (UPS) Study of the Interaction of Potassium with Carbon Monoxide and Benzene on the Pt(111) Surface (Publication 37)

M. Kudo,† E.L. Garfunkel,‡ and G.A. Somorjai

The interaction of potassium with carbon monoxide and benzene has been studied on the Pt(111) crystal surface by UPS. The adsorptive changes reported in previous studies for carbon monoxide and benzene when potassium is coadsorbed are correlated with the UPS results presented here and are explained with the aid of a molecular-orbital analysis. We find that the valence molecular orbitals increase their binding energy slightly when the potassium is coadsorbed, implying a model in which the adsorbates sense the potassium-induced changes in the dipole field at the surface.

†Present address: Institute of Industrial Science, University of Tokyo, Japan.

‡Present address: Wright-Reiman Laboratory, Department of Chemistry, Rutgers University, New Brunswick, New Jersey 08903.

14. Carbon Monoxide-Induced Ordering of Benzene on Rh(111) and Pt(111) Crystal Surfaces (Publication 38)

C.M. Mate and G.A. Somorjai

Carbon monoxide-induced ordering of an organic molecule, benzene, has been studied on the Pt(111) and Rh(111) crystal surfaces using LEED and HREELS. We propose detailed geometries for all the ordered structures of coadsorbed CO and benzene. Ordering in the adsorbed overlayer results from the attractive interaction between coadsorbed CO and benzene.

15. A Comparison of Gas-Phase and Electrochemical Hydrogenation of Ethylene at Platinum Surfaces (Publication 39)

A. Wieckowski,[†] S.D. Rosasco,[†] G.N. Salaita,[†] A. Hubbard,[†] B.E. Bent, F. Zaera,[‡] and G.A. Somorjai

Rates of hydrogenation of ethylene to ethane under gas-solid (G-S) and liquid-solid (L-S) (i.e., electrochemical) conditions at well-defined Pt(111) and smooth polycrystalline Pt surfaces have been measured. The activation energies are 5.9 kcal/mole for the L-S reaction and 10.8 kcal/mole for the G-S reaction. Comparison of the rate laws under appropriate conditions shows that the hydrogenation proceeds by different reaction mechanisms at the two different interfaces. We have used surface-science techniques (LEED, AES, HREELS, temperature-programmed desorption) and electrochemistry (a combination of solution and ultrahigh-vacuum procedures) to characterize the adsorbed species formed under G-S and L-S reaction conditions and to gain insight into the reaction mechanisms. We propose that in hydrogenation at the L-S interface, ethylene is reduced on the Pt surface by adsorbed H atoms, while during hydrogenation at the G-S interface, H atoms must be transferred from the Pt surface through a layer of irreversibly adsorbed ethylene to ethylene that is adsorbed on top of this layer.

[†]Permanent address: Department of Chemistry, University of California, Santa Barbara 93106.

[‡]Present address: Brookhaven National Laboratory, Upton, New York 11973.

CATALYSIS

16. Molecular Ingredients of Heterogeneous Catalysis (Publication 4)

G.A. Somorjai and R.C. Yeates

We have assembled a review and status report of the rapidly developing surface science of heterogeneous catalysis. We describe the experimental results that identified three molecular ingredients of catalysis: (1) structure, (2) carbonaceous deposit, and (3) the oxidation state of surface atoms. The hydrogenation of ethylene at both the gas-solid and liquid-solid interfaces is described.

17. A Model for Vibrational and Translational Energy Accommodation of NO Molecules During Scattering from a Pt(111) Crystal Surface (Publication 40)

M. Asscher,[†] E. Pollak,[‡] and G.A. Somorjai

A model is formulated and applied to the recently measured vibrational and translational accommodation of NO scattered from a Pt(111) crystal surface. The model assumes that the initial adsorption of NO occurs via a precursor state. Experimentally observed memory of the incident energy by the scattered molecules is a result of competition between chemisorption and desorption from the precursor state.

[†]Present address: Department of Physical Chemistry, The Hebrew University of Jerusalem, Israel.

[‡]Present address: Chemical Physics Department, Weizmann Institute of Science, Rehovot, Israel.

18. Energy Redistribution in Diatomic Molecules on Surfaces (Publication 27)

M. Asscher[†] and G.A. Somorjai

Translational and internal degrees of freedom of a scattered beam of NO molecules from a Pt(111) single-crystal surface were measured as a function of scattering angle and crystal temperature in the range 450–1250 K. None of the three degrees of freedom were found to fully accommodate to the crystal temperature, the translational degree being the most

accommodated and the rotational degree of freedom the least. A precursor-state model is suggested to account for the incomplete accommodation of translational and vibrational degrees of freedom as a function of crystal temperature and incident-beam energy. The vibrational accommodation is further discussed in terms of a competition between desorption and vibrational excitation processes, thus providing valuable information on the interaction between vibrationally excited molecules and surfaces. Energy transfer into rotational degrees of freedom is qualitatively discussed.

---

†Present address: Department of Physical Chemistry, The Hebrew University of Jerusalem, Israel.

19. The Reaction of Ethane with Deuterium over Pt(111) Single-Crystal Surfaces (Publication 41)

F. Zaera† and G.A. Somorjai

Deuterium exchange and hydrogenolysis of ethane were studied over Pt(111) surfaces under atmospheric pressures and a temperature range of 475–625 K. Activation energies of 19 Kcal/mole for exchange and 34 kcal/mole for hydrogenolysis were obtained. The exchange-reaction rates displayed kinetic orders with respect to deuterium and ethane partial pressures of −0.55 and 1.2, respectively. The exchange-product distribution was U-shaped, peaking at one and six deuterium atoms per ethane molecule, similar to results reported for other forms of platinum, e.g., supported, films, and foils. The presence of ethylidyne moieties on the surface was inferred from LEED and TDS. A mechanism is proposed to explain the experimental results, in which ethylidyne constitutes an intermediate in one of two competitive pathways.

---

†Present address: Brookhaven National Laboratory, Upton, New York 11973.

20. The Oscillatory Behavior of the CO Oxidation Reaction at Atmospheric Pressure over Platinum Single Crystals: Surface Analysis and Pressure-Dependent Mechanisms (Publication 42)

R.C. Yeates, J.E. Turner,† A.J. Gellman, and G.A. Somorjai

The oscillatory behavior of the catalyzed oxidation of carbon monoxide has been studied over platinum single crystals of (111), (100), and (13,1,1) orientation. Surface properties were examined in ultrahigh vacuum, before and after the reaction, using AES, LEED, and a Kelvin probe for work-function measurements. The oxidation of carbon monoxide was carried out at both low pressure (10^{-4} Torr) and atmospheric pressure. The mechanism for the oscillations was different at high and low pressures. A model is presented for the oscillations appearing in the high-pressure reaction. This model invokes the formation of platinum oxide, the presence of which was determined experimentally. At atmospheric pressure, silicon was always present on the platinum surfaces and was necessary to detect oscillatory behavior.

---

†Present address: Materials Research Laboratory, Hewlett-Packard, Palo Alto, California 94304.

21. Ammonia Synthesis Over Rhenium Single-Crystal Catalysts: Structure Sensitivity, Kinetics, and the Effects of K and O (Publication 43)

M. Asscher,† J. Carrazza, M.M. Khan,‡ K.B. Lewis, and G.A. Somorjai

Ammonia synthesis was investigated over model single-crystal and polycrystalline foil rhenium catalysts at 20-atm reactant pressure and in the 720–900 K temperature range. The structure sensitivity of this reaction on four rhenium single crystals was studied. A remarkable sensitivity to the

catalysts' surface structure was observed, with reactivity ratios of 1:94:920:2820 for the Re(0001), Re(1010), Re(1120), and Re(1121) crystal faces, respectively. The importance of high-coordination metal atom sites both in the first and in the second layers is clearly indicated by these results. An apparent activation energy for the reaction of 20.4 ± 1.1 kcal/mole was observed, regardless of the catalyst surface structure. Kinetic data, pressure-dependence analysis, and isotope effects indicate that, as with the iron catalyst, the rate-limiting step for the reaction is the dissociative chemisorption of the nitrogen molecule. Potassium atoms on the clean rhenium catalysts were found neither to promote nor to poison the reaction. The coadsorption of potassium with oxygen does not suppress the reactivity of the catalyst, and stabilization of the potassium atoms on the surface occurs. The presence of oxygen alone appears to increase the reaction rate.

---

†Present address: Department of Physical Chemistry, The Hebrew University of Jerusalem, Israel.

‡Present address: Advanced Micro Devices, Inc., Sunnyvale, California 94088.

22. Studies of the Kinetics and Mechanisms of Ammonia Synthesis and Hydrodesulfurization on Metal Single-Crystal Surfaces (Publication 44)

A.J. Gellman, M. Asscher,† and G.A. Somorjai

We have studied the ammonia-synthesis reaction over Fe and Re single-crystal surfaces and the hydrodesulfurization (HDS) of thiophene over the Mo(100) single-crystal surface. The studies have been performed using UHV surface-science tools with the capability of exposing the surfaces to high-pressure, high-temperature reaction conditions. The ammonia-synthesis reaction was shown to be extremely sensitive to surface structure on both Fe and Re, favoring surfaces with a rough or open topography. The HDS reaction on the Mo(100) surface has been shown to be similar to that on MoS_2 and appears to proceed via a reaction path that does not produce a strong Mo-S bond as an intermediate species.

---

†Present address: Department of Physical Chemistry, The Hebrew University of Jerusalem, Israel.

23. Work in Progress

LEED studies starting at 20 K explore the temperature-dependent changes of structure and bonding of adsorbed monolayers of molecules (O_2, N_2, NO, CH_4, C_6H_6, and C_6H_5N) on transition-metal crystal surfaces. Similar studies are being carried out using HREELS.

Effects of the coadsorption of sulfur, oxygen, and carbon on the bonding of organic molecules on molybdenum, rhenium, and iron surfaces are being explored at low pressures using electron spectroscopies and thermal desorption.

The catalytic activity of platinum is being modified by using gold, copper, rhenium, and titanium that are evaporated and alloyed with it. Hydrocarbon conversion reactions are being studied.

The influence of potassium on the catalytic behavior of iron and rhenium during ammonia synthesis is being explored.

1984 PUBLICATIONS AND REPORTS

Refereed Journals

1. U. Bardi, P.N. Ross, and G.A. Somorjai, "Ligand Effects for CO and H_2 Chemisorption on a Polycrystalline Pt_3Ti Surface," J. Catal. **85**, 272 (1984); LBL-15603.
2. H.W.K. Tom, C.M. Mate, X.D. Zhu, J.E. Crowell, T.F. Heinz, Y.R. Shen, and G.A. Somorjai, "Surface Studies by Optical Second-Harmonic Generation: The Adsorption of O_2, CO, and Sodium on the Rh(111) Surfaces," Phys. Rev. Lett. **52**, 348 (1984); LBL-16798.
3. B.E. Koel, B.E. Bent, and G.A. Somorjai, "Hydrogenation and H,D Exchange Studies of Ethylidyne (CCH_3) on Rh(111) Crystal Surfaces at 1Atm Pressure Using HREELS," Surf. Sci. **146**, 211 (1984); LBL-17410.
4. R.C. Yeates and G.A. Somorjai, "Molecular Ingredients of Heterogeneous Catalysis," J. Electrochem. Soc. **131**, 228C (1984); LBL-16062.
5. F. Zaera and G.A. Somorjai, "The Effect of Potassium on the Catalyzed Reactions of n-Hexane Over Pt(111) Single Crystal Surfaces," J. Catal. **84**, 375 (1983); LBL-15734.
6. L.H. Dubois and G.A. Somorjai, "Comments on 'Why CO_2 Does Not Dissociate on Rh at Low Temperature' by W.H. Weinberg," Surf. Sci. **128**, L231 (1983).

7. R.C. Yeates and G.A. Somorjai, "The Growth and Alloy Formation of Copper on the Platinum (111) and Stepped (553) Crystal Surfaces. Characterization by LEED, AES, and CO Thermal Desorption," Surf. Sci. **134**, 729 (1983); LBL-16229.
8. M. Salmeron, S. Ferrer, M. Jazzar, and G.A. Somorjai, "Photoelectron-Spectroscopy Study of the Electronic Structure of Au and Ag Overlayers on Pt(100), Pt(111) and Pt(997)," Phys. Rev. B **28**, 6758 (1983); LBL-16942.
9. U. Bardi, P.N. Ross, and G.A. Somorjai, "LEED and AES Study of Structural and Chemisorptive Properties of Zr Overlayers on the Pt(100) Crystal Face," J. Vac. Sci. Techn. A **2**, 40 (1984); LBL-15294.
10. S.M. Davis, F. Zaera, and G.A. Somorjai, "Surface Structure and Temperature Dependence of n-Hexane Skeletal Rearrangement Reactions Catalyzed over Platinum Single Crystal Surfaces: Marked Structure Sensitivity of Aromatization," J. Catal. **85**, 206 (1984); LBL-15826.
11. B.E. Koel, J.E. Crowell, C.M. Mate, and G.A. Somorjai, "An HREELS Study of the Surface Structure of Benzene Adsorbed on the Rh(111) Crystal Face," J. Phys. Chem. **88**, 1988 (1984); LBL-16012.
12. A.J. Gellman, M.H. Farias, M. Salmeron, and G.A. Somorjai, "A Thermal Desorption Study of Thiophene Adsorbed on the Clean and Sulfided Mo(100) Crystal Face," Surf. Sci. **136**, 217 (1984); LBL-15934.
13. M. Asscher, W.L. Guthrie, T.-H. Lin, and G.A. Somorjai, "Molecular Beam Surface Scattering Study of Ammonia Oxidation on a Pt(111) Single Crystal Surface," J. Phys. Chem. **88**, 3233 (1984); LBL-16353.
14. M.H. Farias, A.J. Gellman, R.R. Chianelli, K.S. Liang, and G.A. Somorjai, "The Coadsorption and Reaction of Sulfur, Hydrogen and Oxygen on Clean and Sulfided Mo(100) and on MoS_2," Surf. Sci. **140**, 181 (1984); LBL-16412.
15. F. Zaera and G.A. Somorjai, "The Hydrogenation of Ethylene Over Platinum (111) Single Crystal Surfaces," J. Am. Chem. Soc. **106**, 2288 (1984); LBL-16423.
16. G.A. Somorjai, "The Molecular Surface Science of Heterogeneous Catalysis, History and Perspective," ISISS Proceedings 1983, Springer Series in Chemical Physics **35**, (1984); LBL-16573.
17. T.-H. Lin and G.A. Somorjai, "Angular and Velocity Distributions of HD Molecules Produced by the H_2-D_2 Exchange Reaction on the Stepped Pt(557) Surface," J. Chem. Phys. **81** (2), 704 (1984); LBL-16598.
18. A.J. Gellman, M.H. Farias, and G.A. Somorjai, "The Catalytic Hydrodesulfurization of Thiophene Catalyzed on the Mo(100) Crystal Surface," J. Catal. **88**, 546–548 (1984); LBL-17144.
19. M. Asscher and G.A. Somorjai, "Vibrational Excitation and Deexcitation Rates of Molecules Adsorbed on Metal Surfaces," J. Chem. Phys. **81**, 1507 (1984); LBL-16830.
20. J.W.A. Sachtler and G.A. Somorjai, "Cyclohexane Dehydrogenation Catalyzed by Bimetallic Au-Pt(111) Single Crystal Surfaces," J. Catal. **89**, 35 (1984); LBL-16845.
21. W.T. Tysoe, J. Carrazza, and G.A. Somorjai, "The Adsorption and Catalyzed Reactions of CO and CO_2 on Graphite Surfaces," ACS Division of Fuel Chemistry Symposium on Gasification of Chars and Carbonaceous Materials **29**, 190 (1984); LBL-17004.
22. M. Asscher and G.A. Somorjai, "The Remarkable Surface Structure Sensitivity of the Ammonia Synthesis Over Rhenium Single Crystals," Surf. Sci. **143**, L389 (1984); LBL-17176.
23. M.M. Khan and G.A. Somorjai, "A Kinetic Study of Partial Oxidation of Methane with Nitrous Oxide on a Molybdena-Silica Catalyst," J. Catal. **9**, 1 (1985); LBL-17408.
24. J.J. Maj, C. Colmenares, and G.A. Somorjai, "Thorium Oxide: A New Catalyst for Methanol, Isobutanol, and Light Hydrocarbon Production from Carbon Monoxide and Hydrogen," Appl. Catal. **10**, 313 (1984).

Other Publications

25. G.A. Somorjai, "Surface Science View of Heterogeneous Catalysis: The Past, Present and Future," Plenary Lecture for Interational Congress on Catalysis, Berlin, West Germany, July 1984; LBL-17463.
26. M.A. Van Hove, "Structural Determination of Molecular Adsorbates with Dynamical LEED and HREELS," in *The Structure of Surfaces,* S.Y. Tong and M.A. Van Hove, eds., Proc. ICSOS-1, Springer Series in Surface Science, **2** (1985); LBL-18080.
27. M. Asscher and G.A. Somorjai, "Energy Redistribution in Diatomic Molecules on Surfaces," in *Proc. 17th Jerusalem Symposium on Quantum Chemistry and Biochemistry: Dynamics of Molecule-Surface Interaction,* April 30–May 3, 1984; LBL-17670.

LBL Reports

28. W.T. Tysoe, F. Zaera, and G.A. Somorjai, "On the Absolute Coverage of Ethylene on Pt(111) Single Crystals," submitted to Surf. Sci.; LBL-17122.
29. E.L. Garfunkel, M.H. Farias, and G.A. Somorjai, "The Modification of Benzene and CO Adsorption on Pt(111) by the Coadsorption of Potassium or Sulfur," submitted to J. Am. Chem. Soc.; LBL-17648.

30. C. Zhang, M.A. Van Hove, and G.A. Somorjai, "The Interaction of Oxygen with the Mo(100) and Mo(111) Single-Crystal Surfaces: Chemisorption and Oxidation at High Temperatures," submitted to Surf. Sci.; LBL-17818.
31. S.M. Davis, F. Zaera, B.E. Gordon, and G.A. Somorjai, "Radiotracer and Thermal Desorption Studies of Dehydrogenation and Atmospheric Hydrogenation of Organic Fragments Obtained from ^{14}C-Ethylene Chemisorbed Over Pt(111) Surfaces," submitted to J. Catal.; LBL-17902.
32. D.K. Saldin, J.B. Pendry, M.A. Van Hove, and G.A. Somorjai "The Interpretation of Diffuse LEED Intensities," submitted to Phys. Rev.; LBL-17963.
33. A. Gavezzotti, M. Simonetta, M.A. Van Hove, and G.A. Somorjai, "Adsorbate-Adsorbate Interactions and the Ordering of Organic Monolayers on Metal Surfaces," submitted to Surf. Sci.; LBL-17964.
34. C. Zhang, A.J. Gellman, M.H. Farias, and G.A. Somorjai, "The Adsorbate Induced Faceting of the Mo(111) Surface," submitted to Chem. Phys. Lett.; LBL-18034.
35. J.E. Crowell, W.T. Tysoe, and G.A. Somorjai, "Potassium Co-adsorption Induced Dissociation of CO on the Rh(111) Crystal Surface: An Isotope Mixing Study," submitted to J. Phys. Chem.; LBL-18123.
36. F. Zaera and G.A. Somorjai, "The Chemisorption of O_2, CO, D_2 and C_2H_4 Over Epitaxially Grown Rhenium Crystalline Films," submitted to Surf. Sci.; LBL-18356.
37. M. Kudo, E.L. Garfunkel, and G.A. Somorjai, "A UPS Study of the Interaction of Potassium with Carbon Monoxide and Benzene on the Pt(111) Crystal Surface," submitted to Surf. Sci.; LBL-18364.
38. C. Mate and G.A. Somorjai, "CO-Induced Ordering of Benzene on Rh(111) and Pt(111) Crystal Surfaces," submitted to Chem. Phys. Letters; LBL-18502.
39. A. Wieckowski, S. Rosasco, G. Salaita, A. Hubbard, B.E. Bent, F. Zaera, and G.A. Somorjai, "A Comparison of Gas Phase and Electrochemical Hydrogenation of Ethylene at Platinum Surfaces," submitted to J. Am. Chem. Soc.; LBL-18585.
40. M. Asscher, E. Pollak, and G.A. Somorjai, "A Model for Vibrational and Translational Energy Accommodation in NO-Pt(111) Surface Scattering," submitted to Surf. Sci.; LBL-17409.
41. F. Zaera and G.A. Somorjai, "The Reaction of Ethane with Deuterium Over Platinum (111) Single Crystal Surfaces," submitted to J. Catal.; LBL-17764.
42. R.C. Yeates, J.E. Turner, A.J. Gellman, and G.A. Somorjai, "The Oscillatory Behavior of the CO Oxidation Reaction at Atmospheric Pressure Over Platinum Single Crystals: Surface Analysis and Pressure Dependent Mechanisms," submitted to Surf. Sci.; LBL-17934.
43. M. Asscher, J. Carrazza, M. Khan, K. Lewis, and G.A. Somorjai, "The Ammonia Synthesis Over Rhenium Catalysts. Structure Sensitivity, Kinetics and the Effects of K and O," submitted to J. Catal.; LBL-18200.
44. A.J. Gellman, M. Asscher, and G.A. Somorjai, "Studies of the Kinetics and Mechanism of Ammonia Synthesis and Hydrodesulfurization on Metal Single Crystal Surfaces," submitted to ACS Symp. Ser.; LBL-18289.
45. G.A. Somorjai, "Molecular Ingredients of Heterogeneous Catalysis," Chem. Soc. Rev. (in press); LBL-16983.
46. M. Logan, A.J. Gellman, and G.A. Somorjai, "Hydrogenation of Carbon Monoxide on Mo," submitted to J. Catal.; LBL-17964.
47. E.L. Garfunkel, J. Parmeter, B.M. Naasz, and G.A. Somorjai, "The Hydrogenation of Carbon Monoxide Over Model Rhenium Catalysts: Additive Effects and a Comparison with Iron," submitted to Langmuir; LBL-17965.
48. T.-H. Lin and G.A. Somorjai, "The Dynamics of Atomic Hydrogen and Deuterium Recombination on the Stepped Pt(557) Crystal Surface," J. Phys. Chem. (in press); LBL-16599.
49. J.E. Crowell and G.A. Somorjai, "The Effect of Potassium on the Chemisorption of Carbon Monoxide on the Rh(111) Crystal Face," Appl. Surf. Sci. (in press); LBL-16984.

Invited Talks

50. G.A. Somorjai, "Catalysis for Energy Conversion," University of Lausanne, Switzerland, September 16, 1983.
51. G.A. Somorjai, "Molecular Surface Science: Its Triumphs, Challenging Problems and Future Promise," Colloquium, Department of Chemistry, University of California Berkeley, February 13–14, 1984.
52. M. Asscher and G.A. Somorjai, "Ammonia Synthesis Over Rhenium Catalysts," The California Catalysis Society Spring Meeting 1984, Richmond, March 23, 1984.
53. F. Zaera, B. Bent, and G.A. Somorjai, "The Role of Ethylidyne in the Mechanisms of High Pressure Hydrocarbon Conversion Reactions Over Metallic Surfaces," The California Catalysis Society Spring Meeting 1984, Richmond, March 23, 1984.
54. R.C. Yeates, J.E. Turner, A.J. Gellman, and G.A. Somorjai, "The Oscillatory Behavior of the CO Oxidation Reaction Over Pt Single Crystals," The Cali-

fornia Catalysis Society Spring Meeting 1984, Richmond, March 23, 1984.

55. G.A. Somorjai, "The Birth of a High Technology Industry. The Surface Science of Heterogeneous Catalysis"; "The Structure and Composition of Solid Surfaces and Monolayers of Adsorbed Atoms and Molecules"; and "The Surface Chemical Bond"; The Fred J. Robbins Lectureship, Pomona College, Claremont, California, March 26–28, 1984.
56. G.A. Somorjai, "Active Sites in Catalysis: Active Sites for the Dissociation and Reactions of CO and Other Small Molecules on Solid Surfaces," 30th Industrial Affiliates Symposium, Stanford University, Stanford, California, March 30, 1984.
57. G.A. Somorjai, "The Bonding and Chemistry of Organic Monolayers on Metal Surfaces," The George A. Abbott Lectureship in Chemistry, University of North Dakota, Grand Forks, April 12, 1984.
58. G.A. Somorjai, "Surface Crystallography by Low-Energy Electron Diffraction: Present and Near Future Developments," American Crystallographic Association Annual Meeting, University of Kentucky, Lexington, May 21, 1984.
59. G.A. Somorjai, "Molecular Surface Science: Its Triumphs, Its Challenges and Future Promise," The 11th Annual Dorn Memorial Lecture, Northwestern University, Evanston, Illinois, May 22, 1984.
60. G.A. Somorjai, "Surface Crystallography," American Crystallographic Association Annual Meeting, University of Kentucky, Lexington, May 23, 1984.
61. G.A. Somorjai, "Frontiers of Chemistry, New Excitement, New Challenges," in "Catalysis: Frontier Area of Chemistry," Chemical Sciences and Technology, National Research Council, Washington, D.C., May 25, 1984.
62. G.A. Somorjai, "The Structure of Adsorbed Monolayers. The Surface Chemical Bond," 8th Scandinavian Symposium on Surface Chemistry, University of Lund, Sweden, June 5, 1984.
63. G.A. Somorjai, "The Molecular Surface Science of Heterogeneous Catalysis," University of Louvain, Belgium, June 29, 1984.
64. G.A. Somorjai, "The Surface Science View of Heterogeneous Catalysis: The Past, the Present and the Near Future," Plenary Lecture, International Congress of Catalysis, Berlin, West Germany, July 3, 1984.
65. G.A. Somorjai, "Surface Analysis and Catalysis in Environmental Research," European Institute for Transuranium Elements, Karlsruhe, West Germany, July 10, 1984.
66. G.A. Somorjai, "Surface Science of Energy Conversion," ETH, Zurich, Switzerland, July 11, 1984.
67. M. Asscher, A. Gellman, and G.A. Somorjai, "Studies of the Kinetics and Mechanism of Ammonia Synthesis and Hydrodesulfurization on Metal Single Crystal Surfaces," The New Surface Science in Catalysis Symposium at the Philadelphia American Chemical Society Meeting, Philadelphia, Pennsylvania, August 26–31, 1984.
68. G.A. Somorjai, "Molecular Surface Science of Heterogeneous Catalysis," Congrès de la Société Francaise de Chimie, Nancy, France, September 17, 1984.
69. G.A. Somorjai, "The Surface Chemical Bond," École Nationale Superièure de Chimie de Paris, France, September 21, 1984.
70. A.J. Gellman, D.L. Neiman, and G.A. Somorjai, "Catalytic Hydrotreating on Mo Single Crystal Surfaces," The California Catalysis Society Fall Meeting 1984, Pasadena, October 19, 1984.
71. G.A. Somorjai, "The Relationship Between Surface Chemistry at High Pressures and Low Pressures for Chemisorption and for Catalytic Reactions," University of Pittsburgh, Pennsylvania, October 30–31, 1984.
72. G.A. Somorjai, "The Surface Chemical Bond," Harvard-MIT Seminar, Cambridge, Massachusetts, November 1, 1984.
73. G.A. Somorjai, "Surface Science Problems at High Temperatures," Bay Area High-Temperature Conference, Lawrence Berkeley Laboratory, November 8, 1984.
74. G.A. Somorjai, "Twenty Years of Surface Science: Its Accomplishments and Future Challenges," IBM T.J. Watson Research Center, Yorktown Heights, New York, November 27, 1984.
75. G.A. Somorjai, "The Building of Catalysts: The Molecular Surface Science Approach," Symposium on the "Design and Optimization of Catalysts," American Institute of Chemical Engineers, San Francisco, California, November 25–30, 1984.
76. G.A. Somorjai, "The Surface Science of Catalytic Materials," Exxon Research and Engineering Company, Annandale, New Jersey, and Boston, Massachusetts, November 28, 1984.
77. G.A. Somorjai, "The Roles of Carbon, Sulfur and Alkali Metals as Promoters of Catalyzed Reactions on Metal Surfaces," American Vacuum Society 31st National Symposium, Reno, Nevada, December 7, 1984.
78. G.A. Somorjai, "The Surface Chemical Bond. The Structure and Bonding of Monolayers," Naval Research Laboratory Chemistry Colloquium, Washington, D.C., December 11, 1984.
79. M.A. Van Hove, "Methods of Surface Structure

Determination"; "Types of Surface Structure and Their Recognition in LEED Patterns"; "Performing a Surface Structure Determination"; and "Results of Surface Structure Determination"; Fudan University, Shanghai, People's Republic of China, February 13–20, 1984.

80. M.A. Van Hove, "Modern Methods in Surface Structure Determination" and "Recently Determined Surface Structures," Institute of Physics, Academia Sinica, Beijing, People's Republic of China, February 24, 1984.

81. M.A. Van Hove, "Surface Science of Ceramics," Lawrence Berkeley Laboratory, April 12, 1984.

82. M.A. Van Hove, "Dynamical LEED Calculations for Surface Superlattices with Large Unit Cells and Extension to Disordered Overlayers," American Crystallographic Association Meeting, Lexington, Kentucky, May 23, 1984.

83. M.A. Van Hove, "Benzene on Rh(111) and Other Complex Surface Structures from LEED," University of Milan, Italy, June 13, 1984.

84. M.A. Van Hove, "Structural Determination of Molecular Adsorbates with Dynamical LEED and HREELS," First International Conference on the Structure of Surfaces, Berkeley, California, August 13, 1984.

Nuclear Magnetic Resonance*

Alexander Pines, Investigator

INTRODUCTION

The primary objectives of the nuclear-magnetic-resonance (NMR) program are to develop methods in magnetic-resonance spectroscopy and to use them to study structure and molecular behavior in condensed phases. This objective demands an understanding of the interaction of nuclear spins with each other; with other degrees of freedom such as molecular translations, vibrations, and rotations; and with external radiation such as radiofrequency sources and light. Novel methods developed under the program include multiple-quantum spectroscopy, high-resolution NMR and magic-angle spinning, zero-field NMR, nuclear-magnetic-isotope separation, solid-state NMR imaging, and topical NMR with spatial selectivity. These methods are being applied to understand structure and dynamics at the molecular level in a number of materials, including doped amorphous semiconductors, liquid crystals, polymers, organometallic hydrogen complexes, zeolites, silicate glasses, and surfaces. Some molecular properties change on light excitation, and laser-magnetic double resonance is being developed to examine how these changes dictate the course of photochemical reactions. New methods of propagation and detection are being developed to increase the sensitivity and selectivity, in particular using rapidly switched superconducting fields, Josephson junction devices such as superconducting quantum interference devices (SQUIDs), optical pumping of inert gases, and spatially selective topical coils.

1. Time-Domain Zero-Field NMR and Nuclear-Quadrupole Resonance (NQR) (Publication 29)

D.B. Zax, A. Bielecki, A. Pines, K. Zilm,† and D.P. Weitekamp

Methods are described and demonstrated for detecting the coherent evolution of nuclear-spin observables in zero magnetic field with the full sensitivity of high-field NMR. The principle motivation is to provide a means of obtaining solid-state spectra of the magnetic dipole and electric quadrupole interactions of disordered systems without the line broadening associated with random orientation with respect to the applied magnetic field. Comparison is made to previous frequency-domain and high-field methods. A general density-operator formalism is given for experiments where the evolution period is initiated by a sudden switching to zero field and is terminated by a sudden restoration of the field. Analytical expressions for the signals are given for a variety of simple dipolar and quadrupolar systems, and numerical simulations are performed for up to six coupled spin-1/2 nuclei. Experimental results are reported or reviewed for ^{1}H, ^{2}H, ^{7}Li, ^{13}C, and ^{27}Al nuclei in a variety of polycrystalline materials. The effects of molecular motion and bodily sample rotation are described. Various extensions of the method are discussed, including demagnetized initial conditions and correlation by two-dimensional Fourier transformation of zero-field spectra with themselves or with high-field spectra.

*This work was supported by the Director, Office of Energy Research, Office of Basic Energy Sciences, Materials Sciences Division of the U.S. Department of Energy and the Director's Program Development Funds of the Lawrence Berkeley Laboratory under Contract No. DE-AC03-76SF00098.

†Present address: Department of Chemistry, Yale University, New Haven, Connecticut 06511.

2. Zero-Field NMR Study of $H_2Os_3(CO)_{10}$ (Publication 19)

A. Bielecki, D.B. Zax, M. Kulick, E. Muetterties,† and A. Pines

As a model for the adsorption and reduction of unsaturated hydrocarbons on metal surfaces, the triosmium carbonyl hydride complex $[H_2Os_3(CO)_{10}]$ has been intensively studied. Both x-ray and neutron diffraction methods have been applied to single crystals in an attempt to determine structural parameters. In the x-ray studies, the locations of the hydrogen nuclei could not be determined. Using zero-field NMR, we have studied the relative locations of the ^{1}H nuclei. A spectral simulation (Figure 2-1) clearly indicates a room-temperature structure that is somewhat expanded relative to the low-temperature neutron-diffraction work.

†Deceased.

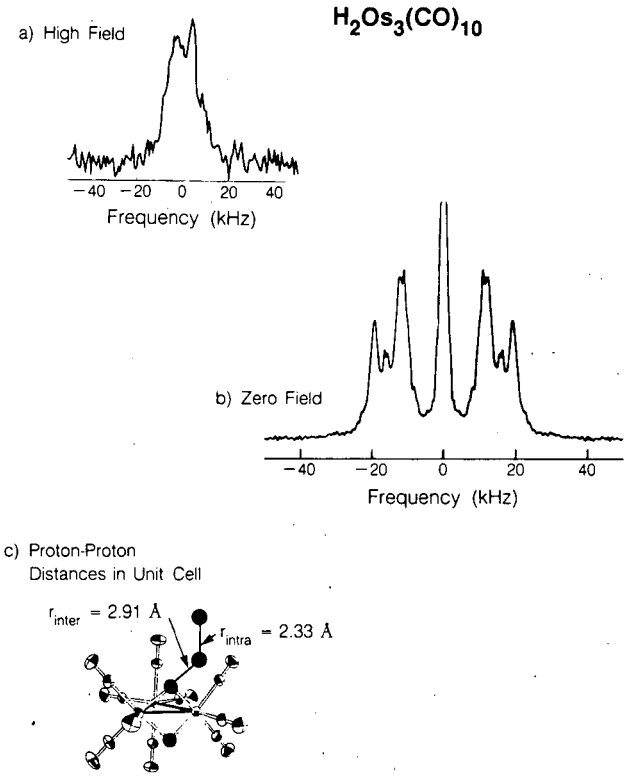

Figure 2-1. High-field (a) and zero-field (b) NMR spectra of protons in solid $H_2Os_3(CO)_{10}$. The proton positions can be precisely determined by zero-field NMR even in this polycrystalline material. (XBL 849-3893)

3. Deuterium Quadrupole Coupling Constants and Asymmetry Parameters from Zero-Field NQR Spectra (Publication 21)

A. Bielecki, J. Millar, A. Thayer, D.B. Zax, and A. Pines

Fourier-transform zero-field NQR allows the detection and assignment of quadrupolar couplings from high-resolution spectra of polycrystalline solids.[1] In particular, the low-frequency ν_0 lines have been observed for the first time. This information is valuable as a tool for understanding structure and bonding in solids and is normally difficult or impossible to obtain with traditional NMR and NQR techniques. With the ability to resolve the low-frequency transitions in quadrupolar systems, values of e^2qQ/h and η may be calculated for inequivalent deuterons. We are studying model compounds to determine deuterium quadrupole coupling parameters. Some representative initial results appear in Table 3-1.

1. A. Bielecki, J.B. Murdoch, D.P. Weitekamp, D.B. Zax, K.W. Zilm, H. Zimmerman, and A. Pines, J. Chem. Phys. **80**, 2232 (1984).

Table 3-1
Deuterium Quadrupole Coupling Constants and Asymmetry Parameters

Compound		e^2qQ/h (kHz)	η
Dimethoxybenzene-d_{10}	methyl[a]	47.9	0.096
	aromatic[b]	178.5	0.045
Dimethylterephthalate-d_{10}	aromatic[a]	178.0	0.044
		180.0	0.025
Diethylterephthalate-d_4	methylene[c]	149.9	0.042
		152.9	0.052
Glycine-d_5	methylene[d]	160.1	0.042
		169.0	0.092
$Ba(ClO_3)_2.HDO$[c]		122.2	0.98

a. A. Bielecki and D. Zax, unpublished results.
b. see Reference 1.
c. J. Millar and A.M. Thayer, unpublished results.
d. A. Bielecki, M. Trecoske, and D. Shykind, unpublished results.

4. Heteronuclear Zero-Field NMR (Publication 4)

D.B. Zax, A. Bielecki, K.W. Zilm,† and A. Pines

We have previously demonstrated the ability of zero-field magnetic resonance to measure dipole-dipole couplings between ^1H nuclei in powdered samples. These couplings can be interpreted in terms of structural parameters. We have extended this work to include couplings to inequivalent nuclei (e.g., ^{13}C). Because of the high-field inequivalence of different types of nuclei, the zero-field spectra may be more complex than those of homonuclear systems. High-field NMR techniques may be used to prepare these systems to simplify the zero-field patterns, as shown in Figure 4-1. This should prove useful in disentangling spectral patterns arising from different functional groups (e.g., ^{13}CH, $^{13}CH_2$, and $^{13}CH_3$) that cannot normally be counted in solid materials.

†Present address: Department of Chemistry, Yale University, New Haven, Connecticut 06511.

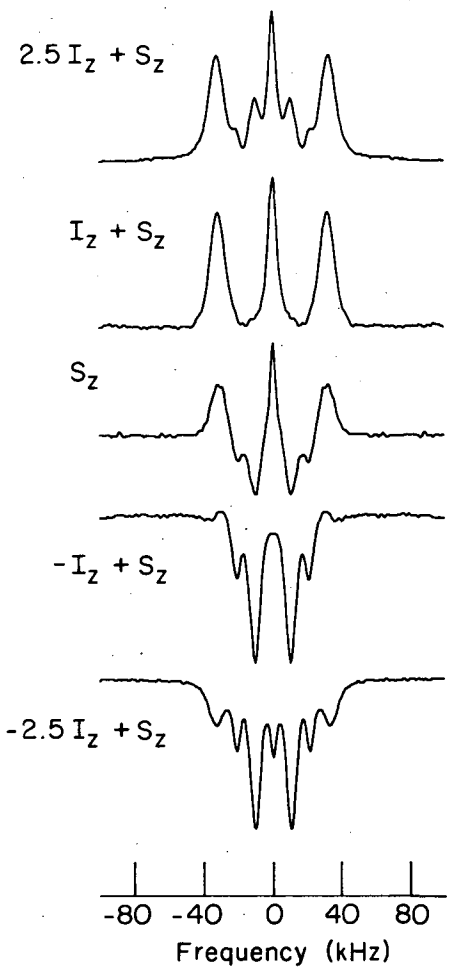

Figure 4-1. Zero-field NMR spectra of the ^{13}C-^1H group in solid polycrystalline calcium formate for different initial conditions of the relative $^1H(I)$ and $^{13}C(S)$ polarization. (XBL 8312-4680)

5. Pulsed Zero-Field NQR (Publication 20)

A. Bielecki, J. Millar, A. Thayer, D.B. Zax, D.P. Weitekamp, and A. Pines

Our laboratory has extended the zero-field NQR experiment[1] through the use of dc magnetic-field pulses on a demagnetized sample to produce evolution in zero field. Under dc pulses, nuclei will respond differently to the applied field due to their different gyromagnetic ratios. This behavior provides for selectivity in the evolution and detection of a given nucleus in a multinuclear spin system. Combined with adiabatic field cycling to zero field, this approach allows for indirect detection of a low γ quadrupolar nucleus via level crossing with an abundant spin-1/2 nucleus such as ^1H. With selection between different nuclei and optimization of the experiment, the proton signal is eliminated in the NQR spectrum. Figure 5-1 illustrates the selective indirect detection obtainable in partially deuterated organic solids.

1. A. Bielecki, J.B. Murdoch, D.P. Weitekamp, D.B. Zax, K.W. Zilm, H. Zimmerman, and A. Pines, J. Chem. Phys. **80**, 2232 (1984).

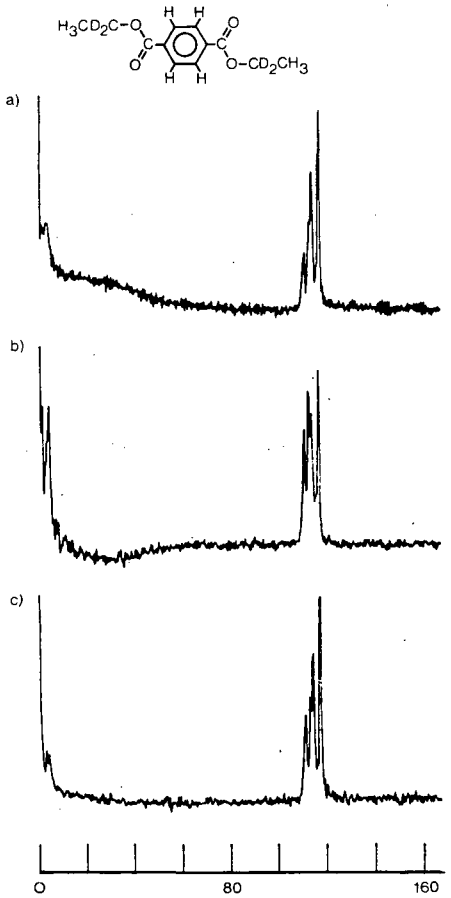

Figure 5-1. High-resolution Fourier-transform NQR spectra of polycrystalline diethylterephthalate-d_4 ($CH_3CD_2CO_2$-C_4H_4-$CO_2CO_2CH_3$). In (c) the dc pulses used allow for selective detection of the deuteron signal, unlike (a) and (b), in which the proton signal also appears as a broad region below 50 kHz. Low-frequency transitions may be observed in (c); these transitions allow for the determination of e^2qQ/h and η for two inequivalent methylene deuterons. (XBL 851-725)

6. Zero-Field NMR Spectrometer (Publication 15)

A. Bielecki, D.B. Zax, K. Zilm,† and A. Pines

An instrument has been designed and built to examine the dynamics of nuclear-spin systems in the absence of applied fields (zero-field NMR) (see Figure 6-1). The motivation for such studies is that they often provide molecular structural information, even with polycrystalline or amorphous samples. The distinctive feature of the instrument is that it can generate magnetic-field cycles in which the field changes rapidly between large values (up to 4 tesla) and negligible values (less than 10^{-5} tesla). The pulsed dc fields for the Fourier-transform experiment can be turned on and off in about one microsecond.

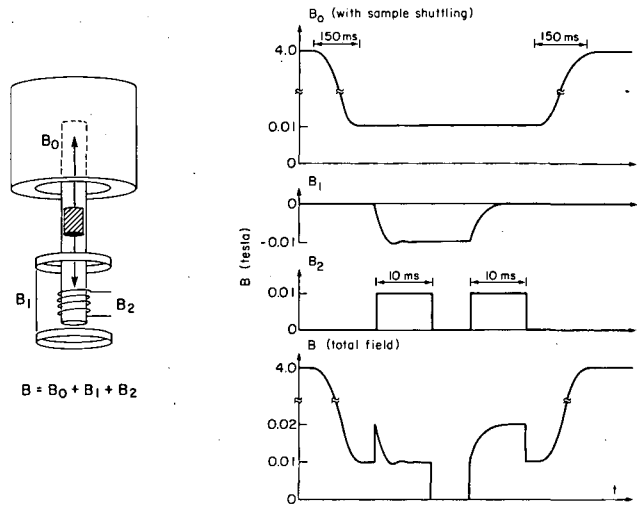

Figure 6-1. Schematic diagram of mechanical shuttling and magnetic-field timing for zero-field NMR spectrometer. (XBL 851-726)

The spectrometer allows time-domain measurements of internuclear dipole-dipole interactions in zero field and is useful as well for the observation of pure NQR spectra. Experimental results have been obtained with a variety of materials. The spectrometer is now being enhanced for direct detection of zero-field NMR with the use of SQUID detectors in collaboration with professor J. Clarke, also of MMRD.

---

†Present address: Department of Chemistry, Yale University, New Haven, Connecticut 06511.

7. Composite Pulses Without Phase Distortion (Publication 12)

R. Tycko, H. Cho, E. Schneider, and A. Pines

The radiofrequency pulses used in transient NMR experiments often contain large unavoidable imperfections, such as inhomogeneities in the amplitude of the applied radiation and offsets from the nuclear-spin transition frequencies. These imperfections can cause significant loss of signal and phase coherence in NMR samples and thus impair the performance of many modern NMR experiments. We have used coherent-averaging theory[1] to design composite multiple-pulse sequences that compensate for pulse imperfections over a broad bandwidth of transition frequencies and radiation amplitudes. These composite pulse schemes, unlike others proposed in the past, have the additional advantage that they

preserve the phase coherence of the spins over their effective bandwidths. This last feature is particularly crucial for experiments such as spin echoes and spatial localization of NMR signals, which require that the response of the spin ensemble be free of phase distortion.

1. U. Haeberlen and J.S. Waugh, Phys. Rev. **175**, 453 (1968).

8. Composite Sequences for Efficient Double-Quantum Excitation (Publication 13)

T.M. Barbara,† R. Tycko, D.P. Weitekamp, and A. Pines

Double-quantum NMR is an important technique for high-resolution NMR in solids. We demonstrate theoretically and experimentally that double-quantum coherence can be excited with nearly maximal efficiency over a large range of spin-coupling strengths in NMR with the use of composite excitation sequences. Such sequences are shown to be directly constructible from existing composite $\pi/2$ pulses (see Figure 8-1). In addition, we give a general procedure for converting a composite excitation sequence to an equivalent, reduced form that contains fewer radiofrequency (rf) pulses and simpler rf phase shifts. Experiments are performed on the proton pair of CH_2Cl_2 oriented in a liquid-crystal solvent. Applications to quadrupolar spin-1 nuclei and other dynamically simple multilevel systems are discussed.

†Present address: Department of Chemistry, University of California, San Diego 92093.

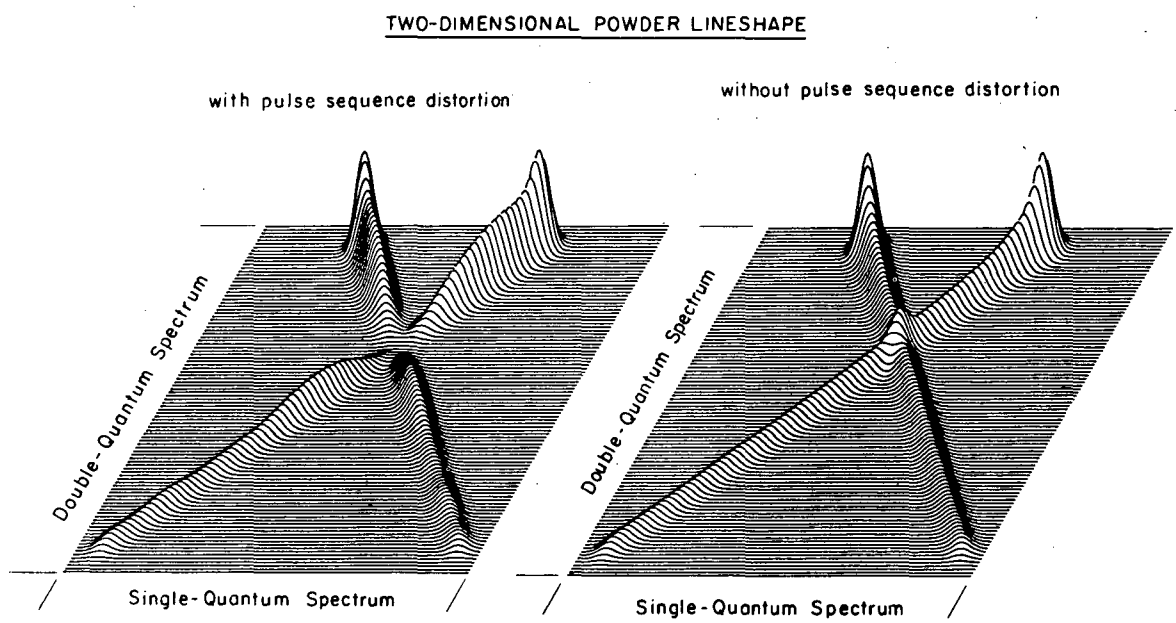

Figure 8-1. Two-dimensional NMR lineshapes for double-quantum excitation with and without pulse-sequence distortion. (XBL 851-933)

9. Broadband Population Inversion and Spin Decoupling in Solid-State NMR (Publication 2)

R. Tycko, E. Schneider, and A. Pines

A universal problem in pulsed NMR is that of exciting nuclear spins and decoupling with a broad range of resonance frequencies using only a single frequency of rf radiation. The theory, simulations, and experimental demonstrations of composite pulses are presented. The composite π pulses are phase-shifted rf pulse sequences designed to invert spins over a larger range of dipole or quadrupole couplings than a conventional π pulse, for a given rf power, in coupled spins such as those that occur in

solid-state NMR. A previously proposed theory for constructing composite pulses is discussed in the specific context of solids. Two particular sequences, $45_0180_{90}90_{180}45_0$ and $180_0180_{120}180_0$, are examined in detail. Their performance in coupled-spin systems of various sizes is evaluated in simulations. Experiments are performed on two solid compounds, $Ba(ClO_3)_2 \cdot H_2O$ and $C_4O_4H_2$. The results reveal markedly less spectral distortion after composite pulse inversion than after conventional π-pulse inversion at low rf powers (see Figure 9-1).

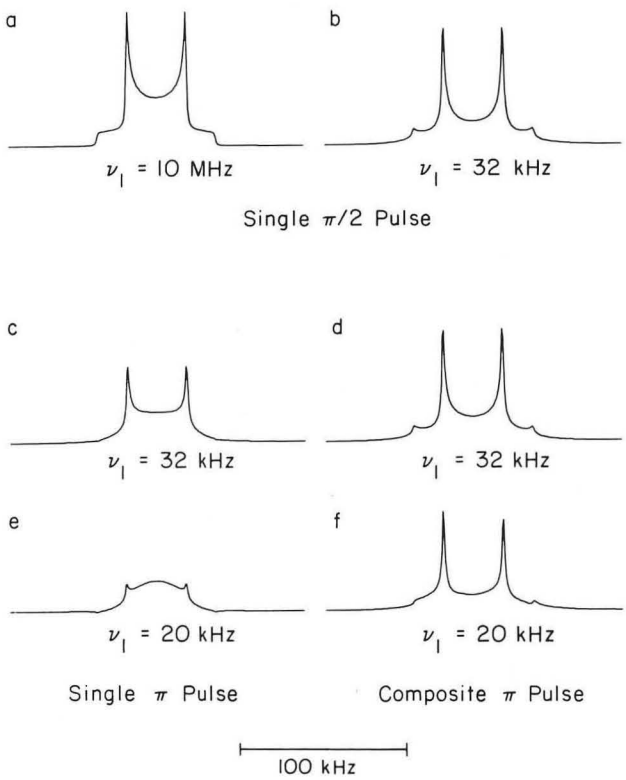

Figure 9-1. Solid-state NMR spectra of proton in $Ba(ClO_3)_2 \cdot H_2O$ by conventional (left) and composite (right) pulses. (XBL 841-304)

10. Fixed-Point Theory of Nonlinear Excitation in Spectroscopy (Publication 18)

R. Tycko, J. Guckenheimer,† and A. Pines

A common requirement in spectroscopy is selective nonlinear excitation over a selected set of values of some parameter (e.g., frequency-excitation amplitude or dipole coupling). We have developed a method of iterations that converges to the desired excitation. This is done by performing transformations on Liouville space for which the desired propagator is a fixed point. A stable, attractive fixed point leads to broadband behavior, and an unstable fixed point leads to narrowband behavior. As an example, the sequence of phases [0,330,60,330,0] leads to π pulses that are broadband both in frequency and excitation amplitude. The behavior of this sequence is illustrated in Figure 10-1, which shows how rapidly the operators corresponding to SO(3), appropriate for a two-level system, converge to the fixed point at π. The broadband inversion characteristic of this scheme is depicted in Reference 1.

†Present address: Department of Mathematics and Applied Science, University of California, Santa Cruz 95064.

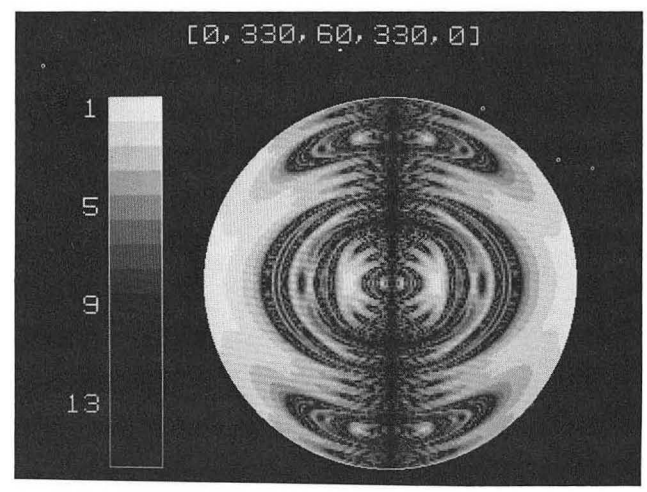

Figure 10-1. Convergence basin for an attractive fixed point at π (equator) in the iterative scheme [0,330,60,330,0]. (XBB 8410-7471)

11. Pulse-Iteration Schemes with Two Fixed Points (Publication 16)

H. Cho, R. Tycko, A. Pines, and J. Guckenheimer[†]

Many applications of NMR require the ability to excite nuclear spins selectively and uniformly depending on their transition frequency, their position in space, or the local radiation amplitude. However, the design and excitation of NMR pulse sequences that can achieve such well-defined selectivity is greatly complicated by the highly nonlinear relationships between the excitation and response for nuclear-spin ensembles in transient NMR experiments. A general fixed-point theory has recently been developed by us for analyzing the nonlinear dynamics of this problem and has been successfully applied to the design of slice-selective pulses for use in NMR imaging. The strategy prescribed by fixed-point theory is to find some iterative mathematical operation that acts on parameters subject to experimental control, and that has the desired selective spin response as a stable fixed point. The extension to more than one fixed point allows the selective irradiation of spatially distributed spins and constitutes the novelty of this work. In the example shown in Figure 11-1, the desired response is the population inversion of the nuclear-spin energy levels over some sharply defined range of radiation amplitudes, and the iteration procedure is a series of phase shifts of the applied radiofrequency radiation calculated using the fixed-point method. The shaping of the response allows selective slicing in topical NMR.

[†]Present address: Department of Mathematics and Applied Science, University of California, Santa Cruz 95064.

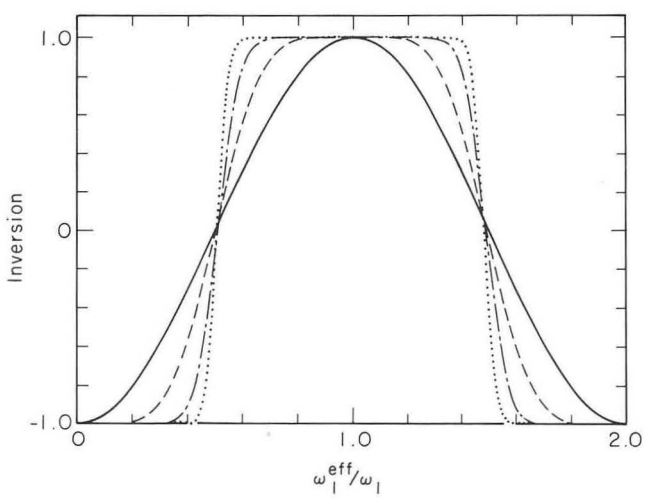

Figure 11-1. Selective slicing in space of NMR irradiation by an iterative scheme with two fixed points: one iteration (straight line); two iterations (dashed line); three iterations (dash-dot line); four iterations (dotted line). (XBL 851-764)

12. Spatial Localization of NMR Signals by Narrowband Inversion (Publications 1 and 17)

J. Baum, R. Tycko, H. Cho, and A. Pines

Surface coils for exciting and detecting NMR signals are often used in place of the traditional solenoid or Helmholtz coils in situations where only a small region of a large sample is of interest. This form of spectroscopy, called topical NMR, is of interest particularly in many *in vivo* studies. We have developed a scheme called NOBLE (narrowband localization of excitation) that limits the detected signal in such a topical NMR experiment to a selected region in space. This procedure relies on a gradient of the radiofrequency field and an iterative phase-cycling scheme that is selective for the field value. An example of the narrowband radiofrequency selectivity afforded by such a scheme is indicated in Figure 12-1. This approach will allow the selective observation of NMR from specific regions of a material or organism, extending the use of NMR imaging for noninvasive diagnostics.

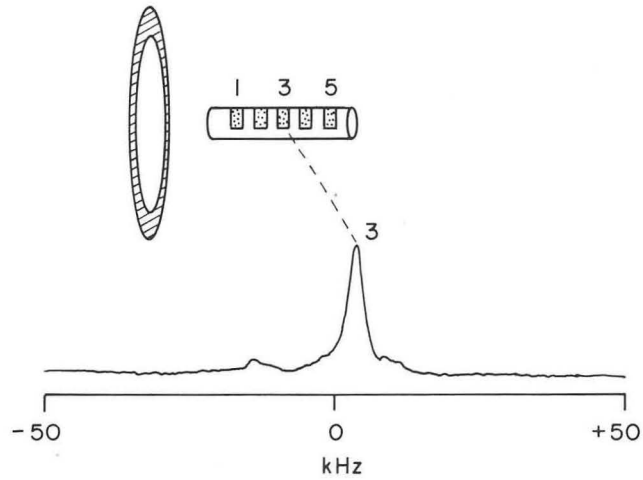

Figure 12-1. Spatially localized NMR signal from a sample of capillary tubes and surface coil arranged as shown. The depth resolution is indicated here by the exciting and detecting signal from position 3 only. (XBL 851-765)

13. Phase-Modulated Pulses for Adiabatic Population Inversion (Publication 3)

J. Baum, R. Tycko, and A. Pines

We have derived a class of continuously phase-modulated radiation pulses that result in coherent population inversion on resonance as well as over a large range of transition frequencies and radiation-field strengths. This is the population inversion analogy to self-induced transparency. Simulations of the inversion properties of the modulated inversion pulse (MIP) are presented in Figure 13-1. We have shown that the inversion behavior can be explained by treating the MIP as a highly efficient adiabatic sweep. Finally, we have presented a method for generating a sequence of phase-shifted radio-frequency pulses from the continuously modulated pulse. The method can be implemented on modern NMR and coherent optical spectrometers.

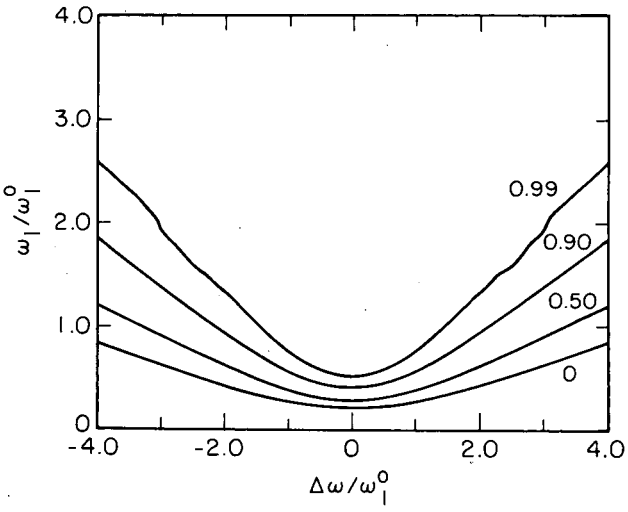

Figure 13-1. Simulated contour plot of population inversion vs. relative resonance offset ($\Delta\omega/\omega_1^0$) and rf amplitude (ω_1/ω_1^0) resulting from the modulated inversion pulse; ω_1^0 is the nominal rf amplitude. Inversion is defined as the negative of the final z component of the spin angular momentum; initially the spin system has a z component of +1. (XBL 8412-5493)

14. Multiple-Quantum NMR Study of Molecular Structure and Ordering in a Liquid Crystal (Publication 6)

S. Sinton,[†] D.B. Zax, J.B. Murdoch,[‡] and A. Pines

Proton multiple-quantum NMR was used to investigate the anisotropic ordering in a magnetic field and molecular structure in the nematic phase, 4-cyano-4′-n-pentyl-d_{11}-b-phenyl (5CB-d_{11}). The multiple-quantum spectra are more highly resolved than is the conventional single-quantum NMR spectrum (see Figure 14-1). This resolution greatly simplifies the analysis. Using the five, six, seven quantum splittings, we obtain the dipolar couplings in 5CB-d_{11} that characterize its structure. The structure exhibits a high degree of symmetry, and a complete analysis reveals that the dihedral angle between the two phenyl rings is 30 ± 2°.

[†]Present address: Exxon Production Research Company, Houston, Texas 77001.

[‡]Present address: Technicare Corporation, Cleveland, Ohio 44101.

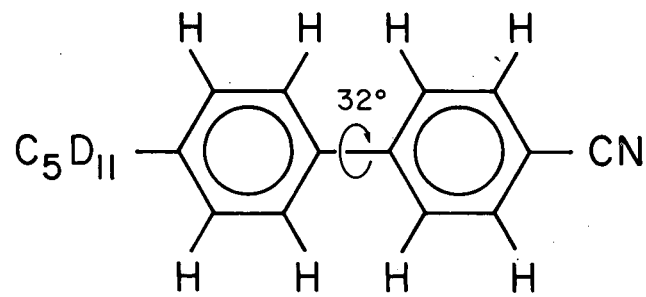

Figure 14-1. Structure of cyanobiphenyl liquid-crystal molecule as deduced from multiple-quantum spectroscopy. (XBL 851-932)

15. Phase Enhancement for Precise Determination of Small rf Phase Angles (Publication 26)

A.N. Garroway† and A. Pines

For multiple-quantum NMR, digital phase shifters generate the nonquadrature phase shifts. Though the required phase increments must be rather small (~1.4°) to separate very high order coherences, these increments must also be set to great precision since, compared to a single-quantum coherence, an n-quantum coherence is n times more sensitive to any phase error. This report indicates qualitatively the effect of digital phase-shifter errors on multiple-quantum spectra and demonstrates a highly accurate method for measuring the relative phase of small rf increments (see Figure 15-1). The method relies on frequency multiplication to enhance these small phase shifts.

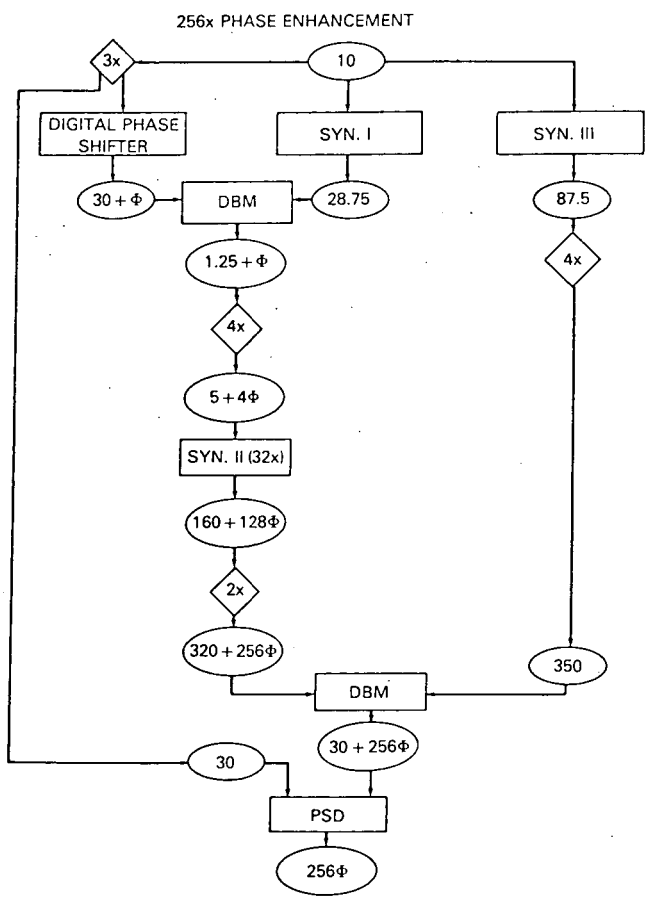

Figure 15-1. Schematic diagram showing enhancement of the rf digital phase for multiple quantum spectroscopy. Frequency multipliers are indicated by 2x, 3x, etc; DBM stands for double balanced mixer. Shown too are the rf frequencies in MHz and the digitally selected phase shift ϕ. (XBL 851-762)

†Permanent address: Code 6120, Naval Research Laboratory, Washington, D.C. 20375.

16. Multiple-Quantum Dynamics in Solid-State NMR (Publication 24)

J. Baum, M.G. Munowitz, A.N. Garroway,† and A. Pines

We have employed multiple-quantum NMR methods to study extended coupling networks in solids,[1,2] hoping both to gain added insight into nuclear-spin dynamics in dipolar solids and to develop new techniques for studying clustering and materials characterization. Shown in Figure 16-1 are a series of ^{1}H multiple-quantum spectra of hexamethylbenzene, which illustrate the distribution of spectral intensity over the various coherence (or transition) orders for increasing excitation times. The progressive development of multiple-quantum coherence with time is found to depend on the formation of multiple-spin correlations throughout the system, a phenomenon also accompanying the familiar free-induction decay. Both the time development and the observed distribution of coherence can be approached statistically, with the spin system described by a time-dependent density operator whose elements are completely uncorrelated at sufficiently long times. Taking this viewpoint, we treat the distribution of coherence in a multiple-quantum spectrum as gaussian and loosely associate its variance with the number of coupled spins effectively interacting up to a certain instant. The observed steady increase in effective system "size" is accounted for by a random-walk model for the time development of the density operator.

†Permanent address: Code 6120, Naval Research Laboratory, Washington, D.C. 20375.

1. D.P. Weitekamp, Adv. Magn. Reson. **11**, 111 (1983).
2. Y.S. Yen and A. Pines, J. Chem. Phys. **78**, 3579 (1983).

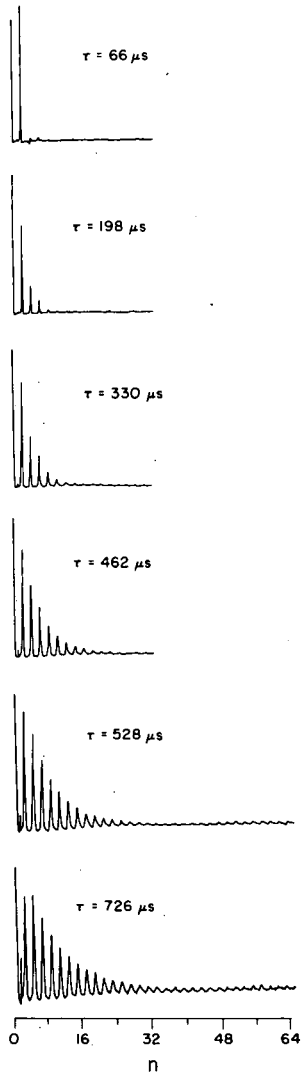

Figure 16-1. 360-MHz ^{1}H multiple-quantum spectra of hexamethylbenzene. Excitation times are as marked. Note that the distribution of spectral intensity over coherence orders n broadens with time. The direct nuclear dipole-dipole interaction makes it possible to excite coherences of very high order. (XBL 8412-5495)

17. Identification of Nuclear Spin Clusters in Solids by Multiple-Quantum NMR (Publication 25)

M.G. Munowitz, J. Baum, A.N. Garroway,† and A. Pines

Multiple-quantum NMR is a method by which a group of coupled spins can be forced to act in concert. With direct dipole-dipole couplings providing a communications network, the collective excitation of nuclear spins both enhances and simplifies the magnetic-resonance problem. We have used such techniques to demonstrate that the existence and sizes of isolated clusters of spins in the solid state can be revealed. The essential point is that a group of n spins can absorb or emit at most n quanta of radiant energy. By studying the time development of multiple-quantum coherence in a solid, we can then ascertain the number of coupled spins effectively excited by the radiation. We expect to use this technique to identify nuclear clusters in naturally occurring dilute systems, found, for example, on surfaces and in inert matrices. An illustrative result for a six-spin system is shown in Figure 17-1. Applications are under way to the study of clustering in device-quality amorphous silicon hydride, together with Professor J. Reimer of the University of California at Berkeley and the Center for Advanced Materials.

†Permanent address: Code 6120, Naval Research Laboratory, Washington, D.C. 20375.

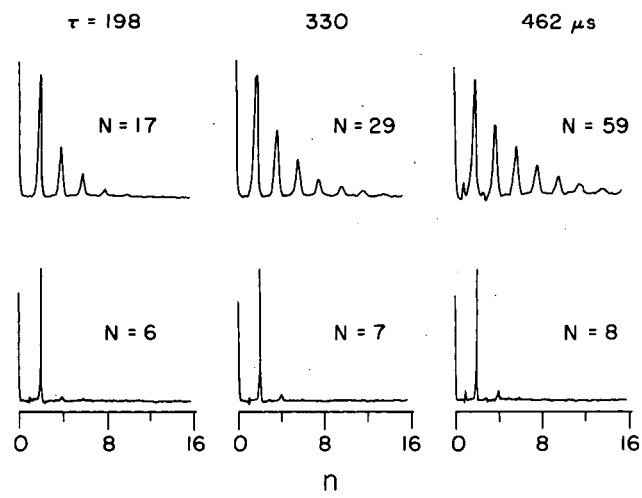

Figure 17-1. 360-MHz ^{1}H multiple-quantum spectra of dimethylnaphthalene (DMN) (bottom) for increasing excitation times. The dilute system is a 5-mole% solid solution of DMN-d_6 in perdeuterated DMN-d_{12}. The partially deuterated molecule has been labeled at the ring positions only, leaving the 6 methyl protons as a dilute, isolated cluster of spins. In contrast to the neat system, the effective spin size N grows very slowly for the cluster, indicating that coherence has been localized only among clusters of 6 interacting spins in the polycrystalline sample. (XBL 8412-5494)

18. NMR Imaging in Solids by Multiple-Quantum Resonance (Publication 7)

A.N. Garroway,[†] *J. Baum, M.G. Munowitz, and A. Pines*

In its most general form, an NMR imaging method uses a magnetic-field gradient to encode the positions of a selected group of nuclear spins with a spatially varying resonant frequency. The degree of spatial resolution ultimately attainable therefore depends on the magnitude of this externally imposed field relative to any local fields internal to the sample. When strong nuclear dipolar fields are naturally present, as they generally are in a rigid solid, very large gradients are necessary, and imaging of solid materials by NMR becomes very difficult. Our approach to this problem is to prepare high-order multiple-quantum coherences that then evolve in the static magnetic-field gradient. In a gradient the nth-order coherence evolves n times faster than the (usual) single-quantum coherence. The effective local dipolar fields are, however, roughly comparable for high- and low-order coherences in very large spin systems. Consequently, imaging in strongly coupled solids can be accomplished even with rather small magnetic gradients. This is analogous to a higher enlargement factor for the NMR "microscope." We illustrate this approach in Figure 18-1 by a ^{1}H cross-sectional image of a simple phantom consisting of two tubes of solid of adamantane for $n \leqslant 14$.

[†]Permanent address: Code 6120, Naval Research Laboratory, Washington, D.C. 20375.

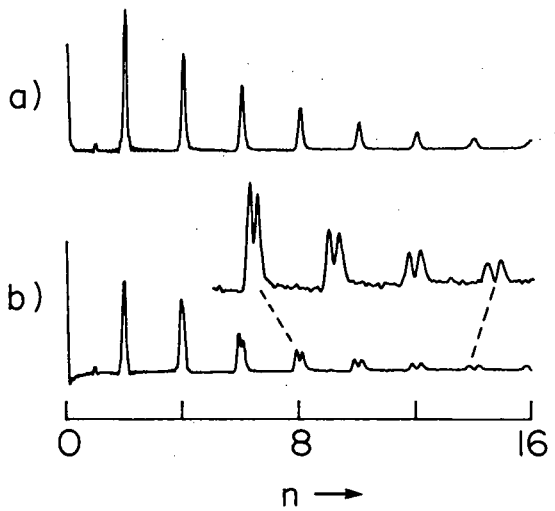

Figure 18-1. Adamantane ^{1}H multiple-quantum spectra recorded at 360 MHz with (b) and without (a) a static z-gradient. The sample, consisting of two cylindrical plugs (1.3 mm dia. × 4 mm long) separated by 2.0 mm, is aligned with its cylindrical axes perpendicular to the direction of the gradient. Even with a small gradient (20 kHz/cm), the two adamantane plugs can be resolved. (XBL 846-2272)

19. Coherence-Transfer-Echo Spectroscopy for High-Resolution Liquid Spectra in Inhomogeneous Fields (Publication 22)

M. Gochin, D.P. Weitekamp, and A. Pines

In regular liquid-state NMR spectroscopy, the natural linewidths are narrow enough that resolution is limited only by the magnetic-field homogeneity. This poses a problem in cases where the sample is large or inherently nonhomogeneous, as in *in vivo* systems. A method has been developed for taking high-resolution spectra irrespective of field homogeneity. The method involves measuring the large chemical-shift spread of carbon resonances via the more sensitive proton nuclei to which these carbons are coupled, and makes use of spin echoes to cancel the effects of the magnetic-field inhomogeneity. An example is shown in the two-dimensional spectrum of Figure 19-1, which depicts the normal low-resolution spectrum on the ω_2 axis

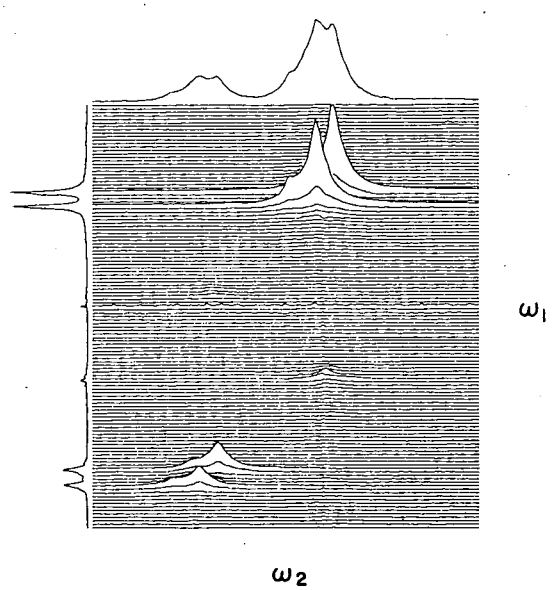

Figure 19-1. A coherence-transfer-echo experiment on neat alcohol (25% 1-^{13}C, 25% 2-^{13}C, 50% ^{13}C) in poor-field inhomogeneity to illustrate the carbon chemical shift and narrow lines along ω_1, and the broad unresolved proton lines along ω_2. (XBL 851-753)

and the high-resolution coherence-transfer spectrum on the ω_1 axis. Spatially selective NMR spectra will now be possible even in the realistically large magnets required for imaging.

20. Molecules on Zeolites (Publication 27)

E. Schneider, M. Trecoske, R. Eckman,† and A. Pines

The molecular-sieve properties of porous solids (e.g., zeolites) are industrially important as catalysts and adsorbents. To better understand this selectivity, solid-state NMR is being used to study the motions and nature of interactions of organic molecules in zeolites. Deuterium is a sensitive probe of the local environment for disordered solids. Progress to date includes building a glass vacuum (10^{-6} Torr) line for sample preparation, refining sorption techniques, and determining high-field ^{2}H and ^{1}H spin-lattice relaxation times (T_1, which must be >1 second to detect the signal) for various samples. A high-sensitivity solid-state NMR probe with variable temperature to lengthen T_1 has been constructed. Theoretical calculations have been made on the effect on various restricted motions on solid-state NMR line shapes (see Figure 20-1).

†Permanent address: Exxon Chemical Company, Baytown, Texas 77520.

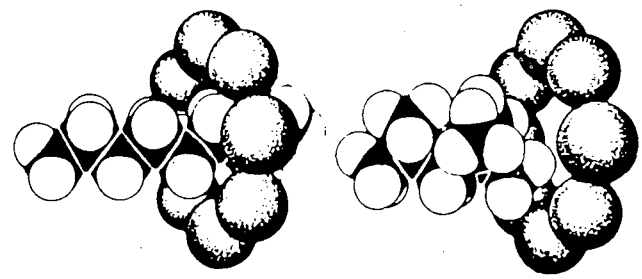

Figure 20-1. Schematic illustration of the entry of straight-chain hydrocarbons and the blockage of branch-chain hydrocarbons at channel apertures. (XBL 851-931)

21. Differentiation Between ^{27}Al Nuclei in Alums by Fourier-Transform Pure NQR (Publication 5)

D.B. Zax, A. Bielecki, A. Pines, and S.W. Sinton†

In light of the successful application of magic-angle spinning (MAS) to studies of ^{29}Si in zeolites, one might expect the same technique to be of considerable use in studies of ^{27}Al. When applied to aluminum, however, MAS generally reveals only the difference between tetrahedral or octahedral sites. The small dispersion in ^{27}Al chemical shifts and the broad lines due to second-order quadrupole coupling limit the applicability of the method. Our approach is, instead, to utilize the chemical sensitivity of pure NQR. High-sensitivity pure NQR measurements are made by our pulsed-field cycling Fourier-transform technique. For a spin-5/2 nucleus, such as ^{27}Al, we expect to observe a pair of lines for each crystalline site. Figure 21-1 illustrates the results for two simi-

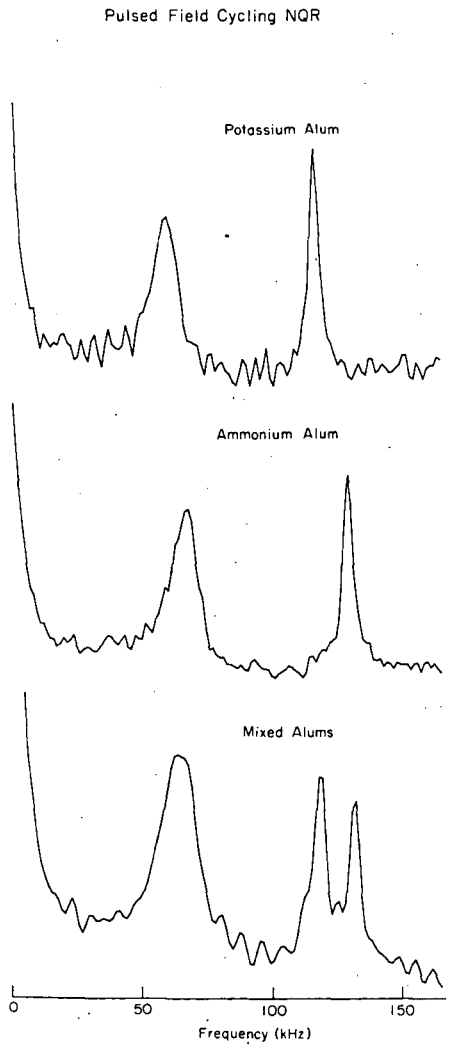

Figure 21-1. ^{27}Al Fourier-transform pure nuclear-quadrupole-resonance spectra of representative alums. Each site contributes two lines to the zero-field spectrum. The asymmetry parameter in the quadrupole tensor, η, was calculated to be 0.17 for potassium alum and ammonium alum. Respective values of 391 and 438 kHz were obtained for the quadrupole coupling constant, $(e^2qQ)/h$, where eQ is the nuclear quadrupole moment, eq is the electric-field gradient, and h is Planck's constant. The pair of high-frequency lines in the mixed sample (56 mol% potassium alum, 44 mol% ammonium alum) clearly indicates the existence of two distinct ^{27}Al sites. (XBL 844-1460)

lar aluminum-containing samples, ammonium and potassium alums. Despite nearly identical crystal structures and high-field MAS NMR spectra, the zero-field NQR experiment clearly differentiates between the two types of aluminum nuclei.[1]

†Present address: Exxon Production Research Company, Houston, Texas 77001.

1. D.B. Zax, A. Bielecki, A. Pines, and S.W. Sinton, Nature **312**, 351 (1984).

22. High-Resolution ^{29}Si NMR Study of Silicate and Aluminosilicate Glasses. The Effect of Network-Modifying Cations (Publication 14)

J.B. Murdoch,† J.F. Stebbins,‡ I.S.E. Carmichael,‡ and A. Pines

The structure of silicate glasses is of interest not only with regard to their commercial applicability but also in that they are frozen approximations of silicate melts, for which a detailed knowledge of silicate speciation is needed to better understand magnetic processes. The effect of network-modifying alkali and alkaline-earth cations on the degree of polymerization is investigated using ^{29}Si MAS NMR. The NMR linewidth is found to increase (reflecting a broader range of silicate environments) as the polarizing power of the cation increases. A similar effect occurs in three-dimensional-framework aluminosilicate glasses: smaller, more highly charged cations create greater variety in the distribution of silicate and aluminate tetrahedra. Linewidths as a function of the silicon-to-aluminum ratio suggest, however, that Lowenstein's aluminum-avoidance principle is largely obeyed. Spectra of three natural silica-rich glasses have been analyzed in terms of the Si/Al ratio and the concentration of paramagnetic species (see Figure 22-1).

†Present address: Technicare Corporation, Cleveland, Ohio 44101.

‡Permanent address: Earth Sciences Division, Lawrence Berkeley Laboratory.

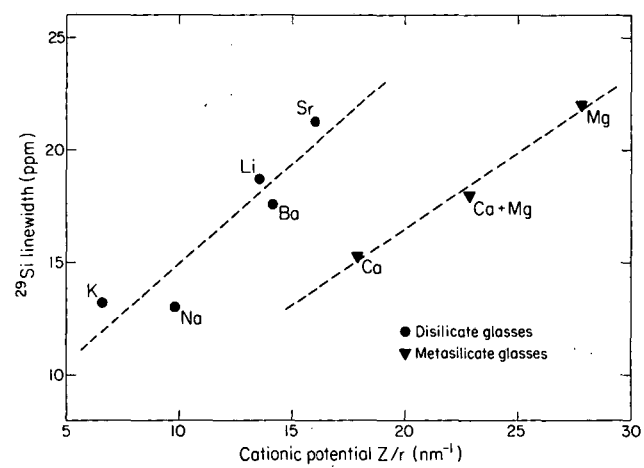

Figure 22-1. Integrated linewidths (peak area/height) of disilicate and metasilicate glasses as a function of the ionic potential (charge/radius) of the network-modifying cation. For $CaMgSi_2O_6$, the cationic potential was assumed to be the average of the values for Ca and Mg. (XBL 842-6945)

23. High-Temperature ^{23}Na, ^{27}Al, and ^{29}Si NMR in Molten Silicates (Publication 28)

J.F. Stebbins,† J.B. Murdoch,‡ E. Schneider, I.S.E. Carmichael,† and A. Pines

We have developed a novel, high-temperature (≥ 1400°C), high-resolution NMR apparatus to study the dynamics of molecular motion and structural rearrangement in molten silicates. We have studied the system Na_2O-Al_2O_3-SiO_2 using ^{23}Na, ^{27}Al, and ^{29}Si NMR. As has been observed in glasses and crystals, chemical-shift values (δ) of ^{29}Si in melts become more negative (greater chemical shielding) with increased polymerization (see Figure 23-1). Similarly, ^{23}Na decreases with increasing O/Na ratio. Spin-spin relaxation times for ^{23}Na and ^{29}Si dramatically decrease with falling temperature until liquid-like spectra become solid-like. ^{27}Al spectra are very broad at all temperatures due to strong quadrupole coupling. We are studying high-temperature liquid-relaxation times as a function of temperature to probe the molecular dynamics of aluminosilicates.

†Permanent address: Earth Sciences Division, Lawrence Berkeley Laboratory.

‡Present address: Technicare Corporation, Cleveland, Ohio 44101.

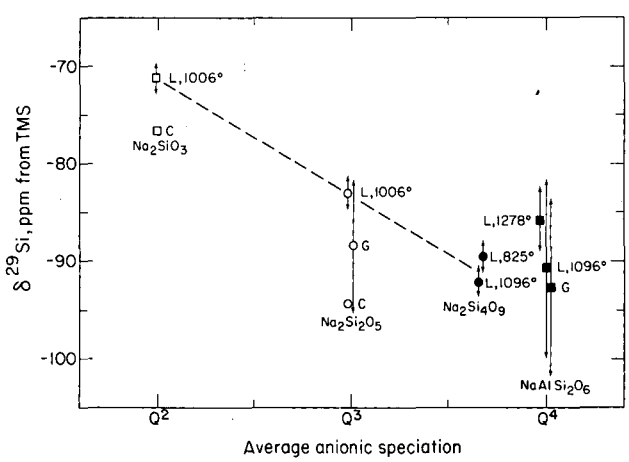

Figure 23-1. ^{29}Si chemical shifts in silicates. Symbols indicate composition. Solid circles: $Na_2Si_4O_9$; open circles: $Na_2Si_2O_5$; solid squares: $NaAlSi_2O_6$; open squares: Na_2SiO_3. L indicates liquid (at temperatures shown), C indicates crystalline solid, and G indicates glass (the latter two at room temperature). Arrows indicate linewidths, not errors. Q_n is the average speciation of the liquid, indicting n other $(Si, Al)_4$ tetrahedral structural groups attached to a given group. (XBL 849-9924)

1984 PUBLICATIONS AND REPORTS

Refereed Journals

1. R. Tycko and A. Pines, "Spatial Localization of NMR Signals by Narrowband Inversion," J. Magn. Reson. **60**, 156 (1984); LBL-17793.
2. R. Tycko, E. Schneider, and A. Pines, "Broadband Population Inversion in Solid-State NMR," J. Chem. Phys. **81**, 680 (1984); LBL-17505.
3. J. Baum, R. Tycko, and A. Pines, "Phase Modulated Pulses for Adiabatic Population Inversion," J. Chem. Phys. **79**, 4643 (1983); LBL-16098.
4. D.B. Zax, A. Bielecki, K.W. Zilm, and A. Pines, "Heteronuclear Zero Field NMR," Chem. Phys. Lett. **106**, 550 (1984); LBL-17506.
5. D.B. Zax, A. Bielecki, A. Pines, and S. Sinton, "Differentiation between ^{27}Al Nuclei in Alums by Fourier Transform Pure NQR," Nature **312**, 351 (1984); LBL-18474.
6. S. Sinton, D.B. Zax, J.B. Murdoch, and A. Pines, "Multiple-Quantum NMR Study of Molecular Structure and Ordering in a Liquid Crystal," Mol. Phys. **53**, 333 (1984); LBL-16685.
7. A.N. Garroway, J. Baum, M.G. Munowitz, and A. Pines, "NMR Imaging in Solids by Multiple-Quantum Resonance," J. Magn. Reson. **60**, 337 (1984); LBL-18173.
8. A. Bielecki, J.B. Murdoch, D.P. Weitekamp, D.B. Zax, K.W. Zilm, and A. Pines, "Fourier Transform Pure Nuclear Quadrupole Resonance by Pulsed Field Cycling," J. Chem. Phys. **80**, 2232 (1984); LBL-17167.
9. J.B. Murdoch, W.S. Warren, D.P. Weitekamp, and A. Pines, "Computer Simulations of Multiple-Quantum NMR Experiments. I. Non-Selective Excitation," J. Magn. Reson. **60**, 205 (1984); LBL-17184.
10. W.S. Warren, J.B. Murdoch, and A. Pines, "Computer Simulations of Multiple-Quantum NMR Experiments. II. Selective Excitation," J. Magn. Reson. **60**, 236 (1984); LBL-17185.
11. R. Tycko and A. Pines, "Iterative Schemes for Broadband and Narrowband Population Inversion in NMR," Chem. Phys. Lett. **111**, 462 (1984); LBL-18103.
12. R. Tycko, H. Cho, E. Schneider, and A. Pines, "Composite Pulses Without Phase Distortion," J. Magn. Reson. **61**, 90 (1985); LBL-17794.

LBL Reports

13. T.M. Barbara, R. Tycko, and D.P. Weitekamp, "Composite Sequences for Efficient Double Quan-

tum Excitation Over a Range of Spin Coupling Strengths," J. Magn. Reson. (in press); LBL-18090.

14. J.B. Murdoch, J. Stebbins, I.S.E. Carmichael, and A. Pines, "High-Resolution ^{29}Si NMR Study of Silicate and Aluminosilicate Glasses, The Effect of Network-Modifying Cations," Amer. Mineralogist (in press); LBL-17537.
15. A. Bielecki, D.B. Zax, K. Zilm, and A. Pines, "Zero Field NMR Spectrometer," LBL-18842.
16. H. Cho, R. Tycko, A. Pines, and J. Guckenheimer, "Pulse Iteration Schemes with Two Fixed Points," LBL-18863.
17. J. Baum, R. Tycko, and A. Pines, "Spatial Selectivity in Topical NMR," LBL-18870.
18. R. Tycko, J. Guckenheimer, and A. Pines, "Fixed Point Analysis of Iterative Excitation Schemes in NMR," submitted to J. Chem. Phys.; LBL-18936.
19. A. Bielecki, D.B. Zax, M. Kulick, E. Muetterties, and A. Pines, "Zero Field Study of $H_2Os_3(CO)_{10}$," LBL-18762.
20. A. Bielecki, J. Millar, A. Thayer, D.B. Zax, and A. Pines, "Pulsed Zero Field NQR," LBL-18812.
21. A. Bielecki, J. Millar, A. Thayer, D.B. Zax, and A. Pines, "Deuterium Quadrupole Coupling Constants and Asymmetry Parameters from Zero Field NQR Spectra," LBL-18993.
22. M. Gochin, D.P. Weitekamp, and A. Pines, "Heteronuclear Coherence Transfer Echo Spectroscopy," LBL-18866.
23. M. Gochin and A. Pines, "Multiple Quantum NMR in Liquid Crystals for Spectroscopic Isomer Separation," LBL-18867.
24. J. Baum, M.G. Munowitz, A.N. Garroway, and A. Pines, "Multiple-Quantum Dynamics in Solid-State NMR," LBL-18813.
25. M.G. Munowitz, J. Baum, A.N. Garroway, and A. Pines, "Identification of Nuclear Spin Clusters in Solids by Multiple-Quantum NMR," LBL-18991.
26. A.N. Garroway, "Phase Enhancement for Precise Determination of Small RF Phase Angles," submitted to J. Magn. Reson.; LBL-18862.
27. E. Schneider, M. Trecoske, R. Eckman, and A. Pines, "Molecules on Zeolites," LBL-18992.
28. J.F. Stebbins, J.B. Murdoch, E. Schneider, I.S.E. Carmichael, and A. Pines, "High Temperature ^{23}Na, ^{27}Al, and ^{29}Si NMR in Molten Silicates," Nature (in press); LBL-18515.
29. D.B. Zax, A. Bielecki, K. Zilm, A. Pines, and D.P. Weitekamp, "Time Domain Zero Field NMR and NQR," submitted to J. Chem. Phys.; LBL-18811.

Invited Talks

30. A. Pines, "NMR and Nonlinear Spin Dynamics," colloquium, Department of Physics, University of Munich, West Germany, March 12, 1984.
31. A. Pines, "NMR and Nonlinear Spin Dynamics," departmental seminar, Department of Chemistry, University of Pennsylvania, Philadelphia, March 26, 1984.
32. A. Bielecki, J.B. Murdoch, D.P. Weitekamp, D.B. Zax, K.W. Zilm, and A. Pines, "Zero Field NMR and NQR," 25th Experimental Nuclear Magnetic Resonance Spectroscopy Conference, Wilmington, Delaware, April 1984.
33. A.N. Garroway, J. Baum, M. Munowitz, and A. Pines, "Multiple Quantum NMR," 25th Experimental Nuclear Magnetic Resonance Spectroscopy Conference, Wilmington, Delaware, April 1984.
34. A. Pines, "New Techniques in Solid State NMR," departmental seminar, Physics Department, University of Stuttgart, West Germany, May 4, 1984.
35. A. Pines, "NMR with Irregular Irradiation," colloquium, Physics Department, University of Ulm, West Germany, May 7, 1984.
36. A. Pines, "Recent Development in NMR by Regular and Irregular Irradiation," physics colloquium, University of Bayreuth, West Germany, May 8, 1984.
37. A. Pines, "Zero Field NMR," departmental seminar, Department of Chemistry, University of California, Irvine, May 21, 1984.
38. A. Pines, "MQ-Zero Field NMR," departmental seminar, School of Chemistry, Georgia Institute of Technology, Atlanta, May 24, 1984.
39. A. Pines, "Zero Field NMR," 7th European Experimental NMR Conference (E.E.N.C.), Palermo, Italy, May 29–June 1, 1984.
40. A. Pines, "Some New Ways of Fooling the Spins," departmental seminar, Huygens Laboratory of Physics, University of Leiden, The Netherlands, June 4, 1984.
41. A. Pines, "NMR with Regular and Irregular Radiation," Chemische Gesellschaft Zurich, Switzerland, June 6, 1984.
42. A. Pines, "NMR with Regular and Irregular Irradiation," department colloquium, Physics Department, University of Berlin, West Germany, June 6, 1984.
43. A. Pines, "NMR with Irregular Radiation," Department of Physics, University of Dortmund, West Germany, June 19, 1984.

44. A. Pines, "NMR with Regular and Irregular Irradiation," Max-Planck Institute of Solid-State Physics, Stuttgart, West Germany, June 26, 1984.
45. A. Pines, "Zero Field NMR," Max-Planck Institute for Polymers and Department of Physics, University of Mainz, West Germany, July 1, 1984.
46. A. Pines and D.B. Zax (speaker), "Zero Field NMR," 26th Rocky Mountain Conference, Denver, Colorado, August 5–9, 1984.
47. A. Pines and D.P. Weitekamp (speaker), "Developments in Solid State Multiple Quantum Spectroscopy," XXII Ampere Congress, Zurich, Switzerland, September 10–15, 1984.
48. D.B. Zax, A. Bielecki, D.P. Weitekamp, K.W. Zilm, and A. Pines, "Time Domain Zero Field Magnetic Resonance," XXII Ampere Congress, Zurich, Switzerland, September 10–15, 1984.
49. J. Baum, A.N. Garroway, M. Munowitz, and A. Pines, "Multiple-Quantum NMR in Solids: Application to Spin Imaging," XXII Ampere Congress, Zurich, Switzerland, September 10–15, 1984.
50. A. Pines, "New Approaches to Volume Selective Excitation in *In Vivo* NMR Spectroscopy," General Electric Company—Medical Systems Operations, Milwaukee, Wisconsin, September 20, 1984.
51. A. Pines, "Irreversibility," Department of Chemistry, University of Oklahoma, Norman, September 27, 1984.
52. A. Pines, "Unusual NMR in Unusual Systems," ACS/SAS Pacific Conference on Chemistry and Spectroscopy, Symposium on Modern NMR Methods, Sacramento, California, October 11, 1984.
53. A. Pines, "Recent Developments in Solid State NMR," Chevron Research Company, Richmond, California, October 19, 1984.
54. A. Pines, "Broadband Nonlinear Excitation in Spectroscopy," Colloquium Series in Nonlinear Systems and Dynamics, Research Group in Nonlinear Systems and Dynamics, Center for Pure and Applied Mathematics, Berkeley, California, October 30, 1984.

Chemical Sciences

FUNDAMENTAL INTERACTIONS

PHOTOCHEMICAL AND RADIATION SCIENCES

Photon-Assisted Surface Reactions, Materials, and Mechanisms*

Gabor A. Somorjai, Investigator

INTRODUCTION

This project explores the photocatalyzed dissociation of water (H_2O) at both the solid-liquid and solid-vapor interfaces to produce hydrogen and oxygen gases. The purposes of these studies are to explore the mechanism of the photon-assisted surface reaction, to characterize the semiconductor catalyst, and to establish the optimum conditions of surface structure, composition, temperature, and electrolyte solution that maximize both the rate of hydrogen and oxygen production and the power-conversion efficiency of the process. Materials used include silicon- and magnesium-doped iron oxides as small particles, thin films, and single crystals.

1. The Characterization of Doped Iron Oxide Electrodes for the Photodissociation of Water: Stability, Optical, and Electronic Properties (Publication 1)

J.E. Turner,† M. Hendewerk, J. Parmeter, D. Neiman, and G.A. Somorjai

We have studied the optical and electronic properties for p-type (Mg-doped) and n-type (Si-doped) iron oxides used in the photoelectrolysis of water. Photocurrent vs. wavelength spectra for these electrodes indicate that α-Fe_2O_3 is the active optical component for both p-type and n-type materials. Band-edge locations for p-type and n-type iron oxides in sodium hydroxide aqueous solution are determined from differential capacitance measurements. The thermodynamic feasibility of the catalytic photodissociation of water without external potential is demonstrated for a short-circuited p/n diode assembly on an energy-level diagram of the electrode/electrolyte interfaces. The open-circuit voltage (V_{oc}) and short-circuit current (I_{sc}) generated by the p/n assembly as a function of the intensity of laser irradiation indicate that these doped iron oxides are low-mobility, high-carrier-density semiconductors. Photooxidation of water at the n-type anode is verified through oxygen detection. Gas evolution is monitored from an operating diode assembly using mass spectrometry and isotopically labeled water ($H_2^{18}O$). Photocurrents from these p/n assemblies show excellent long-term stability in aqueous solution, and Auger analysis of the semiconductor surfaces indicates no evidence of electrode dissolution.

*This work was supported by the Director, Office of Energy Research, Office of Basic Energy Sciences, Chemical Sciences Division of the U.S. Department of Energy under Contract No. DE-AC03-76SF00098.

†Present address: Materials Research Laboratory, Hewlett-Packard, Palo Alto, California 94304.

2. Catalyzed Photodissociation of Water—The First Step in Inorganic Photosynthesis? (Publication 2)

G.A. Somorjai and J.E. Turner†

We have carried out surface-science studies of the complex mechanisms that lead to the photochemical decomposition of water over two transition-metal oxides: strontium titanate (type I) and iron oxide (type II). We have utilized electron-spectroscopy techniques (photoelectron, Auger electron, and electron loss) to monitor the surface composition and oxidation states of surface atoms. Other techniques use a reaction cell that permits monitoring of photocurrents as well as the evolution of gases (H_2 and O_2) generated by the photoreaction. As a result, many of the elementary reaction steps leading to H_2 and O_2 evolution have been identified. For instance, photocatalyzed dissociation of water represents the first important step in photosynthesis: the production of oxygen and a reactive intermedi-

ate, hydrogen. The subsequent reactions of H_2 with CO_2 to produce hydrocarbons or organic molecules containing oxygen are exothermic. These reactions occur readily without illumination on suitable catalysts in the appropriate temperature range.

†Present address: Materials Research Laboratory, Hewlett-Packard, Palo Alto, California 94304.

3. The Catalyzed Photodissociation of Water (Publication 4)

G.A. Somorjai, M. Hendewerk, and J.E. Turner†

The dissociation of water to hydrogen and oxygen requires energy of ΔG_{298} = 228 kJ/mole. By irradiating a semiconductor with light of energy greater than this amount, one may produce electrons in the excited state and electron vacancies at the surface that can perform the photochemical reduction ($2H^+ + 2e^- \rightarrow 2H \rightarrow H_2$) and oxidation ($2OH^- + 2+ \rightarrow H_2O_2 \rightarrow H_2O + (1/2)O_2$).

There are several semiconductors, $SrTiO_3$, TiO_2, CdS, and Fe_2O_3 among them, that can photodissociate water. Some possess sites for both reduction and oxidation, while others carry out the two processes at different surfaces. A reversible solid-state reaction that involves changes in the transition-metal and ion-oxidation state must accompany the splitting of water. Platinum, rhodium, and ruthenium oxide, when deposited on the semiconductor, serve as catalysts that accelerate the water photodissociation. These additives accelerate the recombination of hydrogen and oxygen atoms, shift the semiconductor Fermi level to a more favorable position that improves the thermodynamic feasibility for the process, accelerate electron transport, and inhibit side reactions like the photoreduction of oxygen. Many of the elementary reaction steps leading to photoproduction of hydrogen and oxygen over $SrTiO_3$ and Fe_2O_3 have been identified.

†Present address: Materials Research Laboratory, Hewlett-Packard, Palo Alto, California 94304.

4. Preparation, Characterization, and Photoelectronic Properties of Germanium-Substituted Fe_2O_3 Single Crystals (Publication 5)

K.D. Sieber,† *C. Sanchez, J.E. Turner,*‡ *and G.A. Somorjai*

Single crystals of germanium-substituted Fe_2O_3 were grown using chemical vapor transport with tellurium tetrachloride, and their crystallographic, electrical, magnetic, and photoelectronic properties were measured. Germanium-substituted Fe_2O_3 crystallized with the corundum structure and is an extrinsic n-type semiconductor with a room-temperature resistivity of around 5 Ω cm and an impurity ionization energy of 0.12 eV. Low-temperature susceptibility measurements suggest that insertion of Ge(IV) leads to reduction of iron(III) to iron(II) without spinel-phase inclusion. Photoelectrochemical measurements and determinations of the flatband potential by different techniques suggest that the behavior of Fe_2O_3 photoanodes may be influenced by energy levels in the band gap near the conduction band.

†Present address: Eastman Kodak Company, Rochester, New York 14650.

‡Present address: Materials Research Laboratory, Hewlett-Packard, Palo Alto, California 94304.

5. Preparation, and Electrical and Photoelectrochemical Properties of Magnesium-Doped Iron Oxide-Sintered Discs (Publication 6)

K.D. Sieber,† *C. Sanchez, J.E. Turner,*‡ *and G.A. Somorjai*

Sintered discs of magnesium-substituted iron oxides have been prepared by gel routes or classical solid-state reaction techniques, and their crystallographic, electrical, and photoelectrochemical properties have been examined. The discs, sintered

between 1200 and 1400°C for 20 hours, contain both α-Fe_2O_3 and a spinel phase. The electrical properties of the discs have been correlated with spinel concentration, the electrical resistivity decreasing with increasing spinel content. The materials were found to be consistently n-type by Seebeck voltage measurements. Photoelectrochemical measurements in aqueous solution showed, however, that the sintered disc electrodes exhibit photocathodic currents that are characteristic of p-type semiconductors. Evidence is presented that suggests that inhomogeneities in the near-surface region of the discs are responsible for the observed photoelectrochemical properties.

---

†Present address: Eastman Kodak Company, Rochester, New York 14650.

‡Present address: Materials Research Laboratory, Hewlett-Packard, Palo Alto, California 94304.

6. Work in Progress

The bonding, chemisorption, and photoinduced chemical changes of adsorbed H_2O, H_2, and O_2 over iron oxide single-crystal surfaces are being studied using electron spectroscopies at low pressures to explore the elementary steps of water photodissociation.

The use of transition-metal additives is being investigated as a possible means of increasing the quantum efficiency of the photodissociation of water.

The stability and efficiency of sputtered n-type and p-type iron oxide films for the photodissociation of water are being explored.

1984 PUBLICATIONS AND REPORTS

Refereed Journals

1. J.E. Turner, M. Hendewerk, J. Parmeter, D. Neiman, and G.A. Somorjai, "The Characterization of Doped Iron Oxide Electrodes for Photodissociation of Water: Stability, Optical and Electronic Properties," J. Electrochem. Soc. **131**, 1777 (1984); LBL-16411.
2. J.E. Turner and G.A. Somorjai, "Catalyzed Photodissociation of Water—The First Step of Inorganic Photosynthesis," Die Naturwissenschaften **71**, 575 (1984); LBL-17664.
3. J.E. Turner, M. Hendewerk, and G.A. Somorjai, "The Photodissociation of Water by Doped Iron Oxides: The Unbiased P/N Assembly," Chem. Phys. Lett. **105**, 581 (1984); LBL-16134.

LBL Reports

4. M. Hendewerk, J.E. Turner, and G.A. Somorjai, "The Catalyzed Photodissociation of Water," submitted to *Proc. 2nd Berkeley Catalysis and Surface Science Conf.*, January 11–13, 1984, Lawrence Berkeley Laboratory; LBL-17670.
5. K. Sieber, C. Sanchez, J.E. Turner, and G.A. Somorjai, "Preparation, Characterization, and Photoelectronic Properties of Germanium Substituted Fe_2O_3 Single Crystals," J. Chem. Soc., Faraday Trans. (in press); LBL-18033.
6. K. Sieber, C. Sanchez, J.E. Turner, and G.A. Somorjai, "Preparation, Electrical and Photoelectrochemical Properties of Magnesium Doped Iron Oxide Sintered Discs," Mat. Res. Bull. (in press); LBL-18333.

Invited Talks

7. G.A. Somorjai, "The Catalyzed Photodissociation of Water," Second Berkeley Catalysis and Surface Science Conference, Lawrence Berkeley Laboratory, Berkeley, California, January 13, 1984.
8. G.A. Somorjai, "The Surface Science of Energy Conversion. The Catalyzed Reactions of Water, Carbon and Methane," The Fred J. Robbins Lectureship, Pomona College, Claremont, California, March 29, 1984.
9. G.A. Somorjai, "The Photocatalyzed Dissociation of Water," The George A. Abbott Lectureship in Chemistry, University of North Dakota, Grand Forks, April 13, 1984.
10. G.A. Somorjai, "Adsorption of Energy in Photocatalytic Reactors," NATO Advanced Study Institute Symposium on Fundamentals and Developments of Photocatalytic and Photoelectrochemical Processes, Erice, Italy, May 27, 1984.

Photochemistry of Materials in the Stratosphere*

Harold S. Johnston, Investigator

INTRODUCTION

This research is concerned with fundamental gas-phase photochemistry, with application to chemical species that occur in the stratosphere. Laboratory studies are carried out to obtain optical cross sections, quantum yields, information about microscopic states, and macroscopic rate coefficients for molecules and reactions currently important toward interpreting atmospheric observations. The experimental methods include visible- and ultraviolet-laser flash photolysis, laser resonance absorption, resonance fluorescence, and infrared-diode lasers. Theoretical methods include gas-phase reaction-rate theory and some molecular quantum mechanics. This research has applications to problems of atmospheric ozone and to the role of trace gases other than carbon dioxide on the "greenhouse effect."

1. Unimolecular Decomposition of NO_3 to Form NO and O_2 (Publication 6)†

Harold S. Johnston, C.A. Cantrell, and J.G. Calvert

The nitrate free radical NO_3 has been observed by several investigators in the troposphere at night. It increases during the night much less than predicted in terms of known processes, and there has been a search for an unknown NO_3 scavenger. This article finds evidence in the chemical literature for the thermal decomposition of NO_3 to form nitric oxide and molecular oxygen, (w) $NO_3 + M = NO + O_2 + M$; and the rate is such that this reaction is proposed as a scavenging process in the troposphere. By straightforward reinterpretation of three room-temperature kinetic studies that used reactors of widely different volumes, we find the first-order rate constant at one-atmosphere pressure to be $3 \pm 2 \times 10^{-3}$ sec^{-1}. In a high-temperature shock tube Schott and Davidson evaluated rate constants for (e) $NO_2 + NO_3 = NO + O_2 + NO_2$ and (g) $2NO_3 = 2NO_2 + O_2$, but these values are strongly different from extrapolated results of Graham and Johnston. This difference is ascribed to the unrecognized contribution of reaction w in Schott and Davidson's system, and with this assumption we evaluated the rate constants for w at high temperatures to give the Arrhenius expression 1×10^{-12} exp(-6840/T) cm^3 $molecule^{-1}$ sec^{-1} (see Figure 1-1). This relation implies that the unimolecular reaction has a low frequency factor and a low activation energy, which are related to the presence of a low-lying excited electronic state of NO_3. The rate of this channel of decomposition is compared with the much slower process leading to NO_2 and O as products. Although this article gives strong evidence that the reaction $NO_3 = NO + O_2$ occurs, the quantitative values of rate coefficients are noisy and uncertain, and there are no data concerning the effect of foreign gas pressure. This article points out two methods whereby deliberate studies of this reaction should be able to confirm its existence, establish its rate coefficients, and find its M-gas dependence.

*This work was supported by the Director, Office of Energy Research, Office of Basic Energy Sciences, Chemical Sciences Division of the U.S. Department of Energy under Contract No. DE-AC03-76SF00098.

†C.A. Cantrell and J.G. Calvert were supported by the National Science Foundation at the National Center for Atmospheric Research, Boulder, Colorado.

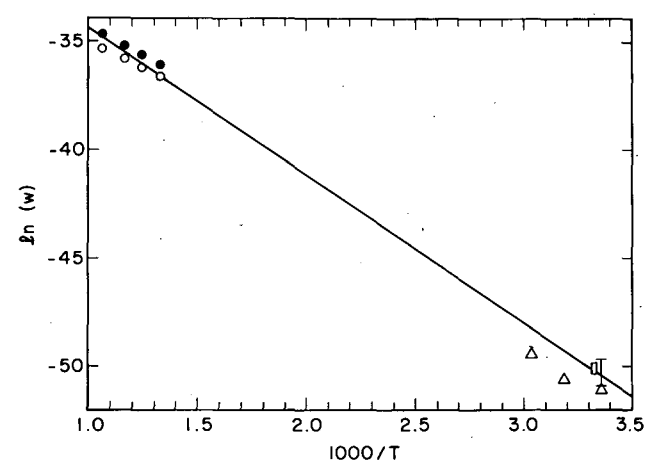

Figure 1-1. Values for the rate constant for $NO_3 \rightarrow NO + O_2$ found by four different methods: Δ, Graham (1975); ○ and ●, Schott and Davidson (1958); [], Cantrell and Calvert (1984); I, Tuazon et al. (1984). The least-squares line gives equal weight to each of 28 values. (XBL 853-1488)

2. Human Effects on the Global Atmosphere (Publication 3)

Harold S. Johnston

This review considers whether human activities can significantly change important functions of the global atmosphere by altering the amount or distribution of certain trace species. It emphasizes two topics: stratospheric ozone and the role of trace species other than carbon dioxide on the "greenhouse effect." Over the past ten years as new information has become available, the predicted effects of increasing chlorofluorocarbons or of increasing stratospheric nitrogen oxides have changed, as indicated by Figure 2-1. The current understanding of this topic is summarized in Table 2-1. Whereas the trends in atmospheric species display compensating features as far as ozone is concerned, all of them except particulate matter move in one direction as far as the effect on surface temperature is concerned.

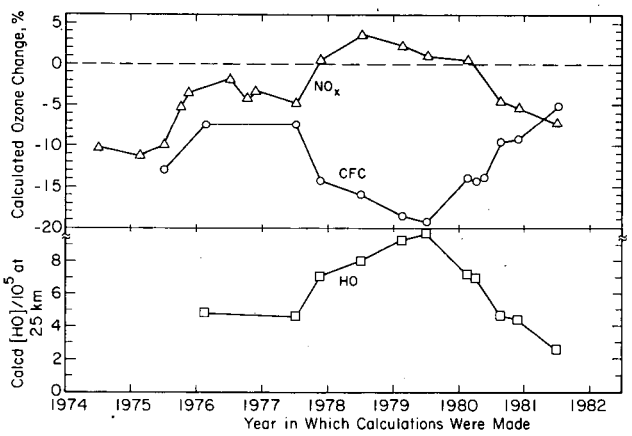

Figure 2-1. History of results of model calculations that differ only in differences in chemistry. The upper curve is the calculated steady-state percentage change of total ozone for an injection of 2000 molecules cm^{-3} sec^{-1} of NO between 19.5 and 20.5 km as the only perturbation (an artificial representation of a large fleet of stratospheric aircraft). The chlorofluorocarbon curve (CFC) is the calculated future steady-state ozone change for the sole perturbation of chlorofluorocarbon manufacture and release at the 1974 level. The lowest curve is the calculated concentration of hydroxyl radicals at 25 km, showing correlation and anticorrelation with the NO and chlorofluorocarbon curves. (XBL 853-1489)

Table 2-1

Effect of various human activites on certain atmospheric functions (+ = increasing effect; − = decreasing effect; ? = unknown effect)

Source	Present trend or status	Effect of increase on: Ozone	Surface temp.
CO_2	+	+	+
CH_4	+	+	+
N_2O	+	−	+
Chlorofluorocarbons	+	−	+
Aircraft below 13 km	+	+	+
Aircraft above 16 km	few	−	?
Particulate matter	+	?	−

3. Work in Progress

The diode laser has been used to measure the high-resolution absorption spectrum of the ν_2 band of the unstable but atmospherically important molecule HOCl. Over 1000 line positions and 300 absolute absorption-line strengths have been measured, and these data are now being interpreted. The pressure-broadening coefficients are being measured for several selected lines.

The "nascent" vibrational distribution of NO_3 is being studied as a result of N_2O_5 and of $ClNO_3$ photolysis by a pulsed ultraviolet laser, and the time-dependent population of excited radicals is followed by laser resonance absorption at the "hot-band" frequencies of the nitrate free radical. The concentration of vibrationally excited NO_3 is observed to increase and then decrease on the submicrosecond scale.

The contribution of intermediate complex formation on negative activation energies is being explored by calculations for a wide range of reactions, for which the second transition state has higher vibration frequencies than the first transition state.

1984 PUBLICATIONS AND REPORTS

Refereed Journals

1. Diane Swanson, Brian Kan, and Harold S. Johnston, "NO_3 Quantum Yields from N_2O_5 Photolysis," J. Phys. Chem. **88**, 3115 (1984); LBL-16951.
2. Harold S. Johnston, Mark Paige, and Francis Yao, "Oxygen Absorption Cross Sections in the Herzberg Continuum and between 206 and 327 K," J. Geophys. Res. **89**, 11661 (1984).
3. Harold S. Johnston, "Human Effects on the Global Atmosphere", Ann. Rev. Phys. Chem. **35**, 481 (1984); LBL-17290.

Other Publications

4. C.A. Cantrell, W.R. Stockwell, L.G. Anderson, K.L. Busarow, D. Perner, A. Schmeltekopf, J.G. Calvert, and H.S. Johnston, "A Kinetic Study of the NO_3-CH_2O Reaction and its Possible Role in the Nighttime Tropospheric Chemistry," submitted to J. Phys. Chem.†
5. D. Perner, A. Schmeltekopf, R.H. Winkler, H.S. Johnston, J.G. Calvert, C.A. Cantrell, and W.R. Stockwell, "A Laboratory and Field Study of the Equilibrium, $N_2O_5 = NO_2 + NO_3$," submitted to J. Geophys. Res.†
6. H.S. Johnston, C.A. Cantrell, and J.G. Calvert, "Unimolecular Decomposition of NO_3 to Form NO and O_2," submitted to J. Geophys. Res.‡

Invited Talks

7. H.S. Johnston, "NO_3," University of Colorado, Boulder, May 1984.
8. H.S. Johnston, "Recent Results of Stratospheric Model Calculations," Denver University, Colorado, June 1984.

---

†Supported by the National Science Foundation at the National Center for Atmospheric Research, Boulder, Colorado.

‡Supported in part by the National Science Foundation at the National Center for Atmospheric Research, Boulder, Colorado.

CHEMICAL PHYSICS

Energy Transfer and Structural Studies of Molecules on Surfaces*

Charles B. Harris, Investigator

INTRODUCTION

The goal of this research is to study the mechanisms that are responsible for the transfer of energy from the excited states of molecules to metal surfaces and to develop new laser techniques for probing molecule-surface interactions. The research program is both theoretical and experimental in character, and it includes nonlinear optical and picosecond laser techniques in addition to a variety of standard surface-science tools for characterizing molecule-surface interactions. The results of this program have a direct bearing on high-speed technological devices and materials, and on problems of general interest such as surface-enhanced photochemistry, the dynamics of surface photoemission, and the optical properties of thin films.

1. Nonclassical Behavior of Energy Transfer from Molecules to Metal Surfaces (Publication 11)

A.P. Alivisatos, D.H. Waldeck, and C.B. Harris

Electronically excited molecules near metal surfaces decay very rapidly. To understand this rapid decay, we can picture the molecule as a point oscillating dipole that nonradiatively transfers energy to the bulk metal electrons through its near field. A simple classical model of this type predicts that the energy transfer from the molecule to the metal will vary as $1/d^3$, where d is the dipole-metal separation. The $1/d^3$ prediction of the classical model has been shown to be valid for the case where the molecule is resonant with metal bulk interband transitions (e.g., Ni(111) and Ag(111) at 3.3 eV).

In this investigation the more general case, where the molecule cannot access metal interband excitations, is considered. In order for the excited molecule to decay via the production of an electronic excitation in the metal, it is necessary that momentum as well as energy be conserved. When the molecule is resonant with an interband excitation, this requirement is satisfied; however, when the molecule contains only enough energy to produce intraband excitations, the situation is more complicated. Then momentum conservation will allow the transfer of molecular energy to metal electrons only at the instant when they are undergoing a collision. If the mean free time between collisions for bulk electrons is very long (e.g., noble metals), then very little energy would be transferred to these electrons. In contrast, electrons localized near the metal surface undergo frequent collisions with the surface potential and are a good sink for the molecular energy. If the molecular energy is transferred primarily to surface rather than bulk electrons, then the energy-transfer rate will scale as $1/d^4$, rather than the usual $1/d^3$ dependence associated with transfer to the bulk.

In order to test this prediction, the lifetime of the first triplet state of biacetyl has been measured as a function of distance from Ag(111). The data as well as various theoretical fits are shown in Figure 1-1. The classical $1/d^3$ model has too shallow a slope and is unable to fit the data under any circumstances. The $1/d^4$ surface-damping model alone provides a better fit to the data, and when radiative-interference effects are included (as they are in the classical model), the surface-damping model provides an excellent fit. This work provides evidence for a classification scheme: molecular excited states that produce intraband electronic excitations transfer energy

*This work was supported by the Director, Office of Energy Research, Office of Basic Energy Sciences, Chemical Sciences Division of the U.S. Department of Energy Under Contract No. DE-AC03-76SF00098.

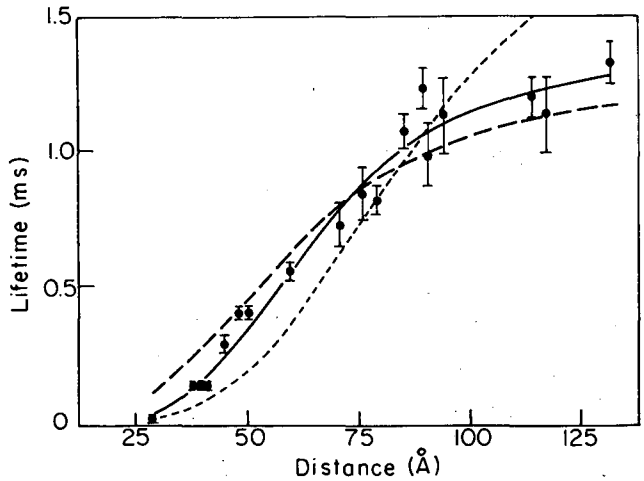

Figure 1-1. Plot of $^3n\pi^*$ biacetyl lifetime versus distance from the Ag(111) surface, in the regime where the surface-damping model is expected to dominate. The long-dash line is the best fit to the classical theory, and the solid line is the best fit to the surface-damping model including radiative effects. The short-dash line is the best fit to the surface-damping model without radiative effects. (XBL 847-7189)

to electrons localized near the metal surface, while those excited molecular states that can access direct interband excitations transfer energy to electrons throughout the bulk of the metal.

2. Nonradiative Damping of Molecular Electronic Excited States by Metal Surfaces (Publication 12)

D.H. Waldeck, A.P. Alivisatos, and C.B. Harris

The interaction of a molecular excited state with a smooth substrate is reviewed. Both theoretical and experimental work is treated. The classical treatment of the interaction is discussed first because of its success in comparison with experiment. The shortcomings of the classical treatment are also presented, together with some recent approaches to correcting these limitations. The experimental work is considered with a focus on the region close to the substrate, less than 500 Å away, because the longer-distance regime has been well reviewed. The possibility of rigorously testing the various corrections to the classical treatment experimentally is also briefly explored.

3. Picosecond Far-Infrared Generation by Parametric Mixing (Publication 13)

M. Berg, C.B. Harris, T.W. Kenney, and P.L. Richards

The study of ultrafast dynamics in the far-infrared has been hampered by the lack of suitable laser sources. This paper reports the generation of picosecond pulses at a 10-Hz repetition rate from 20-200 cm^{-1} with up to 1.6×10^{12} photons/pulse. The far-infrared is generated through the parametric interaction of two visible pulses: a high-power (35 GW/cm^2) picosecond pulse, and a lower-intensity (150 MW/cm^2) nanosecond pulse at a slightly lower frequency. A relatively constant quantum efficiency of 0.1–0.3% is found throughout the infrared frequency range, despite large variations in far-infrared absorption, diffraction, and phonon resonance enhancement.

At the intensities used, simple nonlinear optical equations predict very efficient conversion of the visible picosecond pulse to a far-infrared pulse ~10 ps long. Experimentally, 35–50% depletion of the visible picosecond pulse is observed, However, the quantum conversion to the far-infrared is considerably smaller. As expected for a strongly depleted process, the far-infrared energy is insensitive to the nanosecond power and only linearly dependent on the picosecond power. Although all pulses give significant far-infrared generation, the far-infrared energy shows unexpectedly large pulse-to-pulse fluctuations. If the origin of the losses and fluctuations can be understood, substantial improvements in the average efficiency may be possible.

4. Rapid Solvent-Induced Recombination and Slow Energy Relaxation in a Simple Chemical Reaction: Picosecond Studies of Iodine Photodissociation (Publication 8)†

M. Berg, A.L. Harris, and C.B. Harris

The iodine photodissociation reaction has been a primary model system for studying the effect of solvent dynamics on chemical reactions, yet the time scales involved in this system are still in controversy. Based on new picosecond absorption spectra, the

time scale for atom recombination appears to be ~15 ps. The previously observed slow recovery (>100 ps) of molecular absorption has been shown to be due to both ground-state vibrational relaxation and excited-state trapping in the recombined molecule. Trends in the vibrational relaxation rate and electronic-state relaxation rate measured in different solvents are incorrectly predicted by several current theories. In addition, newly observed absorptions in the blue/UV indicate that both solvent-induced predissociation and vibrational relaxation in the initially excited electronic state occur on a 10–15 ps time scale.

†Supported by the National Science Foundation using DOE equipment.

1984 PUBLICATIONS AND REPORTS

Refereed Journals

1. G.M. Goncher, C.A. Parsons, and C.B. Harris "Photochemistry on Metal Surfaces," J. Phys. Chem. (feature article) **88**, 4200 (1984); LBL-17000.
2. S.M. George, A.L. Harris, M. Berg, and C.B. Harris, "Picosecond Studies of the Temperature Dependence of Homogeneous and Inhomogeneous Vibrational Linewidth Broadening in Liquid Acetonitrile," J. Chem. Phys. **80**, 83 (1984); LBL-15641.
3. M. Berg, A.L. Harris, J.K. Brown, and C.B. Harris, "Generation of Tunable Picosecond Pulses in the Vibrational Infrared by Stimulated Electronic Raman Scattering of Rhodamine Dye Laser Pulses from the 6s-5d Cesium Transition," Opt. Lett. **9**, 50 (1984); LBL-17021.
4. A.L. Harris, J.K. Brown, M. Berg, and C.B. Harris, "Generation of Widely Tunable Nanosecond Pulses in the Vibrational Infrared by Stimulated Raman Scattering from the Cesium 6s-5d Transition," Opt. Lett. **9**, 47 (1984); LBL-17022.

Other Publications

5. D. Ben-Amotz, M. Berg, S.M. George, A.L. Harris, and C.B. Harris, "Picosecond Vibrational Dephasing Experiments in Liquids under High Laser Depletion Conditions," in *Conference Proceedings,* Italy, NATO Advanced Research Workshop on "Applications of Picosecond Laser Spectroscopy to Chemistry," K. Eisenthal, Ed., Reiden, Holland, 1983.†
6. A.L. Harris, M. Berg, J.K. Brown, and C.B. Harris, "A New Picosecond Source in the Vibrational Infrared," in *Proc. Ultrafast Phenomena Conf.,* K.B. Eisenthal, Ed., Optical Society of America, 1984.†
7. M. Berg, A.L. Harris, J.K. Brown, and C.B. Harris, "Iodine Photodissociation in Solution: New Transient Absorptions," in *Proc. Ultrafast Phenomena Conf.,* K.B. Eisenthal, Ed., Optical Society of America, 1984.†
8. M. Berg, A.L. Harris, and C.B. Harris, "Picosecond Studies of Solvent-Induced Predissociation, Vibrational Relaxation, and Electronic Curve Crossing in a Simple Chemical Reaction: Iodine Photodissociation in CCl_4," Phys. Rev. Lett. (in press).†

LBL Reports

9. G.M. Goncher (Ph.D. Thesis), "Enhanced Spectroscopy and Photochemistry of Molecules Adsorbed on Metal Surfaces," LBL-18452.
10. G.M. Goncher, C.A. Parsons, and C.B. Harris, "Enhanced Photochemistry on Metal Surfaces," Materials Research Society (in press); LBL-18420.
11. A.P. Alivisatos, D.H. Waldeck, and C.B. Harris, "Non-Classical Behaviour of Energy Transfer from Molecules to Metal Surfaces: Biacetyl ($^3n\pi^*$)/Ag(111)," J. Chem. Phys. (in press); LBL-18178.
12. D.H. Waldeck, A.P. Alivisatos, and C.B. Harris, "Nonradiative Damping of Molecular Electronic States by Metal Surfaces," Spec. Iss., Surf. Sci., North-Holland, 1984; LBL-19124.
13. M. Berg, C.B. Harris, T.W. Kenney, and P.L. Richards, "Picosecond Far-Infrared Generation by Parametric Mixing," in *Abs. Int. Conf. Lasers 1984;* LBL-19123abs.

Invited Talks

14. Charles B. Harris, "A New IR Picosecond Source and its Applications in Chemical Dynamics," Sixth International Conference on Lasers and Applications, San Francisco, California, December 12–16, 1983.
15. Charles B. Harris, "Energy Transfer and Photochemistry on Metal and Semiconductor Surfaces," Chemistry Department, University of California, Los Angeles, April 9, 1984.
16. Charles B. Harris, "Energy Transfer to Metal and Semiconductor Surfaces," Northern California Chapter of the American Vacuum Society Meeting, May 29, 1984.
17. Charles B. Harris, "A New Picosecond Source in the Vibrational Infrared," Topical Meeting on Ultrafast Phenomena, Optical Society of America, Monterey, California, June 12–15, 1984.

18. M. Berg, A.L. Harris, J.K. Brown, and C.B. Harris, "Iodine Photodissociation in Solution: New Transient Absorptions," Topical Meeting on Ultrafast Phenomena, Optical Society of America, Monterey, California, June 12–15, 1984.
19. Charles B. Harris, "Energy Transfer and Enhanced Photochemistry on Metal and Semiconductor Surfaces," International Symposium on Spectroscopic Studies of Adsorbates on Solid Surfaces, Kwansei Gakuin University, Japan, September 3–5, 1984.
20. A.P. Alivisatos, D.H. Waldeck, and C.B. Harris, "The Electronic Structure of Metals and their Ability to Quench Molecular Excited States," First International Conference on the Structure of Surfaces, Berkeley, California, August 13–16, 1984.
21. G.M. Goncher, C.A. Parsons, and C.B. Harris, "Surface Resonance Enhanced Multiphoton Fragmentation on Rough Metal Surfaces," First International Conference on the Structure of Surfaces, Berkeley, California, August 13–16, 1984.

†Supported by the National Science Foundation using DOE equipment.

Selective Photochemistry*

C. Bradley Moore, Investigator

INTRODUCTION

The fundamental goals of this program are to understand the photophysics and photochemistry that occur following selective excitation of molecules. Of particular interest are the chemical reactions of specifically excited states and the dynamics of energy transfer, both within the isolated molecule and following interactions with surrounding molecules. For low levels of vibrational excitation in small molecules, individual quantum states may be excited, enabling the measurement of reaction and energy-transfer rate constants for each quantum state. For larger or more highly excited molecules, it is usually not possible to excite single eigenstates. Instead, a number of eigenstates are excited simultaneously and a redistribution of the initial vibrational excitation occurs. This process, known as intramolecular vibrational energy redistribution (IVR), has so far proven too rapid for true mode-specific unimolecular reactions to be realized.

Advances in mode-specific chemistry will come from a more complete understanding of the IVR process and the parameters that control its efficiency. By being able to predict the rate of IVR and the path of vibrational energy flow through a molecule, experiments can be designed utilizing molecular systems that maximize the possibilities for mode-specific effects. Studies designed to elucidate the coupling mechanisms and dominant pathways for IVR are currently under way on a number of model systems.

The rates and mechanisms of free-radical reactions are often best studied by flash kinetic spectroscopy using lasers for thermal heating, for photolyzing, and for spectroscopic probing. Reactions can be studied as a function of individual quantum states. A fundamental understanding of these reactions is sought to serve as a basis for modeling combustion processes.

*This work was supported by the Director, Office of Energy Research, Office of Basic Energy Sciences, Chemical Sciences Division of the U.S. Department of Energy under Contract No. DE-AC03-76SF00098.

1. CH Stretch-Bend Interactions in the Trihalomethanes

William H. Green, Warren D. Lawrance, and C. Bradley Moore

Berry and co-workers[1] have shown that the linewidths of CH overtones in benzene first increase with increasing energy, as expected based on the increasing state density, but then go through a maximum and begin to decrease. Thus it appears that the vibrational redistribution rates do not simply increase monotonically with energy. These results have been interpreted by Sibert *et al.*[2] as being due to the presence of specific pathways for the vibrational energy flow from mode to mode. They suggest that the CH stretch and CCH in-plane wag motions are intimately connected through a strong Fermi resonance (anharmonic coupling), and that excitation of the stretch is quickly transferred to a combination of stretch and wag motion. This transfer requires a close proximity of the energy of the vibrations. As the overtone excitation increases, the anharmonicity of the CH overtone alters the energy separation, causing at first an increase in the interaction as the levels come closer in energy, and then a decrease as they pass by each other.

This kind of mechanical resonance in IVR should be quite general in CH-overtone spectra. Our research has focused on the closely related CH-stretch/CH-bend interactions. For the trihalomethanes, the presence of a single CH chromophore and a small number of vibrational modes considerably simplifies the spectra. For example, the strong interaction between the CH stretch and CH bend is clearly demonstrated by the presence of four strong absorption features rather than one for the fifth CH-stretch overtone of $CHCl_2F$ (see Figure 1-1). An analysis of the trihalomethane spectra in terms of a cubic anharmonic coupling between the stretch and bend modes reproduces the observed band positions and intensities. It is clear from this analysis that the interaction between the CH stretch and CH bend is the dominant influence. Furthermore, the coupling constant obtained from the analysis can be broken down into two contributions: the intrinsic anharmonicity of the potential surface for the CH bond, which requires extensive *ab initio* computations to calculate, and the more easily calculable kinetic anharmonicity induced by the pendulum-like motion of the CH bend. The kinetic anharmonicity is the largest contribution to the coupling, in agreement with the assumption of Sibert *et al.* in their calculations on benzene overtone line shapes.

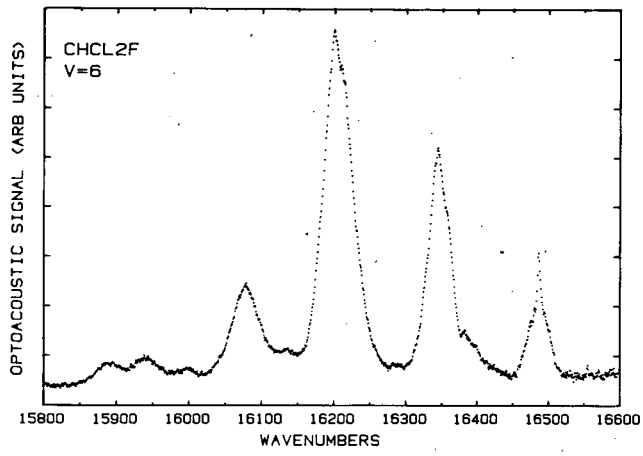

Figure 1-1. The $v_{CH} = 0 \rightarrow 6$ photoacoustic spectrum for CH stretching in $HCFCl_2$. One band would be observed in the absence of coupling; however, the $v_{CH} = 6$ level is strongly coupled to the $v_{CH} = 5$, $v_{bend} = 2$ levels. (XBL 853-1505)

For the halomethanes the CH-stretch/CH-bend interaction is separate from other coupling pathways; it appears as the extra features observed in the spectra. The CH stretch to CH bend IVR rate can be calculated from these data. The linewidths of the isolated features give further information on the coupling to other vibrational motions. It is clear that the motions of the halogens are much less strongly coupled, and the IVR lifetime is correspondingly much longer than for the CH stretch to CH bend energy transfer.

These overtone spectra, and their interpretation in terms of specific pathways for redistribution, highlight the existence of a wide variation in the coupling strengths between different types of nuclear motion, and they are encouraging for those interested in trying to induce reactions along a particular coordinate.

1. K.V. Reddy, D.F. Heller, and M.J. Berry, J. Chem. Phys. **76**, 2814 (1982).

2. E.L. Sibert, W.P. Reinhardt, and J.T. Hynes, Chem. Phys. Lett. **92**, 455 (1982).

2. Recombination of H^+ and OH^- in Pure Liquid Water (Publication 4)

Wesley C. Natzle and C. Bradley Moore

Relaxation times for the $H_2O \rightleftharpoons H^+ + OH^-$ equilibrium are measured as a function of temperature between 0 and 48°C and in H_2O-D_2O mixtures at 25 ± 1°C. Photoionization is produced by a short laser pulse. The measurements test the recombination mechanism proposed by Eigen[1] involving a rate-limiting diffusive encounter between free H^+ and OH^-. The relaxation times range between 233 μs and 14 μs. The corresponding recombination distance is found to be 5.9 ± 0.5 Å independent of temperature and isotopic composition (see Figure 2-1); the result is consistent with Eigen's four-molecule ion-pair intermediate (see Figure 2-2). Encounter rates, diffusive separation rates, overall ionization rates, and the ion-pair equilibrium constant are calculated from the 5.8-Å recombination distance for a range of temperatures and isotopic compositions. This study is part of an investigation of the quantum yield and mechanism for vibrational photochemistry in pure liquid water:

$$H_2O(l) + h\nu \rightarrow H^+(aq) + OH^-(aq).$$

1. M. Eigen, W. Kruse, G. Maas, and L. DeMaeyer, Prog. Reaction Kin. **2**, 285 (1964).

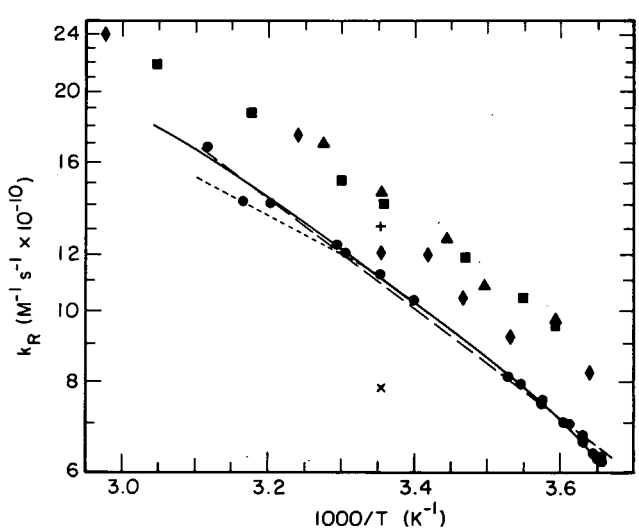

Figure 2-1. Arrhenius plot of $\ln(k_R)$ vs 1000/T for the thermal recombination in pure H_2O. The long-dashed line is a least-squares fit of these data, shown by circles. The solid curve is for $\sigma = 5.8$ Å. The short-dashed line and all other data points are from references in Publication 4 of the publications list. See Publication 4 for detailed references. (XBL 853-1506)

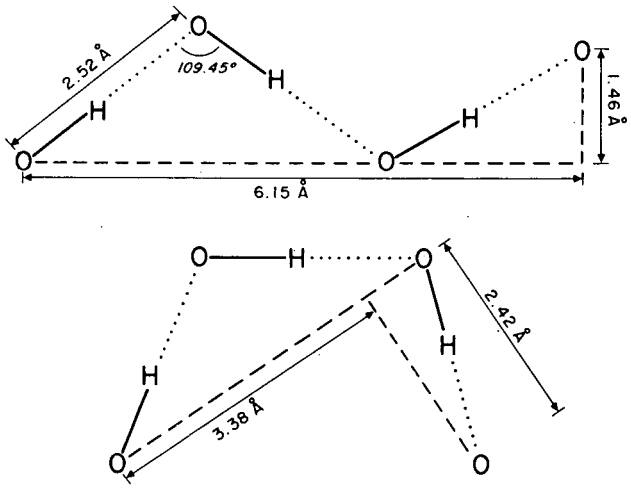

Figure 2-2. The maximum and minimum distance geometry for a linear chain of four hydrogen-bonded water molecules. The net O...O atom distances are 6.32 Å and 4.16 Å. (XBL 853-1507)

1984 PUBLICATIONS AND REPORTS

Refereed Journals

1. A.D. Abbate, T. Kawai, C.B. Moore, and C.-T. Chin, "Activation and Cleaning of Oxide Surfaces by Heating with a CO_2 Laser," Surf. Sci. Lett. **136**, L19 (1984); LBL-16678.
2. A.O. Langford and C.B. Moore, "Reaction and Relaxation of Vibrationally Excited Formyl Radicals," J. Chem. Phys. **80**, 4204 (1984); LBL-17026.
3. A.O. Langford and C.B. Moore, "Collision Complex Formation in the Reactions of Formyl Radicals With Nitric Oxide and Oxygen," J. Chem. Phys. **80**, 4211 (1984); LBL-17027.

LBL Reports

4. W.C. Natzle and C.B. Moore, "Recombination of H^+ and OH^- in Pure Liquid Water," J. Phys. Chem. (in press); LBL-17753.

Invited Talks

5. C.B. Moore, "Laser Flash Kinetic Spectroscopy: Studies of Molecular Structure, Energy Transfer, and Chemical Kinetics of Free Radicals," 1984 Annual Review Symposium, MMRD, LBL, February 6, 1984.
6. C.B. Moore, "Kinetics and Spectroscopy of Formyl and Methylene Radicals," Exxon Research Corporation, Clinton, New Jersey, February 21, 1984.
7. C.B. Moore, "Laser Probes of Unimolecular Reactions," Chemistry Colloquium, Princeton University, Princeton, New Jersey, February 22, 1984.
8. C.B. Moore, "Infrared Spectroscopy and Reaction Kinetics of Free Radicals," Department Seminar, University of Pittsburgh, Pennsylvania, February 22, 1984.
9. C.B. Moore, "Infrared Spectroscopy and Chemical Kinetics," Avco Everett Research Laboratory, Everett, Massachusetts, February 24, 1984.
10. C.B. Moore, "Laser Probes of Unimolecular Reaction Dynamics," American Chemical Society Division of Physical Chemistry Spring Meeting, St. Louis, Missouri, April 9, 1984.
11. C. Bradley Moore and A.O. Langford, "Vibrational Relaxation and Chemical Reaction of Formyl Radicals via Complex Formation," Division of Chemical Sciences Combustion Contractor's Meeting, DOE, Livermore, California, May 22, 1984.
12. C.B. Moore, "Observing and Manipulating Molecules," AAAS Symposium on "Frontiers in Chemistry," New York, May 24, 1984.
13. C.B. Moore and A.O. Langford, "Collision Complex Formation Between Formyl Radicals and Nitric Oxide or Oxygen," American Chemical Society Division of Physical Chemistry Fall Meeting, Philadelphia, Pennsylvania, August 25, 1984.
14. C.B. Moore, "State-Resolved Dynamics of Unimolecular Reactions," Department of Chemistry, University of Illinois at Chicago, October 24, 1984.
15. C.B. Moore, "State-Resolved Unimolecular Reaction Dynamics," Radiation Laboratory, University of Notre Dame, South Bend, Indiana, November 1, 1984.
16. C.B. Moore, "Quantum State to Quantum State—Resolving the Mechanics of Energy Transfer and Chemical Reaction Processes," University Lecture, University of Ottawa, Ontario, November 12, 1984.
17. C.B. Moore, "State Resolved Unimolecular Reaction Dynamics," seminar, Cornell University, Ithica, New York, November 15, 1984.
18. C.B. Moore, "State-Resolved Unimolecular Reaction Dynamics," seminar, University of Toronto, Ontario, November 16, 1984.
19. C.B. Moore, "State-Selected, State-Resolved Unimolecular Processes," physical chemistry seminar, Massachusetts Institute of Technology, Cambridge, November 20, 1984.
20. C.B. Moore, "State-Resolved Dynamics of Unimolecular Reactions," General Motors Corporation, Warren, Michigan, December 13, 1984.

Physical Chemistry with Emphasis on Thermodynamic Properties*

Kenneth S. Pitzer, Investigator

INTRODUCTION

The purpose of this program is the discovery and development of methods of calculating thermodynamic and related properties of important chemical systems by the use of quantum and statistical mechanics together with experimental measurements for key systems. Current efforts include ionized systems, electrolyte solutions, and plasmas. Systems comprising fused salts mixed in any proportion with water or other polar solvents are being studied experimentally and with semiempirical theory. Recent theoretical advances include treatments of the dielectric constant of H_2O and the thermodynamics of ionic solutions in H_2O above its critical temperature, and the critical properties of pure ionic fluids such as NaCl. Earlier advances yielded improved equations for electrolyte solutions; these equations are now being applied to a wide variety of systems of industrial or geological interest, including geothermal brines.

Another general research area is the use of relativistic quantum-mechanical methods to calculate energies, bond distances, and other properties of the ground and excited states of molecules containing very heavy atoms; conventional nonrelativistic methods are inadequate in these situations. Such results are important in both evaluating possible laser systems and modeling catalytic entities including heavy atoms such as platinum.

1. Critical Point and Vapor Pressure of Ionic Fluids Including NaCl and KCl (Publication 1)

Kenneth S. Pitzer

The critical properties and the vapor and liquid densities of NaCl, KCl, and the primitive-model ionic fluid are compared on a corresponding-states basis. In preparation for these comparisons, the vapor density of NaCl at very high temperature is calculated from the accurate molecular parameters. The recent treatment of Gillan is adopted for the primitive model. The liquid properties of KCl and NaCl follow corresponding states exactly, but there is some discrepancy for the ion pair in the vapor. The differences are greater for the primitive model, but again the agreement is quite good for the liquid. Critical properties are reported for all three fluids.

2. Ionic Fluids (Publication 6)

Kenneth S. Pitzer

The statistical mechanics and thermodynamics of ionic fluids are reviewed and discussed on a corresponding-states basis with emphasis on areas of recent advances. First the vapor-liquid and critical properties are considered for pure ionic fluids such as NaCl, as well as for the primitive ionic model. The underlying reasons are discussed for differences between fluids of ions and those of neutral molecules. Then systems involving a solvent are considered, with emphasis on simple systems showing phase separation or with strong ion-pairing. Figure 2-1 shows the general pattern, including the range of ion-pair formation and the reduced temperatures for 1:1 and 2:2 electrolytes in water at various temperatures. Figure 2-2 shows the activities of both H_2O and NaCl under critical conditions at 823 K and 754 bar. Estimates are also presented for the critical curve for the system NaCl-H_2O to the critical point of pure NaCl at 3900 K.

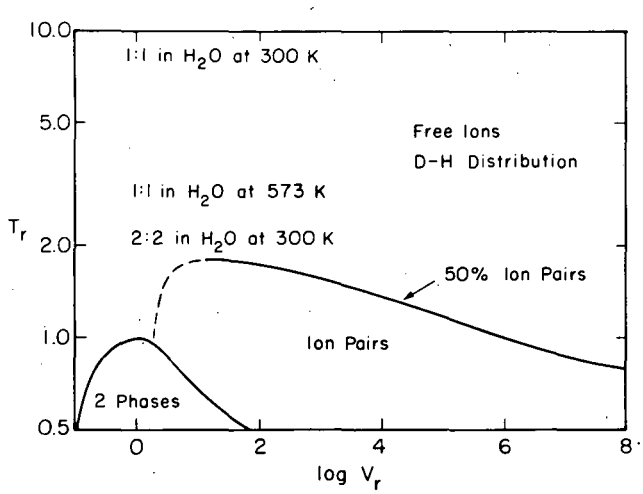

Figure 2-1. The phase boundaries and critical point for an ionic fluid (pure NaCl) on a corresponding-states basis, i.e., as functions of reduced temperature (T_r) and volume (V_r). The range of ion-pair formation and the approximate reduced temperatures for aqueous electrolytes are also shown. (XBL 853-1516)

*This work was supported by the Director, Office of Energy Research, Office of Basic Energy Sciences, Chemical Sciences Division of the U.S. Department of Energy under Contract No. DE-AC03-76SF00098.

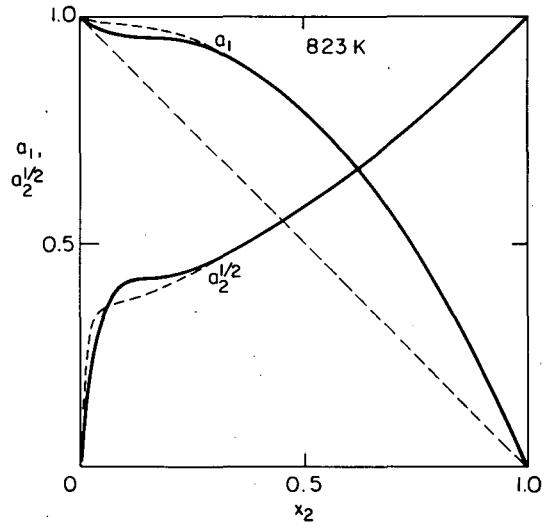

Figure 2-2. The activities of H_2O (a_1) and NaCl (a_2) at 823 K and 754 bar as a function of mole fraction (x_2). The short-dashed curves are extrapolations of a simple equation valid for concentrated solutions; the long-dashed line shows ideal behavior on an ionized basis. (XBL 8310-6475)

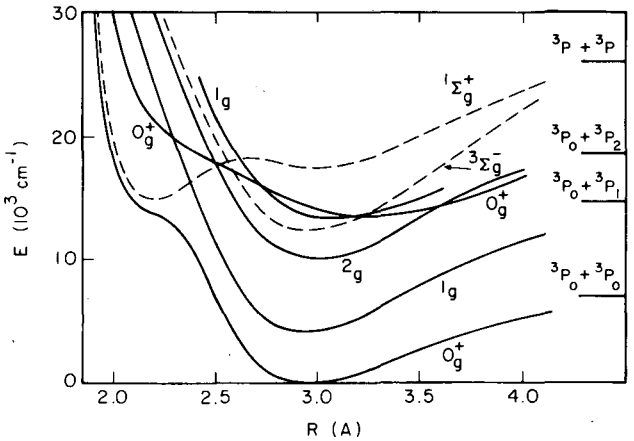

Figure 3-1. Calculated potential-energy (E) curves for g states of Pb_2 as a function of interatomic distance (R). The dashed curves are computed without the spin-orbit term. This spin-orbit term yields a large decrease in energy for the ground O_g^+ state from the $^3\Sigma_g^-$ state. (XBL 853-1515)

3. Relativistic Calculations of Dissociation Energies and Related Properties (Publication 7)

Kenneth S. Pitzer

Methods of calculation of potential-energy curves or surfaces, including dissociation energies, bond distances, and vibration frequencies, are discussed, as are recently obtained results for several molecules. The *ab initio* relativistic methods involve the derivation of "shape-consistent" effective potentials from Dirac-Fock atomic calculations. These effective potentials are averaged and differenced with respect to spin with the differences ($p_{3/2}$ - $p_{1/2}$, etc.) yielding spin-orbit operators. The molecular calculations are then set up in a familiar manner through the SCF stage using spin-averaged effective potentials. The final stage is a configuration-interaction calculation including the spin-orbit terms as well as the electron-repulsion terms.

Calculations that have been made for several low-lying excited states as well as the ground state for Au_2, TlH, Tl_2, Sn_2, and Pb_2 are discussed. Good agreement is obtained with spectroscopic data, and a number of interesting predictions are made. The results for Pb_2 are shown in figures 3-1 and 3-2.

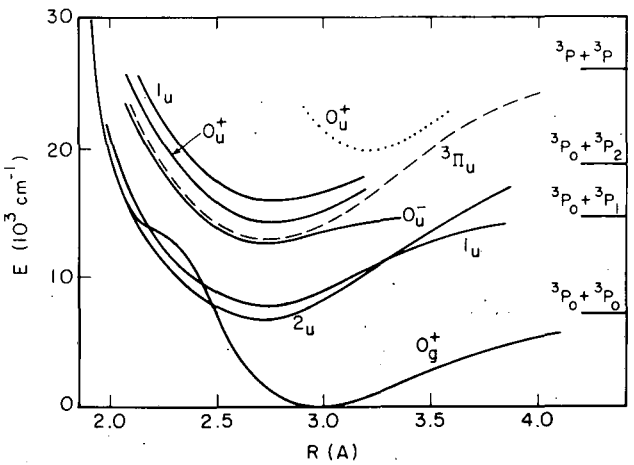

Figure 3-2. Calculated potential-energy (E) curves for u states and the ground O_g^+ state of Pb_2 as a function of interatomic distance (R). An estimated curve at the experimental T_e is also given for the upper O_u^+ state. (XBL 853-1514)

4. The Geometric and Electronic Structure of Small Copper Clusters Cu_n and Cu_n^+ (n = 1–3) by an Effective-Core-Potential Method (Publication 17)

Sheng-Wei Wang

Electronic-structure calculations have been carried out for the total energy of the ground state of Cu_n and Cu_n^+ (n=1–3) clusters. The Cu atom is treated as a one-electron system, and the effect of the core is approximated by a shape-consistent pseudopotential and a semiempirical core-valence, core-core polarization potential. The exchange and correlation energies among the valence electrons are treated by the local-spin-density-functional approximation with and without the self-interaction corrections (SIC). The binding energy and bond distance of Cu_2 calculated with SIC are in almost exact agreement with experimental data. The calculated ionization potentials exhibit even-odd oscillations as a function of n. The potential-energy surfaces of Cu_3 show substantial differences when obtained with and without SIC. The most stable geometry predicted with SIC is an acute triangle with an apex angle of 47° and a long bond length of 5.41 a.u. In terms of a distortion parameter ρ with respect to an equilateral triangle with an equilibrium bond length of 4.78 a.u., $\rho = 0.435$ a.u. This is in reasonable agreement with the experimental value of $\rho = 0.472$ a.u. The calculated binding energy of Cu_3 with respect to fragmentation into Cu atoms is 2.259 eV, compared with the experimental values of 3.108 ± 0.135 or 3.058 ± 0.151 eV. The 27% error is probably due to the use of local exchange-correlation energies and the somewhat small basis set.

5. Work in Progress

Exploratory experiments are in progress seeking critical behavior in ionic systems where one component is a salt melting at moderate temperature. The selection of components is guided by the corresponding-states principle. One system, tetra-n-butylammonium picrate: 1-chloroheptane, has been found that shows critical behavior in the vicinity of 140°C. This picrate salt melts at 91°C and is known to show fully ionic character through its high electrical conductance.

A collaborative program with Lawrence Livermore National Laboratory is in progress for relativistic quantum calculations for UF_6, NpF_6, and PuF_6.

1984 PUBLICATIONS AND REPORTS

Refereed Journals

1. Kenneth S. Pitzer, "Critical Point and Vapor Pressure of Ionic Fluids Including NaCl and KCl," Chem. Phys. Lett. **105**, 484 (1984); LBL-16888.
2. K.S. Pitzer, J.C. Peiper, and R.H. Busey, "Thermodynamic Properties of Aqueous Sodium Chloride Solutions," J. Phys. Chem. Ref. Data **13**, 1 (1984); LBL-15512.†
3. K. Balasubramanian and K.S. Pitzer, "Relativistic Configuration Interaction Calculations for Several Low Lying States of PbO: Comparison with Chemiluminescent Spectra," J. Phys. Chem. **87**, 4857 (1983); LBL-16014.
4. J.H. Yates, W.C. Ermler, N.W. Winter, P.A. Christiansen, K.S. Pitzer, and Y.S. Lee, "*Ab Initio* Potential Energy Curves for the Low-Lying Electronic States of the Argon Excimer," J. Chem. Phys. **79**, 6145 (1983).
5. Kenneth S. Pitzer and Yi-gui Li, "Thermodynamics of Aqueous Sodium Chloride to 823 K and 1 Kilobar (100 MPa)," Proc. Nat. Acad. Sci. USA **80**, 7689 (1983); LBL-16561.†
6. Kenneth S. Pitzer, "Ionic Fluids," J. Phys. Chem. **88**, 2689 (1984); LBL-16991.
7. Kenneth S. Pitzer, "Relativistic Calculations of Dissociation Energies and Related Properties," Int. J. Quantum Chem. **25**, 131 (1984); LBL-14705.
8. K. Balasubramanian and Kenneth S. Pitzer, "Relativistic Quantum Calculations of Low-Lying States of SnH: Comparisons with the Electronic Spectra of SnH and with the Properties of PbH," J. Molec. Spectros. **103**, 105 (1984); LBL-16474.
9. Kenneth S. Pitzer and Yi-gui Li, "Critical Phenomena and Thermodynamics of Dilute Aqueous Sodium Chloride to 823 K," Proc. Nat. Acad. Sci. USA **81**, 1268 (1984); LBL-16831.†
10. Kenneth S. Pitzer and John M. Simonson, "Ion Pairing in a System Continuously Miscible from the Fused Salt to Dilute Solution," J. Am. Chem. Soc. **106**, 1973 (1984); LBL-16315.†
11. K. Balasubramanian and Kenneth S. Pitzer, "Relativistic Quantum Calculations of Low-Lying States of Lead Hydride. Comparisons with Experimental Spectra," J. Phys. Chem. **88**, 1146 (1984); LBL-16562.
12. Rabindra N. Roy, James J. Gibbons, Rick Williams, Lehman Godwin, Gigi Baker, John M. Simonson, and Kenneth S. Pitzer, "The Thermodynamics of Aqueous Carbonate Solutions. II. Mixtures of Potassium Carbonate, Bicarbonate, and Chloride," J.

Chem. Thermodynamics **16**, 303 (1984); LBL-16317.†

Other Publications

13. Kenneth S. Pitzer, "Electron Structure of Molecules with Very Heavy Atoms Using Effective Core Potentials," NATO Adv. Sci. Inst. Ser. B **87**, 403 (1984); LBL-13266.
14. Kenneth S. Pitzer, "Thermodynamics of Condensed Ionic Systems," NATO Adv. Sci. Inst. Ser. C **130**, 165 (1984); LBL-16634.

LBL Reports

15. Kenneth S. Pitzer and J.M. Simonson, "Thermodynamics of Multicomponent Miscible Ionic Systems: Theory and Equations," 1984 Int. Chem. Congress of Pacific Basin Societies, Honolulu, Hawaii, December 16–21, 1984; LBL-17839.†
16. Kenneth S. Pitzer, Joyce Olsen, John M. Simonson, Rabindra N. Roy, James J. Gibbons, and LeAna Rowe, "Thermodynamics of Aqueous Magnesium and Calcium Bicarbonates and Mixtures with Chloride," accepted by J. Chem. and Engr. Data; LBL-17571.†
17. S.W. Wang, "The Geometric and Electronic Structure of Small Copper Clusters Cu_n(n=1–3) by an Effective Core Potential Method," submitted to J. Chem. Phys.; LBL-18155.

Invited Talks

18. Kenneth S. Pitzer, "Thermodynamic Properties of Aqueous NaCl from 273 to 823 K with Estimates for Higher Temperatures," plenary lecture at the International Conference on the Properties of Steam, September 2–7, 1984, Moscow, Russia; to be published in the Proceedings; LBL-18183.†
19. Kenneth S. Pitzer, "Role of Theory and Models in the Best Representation of Properties of Aqueous Electrolytes," national meeting, American Chemical Society, St. Louis, Missouri, April 9, 1984.
20. Kenneth S. Pitzer, "The Thermodynamics of Aqueous Sodium Chloride and of its Mixtures over a Wide Range of Temperature," IUPAC Conference on Chemical Thermodynamics, McMaster University, Hamilton, Ontario, August 15, 1984.

†Supported by the Director, Office of Energy Research, Office of Basic Energy Sciences, Division of Engineering, Mathematics, and Geosciences of the U.S. Department of Energy under Contract No. DE-AC03-76SF00098.

Molecular Interactions*

William A. Lester, Jr., Investigator

INTRODUCTION

This program is directed at extending fundamental knowledge of the interactions and dynamics that govern energy-transfer, reactive, and photodissociative molecular processes with application, where appropriate, to combustion systems. The approach is based on the reliable description of the potential energy surfaces and coupling matrix elements needed in theoretical approaches for the evaluation of cross sections and rates. Emphasis is placed on the use of state-of-the-art Hartree-Fock (HF), multiconfiguration HF (MCHF), and configuration-interaction (CI) *ab initio* methods for the accurate description of molecular interactions. The dynamics studies include fully quantum-mechanical approaches to rotational and vibrational energy transfer in molecules by collision, and an adiabatic approach to single-photon photodissociation of small polyatomic molecules and to chemical reaction.

A novel method that solves the Schroedinger equation stochastically is also being studied to ascertain its usefulness for determining the energy and other molecular properties.

1. Hydrogen Atom Abstraction from Aldehydes: OH + H_2CO and O + H_2CO (Publication 2)†

Michel Dupuis‡ and William A. Lester, Jr.

The essential features of the potential energy surfaces governing hydrogen abstraction from formaldehyde by oxygen atom and hydroxyl radical have been characterized with *ab initio* MCHF and CI wavefunctions. The results are consistent with a very small activation energy for the OH + H_2CO reaction, and with an activation energy of a few kcal/mol for the O + H_2CO reaction. In the transition-state structure of both systems, the attacking oxygen atom is nearly collinear with the attacked CH bond.

*This work was supported by the Director, Office of Energy Research, Office of Basic Energy Sciences, Chemical Sciences Division of the U.S. Department of Energy under Contract No. DE-AC03-76SF00098.

†Michel Dupuis was partly supported by the National Aeronautics and Space Administration under Contract No. A86130B(LML).

‡Present address: IBM Corporation, Scientific and Engineering Computation, Kingston, New York 12401.

2. Static Dipole Polarizability of Electronically Excited Molecules: $H_2(B\ ^1\Sigma_u^+)$ (Publication 3)

R.M. Grimes, M. Dupuis,† and W.A. Lester, Jr.

The dipole polarizability of $H_2(B\ ^1\Sigma_u^+)$ is computed using extended Gaussian basis sets and HF, MCHF, and CI wavefunctions. Electron-correlation contributions are found to be significant (~25%), with the largest contribution arising from angular correlation. With a full CI wavefunction, the components of the dipole polarizability were computed to be (in a.u.): $\alpha\perp = 50$ and $\alpha\| = 257$.

†Present address: IBM Corporation, Scientific and Engineering Computation, Kingston, New York 12401.

3. Fixed-Node Quantum Monte Carlo Study of the H + H_2 Exchange Reaction (Publications 7 and 8)†

Robert N. Barnett, Peter J. Reynolds, and William A. Lester, Jr.

The classical barrier height for the H + H_2 exchange reaction, as well as the energies at other points along the reaction path, are calculated using fixed-node quantum Monte Carlo (FNQMC). Several single-determinant importance functions are used at the saddle-point in order to relate the quality of the importance function to the accuracy and precision of the final result. The computed barrier is an upper bound since the energy of H and of H_2 is obtained exactly by FNQMC. Our best upper bound, 9.70 ± 0.13 kcal/mole, has a mean within 0.1 kcal/mole of the presumed exact value. This best bound is obtained with a single-determinant, double-zeta basis importance function. Contrary to experience with expansion methods, an importance function with a basis set of near-HF quality, as well as one derived from a spin-unrestricted self-consistent-field (SCF) calculation, are among the least efficient and least accurate of the importance functions used. Specifically, a nodal surface appearing in the lowest-energy molecular orbital in these functions apparently increases the FNQMC energy. The FNQMC energy at the other points along the

reaction path is found to agree with the most accurate CI results of Liu[1] to within statistical error.

†Support for R.N. Barnett and P.J. Reynolds was provided by the Office of Naval Research.

1. B. Liu, J. Chem. Phys. **80**, 581 (1984).

4. Chemical Reaction as a Quantum Transition (Publication 10)

Vladimir Z. Kresin, William A. Lester, Jr., Michel Dupuis,† and Christopher E. Dateo

A chemical reaction is treated as a quantum transition from reactants to products. This approach leads to a Franck-Condon-like factor for the evaluation of product energy distributions. Second-quantization representation is used to enable a Hamiltonian for reaction *per se* to be defined. A specific adiabatic method is used to describe the dynamics of nuclear motion. The theory is applied to the reactions HO + D → OD + H and ClI + D → Cl + ID.

†Present address: IBM Corporation, Scientific and Engineering Computation, Kingston, New York 12401.

5. Quantum Monte Carlo Calculation of the Singlet-Triplet Splitting in Methylene (Publication 11)†

Peter J. Reynolds, Michel Dupuis,‡ and William A. Lester, Jr.

The FNQMC method is used to calculate the total energy of CH_2 in the $^3B_1$ and $^1A_1$ states. For both states, the best FNQMC variationally bounded energies lie more than 15 kcal/mole (0.024 hartrees) below the best previous variational calculations. Subtracting these energies to obtain the singlet-triplet splitting yields $T_e = 9.4 \pm 2.2$ kcal/mole. Adjusting for zero-point energies and relativistic effects, we obtain $T_0 = 8.9 \pm 2.2$ kcal/mole. This result is in excellent agreement with the recent direct measurements of McKellar et al.[1] of $T_0 = 9.05 \pm 0.06$ kcal/mole, and of Leopold et al.[2] of ~9 kcal/mole, as well as with recent theoretical investigations that indicate an energy gap of 9–11 kcal/mole. We note that the present results were obtained using only single determinant functions for both states, in contrast to conventional *ab initio* approaches, which must use at least two configurations to properly describe the singlet state. We also present a scheme for iteratively correcting the Monte Carlo procedure that has the potential to reduce variance and increase accuracy.

†Supported in part by the Control Data Corporation under Grant No. 82-CSU-12 in the form of computer time. Support for Peter J. Reynolds was provided by the Office of Naval Research.

‡Present address: IBM Corporation, Scientific and Engineering Computation, Kingston, New York 12401.

1. A.R.W. McKellar, P.R. Bunker, T.J. Sears, K.M. Evenson, R.J. Saykally, and S.R. Langhoff, J. Chem. Phys. **79**, 5251 (1983).

2. D.G. Leopold, K.K. Murray, and W.C. Lineberger, J. Chem. Phys. **81**, 1048 (1984).

6. Work in Progress

By treating a direct bimolecular reaction as a radiationless quantum transition, the probability of reactants forming products in specific quantum states can be written as a Franck-Condon-like factor. This state-to-state approach is being used to predict the product translational and vibrational energy distributions (collinear model) of chemical reactions as a function of vibrational state of reactions. The method has been applied to the reactions H + BrCl → HBr + Cl and Li + FH → LiF + H. For these systems the distributions are found to depend strongly on the ratio of the vibrational frequency of the reactant to that of the product.

1984 PUBLICATIONS AND REPORTS

Refereed Journals

1. M. Dupuis and W.A. Lester, Jr., "Hydrogen Atom Migration in the Oxidation of Aldehydes: $O(^3P)$ + H_2CO," J. Chem. Phys. **80**, 4193 (1984); LBL-16274.
2. M. Dupuis and W.A. Lester, Jr., "Hydrogen Atom Abstraction from Aldehydes: OH + H_2CO and O + H_2CO," J. Chem. Phys. **81**, 847 (1984); LBL-17301.
3. R.M. Grimes, M. Dupuis, and W.A. Lester, Jr., "Static Dipole Polarizability of Electronically Excited Molecules: $H_2(B\ ^1\Sigma_u^+)$," Chem. Phys. Lett. **110**, 247 (1984); LBL-17557.
4. V.Z. Kresin and W.A. Lester, Jr., "Reaction Hamiltonian and the Adiabatic Approach to the Dynamics of Chemical Reaction," Chem. Phys. **90**, 335 (1984); LBL-16739.
5. M. Dupuis and J.J. Wendoloski, "Systematic GVB Study of Harmonic Vibrational Frequencies and

Dipole Moment Derivatives: the Vinyl Radical C_2H_3 and Other Simple Molecules," J. Chem. Phys. **80**, 5696 (1984); LBL-14872.

Other Publications

6. V.Z. Kresin and W.A. Lester, Jr., "Quantum Theory of Polyatomic Photodissociation," accepted by Adv. in Photochem.

LBL Reports

7. R.N. Barnett, P.J. Reynolds, and W.A. Lester, Jr., "Fixed-Node Quantum Monte Carlo Study of the Classical Barrier Height for the $H + H_2$ Exchange Reaction," accepted by J. Chem. Phys.; LBL-17610.
8. P.J. Reynolds, R.N. Barnett, and W.A. Lester, Jr., "Quantum Monte Carlo Study of the Classical Barrier Height for the $H + H_2$ Exchange Reaction: Restricted versus Unrestricted Trial Function," accepted by Int. J. Quan. Chem.; LBL-17611.
9. C.E. Dateo, M. Dupuis, and W.A. Lester, Jr., "*Ab Initio* Study of Cyanogen: the $X\ ^1\Sigma_g^+$, $\tilde{a}\ ^3\Sigma_u^+$, $\tilde{B}\ ^1\Delta_u$, and $\tilde{C}\ ^1\Pi_u$ States," submitted to J. Chem. Phys.; LBL-17676.
10. V.Z. Kresin, W.A. Lester, Jr., M. Dupuis, and C.E. Dateo, "Chemical Reaction as a Quantum Transition," accepted by Int. J. Quan. Chem.; LBL-17715.
11. P.J. Reynolds, M. Dupuis, and W.A. Lester, Jr., "Quantum Monte Carlo Calculation of the Singlet-Triplet Splitting in Methylene," accepted by J. Chem. Phys.; LBL-17823.

Invited Talks

12. W.A. Lester, Jr., "Quantum Monte Carlo for Molecules," Department of Chemistry, University of California, Los Angeles, February 22, 1984; Quantum Chemistry Group, University of Uppsala, Sweden, October 9, 1984.
13. W.A. Lester, Jr., "An Adiabatic Theory of Indirect Photodissociation," meeting on "The Theory of Chemical Reaction Dynamics," Magdelene College, Cambridge, England, July 13–15, 1984.
14. W.A. Lester, Jr., "Directions of Chemical Theory," U.S.-Sweden Workshop on the Future of Chemistry, Saltsjöbaden, Sweden, October 6–7, 1984.
15. W.A. Lester, Jr., "Diffusion Monte Carlo for Molecules," Institute for Theoretical Physics, Stockholm University, Sweden, October 10, 1984.

Spectroscopy and Structures of Reactive Intermediates*

Richard J. Saykally, Investigator

INTRODUCTION

The objective of this research is to develop new techniques for the detection of unstable forms of molecules and to use these techniques to carry out detailed measurements of the structures, properties, and dynamics of these species.

Reactive molecules, including neutral-free radicals and molecular ions, play extremely important roles as reaction intermediates in combustion processes, reactive plasmas, the terrestrial atmosphere, and interstellar space. The transient nature of these reactive species has made their detection and characterization difficult, and comparatively few of these important reactive molecules have been studied in detail.

"Van der Waals molecules" — molecules held together only by very weak dispersion or induction forces, by hydrogen bonds, or by monopole-dipole forces — constitute excellent prototypes of these same weak interactions that dominate the condensed phases. One of the chemical physicist's great dreams has been to bridge the gap from the gas phase, where detailed measurements of isolated species are possible, to the condensed phases, where these measurements are clearly impossible, through the investigation of successively more complex van der Waals aggregates in the gas phase. This dream is still a long way from being realized, as these species, like the reaction intermediates, are extremely difficult to detect and characterize.

Similarly, studies of metal clusters and metal-containing molecules can reveal important features of metal-metal bonds that are inaccessible from studies in the solid. These species are, like the preceding two categories, extremely difficult to study by spectroscopic methods. Metal clusters assume a particularly important role because of possible application to catalysis, and the lack of knowledge regarding their structures and properties is a serious deficiency in accessing such possibilities.

*This work was supported by the Director, Office of Energy Research, Office of Basic Energy Sciences, Chemical Sciences Division of the U.S. Department of Energy under Contract No. DE-AC03-76SF00098.

The primary goal of this research is to carry out detailed investigations of those reaction intermediates that are critical species in the combustion of important fuels. Exactly the same experimental and theoretical techniques employed to study reaction intermediates can be applied to van der Waals molecules and metal molecules; hence, studies of these two crucially important classes of molecules will be undertaken as well, with the long-range objective of correlating the measured properties of these species as a means of understanding condensed phases in more detail.

1. Studies of Astrophysically Important Molecular Ions with Ultrasensitive Infrared Laser Techniques (Publication 5)

R.J. Saykally

We discuss the development of two infrared laser techniques, far-infrared laser magnetic resonance and velocity-modulation infrared-laser spectroscopy. These techniques have demonstrated the capability of studying molecular ions with sufficient precision to produce a positive identification of their corresponding astronomical spectra. We anticipate that in the near future these methods will make it possible to detect, identify, and make detailed studies of spectra of a variety of astrophysically important molecular ions. The extension of astronomical measurements to new ionic species is of obvious importance in understanding the chemistry of the interstellar medium, particularly because most of the ion-molecule reaction data used as the input for modern chemical models have rarely been obtained at the low temperatures appropriate for the interstellar medium. Many of the critically important dissociative-recombination and radiative-association reactions have not been studied at all.

In 1983, Gudeman, Begemann, Pfaff, and myself reported the development of a new method of observing molecular-ion vibration-rotation spectra, called "velocity-modulation laser spectroscopy," and its described application to HCO^+, HNN^+, and H_3O^+. This approach has now been extended to include NH_4^+, H_2F^+, D_3O^+, and DNN^+ in studies at Berkeley; to NH_4^+, H_3O^+, $HCNH^+$, and OH^+ in studies by Oka's groups at Chicago; and to HCO^+ studied by Davies at Cambridge.

The Berkeley laser-magnetic-resonance (LMR) effort has produced extensive rotational spectra of the isovalent series of ions HF^+, HCl^+, and HBr^+. A

detailed analysis of these spectra has revealed structures, spin densities, field gradients, and bonding information for this series. This information will provide an important basis for theoretical studies of the properties of open-shell molecules in general.

More recently, extensive rotational spectra have been measured for the important radical ions OH^+ and H_2O^+. These species are important in combustion and atmospheric chemistry, as well as in astronomy. Figure 1-1 shows a typical LMR rotational spectrum of OH^+, measured in a discharge containing a trace of H_2O in helium. Figures 1-2 and 1-3 show rotational spectra of H_2O^+ for the ortho and para forms, respectively. Analysis of the extensive spectra measured for H_2O^+ and for OH^+ and OD^+ is presently under way and will provide a detailed characterization of the electronic structure of these important reactive intermediates.

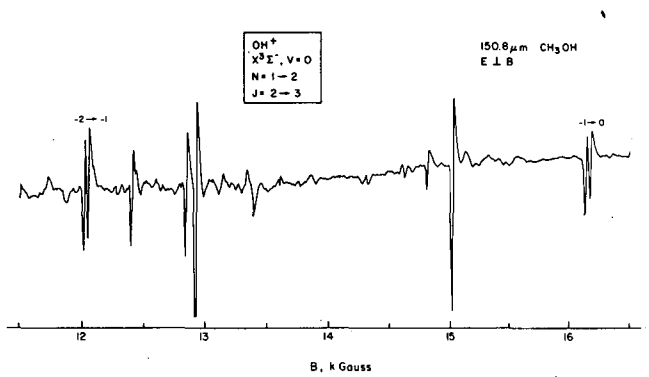

Figure 1-1. Typical LMR rotational spectrum of OH^+. (XBL 853-1508)

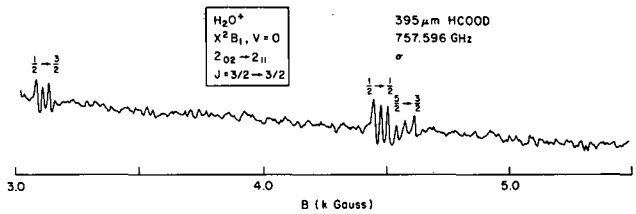

Figure 1-2. LMR rotational spectrum of the ortho form of H_2O^+. (XBL 853-1509)

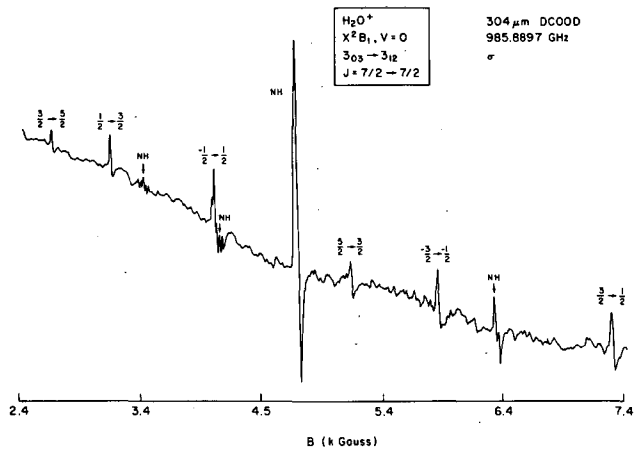

Figure 1-3. LMR rotational spectrum of the para form of H_2O^+. (XBL 853-1510)

2. Work in Progress

A new experiment has been developed in which the vibrational motion of a weak van der Waals bond has been studied in detail for the first time. In this experiment, a supersonic free jet is operated inside the cavity of a far-infrared laser, and an electric field is used to tune energy levels of weakly bound molecules produced in the low temperatures (10 K) of the jet. We have measured the bending vibration of the weakly bound ($\sim$150 cm^{-1}) molecule ArHCl near 35 cm^{-1} with this technique. Over 100 Stark-hyperfine components of several transitions were observed and are presently being analyzed.

1984 PUBLICATIONS AND REPORTS

Refereed Journals

1. R.J. Saykally, Leif Veseth, and K.M. Evenson, "Laser Magnetic Resonance Rotational Spectroscopy of $^2\Sigma$ Radicals: Ethynyl (CCH)," J. Chem. Phys. **80**, 2247 (1984).
2. D.C. Hovde, E. Schafer, Susan E. Strahan, C.A. Ferrari, Douglas Ray, K.G. Lubic, and R.J. Saykally, "Measurement of the Rotational Spectrum of HF^+ by Laser Magnetic Resonance," Molec. Phys. **52**, 245 (1984).
3. L.M. Ziurys, D.P. Clemens, R.J. Saykally, M. Colvin, and H.F. Schaefer, "A Search for Interstellar Silicon Nitride," Astrophys. J. **281**, 219 (1984).
4. C.S. Gudeman and R.J. Saykally, "Velocity Modulation Infrared Laser Spectroscopy of Molecular Ions," Ann. Rev. Phys. Chem. **35**, 387 (1984).

Other Publications

5. R.J. Saykally, "Studies of Astrophysically Important Molecular Ions with Ultrasensitive Infrared Laser Techniques," in *NATO Advanced Study Institute — Molecular Astrophysics, State of the Art and New Directions,* Plenum, New York, 1984.

Invited Talks

6. R.J. Saykally, "Laser Spectroscopy of Molecular Ions," Department of Chemistry, University of Utah, Salt Lake City, November 1983; Department of Chemistry, University of California, Irvine, November 1983.
7. R.J. Saykally, "Infrared Spectroscopy of Molecular Ions," Department of Chemistry, Harvard University, Cambridge, Massachusetts, March 1984; Department of Chemistry, University of Chicago, Chicago, Illinois, April 1984; 39th Symposium on Molecular Spectroscopy, Columbus, Ohio, June 1984; Gordon Research Conference on Radical Cations, Wolfeboro, New Hampshire, June 1984; NATO Advanced Study Institute, Bad Windsheim, West Germany, July 1984.
8. R.J. Saykally, "High-Sensitivity Laser Spectroscopy of Molecular Ions," Symposium on Ultrasensitive Laser Spectroscopy, American Chemical Society National Meeting, Philadelphia, Pennsylvania, August 1984.
9. R.J. Saykally, "Vibrational Modulation Laser Spectroscopy of Molecular Ions," Lasers '84, San Francisco, California, November 27, 1984.

Theory of Atomic and Molecular Collision Processes*

William H. Miller, Investigator

INTRODUCTION

This research is primarily involved with the development of theoretical methods and models for describing atomic and molecular collision processes. Specific topics of interest include the theory of inelastic and reactive scattering, collision processes involving electronically excited atoms or molecules, collisional ionization phenomena, statistical theories of chemical reactions, scattering of atoms and molecules from surfaces, and the interactions of molecular systems with high-power laser radiation.

Much of this research is involved with the development and application of a general semiclassical mechanics that allows one to combine classical mechanics and quantum mechanics in a correct and useful manner. This has been extremely successful in providing an understanding of the various effects that are seen in molecular phenomena, and it also often provides simpler computational methods for carrying out quantitative calculations. Certain research topics are more amenable to a completely quantum-mechanical approach, and these sorts of theoretical techniques are also used.

The ability to understand — and thus to model and predict — chemical kinetic phenomena in the gas phase has widespread practical importance in a number of different areas. Among these are atmospheric chemistry and physics, the interactions of molecules with strong laser fields, and energy-transfer and chemical reactions in flames and combustion.

1. A New Physical Interpretation for Time in Scattering Theory (Publication 7)

Eli Pollak[†] *and William H. Miller*

We show that the collision time may be interpreted as the time average of a flux-flux correlation function. This interpretation leads quantum mechanically to a complex time whose real part is identical to the usual definition as provided by F.T. Smith. The imaginary part is identical, in the semiclassical limit, to the imaginary time associated with tunneling.

*This work was supported by the Director, Office of Energy Research, Office of Basic Energy Sciences, Chemical Sciences Division of the U.S. Department of Energy under Contract No. DE-AC03-76SF00098.

[†]Present address: Chemical Physics Department, Weizmann Institute of Science, Rehovot, 76100, Israel.

2. Coupled-Channel Distorted-Wave Calculations for the Three-Dimensional $H + H_2$ Reaction (Publication 5)[†]

George C. Schatz,[‡] *Lynn M. Hubbard,*[§] *Peter S. Dardi, and William H. Miller*

A method for determining cross sections and other dynamical information based on the use of accurate coupled-channel nonreactive wavefunctions in an evaluation of the distorted-wave reactive-scattering amplitude is developed for three-dimensional atom-diatom reactive collisions and applied to the $H + H_2$ reaction. The nonreactive wave functions are obtained by using a truncated expansion in asymptotic vibration/rotation states to generate coupled-channel equations in terms of the full Hamiltonian. Explicit reduction of the distorted-wave scattering-matrix expression to a real-valued three-dimensional integral is given, and methods for simplifying the calculation through the use of parity decoupling, even/odd decoupling, and the coupled-states approximation are introduced. The application to $H + H_2$ considers the Porter-Karplus potential surface. Comparison of reaction probabilities, opacity functions, and differential and integral cross sections with corresponding results from exact quantum calculations indicates that the coupled-channel distorted-wave method is an excellent approximation as long as the total reaction probability for each partial wave is less than 0.1. Figures 2-1 and 2-2 show sample results. This upper limit occurs at 0.60 eV total energy for $H + H_2$. Above that energy, convergence with basis set size is oscillatory after an initial plateau. The coupled-states distorted-wave method is also found to be an excellent approximation, with results that are indistinguishable in accuracy from coupled-channel distorted-wave results. Extension of these approaches to a nonperturbative evaluation of the scattering matrix elements is discussed.

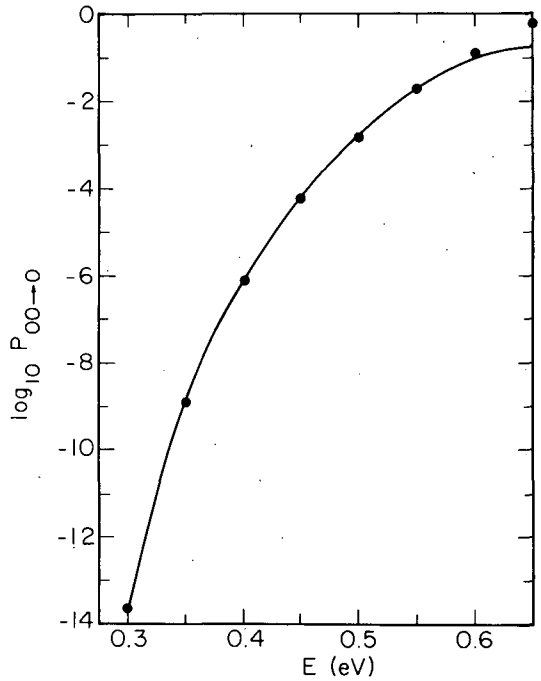

Figure 2-1. Transition probabilities $v = 0$, $j = 0 \to v = 0$ summed over final rotational states with $J = 0$ as a function of total energy. The solid line is the exact quantum results, and the dots are the distorted-wave Born-approximation (DWBA) results. The DWBA results are calculated using 18 vibrational-rotational states: 5,5,4,4. (XBL 8311-4533)

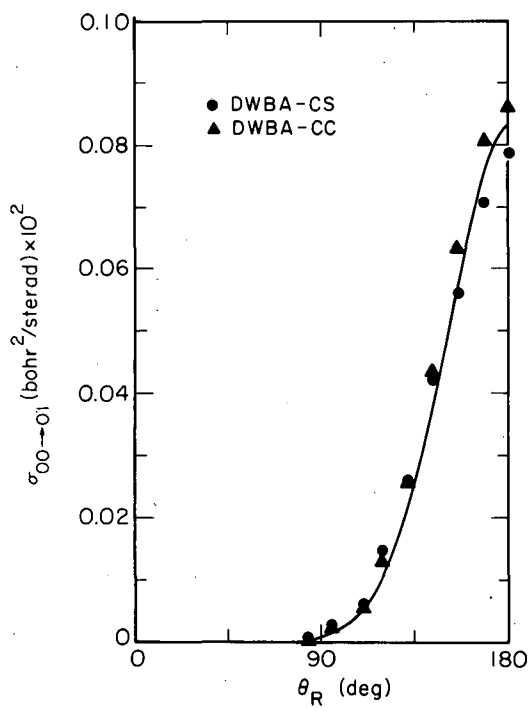

Figure 2-2. Differential cross sections as a function of scattering angle $\theta_R = 180\text{-}\theta$ at total energy $E = 0.5$ eV. The solid line is the exact quantum results. The DWBA-coupled-channel and DWBA-coupled-states results are plotted using the indicated dots. (XBL 8311-4536A)

†Calculations were carried out on a minicomputer supported by the U.S. National Science Foundation grants CHE-81-15109, CHE-81-08990, and CHE-79-20181.

‡Present address: Department of Chemistry, Northwestern University, Evanston, Illinois 60201.

§Present address: Department of Chemistry, Princeton University, Princeton, New Jersey 08540.

3. Application of the Semiclassical-Perturbation Approximation to Scattering from Surfaces. Generalization to Include Phonon Inelasticity (Publication 3)

Lynn M. Hubbard† *and William H. Miller*

The semiclassical-perturbation (SCP) approximation of Miller and Smith[1] is applied to the inelastic scattering of atoms from solid surfaces. Earlier applications of this approach have been to diffraction (i.e., elastic scattering) of He from LiF and to diffraction and rotationally inelastic scattering of H_2 from LiF; the present work is an extension that allows for motion of the surface atoms (and thus phonon inelasticity). Therefore, phenomena that involve energy transfer between the surface and gas molecules can be described. In the present work sticking probabilities are calculated for He-W(110) and Ne-W(110), and the results show that a simple model such as this one can be quite useful in predicting energy transfer in gas-solid scattering systems.

†Present address: Department of Chemistry, Princeton University, Princeton, New Jersey 08540.

1. W.H. Miller and F.T. Smith, Phys. Rev. A **17**, 17 (1978).

4. Classical Models for Electronic Degrees of Freedom: Quenching of $Br^*(^2P_{1/2})$ by Collision with H_2 in Three Dimensions (Publication 1)†

Domenic P. Ali‡ *and William H. Miller*

Three-dimensional classical trajectory calculations have been carried out for the quenching of $Br^*(^2P_{1/2})$ by collision with ground-state H_2, using an approach that describes the electronic as well as heavy-particle (i.e., transition, rotation, vibration) degrees of freedom by classical mechanics. We find a sizeable quenching cross section ($\approx 1/2$ Å^2), with essentially all of the collision products having H_2 vibrationally excited to $v = 1$, i.e., near-resonant E-V

transfer dominates the nonresonant E-T,R processes. This is in agreement with experimental results.

---

†Calculations were carried out on a minicomputer supported by the U.S. National Science Foundation Grant CHE-79-20181.

‡Present address: Department of Chemistry, University of Colorado, Boulder 80309.

5. Work in Progress

Computational methodologies suited to Cray computers are being developed to extend our distorted-wave treatment of state-to-state quantum reactive scattering to a complete solution of the problems. Several new approaches are also being pursued for the "direct" calculation of quantum rate constants, i.e., ways that avoid the explicit solution of the state-to-state reactive-scattering problem.

1984 PUBLICATIONS AND REPORTS

Refereed Journals

1. D.P. Ali and W.H. Miller, "Classical Models for Electronic Degrees of Freedom: Quenching of $Br^*(^2P_{1/2})$ by Collision with H_2 in Three Dimensions," Chem. Phys. Lett. **103**, 470 (1984); LBL-16721.
2. T. Carrington, Jr., L.M. Hubbard, H.F. Schaefer, and W.H. Miller, "Vinylidene: Potential Energy Surface and Unimolecular Reaction Dynamics," J. Chem. Phys. **80**, 4347 (1984).
3. L.M. Hubbard and W.H. Miller, "Application of the Semiclassical Perturbation Approximation to Scattering from Surfaces: Generalization to Include Phonon Inelasticity," J. Chem. Phys. **80**, 5827 (1984); LBL-17095.
4. D.P. Ali and W.H. Miller, "Geminate Recombination of Iodine Atoms in Solution: A Generalized Langevin Treatment Including the Effect of Electronically Inelastic Transitions," Chem. Phys. Lett. **105**, 501 (1984).
5. G.C. Schatz, L.M. Hubbard, P.S. Dardi, and W.H. Miller, "Coupled Channel Distorted Wave Calculations for the Three Dimensional $H + H_2$ Reaction," J. Chem. Phys. **81**, 231 (1984); LBL-17190.
6. W.H. Miller, "Calculation of Semiclassical Eigenvalues with One Arbitrary Trajectory," J. Chem. Phys. **81**, 3573 (1984); LBL-17641.
7. E. Pollak and W.H. Miller, "A New Physical Interpretation for Time in Scattering Theory," Phys. Rev. Lett. **53**, 115 (1984); LBL-18056.
8. T. Carrington, Jr., and W.H. Miller, "Reaction Surface Hamiltonian for the Dynamics of Reactions in Polyatomic Systems," J. Chem. Phys. **81**, 3942 (1984).
9. E. Pollak and W.H. Miller, "A New Physical Interpretation for Time in Scattering Theory," Phys. Rev. Lett. **53**, 115 (1984); LBL-18056.
10. P.S. Dardi and S.K. Gray, "Classical and Quantum Mechanical Studies of Overtone and Multiphoton Absorption of HF in an Intense Laser Field," J. Chem. Phys. **80**, 4738 (1984); LBL-16719.
11. S.-H. Shi, "T-V and V-V Energy Transfer in Collinear Collision of Two Diatomic Molecules — An Application of Label Variable Classical Mechanics," J. Chem. Phys. **81**, 1794 (1984); LBL-17094.

LBL Reports

12. R. Jaquet and W.H. Miller, "Quantum Mechanical Rate Constants via Path Integrals: Diffusion of Hydrogen Atoms on a W(100) Surface," submitted to J. Phys. Chem.; LBL-18167.
13. E. Pollak, "Vibrational Adiabatic Molecules," submitted to Comments At. Mol. Phys.; LBL-17527.
14. E. Pollak, M. Baer, N. AbuSalbi, and D.J. Kouri, "A Model Study of Symmetric Light Atom Transfer Reactions," submitted to J. Chem. Phys.; LBL-18055.
15. E. Pollak, "Harmonic Tunneling Corrections to Sudden and Adiabatic Transition State Theory," submitted to J. Chem. Phys.; LBL-18057.
16. E. Pollak, "Equivalence of Vibrational Sudden and Vibrational Adiabatic Classical Transition State Theory," submitted to Chem. Phys. Lett.; LBL-18168.
17. N. AbuSalbi, D.J. Kouri, M. Baer, and E. Pollak, "A Study of the Quantal Time Delay Matrix in Collinear Reactive Scattering," submitted to J. Chem. Phys.; LBL-18169.

Invited Talks

18. W.H. Miller, "Reaction Dynamics in Polyatomic Systems," International Workshop on Primary Photophysical Processes, Herrsching, West Germany, October 16–21, 1983.
19. W.H. Miller, "Classical and Semiclassical Methods for the Interaction of Molecular Systems with Strong

Radiation Fields," Sixth International Conference on Lasers and Applications, San Francisco, California, December 12–16, 1983.

20. W.H. Miller, "Vinylidene: Potential Energy Surface and Unimolecular Reaction Dynamics," American Chemical Society National Meeting, St, Louis, Missouri, April 8–13, 1984.
21. W.H. Miller, "Recent Developments in the Theory of Quantum Mechanical Reactive Scattering," American Conference on Theoretical Chemistry, Jackson, Wyoming, June 15-20, 1984.
22. W.H. Miller, "Vinylidene: Potential Energy Surface and Unimolecular Reaction Dynamics," 8th International Symposium of Gas Kinetics, Nottingham, England, July 16–20, 1984.
23. W.H. Miller, "Some Recent Developments in Quantum Mechanical Reactive Scattering," International Workshop on Chemical Reaction Dynamics, Cambridge, England, July 13–16, 1984.
24. W.H. Miller, "Recent Progress in Quantum Mechanical Reactive Scattering," 5th European Conference on Dynamics of Molecular Collisions, Jerusalem, Israel, September 3–7, 1984.
25. W.H. Miller, "*Ab Initio* Reaction Dynamics in Polyatomic Systems," Distinguished Lecture Series in Chemistry, Indiana University, Bloomington, October 24, 1984.
26. W.H. Miller, "Reaction Paths and Reaction Surfaces: An Approach to Reaction Dynamics in Polyatomic Systems," Nobel Laureate Symposium, International Chemical Congress of Pacific Basin Societies, Honolulu, Hawaii, December 16–21, 1984.

Photoelectron Spectroscopy*

David A. Shirley, Investigator

INTRODUCTION

This program addresses both experimental and theoretical aspects of electron spectroscopy for the investigation of electronic structure of matter in the gaseous and condensed phases. Research is conducted using both laboratory sources at LBL and synchrotron radiation in the 5–5000 eV energy range available at the Stanford Synchrotron Radiation Laboratory, where there is participation in developing the spectroscopy of this newly accessible range of the electromagnetic spectrum. Time-of-flight measurements with synchrotron radiation are used to measure angular distributions of photoelectrons and resonant photoemission phenomena in the gas phase. Ultrahigh-resolution photoelectron spectroscopy based on molecular beams is yielding new information about small molecules and about the transition from single metal atoms to behavior characteristic of a three-dimensional solid. Employing angle-resolved variable-energy photoemission and electron-energy-loss spectroscopy, this program examines the electronic structure of solids. The program also studies the geometric and electronic structure of surface-adsorbate systems using photoelectron diffraction, angle-resolved photoemission extended fine structure (ARPEFS), and surface extended x-ray absorption fine structure (EXAFS).

1. Observation of a Surface Magnetic Phase Transition on Cr(100) (Publication 8)

L.E. Klebanoff, S.W. Robey, G. Liu,† and D.A. Shirley

We have observed a surface magnetic phase transition on Cr(100) using angle-resolved photoelectron spectroscopy (ARPES). The binding energy of a Cr(100) surface feature displays a temperature dependence that is very similar to that of a ferromagnetic exchange splitting (see Figure 1-1). This observation is consistent with theoretical predictions of a *ferromagnetic* Cr(100) surface.[1–4] The room-temperature ferromagnetic surface exchange potential is estimated to be 0.8 ± 0.1 eV, with an associated surface magnetic moment of 2.4 ± 0.3 μ_B.

†Permanent address: Department of Physics, Zhejiang University, Hangzhou, People's Republic of China.

1. D.R. Grempel, Phys. Rev. B **24**, 3928 (1981).
2. G. Allan, Surf. Sci. Reports **1**, 121 (1981).
3. G. Allan, Phys. Rev. B **19**, 4774 (1979).
4. G. Allan, Surf. Sci. **74**, 79 (1978).
5. D.E. Eastman, F.J. Himpsel, and J.A. Knapp, Phys. Rev. Lett. **40**, 1514 (1978).

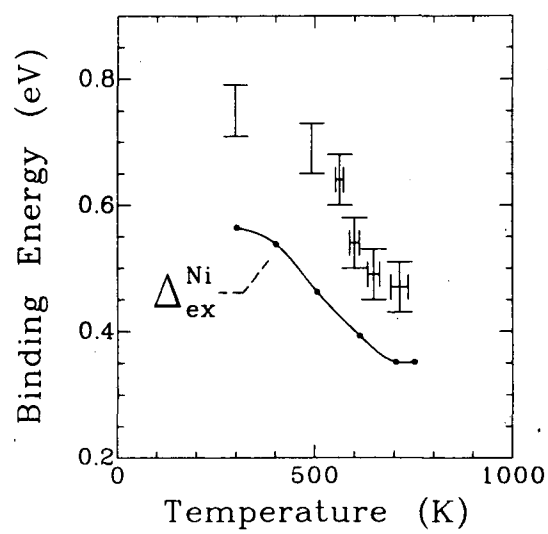

Figure 1-1. Binding energy of the Cr(100) surface features plotted vs. temperature. The solid line is the temperature dependence of the bulk exchange splitting in nickel as measured by ARPES. This curve is reproduced from Figure 2 of Ref. 5 and scaled in energy to our figure. (XBL 8412-5186)

*This work was supported by the Director, Office of Energy Research, Office of Basic Energy Sciences, Chemical Sciences Division of the U.S. Department of Energy under Contract No. DE-AC03-76SF00098. It was performed at the Stanford Synchrotron Radiation Laboratory, which is supported by the Department of Energy, Office of Basic Energy Sciences, and the National Science Foundation, Division of Materials Research.

2. Investigation of the Near-Surface Electronic Structure of Cr(100) (Publication 22)

L.E. Klebanoff, S.W. Robey, G. Liu,† and D.A. Shirley

We used ARPES to study the Cr(100) near-surface electronic structure. ARPES measurements were made of the energy-band dispersions along the [010] direction parallel to the crystal surface. The periodicity of these band dispersions indicates that the valence electrons experience and self-consistently establish antiferromagnetism in the near-surface layers of Cr(100). We also conducted a highly surface-sensitive ARPES measurement of the energy-band dispersions along the [100] direction normal to the surface. The results suggest that the surface magnetic moments, which are coupled ferromagnetically within the surface layer, couple antiferromagnetically to the moments of the atoms in the second layer. Temperature-dependent studies revealed the persistence of near-surface antiferromagnetic order for temperatures up to 2.5 times the bulk Néel temperature. The temperature dependence of this antiferromagnetic order suggests that its thermal stability derives in part from the stability of the Cr(100) ferromagnetic surface phase.

†Permanent address: Department of Physics, Zhejiang University, Hangzhou, People's Republic of China.

3. Effects of Surface Reconstruction and Photon Polarization in Angle-Resolved Photoemission: Applications to Au(001) (Publication 17)

A.E. Schach von Wittenau, R.F. Davis,† J.G. Tobin,‡ M.G. Mason,§ Z. Hussain,‖ and D.A. Shirley

We have obtained normal photoemission spectra from Au(001)-(1 × 1) and Au(001)-(5 × 20) crystal-surface reconstructions using photons ranging in energy from 9 to 32 eV. The Au(001)-(1 × 1) spectra consist almost entirely of direct transition features, with few density-of-states peaks. Using the direct-transition model and calculated bulk-conduction bands as final states, we derive an empirical valence-band map for Au along the Γ-X line, in good agreement with recent self-consistent calculations.

The Au(001)-(5 × 20) spectra are well described as sums of Au(001)-(5 × 20) spectra plus spectra derived from a hexagonal overlayer. Spectra attributed to the hexagonal overlayer are taken to be difference spectra between the Au(001)-(5 × 20) and Au(001)-(1 × 1) spectra. The spacings of the spectral peaks in the difference spectra are well described by crystal field theory plus spin-orbit splitting. These spacings are similar to those found in recent studies of Ag monolayers on Cu(001).

Surface umklapp effects appear to be minimal in both the Au(001)-(1 × 1) and Au(001)-(5 × 20) cases.

†Present address: Polaroid Corporation, Waltham, Massachusetts 02154.

‡Present address: Department of Chemistry, University of Wisconsin, Madison, Wisconsin 53706.

§Present address: Research Laboratory, Eastman Kodak, Rochester, New York 14650.

‖Present address: Department of Physics, University of Petroleum and Minerals, Dhahran, Saudi Arabia.

4. Curved-Wavefront Corrections for Photoelectron Scattering (Publication 24)

J.J. Barton and D.A. Shirley

We derive new, simplified formulas for the scattering of $\ell=1$ spherical waves from central potentials, as a basis for discussing curved-wavefront corrections to single-scattering plane-wave models for ARPEFS and EXAFS. A differential form for the expansion of the screened spherical wave replaces the usual integral form to facilitate the summation over equivalent magnetic sublevels in the scattered wave. Spherical-wave scattering factors are defined and interpreted as corrections to the plane-wave scattering factor. We argue and demonstrate by example that the remarkable success of plane-wave models does not result from reaching the spherical-wave asymptotic limit; instead, adjacent partial-wave corrections cancel for backscattering at high energy. The new scattering formulas allow curved-wavefront numerical calculations to be performed with little more effort than plane-wave formulas.

5. Electron-Energy-Loss Spectroscopy of H_2S Adsorbed on Ni(100) (Publication 10)

A.G. Baca, M.A. Schulz, and D.A. Shirley

H_2S adsorption has been studied on Ni(100) at temperatures between 110–295 K by electron-energy-loss spectroscopy, low-energy electron diffraction (LEED), and Auger spectroscopy. Coverage dependence of the H_2S adsorption, shown in Figure 5-1, has been studied at 110 K. At low coverages H_2S dissociates to S_{ads} + H_{ads}, as evidenced by a S-Ni stretch at 350 cm^{-1} and a H-Ni stretch at ~570 cm^{-1}. At higher coverages two distinct molecular species are observed: H_2S with C_{2v} symmetry (highest coverages), and either HS or H_2S with C_s symmetry (intermediate coverages). The peaks at 2510 and 1170 cm^{-1} are attributed to H_2S, while the peak at 480 cm^{-1} can be due either to HS or to H_2S with C_s symmetry. H_{ads} coexists with the two molecular species and S_{ads}, and a H-Ni stretching frequency that has shifted to 650 cm^{-1} suggests a fourfold hollow site for H_{ads}. A saturation coverage is reached that produces a faint c(2 × 2) LEED pattern, and a comparison with D_2S is made at this coverage. The temperature-dependent spectra shown in Figure 5-2 and other data show dissociation of the molecular species at ~170 K. We also find that H_{ads} recombines and leaves the surface at 220 K.

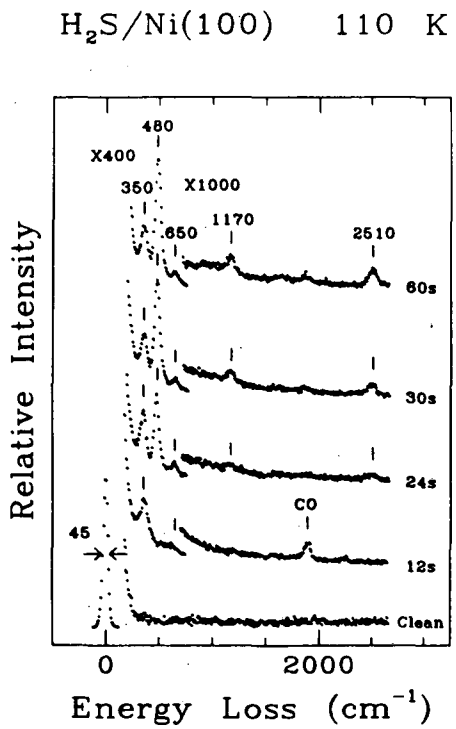

Figure 5-1. Coverage-dependent spectra for H_2S/Ni(100) at 110 K. The number of seconds of exposure to an effusive beam of H_2S is listed at the right of each trace. One second ~0.05–0.1 L; $E_i = E_r = 55°$; $E_o = 1.6$ eV. (XBL 847-2639)

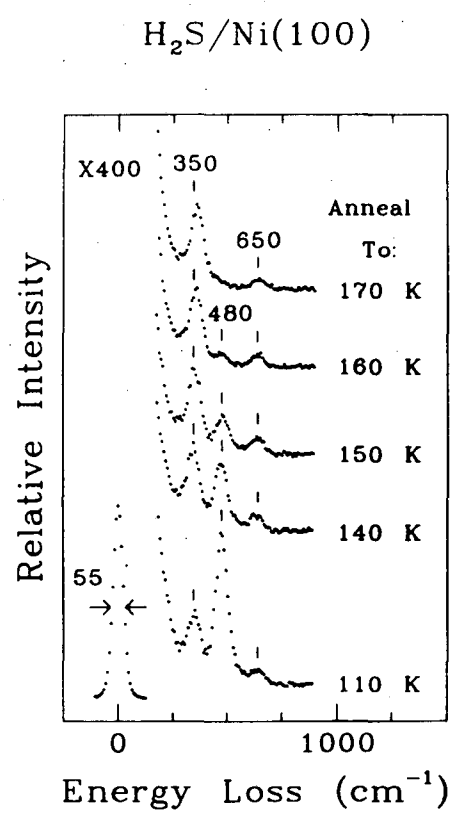

Figure 5-2. Temperature dependence of a saturation coverage of H_2S/Ni(100) with temperatures ranging from 110–170 K. Each spectrum was obtained after annealing to the given temperature for 5 minutes and then cooling back down to 110 K. $E_i = E_r = 55°$; $E_o = 1.6$ eV. (XBL 847-2645)

6. Electron-Energy-Loss Spectroscopy of CH_3NH_2 Adsorbed on Ni(100), Ni(111), Cr(100), and Cr(111) (Publication 21)

A.G. Baca, M.A. Schulz, and D.A. Shirley

Adsorbed CH_3NH_2 has been studied on Ni(100), Ni(111), Cr(100), and Cr(111) at 300 K using electron-energy-loss spectroscopy. The vibrational spectra indicate that molecular CH_3NH_2 exists on all four surfaces with bonding through the nitrogen lone pair, although a substantial amount of dissociation also occurs on the chromium surfaces. Approximately one monolayer of surface species is the stable coverage on each surface at 300 K. The possible existence of coadsorbed dissociation products CH_x and NH_x is discussed. The CN stretch is anomalously broad on Ni(100) and Ni(111) but not detectably broadened on Cr(100), indicating a strong sensitivity of this bond to interactions with the Ni surfaces. A multiplicity of sites is indicated on Cr(111) by the breadth of all the peaks. The loss spectra exhibit striking intensity differences that can be attributed partly to impact scattering and partly to intrinsic differences in the interaction of CH_3NH_2 with the different surfaces. A model explaining the linewidth and intensity differences is proposed.

7. Calculation and Computer Simulation of the Paraboloidal Mirror Analyzer (PMA) (Publication 20)

G. Liu,† J.J. Barton, C.C. Bahr, and D.A. Shirley

A semianalytical method is proposed to calculate the electric field and electron motion inside a paraboloidal electron mirror, the central electron optical component in a new, very high efficiency electron-energy analyzer. The error-of-field calculation is not more than 0.01%, and that of electron-motion calculation is not more than 0.1%. Calculation and computer simulation show that such an electron mirror can give very good angle resolution even for electrons having a wide energy spectrum.

†Permanent address: Department of Physics, Zhejiang University, Hangzhou, People's Republic of China.

8. The Valence Photoelectron Satellites of Neon (Publication 19)

P.A. Heimann, C.M. Truesdale,† H.G. Kerkhoff,‡ D.W. Lindle, T.A. Ferrett, C.C. Bahr, W.D. Brewer,§ U. Becker,‡ and D.A. Shirley

Synchrotron radiation was directed at neon gas, creating Ne^+ ions in "satellite" states characterized by the configurations $1s^22s^22p^4nl$, in addition to the main-line final states $2s^{-1}$ and $2p^{-1}$. Satellite features appearing in the photoelectron spectrum were studied in the near-threshold region with photon energies from 55.2 to 99.7 eV. For three of the satellite peaks, the angular-distribution asymmetry parameter β_i (shown in Figure 8-1) varies with kinetic energy in much the same way as the asymmetry parameter of the 2p line. None of the satel-

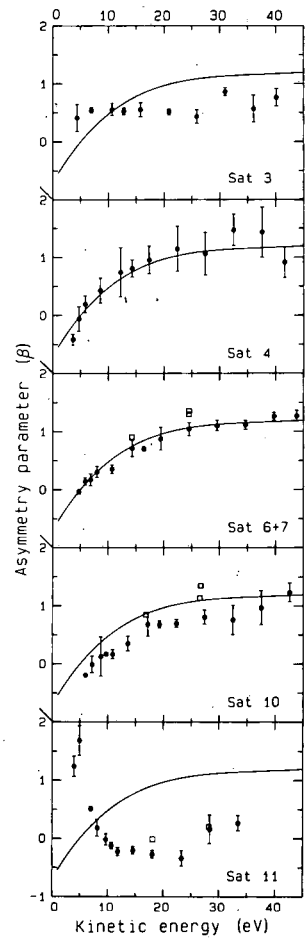

Figure 8-1. Asymmetry parameter of the neon valence satellites as a function of the satellite kinetic energy, with each satellite in a separate panel. The solid lines represent β_{2p} shifted to the equivalent kinetic energy.[1] The open squares display β_i values obtained by Adam.[1] (XBL 8410-4568)

lites have a β_i like that of the 2s line. All the satellite partial cross sections σ_i have kinetic-energy dependences similar to the partial cross section of the 2p main line. However, the σ_i curves are not identical, and some deviation from the 2p intensity behavior is observed. These β_i and σ_i results were used to confirm the previous assignments of the satellite final states in neon and to consider, in general, the energy-dependent behavior of satellites near threshold.

†Present address: Research and Development Division, Corning Glass Works, Corning, New York 14831.

‡Present address: Fachbereich Physik, Technische Universität Berlin, 1000 Berlin 12, West Germany.

§Present address: Institut für Atom und Festkorperphysik, Fachbereich Physik, Freie Universität Berlin, 1 Berlin 33, West Germany.

1. M.Y. Adam, private communication.

9. The Effects of Orbital Collapse on Photoemission from Atomic Eu (Publication 18)

U. Becker,† H.G. Kerkhoff,† D.W. Lindle, P.H. Kobrin,‡ T.A. Ferrett, P.A. Heimann, C.M. Truesdale,§ and D.A. Shirley

Resonant photoelectron spectra of atomic Eu have been measured in the photon-energy ranges of the "4d → 4f" (110–170 eV) and 3d → 4f (1120–1165 eV) excitations. The "4d → 4f" resonance data provide the first determination in a free atom of the decay channels of a "giant resonance" that peaks above its associated threshold. For both inner-shell excitations, decay to single-electron-hole final states (main lines) is the dominant process. However, the relative partial cross sections $\sigma(n\ell)$ for the different main-line final states vary with the initial excitation: decay after 4d excitation leads predominantly to autoionization into the 4f manifold, whereas several open exit channels (4s, 4p, 4d, 4f) participate in the decay following 3d excitation. Figures 9-1 and 9-2 illustrate the measured partial photoionization cross sections for the most important decay channels of the "4d → 4f" and 3d → 4f resonances, respectively.

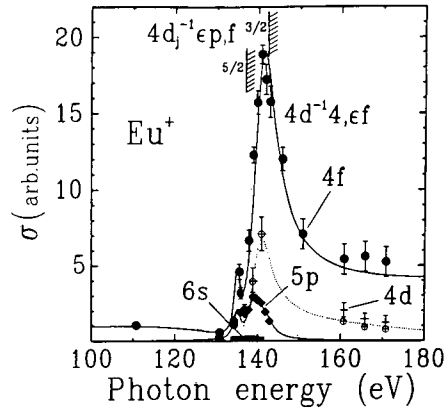

Figure 9-1. Partial cross sections of the 4d (crosses and open circles), 4f (closed circles), 5p (diamonds), and 6s (squares) main lines in the vicinity of the "4d → 4f" giant resonance of atomic Eu. (XBL 853-1512)

†Present address: Institut für Strahlungs- und Kernphysik, Technische Universität Berlin, D-1000 Berlin 12, West Germany.

‡Present address: Rockwell Science Center, Thousand Oaks, California 91360.

§Present address: Research and Development Division, Corning Glass Works, Corning, New York 14831.

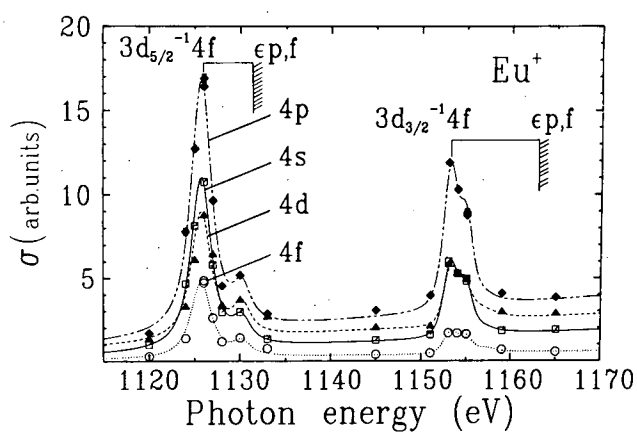

Figure 9-2. Partial cross sections of the 4s (squares), 4p (diamonds), 4d (triangles), and 4f (circles) main lines in the 3d → 4f excitation region. (XBL 853-1513)

10. Shape-Resonance Effects on the Outer- and Inner-Valence Levels of SF_6 in the 54–70 eV Photon-Energy Range (Publication 25)

T.A. Ferrett, M.N. Piancastelli, D.W. Lindle, P.A. Heimann, and D.A.Shirley

Using the time-of-flight synchrotron-radiation-induced photoemission technique, the relative partial photoionization cross sections in the 54–70 eV photon-energy range for both inner-valence and outer-valence orbitals of SF_6 were measured. The goal was to monitor the behavior of all inner- and outer-valence states through a photon-energy range in which a transition from the $3t_{1u}$ inner-valence orbital to the e_g "d-type" shape resonance is expected to take place, namely at ~57 eV, 15 eV above the ionization threshold for the $3t_{1u}$ level. An enhancement of the relative cross section for the $3t_{1u}$ state and possibly for other coupling channels was expected. An enhancement is observed in the photoionization cross section of the inner-valence shell of SF_6, probably corresponding to a transition to the e_g continuum shape-resonant state. This resonant behavior can be attributed mainly to the $3t_{1u}$ state, on the grounds of symmetry-selection rules, but a participation of the $2e_g$ state cross section to the resonance enhancement cannot be ruled out by the experimental findings. No distinct evidence of coupling of the shape-resonant state to any of the outer-valence levels was observed.

11. Chemisorption Geometry of Pyridine on Pt(111) by NEXAFS (Publication 23)

Allen L. Johnson, E.L. Muetterties,[†] J. Stöhr,[‡] and F. Sette[§]

Near edge x-ray absorption fine structure (NEXAFS) measurements were employed to investigate the temperature-dependent geometry of pyridine chemisorbed on the Pt(111) surface. At saturation coverage a low-temperature state with an apparent angle between the ring plane and the surface plane of 52 ± 6° was observed. This state converts (at 300 K) to a state with an angle between the ring plane and the surface plane of 74 ± 10°. An alpha-pyridyl surface state that drives the transformation is proposed.

[†]Deceased.

[‡]Present address: Corporate Research Science Laboratories, Exxon Research and Engineering Company, Annandale, New Jersey 08801.

[§]Present address: Bell Laboratories, Murray Hill, New Jersey 07974.

12. Desulfurization and Structural Transformation of Thiophene on the Pt(111) Surface (Publication 26)

J. Stöhr,[†] J.L. Gland,[†] E.B. Kollin,[†] R.J. Koestner, Allen L. Johnson, E.L. Muetterties,[‡] and F. Sette[§]

The temperature dependence of NEXAFS spectra above the C K-edge and S $L_{2,3}$-edge for thiophene (C_4H_4S) on Pt(111) reveals changes in the chemisorption geometry and the cleavage of the carbon-sulfur bond. Our results suggest the formation of a metallocycle intermediate after desulfurization with the S atom replaced by a Pt surface atom. The NEXAFS results are corroborated by thermal desorption, x-ray photoemission, and electron energy loss data.

[†]Present address: Corporate Research Science Laboratories, Exxon Research and Engineering Company, Annandale, New Jersey 08801.

[‡]Deceased.

[§]Present address: National Synchrotron Light Source, Brookhaven National Laboratory, Upton, New York 11973.

13. NEXAFS Studies of Chemisorbed Hydrocarbons: Bond Lengths with a Ruler (Publication 9)

J. Stöhr,[†] F. Sette,[‡] and Allen L. Johnson

Starting from an established correlation between the σ shape-resonance position in NEXAFS spectra and the intramolecular C-C bond length for gas-phase hydrocarbons, we derive a similar relation for chemisorbed molecules. The linear relation obtained allows us to determine the C-C bond length for chemisorbed molecules from NEXAFS spectra with a ruler to an accuracy of <0.04 Å. Examples are

given for bonding and bond-length changes of C_2H_2 and C_2H_4 on Pt(111).

---

†Present address: Corporate Research Science Laboratories, Exxon Research and Engineering Company, Annandale, New Jersey 08801.

‡Present address: National Synchrotron Light Source, Brookhaven National Laboratory, Upton, New York 11973.

14. Work in Progress

The recent development of the ARPEFS technique of photoelectron diffraction continues to provide exciting breakthroughs. The ARPEFS oscillations are observed by measuring the angle-resolved photoemission intensity as the photon energy—and hence the photoelectron kinetic energy—is scanned. These oscillations are caused by interference between direct and scattered photoelectron currents. Different emission directions pick up scattering signals from different substrate atoms.

Experimental evidence suggests that nearest-neighbor substrate atoms and atoms that backscatter into the detector dominate the ARPEFS spectrum, but theoretical models of the scattering process do not yet give this result. In our latest theoretical model, we are incorporating curved-wavefront corrections, multiple forward scattering, analytic angular integration, and dynamic photoelectron damping with the aim of accurately simulating the measured curves. Among our preliminary results are (1) a new "small-atom" approximation for photoelectron scattering, allowing accurate multiple-scattering, curved-wave calculations to be completed ten times faster than exact formulas, and (2) indications that variable angular apertures will simplify structure determination with ARPEFS.

A complete set of ARPEFS curves for c(2 × 2)S/Ni(110) now being analyzed should provide a critical test for our structural-analysis procedures as well as verify the structure of this system. With rectangular surface sites, this surface is more interesting than the square c(2 × 2)S/Ni(100) surface we have already analyzed; the striking similarity of comparable curves from these surfaces illustrates our deduction that backscattering and neighbor atoms generate the ARPEFS. We have also begun a study of the ARPEFS temperature dependence using this S/Ni(110) surface.

Our new time-of-flight angle-resolved paraboloidal-mirror analyzer (TOFAR-PMA) is fully constructed, including complete computer interfacing, and it has been partially debugged. Its efficiency (10–100 times higher than our present analyzers) spurred its initial construction, but our recent theory work suggests that its variable angular aperture may be equally important.

Our recent experiments in gas-phase photoemission have focused on the study of multielectron processes in atomic and molecular photoionization. Two categories of these studies can be distinguished. First, measurements of photoelectron satellites, which are entirely the result of electron correlation, have indicated the complexity of the kinetic-energy dependences of the satellite cross sections and photoelectron angular distributions. Work has been completed on the 1s shell satellites of the atoms He, Li, Ne, and Ar. These results constitute a major addition to the experimental knowledge of energy-dependent satellite behavior. Second, the role of multielectron effects in inner-shell photoionization has been studied in Xe and SF_6. In Xe, the effect of strong intershell correlation was observed in the 4p angular distribution. For SF_6, the partial multielectron nature of resonances in S 1s and S 2p photoionization has been established, contrary to previous interpretations that only considered one-electron processes. Future work in gas-phase photoemission will continue these investigations. For example, we plan to use a newly constructed threshold electron analyzer to study photoionization processes at and near threshold, with particular emphasis on satellites. In the second category, more work is planned to help understand the effects observed in SF_6. SiF_4 is the next molecule planned for study.

1984 PUBLICATIONS AND REPORTS

Refereed Journals

1. P.H. Kobrin, S. Southworth, C.M. Truesdale, D.W. Lindle, U. Becker, and D.A. Shirley, "Threshold Measurements of the K-Shell Photoelectron Satellites in Ne and Ar," Phys. Rev. A **29**, 194 (1984); LBL-15042.
2. C.M. Truesdale, D.W. Lindle, P.H. Kobrin, U.E. Becker, H.G. Kerkhoff, P.A. Heimann, T.A. Ferrett, and D.A. Shirley, "Core-Level Photoelectron and Auger Shape-Resonance Phenomena in CO, CO_2, CF_4, and OCS," J. Chem. Phys. **80**, 2319 (1984); LBL-15540.
3. C.C. Parks, D.A. Shirley, and G. Loubriel, "Beam-Exposure Dependence and Mechanisms of Photon-Stimulated Desorption from Alkali Fluorides," Phys. Rev. B **29**, 4709 (1984); LBL-16065.
4. J.J. Barton, C.C. Bahr, Z. Hussain, S.W. Robey, L.E. Klebanoff, and D.A. Shirley, "Direct Determination

of Surface Structures From Photoelectron Diffraction," J. Vac. Sci. Technol. A **2**, 847 (1984); LBL-16314.

5. D.J. Trevor, J.E. Pollard, W.D. Brewer, S.H. Southworth, C.M. Truesdale, D.A. Shirley, and Y.T. Lee, "Photoionization Mass Spectroscopy of Ne Dimers," J. Chem. Phys. **80**, 6083 (1984); LBL-17445.
6. D.W. Lindle, P.H. Kobrin, C.M. Truesdale, T.A. Ferrett, P.A. Heimann, H.G. Kerkhoff, U. Becker, and D.A. Shirley, "Inner-Shell Photoemission from the Iodine Atom in CH_3I," Phys. Rev. A **30**, 239 (1984); LBL-16746.
7. P.H. Kobrin, U. Becker, C.M. Truesdale, D.W. Lindle, H.G. Kerkhoff, and D.A. Shirley, "Photoelectron Asymmetries and Two-Electron Satellites Near the 3p → 3d Giant-Resonance Region in Atomic Mn," J. Elect. Spectros. and Rel. Phen. **34**, 129 (1984); LBL-14545.
8. L.E. Klebanoff, S.W. Robey, G. Liu, and D.A. Shirley, "Observation of a Surface Magnetic Phase Transition on Cr(100)," Phys. Rev. B **30**, 1048 (1984); LBL-17722.
9. J. Stöhr, F. Sette, and Allen L. Johnson, "Near-Edge X-Ray-Absorption Fine-Structure Studies of Chemisorbed Hydrocarbons: Bond Lengths with a Ruler," Phys. Rev. Lett. **53**, 1684 (1984); LBL-18723.†
10. A.G. Baca, M.A. Schulz, and D.A. Shirley, "Electron Energy Loss Spectroscopy of H_2S Adsorbed on Ni(100)," J. Chem. Phys. **81**, 6304 (1984); LBL-17986.
11. D.W. Lindle, C.M. Truesdale, P.H. Kobrin, T.A. Ferrett, P.A. Heimann, U. Becker, H.G. Kerkhoff, and D.A. Shirley, "Nitrogen K-Shell Photoemission and Auger Emission from N_2 and NO," J. Chem. Phys. **81**, 5375 (1984); LBL-16861.
12. J.E. Pollard, D.J. Trevor, J.E. Reutt, Y.T. Lee, and D.A. Shirley, "Torsional Potential and Intramolecular Dynamics in the $C_2H_4^+$ Photoelectron Spectra," J. Chem. Phys. **81**, 5302 (1984); LBL-16576.

Other Publications

13. J.J. Barton, C.C. Bahr, Z. Hussain, S.W. Robey, L.E. Klebanoff, and D.A. Shirley, "Angle-Resolved Photoemission Extended Fine Structure," in *The Brookhaven Conference: Advances in Soft X-Ray Science and Technology,* Brookhaven National Laboratory, October 17–20, 1983, SPIE **447**, 82 (1984); LBL-16298.
14. D.A. Shirley, P.H. Kobrin, C.M. Truesdale, D.W. Lindle, T.A. Ferrett, P.A. Heimann, U. Becker, H.G. Kerkhoff, and S.H. Southworth, "Gas-Phase Photoemission with Soft X-Rays: Cross Sections and Angular Distributions," in *The Brookhaven Conference: Advances in Soft X-Ray Science and Technology,* Brookhaven National Laboratory, October 17–20, 1983, SPIE **447**, 150 (1984); LBL-16296.

LBL Reports

15. J.J. Barton, S.W. Robey, C.C. Bahr, and D.A. Shirley, "Surface Structure Determination with ARPEFS," in *Proc. First Int. Conf. on the Structure of Surfaces,* University of California, Berkeley, California, August 13–16, 1984; accepted for publication in *Springer Series in Chemical Physics;* LBL-18236.
16. R.S. Williams, W.J. Gignac, J.G. Nelson, S. Kim, J.G. Tobin, S.W. Robey, and D.A. Shirley, "High Resolution Angle-Resolved Photoemission Study of the Valence Band Structure of Ag(111)," LBL-15135.
17. A.E. Schach von Wittenau, R.F. Davis, J.G. Tobin, M.G. Mason, Z. Hussain, and D.A. Shirley, "Effects of Surface Reconstruction and Photon Polarization in Angle-Resolved Photoemission: Applications to Au(001)," LBL-15913.
18. U. Becker, H.G. Kerkhoff, D.W. Lindle, P.H. Kobrin, T.A. Ferrett, P.A. Heimann, C.M. Truesdale, and D.A. Shirley, "The Effects of Orbital Collapse on Photoemission from Atomic Eu," LBL-16066.
19. P.A. Heimann, C.M. Truesdale, H.G. Kerkhoff, D.W. Lindle, T.A. Ferrett, C.C. Bahr, W.D. Brewer, U. Becker, and D.A. Shirley, "The Valence Photoelectron Satellites of Neon," submitted to Phys. Rev. A.; LBL-18263.
20. G. Liu, J.J. Barton, C.C. Bahr, and D.A. Shirley, "Calculation and Computer Simulation of the Paraboloidal Mirror Analyzer (PMA)," LBL-18216.
21. A.G. Baca, M.A. Schulz, and D.A. Shirley, "Electron Energy Loss Spectroscopy of CH_3NH_2 Adsorbed on Ni(100), Ni(111), Cr(100), and Cr(111)," LBL-18670.
22. L.E. Klebanoff, S.W. Robey, G. Liu, and D.A. Shirley, "Investigation of the Near-Surface Electronic Structure of Cr(100)," submitted to Phys. Rev. B.; LBL-18633.
23. Allen L. Johnson, E.L. Muetterties, J. Stöhr, and F. Sette, "Chemisorption Geometry of Pyridine on Pt(111) by NEXAFS," LBL-18694.
24. J.J. Barton and D.A. Shirley, "Curved Wavefront Corrections for Photoelectron Scattering," LBL-18692.
25. T.A. Ferrett, M.N. Piancastelli, D.W. Lindle, P.A. Heimann, and D.A. Shirley, "Shape-Resonance Effects on the Outer- and Inner-Valence Levels of SF_6 in the Photon-Energy Range 54–70 eV," LBL-18638.

26. J. Stöhr, J.L. Gland, E.B. Kollin, R.J. Koestner, Allen L. Johnson, E.L. Muetterties, and F. Sette, "Desulfurization and Structural Transformation of Thiophene on the Pt(111) Surface," accepted by Phys. Rev. Lett.; LBL-18724.†

Invited Talks

27. D.A. Shirley, "Angle-Resolved Photoemission Extended Fine Structure," Physics Department, Uppsala University, Sweden, February 2, 1984; Chemistry Department, Indiana University, Bloomington, February 22, 1984; Physics Department, William and Mary College, Williamsburg, Virginia, May 4, 1984; Gordon Research Conference on Electron Spectroscopy, Wolfeboro, New Hampshire, July 20, 1984.
28. D.A. Shirley, "Photoelectron Asymmetries and Resonances in Atoms and Molecules," 1984 March Meeting of the American Physical Society, Detroit, Michigan, March 26–30, 1984.
29. J.J. Barton, "Surface Structure Determination with ARPEFS," International Conference on the Structure of Surfaces, University of California, Berkeley, August 13–16, 1984.
30. L.E. Klebanoff, "An ARPES Investigation of Cr(100) Surface Magnetism," SSRL Users Meeting, Stanford, California, October 26, 1984.

†Supported by the Director, Office of Energy Research, Office of Basic Energy Sciences, Chemical Sciences Division of the U.S. Department of Energy under Contract No. DE-AC03-76SF00098, Account 4018.

Crossed Molecular Beams*

Yuan T. Lee, Investigator

INTRODUCTION

The major thrust of this research project is to elucidate detailed dynamics of simple elementary reactions that are theoretically important and to unravel the mechanism of complex chemical reactions or photochemical processes that play important roles in many macroscopic processes. Molecular beams of reactants are used to study individual reactive encounters between molecules or to monitor photodissociation events in a collision-free environment. Most of the information is derived from measurement of the product-fragment energy and angular distributions using various molecular-beam machines designed for these purposes. Recent activities are centered on the following areas: (1) the direct probing of transition states of the F + H_2 and D + H_2 reaction through the experimental observation of quantum-mechanical resonance phenomena; (2) the mechanisms of elementary chemical reactions involving oxygen atoms with unsaturated hydrocarbons; (3) the dynamics of chemical reactions of electronically excited atoms; (4) the primary photochemical processes of polyatomic molecules, radicals, and ions; (5) intramolecular energy transfer of chemically activated and locally excited molecules using overtone-excitation processes; and (6) the interaction potential of open-shell atoms with rare-gas atoms.

1. Reactive Scattering of $O(^3P)$ with Toluene (Publication 4)†

R.J. Baseman,‡ R.J. Buss,§ P. Casavecchia,‖ and Y.T. Lee

In a crossed molecular-beam study, the reaction of $O(^3P)$ + toluene at 9.7 kcal/mole collision energy is shown to give primarily radical products, CH_3 + phenoxy and H + cresoxy, under single-collision conditions. There is no evidence of intersystem crossing to a stable singlet species, cresol, as was previously observed in the O + benzene reaction. The isotropic angular distributions of the product suggest that the mechanism involves formation of a long-lived triplet biradical intermediate.

*This work was supported by the Director, Office of Energy Research, Office of Basic Energy Sciences, Chemical Sciences Division of the U.S. Department of Energy under Contract No. DE-AC03-76SF00098.

†R.J. Baseman was supported by the Fannie and John Hertz Foundation as a Graduate Fellow.

‡Present address: Sperry Univac, Semiconductor Division, St. Paul, Minnesota 55164-0525.

§Present address: Sandia National Laboratory, Albuquerque, New Mexico 87185.

‖Present address: Department of Chemistry, University of Perugia, Perugia, Italy.

2. Infrared Predissociation Spectra of Water Dimer in a Supersonic Molecular Beam (Publication 3)†

Ralph H. Page, Jeremy G. Frey, Y.R. Shen, and Y.T. Lee

The infrared absorption spectrum of the hydrogen-bonded water dimer, $(H_2O)_2$, formed in a supersonic expansion, was recorded in the region of the OH stretch by monitoring the predissociation resulting from the absorption of the radiation. The conditions were such that there was minimal contribution to the observed spectrum from higher water polymers. The observed features show considerable structure, with widths that appear to be limited by the optical resolution of 2 cm^{-1}. A combination band of the OH stretch with the water bend and an overtone of the bending vibration were also observed.

†Jeremy G. Frey was supported by NATO/SERC as a postdoctoral fellow.

3. Photodissociation of 1,2-Chloroiodoethane at 248 and 266 nm; the Enthalpy of Formation of CH_2ClCH_2I (Publication 6)

Timothy K. Minton, Peter Felder, Richard J. Brudzynski, and Yuan T. Lee

The technique of photofragmentation translational spectroscopy has been used to study the photodissociation of CH_2ClCH_2I at excitation wavelengths of 248 and 266 nm. The primary photofragments are C_2H_4Cl and either $I^*(^2P_{1/2})$ or $I(^2P_{3/2})$. A fraction of the chloroethyl radical product contains enough internal excitation after the primary process to undergo secondary dissociation into C_2H_4 and Cl.

By observing the threshold for this secondary process, the reaction enthalpy for $CH_2ClCH_2I \rightarrow C_2H_4 + Cl + I$ was determined, which leads to $\Delta H^{\circ}_{f,0}$ $(CH_2ClCH_2I) = -7.8 \pm 1$ kcal/mole. The center-of-mass (CM) translational-energy distribution of the photofragments was derived for both the I^* and I channels, yielding I^*/I branching ratios of 1.5 at 248 nm and 3 at 266 nm. The translational-energy distribution also revealed that about 50% of the excess energy went into translation. The angular distributions of dissociation products with respect to the laser polarization indicate that the primary photodissociation process for the ground- and excited-state iodine channels at both wavelengths proceeds via a parallel transition — that is, the transition moment must be nearly parallel to the C-I bond.

4. Ultraviolet Photodissociation of C_2F_5Br, C_2F_5I, and 1,2-C_2F_4BrI (Publication 7)

D. Krajnovich, L.J. Butler, and Y.T. Lee

The photodissociation reactions of C_2F_5Br, C_2F_5I, and 1,2-C_2F_4BrI have been studied at 248 and 193 nm using the crossed-laser/molecular-beam technique. Photodissociation of 1,2-C_2F_4BrI was also studied at 266 nm. We find that: (1) C_2F_5Br undergoes C-Br bond fission at 193 nm but does not absorb at 148 nm; (2) C_2F_5I undergoes C-I bond fission at 248 nm but does not absorb at 193 nm; and (3) 1,2-C_2F_4BrI undergoes only C-I bond fission at 248 and 266 nm, but at 193 nm both C-I and C-Br bond fission are observed, with a C-I:C-Br fission ratio of approximately 1.7:1. CM recoil energy and angular distributions are determined for each of these photodissociation reactions. These results, combined with those of other workers, are used to test simple predictions based on molecular-orbital theory. The 266-nm data for C_2F_4BrI provide an approximate value of 19.3 ± 3 kcal/mole for the dissociation energy of C_2F_4Br to $C_2F_4 + Br$. The data also show that all or almost all the iodine produced in the primary C-I bond fission is in the excited $^2P_{1/2}$ state. The prospect of doing bond-selective photochemistry in the ultraviolet is discussed.

5. The Effects of Collision Energy and Vibrational Excitation on H_2^+ + He and HD^+ + He Reactions (Publication 8)†

T. Turner, O. Dutuit,‡ and Y.T. Lee

An experimental study of proton and deuteron transfer in H_2^+ + He and HD^+ + He has been carried out as a function of kinetic and vibrational energy. The data give evidence that, at lower kinetic energies, the spectator-stripping mechanism indeed plays an important role when H_2^+ or HD^+ is vibrationally excited. The H_2^+ (v = 0) reaction has a much smaller cross section than the v = 1–4 reactions and seems to go through intimate, small-impact-parameter collisions involving all the atoms. Investigation of the competition between both the proton- and deuteron-transfer channels for the HD^+ case shows that vibrational enhancement toward forming the HeD^+ product falls off sooner with increasing kinetic energy than does the HeH^+ product, again in accordance with the spectator-stripping model. The higher yield for HeH^+ production at both higher vibrational levels of HD^+ and lower kinetic energy, as well as the behavior of translational energy dependence of HeH^+, seems to indicate the importance of the induced orientation of HD^+ during the collision with He. Because of the displacement of the center of mass from the center of charge in HD^+, the charge-induced dipole interaction between He and HD^+ tends to swing the H atom more toward He during the approach of He and HD^+.

†T. Turner was supported by the Fannie and John Hertz Foundation as a Graduate Fellow.

‡Permanent address: Laboratoire de Resonance Electronique et Ionique, Centre Universitaire d'Orsay, 91405 Orsay, France.

6. Photodissociation of CF_2Br_2 at 248 nm by the Molecular-Beam Method (Publication 9)

D. Krajnovich, Z. Zhang, L. Butler, and Y.T. Lee

The photochemistry of CF_2Br_2 at 248 nm has been studied by the crossed-laser/molecular-beam

technique. The only primary-reaction channel observed is atomic-bromine elimination: $CF_2Br_2 \rightarrow CF_2Br + Br$. Laboratory angular and time-of-flight distributions of the CF_2Br and Br primary products were measured and used to derive CM product-recoil-energy and angular distributions for this reaction. The average CM recoil energy of the products is 21.3 kcal/mole. The shape of the CM angular distribution indicates that the transition-dipole moment is polarized parallel to the Br-Br direction in CF_2Br_2. The molecular-bromine elimination reaction, $CF_2Br_2 \rightarrow CF_2 + Br_2$, does not occur to a measurable extent at 248 nm. However, CF_2 radicals are produced in abundance under collision-free conditions, due to the efficient secondary photodissociation of some of the CF_2Br primary product.

7. Dynamic Resonances in the Reaction of Fluorine Atoms with Hydrogen Molecules (Publications 5 and 10)

D.M. Neumark,[†] A.M. Wodtke, G.N. Robinson, C.C. Hayden,[‡] and Y.T. Lee

The reactions of $F + H_2$, HD, and D_2 were studied in high-resolution crossed-molecular-beam experiments. CM translational-energy and angular distributions were determined for each product vibrational state. In the $F + H_2$ reaction, the v = 3 product showed intense forward scattering while the v = 2 product was backward-peaked. These results, in contrast to the backward scattering of all DF-product vibrational states from $F + D_2$ at the same collision energy, suggest that dynamical resonances play an important role in the reaction dynamics of this system. In the F + HD reaction, the strong forward scattering of HF products and backward scattering of DF products is in agreement with the prediction of a stronger resonance effect for HF formation. The effect of the H_2 rotational excitation and the reactivity of $F(^2P_{1/2})$ are also discussed.

[†]Present address: Department of Chemistry, University of Colorado, Boulder, Colorado 80309.

[‡]Present address: Department of Chemistry, University of Wisconsin, Madison, Wisconsin 53706.

8. The Effect of Collision Energy and Vibrational Excitation on the Reaction $C_2H_2^+ + H_2$ (Publication 15)

T. Turner and Y.T. Lee

The relative efficiencies between the excitation of the C-C stretching vibration and collision energy on the promotion of the H-atom transfer reaction of $C_2H_2^+ + H_2 \rightarrow C_2H_3^+ + H$ have been examined. At low collision energies the reaction is strongly vibrationally enhanced, in agreement with previous thermal-energy studies. Translational energy was found to be not as effective as exciting the C-C stretching vibration in promoting the reaction. The results indicate that the H-atom transfer from H_2 to the C atom should have a late barrier, but the C-C stretching vibration of $C_2H_2^+$ is apparently coupled to the reaction coordinate. Because the C-C bond in $C_2H_3^+$ is expected to be longer than that of $C_2H_2^+$, vibrational energy added to the C-C bond might reduce the barrier for H-atom transfer from H_2 to a C atom in $C_2H_2^+$.

[†]T. Turner was supported by the Fannie and John Hertz Foundation as a Graduate Fellow.

9. Radiative Decay of Vibrationally Excited CH_2^- (Publication 16)[†]

M. Okamura, L.I.C. Yeh, D. Normand,[‡] J.J.H. van den Biesen,[§] S.W. Bustamente,[‖] and Y.T. Lee

We have observed the presence of vibrationally excited CH_2^- created in a discharge by measuring the photodetachment from CH_2^- as it radiatively relaxes in a high-vacuum ion trap. We used a tunable infrared laser to produce photons with energies above and below the expected threshold for removing an electron from the ground state. The time dependence of the photodetachment is consistent with the electron affinity of 5250cm^{-1} (0.65 eV) obtained by Sears and Bunker[1] for the ground state of X^3B_1 methylene. We have tentatively assigned radiative lifetimes for the excited bending vibrations of CH_2^-: 600.ps 10 ± 300 msec for $v_2 = 1$,

80 ± 40 msec for $v_2 = 2$, and 10 ± 5 msec for $v_2 = 3$.

†M. Okamura was supported as a 1982–1983 Regents Fellow. L.I.C. Yeh was supported by the National Science Foundation as a Predoctoral Fellow.

‡Permanent address: C.E.N./Saclay, 91191 Gif-sur-Yvette, France.

§Present address: Philips Research Laboratories, 5600 JA Eindhoven, The Netherlands.

||Present address: Hughes Aircraft Corp., P.O. Box 2999, Torrance, California 90509.

1. T.S. Sears and P.R. Bunker, J. Chem. Phys. **79**, 5265 (1983).

10. Molecular-Beam Studies of the F + H_2 Reaction (Publication 18)

D.M. Neumark,† A.M. Wodtke, G.N. Robinson, C.C. Hayden,‡ and Y.T. Lee

The dynamics of the F + H_2 reaction have been investigated in a high-resolution crossed-molecular-beam study. Differential cross sections and kinetic-energy distributions were obtained for each HF vibrational state. The v = 1 and v = 2 states were predominantly backward scattered, but substantial forward scattering was observed for HF (v = 3) over the range of collision energies accessible in our apparatus, from 0.7 to 3.4kcal/mole. The results strongly suggest that dynamical resonances play a significant role in the reaction dynamics of F + H_2 and that resonance effects are most prominent in the v = 3 product channel. Quantal reactive-scattering calculations on F + H_2 predict that the v = 2 channel should be most strongly affected by resonances. This discrepancy is attributed to inadequacies in the potential-energy surface used in the calculations, and several modifications to the surface are proposed based on the experimental results. Other features of the reaction are also discussed, including the integrated partial cross sections, the effect of H_2 rotation, and the reactivity of $F(^2P_{1/2})$.

†Present address: Department of Chemistry, University of Colorado, Boulder, Colorado 80309.

‡Present address: Department of Chemistry, University of Wisconsin, Madison, Wisconsin 53706.

11. Molecular-Beam Studies of the F + D_2 and F + HD Reactions (Publication 17)

D.M. Neumark,† A.M. Wodtke, G.N. Robinson, C.C. Hayden,‡ K. Shobatake,§ R.K. Sparks,|| T.P. Schafer, and Y.T. Lee

The F + D_2 and F + HD reactions were investigated in a high-resolution crossed-molecular-beam experiment at several collision energies. The DF product from both reactions was predominantly backward scattered, although some forward-scattered DF (v = 4) was observed at the highest energy studied. The HF angular distributions from F + HD were quite different, showing considerable forward-scattered HF (v = 3) and no other identifiable structure. These results disagree with classical trajectory studies, which predict only small variations in the product angular distributions among F + H_2 and its isotopic variants. They agree, however, with the predicted dependence of dynamical resonance effects on isotopic substitution. The results therefore support the conclusions drawn in abstract 10 regarding the role of dynamical resonances in the F + H_2 reaction.

†Present address: Department of Chemistry, University of Colorado, Boulder, Colorado 80309.

‡Present address: Department of Chemistry, University of Wisconsin, Madison, Wisconsin 53706.

§Permanent address: Institute for Molecular Science, Myodaiji, Okazaki 444, Japan.

||Permanent address: Department of Chemistry, California Institute of Technology, Pasadena, California 91125.

12. Photoionization Mass Spectroscopy of Ne Dimers (Publication 2)

*D.J. Trevor,† J.E. Pollard,‡ W.D. Brewer,§ S.H. Southworth,|| C.M. Truesdale,** D.A. Shirley, and Y.T. Lee*

The photoionization-efficiency curve of Ne_2 as a function of wavelength has been obtained between 560 and 620 Å with a synchrotron-radiation photon source. Detailed considerations of the autoioniza-

tion mechanisms and symmetry of the excited states of Ne_2 have led to the partial assignment of those excited electronic states of Ne_2 responsible for the structure observed in its photoionization-efficiency curve. The considerations have also helped to demonstrate the importance of Rydberg states with a $B^2\Pi_g$ core. The lower bound to the dissociation energy of of Ne_2^+ was determined to be 1.24 ± 0.08 eV (28.6 ± 1.8 kcal/mole).

†Present address: Exxon Research and Engineering Company, Annandale, New Jersey 08801.

‡Present address: The Aerospace Corporation, Los Angeles, California 90009.

§Present address: Institut für Atome and Festkorperphysik, Freie Universitat, Berlin, West Germany.

‖Present address: National Bureau of Standards, Washington, D.C. 20234.

**Present address: Department of Applied Physics, Corning Glass Works, Corning, New York 14831.

13. Torsional Potential and Intramolecular Dynamics in the $C_2H_4^+$ Photoelectron Spectra (Publication 20)

J.E. Pollard,† D.J. Trevor,‡ J.E. Reutt, Y.T. Lee, and D.A. Shirley

The 584-Å photoelectron spectrum of ethylene was reexamined at higher resolution using a supersonic molecular-beam source for rotational cooling. The vibrational frequencies of the $C_2H_4^+$ $\tilde{X}$ $^2B_3$ state were measured with improved accuracy, which permitted the torsional potential-energy curve to be characterized. The measured equilibrium torsional angle is 27 ± 2°, and the inversion barrier is 270 ± 150 cm^{-1}. The $\tilde{A}$ $^2B_3$ state is shown to be in reasonable agreement with a recent theoretical calculation that takes into account strong nonadiabatic effects. The correlation function calculated for this state is consistent with this calculation and with recent calculations on the unimolecular dissociation of this state. The $\tilde{B}$ ^2A state correlation function indicates that a rapid decay mechanism is operative. The broadened vibrational structure in the fourth band results from a saddle point in the $\tilde{C}$ $^2B_2$ potential-energy surface from which the ion relaxes to the $\tilde{X}$ state by moving along a repulsive degree of freedom, which in this case is internal rotational. The $\tilde{C}$ state vibrational broadening, as well as the decay of the correlation function, yields a lifetime for this process of 7 fsec.

†Present address: The Aerospace Corporation, Los Angeles, California 90009.

‡Present address: Exxon Research and Engineering Company, Annandale, New Jersey 08801.

14. Work in Progress

We have studied the reactions

$$Na(3^2S_{1/2}, 3^2P_{3/2}, 4^2D_{5/2}, 5^2S_{1/2}) + HCl \rightarrow NaCl + H$$

and

$$Na(3^2S_{1/2}, 3^2P_{3/2}, 4^2D_{5/2}, 5^2S_{1/2}) + O_2 \rightarrow NaO + O$$

in a crossed-molecular-beam machine. The observed differential cross sections depend strongly on the initial electronic state and, for the $4^2D_{5/2}$ state, on the laser-induced orbital alignment.

The dominant feature in the reaction

$$Na(3^2S_{1/2}, 3^2P_{3/2}, 4^2D_{5/2}, 5^2S_{1/2}) + HCl \rightarrow NaCl + H \quad (\Delta H = +4.68 \text{ kcal/mole})$$

is the narrowing of the angular distribution at higher electronic energies.

With higher electronic excitation, the ionic-neutral potential-surface crossing points move out to larger interatomic distances. Since slow electrons dissociate HCl,[1] electron transfer from Na dissociates HCl. In the case of the Na(4d) and Na(5s) levels, the H atom has departed before the Na^+ and Cl^- come together to form a highly vibrationally excited NaCl molecule.

The preferred laser-polarization direction is parallel to the relative-velocity vector, showing that a Σ NaClH molecular state is most important in leading to the NaCl product.

In the reaction

$$Na(3^2S_{1/2}, 3^2P_{3/2}, 4^2D_{5/2}, 5^2S_{1/2}) + O_2 \rightarrow NaO + O \quad (\Delta H = +57.86 \text{ kcal/mole}),$$

the $4^2D_{5/2}$ state reacts to produce NaO, but the $3^2P_{3/2}$ and the $5^2S_{1/2}$ states do not, although the reaction is energetically allowed. Although the reaction takes places at collision energies of 18.1 and 15.9 kcal/mole, it does not occur at 7.1 kcal/mole, implying an entrance-channel barrier of at least 7 kcal/mole.

The laboratory angular distributions are strongly backwards-peaked relative to incoming sodium atoms, showing that collinear and near-collinear approach geometries are favored for the reaction. All the NaO falls within a very restricted angular range — completely within the Newton circle for $Na(4^2D_{5/2}) + O_2 \rightarrow NaO + O^*(^1D)$.

---

1. J.N. Bardsley and J.M. Wadehrs, J. Chem. Phys. **78**, 7227 (1983).

1984 PUBLICATIONS AND REPORTS

Refereed Journals

1. Jeremy G. Frey, "Excited Vibrational States Near Dissociation in Weakly Bound Triatomic Systems," Chem. Phys. Lett. **102**, 421 (1983); LBL-16709.†
2. D.J. Trevor, J.E. Pollard, W.D. Brewer, S.H. Southworth, C.M. Truesdale, D.A. Shirley, and Y.T. Lee, "Photoionization Mass Spectroscopy of Ne Dimers," J. Chem. Phys. **80**, 6083 (1984); LBL-17445.
3. Ralph H. Page, Jeremy G. Frey, Y.R. Shen, and Y.T. Lee, "Infra-red Predissociation Spectra of Water Dimer in a Supersonic Molecular Beam," Chem. Phys. Lett. **106**, 373 (1984); LBL-17512.†
4. R.J. Baseman, R.J. Buss, P. Casavecchia, and Y.T. Lee, "Reactive Scattering of $O(^3P)$ with Toluene," J. Am. Chem. Soc. **106**, 4108 (1984); LBL-17103.‡
5. D.M. Neumark, A.M. Wodtke, G.N. Robinson, C.C. Hayden, and Y.T. Lee, "Experimental Investigation of Resonances in Reactive Scattering: The $F + H_2$ Reaction," Phys. Rev. Lett. **53**, 226 (1984); LBL-17446.
6. Timothy K. Minton, Peter Felder, Richard J. Brudzynski, and Yuan T. Lee, "Photodissociation of 1,2-Chloroiodoethane at 248 and 266 nm; the Enthalpy of Formation of CH_2ClCH_2I," J. Chem. Phys. **81**, 1759 (1984); LBL-17535.
7. D. Krajnovich, L.J. Butler, and Y.T. Lee, "UV Photodissociation of C_2F_5Br, C_2F_5I, and 1,2-C_2F_4BrI," J. Chem. Phys. **81**, 3031 (1984); LBL-17447.
8. T. Turner, O. Dutuit, and Y.T. Lee, "The Effect of Collision Energy and Vibrational Excitation on H_2^+, HD^+ + He Reactions," J. Chem. Phys. **81**, 3475 (1984); LBL-17729.‡
9. D. Krajnovich, Z. Zhang, L. Butler, and Y.T. Lee, "Photodissociation of CF_2Br_2 at 248 nm by the Molecular Beam Method," J. Phys. Chem. **88**, 4561 (1984); LBL-16431.

Other Publications

10. D.M. Neumark, A.M. Wodtke, G.N. Robinson, C.C. Hayden, and Y.T. Lee, "Dynamic Resonances in the Reaction of Fluorine Atoms with Hydrogen Molecules," in ACS Symposium on *Resonances in Electron-Molecule Scattering, van der Waals Complexes and Reactive Chemical Dynamics,* Donald G. Truhlar, Ed., ACS Symp. Ser. **263**, 479 (1984); LBL-17822.
11. R.J. Brudzynski, "Molecular Beam Study of the Unimolecular Decomposition of Toluene," in *Proc. Int. Conf. on Radiationless Transitions,* Newport Beach, California, January 2–7; 1984; LBL-16911abs.
12. Peter Felder, "Photodissociation of Isopropylcycloheptatriene at 266 nm," in *Proc. Int. Conf. on Radiationless Transitions,* Newport Beach, California, January 2–7, 1984; LBL-16912abs.
13. Timothy K. Minton, "Photodissociation of 1,2-chloroiodoethane," in *Proc. Int. Conf. on Radiationless Transitions,* Newport Beach, California, January 2–7, 1984; LBL-16913abs.

LBL Reports

14. Daniel M. Neumark (Ph.D. Thesis), with Y.T. Lee, "High Resolution Reactive Scattering," LBL-16968.
15. T. Turner and Y.T. Lee, "The Effect of Collision Energy and Vibrational Excitation on the Reaction of $C_2H_2^+ + H_2$," J. Chem. Phys. (in press); LBL-17549.‡
16. M. Okamura, L.I.C. Yeh, D. Normand, J. van den Biesen, S.W. Bustamente, and Y.T. Lee, "Radiative Decay of Vibrationally Excited CH_2," accepted by Tetrahedron Symposium in Print, *Recent Aspects of Carbene Chemistry;* LBL-17888.§
17. D.M. Neumark, A.M. Wodtke, G.N. Robinson, C.C. Hayden, K. Shobatake, R.K. Sparks, and Y.T. Lee, "Molecular Beam Studies of the $F + D_2$ and F + HD Reactions," submitted to J. Chem. Phys.; LBL-17809.
18. D.M. Neumark, A.M. Wodtke, G.N. Robinson, C.C. Hayden, and Y.T. Lee, "Molecular Beam Studies of the $F + H_2$ Reaction," submitted to J. Chem. Phys.; LBL-17810.
19. Thomas P. Turner (Ph.D. Thesis), with Y.T. Lee, "The Effect of Collision Energy and Vibrational Excitation on Endothermic Ion-Molecule Reactions," LBL-18082.‡

20. J.E. Pollard, D.J. Trevor, J.E. Reutt, Y.T. Lee, and D.A. Shirley, "Torsional Potential and Intramolecular Dynamics in the $C_2H_4^+$ Photoelectron Spectra," submitted to J. Chem. Phys.; LBL-16576.

Invited Talks

21. Y.T. Lee, "Formation and Decay of Quasi-bound State in Elementary Chemical Reactions," International Conference on Radiationless Transitions, Newport Beach, California, January 2–7, 1984.
22. Y.T. Lee, "Molecular Beam Studies of Elementary Chemical Reactions," University of Ohio, Columbus, Ohio, February 29, 1984.
23. Y.T. Lee, "Photofragmentation Translational Spectroscopy," University of Ohio, Columbus, Ohio, March 1, 1984.
24. D.M. Neumark, "The Observation of Dynamic Resonances in the $F + H_2$ Reaction," 187th American Chemical Society Meeting, St. Louis, Missouri, April 9–12, 1984.
25. Y.T. Lee, "Molecular Beam Studies on Reaction Dynamics," University of Wisconsin, Madison, April 18, 1984.
26. Y.T. Lee, "Energetics of Radicals Involved in Combustion Processes," Department of Energy Combustion Science Contractor's Meeting, Sandia Laboratory, Livermore, California, May 22–23, 1984.
27. Y.T. Lee, "Dynamics and Mechanism of Elementary Chemical Reactions," Symposium on "Frontiers of Chemistry," American Association for Advancement of Science, New York, New York, May 24–27, 1984.
28. Y.T. Lee, "Dynamic Resonances in the $F + H_2$ Reaction," Fifth American Conference on Theoretical Chemistry, Jackson, Wyoming, June 15–20, 1984.
29. Y.T. Lee, "Molecular Collisions and Chemical Kinetics" (three lectures), Workshop on Chemical Kinetics and Laser Chemistry, Shitou, Taiwan, July 16–20, 1984.
30. Y.T. Lee, "Dynamics and Mechanism of Elementary Chemical Reactions," 188th American Chemical Society National Meeting, Philadelphia, Pennsylvania, August 26–28, 1984.
31. L.J. Butler, "Molecular Beam Studies of Photodissociation Dynamics," 188th American Chemical Society National Meeting, Philadelphia, Pennsylvania, August 26–28, 1984.
32. Y.T. Lee, "Direct Probing of the Transition State: Dynamic Resonances in $F + H_2$ Reactions," The Fifth European Conference on Dynamics of Molecular Collisions, Jerusalem, Israel, September 3–7, 1984.
33. Y.T. Lee, "Energetics and Dynamics of Chemical Reactions by Crossed Molecular Beams Experiments," University of Pittsburgh, Pittsburgh, Pennsylvania, September 13, 1984.
34. Y.T. Lee, "Dynamic Resonances in the Reaction of Fluorine Atoms with Hydrogen Molecules," Stanford University, Stanford, California, October 11, 1984.
35. Y.T. Lee, "Molecular Beam Chemistry," 31st G.N. Lewis Memorial Lecture, University of California Berkeley, October 23, 1984.
36. Y.T. Lee, "Primary Dissociation Processes of Polyatomic Molecules," ONR/NRL Workshop on Energetic Materials Initiation Fundamentals, Baltimore, Maryland, October 30–31, 1984.
37. Y.T. Lee, "Dynamic Resonances in Reactive Scattering," University of Illinois, Champagne-Urbana, November 7, 1984.
38. Y.T. Lee, "Molecular Beam Studies of Primary Photochemical Processes," Lasers 1984, San Francisco, California, November 29, 1984.
39. Y.T. Lee, "Crossed Molecular Beam Studies of Dynamics of Chemical Reactions," Academia Sinica, Taipei, Taiwan, December 17, 1984.

---

†Supported partly by NATO/SERC.

‡Supported partly by the Fannie and John Hertz Foundation.

§Supported partly by the National Science Foundation.

Potential-Energy Surfaces for Chemical Reactions*

Henry F. Schaefer III, Investigator

INTRODUCTION

This research program has two goals, related yet distinct. The first goal is the development of new theoretical and/or computational methods for the description of "what electrons are doing in molecules," to use the words of Robert S. Mulliken. Specifically, the single outstanding problem in the field is the correlation problem, that of formulating models for going beyond the single-particle or Hartree-Fock approximation. The second goal of our research is to apply these theoretical methods to significant problems of broad chemical interest. Currently two areas are of special concern: (1) model theoretical studies of chemisorption, metal clusters, and organometallic species, and (2) potential-energy surfaces that govern gas-phase chemical reactions. Research in the former area is ultimately aimed at a truly molecular understanding of catalysis, a subject pertinent to future energy requirements. In the second area research sometimes tends toward molecules that are potentially important in interstellar space, atmospheric chemistry, and the development of high-power laser systems. It is to be emphasized that in recent years theoretical chemistry has become a significant source not only of broad generalities, but also of specific predictions concerning molecular systems that may be very important but inaccessible to experiment.

1. An Energetically Low-Lying Silacyclopropyne Isomer of SiC_2 (Publication 5)†

Roger S. Grev and Henry F. Schaefer III

We have discovered a low-lying cyclic isomer of Si-C-C that is best described as a three-membered ring with a weak carbon-carbon triple bond. In these theoretical studies a double zeta plus polarization (DZ+P) basis set was used initially. At the self-consistent-field (SCF) and two-configuration (TC) SCF levels of theory, the ring structure is a transition state leading to linear Si-C-C. A configuration-interaction (CI) treatment at the SCF-optimized cyclic geometry, however, shows it to lie 1.1 kcal/mole below the linear structure. Extension of the basis set to include a second set of d functions on each atom gives a final prediction that the ring structure lies ~5 kcal below linear Si-C-C. The predicted structures are seen in Figure 1-1. These predictions were subsequently confirmed at Rice University in the laboratory of Professor R.E. Smalley.[1]

*This work was supported by the Director, Office of Energy Research, Office of Basic Energy Sciences, Chemical Sciences Division of the U.S. Department of Energy under Contract No. DE-AC03-76SF00098.

†Supported in part by an unrestricted grant from Energy Conversion Devices, Inc.

1. R.E. Smalley, J. Chem. Phys. **80**, 3566 (1984).

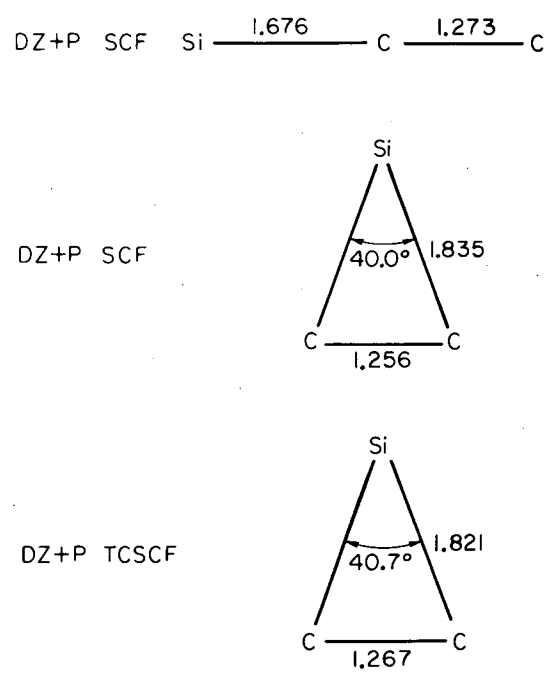

Figure 1-1. Predicted stationary-point geometrical structures for the SiC_2 molecule. All bond distances are given in Å. DZ+P TCSCF describes a two-configuration self-consistent-field (TCSCF) wavefunction, obtained using a double zeta plus polarization (DZ+P) basis set. (XBL 842-606)

2. Vinylidene: Potential-Energy Surface and Unimolecular Reaction Dynamics (Publication 7)

Tucker Carrington, Jr., Lynn M. Hubbard, Henry F. Schaefer III, and William H. Miller

A new quantum-mechanical treatment (with a triple zeta plus polarization basis set, and single and double excitation configuration interaction) has been carried out to determine the equilibrium points and the transition state for the vinylidene ($H_2C{=}C{:}$) → acetylene ($HC{\equiv}$) isomerization. A classical barrier height (i.e,, with no zero-point energy effects) of 6.3 kcal/mol is obtained, and application of the Davidson correction for unlinked clusters reduces this barrier height to 5.4 kcal/mol. Our best estimate is that the true classical barrier lies in the range of 2–4 kcal/mol. The dynamics of the vinylidene/acetylene isomerization is described within the framework of the reaction-path Hamiltonian approach. The lifetime of vinylidene (in its ground vibrational state) with respect to this process is calculated to be 0.24 to 4.6 psec for a classical barrier of 2 to 4 kcal/mol. This lifetime decreases by a factor of ~2 if one quantum of the CH_2 scissors mode of vinylidene is excited, but it is predicted to increase somewhat if a quantum of the C-C stretch is excited. These results are all consistent with the recent experimental observation of vinylidene via photodetachment of $C_2H_2^-$.

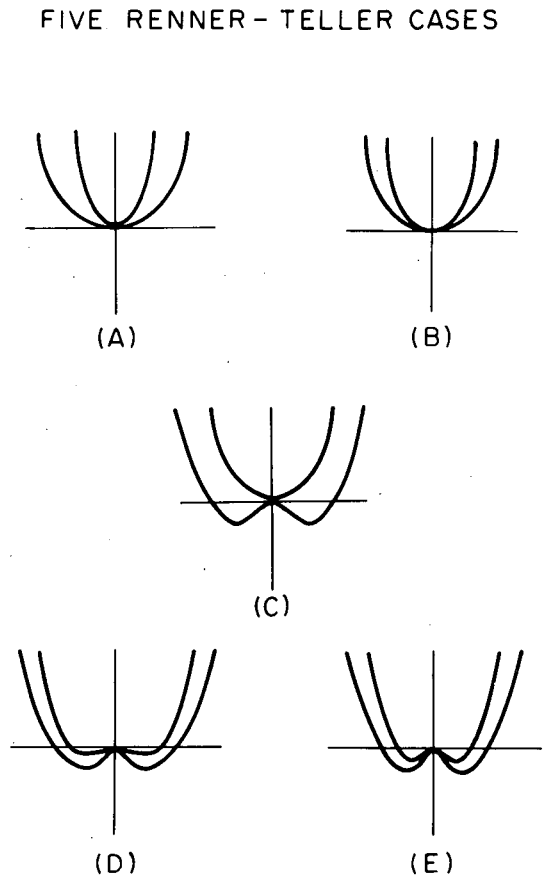

Figure 3-1. Illustrations of the five qualitatively different types of Renner-Teller potential-energy surfaces. See the text for the distinctions between the different cases. (XBL 835-3763)

3. Analytic Second Derivatives For Renner-Teller Potential-Energy Surfaces. Examples of the Five Distinct Cases (Publication 8)†

Timothy J. Lee, Douglas J. Fox, Henry F. Schaefer III, and Russell M. Pitzer‡

Force constants at Renner-Teller stationary points fall into five distinct categories, which are readily explored using symmetry principles and many-electron perturbation theory. By considering the BH_2, CH_2, NH_2, and CuH_2 molecules, examples of all five cases are illustrated via *ab initio* molecular electronic-structure theory. The five Renner-Teller cases are sketched qualitatively in Figure 3-1.

†Supported in part by the National Science Foundation, Grant CHE-8218785.

‡Present address: Department of Chemistry, Ohio State University, Columbus, Ohio 43210.

4. The Cyclic, Two-Hydrogen-Bond Form of the HO_2 Dimer (Publication 9)†

George Fitzgerald and Henry F. Schaefer III

Among possible forms of the hydroperoxyl radical dimer H_2O_4, one of the most appealing and plausible is the six-membered ring. This cyclic isomer of H_2O_4 has been investigated using nonempirical molecular electronic-structure theory. For the lowest triplet state of H_2O_4, the single configuration SCF method was used in conjunction with double zeta (DZ) and DZ+P basis sets. At both levels of theory, the six-membered ring is predicted to be a minimum on the H_2O_4 potential-energy hypersurface. The DZ SCF and DZ+P SCF dimerization energies are 4.5 and 4.9 kcal, respectively. Vibrational frequencies are predicted within the harmonic approximation and compared with the analogous monomer predictions and with the recent experimental findings of

Diem, Tso, and Lee. It is concluded that the cyclic HO_2 dimer is composed of two weak hydrogen bonds, each about one-half the strength of that observed for the water dimer. Figure 4-1 gives the predicted geometry of the HO_2 dimer.

†Calculations were carried out on a minicomputer supported by National Science Foundation Grant CHE-8218785.

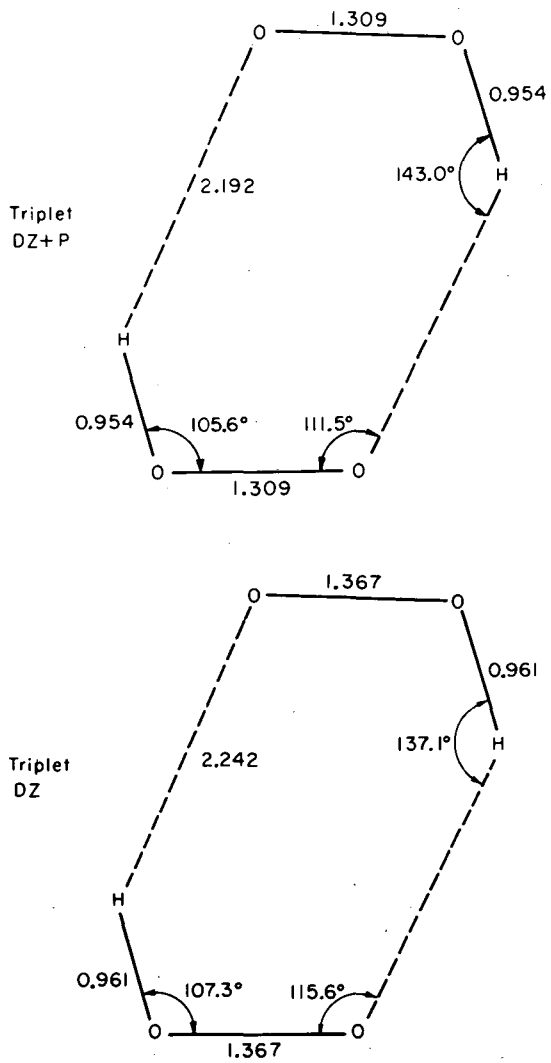

Figure 4-1. Theoretical structures for the ^3B_u cyclic, two-hydrogen-bond form of the HO_2 dimer. All bond distances are in Å. DZ + P SCF refers to the double zeta plus polarization (DZ+P) self-consistent-field (SCF) level of theory. (XBL 841-7550)

5. Vibrational Frequencies for the Classical and Nonclassical Forms of Protonated Acetylene—$C_2H_3^+$ (Publication 13)†

Gwendolyn P. Raine and Henry F. Schaefer III

The equilibrium geometries and harmonic vibrational frequencies of the classical and nonclassical structures of $C_2H_3^+$ have been predicted using *ab initio* molecular electronic structure. SCF methods were used with a DZ+P basis set. For the complete set of normal modes of vibration for both structures, the infrared intensities have been predicted. In addition, for a subset of these harmonic frequencies, actual vibrational fundamentals have been estimated using scaling techniques. The predicted structures of protonated acetylene are seen in Figure 5-1.

†Calculations were carried out on a minicomputer supported by National Science Foundation Grant CHE-8218785.

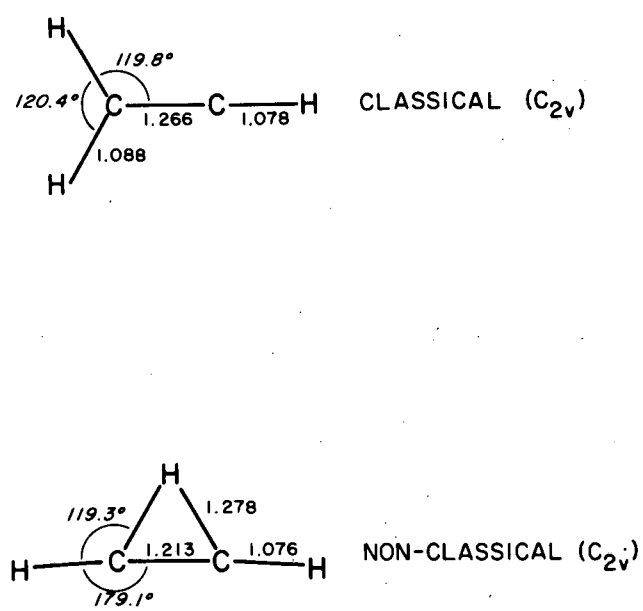

Figure 5-1. Predicted molecular structures for protonated acetylene, $C_2H_3^+$. Bond distances are in Å. (XBL 853-1511)

6. Toward the Laboratory Identification of Cyclopropenylidene (Publication 14)†

Timothy J. Lee, Annik Bunge,‡ and Henry F. Schaefer III

Nonempirical molecular electronic-structure theory has been used to predict the geometries and energetics of the lowest singlet and triplet states of

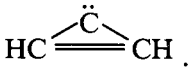

The closed-shell singlet ground state is predicted to lie about 70 kcal/mole below the lowest triplet state. Actually there are two low-lying triplet states, $^3B_1$ and $^3B_2$, which lie very close energetically. Ground-state cyclopropenylidene is predicted to have a dipole moment $\mu \sim 3.4$ debye, making it a very nucleophilic carbene. Vibrational frequencies are predicted for all three low-lying electronic states at the DZ+P SCF or two-configuration (TC) SCF levels of theory. A comparison of the predicted harmonic frequencies of singlet cyclopropenylidene and cyclopropene at the SCF level of theory is made. These predictions should assist in the identification of cyclopropenylidene from matrix-isolation infrared spectroscopy. The ground-state equilibrium geometry is seen in Figure 6-1. Based on these theoretical predictions, cyclopropenylidene was subsequently identified spectroscopically by Reisenauer.[1]

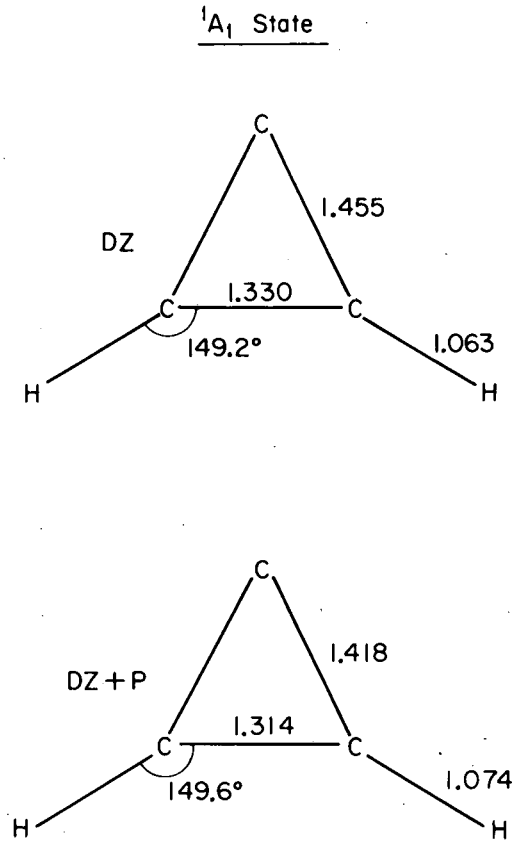

Figure 6-1. Predicted molecular structures for the cyclopropenylidene ground state. Bond distances are in Å. DZ+P refers to the use of a double zeta plus polarization basis set.
(XBL 831-4134)

†Calculations were carried out on a minicomputer supported by National Science Foundation Grant CHE-8218785.

‡Present address: Instituto de Fisica, Departmento de Fisica Teorica, Universidad Nacional Autonoma de Mexico, Apartado Postal 20-364, Mexico 20, D.F.

1. Reisenauer, Angew. Chem. Int. Ed. Engl. (1984).

1984 PUBLICATIONS AND REPORTS

Refereed Journals

1. M.R. Hoffmann, W.D. Laidig, K.S. Kim, D.J. Fox, and H.F. Schaefer, "Electronic Symmetry Breaking in Polyatomic Molecules. Multiconfiguration Self-

Consistent Field Study of the Cyclopropenyl Radical C_3H_3," J. Chem. Phys. **80**, 338 (1984); LBL-14092.

2. G.P. Raine, H.F. Schaefer, and N.C. Handy, "The HO_2^+ Molecular Ion. Geometrical Structure and Vibrational Frequencies," J. Chem. Phys. **80**, 319 (1984); LBL-16717.
3. T.J. Lee and H.F. Schaefer, "Vibrational Frequencies and Infrared Intensities for H_2CN^+, Protonated HCN," J. Chem. Phys. **80**, 2977 (1984); LBL-17098.
4. W.D. Laidig, Y. Yamaguchi, and H.F. Schaefer, "Where to Look for the Electronic Spectrum of Hydrogen Isocyanide, HNC," J. Chem. Phys. **80**, 3069 (1984); LBL-14203.
5. R.S. Grev and H.F. Schaefer, "An Energetically Low-Lying Silacyclopropyne Isomer of SiC_2," J. Chem. Phys. **80**, 3552 (1984); LBL-16718.
6. J.F. Gaw, Y. Yamaguchi, M.A. Vincent, and H.F. Schaefer, "Vibrational Frequency Shifts in Hydrogen-Bonded Systems: The Hydrogen Fluoride Dimer and Trimer," J. Am. Chem. Soc. **106**, 3133 (1984); LBL-17096.
7. T. Carrington, Jr., L.M. Hubbard, H.F. Schaefer, and W.H. Miller, "Vinylidene: Potential Energy Surface and Unimolecular Reaction Dynamics," J. Chem. Phys. **80**, 4347 (1984).
8. T.J. Lee, D.J. Fox, H.F. Schaefer, and R.M. Pitzer, "Analytic Second Derivatives for Renner-Teller Potential Energy Surfaces. Examples of the Five Distinct Cases," J. Chem. Phys. **81**, 356 (1984); LBL-17097.
9. G. Fitzgerald and H.F. Schaefer, "The Cyclic, Two-Hydrogen Bond Form of the HO_2 Dimer," J. Chem. Phys, **81**, 362 (1984); LBL-17526.

Other Publications

10. H.F. Schaefer, "Applications of Molecular Quantum Mechanics to Problems in Chemistry," in *Chemistry for the Future,* H. Grunewald, Ed., Pergamon, Oxford, England, 1984, p. 247; LBL-15762.
11. H.F. Schaefer, *Quantum Chemistry: The Development of Ab Initio Methods in Molecular Electronic Structure Theory,* Clarendon Press, Oxford, England, 1984.
12. C.E. Dykstra and H.F. Schaefer, "Computer Technology in Quantum Chemistry," in *Advanced Theories and Computational Approaches to the Electronic Structure of Molecules,* C.E. Dykstra, Ed., D. Reidel, Dordrecht, Holland, 1984, p. 197.

LBL Reports

13. G.P. Raine and H.F. Schaefer, "Vibrational Frequencies for the Classical and Nonclassical Forms of Protonated Acetylene—$C_2H_3^+$," LBL-18054.
14. T.J. Lee, A. Bunge, and H.F. Schaefer, "Toward the Laboratory Identification of Cyclopropenylidene," LBL-17525.
15. A.C. Scheiner and H.F. Schaefer, "Why the Energetic Minimum Al -Vinylidene is not Observed in Low Temperature Aluminum-Acetylene Reactions," LBL-18061.
16. M.J. Frisch, A.C. Scheiner, H.F. Schaefer, and J.S. Binkley, "The Malonaldehyde Equilibrium Geometry. A Major Structural Shift Due to the Effects of Electron Correlation," LBL-18799.
17. R.S. Grev and H.F. Schaefer, "Geometrical Structure and Vibrational Frequencies of Several Electronic States of Si_2C," LBL-18800.

Invited Talks

18. H.F. Schaefer, Mardi Gras Symposium in Theoretical Chemistry, Tulane University, New Orleans, Louisiana, March 1–2, 1984.
19. H.F. Schaefer, "Spectroscopy, Structures, and Dynamics of Molecular Ions," American Chemical Society, St. Louis, Missouri, April 10, 1984.
20. H.F. Schaefer, "Comparison of *Ab Initio* Quantum Chemistry with Experiment for Small Molecules: State of the Art," American Chemical Society, Philadelphia, Pennsylvania, August 26–30, 1984.
21. H.F. Schaefer, "Chemistry in Texas: The 30th Year of the Welch Foundation," Robert A. Welch Foundation, Houston, Texas, November 5–7, 1984.
22. H.F. Schaefer, Seventh International Conference on Lasers and Applications, Society for Optical and Quantum Electronics, San Francisco, November 26–30, 1984.
23. H.F. Schaefer, "Molecular Electronic Structure Calculations — Methods and Applications," Faraday Division of the Royal Society of Chemistry, University of Cambridge, England, December 11–13, 1984.
24. H.F. Schaefer, Chemistry Department, University of California, Davis, September 27, 1984.
25. H.F. Schaefer, Chemistry Department, University of South Carolina, Columbia, October 5, 1984.
26. H.F. Schaefer, Chemistry Department, Oakland University, Rochester, Michigan, October 25, 1984.
27. H.F. Schaefer, Chemistry Department, Arizona State University, Tempe, November 8, 1984.
28. H.F. Schaefer, Chemistry Department, Florida State University, Tallahassee, November 27, 1984.

ATOMIC PHYSICS

Atomic Physics*

Richard Marrus, Investigator

INTRODUCTION

The atomic-physics group is engaged in spectroscopic and collision studies of fundamental atomic problems. There are five current areas of research: (1) Parity violation in atomic thallium. These experiments test unified theories of the weak and electromagnetic interactions. (2) X-ray spectroscopy of one- and two-electron iron ions. In these experiments, the spectra taken from foil-excited beams show the presence of dielectronic satellites such as those observed in Tokamaks. Our measurements test the calculations of these spectra. (3) Electron capture and loss in solid targets by relativistic uranium beams. These experiments test the relative importance of radiative electron capture and nonradiative charge exchange at high energy. These measurements are important for the design of relativistic heavy-ion accelerators. (4) Measurement of forbidden lifetimes using ion-trapping techniques. The ion trap has proved to be a productive light source for studying forbidden transitions. Forbidden lines are important in the diagnosis of Tokamak plasmas. (5) Measurement of lifetimes of excited states of one- and two-electron ions of high Z. These excited-state measurements test calculations of quantum electrodynamics and relativistic effects in strong electric fields.

1. Parity Nonconservation in Atomic Thallium (Publication 1)

Eugene D. Commins and Persis S. Drell

According to the standard SU(2) × U(1) electroweak model, parity nonconservation (PNC) occurs in an atom because of interference between electromagnetic and neutral-weak amplitudes; it is detected most readily in heavy atoms. Observations of PNC have been reported in optical-rotation experiments in $_{82}$Pb and $_{83}$Bi. However, these atoms are complex, and interpretations of the results in terms of fundamental electroweak couplings are limited by large uncertainties in atomic theory. The single-valence-electron atoms cesium and thallium are considerably simpler, and their theoretical uncertainties are correspondingly smaller. Stark-interference experiments have been carried out on cesium at Paris, France, and on the $6^2P_{1/2} \rightarrow 7^2P_{1/2}$ transition (293 nm) in Tl in our laboratory. In one of our previous experiments, circularly polarized photons were absorbed by ground-state atoms in the presence of an external electric field. Interference between the electric-dipole amplitudes caused by PNC and by the Stark effect resulted in a helicity-dependent polarization of the excited state, the detection of which yielded a measurement of PNC. In the present experiment, we carried out a new Stark-interference measurement that made use of linearly polarized 293-nm photons and crossed electric and magnetic fields. The new technique yielded far more precise results than the old one, and the results had much smaller systematic corrections.

*This work was supported by the Director, Office of Energy Research, Office of Basic Energy Sciences, Chemical Sciences Division of the U.S. Department of Energy under Contract No. DE-AC03-76SF00098.

The final result is a determination of the ratio of the parity-violating electric-dipole moment ϵ_P to the Stark-amplitude coefficient β for the $6^2P_{1/2} \rightarrow 7^2P_{1/2}$ transition,

$$\epsilon_P/\beta = (-1.73 \pm 0.33)i \text{ mV/cm},$$

where $i = \sqrt{-1}$.

2. High-Precision Spectroscopic Study of Heliumlike Iron (Publication 2)

R. Marrus, J.P. Briard, M. Tavernier, and J.P. Desclaux

The x-ray spectrum of foil-excited heliumlike ions shows lines that arise from transitions from doubly excited states and dielectronic satellites. Precision energy measurements are capable of testing discrepant calculations of the energies of these lines. Dielectronic satellites are also important in the diagnosis of plasmas observed in Tokamaks, since their intensity gives a measure of the electron density. Additional interest in the spectrum results from the fact that, at high Z, quantum electrodynamic and relativistic effects give large measurable contributions to the energy separation.

The x-ray spectrum emitted by high-velocity heliumlike iron ions has been studied with a crystal spectrometer. The absolute energies of the $n = 2 \rightarrow n = 1$ lines have been measured with a precision of 40 ppm. Good agreement is found between the experimental results and a multiconfiguration Dirac-Fock calculation. The precision of the measurement is such that for the first time both the magnetic-correlation (spin-spin) energy and the screening of quantum-electrodynamic effects are observed. Dielectronic satellites have been observed and studied in detail by varying the nature and thickness of the targets. Transitions from doubly excited states are also observed. The results are compared with several discrepant calculations of the energies of the lines.

3. Electron Capture By U^{91+} and U^{92+} and Ionization of U^{90+} and U^{91+} (Publication 3)†

Harvey Gould, Douglas Greiner,‡ Peter Lindstrom,‡ T.J.M. Symons,‡ and Henry Crawford§

Measurements were made, at energies of 962 MeV/nucleon and 437 MeV/nucleon, of the cross sections for capture of an electron by U^{92+} (bare uranium nuclei) and U^{91+} and of the cross section for ionizing U^{91+} and U^{90+} in mylar, copper, and tantalum. These are the first experimental cross sections for capture and loss of an electron by a relativistic heavy ion of nuclear charge >18. We find that beams containing nearly 50% bare U^{92+} are produced by stripping 437-MeV/nucleon uranium in a 90-mg/cm^2 thick Cu target, and that beams containing over 85% bare U^{92+} are produced by stripping 962-MeV/nucleon uranium in 150-mg/cm^2 Cu or 85-mg/cm^2 Ta targets (see Figure 3–1).

Relativistic U^{68+} ions are obtained from the Lawrence Berkeley Laboratory's Bevalac, a heavy-ion linear accelerator (the SuperHILAC) and a synchrotron (the Bevatron) operating in tandem.

Figure 3-2 shows the experimental cross sections for capture of an electron by U^{92+} and U^{91+} at 962 MeV/nucleon and 437 MeV/nucleon for different targets. Relativistic uranium captures electrons by radiative electron capture (REC) and by charge exchange. REC is the inverse process of photoionization. The cross section for REC of an electron by U^{92+} is given by the solid line in Figure 3–2. The REC cross section for U^{91+} is about half as large.

The second process for electron capture is nonradiative charge exchange. A relativistic theory for nonradiative capture from a multielectron target does not yet exist. Comparing the data in Figure 3-2 with the REC cross section shows the following

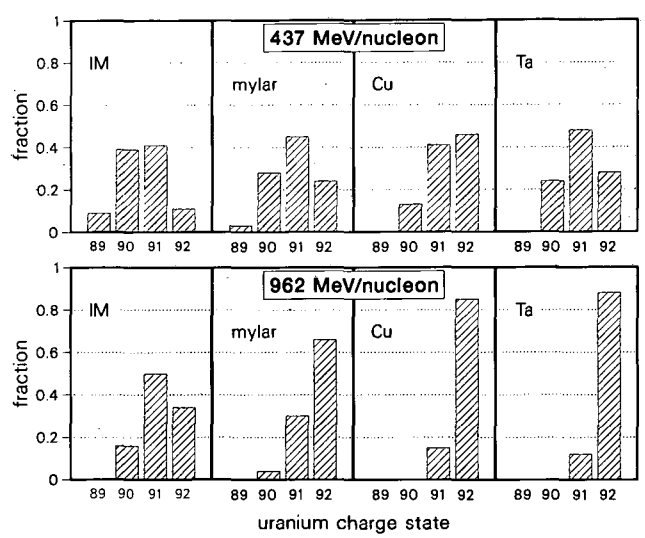

Figure 3-1. Charge-state distributions of uranium at energies of 962 MeV/nucleon and 437 MeV/nucleon for equilibrium-thickness targets of mylar, Cu, and Ta. The height of the bar indicates the percent of ions obtained at each charge state. Note the high percentage (over 85%) of bare uranium nuclei (charge state 92) with Ta and Cu at 962 MeV/nucleon. (XBL 837-10840)

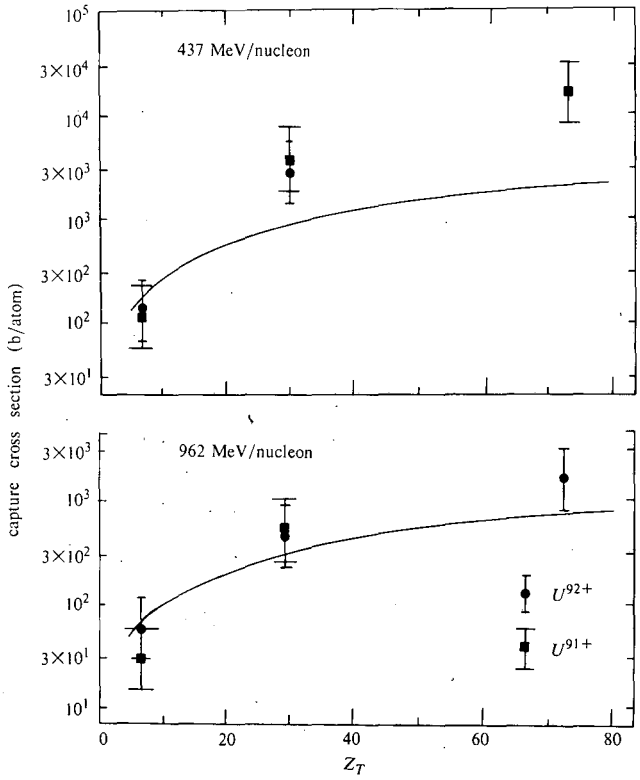

Figure 3-2. Cross sections for electron capture by U^{92+} and U^{91+} at energies of 962 MeV/nucleon and 437 MeV/nucleon as a function of target atomic number Z_T. Experimental points are for mylar, Cu, and Ta. The REC for U^{92+}, from theory, is shown as the continuous curve. (XBL 837-10838)

results: (1) The data are consistent with REC as the dominant capture mechanism for low atomic-number targets. (2) Nonradiative charge exchange becomes important for high atomic-number targets. (3) Nonradiative charge exchange becomes important for lower energies.

†Supported in part by the Office of High Energy and Nuclear Physics, Nuclear Science Division of DOE.

‡Supported by the Nuclear Science Division of DOE.

§Supported by NASA.

4. Radiative-Decay Rates of Metastable ArIII and CuII Ions (Publication 4)

M.H. Prior

The measurement of the radiative lifetimes of metastable ions is an area of study that has remained largely untouched until recently. This is in spite of the fact that the study of forbidden radiation from metastable atomic systems has a long history, extending from the early observations of astrophysical sources (e.g., the nebular lines) to the present diagnostic studies of Tokamak reactor plasmas. The laboratory measurement of metastable-ion radiative lifetimes has mainly used two techniques: decay following beam-foil excitation of fast ions, and observation of emission from pulse-excited trapped ions. The beam-foil approach applies well to highly charged, short-lived metastable states such as H-like 2s ArXVIII, whereas the ion-trap methods have been applied so far to singly and doubly charged ions with lifetimes up to about one minute.

This work reports studies of metastable CuII and ArIII ions (members of the Ni and S isoelectronic sequences) in which the electrostatic ion trap is used for the first time in lifetime measurements. We have observed electric-quadrupole (E2) lines in emission from CuII ions in the $3d^94s$ $^1D_2$ and $^3D_2$ states (see Figure 4–1), and the 3109-Å magnetic-dipole (M1) line emitted by ArIII ions in the $3p^4$ $^1S_0$ state. To our knowledge these are the first laboratory observations of these lines, although the ArIII line and the 3807-Å line from $^1D_2$ CuII have been seen in emission from astrophysical sources.

The decay of the forbidden lines following excitation has yielded the lifetimes (or total radiative-decay rates) for the upper levels. The results for the total radiative rates are: ArIII $\gamma(^1S_0) = 9.2 \pm 2.3$ sec^{-1}, CuII $\gamma(^3D_2) = 0.14 \pm 0.28$ sec^{-1}, and CuII

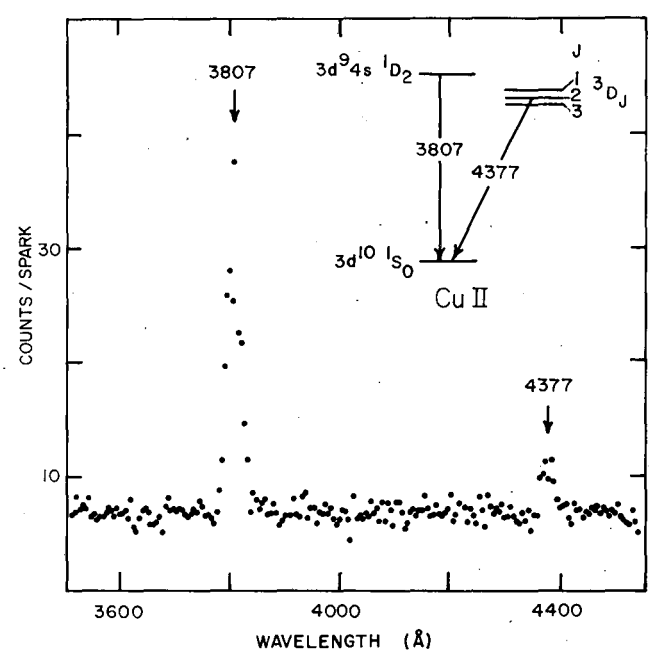

Figure 4-1. Spectrometer scan showing the CuII E2 lines studied. The energy-level diagram shows the ground and first-excited configuration levels. The 3807-Å line represents the $^1D_2$ state, and the 4377-Å line represents the $^3D_2$ state. (XBL 846-2486)

$\gamma(^1D_2) = 1.95 \pm 0.24\ sec^{-1}$. These results are in reasonable agreement with theoretical calculations.

5. Work in Progress

A precision measurement of the lifetime of the 2^1S_0 state in Kr^{34+} is under way. This state decays by two-photon (2E1) emission, and the experiment will test the relativistic theory of 2E1 decay for the first time.

Work on charge-changing cross sections is continuing, with the goal of determining nonradiative-capture cross sections for relativistic very heavy ions. This work will be done using beams of bare nuclei and very low and very high atomic-number targets.

A measurement of the $2^3P_0-2^3S_1$ fine-structure splitting of heliumlike uranium is being performed as a test of quantum electrodynamics. The experiment is designed to measure the splitting to 2% and eventually to 0.1%.

A beam line is currently under construction at the LBL electron cyclotron resonance (ECR) source. This line will initially be used to perform laser spectroscopic studies on Ar^{14+}.

Work continues on parity nonconservation in atomic thallium. The ultimate goal of this research is to determine the electric-dipole moment ϵ_P that arises from neutral weak-electromagnetic interference. Since the quantity actually measured in that experiment is $\epsilon_{P/\beta}$, where β is the Stark-amplitude coefficient, it is necessary to measure the latter quantity separately. We have constructed and are now operating an experiment for this purpose. The apparatus employs the same laser system as in the PNC experiment (Abstract 1), and also a long cell with a pair of parallel electric-field plates, inside an oven of precisely known temperature. Absorption of 293-nm light is measured as a function of electric-field strength and thallium-vapor density. The latter is calibrated by a pair of auxiliary allowed transitions with known oscillator strengths.

This work is now yielding very precise and satisfactory data and should be concluded successfully in early spring 1985.

1984 PUBLICATIONS AND REPORTS

Refereed Journals

1. Persis S. Drell and Eugene D. Commins, "Parity Nonconservation in Atomic Thallium," Phys. Rev. Lett. **53**, 968 (1984).
2. R. Marrus, J.P. Briard, M. Tavernier, and J.P. Desclaux, "High Precision Spectroscopic Study of Heliumlike Iron," Phys. Rev. A**29**, 3143 (1984).
3. H. Gould, D. Greiner, P. Lindstrom, T.J.M. Symons, and H. Crawford," Electron Capture by U^{91+} and U^{92+} and Ionization of U^{90+} and U^{91+}," Phys. Rev. Lett. **52**, 180 (1984); errata **52**, 1654 (1984).
4. M.H. Prior, "Radiation Decay Rates of Metastable ArIII and CuII Ions," Phys. Rev. A**30**, 3051 (1984).

Other Publications

5. H. Gould, D. Greiner, P. Lindstrom, T.J.M. Symons, and H. Crawford, "Charge Changing Cross Sections of Relativistic Uranium," in *Proc. 9th Int. Conf. on Atomic Physics*, University of Seattle, Washington, July 23–27, 1984; LBL-17627abs.

LBL Reports

6. H. Gould, "Atomic Physics—Testing Quantum Electrodynamics," in *The Tevalac: A National Facility for Relativistic Heavy-Ion Research to 10 GeV per Nucleon with Uranium*, LBL PUB-5081, pp. 19–20.
7. M.H. Prior, "Radiative Decay Rates of Metastable ArIII and CuII Ions," LBL-18048.

Invited Talks

8. R. Marrus, "Experiments with One- and Two-Electron Ions of High-Z," Oregon State University, Corvallis, April 26, 1984.
9. R. Marrus, "Forbidden Transitions in One- and Two-Electron Ions of High-Z," University of Paris, France, June 7, 1984.
10. R. Marrus, "Two-Photon Decay," Physics Department, GANIL Accelerator, Caen, France, June 14, 1984.
11. H. Gould, "Charge States of Relativistic Uranium," Washington Meeting, American Physical Society, April 25, 1984; Bull. Am. Phys. Soc. **29**, 730 (1984); LBL-17275abs.
12. H. Gould, "Observation of U^{92+} and Atomic Physics Experiments with Highly Stripped Uranium," Atomic Physics Seminar, University of Virginia, Charlottesville, May 1, 1984.
13. H. Gould, "Atomic Physics with U^{92+}," Physics Division Group A Seminar, Lawrence Berkeley Laboratory, June 4, 1984.
14. H. Gould, "Spectroscopy of One- and Two-Electron Uranium," International Conference on the Physics of Highly Ionized Atoms, Oxford, England, July 2–5, 1984; LBL-18143.

15. M.H. Prior, "Atomic Physics with Trapped Multiply Charged Ions," Annual Meeting, American Physical Society, Division of Electron and Atomic Physics, Storrs, Connecticut, May 30–June 1, 1984.
16. P.S. Drell, Cornell University, Ithica, New York; Fermi National Accelerator Laboratory, Batavia, Illinois; University of Chicago, Illinois; University of Wisconsin, Madison; Yale University, New Haven, Connecticut; Princeton University, Princeton, New Jersey; Columbia University, New York City; Stanford Linear Accelerator Center, Stanford, California; Lawrence Berkeley Laboratory.
17. E.D. Commins, "Parity Violation in Atomic Thallium," University of California, San Diego; University of California Berkeley; Fermi National Accelerator Laboratory, Batavia, Illinois.

PROCESSES AND TECHNIQUES

CHEMICAL ENERGY

Formation of Oxyacids of Sulfur from SO_2*

Robert E. Connick, Investigator

INTRODUCTION

The research is concerned primarily with the fundamental chemistry of sulfur species formed from sulfur dioxide in aqueous solution and the reactions of these species. This chemistry is of particular importance in the problems associated with atmospheric pollution by sulfur dioxide and the resulting formation of acid rain. Recent research has elucidated the kinetics of the exchange of oxygen atoms between bisulfite ion and water, using the nuclear magnetic resonance (NMR) of oxygen-17 for following the reaction. In work supported by The Electric Power Research Institute, the kinetics of the oxidation of bisulfite ion by oxygen has been studied. Work remains to be done on the latter project, and additional oxidation-reduction reactions of bisulfite ion should be investigated. Of particular interest are such reactions involving two or more oxidation states of sulfur. A secondary and not closely related goal is to determine the factors controlling rates of substitution reactions in the first coordination sphere of metal ions in solution. The research is being pursued both through the measurement of such rates with NMR and by computer modeling of such processes.

1. The Kinetics of Oxygen Exchange Between Bisulfite Ion and Water as Studied by Oxygen-17 NMR Spectroscopy (Publication 1)

Robert E. Connick and David A. Horner†

The nuclear magnetic relaxation times of oxygen-17 have been measured in aqueous sodium bisulfite solutions in the pH range from 2.5 to 5 as a function of temperature, pH, and S(IV) concentration, at an ionic strength of 1.0M. The rate law for oxygen exchange between bisulfite ion and water was obtained from an analysis of the data and is consistent with oxygen exchange occurring via the reaction of SO_2 with water to form bisulfite ion and hydrogen ion. The value of the rate constant is in essential agreement with the results of a previous determination by relaxation measurements.

Direct NMR spectroscopic evidence was found for the existence of two isomers of bisulfite ion: one with the proton bonded to the sulfur (HSO_3^-) and the other with the proton bonded to an oxygen (SO_3H^-). The relative amounts of the two isomers were determined as a function of temperature, and the rate and mechanism of oxygen exchange between the two was investigated. One of the two isomers, presumably SO_3H^-, exchanges oxygens with water much more rapidly than does the other.

A two-pulse sequence was developed that greatly diminished the solvent peak in the NMR spectrum. This pulse sequence allowed accurate measurements of the linewidth of the solute peak to be made.

*This work was supported by the Director, Office of Energy Research, Office of Basic Energy Sciences, Chemical Sciences Division of the U.S. Department of Energy under Contract No. DE-AC03-76SF00098.

Mathematical expressions were derived for the linewidth of the solute peak in the presence of chemical exchange of nuclei between the solvent and solute environments.

---

†Present address: Department of Chemistry, North Central College, Naperville, Illinois 60566.

2. Work in Progress

Previously, evidence was found that the bis nickel-iminodiacetate complex undergoes racemization of the cis and trans forms through a Bailar twist. A careful study of the coalescence of the ^{13}C NMR peaks of the carboxylate groups indicates that the two different carboxylate carbons of the cis species are isomerizing a little faster than expected if the isomerization always goes from cis to trans to cis. This effect is evidence that the Bailar twist can also occur by cis to cis where the two nitrogens would have to slide past each other, rather than having just nitrogen-oxygen eclipses in the cis to trans to cis case.

To characterize the relaxation phenomena of the ^{17}O and ^{13}C nuclei in nickel complexes of iminodiacetate, methyl iminodiacetate, and ethyl iminodiacetate, a study is being made of the corresponding zinc complexes where the possible modes of relaxation are more restricted. It will be possible to obtain the tumbling times of the whole complex as well as indications of internal motions of the methyl and ethyl groups on the latter two complexes. The tumbling times should be applicable to the nickel complexes and will therefore aid in the interpretation of the nickel relaxation and the isomerization process.

1984 PUBLICATIONS AND REPORTS

LBL Reports

1. D.A. Horner (Ph.D. Thesis), "The Kinetics of Oxygen Exchange Between Bisulfite Ion and Water as Studied by Oxygen-17 Nuclear Magnetic Resonance Spectroscopy," LBL-18297.

Catalytic Hydrogenation of CO*

Gabor A. Somorjai and Alexis T. Bell, Investigators

INTRODUCTION

The purpose of this program is to develop an understanding of the fundamental processes involved in catalytic conversion of carbon monoxide and hydrogen to gaseous and liquid fuels. Attention is focused on defining the factors that limit catalyst activity, selectivity, and resistance to poisoning, and the relationship between catalyst composition/ structure and performance. To meet these objectives, a variety of surface diagnostic techniques are used to characterize supported and unsupported catalysts before, during, and after reactions. These techniques include low-energy electron diffraction (LEED), Auger electron spectroscopy (AES), x-ray photoelectron spectroscopy (XPS), electron-energy-loss spectroscopy (EELS), infrared spectroscopy (IRS), and temperature-programmed desorption (TPD). The information thus obtained is combined with detailed studies of reaction kinetics to elucidate reaction mechanisms and the influence of modifications in catalyst composition and/or structure on the elementary reactions involved in carbon monoxide hydrogenation.

1. Methanol Production from Carbon Monoxide and Hydrogen on Thorium Dioxide (Publications 1 and 11)

J.J. Maj, C. Colmenares, and G.A. Somorjai

High-surface-area ThO_2 catalysts ($\sim$120 m^2/g) were prepared by a precipitation method and characterized by x-ray diffraction, Brunauer-Emmett-Teller surface area, transmission electron microscopy, XPS, and AES. Thoria precipitated from Na_2CO_3 (Na-ThO_2) and $(NH_4)_2CO_3$ (NH_4-ThO_2) was crystalline with particle size $>$5 nm and active for the production of mostly methanol and small amounts of isobutanol, isobutane, methane, and ethane/ethene. On the other hand, ThO_2 precipitated with K_2O_3 formed large shards with a glassy appearance and very small surface area (1.7 m^2/g); this catalyst was inactive for methanol production. Both x-ray diffraction and XPS measurements showed that Na-ThO_2 and NH_4-ThO_2 catalysts were ThO_2 after calcination in air at 520 K. XPS and AES measurements disclosed that the Na-ThO_2 catalyst contained $\sim$10 atm% ionic sodium present as Na_2O. This catalyst showed a higher activity for isobutanol synthesis than the sodium-free thoria, while producing comparatively less isobutane.

Synthesis experiments were carried out in a copper-lined tubular reactor as a function of gas mixture ($2H_2/CO$ and H_2/CO), pressure (2.0–6.5 MPa), and temperature (570–635 K) at a flow rate of 1.8 m^3/hr-kg cat. (5000 hr^{-1}). Changing the flow rate between 5000 and 10,000 hr^{-1} had little effect on the synthesis reaction. Both Na-ThO_2 and NH_4-ThO_2 produced $\sim$1 mole% methanol in the effluent gas under optimum conditions ($2H_2/CO$ at 5.4 MPa, 600 K, 5000 hr^{-1}); this corresponds to $\sim$3% carbon conversion (0.8 kg CH_3OH/l cat.-hr). Both catalysts showed little tendency for gaseous hydrocarbon production, and their selectivity varied between 85% and 95%.

The effect of reactant pressure on the rate of methanol formation was tested by both a power dependence and a fit to the Natta model for ZnO/Cr_2O_3 and $CuO/ZnO/Cr_2O_3$. In both cases hydrogen was found to be more strongly adsorbed than carbon monoxide.

2. Hydrogenation of Carbon Monoxide on Mo(100) Single Crystals and Polycrystalline Foils (Publication 12)

M. Logan, M. Gellman, and G.A. Somorjai

The hydrogenation of carbon monoxide over (100) oriented single crystals and polycrystalline molybdenum catalysts produces primarily methane, ethene, and propene. The rates of formation of all products were found to be the same for both the (100) single crystals and polycrystalline foils, suggesting that the reaction is structure-insensitive. The

*This work was supported by the Director, Office of Energy Research, Office of Basic Energy Sciences, Chemical Sciences Division of the U.S. Department of Energy under Contract No. DE-AC03-76SF00098.

dependence of the rate of formation of methane on reactant pressure was found to be

$$r_{CH_4} = KP_{CO}^{0.32 \pm 0.5} P_{H_2}^{1.0 \pm 0.1}.$$

The unusual positive CO pressure dependence points to a mechanism of methanation that is different from that on other transition-metal methanation catalysts (Fe, Ru, Ni), although the activation energy for the reaction is similar, 24 kcal/mol. Adding K to the surface at coverages of less than 0.3 monolayer increased the overall reaction rate and enhanced the olefin-to-paraffin ratio. The addition of S to the surface decreased the hydrogenation rate but, for coverages up to ~0.25 monolayer, increased the ratio of ethene to methane by as much as a factor of 5.

3. Partial Oxidation of Methane with Nitrous Oxide over V_2O_5-SiO_2 Catalyst (Publication 13)

K.J. Zhen, M.M. Khan, C.H. Mak, K.B. Lewis, and G.A. Somorjai

The partial oxidation of methane to methanol and formaldehyde can be achieved selectively on silica-supported vanadium pentoxide catalysts in the 460–500°C temperature range in a reactant mixture of CH_4, N_2O, and H_2O at 1 atm total pressure. The selectivity to CH_3OH and HCHO can be 100% at 460°C at low conversions (~0.2%) and contact time (1.2 sec). More CO is produced with increasing temperature, contact time, and conversion. The activation energies are 22 ± 2 kcal/mole, 40 ± 4 kcal/mole, and 47 ± 4 kcal/mole for the production of HCHO, CH_3OH, and CO, respectively. The rate equations are

$$\text{Rate } (CH_3OH) \sim (CH_4)^{1/2}(N_2O)^{1/2}(H_2O)^{1/2},$$

$$\text{Rate } (HCHO) \sim (CH_4)^{1/2}(N_2O)^{1/3}, \text{ and}$$

$$\text{Rate } (CO) \sim (CH_4)^{1/2}(N_2O)(H_2O)^{-1}.$$

Oxygen does not react when it is added to the reaction mixture. The products form by parallel reaction paths that are different from the sequential oxidation mechanism of methane on molybdena and in a lower temperature range than on molybdenum oxide.

4. Studies of Carbon- and Hydrogen-Containing Adspecies Present During CO Hydrogenation over Unsupported Ru, Ni, and Rh (Publication 17)

P. Winslow and A.T. Bell

Isotopic tracer studies have been conducted to determine the coverages of adsorbed CO, carbon, and hydrogen on the surfaces of unsupported Ru, Rh, and Ni powders during CO hydrogenation. Two forms of hydrogen are observed on each catalyst at 298 K. A low-energy form is in equilibrium with the gas phase and is rapidly displaced from the surface by CO adsorption. The high-energy form is not in equilibrium with the gas phase and is not displaced by CO adsorption. Adsorbed carbon and CO are also observed on each catalyst. It is demonstrated that high activities for methanation correlate with $\theta_C\theta_D$, the product of the surface coverages of active carbon and hydrogen.

5. The Characterization of Carbonaceous Species on Ruthenium Catalysts with ^{13}C Nuclear Magnetic Resonance (NMR) (Publications 21 and 22)

T.M. Duncan, P. Winslow, and A.T. Bell

^{13}C NMR spectroscopy has been applied to the study of carbon species deposited on supported and unsupported ruthenium catalysts during CO hydrogenation. Four forms of nonoxygenated carbon on the substrate have been identified, designated C_α, $C_{\beta 1}$, $C_{\beta 2}$, and unreactive carbon. Correlation of isotropic shifts, nuclear dipolar interactions, and anisotropy of chemical shielding leads to a description of each carbon species. C_α is interpreted as carbidic carbon atoms distributed in a variety of sites located on or below the metal surface. $C_{\beta 1}$ and $C_{\beta 2}$ are alkyl groups attached to the catalyst and are differentiated by their relative mobilities and interconversion to other forms. $C_{\beta 1}$ reorients at room temperature but is quenched at 110 K. $C_{\beta 2}$ is motionally averaged at 110 K and is selectively depleted by purging the catalyst with an inert gas. Characterization of $C_{\beta 1}$ by magic-angle-spinning ^{13}C NMR reveals individual peaks for CH_2 and CH_3 groups. From these spectra, it is confirmed that the alkyl groups are attached to the metal and have an

average chain length of four to five carbon atoms. The nonreactive carbon has a ^{13}C NMR spectrum similar to that of turbostratic graphite. The relationships of the different carbon species to each other are discussed.

6. Characterization of the Preparation of Pd/SiO_2 and Pd/La_2O_3 by Laser Raman Spectroscopy (Publication 5)

S.S. Chan and A.T. Bell

Multichannel laser Raman spectroscopy has been used to characterize the chemistry occurring during the preparation of silica- and lanthanum oxide-supported palladium catalysts from $PdCl_2$. The results show that the structure of lanthanum oxide is a strong function of its state of hydration, and evidence is reported for structures bridging the extremes of $La(OH)_3$ and La_2O_3. $PdCl_2$, used as the source of Pd, undergoes a change in crystal structure and then conversion to PdO when heated in air up to 773 K. Silica-supported $PdCl_2$ undergoes a similar set of transformations. The spectrum of the lanthanum oxide-supported $PdCl_2$ is quite different from that supported on silica, but the exact structure of the supported species cannot be determined. Calcination produces a new species that is believed to be a mixed metal oxide of La and Pd.

7. Studies of the Interactions of H_2 and CO with Pd/SiO_2 and Pd/La_2O_3 (Publications 6 and 19)

J.S. Rieck, R.F. Hicks, Q.-J. Yen, and A.T. Bell

The interactions of H_2 and CO with Pd/SiO_2, Pd/La_2O_3, and lanthana-promoted Pd/SiO_2 have been investigated using TPD, temperature-programmed surface-reaction spectroscopies, and IRS. In the presence of lanthana, a portion of the lanthana in close contact with the Pd particles undergoes reduction to form LaO_x moieties. These species cause a reduction in the absolute magnitude of H_2 and CO adsorption, as well as a change in the distribution of adstates relative to that observed for Pd/SiO_2. The latter effect is relatively small for H_2 but is quite significant for CO, for which adsorption into strongly bound states is suppressed more extensively than adsorption into weakly bound states. The LaO_x moieties also facilitate the dissociation of CO, a key step in CO methanation; as a consequence, the synthesis of CH_4 over Pd/La_2O_3 and lanthana-promoted Pd/SiO_2 is much more rapid than that over Pd/SiO_2. The change in the distribution of adsorbed H_2 and CO under synthesis conditions, brought about by LaO_x, also contributes to the higher selectivity of the lanthana-containing catalysts for methanol synthesis.

8. Effects of Metal-Support Interactions on the Hydrogenation of CO over Pd/SiO_2 and Pd/La_20_3 (Publications 7 and 16)

R.F. Hicks and A.T. Bell

A study of CO hydrogenation over Pd/SiO_2 and Pd/La_2O_3 has been carried out to identify the effects of Pd dispersion, Pd morphology, and support composition on the catalytic activity of supported Pd. The specific activity of each catalyst for methanol and methane synthesis was determined from microreactor studies carried out at a fixed set of reaction conditions. Palladium dispersion was measured by H_2-O_2 titration, and the morphology of the Pd crystallites, as expressed by the distribution of Pd(100) and Pd(111) planes, was determined from *in situ* infrared spectra of adsorbed CO. The crystallite morphology of the Pd/SiO_2 catalysts is the same, independent of Pd weight loading: 90% of the surface comprises Pd(100) planes, and 10% of the surface comprises Pd(111) planes. By contrast, the crystallite morphology of the Pd/La_2O_3 catalysts changes with Pd loading. Primarily Pd(100) planes are exposed at low weight loadings, while Pd(111) planes are exposed at high weight loadings. The Pd dispersion has little effect on the methanol turnover frequency over both Pd/SiO_2 and Pd/La_2O_3, for dispersions between 10% and 30%. On the other hand, the methane turnover frequency is independent of Pd dispersion over Pd/SiO_2, but it increases with decreasing dispersion over Pd/La_2O_3. The Pd morphology also influences the specific activity of Pd/La_2O_3 for methanol synthesis. Pd(100) is nearly three times more active than Pd(111). For a fixed morphology, the specific methanol-synthesis activity of Pd/La_2O_3 is a factor of 7.5 greater than that of Pd/SiO_2.

Studies of the kinetics of methanol synthesis over Pd/SiO_2 and Pd/La_2O_3 show that the activation energy and the orders with respect to H_2 and CO partial pressures are essentially the same for both catalysts. This result suggests that the methanol

reaction mechanism is unaffected by support composition. The higher specific activity of Pd/La_2O_3 relative to Pd/SiO_2 for methanol synthesis is attributed to differences in the relative strengths of H_2 and CO adsorption. The rate expressions for methane synthesis over Pd/SiO_2 and Pd/La_2O_3 differ significantly. This difference strongly suggests that the methane reaction mechanism for the two catalysts is different, or alternatively that the mechanism is the same but the rate-limiting step is different.

9. Electron Microscopy Study of the Interactions of Rhodium with Titania (Publication 18)

A.K. Singh, N.K. Pande, and A.T. Bell

Transmission electron microscopy has been used to study strong metal-support interactions in the Rh/TiO_2 system. Selected-area electron diffraction and x-ray diffraction were used to characterize the TiO_2 support as a function of reduction temperature. A specially prepared sample of TiO_2-promoted Rh/SiO_2 was examined to study the interaction of TiO_2 with Rh metal particles. TPD experiments were performed on the Rh/TiO_2- and TiO_2-promoted Rh/SiO_2 samples to investigate the adsorption of H_2 and CO as a function of catalyst-reduction temperature. The suppression of H_2 and CO chemisorption with increasing reduction temperature observed for both samples is attributed to a physical blockage of Rh surface sites by TiO_x moieties.

1984 PUBLICATIONS AND REPORTS

Refereed Journals

1. J.J. Maj, C. Colmenares, and G.A. Somorjai, "Thorium Oxide: A New Catalyst for Methanol, Isobutanol, and Light Hydrocarbon Production from Carbon Monoxide and Hydrogen," Appl. Catal. **10**, 313 (1984).
2. J.S. Rieck and A.T. Bell, "Influence of Adsorption and Mass Transfer Effects on Temperature Programmed Desorption from Porous Catalysts," J. Catal. **85**, 143 (1984); LBL-16701.
3. P. Winslow and A.T. Bell, "Applications of Transient Response Techniques for Quantitative Determination of Adsorbed Carbon Monoxide and Carbon Present on the Surface of a Ruthenium Catalyst During Fischer-Tropsch Synthesis," J. Catal. **86**, 158 (1984); LBL-16265.
4. T.H. Fleisch, R.F. Hicks, and A.T. Bell, "Characterization of Pd/SiO_2 and Pd/La_2O_3 Methanol Synthesis Catalysts by X-Ray Photoelectron Spectroscopy," J. Catal. **87**, 398 (1984); LBL-16570.
5. S.S. Chan and A.T. Bell, "Characterization of the Preparation of Pd/SiO_2 and Pd/La_2O_3 by Laser Raman Spectroscopy," J. Catal. **89**, 433 (1984); LBL-17460.
6. R.F. Hicks, Q.-J. Yen, and A.T. Bell, "Effects of Metal-Support Interactions on the Chemisorption of H_2 and CO on Pd/SiO_2 and Pd/La_2O_3," J. Catal. **89**, 498 (1984); LBL-17325.
7. R.F. Hicks and A.T. Bell, "Effects of Metal-Support Interactions on the Hydrogenation of CO over Pd/SiO_2 and Pd/La_2O_3," J. Catal. **90**, 205 (1984); LBL-17495.

Other Publications

8. P. Winslow and A.T. Bell, "Studies of the Surface Coverage of Ruthenium by Carbon and Hydrogen Adspecies during CO Hydrogenation," in *Proc. 8th Int. Congress on Catalysis,* Vol. III, Verlag Chemie, Weinheim, Germany, 1984, p. 175; LBL-17199.
9. A.T. Bell, "Fourier-Transform Infrared Spectroscopy in Heterogeneous Catalysis," in *Chemistry and Physics of Solid Surfaces,* V.R. Vanselow and R. Howe, eds., Springer Verlag, New York, 1984, p. 23.
10. A.T. Bell, "Mechanisms of Fischer-Tropsch Synthesis," in *Heterogeneous Catalysis,* B.L. Shapiro, Ed., Texas A&M University Press, College Station, Texas, 1984, p. 211.
11. J. Maj, C.A. Colmenares, and G.A. Somorjai, "Methanol Production from Carbon Monoxide and Hydrogen on Thorium Dioxide," submitted to J. Catal.

LBL Reports

12. M. Logan, A. Gellman, and G.A. Somorjai, "Hydrogenation of Carbon Monoxide on Mo(100) Single Crystals and Polycrystalline Foils," submitted to J. Catal.; LBL-17952.
13. K.J. Zhen, M.M. Khan, C.H. Mak, K.B. Lewis, and G.A. Somorjai, "Partial Oxidation of Methane and Nitrous Oxide over V_2O_5-SiO_2 Catalyst," submitted to J. Catal.; LBL-18493.
14. E.L. Garfunkel, J. Parmeter, B.M. Naasz, and G.A. Somorjai, "The Hydrogenation of Carbon Monoxide Over Model Rhenium Catalysts: Additive Effects and Comparison with Iron," submitted to Langmuir; LBL-17965.

15. M.A. Logan and G.A. Somorjai, "Deuterium Isotope Effects on Hydrogenation of Carbon Monoxide over Rhodium," submitted to J. Catal.; LBL-18717.
16. R.F. Hicks and A.T. Bell, "Kinetics of Methanol and Methane Synthesis over Pd/SiO_2 and Pd/La_2O_3," J. Catal. (in press); LBL-17498.
17. P. Winslow and A.T. Bell, "Studies of Carbon- and Hydrogen-Containing Adspecies Present During CO Hydrogenation over Unsupported Ru, Ni, and Rh," submitted to J. Catal.; LBL-18233,
18. A.K. Singh, N.K. Pande, and A.T. Bell, "Electron Microscopy Study of the Interactions of Rhodium with Titania," submitted to J. Catal.; LBL-18583.
19. J.S. Rieck and A.T.Bell, "Studies of the Interactions of H_2 and CO with Silica- and Lanthana-Supported Palladium," submitted to J. Catal.; LBL-18689.
20. A.T. Bell, "Infrared Spectroscopy of High Area Catalytic Surfaces," in *Vibrational Spectroscopy of Molecules on Surfaces,* Vol. 4 of *Methods of Surface Characterization,* J.T. Yates, Jr., Ed. (in press); LBL-18556.
21. T.M. Duncan, P. Winslow, and A.T. Bell, "The Characterization of Carbonaceous Species on Ruthenium Catalysts with ^{13}C Nuclear Magnetic Resonance Spectroscopy," submitted to J. Catal.; LBL-18827.
22. T.M. Duncan, J.A. Reimer, P. Winslow, and A.T. Bell, "The Characterization of Alkyl Intermediates on Silica-Supported Ruthenium with ^{13}C Nuclear Magnetic Resonance Spectroscopy," submitted to J. Catal.; LBL-18828.

Invited Talks

23. G.A. Somorjai, "Molecular Surface Science: Its Triumphs, Its Challenges and Future Promises," The 11th Annual John Dorn Memorial Lecture, Northwestern University, Evanston, Illinois, May 1984.
24. G.A. Somorjai, "Organic Surface Species in Catalytic C_1-Chemistry and Methods of Investigation," Symposium on C_1 Chemistry, Karlsruhe, West Germany, July 1984.
25. M.A. Logan, A.J. Gellman, and G.A. Somorjai, "Hydrogenation of Carbon Monoxide on Clean and Promoted Molybdenum Surfaces," California Catalysis Society Meeting, Pasadena, October 1984.
26. A.T. Bell, "Applications of Transient Response Techniques to Studies of Catalyzed Reactions," Department of Chemical Engineering, University of Texas, Austin, February 1984.
27. A.T. Bell, "Influence of Metal-Support Interactions on the Interaction of H_2, CO, and NO with Silica- and Lanthana-Supported Pd," California Catalysis Society Meeting," Richmond, March 1984.
28. A.T. Bell, "Mechanisms of Fischer-Tropsch Synthesis," Second Annual IUCCP Symposium, Texas A&M University, College Station, April 1984.
29. A.T. Bell, "Isotopic Tracer Studies of Hydrocarbon Synthesis over Ruthenium," American Chemical Society Meeting, St, Louis, Missouri, April 1984.
30. A.T. Bell, "Modern Methods for Characterizing Group VIII Metal Catalysts," 1984 Donald L. Katz Lecture, Department of Chemical Engineering, University of Michigan, Ann Arbor, April 1984.
31. A.T. Bell, "Advances in Understanding the Catalytic Conversion of CO and H_2 to Synthetic Fuel," 1984 Donald L. Katz Lecture, Department of Chemical Engineering, University of Michigan, Ann Arbor, April 1984.
32. A.T. Bell, "Effects of Reduction and Reaction Conditions on the Performance of Iron Catalysts for Fischer-Tropsch Synthesis," American Institute of Chemical Engineering Meeting, Anaheim, California, May 1984.
33. A.T. Bell, "Recent Studies of Hydrocarbon and Alcohol Synthesis from CO and H_2," General Motors Technical Center, Warren, Michigan, June 1984.
34. A.T. Bell, "Characterization of Carbon- and Hydrogen-Containing Species Formed During Fischer-Tropsch Synthesis over Group VIII Metals," Instituto de Catalisis y Petroleoquimica, Madrid, Spain, June 1984; Department of Chemistry, University of Lyon, France, July 1984.
35. A.T. Bell, "Studies of the Surface Coverage of Ruthenium by Carbon- and Hydrogen-Containing Adspecies during CO Hydrogenation," 8th International Congress on Catalysis, Berlin, West Germany, July 1984.
36. A.T. Bell, "Mechanisms of Fischer-Tropsch Synthesis," Symposium on C_1 Chemistry, Karlsruhe, West Germany, July 1984.
37. A.T. Bell, "Effects of Metal-Support Interactions on CO Hydrogenation over Palladium Catalysts," Institute de Catalyse, Lyon, France, July 1984; Department of Chemical Engineering, Northwestern University, Evanston, Illinois, October 1984; Department of Chemical Engineering, University of Notre Dame, South Bend, Indiana, October 1984.
38. A.T. Bell, "Identification of Carbon- and Hydrogen-Containing Adspecies Formed During CO Hydrogenation over Ru, Rh, Pd, and Ni," American Chemical Society Meeting, Philadelphia, August 1984.
39. A.T. Bell, "Applications of Transient Response Techniques to Studies of Catalyzed Reactions,"

Department of Chemical Engineering, The University of Arizona, Tucson, September 1984; Department of Chemical Engineering, Iowa State University, Ames, September 1984.

40. A.T. Bell, "Recent Studies of the Mechanism of Carbon Monoxide Hydrogenation over Group VIII Metals," New York Catalysis Society, Newark, New Jersey, October 1984.
41. A.T. Bell, "The Role of Metal-Support Interactions in the Design of Supported-Metal Catalysts," American Institute of Chemical Engineers Meeting, San Francisco, California, November 1984.
42. A.T. Bell, "Applications of Transient Response Techniques to the Study of CO Hydrogenation over Group VIII Metals," American Institute of Chemical Engineers Meeting, San Francisco, California, November 1984.
43. A.T. Bell, "Reaction Mechanisms and the Interpretation of Complex Rate Processes," American Institute of Chemical Engineers Meeting, San Francisco, California, November 1984.
44. A.T. Bell, "Physical and Chemical Evidence for Metal-Support Interactions," 1984 International Chemical Congress of Pacific Basin Societies, Honolulu, Hawaii, December 1984.
45. A.T. Bell, "Influence of Metal-Support Interactions on the Synthesis of Oxygenated Compounds over Pd and Rh," 1984 International Chemical Congress of Pacific Basin Societies, Honolulu, Hawaii, December 1984.

Organometallic Chemistry of Coal Conversion*

K. Peter C. Vollhardt, Investigator

INTRODUCTION

The purpose of this work is to apply organometallic processes and techniques to the solution of problems concerned with the conversion of coal and coal-related molecules to liquid and gaseous fuels. In addition, novel organometallic systems are being constructed that might serve to activate small molecules of industrial relevance to carbon-carbon and carbon-heteroatom bond formation. The potential of selected systems as photostorage devices is also being explored.

Work concerned with the transition-metal and Lewis-acid-promoted activation of benzene and related aromatic molecules to rearrangements and degradation has been completed. In addition, a project elucidating the mechanistic details by which carbon-carbon bond breaking and bond making occurs in the coordination sphere of cyclobutadiene-complexed cobalt systems has reached its final stage. New efforts are concentrating on the exploitation of the novel chemistry of fulvalene dimetal complexes. This work has led to the discovery of several unprecedented rearrangements and new reactions, and to the activation of small molecules.

1. First Photosubstitution Chemistry of Fulvalene-Bridged Metal-Metal-Bonded Carbonyls. Synthesis and Structural Determination of Novel Homo- and Heterobimetallic Alkyne Complexes (Publication 1)†

James S. Drage, Mats Tilset, K. Peter C. Vollhardt, and Timothy W. Weidman

Irradiation of the carbonyl(η^5:η^5-fulvalene)dimetal complexes of molybdenum, tungsten, and ruthenium in the presence of alkynes gives complexes of different respective composition and structure not only within the series but also in comparison with corresponding (η^5-cyclopentadienyl)metal carbonyl dimers. (η^5:η^5-$C_{10}H_8$)$(CO)_5$MoRu furnishes a novel reactive dinuclear (alkyne)metal oxo complex. This molecule is active in the oxidation of hydrogen and/or carbon monoxide and possibly other organic moieties. Three compounds of novel composition have been characterized by x-ray structural methods.

*This work was supported by the Director, Office of Energy Research, Office of Basic Energy Sciences, Materials Sciences Division of the U.S. Department of Energy under Contract No. DE-AC03-76SF00098.

†Mats Tilset was supported by a Royal Fellowship of Norway.

2. Studies on the Reaction of Benzene and Other Hydrocarbons with Aluminum Trichloride (Publication 2)

Yee-Hing Lai, Linda S. Benner, and K. Peter C. Vollhardt

A detailed analysis of the volatile hydrocarbons obtained from the reaction of benzene and $AlCl_3$ was performed. Several experiments point to the intermediacy of phenylcyclohexane as a primary product. ^{13}C-^{12}C exchange was observed using a 1:1 mixture of $^{13}C_6H_6$ and $^{12}C_6H_6$. Hydrogenation was predominant when polybenzenoids were reacted with $AlCl_3$ in the presence of PtO_2/H_2. Cycloalkanes, however, underwent mainly ring-contraction reactions. The effect of transition metals and added ligands on these results was of a quantitative but not qualitative nature. It is clear that many of the reported reactions will play a significant role in any process that attempts to liquefy coal or heavy-petroleum hydrocarbons in the presence of Lewis acids. A successful method for hydroliquefaction of coal would seem to depend on the search for a bifunctional catalyst having complementary properties of Lewis-acid and hydrogenation activity.

3. Thermally Induced Diastereoisomerization of (Cyclobutadiene)cobalt Complexes as a Probe for the Reversibility of Their Formation from Complexed Alkynes (Publication 3)

Guy A. Ville,† K. Peter C. Vollhardt, and Mark J. Winter‡

The synthesis and separation of a series of racemic diastereomers of formula $Co[\eta^4$-$CR^1CR^2CR^3CR^4](\eta$-$C_5H_5)$ by cocyclization of $Co(CO)_2(\eta$-$C_5H_5)$, $Me_3SiC_2SiMe_3$ (btmse), and HC_2CHMeR is described. Gas- and solution-phase

pyrolyses of pairs of diastereomers reveal extensive mutual interconversions. A crossover experiment demonstrates the unimolecular character of the reaction, and studies on enantiomerically enriched systems show that the cobalt unit is the site of diastereoisomerization rather than the alternative carbon chiral center. Kinetic, crossover, and silicon and ^{13}C-labeling experiments furnish results that are best interpreted by assuming that the cyclobutadiene rings open directly to bis(alkyne)cobalt species without the intermediacy of cobaltacyclopentadiene intermediates.

---

†Present address: C.N.R.S. ER84, Universite Pierre et Marie Curie, 75005, Paris, France.

‡Present address: Department of Chemistry, The University, Sheffield, S3 7HF United Kingdom.

4. Work in Progress

The remarkable photochemistry of fulvalene diruthenium tetracarbonyl is being explored extensively, including the measurement of quantum yields and the determination of quantitative data. A new tetranuclear cluster, which appears to be an intermediate in the photochemical activation of this system, has been isolated and characterized by x-ray crystallography.

The thermochemistry and photochemistry of fulvalene dimolybdenum hexacarbonyl has been subjected to extensive examination. This has included the synthesis of several reactive species that function as models for surface-catalyzed reactions. Deuterium isotopic labeling and kinetic results have helped to pinpoint the mechanism of a remarkable thermal extrusion of propene from a 2-oxocyclopentylidene dimolybdenum system. This work has led to the discovery of an unprecedented mode for hydrocarbon generation from dinuclear metal systems.

1984 PUBLICATIONS AND REPORTS

Refereed Journals

1. J.S. Drage, M. Tilset, and K.P.C. Vollhardt, "First Photosubstitution of Fulvalene-Bridged Metal-Metal Bonded Carbonyls. Synthesis and Structural Determination of Novel Homo- and Heterobimetallic Alkyne Complexes," Organometallics **3**, 812 (1984); LBL-17007.†
2. Y.-H. Lai, L.S. Benner, and K.P.C. Vollhardt, "Studies on the Reaction of Benzene and Other Hydrocarbons with Aluminum Trichloride," Fuel **63**, 231 (1984); LBL-15606.
3. G.A. Ville, K.P.C. Vollhardt, and M.J. Winter, "Thermally Induced Diastereoisomerization of (Cyclobutadiene)cobalt Complexes as a Probe for the Reversibility of Their Formation from Complexed Alkynes," Organometallics **3**, 1177 (1984); LBL-17006.
4. K.P.C. Vollhardt and T.W. Weidman, "Efficient Syntheses of New Fulvalene-Bridged Carbonyl Complexes of Cobalt, Ruthenium, Chromium, Molybdenum, and Tungsten," Organometallics **3**, 82 (1984); LBL-17005.
5. K.P.C. Vollhardt and Z.-Y. Yang, "Nickel-Catalyzed Reduction of Carbon Monoxide by Hexamethyldisilane: A New Reaction Leading to a Novel Synthesis of Siloxanes," Angew. Chem., Int. Ed. Engl. **23**, 460 (1984); LBL-17913.‡

LBL Reports

6. J.S. Drage and K.P.C. Vollhardt, "Synthesis, Structure, and Dynamic Properties of a Fulvalene-Bound Fischer-Type Carbene Complex. A Novel Thermal Elimination of Propene," Organometallics, in press; LBL-18239.
7. J.S. Drage and K.P.C. Vollhardt, "The Mechanism of the Thermal Extrusion of Sulfur Dioxide from (η^5-Cyclopentadienyl)cobalt η^4-Thiophene 1,1-Dioxides to Complexed Cyclobutadienes," Organometallics, in press; LBL-18184.

Invited Talks

8. K.P.C. Vollhardt, "Remarkable Rearrangements in the Coordination Sphere of Transition Metals," Badische Anilin und Sodafabriken, Ludwigshafen, West Germany, January 11, 1984; Technical University, Munich, West Germany, January 19, 1984; Princeton University, Princeton, New Jersey, February 29, 1984.
9. K.P.C. Vollhardt, "Cobalt-Mediated Total Synthesis," Johns Hopkins University, Baltimore, Maryland, February 28, 1984; Duke University, Durham, North Carolina, March 1, 1984; University of Hawaii (Distinguished Visitor Lecturership), Honolulu, March 12–16, 1984.
10. K.P.C. Vollhardt, "The Remarkable Chemistry of Fulvalene Dimetals," University of California, Santa Cruz, October 1, 1984; University of California, Santa Barbara, October 5, 1984; University of California, San Diego, October 22, 1984.
11. K.P.C. Vollhardt, "Transition Metal Catalyzed

Approaches to the Total Synthesis of Natural and Unnatural Molecules," Samuel McElvain Lecturer, University of Wisconsin, Madison, October 8–9, 1984.

†Mats Tilset was supported by a Royal Fellowship of Norway.

‡Equipment funds were supported by the National Science Foundation.

Synthetic and Physical Chemistry*

William L. Jolly, Investigator

INTRODUCTION

The purpose of this project is to use photoelectron spectroscopy to determine the nature of the bonding in significant inorganic and organometallic compounds. By measuring core-electron binding energies of appropriate transition-metal compounds, it is possible to study the interaction of metal d electrons with various ligands and to identify various modes of ligand-metal bonding that have analogues in the intermediates of catalyzed organic reactions. Core binding energies can also be used in conjuction with valence-shell ionization potentials to quantify the bonding or antibonding character of molecular orbitals.

1. Applications of the Equivalent-Cores Approximation. Determining Proton Affinities and Isocyanide-to-Nitrile Isomerization Energies from Core Binding Energies (Publication 1)

David B. Beach, Charles J. Eyermann, Steven P. Smit, Si Fen Xiang, and William L. Jolly

Core binding energies were determined for the following gas-phase molecules: CH_2CCH_2, CH_2CO, BH_3CO, HNCO, CH_3CN, CH_3NC, NH_2CN, t-BuNC, and C_6H_5NC. By use of the equivalent-cores approximation, these data and data from the literature were used to calculate the proton affinities of N_2O, CO_2, HCCF, NCF, NH_2CN, CH_2N2, HNCO, CH_2CO, HN_3, CH_3NC, and CH_3CN with an estimated accuracy of $\pm$ 7 kcal mol^{-1}. By a similar method, the isocyanide-to-nitrile isomerization energies for CH_3NC, t-BuNC, and C_6H_5NC were calculated to be -30, -27, and -28 kcal mol^{-1}, respectively.

*This work was supported by the Director, Office of Energy Research, Office of Basic Energy Sciences, Chemical Sciences Division of the U.S. Department of Energy under Contract No. DE-AC03-76SF00098.

2. Core Binding Energies of the Boron Trihalides, Lewis Acidities of the Boron Trihalides, and Heats of Formation of Carbonium Ions (Publication 2)

David B. Beach and William L. Jolly

The core-electron binding energies of the boron trihalides have been redetermined. It has been known for many years that the Lewis acidity of the boron halides increases in the order $BF_3 << BCl_3 < BBr_3$, which is opposite to the order expected from the relative electronegativities of the halogens. To rationalize this acidity trend, it has generally been assumed that halogen-boron π bonding increases on going from BBr_3 to BF_3. The present data constitute direct experimental evidence for this trend in π bonding. By considering the core bonding energies, we have been able not only to interpret the interactions of the "nonbonding" p orbitals, but also to reassign the valence photoelectron spectrum.

The boron 1s binding energies, the heats of formation of the boron compounds, and the heats of formation of the corresponding carbonium ions were used to calculate the core replacement energies Δ_C for BF_3, BCl_3, BBr_3, and BH_3CO. The average Δ_C value (186.91 eV) may now be confidently used to calculate heats of formation of carbon-containing cations with an uncertainty of 4 or 5 kcal mol^{-1}.

3. A Study of σ and π Bonding in Iron Tetracarbonyl Complexes (Publication 3)

David B. Beach, Steven P. Smit, and William L. Jolly

Core-electron binding energies have been measured for a series of monosubstituted iron carbonyls of the formula $Fe(CO)_4L$, where L = pyridine, trimethylphosphine, acrolein, methyl acrylate, dimethyl maleate, 1,1-dichloroethylene, and trans-1,2-dichloroethylene. The core binding energies have been used in conjunction with available valence-orbital ionization potentials to compare the bonding properties of the ligands with carbon monoxide. The method led to the following conclusions: (1) The Fe $d_{x^2-y^2}$, d_{xy} orbitals of the axially coordinated pyridine and trimethylphosphine complexes do not interact with the axial ligands, whereas the Fe d_{xy}, d_{yz} orbitals in these complexes are destabilized by about 0.3 eV relative to $Fe(CO)_5$ because of the loss of the strongly back-bonding CO ligand. (2) The

replacement of CO in the equatorial plane with an olefin having electron-withdrawing substituents causes the Fe $d_{x^2-y^2}$, d_{xy} orbitals to be stabilized by 0.2–0.4 eV relative to $Fe(CO)_5$, whereas the Fe d_{xz}, d_{yz} orbitals are destabilized by about 0.3 eV because of their orthogonality to the olefin π^* orbitals. (3) The olefin π orbitals are stabilized by about 0.6 eV by coordination to the $Fe(CO)_4$ fragment, indicating significant σ interaction.

4. An X-Ray Photoelectron Spectroscopic (XPS) Study of Sulfur-Nitrogen-Fluorine Compounds (Publication 4)

David B. Beach, William L. Jolly, Rudiger Mews, and Alfred Waterfeld

The gas-phase core binding energies of NSF, NSF_3, and several compounds of the types NSF_2R and F_2SNR have been determined. Qualitative interpretation of the data shows that $N(p\pi) \rightarrow S(d\pi)$ bonding is probably important in the NSF_2R compounds and in NSF_3, that the bonding of the sulfur atom in NSF is similar to that in SO_2, and that the nitrogen atom of NSF_3 is more negatively charged than that of NSF (in spite of a stronger N-S bond in NSF_3). Quantitative interpretation of the data for NSF and NSF_3, together with valence ionization potentials in the literature, show that the HOMO of each molecule has principally nitrogen 2p character and is stabilized by interaction with a higher-lying sulfur 3d orbital. The approximate atomic-orbital contributions to the other molecular orbitals of these molecules are deduced.

5. Pi Bonding in Trisilylamine and Related Compounds (Publication 5)

David B. Beach and William L. Jolly

By use of both core and lone-pair ionization potentials, it is shown that the nitrogen $2p\pi$ orbitals in trisilylamine, tris(trimethylsilyl)amine, and bis(trimethylsilyl)amine undergo net stabilizing interactions with other orbitals of the same symmetry in the molecules. Similarly, it has been shown that the sulfur $3p\pi$ orbital of disilyl sulfide undergoes a net stabilization. Although the oxygen $2p\pi$ and selenium $4p\pi$ orbitals in disilyl ether and disilyl selenide, respectively, are slightly destabilized, comparison with the data for the methyl compounds suggests that the lone pairs of the silyl compounds also undergo a stabilizing interaction with higher-lying empty orbitals. It is argued that the empty $d\pi$ orbitals of the silicon atoms in all these compounds interact with the $p\pi$ lone pairs, causing stabilization of the lone pairs and a drift of electron density to the silicon atoms.

6. Work in Progress

The molecule CF_3NC is potentially a very strong π-acceptor ligand, and we are studying the XPS spectra of this molecule and its transition-metal complexes to evaluate its π-acceptor ability. We are studying the bonding in various BH_3 adducts to determine the nature and extent of π bonding in these compounds. We hope to investigate short-lived radical species by XPS, using a new electric-discharge system.

1984 PUBLICATIONS AND REPORTS

Refereed Journals

1. D.B. Beach, C.J. Eyermann, S.P. Smit, S.F. Xiang, and W.L. Jolly, "Applications of the Equivalent Cores Approximation. The Determination of Proton Affinities and Isocyanide-to-Nitrile Isomerization Energies from Core Binding Energies," J. Am. Chem. Soc. **106**, 536 (1984); LBL-16345.
2. D.B. Beach and W.L. Jolly, "Core Binding Energies of the Boron Trihalides, Lewis Acidities of the Boron Trihalides, and Heats of Formation of Carbonium Ions," J. Phys. Chem. **88**, 4647 (1984); LBL-17407.
3. D.B. Beach, S.P. Smit, and W.L. Jolly, "A Study of σ and π Bonding in Iron Tetracarbonyl Complexes," Organometallics **3**, 556 (1984); LBL-16771.
4. D.B. Beach, W.L. Jolly, R. Mews, and A. Waterfeld, "An X-Ray Photoelectron Spectroscopic Study of Sulfur-Nitrogen-Fluorine Compounds," Inorg. Chem. **23**, 4080 (1984); LBL-17606.
5. D.B. Beach and W.L. Jolly, "Pi Bonding in Trisilylamine and Related Compounds," Inorg. Chem. **23**, 4080 (1984); LBL-17980.
6. W.R. Tikkanen, C. Kruger, K.D. Bomben, W.L. Jolly, W.C. Kaska, and P.C. Ford, "Synthesis, Characterization, and X-ray Molecular Structures of Mono- and Dinuclear Copper Complexes with 2,7-Bis(2-pyridyl)-1,8-naphthyridine," Inorg. Chem. **23**, 3633 (1984).

Other Publications

7. W.L. Jolly, *Modern Inorganic Chemistry*, McGraw-Hill, New York, 1984.

LBL Reports

8. D.B. Beach and W.L. Jolly, "A Photoelectron Spectroscopic Study of the Bonding in Borane Adducts," LBL-17669.
9. D.B. Beach, R. Bertoncello, G. Granozzi, and W.L. Jolly, "Transition Metal-Isocyanide Bonding: A Photoelectron Spectroscopic Study of Iron Tetracarbonyl Isocyanide Complexes," LBL-18121.
10. D.B. Beach, W.L. Jolly, and D. Lentz, "An X-Ray Photoelectron Spectroscopic Study of Trifluoromethyl Isocyanide. Back Bonding, Fluorine Lone-Pair Ionization Potentials, and the $CF_3NC \rightarrow CF_3CN$ Isomerization Energy," LBL-18120.

Invited Talks

11. W.L. Jolly, "Photoelectron Spectroscopy for Chemists," Chemistry Department, Rice University, Houston, Texas, April 17, 1984; Chemistry Department, University of Texas, Austin, April 18, 1984; Chemistry Department, University of California, Los Angeles, June 6, 1984.
12. W.L. Jolly, "What Are the Important Features of Inorganic Chemistry?" Symposium on Inorganic Chemistry, Eighth Biennial Conference on Chemical Education, Storrs, Connecticut, August 5–10, 1984.

Chemistry and Morphology of Coal Liquefaction*

Heinz Heinemann, Investigator, with A.T. Bell, R.H. Fish, and G.A. Somorjai, Investigators

For the complete entry under this title, see "Chemistry and Morphology of Coal Liquefaction" in the Fossil Energy Section of this Annual Report.

Electrochemical Systems*

John Newman, Investigator

INTRODUCTION

This program includes investigation of fluid flow and electrochemical transport, analysis of mass-transfer rates and current distribution, design of practical electrochemical systems, and investigation of corrosion processes. Coupled-kinetic, mass-transfer, and fluid-flow phenomena are investigated in semiconductor electrode systems, with emphasis on the optimization of configurational and operating parameters of liquid-junction photovoltaic cells.

1. Work in Progress

A rotating-disk electrode has been used to determine the diffusion coefficient of the mercuric chloride complex $HgCl_4^{--}$ in NaCl solution. The diffusion-coefficient data have been combined with experimental results already obtained from a bench-scale porous-electrode reactor of reticulated vitreous carbon (RVC). The combined data determine a dimensionless mass-transfer-coefficient correlation useful in the scale-up of metal-ion removal processes employing RVC reactors.

Development of a general procedure for modeling the behavior of electrochemical systems during cyclic voltammetry has been completed. A quick algorithm for the calculation of the appropriate superposition integrals has been implemented on a minicomputer, and the procedure has been used to extend the analysis begun last year of the voltammograms of the iodine-iodide-triiodide redox system in propylene carbonate.

A software package to facilitate the development of computer programs for solving one-dimensional boundary-value problems has been written. The package, BandAid, provides support for a reliable system of program development for problems that may be solved by a finite-difference approach employing the banded-matrix algorithm BAND (developed by John Newman). The code is written in ANSI-standard Pascal and has been implemented on a VAX 11/780 minicomputer.

1984 PUBLICATIONS AND REPORTS

Refereed Journals

1. Mark E. Orazem and John Newman, "Mathematical Modeling of Liquid-Junction Photovoltaic Cells: I. Governing Equations," J. Electrochem. Soc. **131**, 2551–2556 (1984); LBL-16210.
2. Mark E. Orazem and John Newman, "Mathematical Modeling of Liquid-Junction Photovoltaic Cells: II. Effect of System Parameters on Current-Potential Curves," J. Electrochem. Soc. **131**, 2574–2582 (1984); LBL-16211.
3. Mark E. Orazem and John Newman, "Mathematical Modeling of Liquid-Junction Photovoltaic Cells: III. Optimization of Cell Configurations," J. Electrochem. Soc. **131**, 2582–2589 (1984); LBL-16212.
4. Mark E. Orazem and John Newman, "Activity Coefficients of Electrons and Holes in Semiconductors," J. Electrochem. Soc. **131**, 2715–2717 (1984); LBL-16786.
5. Mark E. Orazem and John Newman, "Primary Current Distribution and Resistance of a Slotted-Electrode Cell," J. Electrochem. Soc. **131**, 2857–2861 (1984); LBL-15494.

Other Publications

6. Karrie Hanson, Michael Matlosz, John Newman, and Charles Tobias, "Theory of Cyclic Voltammetry for Reactions Having Complex Stoichiometry," in *Proc. Int. Soc. Electrochem.*, Berkeley, California, August 5–10, 1984 (ext. abs.); LBL-17952.

*This work was supported by the Director, Office of Energy Research, Office of Basic Energy Sciences, Chemical Sciences Division of the U.S. Department of Energy under Contract No. DE-AC03-76SF00098.

High-Energy Oxidizers and Delocalized-Electron Solids*

Neil Bartlett, Investigator

INTRODUCTION

The main aim of this program is the synthesis and characterization of new materials that may have value in electrochemical applications. The synthetic work tests models and theories that correlate physical properties (such as electrical conductivity) with chemical composition and structure. The present emphasis is on the study of two-dimensional extended-atomic networks such as those derived from graphite, layer-form boron nitride, and their relatives. Electron oxidation of such materials (with accompanying intercalation to form salts) generates durable and conductive materials (some conducting better than aluminum). Chemical, stoichiometric, and structural requirements for the best conductivity are being defined. The layered materials can often be oxidized (and intercalated) electrochemically in a reversible process. Some of these materials (e.g., $C_xF_{1-\delta}\cdot\delta HF$) may be useful for high-energy electrodes. Physical and chemical studies are being applied to such materials to determine the structure and bonding changes that accompany oxidation and reduction. Salts that are either proton conductors or fluoride-ion conductors, and that are resistant to oxidation but are not metallic, are being sought as solid electrolytes for use with the metallic layer-material salts.

1. Fluoride-Ion Affinities, Electron Affinities, and Lattice Energies (Publications 4 and 11)

Thomas E. Mallouk, Guy L. Rosenthal, Gerhard Müller, Raymond Brusasco, and Neil Bartlett

In order to provide a set of data to evaluate the thermodynamics of the intercalation of graphite by oxidizing fluorides, salts preparable from gaseous fluoride precursors were studied. The enthalpy of dissociation was measured if not otherwise known. It was thus possible to obtain the fluoride-ion affinity or the electron affinity from a knowledge of the fluorobasicities or ionization potential and the lattice energies of the salts. The evaluation of the latter gave the greatest trouble. So that the electrostatic term could be calculated reliably, the crystal structures were determined. The London energy terms were evaluated semiempirically. Perhaps the most useful finding from this study was that the lattice energies of salts A^+X^- ranging from LiF to CsI and $NOUF_6$ are in linear relationship to the inverse of the cube root of the formula-unit volume in the crystal. This correlation is shown in Figure 1-1. The correlation is particularly good among members of a given structural family, e.g. LiF or CsCl. The dispersion-energy term is large in cases where the ions are highly polarizable or strongly coordinating (e.g., TlCl and SF_3BF_4). In such cases the lattice energies are greater than indicated by the formula unit volume. This is a more valuable empirical relationship than any previously available since cationic and anionic radii were usually required. Formula unit volumes are readily estimated, if not known.

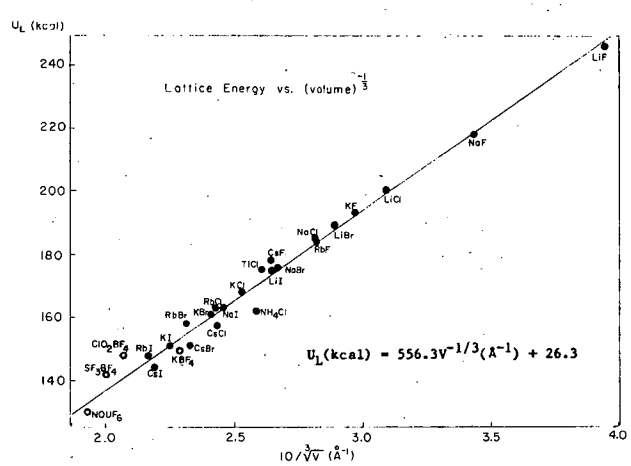

Figure 1-1. Lattice energies vs. (molecular volume)$^{-1/3}$; open circles are for this work; shaded circles are for lattice energies given by Kapustinski.[1] (XBL 835-9968)

1. Kapustinski, Zh. Fiz. Khim. 5, 59 (1934).

*This work was supported by the Director, Office of Energy Research, Office of Basic Energy Sciences, Chemical Sciences Division of the U.S. Department of Energy under Contract No. DE-AC03-76SF00098.

2. Raman, Infrared, and Nuclear Magnetic-Resonance (NMR) Studies of the Graphite Hydrofluorides $C_xF_{1-\delta}(HF)_\delta$ ($2 \leqslant x \leqslant 5$) (Publication 7)

T. Mallouk, B.L. Hawkins, M.P. Conrad, K. Zilm, G.E. Maciel, and N. Bartlett

Raman spectra of $C_xF_{1-\delta}(HF)_\delta$ ($x|\delta \approx 12$) show bands at 1600, 1355, and 839 cm^{-1}. Graphite itself has an (E_{2g}-like) in-plane-motion Raman band at 1581 cm^{-1} and an out-of-plane-motion band at 848 cm^{-1}. In addition, in small-crystallite graphite, a broad band observed at ~1355 cm^{-1} has been attributed to an in-plane breathing motion. From these observations it has been concluded that the carbon-atom sheets in $C_xF_{1-\delta}(HF)_\delta$ are as flat as in graphite and that the domain size in those materials yielding the Raman spectra is in the 50–100 Å range. Variable-contact-time cross-polarized magic-angle-spinning ^{13}C NMR spectra have been obtained for x = 2.05 and 3.70. In both spectra, two peaks ($+135/10^6$ and $+188/10^6$ chemical shift from tetramethyl silane) are seen; they are attributed, respectively, to graphitic and C-F carbons. The ratio of graphitic to C-F carbon atoms has been found to be 1.6(2):1 in $C_{2.05}F_{0.82}(HF)_{0.18}$. The bonding of fluorine to carbon is highly ionic. Since the binding within the graphitic layers is essentially the same as in pristine graphite, the C-C π-bond is preserved. This will be so if the carbons make, in the language of valence-bond theory, one-electron dative bonds to the fluorine atoms. These electrons bestow a partial negative charge on the fluorine atoms and are at the same time used in π-bonding within the carbon network. Such π-electrons employed in the binding of F atoms must be strongly localized near the fluorine. Charge carriers (electrons) must therefore have low mobility at such centers in the π system. This low mobility can account for the conductive character of C_3F and the insulating character of C_2F, if the structural models shown in Figure 2-1 are valid. For the C_3F model it is necessary to assume that the F atom attachment on one side of the sheet is *ortho* to that of the other. In that case chains of nonfluorinated π system remain to provide the high-mobility pathways for the charge carriers.

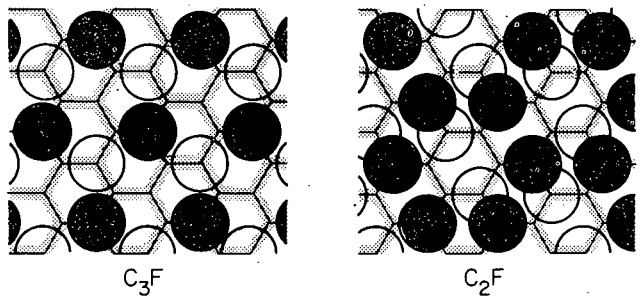

Figure 2-1. Structural models for C_3F and C_2F. The unshaded circles represent the fluorine atoms on one side of a carbon-atom sheet, and the shaded circles represent the fluorine atoms of a like adjacent sheet in positions of closest packing. (XBL 852-1384)

3. Reversible Intercalation of $C_{14}AsF_6$ by AsF_5 and AsF_3 and Accompanying Changes in Structure and Electrical Conductivity (Publications 8 and 10)

Fujio Okino and Neil Bartlett

Treatment of chips of highly oriented pyrolytic graphite (HOPG) suitable for conductivity measurements employed an AsF_5:F_2 molar ratio of 2:1 at ~20°. It was necessary to use low gas pressures (<3 atmospheres) at the onset to avoid the addition of excess fluorine. (Addition of fluorine beyond the stoichiometry for AsF_6^- led to marked decrease in conductivity.) Chips (~5 × 5 × 0.03 mm) of first-stage $C_{14}AsF_6$ made in this way have the structure in which the threefold sets of F ligands of the AsF_6^- are nestled in contiguous hexagons of the enclosing graphite sheets. As a consequence of the nestling and the D_{3d} symmetry of the nestled AsF_6^-, the enclosing sheets are staggered with respect to one another. The *ab*-plane specific conductivity of $C_{14}AsF_6$ measured by a contactless radio-frequency (1 kHz) inductive technique showed it to be ten times better than that of pristine graphite and comparable with the first-stage materials made from graphite and AsF_5 commonly referred to as C_xAsF_5. Treatment of $C_{14}AsF_6$ with AsF_5 at ~20° yields (<2 hrs) expanded solids (c_o ~ 8.0 Å) with composition $C_{14}AsF_6 0.5AsF_5$. X-ray-diffraction data show that the carbon-atom sheets in the latter are eclipsed (no AsF_6^- nestling). The electrical conductivity is

comparable with that of $C_{14}AsF_6$. The AsF_5 of $C_{14}AsF_6 0.5AsF_5$ is quickly lost to vacuum and the nestled-structure $C_{14}AsF_6$ material recovered. This rapid uptake and loss of AsF_5 contrasts with the very slow uptake (ultimately to composition $\sim C_{14}AsF_6 0.5AsF_3$) and loss of AsF_3. The difference in ease of uptake is attributed to the strong fluoroacidity of AsF_5 ($AsF_6^- + AsF_5 \rightleftharpoons As_2F_{11}^-$), which thus provides a mechanism for transport within the graphite. The more basic fluoride, AsF_3, is unable to form such complex species, and its addition to, or loss from, the AsF_6^- salts depends on the redox interaction $AsF_3 + 2AsF_6^- \rightleftharpoons 3AsF_5 + 2e$.

4. Antimonypentafluoroorthotellurates: Antimony(III)trispentafluoroorthotellurate, Antimony(V)pentakispentafluoroorthotellurate, and Some Salts of the Hexakispentafluoroorthotelluroantimonate(V) Anion, $A^+Sb(OTeF_5)_6^-$ (Publication 9)

W. Tötsch and N. Bartlett

$Sb(OTeF_5)_3$ has been prepared from SbF_3 and $B(OTeF_3)_3$. Contrary to a previous report, it is a low-melting, sublimable solid. It interacts with Cl_2 and Br_2 to give $SbCl_4^+Sb(OTeF_5)_6^-$ and $SbBr_4^+Sb(OTeF_5)_6^-$, respectively. $Sb(OTeF_5)_3$ and $Xe(OTeF_5)_2$ yield antimony(V)pentakispentafluoroorthotellurate, $Sb(OTeF_5)_5$, which is unstable at room temperature. ^{19}F NMR at $-20°C$ suggests an ionic formulation: $Sb(OTeF_5)_4^+ Sb(OTeF_5)_6^-$. Salts containing the new anion $Sb(OTeF_5)_6^-$ have been synthesized in 3 ways: (1) from $Sb(OTeF_5)_5$ and an appropriate pentafluoroorthotellurate: $Sb(OTeF_5)_5 + NMe_4^+OTeF_5^- = NMe_4^+Sb(OTeF_5)_6^-$; (2) from $SbCl_4^+Sb(OTeF_5)_6^-$ and a corresponding chloride: $SbCl_4^+Sb(OTeF_5)_6^- + CsCl = Cs^+Sb(OTeF_5)_6^- + SbCl_5$; and (3) oxidatively using a mixture of $Sb(OTeF_5)_5$ and $Xe(OTeF_5)_2$: $1/2\ Xe(OTeF_5)_2 + Sb(OTeF_5)_5 + C_6F_6 = C_6F_6^+Sb(OTeF_5)_6^- + 1/2\ Xe$. The novel $Sb(OTeF_5)_6^-$ anion has high thermodynamic stability, and its large size (anion volume ~ 660 Å^3) and high symmetry should be useful in stabilizing delocalized-electron cations.

5. Work in Progress

X-ray-powder diffraction data from the solids in contact with liquid hydrogen fluoride have established the existence of the previously unknown first-stage salts $C_xF(HF)_y^-$. The first-formed first-stage salts, which are black, are characterized by a hexagonal unit cell with dimensions a = 2.459 Å and c = 6.4 Å. Such materials fall, *in vacuo*, to a second-stage salt of composition C_{14} to $C_{16}HF_2$, but addition of HF restores the first-stage salt. As the oxidative fluorination of the graphite proceeds, attachment of fluorine to the carbon occurs, and another first-stage product appears that coexists with the first. It is characterized by a hexagonal unit cell with dimensions a = 2.459 Å and c = 7.5 to 6.7 Å. As before, removal of HF yields the second-stage salt $C_{16}HF_2$ from the c = 6.4 Å first-stage material. The other first-stage material yields $C_xF_{1-\delta}(HF)_\delta$. The latter takes up HF (with appropriate increase in the c_o dimension). This reversible uptake of HF by $C_xF_{1-\delta}(HF)_\delta$ amounts to 0.5 HF for each F. Spectra of $C_xF_{1-\delta}(HF)_\delta$ ($x{:}\delta \approx 12{:}1$) determined with electron spectroscopy by chemical analysis (ESCA) have revealed two C1s binding energies. One of the binding energies (284.2 eV) is no more than +0.3 eV greater than the C1s binding energy of pristine graphite carbon, and the other binding energy (287.4 eV) indicates carbon bound to the electron-withdrawing F ligand. The binding energy of the F1s (686.3 eV) is between that for F in LiF (684.9 eV) and F in Teflon (689.1, 689.6 eV) and indicative of the semi-ionic F ligand.

1984 PUBLICATIONS AND REPORTS

Refereed Journals

1. Neil Bartlett, Sam Yeh, Kostantinos Kourtakis, and Tom Mallouk, "The Fluorobasicities of ReF_7 and IF_7 as Measured by the Enthalpy Change $\Delta H°(EF_{7(g)} \rightarrow EF_6^+{}_{(g)} + F_{(g)}^-)$," J. Fluorine Chem. **26**, 97 (1984); LBL-17081.
2. G.L. Rosenthal, T.E. Mallouk, and Neil Bartlett, "Intercalation of Graphite by Silicon Tetrafluoride and Fluorine to Yield a Second-Stage Salt $C_{24}SiF_5$," Syn. Met. **9**, 433 (1984); LBL-15457.
3. Thomas E. Mallouk, Bernard Desbat, and Neil Bartlett, "Structural Studies of Salts of Cis and Trans μ-Fluoro-Bridged Polymers of of GeF_5^- and of GeF_5^- Monomer," Inorg. Chem. **23**, 3160 (1984); LBL-13816.
4. Thomas E. Mallouk, Guy L. Rosenthal, Gerhard Müller, Raymond Brusasco, and Neil Bartlett, "Fluoride Ion Affinities of GeF_4 and BF_3 from Thermodynamic and Structural Data for $(SF_3)_2GeF_6$, ClO_2GeF_5, and ClO_2BF_4," Inorg. Chem. **23**, 3167 (1984); LBL-13817.

Other Publications

5. Neil Bartlett, "Noble-Gas Chemistry and The Periodic System of Mendeleev," Mendeleev Chem. J. **28** (6), 628 (1983).
6. Neil Bartlett, "Xeno," in Vol. X of *Enciclopedia della Chimica,* Uses Edizioni Scientifiche Firenze, 1983, p. 584.

LBL Reports

7. T. Mallouk, B.L. Hawkins, M.P. Conrad, K. Zilm, G.E. Maciel, and N. Bartlett, "Raman, Infrared and N.M.R. Studies of the Graphite Hydrofluorides $C_xF_{1-\delta}(HF)_\delta$ ($2 \leqslant x \leqslant 5$)," Phil. Trans. Royal Soc., London (in press); LBL-17951.
8. F. Okino and N. Bartlett, "Reversible Intercalation of $C_{14}AsF_6$ by AsF_5 and AsF_3 and Accompanying Changes in Structure and Electrical Conductivity," submitted to Syn. Met.; LBL-18920.
9. W. Tötsch and N. Bartlett, "Antimonypentafluoroorthotellurates: Antimony(III)trispentafluoroorthotellurate, Antimony(V)pentakispentafluoroorthotellurate and Some Salts of the Hexakispentafluoroorthotelluroantimonate(V) Anion, $A^+Sb(OTeF_5)_6^-$," submitted to Inorg. Chem.; LBL-18904.
10. F. Okino (Ph.D. Thesis), with N. Bartlett, "Compositional, Structural, and Physical Studies of Some Graphite Hexafluoroarsenates and their Relatives," LBL-18261.
11. G.L. Rosenthal (Ph.D. Thesis), with N. Bartlett, "Electron-Oxidation of Graphite by Fluorospecies," LBL-15607.
12. S.M. Yeh (Ph.D. Thesis), with N. Bartlett, "Application of Powerful Oxidizers in the Synthesis of New High-Oxidation-State Actinide and Related Species," LBL-13346.

Invited Talks

13. N. Bartlett, "The Intercalation of Graphite by Fluorides and Fluorine: Thermodynamic, Kinetic and Bonding Aspects," Colloquium, Department of Chemistry, University College, London, England, February 29, 1984.
14. N. Bartlett, "Noble-Gas Chemistry," "Studies in Electron Oxidation: From O_2^+ Salts to Synthetic Metals," and "Thermodynamic and Kinetic Aspects of the Intercalations of Graphite by Fluorine and Fluorides, and Novel Bonding of Fluorine to Carbon," Renaud Lectures, Michigan State University, East Lansing, May 8–10, 1984.
15. N. Bartlett, "Electrical and Magnetic Properties of Low Dimensional Solids," The Royal Society: A Meeting for Discussion, London, England, May 31–June 1, 1984.
16. N. Bartlett, "Intercalation of Graphite by Fluorides and Fluorine: Structural, Thermodynamic and Kinetic Aspects," Colloquium, University of California, Santa Barbara, May 15, 1984.
17. N. Bartlett, "Thermodynamic, Structural and Electrical Aspects of the Intercalation of Graphite by Fluorides and Fluorine," Chemistry Department, University of Glasgow, Scotland, March 8, 1984.
18. N. Bartlett, "Intercalation of Graphite by Fluorides and Fluorine," Inorganic Chemistry Seminar, University of Leeds, England, June 4, 1984; Inorganic Chemistry Seminar, University of Nottingham, England, June 8, 1984; Inorganic Chemistry Seminar, Oxford University, England, June 11, 1984; Department of Chemistry, Institut Jožef Stefan, Ljubljana, Yugoslavia, June 27, 1984.
19. N. Bartlett, "The Stabilization of High Oxidation States" and "Salts of Cationic Graphite: Thermodynamic, Structural, and Electrical Aspects of the Intercalation of Graphite by Fluorides or Fluorine," 1984–85 Louis Nicolas Vauquelin Lectures, University of Texas, Austin, October 22–23, 1984.
20. N. Bartlett, "Evidence for Novel Bonding of Fluorine to Carbon in Intercalated Graphite Compounds," Inorganic Chemistry Seminar, Department of Chemistry, University of California Berkeley, September 7, 1984.
21. N. Bartlett, "Intercalation of Graphite by Oxidizing Fluorides and Fluorine: Thermodynamic, Structural and Conductance Features," 3rd International Symposium on Clathrate Compounds and Molecular Inclusion Phenomena and 2nd International Symposium on Cyclodextrins, Tokyo, Japan, July 23–27, 1984.
22. N. Bartlett, "The Intercalation of Graphite by Fluorides and Fluorine: Thermodynamic, Structural and Electrical Aspects," and "Thermodynamic and Structural Features of the Intercalation of Graphite by Oxidizing Fluorides," Electrochemical Society Meeting, July 31, 1984; Kyoto University, Japan, July 30, 1984.

Transition-Metal-Catalyzed Conversion of CO, NO, H_2, and Organic Molecules to Fuels and Petrochemicals*

Robert G. Bergman, Investigator

INTRODUCTION

The goal of this project is the discovery of new chemical reactions in which transition metals interact with organic materials, and the understanding of how these reactions work. The approach begins with the synthesis and structural characterization of new types of stable organotransition-metal complexes. Following that the self-reactions of these materials (induced, for example, by heat or light) are investigated, as well as their reactions with small molecules and organic compounds. A recent discovery on this project was the finding that certain classes of hydridoiridium and -rhodium complexes undergo oxidative addition into the carbon-hydrogen bonds of completely saturated hydrocarbons. This is the first example of this long-sought reaction, and work on this project is now directed at examining the scope, selectivity, and mechanism of this reaction. In the rhodium series, an example of the rearrangement of a C-H to a C-C activation product has been found. Efforts are now being directed at converting the alkyl(hydrido)iridium products of the oxidative addition into functionalized organic molecules. In addition, the synthesis and chemistry of several related, but structurally more complex, hydridoiridium complexes have been examined this year.

*This work was supported by the Director, Office of Energy Research, Office of Basic Energy Sciences, Chemical Sciences Division of the U.S. Department of Energy under Contract No. DE-AC03-76SF00098.

1. Synthesis of Trimethylphosphine-Substituted Pentamethylcyclopentadienyliridium Hydride Complexes; Protonation and Deprotonation of $(C_5(CH_3)_5)Ir(P(CH_3)_3)H_2$ (Publication 10)

Thomas M. Gilbert and Robert G. Bergman

Trimethylphosphine reacts with $[(C_5(CH_3)_5)Ir]_2(\mu\text{-}H)_3A$, where A = PF_6 or BF_4 (**1** in Figure 1-1) to yield the monohydride-bridged dimer $[(C_5(CH_3)_5)Ir(P(CH_3)_3)(H)]_2(\mu\text{-}H)A$ (**2**), which has been characterized by a single-crystal x-ray diffraction study. Reaction of $2{\cdot}BF_4$ with a third equivalent of $P(CH_3)_3$ at elevated temperature gives the monomeric species $(C_5(CH_3)_5)Ir(P(CH_3)_3)H_2$ (**4**) and $(C_5(CH_3)_5)Ir(P(CH_3)_3)_2HBF_4$. Reduction of dimer **2** with $LiEt_3BH$ yields two equivalents of **4**.

Protonation of dihydride **4** occurs with $HBF_4{\cdot}OEt_2$ to give $(C_5(CH_3)_5)Ir(P(CH_3)_3)H_3BF_4$ (**5**), the first example of a cationic iridium (V) complex. Low-temperature ^1H nuclear magnetic-resonance studies reveal an anomalously large H-H coupling constant, suggesting potentially interesting structural features.

Deprotonation of dihydride **4** with t-BuLi/pmdeta leads to $(C_5(CH_3)_5)Ir(P(CH_3)_3)H[Li(pmdeta)_x]$, which reacts with alkylating agents to yield complexes of the type $(C_5(CH_3)_5)Ir(P(CH_3)_3)(R)(H)$. This route provides a method of synthesizing alkyl hydride compounds in good yield.

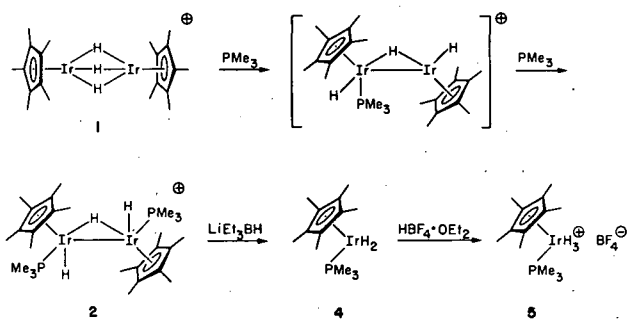

Figure 1-1. Reaction of $[(C_5(CH_3)_5)Ir]_2(\mu\text{-}H)_3A$ (A = PF_6 or BF_4), compound **1**, with trimethylphosphine, to form the monohydride-bridged dimer **2**. (XBL 853-1490)

2. (Pentamethylcyclopentadienyl)iridium Polyhydride Complexes: Synthesis of Intermediates in the Mechanism of Formation of $(C_5(CH_3)_5)IrH_4$, and the Preparation of Several Iridium (V) Compounds (Publication 11)

Thomas M. Gilbert, Frederick J. Hollander, and Robert G. Bergman

Reaction of $LiBH_4$ with $[(C_5(CH_3)_5)Ir]_2(\mu\text{-}H)_3PF_6$ (**1** in Figure 2-1) results in the formation of the borohydride-bound dimer $[(C_5(CH_3)_5)Ir]_2H_3BH_4$ (**2**, R = H), for which a single-crystal x-ray diffraction study shows the borohydride moiety bridging the two metal centers in a unique fashion. Hydrolysis of this complex yields the formally iridium (IV) dimer $[(C_5(CH_3)_5)IrH_3]_2$.

Use of the more nucleophilic reducing agent $LiEt_3BH$ in this reaction leads to the mononuclear salt $(C_5(CH_3)_5)IrH_3[Li(THF)_x]$ (**5**), the anion of which may be hydrolyzed to the iridium (V) complex $(C_5(CH_3)_5)IrH_4$ (**6**). The overall mechanism of the formation of tetrahydride **6** can be understood based on these results.

Deprotonation of **6** with t-BuLi in the presence of pmdeta leads to the sequestered salt $(C_5(CH_3)_5)IrH_3[Li(pmdeta)]$. Silyl- or stannylation of the anion occurs with $Me_3SiO_3SCF_3$, Me_3SnCl, and Ph_3SnBr to yield the new iridium (V) polyhydrides $(C_5(CH_3)_5)IrH_3SiMe_3$, $(C_5(CH_3)_5)IrH_3SnMe_3$, and $(C_5(CH_3)_5)IrH_3SnPh_3$, the last of which was characterized structurally by a single-crystal x-ray diffraction study.

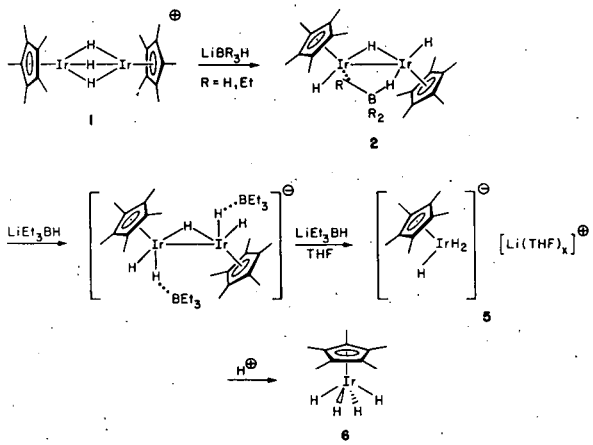

Figure 2-1. Reaction of $[(C_5(CH_3)_5)Ir]_2(\mu\text{-}H)_3PF_6$, compound **1**, with $LiBH_4$, to form the borohydride-bound dimer **2**.
(XBL 853-1491)

3. Rapid Intramolecular Rearrangement of a Hydrido(cyclopropyl)rhodium Complex to a Rhodacyclobutane. Independent Synthesis of the Metallacycle by Addition of Hydride to the Central Carbon Atom of a Cationic Rhodium π-Allyl Complex (Publication 9)

Roy A. Periana and Robert G. Bergman

The product of rhodium-based C-H activation of cyclopropane, Cp*(L)Rh(R)H (**2** in Figure 3-1; R = cyclopropyl; Cp* = C_5Me_5; L = PMe_3) is converted at temperatures above 0°C to the rhodacyclobutane $Cp^*(L)Rh(CH_2)_3$ (**3**) formed by insertion of rhodium into the cyclopropane C-C bond. The metallacycle **3** was characterized by x-ray diffraction and has a nearly planar 4-membered ring. It can be synthesized independently by first preparing the cationic π-allyl complex $[Cp^*(L)Rh(C_3H_5)]^+BF_4^-$ (**5**) and then treating it with sodium borohydride or lithium triethylborohydride. The latter reaction is only the second example of a π-allyl system that adds nucleophiles to the center, rather than the end, of the three-carbon chain. Carrying out the thermolysis of hydride **2** in benzene solvent, rather than in cyclopropane solvent, still leads to 50% of **3** along with 50% $Cp^*(L)Rh(C_6H_5)H$ and cyclopropane by reductive elimination. Because "Cp*RhL" would have been completely trapped by benzene under these conditions, the rhodium atom and C_3 fragment must remain associated with one another during the conversion; i.e., it must be a truly intramolecular rearrangement.

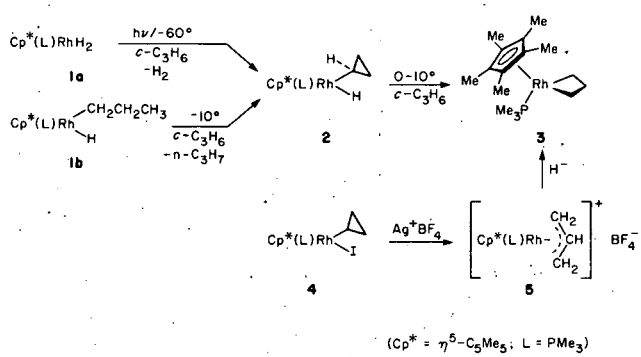

Figure 3-1. Two methods of synthesizing the metallacycle **3**.
(XBL 853-1492)

4. Work in Progress

Several areas opened up by initial discoveries of alkane activation using transition-metal complexes are now being pursued. Systems based on other metals are being explored, and a cyclopentadienylrhenium complex capable of intermolecular C-H insertion has been uncovered. In experiments on substrates other than alkanes, alcohols, organic halides, and alkenes have proved to be reactive and often lead to products in which the functional groups in the organic molecules participate in the C-H activating reaction. Experiments are under way designed to understand in detail the mechanisms of insertion into alkane C-H bonds and to relate this process to its microscopic reverse, the reductive elimination of alkanes from hydrido(alkyl)metal complexes. Finally, studies are in progress aimed at developing methods for converting the products of alkane activation into functionalized organic molecules and to understand the relationship between homogeneous and heterogeneous C-H insertion processes.

1984 PUBLICATIONS AND REPORTS

Refereed Journals

1. R.G. Bergman, "Activation of Alkanes in Homogeneous Solution Using Organotransition Metal Complexes," Science **223**, 902 (1984); LBL-16320.
2. E.N. Jacobsen and R.G. Bergman, "Synthesis, Crystal and Molecular Structure, and Reactions of a Bridging Vinylidene Dicobalt Complex. Reaction with Molybdenum Hydrides to Give a Heteronuclear Cluster Complex," Organometallics **3**, 329 (1984).†
3. M.J. Wax, J.M. Stryker, J.M. Buchanan, C.A. Kovac, and R.G. Bergman, "Reversible C-H Insertion/Reductive Elimination in (η^5-Pentamethylcyclopentadienyl(trimethylphosphine)iridium Complexes. Use in Determining Relative Metal-Carbon Bond Energies and Thermally Activating Methane," J. Am. Chem. Soc. **106**, 1121 (1984); LBL-16617.
4. R.A. Periana and R.G. Bergman, "Oxidative Addition of Rhodium to Alkane C-H Bonds: Enhancement in Selectivity and Alkyl Group Functionalization, and the First Structurally Characterized Derivative of a C-H Insertion Product," Organometallics **3**, 508 (1984); LBL-16548.
5. A.H. Janowicz, R.A. Periana, J.M. Buchanan, C.A. Kovac, J.M. Stryker, M.J. Wax, and R.G. Bergman, "Oxidative Addition of Soluble Iridium and Rhodium Complexes to Carbon-Hydrogen Bonds in Methane and Higher Alkanes," Pure Appl. Chem. **56**, 13 (1984); LBL-18170.
6. W.P. Weiner, F.J. Hollander, and R.G. Bergman, "The Synthesis, Structure and Reactivity of Sodium(η^5-Cyclopentadienyl)nitrosylcobaltate," J. Am. Chem. Soc. **106**, 7462 (1984).†
7. N.E. Schore, C.S. Ilenda, M.A. White, H.E. Bryndza, M.G. Matturro, and R.G. Bergman, "Carbon-Carbon Bond Formation in Dinuclear Dialkyl Complexes. Reactions of $[CpCo(CO)R]_2$ (R = CH_3, CH_2CH_3, CH_2CF_3) and $(C_{11}H_{10})Co_2(CO)_2(CH_3)_2$ with Carbon Monoxide and Triphenylphosphine," J. Am. Chem. Soc. **106**, 7451 (1984).†
8. M.D. Seidler and R.G. Bergman, "Synthesis of Dialkylruthenium Nitrosyls and Thermal Conversion to Ruthenium Oximate, Carboxamide and Cyano Complexes," J. Am. Chem. Soc. **106**, 6110 (1984).‡
9. R.A. Periana and R.G. Bergman, "Rapid Intramolecular Rearrangement of a Hydridocyclopropylrhodium Complex to a Rhodacyclobutane. Independent Synthesis of the Metallacycle by Addition of Hydride to the Central Carbon Atom of a Cationic Rhodium π-Allyl Complex," J. Am. Chem. Soc. **106**, 7272 (1984); LBL-18171.

LBL Reports

10. T.M. Gilbert and R.G. Bergman, "Synthesis of Trimethylphosphine-Substituted Pentamethylcyclopentadienyliridium Hydride Complexes; Protonation and Deprotonation of $(C_5(CH_3)_5)Ir(P(CH_3)_3)H_2$," submitted to J. Am. Chem. Soc.; LBL-18844.
11. T.M. Gilbert, F.H. Hollander, and R.G. Bergman, "(Pentamethylcyclopentadienyl)iridium Polyhydride Complexes: Synthesis of Intermediates in the Mechanism of Formation of $(C_5(CH_3)_5)IrH_4$, and the Preparation of Several Iridium (V) Compounds," submitted to J. Am. Chem. Soc.; LBL-18845.

Invited Talks

12. R.G. Bergman, "Organotransition Metal Complexes," Department of Chemistry, University of Houston, Texas, January 23, 1984.
13. R.G. Bergman, "C-H Activation," Department of Chemistry, University of Southern California, Los Angeles, February 10, 1984; Department of Chemistry and Biochemistry, University of California, Los Angeles, February 16, 1984; Department of Chemistry, Carleton College, Northfield, Minnesota, April 6, 1984; Department of Chemistry, University of California, San Diego, April 23, 1984.

14. R.G. Bergman, "Transformations of Organic Compounds Mediated by Organometallic Complexes," Department of Chemistry, University of Alberta, Edmonton, March 5, 1984; Department of Chemistry, University of British Columbia, Vancouver, March 6, 1984; Department of Chemistry, University of Victoria, British Columbia, March 8, 1984.
15. R.G. Bergman, "Oxidative Addition of Soluble Organotransition Metal Complexes to C-H Bonds in Alkanes," Industrial Associates Conference, California Institute of Technology, Pasadena, March 25, 1984.
16. R.G. Bergman, "Metallacycles," Chemistry Research Conference, Division of Chemistry, California Institute of Technology, Pasadena, March 28, 1984; Department of Chemistry, Cornell University, Ithaca, New York, April 2, 1984; Department of Chemistry, University of Rochester, New York, April 3, 1984.
17. R.G. Bergman, "Oxidative Addition of Soluble Transition Metal Complexes to C-H Bonds in Alkanes," Kirkwood Symposium, Department of Chemistry, Yale University, New Haven, Connecticut, April 4, 1984.
18. R.G. Bergman, "C-H Activation," Section of Organometallic Chemistry, New York Academy of Sciences, New York, April 5, 1984.
19. R.G. Bergman, "Activation of C-H and C-C Bonds in Alkanes Using Soluble Transition Metal Complexes," John Howard Appleton Lecture, Department of Chemistry, Brown University, Providence, Rhode Island, May 4, 1984.
20. R.G. Bergman, "Synthesis of Dialkylruthenium Nitrosyls and their Thermal Conversion to Ruthenium Oximate, Carboxamides and Cyano Complexes," NSF Organometallic Chemistry Workshop, University of North Carolina, Chapel Hill, May 31, 1984.
21. R.G. Bergman, "Activation of Carbon-Hydrogen Bonds Using Soluble Organotransition Metal Complexes," Conference on Reaction Mechanisms, Duke University, Durham, North Carolina, June 6, 1984.
22. A.H. Janowicz, C.A. Kovac, M.J. Wax, J.M. Buchanan, J.M. Stryker, J.C. Hayes, R.A. Periana, P.F. Seidler, T.T. Wenzel, and R.G. Bergman, "Oxidative Addition of Transition Metals to Alkane C-H Bonds," Symposium on Organometallic Chemistry and Catalysis, University of California, Santa Cruz, August 6, 1984.
23. R.G. Bergman, "Alkane Activation by Homogeneous Systems," Gordon Research Conference on Organometallic Chemistry, Proctor Academy, Andover, New Hampshire, August 13–17, 1984.
24. R.G. Bergman, "Transformations of Organic Compounds Induced by Organotransition Metal Complexes," Symposium on Recent Developments in Organic Chemistry, American Chemical Society Annual Meeting, Philadelphia, Pennsylvania, August 28, 1984.
25. R.G. Bergman, "Cluster Expansion Reactions of Dinuclear Vinylidene Complexes with Transition Metal Hydrides," Edward Clark Lee Lecture, University of Chicago, Illinois, November 5, 1984.
26. R.G. Bergman, "The Use of Organometallic Complexes in the Formation and Cleavage of C-H and C-C Bonds," Symposium on Recent Developments in Homogeneous and Heterogeneous Catalysis, International Chemical Congress of Pacific Basin Societies, Honolulu, Hawaii, December 17, 1984.

---

†Supported by the National Science Foundation (Grant No. CHE79-26291)

‡Supported by the National Institute of Health (Grant No. GM-25459)

CHEMICAL ENGINEERING SCIENCES

High-Pressure Phase Equilibria in Hydrocarbon-Water (Brine) Systems*

John M. Prausnitz, Investigator

INTRODUCTION

Phase equilibria are required for the efficient design of large-scale separation processes (e.g., distillation and extraction) in the chemical and related industries. In this context, "efficient" refers to optimum use of raw materials and to conservation of energy.

Since the variety of technologically important fluid mixtures is extremely large, it is not possible to obtain all desired equilibria from experiment. Therefore, the objective of this research is to develop molecular thermodynamics to interpret and correlate selected phase-equilibrium data toward reliable general prediction of phase equilibria for engineering. The correlations are expressed through semitheoretical physicochemical models in a form suitable for computer-aided process design. In this research, particular attention is given to those systems that are of primary interest in energy-related industries, especially those concerned with fossil fuels and fossil-fuel/water mixtures.

Development of molecular thermodynamics calls for a combination of theoretical, computational, and experimental work. It also demands simultaneous awareness of both progress in molecular science and realistic requirements for engineering design.

1. Phase Equilibria for Mixtures Containing Very Many Components. Development and Application of Continuous Thermodynamics (Publications 7, 13, and 14)

R.L. Cotterman, R. Bender,†, D. Dimitrelis, and J.M. Prausnitz

For some multicomponent mixtures, where detailed chemical analysis is not feasible, the composition of the mixture may be described by a continuous distribution function of some convenient macroscopic property such as normal boiling point or molecular weight. To attain a quantitative description of phase equilibria for such mixtures, this work has developed thermodynamic procedures for continuous systems. The procedure is called continuous thermodynamics. To illustrate, continuous thermodynamics is used to calculate dew points for natural-gas mixtures, solvent loss in a high-pressure absorber, and liquid-liquid phase equilibria in a polymer-fractionation process.

Computational methods have been developed to satisfy phase equilibria and material balances required for flash calculations. The perturbed-hard-chain equation of state has been modified and extended for representing thermodynamic properties of high-boiling fluids.

Continuous thermodynamics provides a rational method for calculating phase equilibria where complete chemical analysis is not available but where composition can be given by some statistical description. While continuous thermodynamics is only the

*This work was supported by the Director, Office of Energy Research, Office of Basic Energy Sciences, Chemical Sciences Division of the U.S. Department of Energy under Contract No. DE-AC03-76SF00098.

logical limit of the well-known pseudocomponent method, it is more efficient than that method because required computer time is often lower and arbitrary selection of pseudocomponents is avoided, as is required in conventional methods.

†Present address: BASF, Willstätt, West Germany.

2. Phase Equilibria for High-Boiling Fossil-Fuel Distillates (Publications 10 and 11)

G.L. Alexander, B.J. Schwarz, A.L. Creagh, and J.M. Prausnitz

An experimental procedure is developed for characterizing high-boiling, distillable fossil-fuel mixtures to facilitate estimation of thermodynamic properties for process-design calculations. A mixture is first separated into narrow-boiling fractions using a spinning-band column operating at low pressure and high reflux. Each fraction is considered to be a pseudocomponent of the mixture. Each pseudocomponent is characterized by structural properties per average molecule: carbon, alpha hydrogen, beta hydrogen, gamma hydrogen, hydroxyl, ether oxygen, primary amine, secondary amine, pyridinic nitrogen, and thiophenic sulfur. These structural properties are obtained from elemental analysis, proton nuclear-magnetic-resonance (NMR) spectra, infrared spectra, and cryoscopic measurements. The proposed characterization procedure is illustrated with an Exxon Donor-Solvent product, a Lurgi creosote, five crude-oil fractions from Belridge, California, and five crude-oil fractions from Hendrick Station, Texas.

The molecular-structure properties obtained from characterization data can be used to calculate constants for an equation of state. The Redlich-Kwong-Soave equation is used to calculate phase equilibria for systems containing characterized high-boiling fossil-fuel distillate fractions. Limited experimental data for a few petroleum fractions indicate that calculated vapor pressures using structural data are comparable to those using specific gravity and normal boiling point. The additional use of one boiling-point datum improves the accuracy of vapor-pressure calculations by an order of magnitude. The results of this study suggest that, for petroleum fractions, structural data for characterization do not provide significantly improved correlation of vapor pressures when that correlation is based on a simple model like the Soave equation. For effective use of structural characterization data, it may be advantageous to direct attention to coal-derived liquids and to base correlations on a molecular model more suitable for mixtures of large molecules.

3. Phase Equilibria for Strongly Nonideal Mixtures from an Equation of State with Density-Dependent Mixing Rules (Publication 17)

D. Ludecke† and J.M. Prausnitz

An equation of state of the van der Waals form represents vapor-liquid and liquid-liquid equilibria in binary, particularly aqueous, mixtures. The Mansoori-Carnahan-Starling expression is used for the repulsive part of the equation of state, while the attractive part uses a simple van der Waals form. For a mixture, the usual (density-independent) quadratic mixing rule is used for the leading attractive term, but a density-dependent correction is added to allow for noncentral intermolecular forces of dissimilar components at high densities. This procedure gives the necessary quadratic mole-fraction dependence of the second virial coefficient at low densities but also includes cubic terms for representation of phase equilibria at liquid-like densities. Good results are obtained for vapor-liquid and liquid-liquid equilibria in binary systems containing water, hydrocarbons, phenol, pyridine, and methanol. However, extension to liquid-liquid equilibria in ternary systems is not successful, because the equation of state is not able to properly represent phase equilibria of binary systems at conditions only slightly removed from binary liquid-phase instability. At these conditions, the equation of state erroneously predicts a two-liquid region. For further progress toward application of equations of state to ternary liquid-liquid equilibria, it will be necessary to introduce some fundamental modifications toward better representation of phase behavior in the critical region.

† Present address: Lehrstuhl für Metallurgie der Kernbrennstoffe und Theoretische Hüttenkunde, Technische Hochschule Aachen, West Germany.

4. Solubilities of Nonpolar Solutes in Water and Methanol (Publication 19)

J.O. Wong and J.M. Prausnitz

Since many chemical processes are concerned with dilute solutions in water or methanol, an analytical correlation of solubilities may be useful for computer-aided design. Such a correlation is presented here. Based on a perturbed-hard-sphere equation of state, this correlation gives Henry's constants for nonpolar solutes over a wide temperature range. Unlike most other correlations of solubilities, the one presented here correctly reproduces the often-observed maximum when Henry's constant is plotted against temperature.

5. A Simple Equation of State of the van der Waals Form (Publication 20)

J.O. Wong and J.M. Prausnitz

When the Carnahan-Starling equation of state for hard spheres is combined with a simple attractive term, the molecular-size parameter b for argon (as obtained from critical data) is much closer to the "correct" value than that obtained from the empirical Redlich-Kwong equation.

For the critical isotherm for argon, the best simple form of the attractive term lies between the two common forms, proposed by van der Waals and by Redlich. At constant temperature, the attractive contribution to the compressibility factor is proportional to $(v + 0.2b)^{-1}$, where v is the molar volume. This proportionality is in agreement with results for a square-well fluid recently reported by Sandler.

6. Donor-Number Estimation via Proton NMR Shift of Chloroform (Publication 15)

S. Hahn,[†] W.M. Miller, R.N. Lichtenthaler,[‡] and J.M. Prausnitz

A linear correlation was determined between the proton NMR shift of chloroform, dilute in a solvent, and the donor number (DN) of that solvent. Results are given for water and for 14 organic solvents. The best straight line is given by $\Delta\delta_{CHCl3} = 0.2575 - 0.0521DN$, where $\Delta\delta_{CHCl3}$ is the shift of pure chloroform relative to that of the chloroform in dilute solution. Donor numbers of several solvents were estimated from the correlation.

[†]Present address: Department of Chemical Engineering, University of Illinois, Urbana.

[‡]Present address: Physikalisch-Chemisches Institut der Universität, Heidelberg, West Germany.

7. Vapor Pressures and Saturated-Liquid Volumes for Heavy Fossil-Fuel Fractions from a Perturbed-Hard-Chain Equation of State (Publication 18)

A. Wilhelm[†] and J.M. Prausnitz

A semitheoretical equation of state is used to correlate residual thermodynamic properties of heavy hydrocarbons. The correlation requires three characteristic molecular parameters obtained from liquid-density and vapor-pressure data. These parameters are presented for 61 hydrocarbons with molecular weights to 560 g/mole; they are correlated with molecular weight and structural features. The correlation is extended to narrow-boiling fractions; molecular parameters for such fractions are obtained from experimental characterization data (molecular weight, aromaticity, naphthenicity, and number of methyl groups per molecule). Calculated vapor pressures and liquid densities are in reasonable agreement with new experimental results obtained from Belridge crude oil. The correlation can probably be improved through better characterization data obtained, for example, from carbon-13 NMR spectra.

[†]Present address: Lurgi Kohle- und Mineraloeltechnik GmbH, 6000 Frankfurt, West Germany.

8. Molecular Thermodynamics of Gas Solubility (Publication 16)

Y. Hu,[†] Y.N. Xu,[†] and J.M. Prausnitz

A molecular-thermodynamic model has been established for the solubilities of gases in nonpolar and polar solvents and in aqueous solutions of electrolytes. To obtain an expression for the Helmholz energy of the mixture, the pure components are first mixed isothermally to form an ideal gas mixture. Then each particle in the mixture is inflated into a hard sphere. Finally, all particles are charged with an appropriate potential to form a real liquid mixture; this charging step is based on an ordered first coordination shell and a random mixture beyond that first shell. This model agrees well with computer-simulation data. Calculated and observed

Henry's constants are in good agreement over a wide range of temperature for various gases in benzene, cyclohexane, n-hexane, hexadecane, and water, and in aqueous solutions of NaCl and KOH.

---

†Present Address: East China Institute of Chemical Technology, Shanghai, People's Republic of China.

9. Work in Progress

An apparatus has been constructed for measuring mutual solubilities and vapor pressures for liquid-liquid systems in the region ambient to 200°C. Both phases are sampled and analyzed using gas-liquid chromatography.

The apparatus has been used to obtain data for binary systems in the 100–200°C range. Special care must be taken to assure reliable sampling because mutual solubilities are very small; it is especially important to avoid entrainment, phase change (due to temperature gradients or pressure drop), and adsorption when removing samples for chemical analysis.

Experimental results have been reported for binary aqueous mixtures containing benzene, toluene, and m-xylene. New experimental results have been obtained for water-thiophene.

A semitheoretical method has been established for superimposing the residual thermodynamic properties of pure water and methane over wide ranges of pressure (0.01 to 1000 MPa) and temperature (triple point to twice the critical temperature), as reported in Publication 6. Experimental studies are now in progress. High-pressure vapor-liquid equilibria for water-methane have been measured for two temperatures (117°C and 140°C) at pressures to 870 bar.

1984 PUBLICATIONS AND REPORTS

Refereed Journals

1. E. Bender, U. Klein, W. Schmitt, and J.M. Prausnitz, "Thermodynamics of Gas Solubility: Relation Between Equation-of-State and Activity-Coefficient Models," Fluid Phase Equilibria **15**, 241 (1984); LBL-17152.
2. A. Monge and J.M. Prausnitz, "Solubilities of Heavy Fossil Fuels in Compressed Gases. Calculation of Dew Points in Tar-Containing Gas Streams," IEC Proc. Des. Dev. **23**, 226 (1984); LBL-15015.
3. D.K. Joshi and J.M. Prausnitz, "Supercritical Fluid Extraction with Mixed Solvents," AIChE J. **30**, 522 (1984); LBL-17154.
4. Y. Hu, D. Lüdecke, and J.M. Prausnitz, "Molecular Thermodynamics of Fluid Mixtures Containing Molecules Differing in Size and Potential," Fluid Phase Equilibria **17**, 217 (1984); LBL-16803.
5. Y. Hu, E. Azevedo, D. Lüdecke, and J.M. Prausnitz, "Thermodynamics of Associated Solutions: Henry's Constants for Nonpolar Solutes in Water," Fluid Phase Equilibria **17**, 303 (1984); LBL-16804.
6. E.R. Larsen and J.M. Prausnitz, "High-Pressure Phase Equilibria for the Water/Methane System," AIChE J. **30**, 732 (1984); LBL-15501.
7. R.L. Cotterman, D. Dimitrelis, and J.M. Prausnitz, "Supercritical-Fluid Extraction Calculations for High-Boiling Petroleum Fractions Using Propane. Application of Continuous Thermodynamics," Ber. Bunsenges. Phys. Chem. **88**, 796 (1984); LBL-17769.
8. G.T. Caneba, D.S. Soong, and J.M. Prausnitz, "Diffusion and Sorption of Cyclohexane Vapor in SBS and SBR Copolymers," J. Macromol. Sci.-Phys. **B22**, 693 (1984).
9. M.S. Majerus, D.S. Soong, and J.M. Prausnitz, "Experimental Measurements and Monte-Carlo Simulation of Water Diffusion into Epoxy Matrices," J. Appl. Polymer Sci. **29**, 2453 (1984).

LBL Reports

10. G.L. Alexander, A.L. Creagh, and J.M. Prausnitz, "Phase Equilibria for High-Boiling Fossil-Fuel Distillates 1. Characterization," submitted to IEC Fund.; LBL-18806.
11. G.L. Alexander, B.J. Schwarz, and J.M. Prausnitz, "Phase Equilibria for High-Boiling Fossil-Fuel Distillates 2. Correlation of Equation-of-State Constants with Characterization Data for Phase-Equilibrium Calculations," submitted to IEC Fund.; LBL-18807.
12. F.E. Anderson and J.M. Prausnitz, "Mutual Solubilities and Vapor Pressures for Hydrocarbon-Water Systems," LBL-17333.
13. R.L. Cotterman, R. Bender, and J.M. Prausnitz, "Phase Equilibria for Mixtures Containing Very Many Components. Development and Application of Continuous Thermodynamics," accepted by IEC Proc. Des. Dev.; LBL-16940.
14. R.L. Cotterman and J.M. Prausnitz, "Flash Calculations for Continuous or Semi-Continuous Mixtures Using an Equation of State," accepted by IEC Proc. Des. Dev.; LBL-17770.
15. S. Hahn, W.M. Miller, R.N. Lichtenthaler, and J.M. Prausnitz, "Donor Number Estimation via Proton NMR Shift of Chloroform," submitted to J. Solution Chem.; LBL-18305.

16. Y. Hu, Y.N. Xu, and J.M. Prausnitz, "Molecular Thermodynamics of Gas Solubility," submitted to Fluid Phase Equilibria; LBL-18765.
17. D. Ludecke and J.M. Prausnitz, "Phase Equilibria for Strongly Nonideal Mixtures from an Equation of State with Density-Dependent Mixing Rules," submitted to Fluid Phase Equilibria; LBL-18269.
18. A. Wilhelm and J.M. Prausnitz, "Vapor Pressures and Saturated-Liquid Volumes for Heavy Fossil-Fuel Fractions from a Perturbed-Hard-Chain Equation of State," accepted by Fuel; LBL-18757.
19. J.O. Wong and J.M. Prausnitz, "Solubilities of Nonpolar Solutes in Water and in Methanol," LBL-18164.
20. J.O. Wong and J.M. Prausnitz, "Comments Concerning a Simple Equation of State of the van der Waals Form," submitted to Chem. Eng. Comm.; LBL-18460.

Invited Talks

21. J.M. Prausnitz, "Creativity in Chemical Engineering Education," American Institute of Chemical Engineers Meeting, Atlanta, Georgia, March 1984.
22. J.M. Prausnitz, "Molecular Thermodynamics for Chemical Process Design," Georgia Institute of Technology, Atlanta, March 1984; Lindsay Memorial Lecture, Texas A&M University, College Station, April 1984; Warren McCabe Memorial Lecture, North Carolina State University, Raleigh, December 1984.
23. J.M. Prausnitz, "Molecular Thermodynamics: A Bridge Between Chemistry and Chemical Engineering," Keynote Address, Annual Meeting of the Council for Chemical Research, Oakland, California, September 1984.
24. J.M. Prausnitz, "Thermodynamics of Complex Fluid Mixtures," Chemical Engineering Department Colloquium, University of California Berkeley, February 1984.
25. J.M. Prausnitz, "Equations of State from Generalized van der Waals Theory," Symposium in Memory and Appreciation of Otto Redlich, American Institute of Chemical Engineers Annual Meeting, San Francisco, California, November 1984.

Nuclear Sciences

LOW-ENERGY NUCLEAR SCIENCES

HEAVY-ELEMENT CHEMISTRY

Actinide Chemistry*

Norman M. Edelstein, Richard A. Andersen, Neil Bartlett, John G. Conway, Kenneth N. Raymond, Glenn T. Seaborg, Andrew Streitwieser, Jr., David H. Templeton, and Allan Zalkin, Investigators

INTRODUCTION

The purpose of this project is to study actinide materials in order to provide the basic knowledge necessary for their safe and economic use in present and future technology. The program includes the preparation of new gaseous, liquid, and solid phases and studies of their physical and chemical properties. Techniques for characterization include x-ray diffraction, optical and vibrational spectroscopy, magnetic resonance, and magnetic susceptibility. Equilibrium and kinetic data for complex formation are measured. From these complementary studies, new insights into the structural and chemical principles of actinide compounds are obtained with which to design new synthetic schemes to produce new materials.

A major aspect of the program is the design and synthesis of sequestering agents for actinide ions. These compounds are intended for use in the treatment of actinide poisoning and for possible application in the treatment of spent reactor fuels. Preparative, structural, and physical studies of new types of organoactinide, related organolanthanide, and new actinide inorganic complexes are continuing. Studies on optical spectra of free ions and actinide ions in crystals are being pursued in order to understand their electronic structure.

SPECIFIC SEQUESTERING AGENTS FOR THE ACTINIDES

1. Actinide-Specific Complexing Agents: Their Structural and Solution Chemistry (Publication 1)

Kenneth N. Raymond, Gwen E. Freeman, and Mary J. Kappel

The synthesis of a series of tetracatecholate ligands designed to be specific for Pu(IV) and other actinide(IV) ions is reviewed. Spectroscopic results indicate that the tetracatecholates 3,4,3-LICAM(S) [N^1,N^5,N^{10},N^{14}-tetrakis(2,3-dihydroxy-4-carboxybenzoyl)tetraazatetradecane, tetrasodium salt] and 3,4,3-LICAM(C) [N^1,N^5,N^{10},N^{14}-tetrakis(2,3-dihydroxy-5-sulfobenzoyl)tetraazatetradecane, tetrasodium salt] (see Figure 1-1) form complexes with Am(III). The Am(IV)/(III)-catecholate couple (where the catecholate is 3,4,3,-LICAM(S) or 3,4,3-LICAM(C)) is not observed, but it may not be observable due to the large currents associated with ligand oxidation.

*This work was supported by the Director, Office of Energy Research, Office of Basic Energy Sciences, Chemical Sciences Division of the U.S. Department of Energy under Contract No. DE-AC03-76SF00098.

However, within the potential range where ligand oxidation does not occur, these experiments indicate that the reduction potential of free Am(IV)/(III) is probably ≥ +2.6 V vs. normal hydrogen electrode or higher. Proof of the complexation of americium in the trivalent oxidation state by 3,4,3-LICAM(S) and 3,4,3-LICAM(C) eliminates the possibility that the tetracatecholates stabilize Am(IV) *in vivo*.

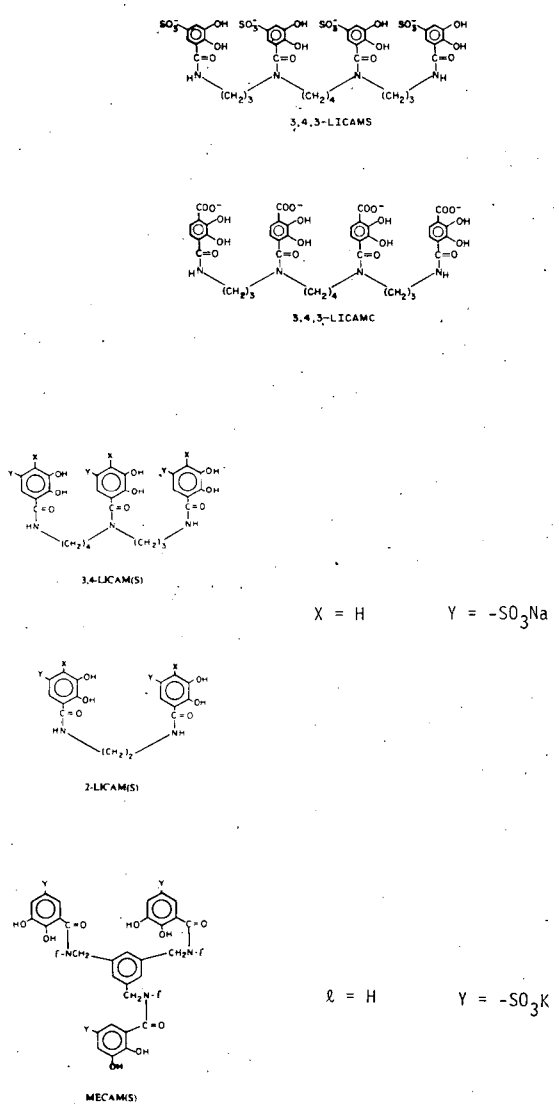

Figure 1-1. Structures of 3,4,3-LICAM(S) (shown as 3,4,3-LICAMS), 3,4,3-LICAM(C) (shown as 3,4,3-LICAMC), 3,4-LICAM(S), 2-LICAM(S), and MECAM(S). (XBL 8412-5440)

2. Specific Sequestering Agents for the Actinides: 10. Enhancement of ^{238}Pu Elimination from Mice by Poly(catechoylamide) Ligands (Publication 2)†

Patricia W. Durbin, Nylan Jeung, E. Sarah Jones, Frederick L. Weitl, and Kenneth N. Raymond

Macromolecules containing four sulfonated catechoyl (2,3-dihydroxybenzoyl) groups are effective for decorporation of newly acquired Pu(IV). However, multiple injections in mice and single injections in dogs of 30 μmole/kg of 3,4,3-LICAM(S) (see Figure 1-1), the most effective sulfonated poly(catechoylamide) ligand, indicated that it would be toxic, so the ligand structure was modified. Each ligand was injected into mice (30 μmole/kg, intraperitoneally) one hour after an intravenous (iv) injection of ^{238}Pu(IV) citrate. The mice were killed 24 hours after the Pu injection. Excreta and tissues were analyzed for Pu by the following methods: (1) The number of catechoyl groups per molecule was reduced to suppress affinity for Fe(III). Net excretion (treated minus control) of 55% of the injected Pu was promoted by tetrameric 3,4,3-LICAM(S) (see Figure 1-1), with 51% promoted by trimeric 3,4-LICAM(S), 22% by dimeric 2-LICAM(S), and 7.4% by the monomer Tiron. (2) A mesitylene platform was substituted for the linear backbone. Net Pu excretion promoted by MECAM(S) (see Figure 1-1), a structurally less flexible trimer, was only 26%, and excretion was delayed. (3) A carboxyl substituent on the catechoyl groups reduced the acidity and hydrophilicity of the ligands. Tetrameric 3,4,3-LICAM(C) (see Figure 1-1) promoted 63% net Pu excretion, and one-third of the excretion was fecal. The Pu contents of liver and skeleton were 33% and 44% of their respective 1-hour control value compared to 51% and 44%, respectively, for $CaNa_3$-DTPA. Mice given 30 μmole/kg of 3,4,3-LICAM(C) 20 times in 4 weeks showed no ill effects. (4) Large N-terminal alkane substituents added to 3,4,3-LICAM(C) increased ligand lipophilicity, hindered Pu chelation, and delayed excretion.

†Biological investigations supported by National Cancer Institute (NCI) Grant NCI CAN 1-8422552 (1981) and National Institute of Environmental Health Sciences grants ESO2698-01 and ESO2698-02 (1982-).

3. Removal of Pu and Am from Beagles and Mice by 3,4,3-LICAM(C) or 3,4,3-LICAM(S) (Publication 3)†

R.D. Lloyd, F.W. Bruenger, C.W. Mays, D.R. Atherton,‡ C.W. Jones, G.N. Taylor, W. Stevens,§ P.W. Durbin, N. Jeung, E.S. Jones, M.J. Kappel, K.N. Raymond, and F.L. Weitl

Decorporation of Pu and Am by tetrameric catechoylamide (CAM) ligands has been investigated in beagles and mice. Eight dogs were injected iv with $^{237+239}$Pu(IV) + ^{241}Am(III) citrate; 30 minutes later, pairs of dogs were injected iv with 30 μmole/kg of 3,4,3-LICAM(C), 3,4,3-LICAM(S) (see Figure 1-1), $CaNa_3$-DTPA, or each of the latter two ligands. Blood was sampled and excreta were collected for 7 days, at which time the dogs were sacrificed and nuclide retention in liver and nonliver tissue was measured. Groups of five mice were each given ^{238}Pu(IV) or ^{241}Am(III) citrate iv; 3 minutes later 30 μmole/kg of a CAM ligand was injected intraperitoneally. The mice were killed at 24 hours, and separated excreta and tissues were analyzed. In the dogs, the average retention at 7 days of the injected Pu and Am, respectively, was as follows: 12% and 70% after treatment with a CAM ligand alone; 30% and 20% after DTPA treatment; 12% and 20% after LICAM(S) plus DTPA treatment; and 90% and 89% without a ligand. In the mice, mean retention of the injected Pu and Am, respectively, was as follows: 14% and 66% after treatment with LICAM(C); 21% and 54% after LICAM(S); and 91% and 87% without a ligand. In both species, about 99% of net Pu excretion (excretion with ligand minus excretion without ligand) promoted in 24 hours by DTPA or LICAM(S) was in the urine, where about 10% of net Pu excretion promoted by the less hydrophilic LICAM(C) was in the feces. Delayed excretion of both Am and Pu was significant in all ligand-treated dogs. Comparison of the nuclide content of tissues of ligand-treated mice with those of mice killed 3 minutes after nuclide injection indicated that the CAM ligands chelated circulating Pu and Am and prevented further deposition. In addition, the CAM ligands removed much of the presumably loosely bound Pu present in liver and skeleton at the time of ligand injection. LICAM(C) was more effective in removing Pu from the liver, and LICAM(S) was more effective in removing Pu from the skeleton. Moderate to severe uremia and histological evidence of cell killing in the distal tubules of the kidney were observed in the four dogs injected once with 30 μmole/kg of LICAM(S). However, blood urea nitrogen levels were normal, and no lesions were found in any tissue of two dogs given one injection or mice given 20 injections of 30 μmole/kg of LICAM(C). LICAM(C) is less acidic than LICAM(S), which reduces its ability to chelate Fe(III) at the pH of tubular urine, and its lesser hydrophilicity allows diversion of some ligand to the gastrointestinal tract and away from the kidneys.

---

†Supported by National Cancer Institute (NCI) Grant 1 RO1 CA28314-01, U.S. Department of Energy Contract DE-AC02-76EV00119, NCI Grant NCI CAN 1-8422552, and National Institute of Environmental Health Sciences grants ESO2698-01 and ESO2698-02.

‡Deceased.

§Present address: Radiobiology Laboratory, University of Utah, Salt Lake City, Utah 84112.

SYNTHETIC AND STRUCTURAL STUDIES OF ACTINIDES AND OTHER COMPOUNDS

4. Preparation of $[Yb(C_5Me_5)_2]_2[Co_3(C_5H_4R)_2(\mu_3\text{-}CO)_4]$, where R = H, Me, or $SiMe_3$; An Example of a Hexagonal-Planar, 47-Electron Transition-Metal Fragment (Publication 8)

J.M. Boncella and R.A. Andersen

The divalent ytterbium metallocene $(Me_5C_5)_2Yb(OEt_2)$ reacts with $(RC_5H_4)Co(CO)_2$ (R = H, Me, or $SiMe_3$), an eighteen-electron, mononuclear transition-metal carbonyl, to give the unusual compounds of composition $[(Me_5C_5)_2Yb]_2[(RC_5H_4)_2Co_3(CO)_4]$. The crystal structure of the derivative where R = $SiMe_3$ is shown in the Figure 4-1. The other derivatives are presumably similar since they show a single ν(CO) at ~1570 cm^{-1}. The averaged Yb-C distance of 2.59(2) Å, and the paramagnetism μ(5-30 K) = 4.5 B.M., show that the ytterbium atoms are trivalent and the electron-transfer process results in a novel cluster-forming reaction. The cluster fragment $[(RC_tH_4)_2Co_3(CO)_4]^{=}$ is an example of a planar, 47-electron cluster.

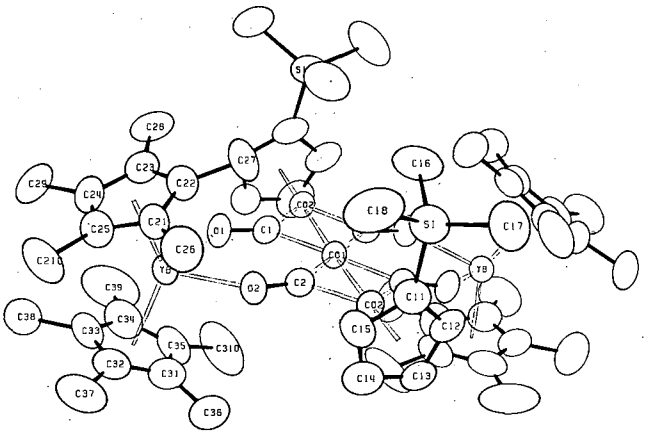

Figure 4-1. ORTEP drawing of the compound $[(Me_5C_5)_2Yb]_2[(RC_5H_4)_2Co_3(CO)_4]$, where R = $SiMe_3$.
(XBL 826-10527)

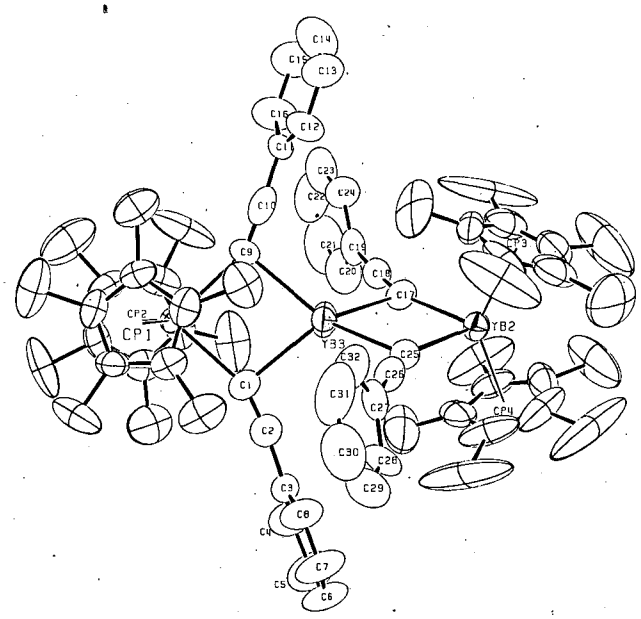

Figure 5-1. ORTEP drawing of the complex $(Me_5C_5)_4Yb_3(\mu\text{-}C{\equiv}CPh)_4$.
(XBL 832-8247)

5. Reaction of $M(C_5Me_5)_2(OEt_2)$, where M = Eu or YB, with Phenylacetylene; Formation of Mixed-Valence $Yb_3(C_5Me_5)_4(\mu\text{-}C \equiv CPh)_4$ and $Eu_2(C_5Me_5)_2(\mu\text{-}C \equiv CPh)_2(thf)_4$ (Publication 7)

J.M. Boncella, T.D. Tilley, and R.A. Andersen

The divalent ytterbium metallocene $(Me_5C_5)_2Yb(OEt_2)$ reacts with phenylacetylene to give the novel mixed-valence complex $(Me_5C_5)_4Yb_3(\mu\text{-}C{\equiv}CPh)_4$. The crystal structure of the complex is shown in Figure 5-1. This complex is the only molecular mixed-valence complex of a lanthanide molecule that has ever been described. The terminal ytterbium atoms are trivalent, and the central ytterbium atom is divalent. Magnetic-susceptibility studies show that the complex is a trapped-valence compound; i.e., there is no electron exchange between the Yb(III) centers. By way of contrast, the divalent europium metallocene $(Me_5C_5)_2Eu(OEt_2)$ does not undergo an electron-transfer reaction with phenylacetylene, but instead it simply undergoes a ring-substitution reaction to give $(Me_5C_5)_2Eu_2(\mu\text{-}C{\equiv}CPh)_2(thf)_4$. The crystal structure of this compound is shown in Figure 5-2.

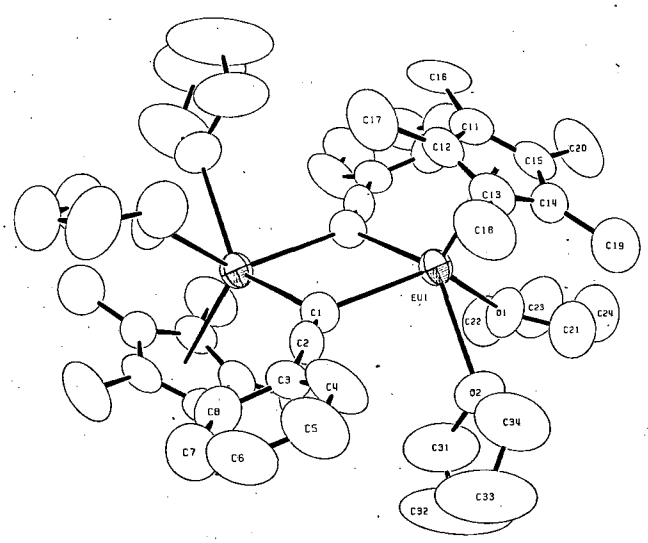

Figure 5-2. ORTEP drawing of the complex $(Me_5C_5)_2Eu_2(\mu\text{-}C{\equiv}CPh)_2(thf)_4$.
(XBL 832-8246)

6. Preparation of $Yb[N(SiMe_3)_2]_2(AlMe_3)_2$; A Complex with Four Yb-Me-Al Interactions (Publication 26)

J.M. Boncella and R.A. Andersen

Two molar equivalents of trimethylaluminum react with $Yb_2[N(SiMe_3)_2]_2[\mu\text{-}N(SiMe_3)_2]_2$ in pentane to give yellow crystals of $Yb[N(SiMe_3)_2]_2(AlMe_3)_2$. The crystal structure is shown in Figure 6-1. The structure may be analyzed in the following way. The lone pair of electrons on each of the silylamido groups acts as a Lewis base toward each Me_3Al unit. Two methyl groups on each aluminum atom [C(1), C(2), C(5), and C(6)] then form four three-center/two-electron bridge bonds between the aluminum and ytterbium atom. The Al-C distances range from 2.009(2) to 2.029(1) Å, and the Yb-C distances range from 2.756(2) to 3.202(3) Å. In addition the carbon atoms C(12, 21) on Si(1, 2) also form bridge bonds with the ytterbium atom, with a Yb-C distance of 3.039(2) and 3.067(2) Å. Thus the molecule is eight coordinate, though the geometry is greatly distorted from any regular polytopyl form.

7. Electron-Transfer Reactions of Trivalent Uranium; Preparation and Structure of $(MeC_5H_4)_3U{=}NPh$ and $[(MeC_5H_4)_3U]_2(\mu\text{-}\eta^1,\eta^2\text{-}PhNCO)$ (Publication 27)

J.G. Brennan and R.A. Andersen

The trivalent uranium metallocene $(MeC_5H_4)_3U(thf)$ undergoes an electron-transfer reaction with phenylisocyanate to give the molecule $[(MeC_5H_4)_3U]_2(\mu\text{-}\eta^1,\eta^2\text{-}PhNCO)$ based on tetravalent uranium. The crystal structure is shown in Figure 7-1. (The MeC_5H_4 groups are omitted for clarity.) More interestingly, phenyl- or trimethylsilyl-azide reacts with $(MeC_5H_4)_3U(thf)$ to give the novel complexes $(MeC_5H_4)_3U{=}NR$, where R = Ph or $SiMe_3$, the result of a two-electron transfer process. The crystal structure is shown in Figure 7-2 (one ring, C(19)-C(23), is disordered). This novel complex is the first example of a pentavalent uranium organoimide that has been prepared. The U-N distance of 2.019(6) Å is the shortest U-N distance ever found. The near-linear U-N-C(1) angle of 167.4(6)° suggests that the U-N bond is a triple bond and that it should be formulated as $U{\leftrightarrows}\ddot{N}R$.

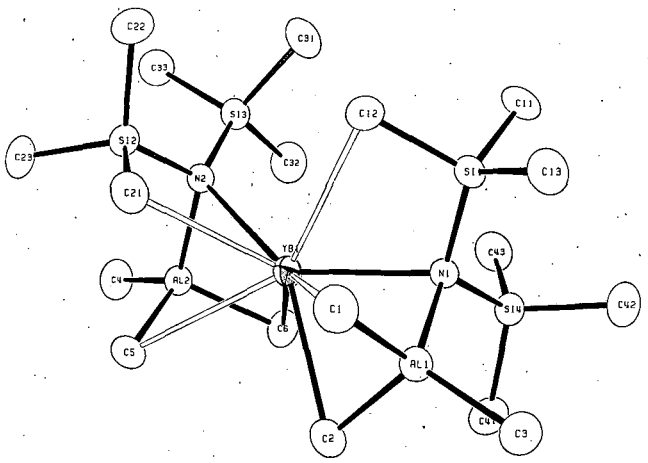

Figure 6-1. ORTEP drawing of the complex $Yb[N(SiMe_3)_2]_2(AlMe_3)_2$. (XBL 847-3160)

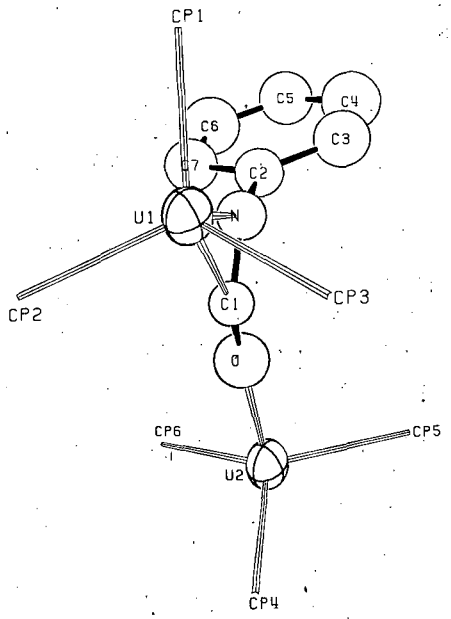

Figure 7-1. ORTEP drawing of the complex $[(MeC_5H_4)_3U]_2(\mu\text{-}\eta^1,\eta^2\text{-}PhNCO)$. (XBL 847-3149)

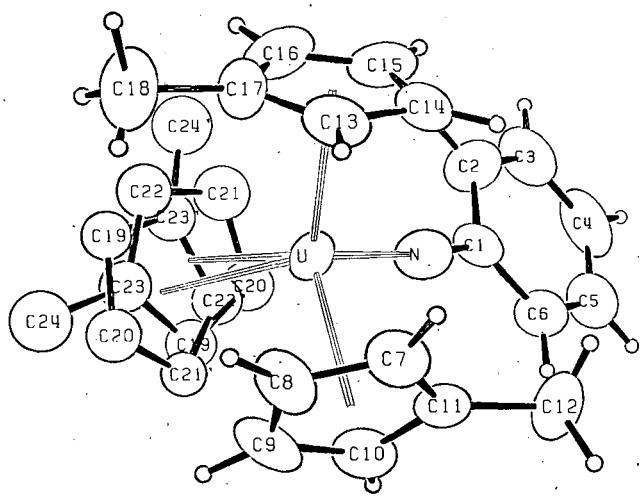

Figure 7-2. ORTEP drawing of the complex $(MeC_5H_4)_3U{=}NR$. (XBL 847-3151)

8. Cerocene, di-π-[8]annulenecerium(IV) (Publication 46)

Andrew Streitwieser, Jr., Steven A. Kinsley, Robert M. Moore, Jr., and John Rigsbee

The synthesis of cerocene, di-π-[8]annulenecerium(IV), by Greco, Cesca, and Bertolini[1] has been reproduced. Conversion of bis[8]-annulenecerate(III) ion to cerocene has been accomplished electrochemically, and by chemical oxidation with nitrosyl fluoroborate, oxygen, and silver ion. Cerocene reacts slowly with UCl_4 to give uranocene; this behavior is similar to that of thorocene and unlike the di-π-[8]annulenelanthanate(III) anions that react rapidly with UCl_4. Cerocene also hydrolyzes in wet thf more slowly than thorocene to produce a mixture of 80% 1,3,5- and 20% 1,3,6-cyclooctatrienes. A sample of cerocene was sent to Professor I. Fragala, University of Catania, Italy, for measurement of the photoelectron spectrum and comparison with the Xα computation of Rösch.[2] The results, summarized in Table 8-1, show excellent agreement and indicate substantial ring-metal covalency in cerocene involving 4f orbitals.

Table 8-1
Ionization energies of cerocene

Band label	Ionization Energy (I.E.) (eV)	ΔI.E. (eV)	Xα Transition-State Energy[1] (eV)	Xα ΔE (eV)
a	6.75	0	6.31 (e_{2u})	0
a′	6.92[a]	-	-	-
b	7.68	0.93	7.20 (e_{2g})	0.89
b′	(7.81)[a]	-	-	-
e	9.98	3.23	9.42 (e_{1u})	3.11
e′	10.32	3.57	9.84 (e_{1g})	3.53

a. Fine structure; shoulders are in parentheses.

1. A. Greco, S. Cesca, and G. Bertolini, J. Organometal. Chem. **113**, 321 (1976).
2. N. Rösch and A. Streitwieser, Jr., J. Am. Chem. Soc. **105**, 7237 (1983); N. Rösch, Inorg. Chim. Acta. **94**, 297 (1984).

9. [8]annulene Derivatives of Actinides and Lanthanides (Publication 29)

Andrew Streitwieser, Jr., and Steven A. Kinsley

A number of [8]annulene actinide and lanthanide compounds are now known at oxidation levels of the central metal of +2, +3, and +4. Several structures have been established for these compounds. The [8]annulene ring is generally present as a planar octagonal ring of carbons with the metal centrally located. Many structures are those of sandwich compounds with the metal located between parallel rings. The original system, uranocene, is the most stable and the most thoroughly studied of these compounds. Only limited chemistry has been explored so far with these systems; in the sandwich compounds the large rings hinder coordination at the central metal. Uranocene is paramagnetic and shows a wide range of ^1H chemical shifts that have been

particularly useful in studies of structure and electronic structure. Especially valuable are derived barriers for a number of dynamic processes. These energies provide significant new information concerning intramolecular interactions.

10. The Disordered Structure of Dibenzouranocene (Publication 22)

A. Zalkin, D.H. Templeton, R. Kluttz, and A. Streitwieser, Jr.

Crystals of $[C_8H_6(C_4H_4)]_2U$ are monoclinic, $P2_1/c$, with cell dimensions a = 9.524(4) Å, b = 8.558(4) Å, c = 11.758(6) Å, β = 113.52(4)°, Z = 2, and R = 0.052 for 944 observed reflections. The uranium atom is sandwiched by two planar benzo-[8]annulene ligands (see Figure 10-1) that are about 6° from an eclipsed configuration. The molecules pack in the crystal in a disordered manner, with the uranium atom sometimes on one side of the center of symmetry and sometimes on the other.

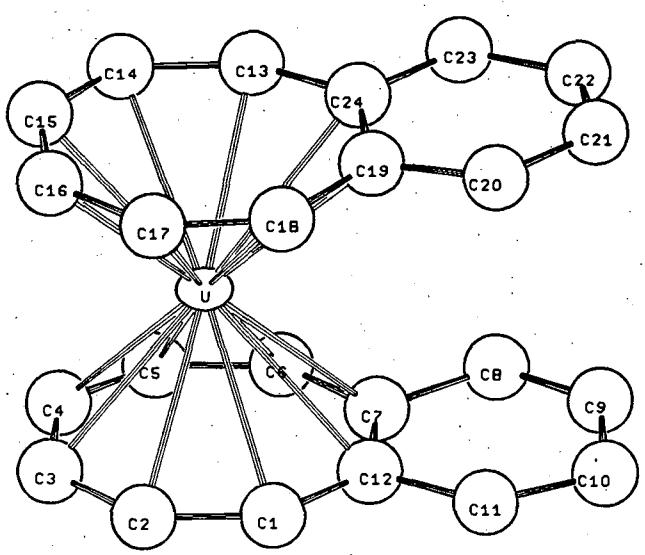

Figure 10-1. Molecular structure of dibenzouranocene. (XBL 816-10255)

11. The Structure of Tris(methylcyclopentadienyl)uranium(III)trimethylphosphine, $(CH_3C_5H_4)_3U.P(CH_3)_3$ (Publication 23)

J.G. Brennan and A. Zalkin

Crystals of $(CH_3C_5H_4)_3U.P(CH_3)_3$ are monoclinic, Cc, with cell dimensions a = 13.949(5) Å, b = 9.280(4) Å, c = 16.194(6) Å, and β = 104.09(4)°. For Z = 4, D_x = 1.80 g/cm^3. The structure is refined to an R factor of 0.024 for 1568 reflections. The structure consists of uranium-centered monomolecular units in which the uranium atom is coordinated in a pentahapto fashion to three cyclopentadiene rings and to the phosphorus atom of the trimethylphosphine molecule (see Figure 11-1). The average U-C distance is 2.79 ± 0.06 Å, and the U-P distance is 2.972(6) Å.

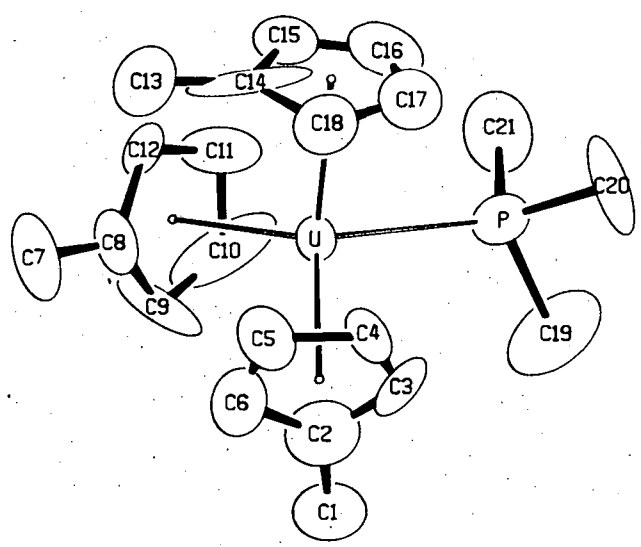

Figure 11-1. ORTEP drawing of tris(methylcyclopentadienyl)-uranium(III)trimethylphosphine. (XBL 853-1493)

12. Tertiary Phosphine Complexes of Tetravalent and Trivalent Uranium Methyltrihydroborates; the Crystal Structures of Tetrakis(methyltrihydroborato)uranium(IV)1,2-dimethylphosphinoethane and Tris(methyltrihydroborato)uranium(III)bis(1,2-dimethylphosphinoethane) (Publication 24)

J. Brennan, R. Shinomoto, A. Zalkin, and N.M. Edelstein

$(CH_3BH_3)_4U[(CH_3)_2PCH_2CH_2P(CH_3)_2]$ (see Figure 12-1) and $(CH_3BH_3)_3U[(CH_3)_2PCH_2CH_2P(CH_3)_2]_2$ (see Figure 12-2) have been synthesized and their molecular structures determined by single-crystal x-ray diffraction. The space groups, unit cell parameters, and R factors are as follows: $(CH_3BH_3)_4U[(CH_3)_2PCH_2CH_2P(CH_3)_2]$ is monoclinic, $P2_1/c$, with a = 9.439(3) Å, b = 14.023(4) Å, c = 16.596(2) Å, β = 97.48(4)°, Z = 4, D_x = 1.536 g/cm^3, and R = 0.024 for 3976 reflections. $(CH_3BH_3)_3U[(CH_3)_2PCH_2CH_2P(CH_3)_2]_2$ is tetragonal, $P4_32_12$, with a = 11.297(4) Å, c = 23.03(2) Å, Z = 4, D_x = 1.412 g/cm^3, and R = 0.024 for 1960 reflections. Both complexes are unimolecular in the crystalline state. The uranium(IV) atom is coordinated to four BH_3CH_3 groups through tridentate hydrogen bridges, and to two P atoms of the $(CH_3)_2PCH_2CH_2P(CH_3)_2$ ligand. The uranium(III) complex is coordinated to three BH_3CH_3 groups through tridentate bridges, and to four P atoms from the $(CH_3)_2PCH_2CH_2P(CH_3)_2$ ligands. The U-B distances for the U(IV) and U(III) complexes average 2.57 ± 0.01 Å and 2.63 ± 0.02 Å, respectively; the U-P distances for the U(IV) and U(III) complexes average 3.02 ± 0.01 Å and 3.13 ± 0.06 Å, respectively.

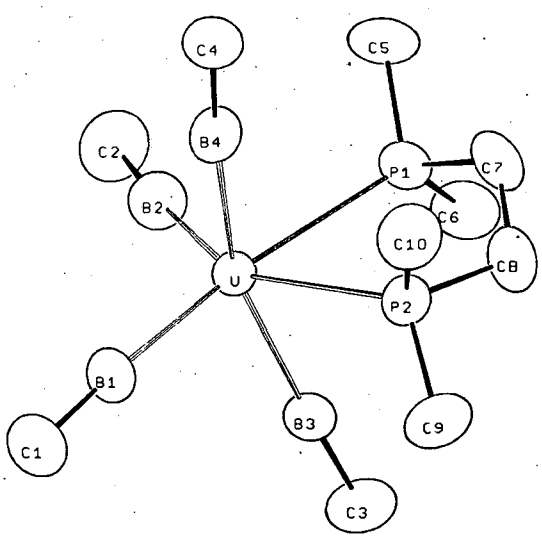

Figure 12-1. ORTEP drawing of $U(BH_3CH_3)_4.DMPE$. (XBL 834-9360)

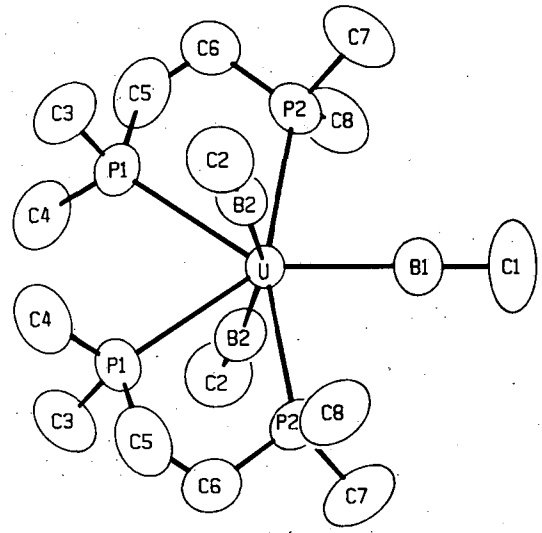

Figure 12-2. ORTEP drawing of $U(BH_3CH_3)_3.(DMPE)_2$. (XBL 841-8)

13. Bridging of Thorium by Hydrogen Atoms of Methyltrihydroborate Groups; The Crystal Structures of Bis[tetra(methyltrihydroborato)-thorium(IV)]etherate and Bis[tetra(methyltrihydroborato)thorium(IV)tetrahydrofuranate] (Publication 25)

R. Shinomoto, J.G. Brennan, N.M. Edelstein, and A. Zalkin

Dimeric complexes of $Th(CH_3BH_3)_4$ with diethyl ether and tetrahydrofuran have been synthesized and the molecular structures determined by x-ray diffraction. $[Th(BH_3CH_3)_4]_2.O(C_2H_5)_2$ (see Figure 13-1) is monoclinic, $P2_1/c$, with cell dimensions a = 20.163(5) Å, b = 10.353 Å, c = 14.583(3) Å, β = 104.47°, Z = 4, D_x = 1.73 g/cm^3, and R = 0.024 for 2265 reflections. $[Th(BH_3CH_3)_4.OC_4H_8]_2$ (see Figure 13-2) is monoclinic, $P2_1/n$, with cell dimensions a = 12.506(4) Å, b = 11.533(4) Å, c = 11.662(4) Å, β =

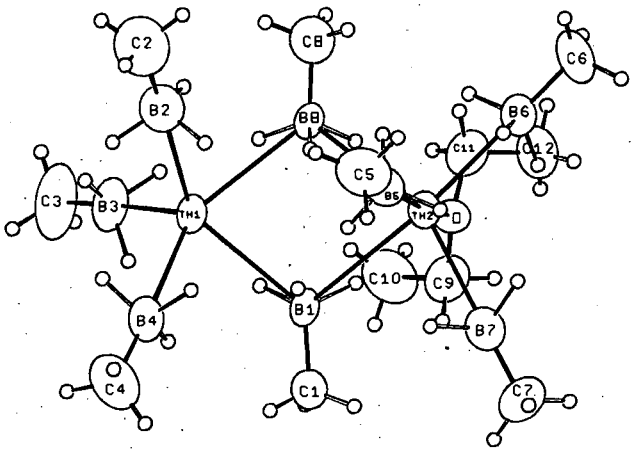

Figure 13-1. ORTEP drawing of $[Th(BH_3CH_3)_4]_2 \cdot O(C_2H_5)_2$. (XBL 835-9692)

99.06(2)°, Z = 4, D_x = 1.68 g/cm^3, and R = 0.019 for 1923 reflections. The thorium atoms are bridged by two BH_3CH_3 ligands through one of the hydrogen atoms of each BH_3 group; the Th-Th distances are 4.445(1) and 4.917(1) Å for the ether and tetrahydrofuran complexes, respectively. The Th-B distances range from 2.47 to 2.61 Å for the terminal BH_3CH_3 groups. The coordination number for Th is 13 for one of the two Th atoms in the ethyl ether complex and 14 for all the others. Nuclear-magnetic-resonance (NMR) and infrared (IR) spectroscopy suggest that the dimeric structure is not maintained in solution.

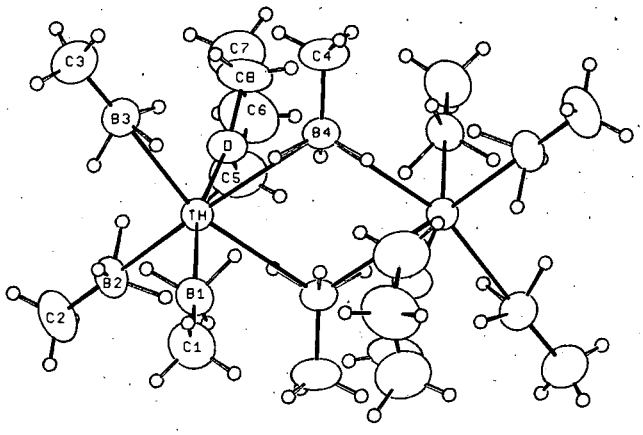

Figure 13-2. ORTEP drawing of $[Th(BH_3CH_3)_4 \cdot OC_4H_8]_2$. (XBL 835-9691)

14. Structure of Monoclinic Sodium Holmium Ethylenediaminetetraacetate Octahydrate: Disorder Induced by Radiation (Publication 38)†

L.K. Templeton, D.H. Templeton, and A. Zalkin

Crystals of the title compound appear to be orthorhombic, like the analogous salts of elements lanthanum through gadolinium, but on close inspection they are found to be monoclinic, space group Fd11, with cell dimensions a = 19.333(3) Å, b = 35.366(6) Å, c = 12.106(2) Å, α = 90.40(10)°, and R = 0.026 for 4843 reflections. The atomic positions are very similar to those in the orthorhombic crystals (space group Fdd2). The monoclinic symmetry comes from ordering of water molecules in alternate sites that are occupied randomly in the orthorhombic structure (see Figure 14-1). Exposure to x rays induces disorder that makes the crystals more nearly orthorhombic, with the angle α approaching 90°. The dysprosium compound of the same composition is also monoclinic.

†Supported in part (a salary) by the National Science Foundation.

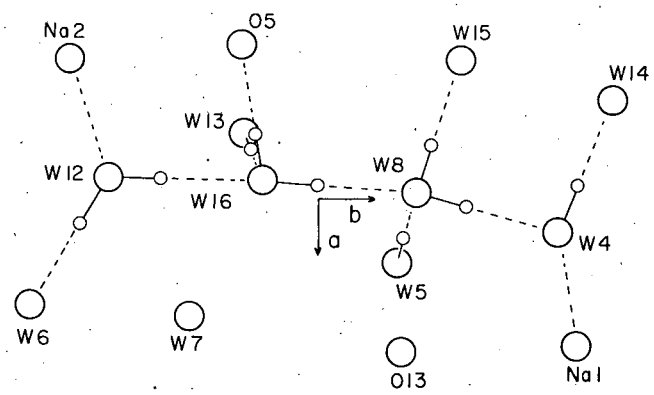

Figure 14-1. Hydrogen bonding in $NaHo(edta).8H_2O$. In the model for the radiation-induced disorder, some of the bonds to O(5) and W(15) are broken, new bonds are formed to W(7) and O(13), and the average structure approaches orthorhombic symmetry with a twofold axis at the center of the figure. (XBL 853-1494)

15. Structure of Zinc (+)-Tartrate 2.5-Hydrate, and Anomalous Scattering by Zinc (Publication 36)†

L.K. Templeton, D.H. Templeton, D. Zhang,‡ and A. Zalkin

In a search of crystals suitable for study of anomalous x-ray scattering with synchrotron radiation, crystals of this zinc salt were prepared and their structure was determined. It is orthorhombic, $P2_12_12_1$, with cell dimensions a = 11.256(3) Å, b = 18.021(7) Å, and c = 7.960(3) Å. The structure consists of cyclic double chelates (see Figure 15-1) that are linked by additional strong coordination of each zinc to a carboxyl oxygen atom of an adjacent group and further by hydrogen bonds. The average Zn-O distances are 2.040(14) Å (carboxyl), 2.158(24) Å (hydroxyl), and 2.059(4) Å (water). The anomalous scattering term f′ for zinc is measured as 1.47(3) electrons/atom for Mo Kα radiation.

†Supported in part (a salary) by the National Science Foundation.

‡On leave from Chemistry Division, East China Engineering Institute, Nanjing, Jiangsu, People's Republic of China.

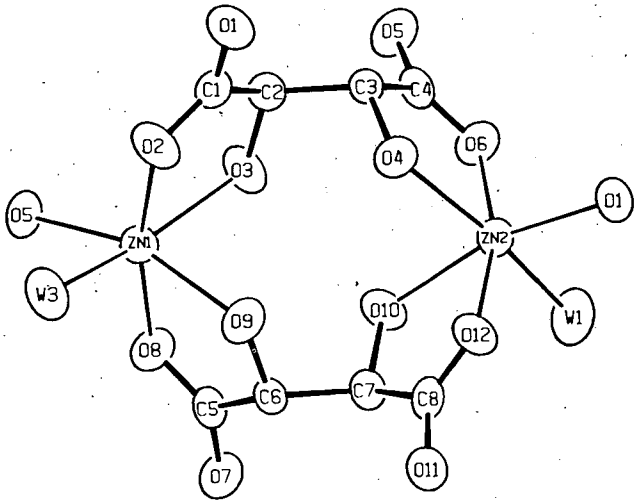

Figure 15-1. Cyclic double chelate in zinc (+)-tartrate.

(XBL 853-1487)

16. Refinement of the Trigonal Crystal Structure of Lanthanum Trifluoride with Neutron-Diffraction Data (Publication 34)

A. Zalkin and D.H. Templeton

Trigonal crystals of LaF_3 are prone to twinning by a twin law that does not affect the macroscopic optical properties or the angles at which diffraction occurs. This twinning has often escaped notice and has led to errors about the symmetry of this important structure type. In a recent report of neutron-diffraction work, Gregson et al.[1] asserted that their data ruled out the trigonal structure (space group $P\bar{3}c1$), and they refined R to 0.042 in the hexagonal space group $P6_3cm$ using 25 independent parameters. When twinning is allowed for in the calculations, R is reduced to 0.026 with only 21 parameters. This refinement confirms the structure determined earlier by x-ray diffraction and gives somewhat more precise values of the parameters.

1. D. Gregson, C.R.A. Catlow, A.V. Chadwick, G.H. Lander, A.N. Cormack, and B.E.F. Fender, Acta Cryst. B **39**, 687 (1983).

PHYSICAL AND SPECTROSCOPIC PROPERTIES

17. Uranium Spectrum Between 1.8 and 5.5 Microns Emitted from a Hollow Cathode (Publication 10)†

John G. Conway, Earl F. Worden,‡ James W. Brault,§ Robert P. Hubbard,§ and Jeremy J. Wagner§

The emission spectrum of uranium has been observed in the infrared from 1.8 to 5.5 μm using the McMath Fourier-transform spectrometer at the Kitt Peak National Observatory and a water-cooled hollow-cathode lamp. The wavenumber, wavelength, and relative intensity of 4418 lines between 1817 and 5598 cm^{-1} that can be classified as

transitions between known levels of the first and second spectra of uranium have been tabulated. In addition, wavenumbers and intensities of 4744 lines that cannot be classified in this manner are listed. Most of these are believed to be uranium-emission lines. Isotope shifts are reported for 196 lines.

†Travel expenses and E.F. Worden's salary were supported by the Lawrence Livermore National Laboratory under Contract W-7405-ENG-48.

‡Permanent address: Lawrence Livermore National Laboratory, Livermore, California 94550.

§Permanent address: Kitt Peak National Observatory, Tucson, Arizona 85726.

18. Crystal-Field Analysis of Tm^{3+} and Yb^{3+} in YPO_4 and $LuPO_4$ (Publication 11)

P.C. Becker, T. Hayhurst,† G. Shalimoff, J.G. Conway, N. Edelstein, L.A. Boatner,§ and M.M. Abraham§

The optical and near-infrared absorptions of dilute Tm^{3+} and Yb^{3+} impurities in YPO_4 and $LuPO_4$ single crystals have been measured at liquid-helium and nitrogen temperatures. For Tm^{3+}, the spectral region from 5,000 to 38,000 cm^{-1} was examined, and Zeeman spectra were obtained in the visible region. The observed transitions were assigned and fit to a semiempirical Hamiltonian with adjustable parameters via a least-squares procedure. Satisfactory fits and good agreement between the calculated and measured g values were obtained. For Yb^{3+}, there are more parameters than experimental levels, so ζ, B_0^2, B_0^4, and B_4^4 were adjusted, while B_0^6 and B_4^6 were fixed at the values found for Tm^{3+}. Energy levels and Zeeman splittings calculated with these parameters are in good agreement with the measured quantities.

†Present address: The Aerospace Corporation, Los Angeles, California 90009.

§Present address: Solid State Division, Oak Ridge National Laboratory, Oak Ridge, Tennessee 37830.

19. Future Directions in Solid-State Lanthanide and Actinide Chemistry (Publication 16)

L.R. Morss† and N. Edelstein

Recent accomplishments are reviewed, and current challenges in the syntheses and elucidation of the bonding and electronic structure of metals, inorganic compounds, and organometallic compounds containing the rare-earth and actinide elements are identified.

† Present address: Chemistry Division, Argonne National Laboratory, Argonne, Illinois.

20. Electronic Structure and Optical Spectroscopy of f^n Ions and Compounds (Publication 48)

Norman Edelstein

The electronic structure of the actinides and lanthanides is reviewed. The assignments of f^n spectra in the visible and near-infrared regions and the fitting of these spectra to the parameters of a phenomenological Hamiltonian are discussed. From the wavefunctions obtained from this type of analysis, magnetic-susceptibility data can be calculated. Examples are given from recent work on $Cp_3Ln{\cdot}L$ ($Cp = C_5H_5$, L = base) compounds. Slater and spin-orbit parameters obtained from the analyses of free-ion spectra and from the same ion in compounds are compared.

21. The Electronic Structure of Organometallic Complexes of the f Elements: IX. Assignment of the Observed Faraday A Terms in the Magnetic Circular Dichroism (MCD) Spectra of Tris(η^5-cyclopentadienyl)-praseodymium(III)adducts (Publication 31)

H.-D. Amberger, W. Jahn, and N.M. Edelstein

In the low-temperature MCD spectra of tris(η^5-cyclopentadienyl)-praseodymium(III)adducts, some Faraday A terms of positive and negative signs, respectively, could be observed. As the singlet CF ground state is of A_1 symmetry, the observed Faraday A terms are due to transitions to excited E states. From the selection rules for MCD spectroscopy, the dominant $|\pm J_z\rangle$ values in the eigenvectors of the excited E states could be determined. From this information a number of levels were assigned and a preliminary set of Slater, spin-orbit, and crystal-field parameters were derived.

22. The Electronic Structure of Organometallic Complexes of the f Elements: XI. Absorption Spectrum and Parameterization of the Crystal-Field Splitting Pattern of a Methyltetrahydrofuran Adduct Derived from Tris(η^5-cyclopentadienyl)-praseodymium(III) (Publication 30)

H.-D. Amberger, H. Schultze, and N.M. Edelstein

The low-temperature absorption spectrum of tris(η^5-cyclopentadienyl)-praseodymium(III) dissolved in a 2-methyltetrahydrofuran glass has been measured. The observed transitions, along with the previously reported MCD transitions, have been assigned and fit to the parameters of a semiempirical Hamiltonian with a root-mean-square deviation of 27.2 cm^{-1} for 40 levels. The experimental and calculated magnetic susceptibilities of Cp_3Pr·butyl acetate (which has an optical spectrum very similar to that of Cp_3Pr·Methf) as a function of temperature are also given (see Figure 22-1).

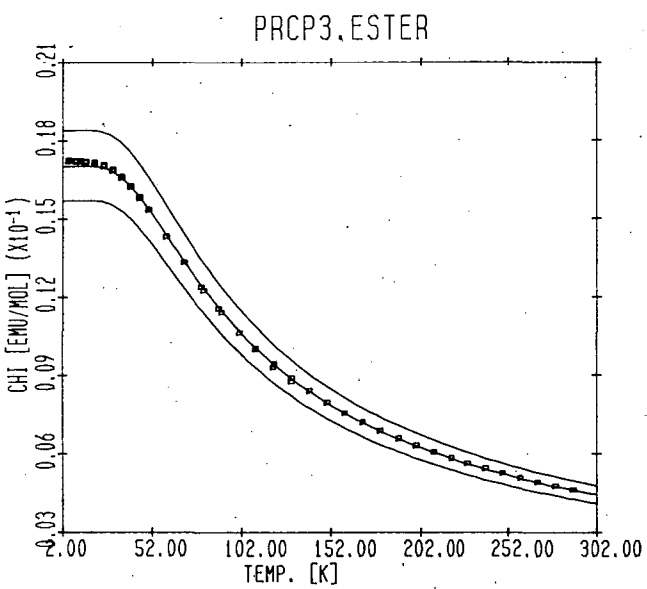

Figure 22-1. Calculated and experimental magnetic susceptibilities of Cp_3Pr·butyl acetate as a function of temperature. The continuous lines are calculated for k = 1.0, 0.975, and 0.95 from top to bottom, where k is the orbital reduction factor. The squares are experimental points. (XBL 8410-4125)

23. The Electronic and Magnetic Properties of Am and Cm (Publication 32)

Norman Edelstein

A review of the present status of the analyses of the optical spectra of Am and Cm in various oxidation states is given. From these analyses, the magnetic properties of the ground states of these ions can be determined. These predicted values are compared with the various magnetic measurements available.

24. The Ionization Potential of Neutral Iron, Fe I, by Multistep Laser Spectroscopy (Publication 18)

E.F. Worden,† B. Comaskey,† J. Densberger,† J. Christensen,† J.M. McAfee,† J.A. Paisner,† and J.G. Conway

Three-step laser excitation was used to populate and observe members of Rydberg series in neutral iron with high effective quantum numbers. These series converge to the ground and first-excited state of singly ionized iron. The photoionization threshold was also observed. Analyses of the Rydberg series yielded the value 63,737(1) cm^{-1} or 7.9024(1) eV as the ionization potential of neutral iron.

---

†Permanent address: Lawrence Livermore National Laboratory, Livermore, California 94550.

1984 PUBLICATIONS AND REPORTS

Refereed Journals

1. K.N. Raymond, G.E. Freeman, and M.J. Kappel, "Actinide-Specific Complexing Agents: Their Structural and Solution Chemistry," Inorg. Chim. Acta **94**, 193–204 (1984).
2. P.W. Durbin, N. Jeung, E.S. Jones, F.L. Weitl, and K.N. Raymond, "Specific Sequestering Agents for the Actinides. 10. Enhancement of ^{238}Pu Elimination from Mice by Poly(catechoylamide) Ligands," Rad. Res. **99**, 85–105 (1984).

3. R.D. Lloyd, F.W. Bruenger, C.W. Mays, D.R. Atherton; C.W. Jones, G.N. Taylor, W. Stevens, P.W. Durbin, N. Jeung, E.S. Jones, M.J. Kappel, K.N. Raymond, and F.L. Weitl, "Removal of Pu and Am from Beagles and Mice by 3,4,3-LICAM(C) or 3,4,3-LICAM(S)," Rad. Res. **99**, 106–128 (1984).
4. P.G. Edwards, R.A. Andersen, and A. Zalkin, "Tetraalkyl-Phosphine Complexes of the f-block Metals: Crystal Structures of $Th(CH_2Ph)_4(Me_2PCH_2CH_2PMe_2)$ and $U(CH_2PH)_3Me(Me_2PCH_2CH_2PMe_2)$," Organometallics **3**, 293 (1984); LBL-15890.
5. T.D. Tilley, R.A. Andersen, and A. Zalkin, "Divalent Lanthanide Chemistry; Preparation and Crystal Structures of Sodium Tris[bis(trimethylsilyl)amido]-Europate(II) and -Ytterbate(II), $NaM[N(SiMe_3)_2]_3$," Inorg. Chem. **23**, 2271 (1984); LBL-15886.
6. J.M. Boncella and R.A. Andersen, "Bis(pentamethylcyclopentadienyl) Ytterbium(II) as a Lewis Acid and Electron-Transfer Ligand; Preparation and Crystal Structure of $[Yb(C_5Me_5)_2(\mu\text{-}CO)_xMn(CO)_{5-x}]_y$ Where x and y are Two and x is Three and y is Infinite," Inorg. Chem. **23**, 432 (1984).
7. J.M. Boncella, T.D. Tilley, and R.A. Andersen, "Reaction of $M(C_5Me_5)_2(OEt_2)$, M = Eu or Yb, with Phenylacetylene; Formation of Mixed-Valence $Yb_3(C_5Me_5)_4(\mu\text{-}C{\equiv}CPh)_4$ and $Eu_2(C_5Me_5)_4(\mu\text{-}C{\equiv}CPh)_2(thf)_4$," J. Chem. Soc. Chem. Comm. 710 (1984); LBL-17335.
8. J.M. Boncella and R.A. Andersen, "Preparation of $[Yb(C_5Me_5)_2]_2[Co_3(C_5H_4R)_2(\mu_3\text{-}CO)_4]$, R = H, Me, $SiMe_3$; An Example of a 47-Electron Transition Metal Fragment with a Hexagonal Planar Cobalt Atom," J. Chem. Soc. Chem. Comm. 809 (1984); LBL-17336.
9. C.H.H. Van Deurzen, K. Rajnak, and J.G. Conway, "Uranium Five (Uv), the $^1S_0$ Level, and a Parametric Analysis of the $5f^2$ Configuration," J. Opt. Soc. Am. B **1**, 45 (1984); LBL-15924.
10. J.G. Conway, E.F. Worden, J.W. Brault, R.P. Hubbard, and J.J. Wagner, "Uranium Spectrum Between 1.8 and 5.5 Microns Emitted from a Hollow Cathode," Atom Data and Nucl. Data Tables **31**, 299 (1984); LBL-15764.
11. P.C. Becker, T. Hayhurst, G. Shalimoff, J.G. Conway, N. Edelstein, L.A. Boatner, and M.M. Abraham, "Crystal Field Analysis of Tm^{3+} and Yb^{3+} in YPO_4 and $LuPO_4$," J. Chem. Phys. **81**, 2872 (1984); LBL-17443.
12. K. Rajnak, E. Gamp, R. Banks, R. Shinomoto, and N. Edelstein, "Optical and Magnetic Properties of Uranium and Neptunium Borohydrides and Tetrakismethylborohydrides," Inorg. Chem. **95**, 29 (1984); LBL-16234.
13. K. Rajnak, R.H. Banks, E. Gamp, and N. Edelstein, "Analysis of the Optical Spectrum of $Np(BD_4)_4$ Diluted in $Zr(BD_4)_4$ and the Magnetic Properties of $Np(BH_4)_4$ and $Np(BH_3CH_3)_4$," J. Chem. Phys. **80**, 5951 (1984); LBL-16486.
14. K. Rajnak, E. Gamp, R. Shinomoto, and N. Edelstein, "Optical and Magnetic Properties of Uranium Borohydride and Tetrakismethylborohydride," J. Chem. Phys. **80**, 5942 (1984); LBL-16460.
15. E. Gamp and N. Edelstein, "Effects of Small Distortions on the EPR of the Γ_6 State (T_d Symmetry) of $Np(BH_3CH_3)_4$ Diluted in $Zr(BH_3CH_3)_4$," J. Chem. Phys. **80**, 5963 (1984); LBL-16484.
16. L.R. Morss and N. Edelstein, "Future Directions in Solid State Lanthanide and Actinide Chemistry," J. Less-Common Metals **100**, 15 (1984); LBL-17682.
17. J.-J. Girerd, G.C. Papaefthymiou, A.D. Watson, E. Gamp, K.S. Hagen, N. Edelstein, R.B. Frankel, and R.H. Holm, "Electronic Properties of the Linear Antiferromagnetically Coupled Clusters $[Fe_3S_4(SR)_4]^{3-}$, Structural Isomers of the $[Fe_3S_4]^+$ Unit in Iron-Sulfur Proteins," J. Am. Chem. Soc. **106**, 5941 (1984); LBL-17808.
18. E.F. Worden, B. Comaskey, J. Densberger, J. Christensen, J.M. McAfee, J.A. Paisner, and J.G. Conway, "The Ionization Potential of Neutral Iron, Fe I, by Multistep Laser Spectroscopy," J. Opt. Soc. Am. B **1**, 314 (1984); UCRL-89701.

Other Publications

19. D. Zhang, D.H. Templeton, and A. Zalkin, "Copper(II) (+)-Tartrate Trihydrate," Abs. PA21, American Crystallographic Association Meeting, Lexington, Kentucky, May 20–25, 1984.†
20. D.H. Templeton and L.K. Templeton, "Polarization of Synchrotron Radiation," Abs. V2, American Crystallographic Association Meeting, Lexington, Kentucky, May 20–25, 1984.†
21. D.H. Templeton and L.K. Templeton, "Polarization Anisotropy of Anomalous Scattering," Abs. 15.4-1, XIIIth Congress, International Union of Crystallography, Hamburg, Germany, August 9-18, 1984; Acta Cryst. A**40**, C-397 (1984).†
22. S.A. Kinsley and A. Streitwieser, Jr., "[8]Annulene Derivatives of Actinides and Lanthanides," in *Organometallics of the f-Elements,* T.J. Marks and I. Fragala, eds., D. Reidel Publishing Co., Dordrecht, Holland (in press).

LBL Reports

23. A. Zalkin, D.H. Templeton, R. Kluttz, and A. Streitwieser, Jr., "The Disordered Structure of Dibenzouranocene, $[C_8H_6(C_4H_4)]_2U$," submitted to Acta Cryst.; LBL-16381 Rev.
24. J.G. Brennan and A. Zalkin, "Structure of Tris(methylcyclopentadienyl)uranium(III)trimethylphosphine, $(CH_3C_5H_4)_3U.P(CH_3)_3$," submitted to Acta Cryst.; LBL-18348.
25. J.G. Brennan, R. Shinomoto, A. Zalkin, and N.M. Edelstein, "Preparation of Tertiary Phosphine Complexes of Tetravalent and Trivalent Uranium Methyltrihydroborates; The Crystal Structures of Tetrakis(methyltrihydroborato)uranium(IV)1,2-dimethylphosphinoethane) and Tris(methyltrihydroborato)uranium(III)bis(1,2-dimethylphosphinoethane)," accepted by Inorg. Chem.; LBL-17900.
26. R. Shinomoto, J.G. Brennan, N.M. Edelstein, and A. Zalkin, "Bridging of Thorium by Hydrogen Atoms of Methyltrihydroborate Groups; The Crystal Structures of Bis[tetra(methyltrihydroborato)thorium(IV)]-etherate and Bis[tetra(methyltrihydroborato)thorium(IV)-tetrahydrofuranate]," submitted to Inorg. Chem.; LBL-16169.
27. J.M. Boncella and R.A. Andersen, "Preparation of $Yb[N(SiMe_3)_2]_2[AlMe_3]_2$; A Complex with Four Yb-Me-Al Interactions," LBL-18196.
28. J.G. Brennan and R.A. Andersen, "Electron-Transfer Reactions of Trivalent Uranium; Preparation and Structure of $(MeC_5H_4)_3$ U=NPh and $[(MeC_5H_4)_3U]_2[\mu\text{-}\eta^1,\eta^2\text{-PhNCO}]$," LBL-18353.
29. S.A. Kinsley, A. Streitwieser, Jr., and A. Zalkin, "Dipotassium Bis[8]annulene-ytterbium(II) and -Calcium(II)," Organometallics (in press); LBL-18122.
30. H.-D. Amberger, H. Schultze, and N. Edelstein, "The Electronic Structure of Organometallic Complexes of the f Elements XI. Absorption Spectrum and Parameterization of the Crystal Field Splitting Pattern of a Methyltetrahydrofuran Adduct Derived from Tris(η^5-cyclopentadienyl)-praseodymium(III)," accepted by Spectrochim. Acta; LBL-18253.
31. H.-D. Amberger, W. Jahn, and N.M. Edelstein, "The Electronic Structure of Organometallic Complexes of the f Elements IX. Assignment of the Observed Faraday A Terms in the MCD Spectra of Tris(η^5-cyclopentadienyl)-praseodymium(III)adducts," accepted by Spectrochim. Acta; LBL-17478.
32. N. Edelstein, "The Electronic and Magnetic Properties of Am and Cm," in *Proc. Int. Symp. on Americium and Curium Chem. and Tech.*, 1984 International Chemical Congress of Pacific Basin Societies, Honolulu, Hawaii, December 16–21, 1984 (in press); LBL-18778.
33. Ronald Steven Shinomoto (Ph.D. Thesis), "Methyltrihydroborate Complexes of the Lanthanides and Actinides," LBL-18730.
34. A. Zalkin and D.H. Templeton, "Refinement of the Trigonal Crystal Structure of Lanthanum Trifluoride with Neutron Diffraction Data," accepted by Acta Cryst.; LBL-17563.
35. D.H. Templeton and L.K. Templeton, "Tensor X-Ray Optical Properties of the Bromate Ion," accepted by Acta Cryst.; LBL-18088.†
36. L.K. Templeton, D.H. Templeton, D. Zhang, and A. Zalkin, "Structure of Zinc (+)-Tartrate 2.5-Hydrate, $Zn(C_4H_4O_6)(H_2O)_{2.5}$, and Anomalous Scattering by Zinc," accepted by Acta Cryst.; LBL-18094.†
37. G. Chapuis, D.H. Templeton, and L.K. Templeton, "Solving Crystal Structures using Several Wavelengths from Conventional Sources. Anomalous Scattering by Holmium," accepted by Acta Cryst.; LBL-18323.†
38. L.K. Templeton, D.H. Templeton, and A. Zalkin, "Structure of Monoclinic Sodium Holmium Ethylenediaminetetraacetate Octahydrate: Disorder Induced by Radiation," accepted by Acta Cryst.; LBL-18423.†
39. D.H. Templeton and L.K. Templeton, "X-Ray Dichroism and Anomalous Scattering of Potassium Tetrachloroplatinate(II)," submitted to Acta Cryst.; LBL-18652.†

Invited Talks

40. K.N. Raymond, "Actinides in the Environment—The Design of Actinide-Specific Sequestering Agents," Workshop on Toxic Metals in the Environment, Seattle, Washington, January 19, 1984.
41. K.N. Raymond, "Transferrin Coordination Chemistry—Actinides and Iron?" Gordon Conference on Metals and Biology, Santa Barbara, California, January 30, 1984.
42. K.N. Raymond, "Actinide Specific Sequestering Agents," Chemistry Department, Cornell University, Ithica, New York, April 30, 1984; Biochemistry Department, University of Wisconsin, Madison, May 30, 1984; Chemistry Department, University of Michigan, Ann Arbor, October 2, 1984; Chemistry Department, University of Illinois, Champaign, October 4, 1984; Chemistry Department, Northwestern University, Evanston, Illinois, October 5, 1984; Frontier in Chemistry Program, Wayne State University, Detroit, Michigan, October 22, 1984; Chemistry Department, Rutgers University, New Brunswick, New Jersey, October 23, 1984.

43. K.N. Raymond, "Plutonium Complexation and the Environment," Department of Environmental Engineering, Stanford University, Stanford, California, November 9, 1984.
44. D.H. Templeton, "X-Ray Scattering," Workshop on New Directions in Soft X-Ray Photoabsorption, Asilomar, California, April 8–11, 1984.†
45. R.A. Andersen, "Recent Advances in Organometallic f-Element Chemistry," University of Southern California, Los Angeles, March 20, 1984; National Science Foundation Organometallic Workshop, University of North Carolina, Chapel Hill, May 30, 1984; International Conference on Coordination Chemistry, University of Colorado, Boulder, July 30, 1984; China-Japan-U.S. Symposium on Organometallic Chemistry and Catalysis, University of California, Santa Cruz, August 6, 1984; Gordon Research Conference in Organometallic Chemistry, Wolfeboro, New Hampshire, August 13, 1984; NATO Summer School on Organometallics of the f-Elements, Maratea, Italy, September 10, 1984; Pacific Conference on Chemistry and Spectroscopy, Sacramento, California, October 12, 1984; University of Victoria, British Columbia, October 23, 1984; University of Alberta, Edmonton, October 25, 1984; Amoco Chemical Company, Naperville, Illinois, November 1, 1984; University of Chicago, November 2, 1984; University of Illinois, Champaign-Urbana, November 6, 1984.
46. Andrew Streitwieser, Jr., "[8]Annulene Derivatives of Actinides and Lanthanides," NATO Advanced Study Institute on "Organometallics of the f-Elements," Maratea, Italy, September 10, 1984.
47. John G. Conway, "Free-Ion Spectra of Interest to Solid and Solution Spectroscopists," International Symposium on Rare Earth Spectroscopy, Wroclaw, Poland, September 10, 1984.
48. N. Edelstein, "Electronic Structure and Optical Spectroscopy of f^n Ions and Compounds," NATO Advanced Study Institute, "Fundamental and Technological Aspects of Organo-F-Element Chemistry," Acquafredda di Maratea, Italy, September 10, 1984; LBL-18582.

†Supported in part by the National Science Foundation.

Fossil
Energy

A Review of Unsolved Problems of Pressing Importance in Fluid Mechanics Affected Erosion*

Joseph A.C. Humphrey, Investigator

INTRODUCTION

The purpose of this study has been to document the relative importance of fluid-mechanics phenomena, especially turbulence, in the erosive wear of materials by solid-particle impact. Many systems of practical or engineering interest involve the motion of solid particles suspended in a turbulent fluid medium. When the particles have inertia numbers of order unity, they respond to high-frequency fluctuations in the fluid motion. Depending on the specific configuration of interest, this effect can result in enhanced or mitigated erosion. Thus, for example, theoretical calculations show that the overall erosive action of a particle-laden air jet can be substantially reduced by increasing the radial component of turbulent diffusion acting directly on the fluid and, through the fluid, on the particles. However, the position of maximum wear also varies with the magnitude of the turbulent diffusion, and regions of an impinged surface previously undergoing relatively little erosion may suddenly experience drastic increases in wear. This review identifies some of the problem areas requiring immediate attention, as well as various unresolved fundamental issues involving longer-term research commitments. Because the prediction of erosion in curved pipes requires a knowledge of the flow field, an experimental study of the turbulent flow through a 180° curved pipe was performed. The correct modeling of the effects of fluid mechanics on erosion continues to be hampered by the lack of suitable experimental data.

1. The Influence of Turbulence on Erosion by a Particle-Laden Fluid Jet (Publication 1)

S. Dosanjh and J.A.C. Humphrey

Very few investigations on wear by particle impact have accounted for the influence of turbulence on erosion. In this study, the effects of turbulent diffusion on particle dispersion, and hence erosion, are demonstrated numerically. Variations imposed on the level of turbulence intensity in a particle-laden jet impinging normally on a flat wall show a strong dependence of wear parameters on turbulence intensity. Impacting particle velocities, trajectories, and surface densities are predicted from Lagrangian equations of motion. Eulerian equations are used to describe fluid motion, with the turbulence viscosity evaluated from a k-ϵ model of turbulence. Nonessential complexities are avoided by assuming one-way coupling between phases and using an adjusted Stokes' drag relation. Numerical calculations reveal that the relative rate of erosion decreases and the location of maximum wear is displaced toward the stagnation point as the turbulence intensity increases. Efforts to remove present model limitations have been hindered by the lack of suitable experimental data.

2. Developing Turbulent Flow in a 180° Curved Pipe and its Downstream Tangent (Publication 2)

J. Azzola and J.A.C. Humphrey

Laser-Doppler measurements of the longitudinal and circumferential velocity components are reported for developing turbulent flow in a strongly curved 180° pipe and its downstream tangent. In the bend, the mean longitudinal velocity component changes little after $\theta = 90°$, but the circumferential component never achieves a fully developed state. Similar behavior is observed in the normal stresses, with large levels of flow anisotropy arising everywhere in the bend and downstream tangent. Between $\theta = 90°$ and $X/D = 5$, the circumferential velocity profiles display reversals of the secondary flow that are essentially independent of the Reynolds number. Ostensible differences between turbulent flows through pipes of circular and square cross sections are revealed by comparing present results with the measurements of Chang et al.[1] Although limited in extent, the data should serve to guide and test theoretical developments for modeling developing turbulent flows in curved pipes.

*This work was supported by the Assistant Secretary for Fossil Energy Research, Advanced Research and Technology Development Program, U.S. Department of Energy under Contract No. DE-AC03-76SF00098.

1. S.M. Chang, J.A.C. Humphrey, and A. Modavi, Physico Chemical Hydrodynamics **4**, 243–269 (1983).

3. Work in Progress

Theoretical work has focused on removing model limitations arising from a diluteness assumption. In particular, work is under way to understand how particle-particle and particle-wall interactions affect the flow structure and erosion at walls.

Experimental work has focused on the lack of an adequate data base for testing the validity of the theoretical findings. An experiment involving a particle-laden jet impinging on a surface is being designed to gather data in this area. The objective of the experiment is to qualify and quantify the response of erosion to carefully controlled changes in the fluid-mechanic conditions. Measurements of the fluid and particle motions will be obtained with a laser-Doppler velocimeter.

1984 PUBLICATIONS AND REPORTS

LBL Reports

1. S. Dosanjh and J.A.C. Humphrey, "The Influence of Turbulence on Erosion by a Particle-Laden Fluid Jet," submitted to Wear; LBL-17247.
2. J. Azzola and J.A.C. Humphrey, "Developing Turbulent Flow in a 180° Curved Pipe and Its Downstream Tangent," submitted to Heat and Fluid Flow; LBL-17681.

Invited Talks

3. S. Dosanjh, "The Influence of Turbulence on Erosion by a Particle-Laden Fluid Jet," Annual Meeting, American Institute of Chemical Engineers, San Francisco, California, November 25–30, 1984; based on LBL-17247.
4. J.A.C. Humphrey, "Developing Turbulent Flow in a 180° Curved Pipe and Its Downstream Tangent," Second International Symposium on Applications of Laser Anemometry to Fluid Mechanics, Lisbon, Portugal, July 2–4, 1984; based on LBL-17681.
5. J.A.C. Humphrey, "A Review of Current Research Activities by the Author in Berkeley," Southwest Research Institute, San Antonio, Texas, February 1984.
6. J.A.C. Humphrey, "Tecnicas Experimentales y Metodos Computacionales Desarrollados en Mis Actividades de Investigacion en la Universidad de California en Berkeley" (in Spanish), Escuela de Ingenieros Industriales de Zaragoza, Spain, June 1984.
7. J.A.C. Humphrey, "Modeling Erosion by a Particle-Laden Fluid Jet," Department of Mechanical Engineering, Instituto Superior Tecnico, Lisbon, Portugal, May 1984.

Electrode Surface Chemistry*

Philip N. Ross, Investigator

INTRODUCTION

Commercialization of phosphoric acid fuel-cell technology requires a capital-cost reduction and an extension of power-section life compared to currently available technology. Significant capital-cost reduction can be achieved if an oxygen-reduction catalyst that is catalytically more active than Pt supported on graphitized carbon black can be developed. Toward this end, extensive fundamental studies of Pt electrochemistry are being conducted to learn how Pt activity depends on temperature, acid anion, water concentration, and surface structure (morphology). Surface studies of gas-phase oxygen adsorption by x-ray photoemission spectroscopy (XPS) suggest that modification of the adsorptive properties of Pt by the substitution of ligands to the Pt coordination sphere could result in enhanced Pt catalysts. The objective of the present research is to develop the physical and chemical understanding of oxygen-platinum-ligand interaction necessary for the rational selection of alloying components. Fundamental studies of the alloy-electrolyte interface using modern surface-science techniques should provide the means to optimize the alloy ligand or to redirect the search for more active materials along the most rational paths. Alloying may have significant beneficial effects on electrode performance above and beyond effects on the oxygen-reduction kinetics, e.g., reduced Pt dissolution and surface-area loss. These additional alloying effects will also be studied at the atomic level, e.g., surface reconstruction and surface self-diffusion.

*This work was supported by the Assistant Secretary for Fossil Energy, Office of Coal Fuel Cells, Advanced Concepts Division of the U.S. Department of Energy under Contract No. DE-AC03-76SF00098, through the Fuel Cell Project Office, NASA Lewis Research Center, Cleveland, Ohio.

1. Superlattice LEED Patterns Observed from [111] and [100] Oriented Single Crystals of $TiPt_3$ (Publication 4)

U. Bardi† and P.N. Ross

We report the observations by low-energy electron diffraction (LEED) of ordered surface structures for $TiPt_3$ single crystals of orientation [111] and [100]. Superlattice patterns arising from the orderly substitution of Ti in the Pt lattice were observed at temperatures up to ~1200 K, the highest temperature we could achieve in our apparatus. The observation of these superlattice patterns of temperature-independent symmetry is an indication that long-range order occurs in the surface as well as in the bulk and that the surface structure is most probably a regular termination of the bulk structure.

The bulk structure for cubic $TiPt_3$ ($AuCu_3$ Ll_2-type) is shown in Figure 1-1, along with the surface structures expected for simple termination of the bulk structure in planes normal to [111] and [100]. In the $TiPt_3$ structure, Ti atoms substitute for Pt at the corners of the fcc unit cell, producing an ABA sequence of planes normal to [100]. These {100} planes alternately have 50% Ti and 100% Pt compo-

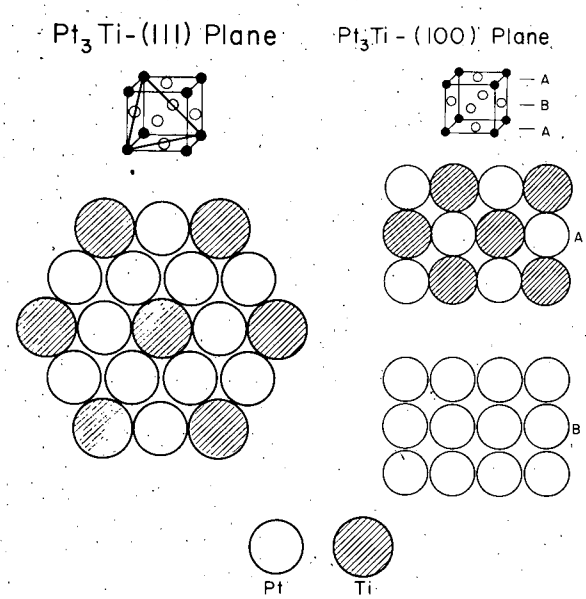

Figure 1-1. Top: fcc unit cell of $TiPt_3$, showing orderly substitution of Ti atoms (dark circles) for Pt at the corners. Left: ideal configuration of a (111) plane of $TiPt_3$. Right: ABA alternations of planes normal to [001]. (XBL 8211-1348A)

sition, and thus there are two inequivalent regular terminations possible, which we designate as the (100) and the (200) terminations, respectively. The {111} planes are all equivalent compositionally. The bulk lattice parameter for $TiPt_3$ is 0.3906 nm, a less than 1% contract of the Pt lattice. Thus the fundamental diffraction beams should be located at nearly the same position on the LEED screen as for the pure Pt crystal, and superlattice beams for ideal (111) and (100) terminations of the bulk lattice would be at half-order positions. Half-order superlattice spots were observed over a wide range of beam energies, from 40 to 200 eV, with relative intensities that were not significantly different at the lowest beam energy than at the highest. This result indicated that the surface termination was (100) rather than (200). The Ti/Pt Auger electron spectroscopy (AES) peak ratios suggested this was the case as well. LEED dynamical-intensity analysis indicated that the (100) surface is actually buckled, with Ti atoms recessed from the surface plane (contracted into the pure Pt plane below).

†Present address: Department of Chemistry, University of Florence, Italy.

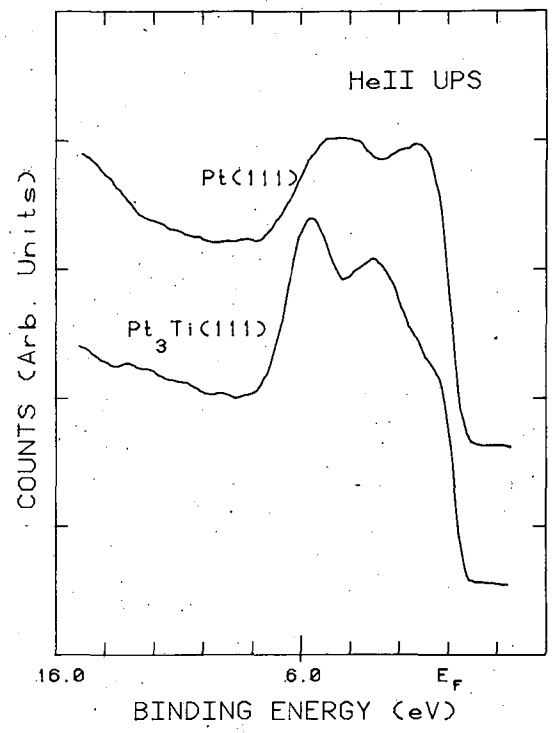

Figure 2-1. He (II) photoemission spectra comparing Pt_3Ti (111) to Pt (111). (XBL 844-1327)

2. Valence-Band and Core-Level Electronic States in Pt_3Ti (Publication 2)

G.N. Derry† and P.N. Ross

Photoemission data for the valence band, the Pt4f states, and the Ti2p states were obtained for intermetallic Pt_3Ti. Relative to the Pt valence band, the Pt_3Ti band shows a decrease in the density of states just below the Fermi level and a shift of the centroid to higher (binding) energy (see Figure 2-1). Ti2p and Pt4f binding energies showed relatively large shifts with respect to pure metals. These changes in the valence-band density of states and core-level binding energies are shown to arise from hybridization of the d-orbitals in both metals to form strong intermetallic bonds. Bond formation is accompanied by charge transfer from Ti to Pt, leaving the Ti atoms in approximately a +1 valence state.

†Present address: Department of Physics, University of North Carolina, Chapel Hill.

3. Initial States of Oxidation of the $Pt_3Ti(111)$ and (100) Single-Crystal Surfaces (Publication 5)

U. Bardi† and P.N. Ross

The process of segregation of titanium oxides onto the surface of Pt_3Ti on exposure to oxygen at different pressures and temperatures was studied by LEED and AES. Oriented (111) and (100) monocrystals as well as polycrystals were synthesized for study. Qualitatively similar behavior was observed with all three types of surfaces, with three stages of oxidation observed on each surface (refer to stages in Figure 3-1). A layer of stoichiometry close to TiO segregated onto the surface in the initial (Stage I) stage of oxidation, depleting the subsurface region of the alloy in Ti. The TiO formed a compact, epitaxial monolayer that completely blocked the metallic surface for chemisorption by carbon monoxide. Further oxidation (Stage II) caused formation of a multilayer of $TiO_{1.2}$, an oxide with an orthorhombic structure derived from TiO by removing Ti atoms to form an ordered-vacancy lattice.

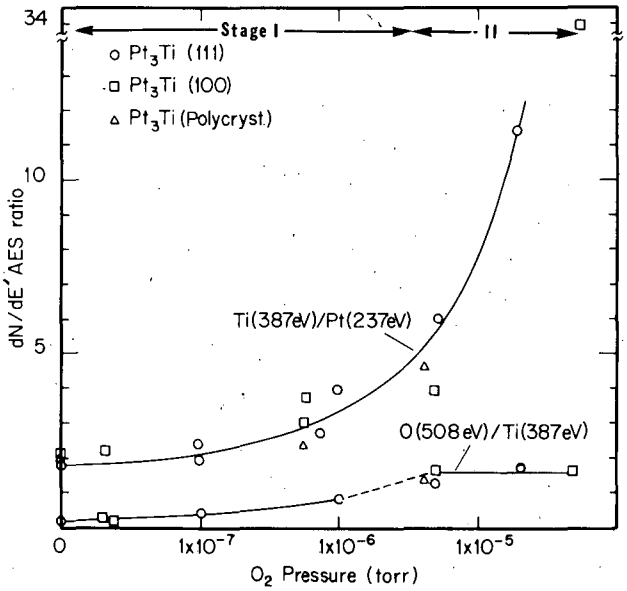

Figure 3-1. AES peak ratios for the first two stages of oxidation of Pt_3Ti. Oxygen dosing was isothermal at 773 K for 30 seconds. (XBL 843-1229A)

Finally, oxidation at the relatively extreme conditions of atmospheric pressure and relatively high (>1000 K) temperature caused formation of thick TiO_2 (rutile) overlayers (Stage III).

†Present address: Department of Chemistry, University of Florence, Italy.

4. Work in Progress

These previous studies have clearly shown two important properties of Pt Group IVb intermetallic surfaces: (1) There is a strong ligand effect from the intermetallic bonding in the chemisorption of reducing gases like hydrogen and carbon monoxide. (2) The intermetallic surface is unstable with respect to oxidizing conditions like that of a fuel-cell cathode. Further studies are in progress to determine the composition and structure of the surface formed by electrochemical oxidation using the gas-phase oxidation-formed surfaces as a guide. Also, studies directed at relating the behavior of bulk surfaces to supported bimetallic clusters (the practical catalyst) are under way. These studies will utilize XPS and EXAFS (extended x-ray absorption fine structure) in characterizing changes to the state of the base metal and the coordination about the Pt surface atoms during use as a fuel-cell cathode catalyst.

1984 PUBLICATIONS AND REPORTS

Refereed Journals

1. U. Bardi, P. Ross, and G. Somorjai, "LEED and AES Study of Structural and Chemisorptive Properties of Zr Overlayers on Pt(100)," J. Vac. Sci. Technol. A **2**, 45 (1984); LBL-15294.
2. G. Derry and P.N. Ross, "Valence Band and Core-Level Electronic States in Pt_3Ti," Solid State Commun. **52**, 151 (1984); LBL-17357.
3. G. Derry and P.N. Ross, "High Coverage States of Oxygen Adsorbed on Pt(100) and Pt(111) Surfaces," Surf. Sci. **140**, 165–180 (1984); LBL-15231 Rev.
4. U. Bardi and P.N. Ross, "Superlattice LEED Patterns Observed from [111] and [100] Oriented Single Crystals of $TiPt_3$," Surf. Sci. **146**, L555 (1984); LBL-17356.

LBL Reports

5. U. Bardi and P.N. Ross, "Initial Stages of Oxidation of the Pt_3Ti(111) and (100) Single Crystal Surfaces," J. Vac. Sci. Technol. A (in press); LBL-17869.
6. G. Derry and P.N. Ross, "A Work Function Change Study of Oxygen Adsorption of Pt(111) and Pt(100)," J. Chem. Phys. (in press); LBL-16409 Rev.

Invited Talks

7. P.N. Ross, "New Catalysts and New Electrolytes for Acid Fuel Cells," Symposium on the New Surface Science of Catalysis, American Chemical Society National Meeting, Philadelphia, Pennsylvania, August 1984.

Studies of Materials Erosion in Coal Conversion and Utilization Systems*

Alan V. Levy, Investigator

INTRODUCTION

The mechanisms and rates of surface loss of materials used for the containment of gas and liquid-solid particle flows in coal conversion and utilization systems were investigated in a generic research program. Portions of the operating environments of components where erosion degradation occurs — in coal gasification and liquefaction processes, fluidized-bed combustion, and advanced pulverized-coal boilers — were simulated to investigate the behavior of candidate alloys and protective coatings. Tests were carried out using flat specimens of various engineering materials with varying compositions and morphologies over a range of controlled test conditions. Rate and mechanisms of surface loss were determined, and models governing the degradation were developed. The fluid mechanics of two-phase flows were established for use in conjunction with the models to predict erosion rates in various containment geometries.

1. Elevated Temperature Erosion of Steels (Publication 4)

Johnny Yan and Alan Levy

Heat treatable stainless steels were erosion tested at temperatures near their heat treatment temperatures in a nitrogen-gas atmosphere, and the resulting erosion rates were compared to lower chromium content steels and non-heat treatable stainless steels. The austenitic stainless steels eroded much less than both the ferritic and precipitation hardened stainless steels and the lower chromium-content steels at all test temperatures. This result was further proof that strength and hardness do not relate directly to erosion resistance in ductile metals, but that ductility does relate directly to erosion resistance.

The velocity exponent for the erosion of 310SS at 800°C is one-half that measured for room temperature erosion. This result indicates that the absorption of the impacting particle's kinetic energy by the eroding metal surface is different from that occurring at room temperature. This means that erosion models now used for room temperature erosion must be significantly modified for elevated temperature erosion prediction. There was no indication that eroding a material at its heat treatment temperature changes the nature or rates of erosion beyond the straight effect of test temperature on erosion.

2. Erosion of Protective Coatings (Publication 5)

Greg Hickey and Alan Levy

Seven different coating systems that are used to protect chemical process plant components from elevated temperature corrosion were erosion tested at room temperature and two elevated temperatures. Four of the coating systems were diffusion type, i.e., aluminized, chromized, carbonized, on carbon steels; the other three were plasma-sprayed nickel or iron base alloys on mild steel. The coatings had different erosion resistance rankings as a function of test temperature and impingement angle, with no single coating superior at all conditions.

The presence of both hard and soft phases in the coatings' microstructures negated the established relationship between the erosion of ductile and brittle materials as a function of impingement angle. A decrease in the steady state erosion rate occurred when the test temperature was increased from 20 to 500°C. Thus, previously accepted relationships between material erosion rates and test conditions did not apply to the erosion of corrosion-protection systems on steels.

3. Combined Erosion-Corrosion (Publication 6)

Yong-Fa Man and Alan V. Levy

The mechanisms of combined erosion-corrosion (E-C) of iron-chromium alloys at elevated test temperatures to 900°C have been determined as a function of several test variables. The understanding gained of how the corrosion scales formed and were removed in the E-C process was used to explain the material loss rates that occurred at different test conditions.

*This work was supported by the U.S. Department of Energy under DOE/FE AA 15 10 10 0, Advanced Research and Technical Development, Fossil Energy Materials Program, Work Breakdown Structure Element LBL-3.5 under Contract No. DE-AC03-76SF00098.

The primary nucleation and growth mechanism in E-C is the nucleation and growth of oxide scale nodules that occur at the locations of early erodent particle impacts. The lateral growth of the nodules to eventually cover the E-C surface develops a scale integrity that varies with the impingement angle and velocity of the erodent particles as well as with the test temperature. The resulting degree of scale integrity determines whether scale loss occurs by a slow cracking and chipping mechanism or by a fast, periodic spalling mechanism. These two scale loss mechanisms determine the rate of sound metal loss in the E-C of iron-chromium alloys. The development of a strong relationship between scale morphology and material loss rate is an important step toward predicting E-C rates and developing more E-C resistant materials.

1984 PUBLICATIONS AND REPORTS

Other Publications

1. A. Levy, E. Slamovich, and N. Jee, "Elevated Temperature Erosion-Corrosion of Steels," in *Proc. Int. Congress of Metallic Corrosion,* Toronto, Ontario, June 1984; LBL-17243.
2. A. Levy and Y.F. Man, "Elevated Temperature Erosion-Corrosion of 9Cr/1Mo Steel," in *Proc. AIME High Temperature Corrosion in Energy Systems,* Detroit, Michigan, September 1984; LBL-18254.
3. A. Levy, N. Jee, and G. Sorell, "The Erosivity of Coal Particles in Coal Solvent Slurries," in *Proc. ASTM Inter Symposium on Slurry Erosion,* Denver, Colorado, June 1984; LBL-17908.

LBL Reports

4. A. Levy, J. Yan, and J. Patterson, "Elevated Temperature Erosion of Steels," LBL-18256.
5. A. Levy and G. Hickey, "Erosion of Corrosion Resistant Surface Treatments on Alloy Steels," LBL-18255.
6. A. Levy and Y.F. Man, "Corrosion-Erosion Rates/Mechanisms of 9Cr/1Mo Steel," LBL-17991.
7. A. Levy and Y.F. Man, "The Effect of Temperature on the Corrosion-Erosion of 9Cr/1Mo Steel," LBL-18641.
8. A. Levy and Y.F. Man, "Surface Degradation of Ductile Metals in Elevated Temperature Gas-Particle Streams," LBL-18686.
9. A. Levy and N. Jee, "Sliding Wear of Ceramic Coating Systems," LBL-18915.
10. A. Levy and Y.F. Man, "Nodular Scale Formation in Erosion-Corrosion of Iron-Chromium Alloys," LBL-18916.
11. A. Levy, "Erosion of the Same Material in Both Ductile and Brittle Modes," LBL-18917.
12. A. Levy and G. Hickey, "Morphology of Eroded Corrosion Protection Coating Systems," LBL-18918.

Invited Talks

13. A. Levy, "Accomplishments of the DOE Combustion Zone Durability Program (CZDP)," ASME Energy Technology Conference, New Orleans, Louisiana, February 1984.
14. A. Levy, "Erosion-Corrosion of Scales," Metals Properties Council Workshop on Understanding Erosion-Corrosion, St. Louis, Missouri, March 1984.
15. A. Levy, E. Slamovich, and N. Jee, "Combined Erosion and Corrosion of Chromium Bearing Steels at High Temperature," National Association of Corrosion Engineers (NACE) Annual Meeting, New Orleans, Louisiana, April 1984.
16. A. Levy, M. Landkof, D. Boone, R. Gray, and E. Yaniv, "The Effect of Surface Doping on the Oxidation of Chromia Former Alloys," NACE Annual Meeting, New Orleans, Louisiana, April 1984.
17. A. Levy, P. Yau, and N. Jee, "Erosion of Steels in Coal-Solvent Slurries," NACE Annual Meeting, New Orleans, Louisiana, April 1984.
18. A. Levy and E. Slamovich, "Combined Corrosion-Erosion of Steels in Oxidizing Environments," NACE Annual Meeting, New Orleans, Louisiana, April 1984.
19. A. Levy, D. Boone, and A. Davis, "Erosion of Ceramic Thermal Barrier Coatings," NACE Annual Meeting, New Orleans, Louisiana, April 1984.
20. G. Hickey and A. Levy, "Erosion of Protective Surface Treatments and Coatings on Steels," AIME-TMS Fall Meeting, Detroit, Michigan, September 1984.
21. A. Levy and J. Yan, "Elevated Temperature Erosion of Heat Treated Alloys," AIME-TMS Fall Meeting, Detroit, Michigan, September 1984.
22. A. Levy, "Ductile and Brittle Erosion Behavior of the Same Material," AIME-TMS Fall Meeting, Detroit, Michigan, September 1984.
23. A. Levy, "Erosion of Metals, Oxide Scales, and Protective Coatings," Seminar at United Technologies Research Center, East Hartford, Connecticut, December 1984.

Chemistry and Morphology of Coal Liquefaction*

Heinz Heinemann, Investigator, with A.T. Bell, R.H. Fish, and G.A. Somorjai, Investigators

INTRODUCTION

This program is designed to look at the basic chemistry and physics of the transformation of coal and coal liquids during processing. It involves investigators of different disciplines and a great variety of instruments that can be brought to play in the different tasks of the project. During the past year, work on the subproject "Selective Synthesis of Gasoline-Range Components from Synthesis Gas" was completed. The continuing investigation of catalyzed graphite gasification at low temperatures resulted in the discovery that a truly catalytic reaction can be achieved by using certain transition-metal oxides as cocatalysts with KOH. This discovery overcomes the previously limiting stoichiometric formation of a phenolate species, which is decomposed by the metal oxide. Work has also continued on the selective hydrogenation of polynuclear nitrogen-containing aromatics. Two results were found: (1) the catalyst is not poisoned by most compounds that can be found in coal liquids, and (2) cresols actually act as promotors.

1. Selective Synthesis of Gasoline-Range Components from Synthesis Gas (Publications 4 and 5)

A.T. Bell, with R.A. Dictor, W. Canella, and Heinz Heinemann

The investigations of iron-based catalysts for Fischer-Tropsch synthesis were completed during the past year. This work was aimed at understanding the effects of catalyst composition and reaction conditions on the distribution of products formed and the kinetics of their formation. Studies were conducted in both a fixed-bed reactor and a well-stirred autoclave, each of which was equipped with an on-line gas chromatograph for product analysis. Since similar results were obtained with both reactors, these will be discussed together.

Six unsupported iron catalysts were examined: iron powder, precipitated iron, potassium-promoted precipitated iron, hematite (Fe_2O_3), potassium-promoted hematite, potassium-promoted fused iron (actually Fe_2O_3), and cementite (Fe_3C). In each case, the catalyst was either reduced or calcined prior to being subjected to synthesis gas. The four unpromoted catalysts exhibited very similar behaviors. Following reduction in H_2, each catalyst exhibited a very high activity for Fischer-Tropsch synthesis. The high initial activity could not be maintained, and the activity declined to a nearly steady-state level in about 24 hours, when the activity was about one tenth of that observed originally. A linear Schulz-Flory distribution of hydrocarbon products was observed. The probability of chain growth α increased with decreasing partial pressure of H_2, increasing partial pressure of CO, and decreasing temperature. For the range of conditions examined, α varied between 0.47 and 0.61. The products produced over each catalyst were remarkably similar, consisting primarily of α-olefins and n-paraffins. Methyl-branched α-olefins and straight-chained β-olefins were observed in lesser concentrations, as was CH_3OH. No higher aldehydes or alcohols were observed. The proportion of paraffins and β-olefins was a strong function of gas velocity, indicating that these products are formed via secondary processes from α-olefins. X-ray analysis of the spent catalyst suggested that the active catalyst consists of the host material (e.g., Fe_3O_4, Fe, Fe_3C), on the surface of which are small particles of x-Fe_5C_2, ϵ'-$Fe_{2.2}C$, and Fe.

Potassium promotion resulted in a product distribution made up of two Schulz-Flory distributions crossing at n = 7 to 8. The value of α for n = 1 to 8 was virtually the same as that for the unpromoted catalyst, while that for n > 8 was noticeably greater. The α for the light products responded to changes in reaction conditions in a manner identical to that observed for the unpromoted catalysts, while the α for the heavier products was virtually unaffected by reaction conditions.

Studies of catalyst surface area revealed that, on reduction, the Brunauer-Emmett-Teller surface area of the fused iron catalyst increased, while that of precipitated iron decreased. This is understandable. In the former case, reduction results in the formation and growth of pores in the fused iron (oxide) matrix.

*This work was jointly supported by the Director, Office of Energy Research, Office of Basic Energy Sciences, Chemical Sciences Division, and the Assistant Secretary for Fossil Energy, Office of Coal Research, Liquefaction Division of the U.S. Department of Energy under Contract No. DE-AC03-76SF00098, through the University Contracts Management Division of the Pittsburgh Energy Technology Center, Pittsburgh, Pennsylvania.

In the latter case, reduction brings about a sintering of the iron particles. Retention of the high initial surface area of precipitated iron could be achieved by calcining the catalyst and then bringing it on stream without reduction. When this is done, the catalyst activity per gram of iron is tenfold higher than that observed for reduced precipitated iron, and little deactivation occurs following attainment of the maximum activity. The product distribution is identical irrespective of whether the precipitated iron catalyst is reduced or calcined prior to use.

Supported iron catalysts were prepared without potassium promotion. The specific activities of these catalysts were found to decrease in the following order: $Fe/TiO_2 > Fe/SiO_2 > Fe/Al_2O_3 >$ Fe/Y-Zeolite $>$ Fe/MgO. The variation in activity can be attributed primarily to metal-support interactions. In all cases, the product distribution was characterized by a single value of α that was quite sensitive to reaction conditions. The magnitude of α was comparable to that for the unpromoted bulk iron catalysts.

The kinetics of hydrocarbon synthesis over all of the catalysts studied could be represented by the expression

$$R_{C_n} = R_{C_1}^{\alpha n-1} = k_{C_1} P_{H_2}^{X_1} P_{CO}^{Y_1 \alpha n-1} ,$$

where

$$\alpha = \alpha(P_{H_2}, P_{CO}).$$

The global activation energy was found to be constant up to 300°C. At higher temperatures the catalyst underwent deactivation due to the rapid buildup of free carbon. The temperature at which deactivation set in could be extended slightly by raising the H_2 partial pressure.

2. Catalyzed Low-Temperature Reaction of Carbon and Water (Publication 1)

G.A. Somorjai, with W.T. Tysoe, J. Carrazza, and Heinz Heinemann

Research has been concentrated in two major areas: (1) exploratory experiments using a flow reactor to discover effective catalysts for the gasification of graphite with steam, and (2) studies of the interaction of different molecules with graphite using a high-pressure surface-science apparatus.

In the flow-reactor experiments, it was previously reported that the gasification of graphite with steam below 950 K, when KOH is present on the surface, ceases after the formation of 0.5 mole of H_2 per mole of KOH adsorbed. It was suggested that the reaction was limited by the formation of a stable potassium phenolate intermediate. In order to overcome this situation, work done during this year was aimed at discovering a way to decompose this surface intermediate so that the process would be carried out catalytically below 900 K.

We found that mixtures of transition-metal oxides coadsorbed with KOH on graphite were good catalysts for the gasification of graphite with steam below 900 K. Figure 2-1 shows the rate of gas production at 900 K for 9 different mixtures. KOH/NiO and KOH/Fe_2O_3 presented the largest activity for this reaction; these mixtures were studied in greater detail.

While KOH adsorbed alone on graphite behaved as a reactant for the gasification of graphite with steam, NiO and Fe_2O_3 adsorbed alone (no KOH present) have no activity for this process. The fact that the mixture of them (KOH/NiO or KOH/Fe_2O_3) is a catalyst at temperatures below 900 K suggests that there is a cooperative effect between the components.

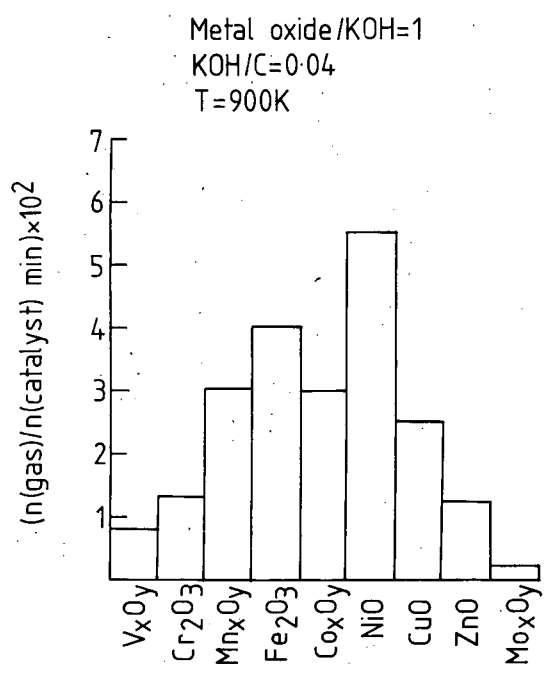

Figure 2-1. Relative gas-production rates of various KOH co-catalyst stems, normalized to metal oxide/KOH. All oxides were coadsorbed with KOH on graphite at 900 K. The activity rate for KOH adsorbed alone on graphite was 0.04. (XBL 848-8581)

The rate of gas production for the gasification of graphite with steam at 859 K, when either KOH/NiO or KOH/Fe_2O_3 were adsorbed on graphite, was followed up to a graphite conversion of 24% (24 moles of CO_2 produced per mole of catalyst adsorbed on the surface). Because more than 24 turnovers of gas can be produced at 860 K, we conclude that NiO/KOH and Fe_2O_3/KOH are indeed good catalysts for the gasification of graphite with steam.

The major gas products obtained for this process in the presence of either KOH/NiO or KOH/Fe_2O_3 are H_2 and CO_2 in the ratio of H_2 to CO_2 equal to 2.2 ± 0.5. CH_4 is initially produced in a ratio of CH_4 to H_2 equal to 0.04 ± 0.01, but its production decreased with time up to a ratio of CH_4 to H_2 equal to 4×10^{-3}. CO was produced at temperatures above 900 K; however, the ratio of CO to CO_2 produced was far below the value expected at equilibrium. This suggests that the gasification process is controlled by the kinetics of a surface reaction.

The activity of Ni metal adsorbed alone on graphite for the gasification of graphite with steam was studied in an isothermal experiment at 859 K. The initial gas production is an order of magnitude faster than in the case of KOH and NiO coadsorbed on graphite; but while in the last case the reaction is still going after 24% of the graphite has been gasified, the reaction stops after 11% conversion when Ni metal is present on the surface. Further work will be done to understand why the reaction stops in the presence of Ni metal.

Three major studies were done using the ultrahigh-vacuum/high-pressure-cell system. The interaction of CO and CO_2 with graphite was studied using thermal desorption (TDS), Auger electron (AES), and x-ray photoelectron (XPS) spectroscopies. The deposition of K on graphite was also monitored using AES. Finally, the presence of a potassium phenolate intermediate on the surface after reaction of a KOH-loaded graphite sample with steam was confirmed using XPS.

3. Chemistry of Coal Solubilization and Liquefaction (Publication 2)

R.H. Fish, with A.D. Thormodsen and Heinz Heinemann

The reduction mechanism of quinoline with deuterium gas was recently elucidated with homogeneous Wilkinson's catalyst. We found the deuterium-incorporation pattern shown in compound 6 in Figure 3-1. In contrast, compound 7 shows the deuterium pattern (as determined by nuclear magnetic resonance (NMR) and multispectral (MS) analysis) obtained with 2% cross-linked polystyrene-divinylbenzene (PS-DVB) Wilkinson's catalyst. The pertinent difference is the lack of aromatic C-H exchange (C_8) for the polymer-supported catalyst. But the stereochemistry at the 3,4-double bond (cis) is similar for both forms of the catalyst, as is the reversible dehydrogenation of the reduced carbon-nitrogen bond (positions 1 and 2) to provide 1.6 D at position 2 via quinoline-2-d. Moreover, reaction of the product, 1,2,3,4-tetrahydroquinoline, with PS-DVB Wilkinson's catalyst under similar deuteration conditions also shows, by NMR and MS analysis, no exchange of the aromatic hydrogen at position 8 (6.42 ppm). This result is in contrast to the homogeneous-catalyst result. Again, steric requirements surrounding the active metal center of the polymer-supported catalyst may be responsible for the lack of aromatic C-H exchange.

Another objective of this work was to determine whether the selectivity for the nitrogen heterocyclic ring (with quinoline as the example) would prevail in the presence of other coal-liquid constituents. The model coal liquid, dissolved in benzene and containing 30 wt% pyrene, 5 wt% tetralin, 38 wt% methylnaphthalene, 17 wt% m-cresol, 7.5 wt% quinoline, and 2.5 wt% x-methylpyridine, was hydrogenated with the 2% PS-DVB Wilkinson's beads to provide 1,2,3,4-tetrahydroquinoline as the only reduction product (initial rate 0.42%/min). Removal of 2-methylpyridine had no effect on the initial rate, in contrast to the competitive inhibition on quinoline by the pyridine derivative in the homogeneous reaction. Interestingly, reduction of quinoline alone, at a similar substrate-to-metal ratio as in the model coal liquid, provided an initial rate (0.18%/min) that was approximately 2.2 times slower than the rate of quinoline in the presence of the model-coal-liquid constituents.

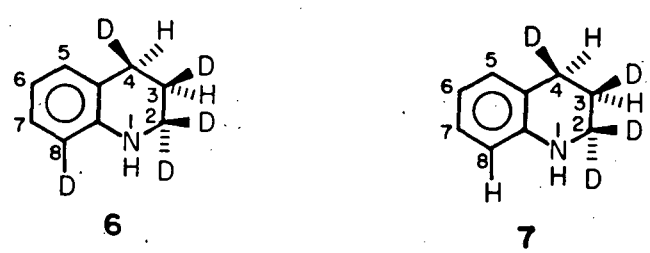

Figure 3-1. Deuterium-incorporation pattern of quinoline reduced with deuterium gas. (6) Pattern found when homogeneous Wilkinson's catalyst was used. (7) Pattern found when 2% cross-linked PS-DVB Wilkinson's catalyst was used. (XBL 8311-4461)

We have been able to confirm that p-cresol, a constituent in a model coal liquid containing pyrene (30 wt%), tetralin (5 wt%), methylnaphthalene (38 wt%), p-cresol (17 wt%), quinoline (7.5 wt%), and methylpyridine (2.5 wt%) enhances the rate of quinoline hydrogenation by a factor of approximately two. In addition, 2-methylpyridine had no effect on the quinoline reduction rate, which is in contrast to its effect when using a homogeneous catalyst. Thus, p-cresol might be useful in hydroprocessing coal liquids.

The above-mentioned result emphasizes the highly selective reaction taking place in the presence of other functionalities; i.e., the regiospecific reduction of the nitrogen heterocyclic ring as well as the rate-enhancement phenomena. The result also provides dramatic evidence for the potential usefulness of polymer-supported catalysts in synthetic-fuel (hydroprocessing) applications.

1984 PUBLICATIONS AND REPORTS

Refereed Journals

1. F. Delannay, W.T. Tysoe, H. Heinemann, and G.A. Somorjai, "Distribution of Reaction Products in the KOH Initiated Low Temperature Steam Gasification of Graphite," Appl. Catal. **10**, 111–113, 1984; LBL-16050.
2. F. Delannay, W.T. Tysoe, H. Heinemann, and G.A. Somorjai, "The Role of KOH in the Low-Temperature Steam Gasification of Graphite: Identification of the Reaction Steps," Carbon **22** (4–5), 401 (1984); LBL-16049.
3. W.T. Tysoe, J. Carrazza, and G.A. Somorjai, "The Adsorption and Catalyzed Reactions of CO and CO_2 on Graphite Surfaces," ACS Div. Fuel Chem. Symp. on Gasification of Chars and Carbonaceous Materials **29** (2), 190 (1984); LBL-17004.

Other Publications

4. *Proc. 2nd Berkeley Catalysis and Surface Science Conf.*, G.A. Somorjai and Heinz Heinemann, eds.; Catal. Rev.—Sci. Eng. **26**, 298–728, 1984.
5. J. Maj, C. Colmenares, and G.A. Somorjai, "Methanol Production from Carbon Monoxide and Hydrogen on Thorium Dioxide," submitted to J. Catal.
6. W.J. Canella (Ph.D. Thesis), "Factors Influencing Kinetics and Product Distribution in Fischer-Tropsch Synthesis over Iron Catalysts."
7. R.A. Dictor (Ph.D. Thesis), "Study of Fischer-Tropsch Synthesis over Iron Based Catalysts using a Well-Stirred Reactor."

LBL Reports

8. R.H. Fish, J.L. Tan, and A.D. Thormodsen, "Homogeneous Catalytic Hydrogenation. 2. Selective Reductions of Polynuclear Heteroatomic Compounds Catalyzed by Chloro(tristriphenylphosphine)rhodium (I)," J. Org. Chem. (in press); LBL-15596.
9. K.-J. Zhen, M.M. Khan, C.-H. Mak, K.B. Lewis, and G.A. Somorjai, "Partial Oxidation of Methane with Nitrous Oxide over V_2O_5-SiO_2 Catalyst," LBL-18493.

Invited Talks

10. W.T. Tysoe, J.E. Crowell, and G.A. Somorjai, "Isotope Scrambling Studies of Alkali Effects on CO Adsorption on Rh(111)," California Catalysis Society Spring Meeting 1984, Richmond, California, March 23, 1984.
11. J. Carrazza, W.T. Tysoe, H. Heinemann, and G.A. Somorjai, "Gasification of Graphite with Steam Catalyzed by a Mixture of Potassium Hydroxide and Transition Metal Oxides Below 900 K," California Catalysis Society Fall Meeting 1984, October 18, 1984.

Energy Storage Systems

ELECTROCHEMICAL ENERGY STORAGE

Lutgard C. De Jonghe, James W. Evans, Rolf H. Muller,
John Newman, Philip N. Ross, and Charles W. Tobias, Investigators

Surface Morphology of Metals in Electrodeposition*

Charles W. Tobias, Investigator

INTRODUCTION

The objective of this project is to gain understanding of the partial processes and their interactions involved in the deposition and dissolution of metals by electrolysis. Of particular interest are the influence of hydrodynamic flow on electrocrystallization and the distribution of charge-transfer rates on advancing and receding metal profiles, as determined by the electric and concentration field in the solution, and by the kinetics of the charge-transfer reaction. Control of the morphology of metallic deposits has been traditionally affected by addition agents that interfere with the crystallization process. In energy-storage applications, however, other means may have to be employed for the control of morphology. Rotating disk electrodes and planar electrodes in channel-type electrolyzers are used for the preparation of metal deposits, over large ranges of solution properties and hydrodynamic conditions, with potentiostatic or galvanostatic control. The genesis of surface textures is studied, using *in situ* motion picture microphotography, videorecording, and *post mortem* examination by electromicroscopy.

1. Studies on Zinc Nodules Electrodeposited from Acid Electrolytes (Publication 13)

Rolfe Anderson and Charles W. Tobias

The development of morphology of electrodeposited zinc was investigated by studying the initial stages of deposition. Zinc was deposited galvanostatically from 1.0M $ZnCl_2$ electrolyte ($0.7 < pH < 4.6$) on rotating-disk electrodes at current densities from 5 to 130 ma/cm^2. Pine glassy carbon, Union Carbide pyrolytic graphite, Gould pyrolytic graphite, Exxon graphite-loaded polymer, and platinum substrates were used. The number densities of nodules (with diameters greater than 1 μm) typically encountered during incipient morphological development were measured using scanning electron microscopy and image analysis. Nodule densities up to 7×10^4 nodules/mm^2 were measured. The results may be summarized as follows: (1) Nucleation processes were discernable through cyclic voltammetry (see Figure 1-1). (2) Potential-step kinetic measurements yielded exchange-current densities on the order of 1 ma/cm^2. (3) The nodule density increased with surface overpotential at a rate from 200 to 1000 nodules/mm^2 $\times$ mv. (4) The potential between the working and reference electrodes exhibited a transient potential peak during the first few seconds of deposition. The relative magnitude of the peak potential is inversely related to the number of available nucleation sites. (5) A parallel exists between the magnitude of this peak and the number density

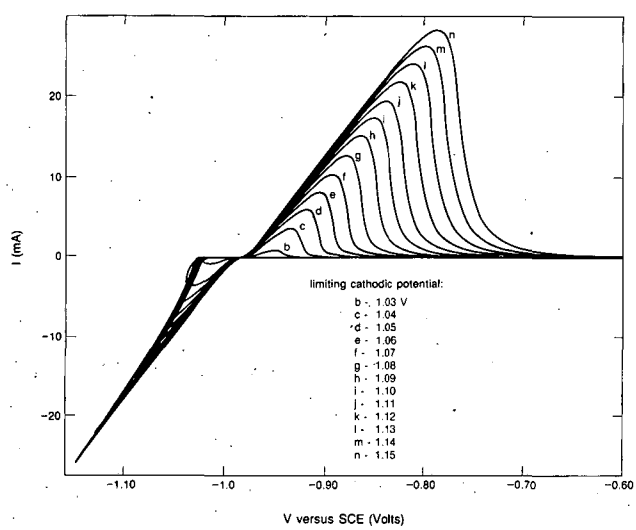

Figure 1-1. Cyclic voltammograms of zinc deposition on Union Carbide pyrolytic graphite. The electrolyte is 3.0M $ZnCl_2$, reagent grade. The sweep rate is 50 mV/sec. (XBL 849-10861)

*This work was supported by the Assistant Secretary of Conservation and Renewable Energy, Office of Energy Systems Research, Energy Storage Division of the U.S. Department of Energy under Contract No. DE-AC03-76SF00098.

of nodules on a given substrate. The substrates, ranked in order of decreasing activity towards zinc nucleation, are Union Carbide HOPG pyrolytic graphite, platinum, Gould pyrolytic graphite, and Exxon graphite-loaded polymer and Pine glassy carbon.

2. A Model for Current Distribution with Passivating Kinetics (Publication 16)

John Dukovic and Charles W. Tobias

No general model presently exists for current distribution in electrochemical systems that exhibit passivity. We have developed a treatment which (1) incorporates the detailed active-passive current-voltage characteristics, (2) handles arbitrary two-dimensional and axisymmetric geometries, and (3) covers conditions of partial passivity of the electrode.

The steady-state, potential-theory model uses a trapezoidal-curve fit of the active-passive polarization curve of the electrode that can be obtained from a rotating disk experiment. The finite-element method is used in a relaxed-iteration scheme with the active-passive characteristic entered as a natural boundary condition.

The model was tested against experimental data obtained on a rotating cylindrical segmented cathode. The experiments produced a stable coexistence of active and passive regions on the Ni anode, dissolving in H_2SO_4. The outcome of one such experiment is given by the step profile in Figure 2-1. The current distribution calculated by the model is plotted for comparison. Both the magnitude and the overall character of the profile are predicted relatively well by the model, but there is some discrepancy in the location of the active-passive transition. Agreement between theory and experiment is probably limited by reproducibility in the preparation of the anode surface.

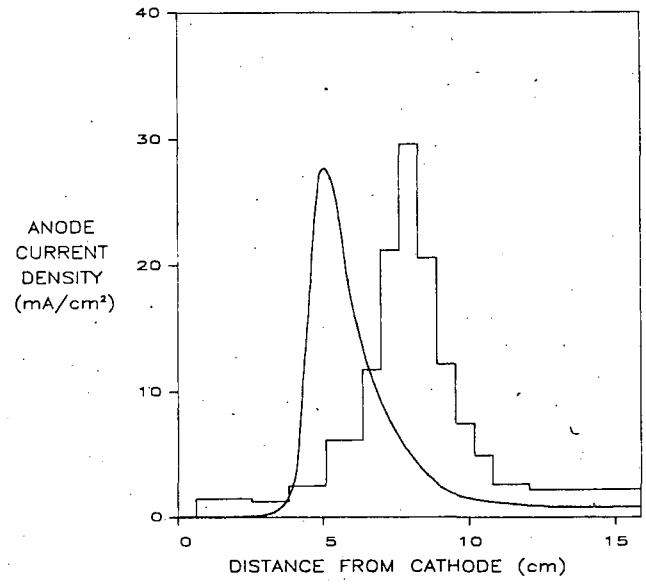

Figure 2-1. Current distribution on a rotating cylindrical nickel anode with a doughnut-shaped cathode located coaxially near one end of the cylinder. The step profile depicts the measured amount of nickel loss; the smooth curve gives a calculated distribution of metal loss using a theoretical model. (XBL 853-1499)

3. Work in Progress

Previous work on the micromorphology of zinc deposited from acidic solutions under forced convection[1] is being extended by *in situ* photomicrography to determine the mass-transfer mechanisms involved in the development of surface striations on different substrates. Contrary to indications in the literature, high (>90%) current efficiencies have been determined for zinc deposition on pyrolytic graphite. (Laura McVey, Rolf H. Muller, and Charles W. Tobias)

1. J. Faltemier, with C.W. Tobias, LBL-16485.

Metal Couples in Non-Aqueous Electrolytes*

Charles W. Tobias, Investigator

INTRODUCTION

The objective of this project is to explore practical alternatives to high-temperature molten-salt systems for the efficient electrochemical reduction and oxidation of reactive metals. Recent developments in advanced primary cells and projected high-energy rechargeable battery systems involve the use of alkali-metal negatives. To expand the possibilities for application of reactive metals at near-ambient temperatures, new ionizing media must be sought that have high decomposition potentials and are capable of dissolving ionic compounds. The propylene carbonate family of solvents has been demonstrated in this laboratory to allow the reduction of alkali metals at room temperature with reasonably high efficiency. However, solvent stability in the presence of reactive metals remains a critical issue, especially in the case of rechargeable galvanic-cell applications. Current work includes the exploration of the reduction of magnesium, the study of viable reactions for the positive electrode, and the investigation of the role of cosolvents in improving stability, solubility, and conductivity. Under the support of the Office of Basic Energy Sciences, novel solvent-purification techniques are being evaluated. A related project under the direction of Rolf H. Muller concerns the chemical nature of surface films on alkali metals in propylene carbonate electrolytes.

1. On Halogen Electrochemistry in Propylene Carbonate (PC) (Publication 12)

Karrie J. Hanson and Charles W. Tobias

UV-visible spectroscopy experiments of iodine and bromine solutions have demonstrated that the stable form of the halogen in PC is the trihalide. In the case of iodine, the equilibrium constant of the disproportionation reaction at 25°C was determined to be 0.85. Gas-chromatography analysis showed that chlorine attacks even dried, distilled PC (less than 7 ppm water), and that the extent of the reaction increases with increasing water content of the solvent. However, solutions of iodine in PC are stable for several months.

Conductivity experiments were performed to determine the extent of ion-pair formation of KI and KBr in PC. In addition, the conductivity of these solutions was measured as a function of the concentration of the corresponding halogen. Increased conductivity was noted for each solution, and a maximum was observed for equimolar iodide and iodine concentrations.

Cyclic voltammograms of KI in supported ($KAsF_6$) PC show two anodic peaks. To characterize the voltammograms, the following sequence of reactions is proposed:

$$3I^- \rightarrow I_3^- + 2e^- \quad (1)$$

$$2I_3^- \rightarrow 3I_2 + 2e^- \quad (2)$$

*This work was supported by the Assistant Secretary of Conservation and Renewable Energy, Office of Energy Systems Research, Energy Storage Division of the U.S. Department of Energy under Contract No. DE-AC03-76SF00098.

The validity of this mechanism was tested in an optically transparent thin-layer cell by performing simultaneous cyclic voltammetry and UV-visible spectroscopy at a narrow-mesh gold working electrode. The sequence of formation and disappearance of triiodide and iodine according to reactions (1) and (2) was confirmed by the spectral scans repeated at 30-second intervals.

A transport model for the simulation of the voltammograms was developed in collaboration with M. Matlosz and J. Newman. The model takes into account the following: the presence of two electron-transfer steps; the fact that these steps have a complex (i.e., not 1:1) stoichiometry; the effect of mass transfer of the three species; and the kinetics of the charge-transfer reactions. The results (see Figure 1-1) indicate that reaction (1) is kinetically inhibited while reaction (2) is reversible.

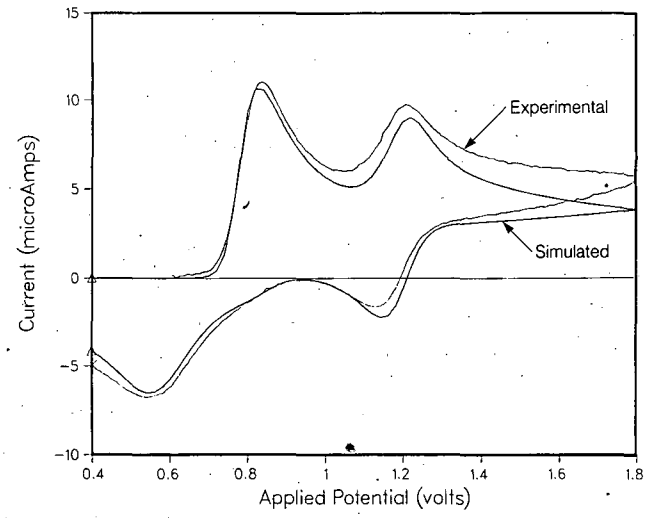

Figure 1-1. A comparison of an experimental cyclic voltammogram of the $I^-/I^{3-}/I_2$ system in propylene carbonate with a simulated voltammogram. Electrolyte: 0.004M KI, 0.5M $KAsF_6$. Electrode area: 0.057 cm^2. All diffusion coefficients: 2×10^{-6} cm^2/sec. Sweep rate: 100 mV/sec. Reaction (1) (see text) is kinetically inhibited (i_o: 6.5×10^{-5} A/cm^2, $\alpha = 0.2$); reaction (2) (see text) is reversible. (XBL 847-7739)

Engineering Analysis of Electrolytic Gas Evolution*

Charles W. Tobias, Investigator

INTRODUCTION

Electrolytic gas evolution is among the most common reaction types in electrolysis and in advanced rechargeable batteries. Modern applications in energy storage and transmission (e.g., hydrogen) require much higher energy efficiency and lower capital cost than achieved in gas-generating processes in the past. This project is directed toward the quantitative description of partial processes and their interactions involved in the nucleation, coalescence, and detachment of gas bubbles. Of special interest are the effects of moving individual bubbles and of gas-electrolyte emulsions on ohmic cell resistance and on mass transport of charged and uncharged species to and from electrode surfaces. A thorough understanding of the physical processes involved in the liberation and movement of gases at electrodes and in the electrolyte should lead to improved energy efficiency and lower capital costs in process and device technology.

1. Current Distribution at an Electrode with an Attached Bubble (Publication 20)

John Dukovic and Charles W. Tobias

There has been continued interest in the effect of gas evolution on the performance of electrolytic cells. Existing theory for the effect of attached bubbles on an electrode reaction is limited to the primary current distribution.[1] We have advanced a model that takes into account local concentration overpotentials due to charged and uncharged species as well as charge-transfer overpotentials. The tertiary current distribution is substantially different from the primary case. In particular, the concentration overpotential of dissolved gas is substantially reduced near the bubble, causing an effective attraction of current to the region nearest to the point of attachment. The pseudo-steady-state analysis accounts for migration and diffusion of each dissolved species in the vicinity of a single attached bubble within a Nernst diffusion layer. The resulting coupled-boundary-value problem is solved by a finite-element routine. Figure 1-1 shows the case of hydrogen evolution in 5.0M KOH at 100 mA/cm^2 for a 10-micron tangent bubble within a 50-micron boundary layer. The current distribution is plotted for various values of exchange current density. For cases of fast kinetics, the attached bubble causes a pronounced enhancement in local current density. For slower kinetics this enhancement is reduced until, in the irreversible limit (Tafel kinetics), product transport does not influence the rate, and hence there is no enhancement effect.

1. P.J. Sides and C.W. Tobias, J. Electrochem. Soc. **127**, 288–291 (1980).

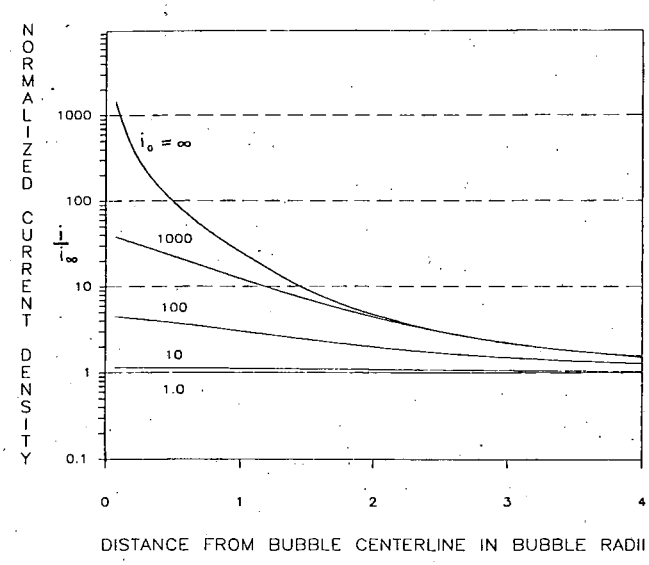

Figure 1-1. Effect of charge overpotential on the current distribution under a spherical hydrogen bubble attached to an electrode surface on which hydrogen ions are discharged. $\beta = 0.5$; i_o is given in mA/cm^2; $i_{ave} = 100$ mA/cm^2, i_∞ = current density at a great distance from the bubble, which has a diameter of 10 microns. Electrolyte: 5M KOH. (XBL 853-1503)

*This work was supported by the Assistant Secretary of Conservation and Renewable Energy, Office of Energy Systems Research, Energy Storage Division of the U.S. Department of Energy under Contract No. DE-AC03-76SF00098.

2. Work in Progress

An electrolytic cell has been designed and constructed in which two identical (e.g., H_2-H_2) or different (H_2-O_2) gas bubbles generated on microelectrodes facing each other may be evolved at suitably low rates. This cell allows the observation of coalescence phenomena as the spherical bubbles come into contact. Preliminary results indicate that for bubbles smaller than 1 mm in diameter, the coalescence event is completed within 10^{-5} sec and that earlier observations, here and elsewhere, that reported that bubbles could touch without immediate coalescence may have resulted from slight axial misalignment.

The effect of electrode morphology and attitude on bubble size and residence time is being studied using high-speed cinematography. Electrodes of various geometries—flat horizontal, flat vertical, ridges, and spheres—are masked with an insulating material so that a single row of bubbles can be viewed from the side. Overpotential measurements are obtained from the unmasked smooth and textured electrodes.

Three new sets of micromosaic electrodes have been produced for us by Hewlett-Packard and Bell Laboratories. For these electrodes more stable materials such as tantalum silicide and titanium/palladium/gold have been used to replace the aluminum and chromium in the original version, hopefully increasing the useful life of these valuable experimental tools. (Gina Whitney, Steven Elliott, and Charles W. Tobias)

1984 PUBLICATIONS AND REPORTS

Other Publications

1. D.W. Dees and C.W. Tobias, "Experimental Observations of Free Convection Mass Transfer to a Horizontal Surface with a Micro-Mosaic Electrode," Electrochem. Soc. Meeting, Cincinnati, Ohio, May 6–11, 1984, Ext. Abstr. 84-1, pp. 535–536; based on LBL-16176.
2. D.W. Dees and C.W. Tobias, "Mass Transfer at Gas Evolving Surfaces: A Microscopic Study," in *Proc. Int. Soc. Electrochem. Meeting,* Berkeley, California, August 5–10, 1984, Ext. Abstr., pp. 717–719; based on LBL-16176.
3. C.A. Coughanowr, R.H. Muller, and C.W. Tobias, "Electrochemical Machining of Cemented Titanium Carbide," in *Proc. Int. Soc. Electrochem. Meeting,* Berkeley, California, August 5–10, 1984, Ext. Abstr., pp. 667–669; based on LBL-13682.†
4. K.J. Hanson, M. Matlosz, J. Newman, and C.W. Tobias, "Theory of Cyclic Voltammetry for Reactions Having Complex Stoichiometry," in *Proc. Int. Soc. Electrochem. Meeting,* Berkeley, California, August 5–10, 1984, Ext. Abstr., pp. 950–952; based on LBL-18335.
5. J. Thonstad and C.W. Tobias, "On the Coalescence of Electrolytic Gas Bubbles," in *Proc. Int. Soc. Electrochem. Meeting,* Berkeley, California, August 5–10, 1984, Ext. Abstr., pp. 950–952.
6. K.J. Hanson and C.W. Tobias, "The Electrochemistry of the Iodide/Tri-Iodide/Iodine Redox System in Propylene Carbonate," Electrochemical Society Meeting, New Orleans, Louisiana, October 7–12, 1984, Ext. Abstr. 140, pp. 211–212; based on LBL-18335.
7. Patents: Process for Producing Ozone, U.S. Patent No. 4,375,395 (1983) (with P.C. Foller and M.L. Goodwin); Canadian Patent No. 1,170,616 (1984).‡
8. F.R. McLarnon, R.H. Muller, and C.W. Tobias, "Interferometric Study of Combined Forced and Natural Convection" (Discussion), J. Electrochem. Soc. **120**, 1444 (1984).†

LBL Reports

9. R.E. Acosta, R.H. Muller, and C.W. Tobias, "Transport Processes in Narrow Gap Channels," accepted by J. AICh.E.; LBL-16067.†
10. C.A. Coughanowr, B.A. Dissaux, R.H. Muller, and C.W. Tobias, "Electrochemical Machining of Refractory Materials," submitted to J. Appl. Electrochem.; LBL-18365.†
11. F.R. McLarnon, R.H. Muller, and C.W. Tobias, "Interferometric Observation of Turbulent Mass Transfer in Channel Flow," submitted to J. Electrochem. Soc.; LBL-18575.†
12. K.J. Hanson (Ph.D. Thesis), with C.W. Tobias, "On the Electrochemistry of Halogen Electrodes in Propylene Carbonate," LBL-18335.
13. R.C. Anderson (M.S. Thesis), with C.W. Tobias, "Studies on Zinc Electrodes Electrodeposited from Acid Electrolytes," LBL-18646.
14. D.S. Fischl, K.J. Hanson, R.H. Muller, and C.W. Tobias, "Mass Transfer Enhancement by Small Flow Obstacles in Electrochemical Cells," submitted to Chem. Eng. Commun.; LBL-18476.
15. M.W. Verbrugge and C.W. Tobias, "A Mathematical Model for the Periodic Electrodeposition of Multicomponent Alloys," submitted to J. Electrochem. Soc.; LBL-17739.
16. J.O. Dukovic and C.W. Tobias, "A Model for Current Distribution with Passivating Kinetics," LBL-18819.

Invited Talks[§]

17. C.W. Tobias, "Introduction to the Norbert Ibl Symposium on Electrochemical Engineering," International Society of Electrochemistry, 35th Meeting, Berkeley, California, August 5–10, 1984; Ext. Abstr. B1-1.
18. C.W. Tobias (presented by J. Thonstad), "The Coalescence of Electrolytic Gas Bubbles," International Meeting on Electrolytic Bubbles, London, England, September 13–14, 1984.
19. C.W. Tobias (presented by P.J. Sides), "Current Distribution Around, and Resistance Presented by, Gas Bubbles Adhering to an Electrode Surface," International Meeting on Electrolytic Bubbles, London, England, September 13–14, 1984.[†]
20. C.W. Tobias (presented by J.O. Dukovic), "Current Distribution at an Electrode with an Attached Bubble," International Meeting on Electrolytic Bubbles, London, England, September 13–14, 1984.

[†]Supported by the Director, Office of Energy Research, Office of Basic Energy Sciences, Materials Sciences Division of the U.S. Department of Energy under Contract No. DE-AC03-76SF00098.

[‡]Supported entirely by University funds.

[§]See further list of papers presented under "Other Publications."

Surface Layers on Battery Materials*

Rolf H. Muller, Investigator

INTRODUCTION

The purpose of this work is to provide direct experimental information about the formation and properties of surface layers on battery-electrode materials and to find new means for controlling properties of surface layers that enhance performance and cycle life. Present studies are concerned with anodic oxide formation and the behavior of lithium in different ambient-temperature nonaqueous electrolytes. A more broadly based research program, supported by the Office of Basic Energy Sciences, Division of Materials Sciences, DOE, is described in the sections "Electrochemical Phase Boundaries," R.H. Muller, Investigator, and "Electrochemical Processes," C.W. Tobias, Investigator.

1. Composition of Surface Layers on Li Electrodes in Propylene Carbonate and $LiClO_4$ of Very Low Water Content (Publication 5)

Gholamabbas Nazri† and Rolf H. Muller

Surface layers formed on Li in $LiClO_4$ with <1 ppm water content have been analyzed. Infrared (IR) spectroscopy showed the formation of Li_2CO_3 and a polymeric compound. Analysis by electron spectroscopy for chemical analysis (ESCA) of the surface layer on electrochemically deposited Li on a Cu substrate indicated the formation of two types of carbon compounds, related to the formation of Li_2CO_3 and polymer. ESCA analysis also showed that $LiClO_4$ decomposes to chlorine compounds with lower valency, with the higher-valent chlorine found in the outer film regions and the lower-valent chlorine found in the inner regions (see Figure 1-1). *In situ* x-ray diffraction confirmed the formation of Li_2CO_3 and polymeric compounds. A scanning electron microscope study of the surface of electrodeposited Li showed a porous structure.

*This work was supported by the Assistant Secretary of Conservation and Renewable Energy, Office of Energy Systems Research, Energy Storage Division of the U.S. Department of Energy under Contract No. DE-AC03-76SF00098.

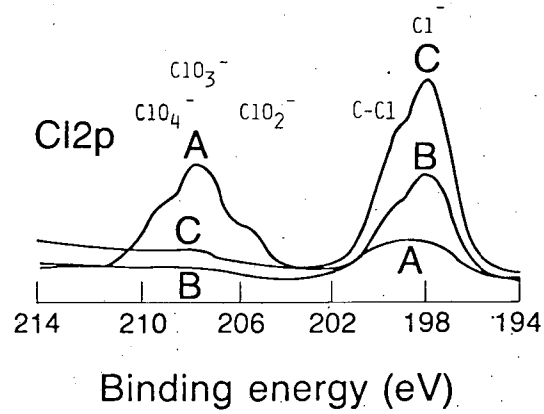

Figure 1-1. X-ray photoelectron spectroscopy spectra of Cl_{2p} in the surface layer formed on Li, electrochemically deposited from propylene carbonate at 1M $LiClO_4$, indicating the decomposition of ClO_4 ions. (A) top surface, (B) after 10 min. sputtering, and (C) after 20 min. sputtering. Sputtering rate 8 Å/min. (XBL 8401-6754)

†Present address: General Motors Technical Center, Warren, Michigan 48090.

2. *In Situ* X-Ray Diffraction of Surface Layers on Lithium in Nonaqueous Electrolyte (Publication 2)

Gholamabbas Nazri† and Rolf H. Muller

In situ x-ray diffraction has been applied to the study of surface layers formed on lithium during deposition from nonaqueous electrolytes. The properties of surface layers are important for the charge and discharge behavior of lithium electrodes in ambient-temperature batteries. Because of the high reactivity of lithium, use of *in situ* techniques for the characterization of surface layers is essential.

A collimated x-ray beam was directed toward the electrode surface at a glancing angle (6° from the surface) in order to enhance sensitivity for the surface region, and the diffracted x rays were measured by a rotating detector. The cell containing the electrode was made of polypropylene and contained the working electrode of 1.9 cm diameter in the center, surrounded by a 3-mm wide counter electrode. A lithium reference electrode of 3 mm diameter was located between the working and counter electrodes. The electrolyte could be injected and removed from the cell by two syringes, connected to the cell with Teflon spaghetti tubing. Electrodes and electrolyte were separated from the atmosphere by a

polyethylene or Mylar window 0.3 mm thick, through which the x-ray beam entered and exited. Permeation of water through the cell window from air over the time of the measurements was found to be negligible.

Surface layers formed on lithium during its cathodic deposition at 1 mA/cm^2 from 1.5M $LiCl_4$ on a nickel substrate. Formation of lithium carbonate was shown by the increasing size of a characteristic sharp diffraction peak (see Figure 2-1); a broad peak at low diffraction angle (20°) is characteristic of the appearance of polymeric compounds. The identification of the two film materials agrees with earlier analyses by IR spectroscopy and ESCA.[1] The formation of Li_2O has also been observed in the presence of trace amounts of water.

†Present address: General Motors Technical Center, Warren, Michigan 48090.

1. G. Nazri and R.H. Muller, Electrochem. Soc. Meeting, Washington, D.C., October 9–14, 1983, Ext. Abs. No. 61.

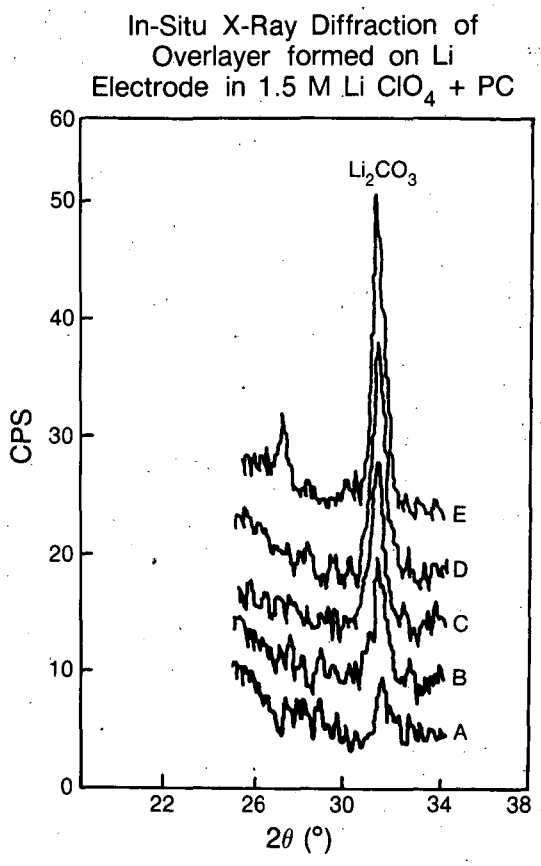

Figure 2-1. *In-situ* x-ray diffraction pattern from the surface layer formed on Li electrochemically deposited on a Ni substrate observed during deposition, after (A) 5 min., (B) 10 min., (C) 15 min., (D) 20 min., and (E) 25 min. The peak indicates Li_2CO_3 formation. (XBL 848-8559)

3. Stability of Nonaqueous Electrolytes for Ambient-Temperature Rechargeable Lithium Cells (Publication 3)

G. Nazri† and R.H. Muller

Three tests have been used to determine the stability of solutions of two nonaqueous solvents—propylene carbonate and 2-methyltetrahydrofuran—and their solutions of $LiAlCl_4$, $LiAsF_6$, and $LiClO_4$ in contact with lithium. The procedures identify the effect of surface layers, open-circuit stand, and anodic and cathodic polarization. They employ (1) contact with liquid Li amalgam and solid-sheet Li, (2) open-circuit potential measurements of cathodic deposits (see Figure 3-1), and (3) anodic dissolution of deposits with ramped potential. The stability of the solvents is found to depend on the dissolved electrolyte. Polymeric materials containing other products of the reaction between metal and electrolytes have been identified by x-ray diffraction.

†Present address: General Motors Technical Center, Warren, Michigan 48090.

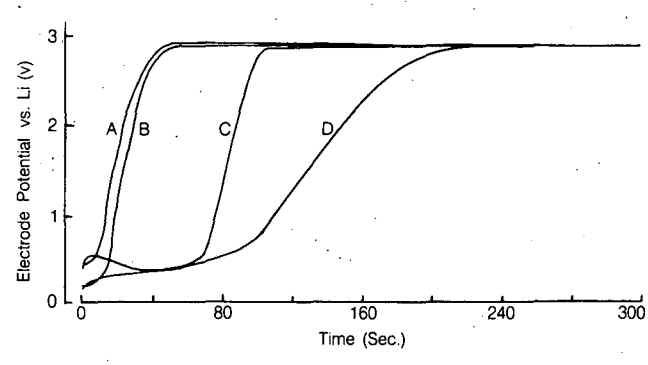

Figure 3-1. Open-circuit potential (compared to Li) of electrochemically deposited Li on Cu in 2-methyl tetrahydrofuran, 1M $LiClO_4$, showing the reaction of Li with the electrolyte. The deposit thickness for compact layer, based on the charge passed, is 100 Å (A), 200 Å (B), 500 Å (C), and 1000 Å (D). (XBL 841-499A)

4. Work in Progress

An earlier study of the anodic formation of silver oxide[1] is being extended by the use of spectroscopic ellipsometry to the initial stages of oxide formation, in order to clarify film-growth mechanisms and optical models. Of particular interest is an assignment of oxidation peaks in the cyclic voltammogram to different stages of film formation.

1. R. Muller and C. Smith, Surf. Sci. **96**, 375 (1980).

1984 PUBLICATIONS AND REPORTS

Other Publications

1. G. Nazri and R.H. Muller, "Surface Layers on Lithium in Organic Battery Electrolytes," in *Proc. Int. Soc. Electrochem. Meeting*, Berkeley, California, August 5–10, 1984, Ext. Abstr. A4-16; LBL-17710.

LBL Reports

2. G. Nazri and R.H. Muller, "*In Situ* X-Ray Diffraction of Surface Layers on Lithium in Nonaqueous Electrolyte," submitted to J. Electrochem. Soc.; LBL-18194.
3. G. Nazri and R.H. Muller, "Stability of Nonaqueous Electrolytes for Ambient-Temperature Rechargeable Lithium Cells," submitted to Chem. Engr. Comm.; LBL-18497.
4. F. Schwager, Y. Geronov, and R.H. Muller, "Ellipsometric Studies of Surface Layers on Lithium," submitted to J. Electrochem. Soc.; LBL-13656 Rev.
5. G. Nazri and R.H. Muller, "Composition of Surface Layers on Li Electrodes in PC, $LiClO_4$ of Very Low Water Content," submitted to J. Electrochem. Soc.; LBL-18197.
6. G. Nazri and R.H. Muller, "Effect of Residual Water in Propylene Carbonate on the Nature of Films Formed on Lithium," submitted to J. Electrochem. Soc.; LBL-16094.

Electrode Kinetics and Electrocatalysis*

Philip N. Ross, Investigator

INTRODUCTION

Complex electrochemical reactions in which chemical bonds are broken and/or formed are invariably catalytic, with electrode kinetics varying by many orders of magnitude for different electrode materials. The structural conformation of the electrode material can also have a pronounced effect on electrode kinetics. The structural effects complicate the optimization of catalytic materials for technological applications and are not effects that are well understood. The study of structure-related effects in electrocatalysis is a central theme in our research.

Metal/metal-ion (Me/Me^{Z+}) couples form the largest class of negative-electrode types for batteries. The kinetics of Me/Me^{Z+} couples used in batteries are relatively rapid, but they are not usually controlled by only a charge-transfer step. These reactions are often quasireversible, in the sense that they proceed at high rate and small overpotential, but they do not follow "ideal" charge-transfer-rate expressions. Phenomena frequently cited as contributing to the "nonideal" behavior of Me/Me^{Z+} systems are critical nucleation, intermediate or precursor formation, and impurity adsorption. The structural transformations to the metallic surface as a result of cyclic Me^{Z+} formation are not well known, particularly at the atomic scales of structure. Yet these structural transformations may control critical phenomena in Me/Me^{Z+} cyclability.

Bifunctional air electrodes, which both consume and evolve oxygen, are especially attractive positive electrodes that can be coupled with Zn negative electrodes to form high-energy-density (150–200 Wh/kg) ambient-temperature batteries. Bifunctional air electrodes require the development of catalytic materials that are both active and corrosion-resistant over a demanding range of electrode potentials. Electrode structures based on catalyzed carbon black appear attractive on the basis of cost. The corrosion resistance of different carbons is under investigation.

*This work was supported by the Assistant Secretary of Conservation and Renewable Energy, Office of Energy Systems Research, Energy Storage Division of the U.S. Department of Energy under Contract No. DE-AC03-76SF00098.

1. Underpotential Metal Deposition on Single-Crystal Substrates Prepared in Ultrahigh Vacuum (UHV) (Publication 3)

P. Andricacos† and P.N. Ross

It is of considerable fundamental interest to determine whether electrode processes respond uniquely to long-range order on the surface. In chemisorption phenomena, it is well known that short-range order, which establishes the adsorption-site symmetry, plays an important role in determining the strength of bonding of adsorbates. The role of long-range order is not as well understood and has not been the subject of systematic investigation. Only recently have surface-structure methods for long-range order determination been developed for low-energy electron diffraction (LEED). These developments in LEED analysis have renewed interest in studies of the effects of long-range order on adsorption phenomena. The underpotential deposition (UPD) of one metal on another is a type of adsorption phenomenon that occurs in electrodeposition. To examine the role of long-range surface order in UPD requires a unique experimental apparatus that permits direct transfer of crystals from UHV, where the surface order can be both tailored and determined, into an electrochemical cell. Such an apparatus has been developed in our laboratory.

We report here a study by cyclic voltammetry of UPD on well-ordered surfaces prepared in and transferred from UHV. LEED was used to characterize the range of order in the substrate surface before and after UPD. The voltammetry of Cu UPD on the well-ordered low-index surfaces of Pt are shown in Figure 1-1. A LEED spot-profile analysis of these low-index substrates indicated that these surfaces had long-range order (~100-Å perfectly ordered domains). Post-UPD LEED analysis of the Pt surfaces emersed at ~0.6 V vs. Cu/Cu(II) indicated Cu UPD had a minimal residual effect on the surface structure, indicating that Pt-Cu place exchange ("alloying") did not occur during Cu UPD. The voltammetry of Cu UPD on oriented Pt surfaces with only short-range order is shown in Figure 1-2. These surfaces were produced either by anodic cycling of the Pt or by UHV treatment with argon-ion bombardment; both treatments produced similar types of surface structures. The comparison of Figures 1-1 and 1-2 reveal the short-range and long-range order in the surface. In the short-range order, the orientation of the crystal (zone axis) determines the local symmetry of the majority of adsorption (adatom)

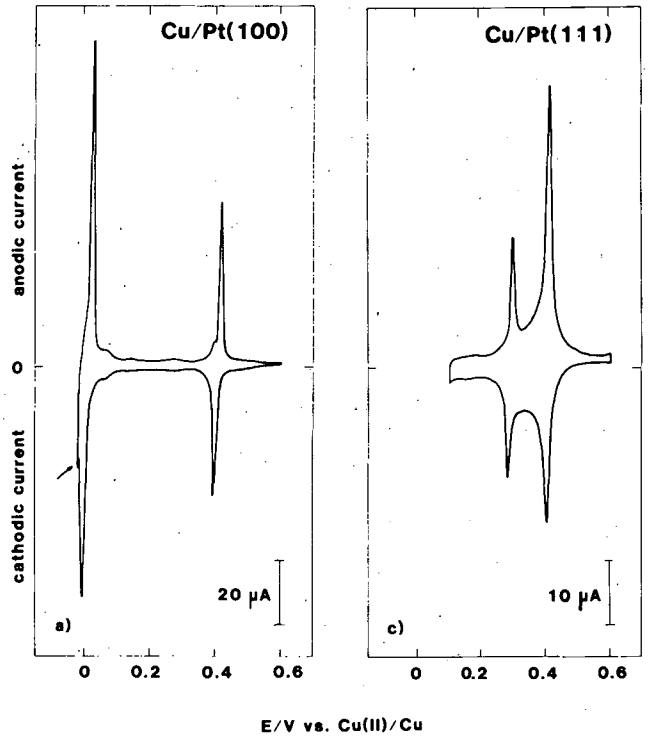

Figure 1-1. Cyclic voltammetry on Pt single crystals in 0.3M HF + 7.8 × 10^{-4}M Cu(II) at 10 mV·sec^{-1}. The contact area was the same on each crystal, but the absolute value was not accurately known (~0.3 cm^2). The arrow in (a) indicates the beginning of bulk deposition. (XBL 841-267A)

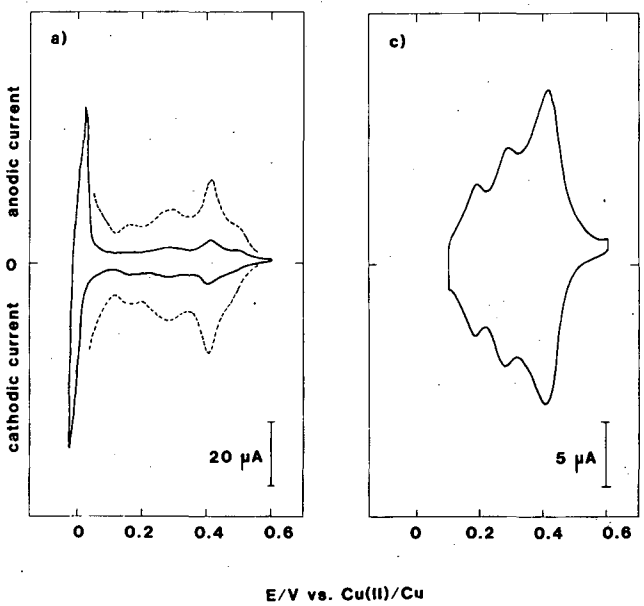

Figure 1-2. Cyclic voltammetry on anodically pretreated Pt single-crystal surfaces using the same conditions shown in Figure 1-1. Anodic pretreatment was 10 times from −0.25 to 1 V at 100 mV·sec^{-1}. Similar voltammetry was observed on single crystals that were ion bombarded but not annealed. (XBL 841-269A)

sites on the surface. The UPD peaks occur at the same potentials on both the short-range and long-range ordered surfaces, indicating, as expected, that the adsorption energy is determined by site symmetry due to the highly localized nature of adsorption bonding. Steps (or dislocations) have the effect of introducing sites with different adsorption energies. Long-range order appears to have a second-order effect that is manifested in the peak widths.

---

† Present address: IBM T.J. Watson Research Center, Yorktown Heights, New York 10598.

2. Auger Electron Spectroscopy (AES) and Thermal-Desorption Spectroscopy (TDS) Studies of Electrochemically Oxidized Pt(100) (Publication 6)

F.T. Wagner† and P.N. Ross

Anodic films formed on Pt(100) in 0.3M HF using a thin-layer electrochemical cell within a vacuum envelope were emersed and transferred to ultrahigh vacuum for study by AES and TDS. Comparison of the oxygen coverage determined in vacuum by AES with the oxygen coverage determined in solution by coulometry indicated that only films formed above 1.1 V versus the reversible hydrogen electrode (RHE) survived emersion and evacuation. As the emersion potential increased above 1.1 V (RHE), the integrated H_2O and O_2 thermal-desorption signals increased in parallel, with a constant O:H_2O stoichiometry consistent with the formation of a hydroxide-type layer, i.e., $Pt(OH)_x$. The oxygen coverage determined by both AES and TDS saturated at an emersion potential of 1.9 V (RHE) with formation of a surface phase containing 2.3 O/Pt and ~2 H_2O/Pt. X-ray photoemission spectroscopy (XPS) and secondary-ionization mass spectroscopy (SIMS) analysis of this surface phase indicated that it is probably $Pt(OH)_4$ rather than $PtO_2 \cdot 2H_2O$. Kinetic analysis of TDS lineshapes indicated that a perimeter-controlled desorption model gave the best overall fit of lineshapes. This model indicates a growth mode for anodic films involving island formation and fusion, with the reverse process occurring on reduction. The water-desorption-peak temperature was 400 K, independent of film thickness, and a temperature much higher than that reported for surface-adsorbed hydroxyl groups produced by low-temperature (100 K) gas-phase coadsorption of O_2 and H_2O. The higher temperature for desorption is ascribed to the

incorporation of hydroxyls into a surface phase with displacement of Pt atoms from their metallic lattice positions, i.e., place-exchange. Oxygen was evolved from the dehydrated anodic films at much lower temperatures than from gas-phase chemisorbed oxygen. The oxygen-peak temperature difference is also ascribed to the subsurface state, but in this case (anhydrous oxide) the bulk phase has a heat of formation lower than the heat of adsorption. This unusual thermochemistry of the platinum-oxygen system is suggested to be the key to understanding the electrocatalytic properties of platinum.

---

†Present address: General Motors Research and Development Laboratory, Warren, Michigan 48095.

3. Work in Progress

The catalytic effect of the impregnation of acetylene black by oxides of cobalt, iron, and nickel is being determined. Cobalt oxide was found to have a deleterious catalytic effect on carbon corrosion, while iron and nickel appear to have little or no effect on carbon corrosion. However, if cobalt oxide is removed from the oxide mix, the oxygen-evolution (charging) rate is adversely affected, so an equivalent replacement must be found. Recent experiments have indicated that chromium oxide is an equally effective evolution catalyst to cobalt oxide, and its effect on carbon corrosion is under study. Recent experiments have also indicated that graphitized thermal blacks exhibited significantly lower corrosion rates at oxygen-evolution potentials than acetylene black. Studies of iron-, chromium-, and nickel-catalyzed graphitized thermal black are in progress.

1984 PUBLICATIONS AND REPORTS

Refereed Journals

1. P.N. Ross and H. Sokol, "The Corrosion of Carbon Black Anodes in Alkaline Electrolyte: I. Acetylene Black and the Effect of Cobalt Catalyzation," J. Electrochem. Soc. **131**, 1742 (1984); LBL-16520.
2. P.N. Ross and P. Andricacos, "Diffusion Controlled Multisweep Cyclic Voltammetry: III. Deposition of Silver on Stationary and Rotating Disk Electrodes," J. Electrochem. Soc. **131**, 1531 (1984); LBL-16734.
3. P. Andricacos and P.N. Ross, "The Underpotential Deposition of Cu on Pt Single Crystals Prepared in an Ultra-High Vacuum System," J. Electroanalytical Chem. **167**, 301 (1984); LBL-17355.

Other Publications

4. P.N. Ross and F.T. Wagner, "The Application of Surface Physics Techniques to the Study of Electrochemical Systems," Chapter 2 in *Advances in Electrochemistry and Electrochemical Engineering,* Vol. **13**, H. Gerischer and C.W. Tobias, eds., Wiley-Interscience, New York, 1984, pp. 69–113; LBL-16235.

LBL Reports

5. F.T. Wagner and P.N. Ross, "LEED Spot Profile Analysis of Electrochemically Cycled Pt(100) and (111) Surfaces," submitted to Surf. Sci.; LBL-18498.
6. F.T. Wagner and P.N. Ross, "AES and TDS Studies of Electrochemically Oxidized Pt(100)," submitted to Appl. Surf. Sci.; LBL-17971.
7. P. Ross, "Corrosion of Carbon in Gas Evolving Electrodes," LBL-17851.

Invited Talks

8. P.N. Ross, "Carbon Corrosion in Gas Evolving Electrodes," International Society of Electrochemistry, 35th Meeting, Berkeley, California, August 5–10, 1984.
9. P.N. Ross, "Surface Science Means to Electrochemical Ends," Third Electrochemical Study Group, Fritz-Haber Institute, Berlin, West Germany, July 9–20, 1984.

Electrical and Electrochemical Behavior of Particulate Electrodes*

J.W. Evans, Investigator

INTRODUCTION

This work is concerned with the use of particulate electrodes (especially zinc) in the storage of electrical energy. One of the major difficulties encountered in the use of monolithic (e.g., slab-like) zinc electrodes in batteries is the change in the morphology of the electrode as the battery is cycled. For example, there is a tendency for zinc to form nodular or dendritic growths; this growth can impact battery performance by forming shorts or by penetrating cell diaphragms. These problems might be overcome by use of a particulate electrode where the zinc is present either as particles or as a thick coating on a particle substrate; the morphology and mechanical integrity of the particle is then of less concern.

One possible particulate electrode is a fluidized-bed electrode where zinc particles are maintained in a state of agitated suspension by the upward-flowing electrolyte. Such electrodes have been the main subject of this investigation to date. The behavior of a fluidized-bed electrode is very different from that of a conventional (monolithic) electrode. The latter operates at a nearly uniform and constant (or slowly varying) potential, while, in contrast, the potential at a point within the fluidized-bed electrode shows rapid fluctuations with time. Furthermore, if the potential fluctuations at a point are averaged over time, then this average potential varies with position in the electrode. These changes in potential affect the electrochemistry of zinc deposition and the morphology of the deposit. This investigation is concerned with these effects, as well as with the engineering issues of cell design and the production of zinc particles.

1. Fluidized-Bed Electrodeposition of Zinc (Publication 2)

V. Jiricny, T. Huh, and J.W. Evans

Experiments have been carried out in which zinc has been deposited in a laboratory fluidized-bed electrode at superficial current densities up to 10,000 A/m^2. The electrode has been shown to yield zinc deposits at current efficiencies and electric-power consumptions comparable with those of conventional cells operated at much lower current densities. Electrolytes used have been both "pure" acidified zinc sulfate solutions and ones containing impurities frequently found in commercial electrolytes (nickel, antimony, etc.). Preliminary experiments have been carried out in which the fluctuating electrolyte and particle potentials within the fluidized cathode have been studied. Analysis of the potential transients reveals two different kinds of bed behavior.

2. Potential Distributions and Transients in Particulate Electrodes of Possible Use in Energy Storage (Publication 3)

T. Huh and J.W. Evans

The use of a fluidized zinc electrode for battery applications is being examined. A preliminary engineering design reveals an energy density of 156 Wh/kg zinc plus electrolyte and an average power density of 53 W/kg for a 15-kWh battery designed for an average discharge power of 5 kW.

Considerable research has been carried out on the gross behavior of the particulate electrode, especially the fluidized-bed electrode, since its invention in the late 1960s. However, research on the transient behavior of such electrodes is still sparse. In the present research project, the potential transients in both the fluidized-bed electrode and the moving-bed

*This work was supported by the Assistant Secretary of Conservation and Renewable Energy, Office of Energy Systems Research, Energy Storage Division of the U.S. Department of Energy under Contract No. DE-AC03-76SF00098.

electrode were analyzed, and the variations of these transients with position in the electrodes were determined.

Due to the characteristic hydrodynamic behavior of the two media (particles and electrolyte) in the particulate electrode, potential transients are inherent. Not only is the overall electrode performance affected by the potential transients, but also the electrochemical-reaction rates are affected, because the electrochemical reaction taking place at the particle surface is proceeding under an unsteady-state condition.

In the fluidized-bed electrode, the potential fluctuations of different kinds of particles show distinct differences in behavior, and these fluctuations are also affected by bed expansion and applied current density, i.e., local resistivity and local electric field. The manner in which the potentials are distributed throughout the volume of the electrode is influenced by both ionic conduction in the electrolytes and electronic conduction from particle to particle. Figure 2-1 shows the transient behaviors of the particle potential, electrolyte potential, and local overpotential for the Zn deposition reaction onto Sorapec (zinc-coated polymer) particles with a current density (superficial current density at the active area of the diaphragm) of 200mA/cm^2 and a bed expansion of about 30%. Figure 2-2 shows the statistical analysis of the particle potential fluctuations of Figure 2-1. The particle and electrolyte potential fluctuations are seen as composed of two different behaviors, a low-frequency large-amplitude fluctuation and a broad-band fluctuation. This difference becomes clear from the power-density spectrum of Figure 2-2, which is composed of low-frequency "flicker" noise and wide-frequency-band white noise.[1] Figure 2-3 is from the Zn dissolution reaction with about 25% bed expansion. The left and center panels show the tran-

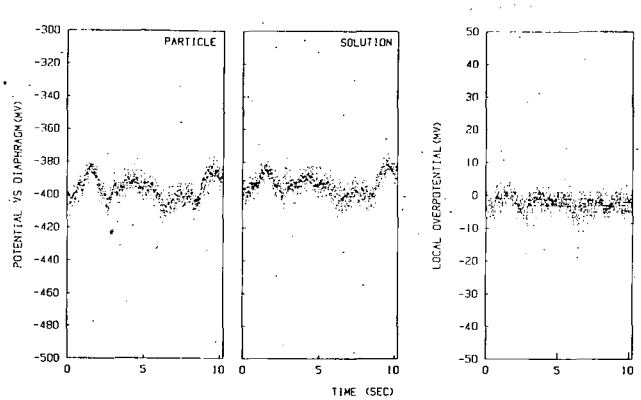

Figure 2-1. Fluctuations of particle and electrolyte potential and of local overpotential measured in a fluidized particulate electrode consisting of zinc-coated plastic spheres. (XBL 853-1495)

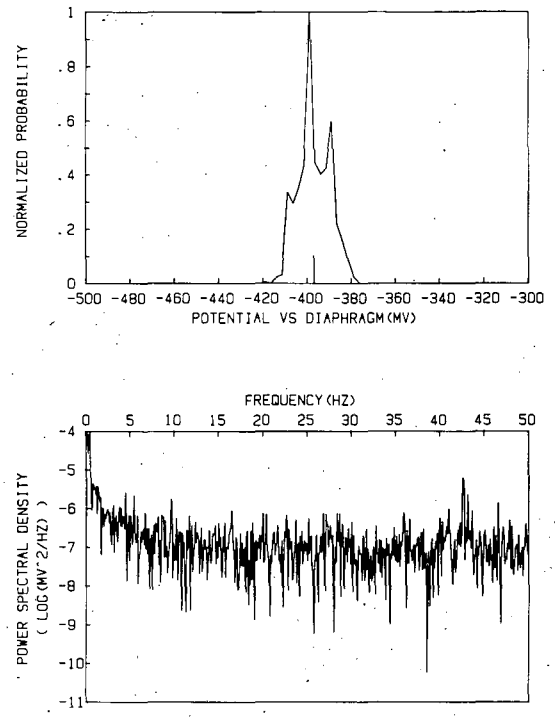

Figure 2-2. Statistical analysis of the particle potential fluctuations of Figure 2-1. (XBL 853-1496)

sients of the zinc-coated Cu particles and the Sorapec particles, respectively, with current density of 100 mA/cm^2. The right panel shows the transient of the Sorapec particles with 200 mA/cm^2 current density. The effect of different particle density and of different local electric field can be seen. The standard deviations are 16.5 mV and 2.4 mV, respectively, for Zn-coated Cu and Sorapec at 100 mA/cm^2. This difference can be explained by the different hydrodynamics of the fluidized bed, which depends on the density differences between the two media. For the heavy zinc-coated copper particles, the fluidized bed undergoes "bubbling" behavior because of the large density difference. Because of those bubbles (which are not gas bubbles but regions of low particle concentration), the local resistivity of the bed will fluctuate. This fluctuation of Zn-coated Cu particles is dominated by flicker noise, but this flicker noise is less for Sorapec particles. However, this flicker noise is synchronous in the particles and electrolyte. That is, the local reaction rate, which is a function of local overpotential, will not be affected directly. This can be seen, for example, in the almost flat band of the overpotential transient in Figure 2-1. Figure 2-4 shows the time-averaged overpotential distribution through the bed. As expected from mathematical models for porous electrodes, the reaction rate in both anodic and

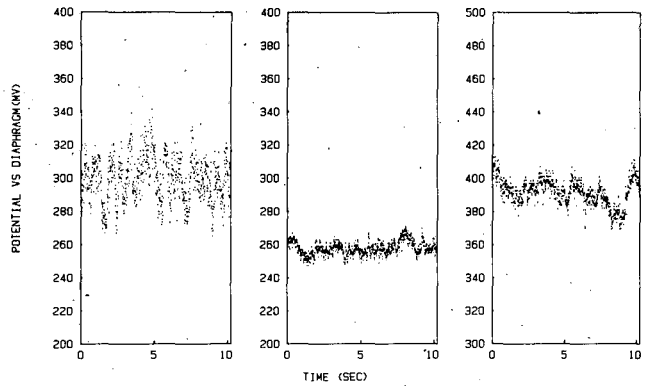

Figure 2-3. Fluctuations of particle potentials from zinc dissolution reaction with about 25% bed expansion. Left panel: transients of the zinc-coated Cu particles, 100 mA/cm^2 current density. Center panel: transients of the Sorapec particles, 100 mA/cm^2 current density. Right panel: transients of the Sorapec particles, 200 mA/cm^2 current density. (XBL 853-1497)

cathodic reactions is higher at the current feeder and diaphragm side than at the center of the bed.

1. It is suggested that low-frequency flicker noise is caused by large-scale hydrodynamic behavior of the bed, while the white noise is due to smaller-scale stochastic phenomena such as interparticle conduction during collision.

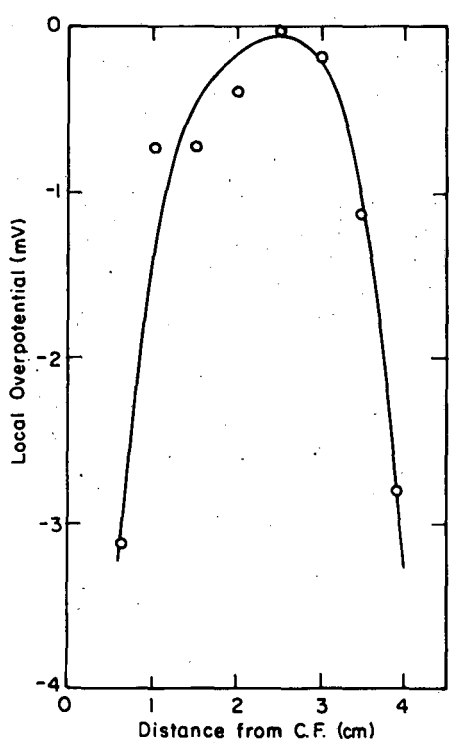

Figure 2-4. Variation of time-averaged overpotential with distance from current feeder (C.F.) in a fluidized bed of zinc-coated plastic spheres onto which zinc is being deposited cathodically. (XBL 853-1498)

3. Fluidized-Bed Electrowinning of Zinc from Chloride Electrolytes (Publication 4)†

Nigel E. Tuffrey, V. Jiricny, and J.W. Evans

The fluidized-bed electrowinning of zinc from chloride electrolytes has been studied in a laboratory cell. The cell has been operated at superficial current densities in the range 1,200–7,500 A/m^2 with catholytes containing up to 62 kg/m^3 Zn and up to 28 kg/m^3 HCl. Anolytes examined contained 59 kg/m^3 NaCl and up to 100 kg/m^3 HCl; in some instances the anolyte had the same composition as the catholyte. Both "pure" catholytes and ones with deliberate additions of impurities (Ni, Co, and Sb) were used. Pure solutions yielded current efficiencies and power consumptions comparable to or better than those of cells with conventional electrodes. Antimony (particularly in combination with Ni and Co) has a detrimental effect on cell performance; this detrimental effect was largely alleviated by simultaneous additions of glue.

†Dr. Jiricny, who played an advisory role in this research, was supported by The National Science Foundation.

4. Work in Progress

Rotating-disc experiments are in progress to determine the effects of potential fluctuations (such as those encountered in particulate electrodes) on the morphology of electrodeposited zinc. This is being done using a potentiostat controlled by a microcomputer in which data on potential fluctuations in a fluidized-particulate electrode are stored. Fluctuation of the current density of the rotating-disc electrode about some mean yields a very different morphology from that obtained at a constant current density equal to this mean. A cell has been constructed with a fluidized zinc electrode and an air-counter electrode to allow engineering evaluations of the particulate-electrode concept.

1984 PUBLICATIONS AND REPORTS

Refereed Journals

1. R. Moreau and J.W. Evans, "An Analysis of the Hydrodynamics of Aluminum Reduction Cells," J. Electrochem. Soc. **131**, 2251 (1984).

Other Publications

2. V. Jiricny, T. Huh, and J.W. Evans, "Fluidized Bed Electrodeposition of Zinc," in *Proc. Spring Meeting Electrochem. Soc.,* Cincinnati, Ohio, May 1984.
3. T. Huh and J.W. Evans, "Potential Distributions and Transients in Particulate Electrodes of Possible Use in Energy Storage," in *Proc. DOE Battery and Electrochemical Contractors Conf.,* Washington, D.C., June 1984; *Proc. Int. Soc. Electrochem. Meeting,* Berkeley, California, August 5–10, 1984, Ext. Abs. A4-11.

LBL Reports

4. N.E. Tuffrey, V. Jiricny, and J.W. Evans, "Fluidized Bed Electrowinning of Zinc from Chloride Electrolytes," LBL-18738.

Electrochemical Properties of Solid Electrolytes*

Lutgard C. De Jonghe, Investigator

INTRODUCTION

Solid electrolytes can find application in a number of energy-producing or energy-storing devices, including high-energy-density batteries. Sodium beta″-alumina ceramic electrolytes are used in one important application as a solid membrane in an electrochemical battery using sodium metal and sodium polysulfide as storage electrodes at ~300°C. Degradation of the solid electrolytes is a potentially life-limiting factor for such batteries and has been a hindrance to large-scale commercialization of the system. The origins of electrochemical degradation phenomena of the sodium beta″-alumina solid electrolytes, therefore, have been studied in this program, and means have been sought to define the cell operating conditions under which such degradation is minimal or absent. One form of electrolyte failure involves the catastrophic propagation of a sodium-filled crack. This type of failure may be assisted by the presence of residual mechanical stresses in the ceramic or by mechanical stresses that arise during the operation of the cell. The interaction of such stresses with the electrolytically driven crack propagation has thus been analyzed. One possible improvement of the properties of the electrolyte involves its strengthening by a dispersion of fine zirconia particles. Such electrolytes are under investigation. Additionally, various electrode impurities may adversely affect the cell operation; the effects of such impurities on failure initiation and on electrolyte/electrode-interface electrochemical behavior have been studied. Significant interface polarization has been known to correlate with electrolyte degradation, but the mechanisms of this polarization are not known.

1. Solid-Electrolyte Degradation with Applied Stress (Publication 3)

D.C. Hitchcock and L.C. De Jonghe

When solid-electrolyte degradation by crack propagation is caused by Poiseuille pressure, generated by the electrolytic deposition of metallic sodium inside a pre-existing surface flaw, an applied mechanical stress affects the degradation process in two ways. First, it will change the width of the crack, thereby changing the Poiseuille pressure. Second, it will contribute to the stress intensity at the crack tip. An analysis of the crack-propagation process under the combined influence of the electrolytically generated and applied mechanical stresses yields the result that the total stress-intensity factor at the crack tip is simply the sum of the independent stress-intensity factors. This result can be used to predict the current-density failure thresholds for electrolytes in service conditions where combinations of electrolytic and mechanical stresses exist.

2. Electrochemical Processes at the Sodium/Sodium Beta″-Alumina Interface (Publication 4)

C. Mailhe

The electrochemical characteristics of interfaces and electrochemical cell behavior can be deduced from an analysis of current-potential data. The current-potential curves were determined for Na/Na cells of cylindrical design incorporating a sodium beta″-alumina electrolyte tube separating the inner (working) and the outer (counter) electrodes. The inner electrode was prepared by electrolyzing sodium into the tube from the counter electrode. A three-electrode system permitted the observation of the electrochemical response of the sodium/solid-electrolyte interface. The concentration of the oxygen

*This work was supported by the Assistant Secretary of Conservation and Renewable Energy, Office of Energy Systems Research, Energy Storage Division of the U.S. Department of Energy under Contract No. DE-AC03-76SF00098.

in the working electrode was controlled by the addition of sufficient Na_2O_2 for oxygen saturation, or by the addition of a metal foil, such as vanadium, to bring the oxygen fugacity to the metal/oxide equilibrium value. Experiments were performed at 350°C, where the solubility of Na_2O is 215 ppm of oxygen, and at 160°C, where the corresponding solubility is about 4 ppm. The resistances for filling and emptying the electrolyte tubes were determined from the current-potential curves and were designated Rc and Rd, respectively. Figure 2-1 gives an example of these curves. For all cases where asymmetric polarization was observed, the resistance for discharge was found to be greater than for charge, e.g., Rd/Rc > 1.

At the operating temperature of the sodium/sulfur battery (350°C), the presence of oxides increased the Na/solid-electrolyte interface resistance. The introduction of an oxygen-gettering metal such as vanadium that can reduce Na_2O to Na at that temperature decreased the interface resistance significantly. A film of Na_2O, formed at the Na/electrolyte interface, was probably responsible for the relatively high value of the electrochemical-interface resistance. Other metals were found to have a similar action in proportion to their oxide/metal equilibrium oxygen fugacity.

At lower temperatures the effects of the Na_2O formation was considerably more pronounced than at 350°C, as shown in Figure 2-2, and the kinetics of various interface reactions were substantially slowed.

The observations led to the conclusion that the control of the oxygen fugacity is an important factor in prolonging the useful lifetime of sodium beta″-alumina in service conditions, and that such control can be achieved through the addition of suitably reducing metal getters such as vandium, titanium, zirconium, or their alloys. A patent has been applied for.

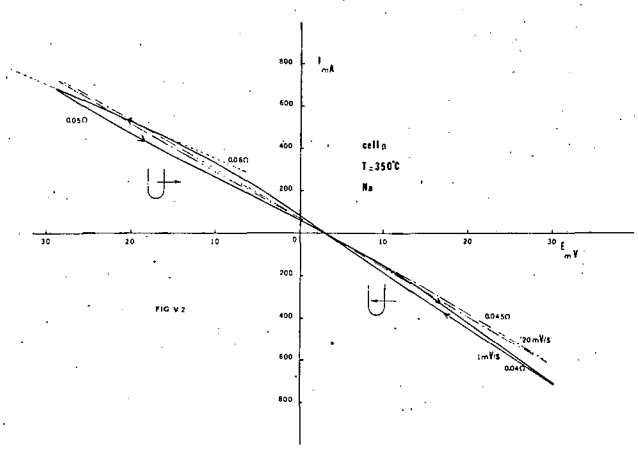

Figure 2-1. Current-voltage curve of a Na/Na cell at 350°C. Cell cycling was done at 1 and 20 mV/sec. (XBL 845-1678)

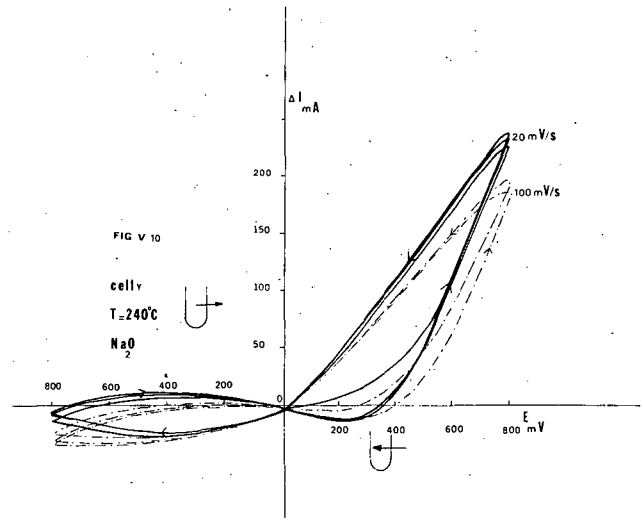

Figure 2-2. Current-voltage curve of a Na/Na cell at 240°C. A large part of the ohmic behavior has been electronically suppressed to highlight the deviations. Cell cycling was done at 20 and 100 mV/sec. (XBL 845-1683)

3. Work in Progress

Ongoing work concerns the examination of the effects of water in the breakdown initiation at both the sodium and the sulfur sides of the electrolytes under dynamic cell conditions; the comparison of the critical-current densities for breakdown initiation of zirconia-toughened and single-phase electrolytes; the examination of slow degradation phenomena; and a quantification of the effects of dissolved oxygen on the reduction processes at the sodium electrode.

1984 PUBLICATIONS AND REPORTS

Refereed Journals

1. Lutgard C. De Jonghe, A. Buechele, and M. Armand, "Oxygen Interstitial Transport and Chemical Coloration in Sodium Beta-Alumina," Solid State Ionics **9**, 165 (1983); LBL-15308.
2. D. Hitchcock and L.C. De Jonghe, "Fracture Toughness Anisotropy of Sodium Beta-Alumina," J. Am. Ceram. Soc. **66**, C204 (1983); LBL-16115.

LBL Reports

3. D.C. Hitchcock and L.C. De Jonghe, "Solid Electrolyte Degradation with Applied Stress," LBL-18218.

4. C. Mailhe (M.S. Thesis), "Electrochemical Processes at the Sodium/Sodium Beta″-Alumina Interface," LBL-17687.

Invited Talks

5. L.C. De Jonghe, "Degradation of Solid Electrolytes," Gordon Research Conference, New London, New Hampshire, July 1984.
6. L.C. De Jonghe, "Recent Work on Solid Electrolytes at LBL," Sandia National Laboratory, Albuquerque, New Mexico, November 1984.
7. C. Mailhe and L.C. De Jonghe, "Influence of Oxygen on Sodium/Beta″-Alumina Interface Polarization," American Ceramic Society Meeting, San Francisco, California, October 1984.
8. D.C. Hitchcock and L.C. De Jonghe, "Electrolytic Degradation of Beta″-Alumina with Controlled Flaws," American Ceramic Society Meeting, San Francisco, California, October 1984.
9. L.C. De Jonghe, "Solid Electrolyte Degradation Experiments," DOE-EPRI Workshop on Na/S Batteries, Sandia National Laboratory, Albuquerque, New Mexico, March 1984.
10. L.C. De Jonghe, "Degradation of Solid Electrolytes," International Society of Electrochemistry Meeting, Berkeley, California, August 1984.

Analysis and Simulation of Electrochemical Systems*

John Newman, Investigator

INTRODUCTION

This program includes the investigation of efficient and economical methods for electrical-energy conversion and storage, development of mathematical models to predict the behavior of electrochemical systems and to identify important process parameters, and experimental verification of the completeness and accuracy of the models. Specific projects include analysis of the thin-gap flow cell for electrochemical synthesis and energy storage, mathematical modeling of the Li-Al/FeS battery and the Li-Si/FeS_2 battery, study of transport processes in sodium polysulfide melts, alternating-voltage measurements on the dissolution of zinc, and modeling and measuring the response of a redox system to alternating current in a flow-through porous electrode.

1. The Corrosion of a Zinc Rotating Disk in One-Molar Hydrochloric Acid (Publication 5)

Alan Hauser

The corrosion of a zinc rotating disk in one-molar hydrochloric acid has been studied using a potentiodynamic-polarization method. The relationship between the electrochemical behavior of zinc and its corrosion rate in an oxygen-free, aqueous solution is described. The principles of the corrosion process presented here emphasize how important it is that engineers understand the underlying fundamental electrochemical concepts. Both experimental and theoretical treatments of the corrosion process have been investigated.

Experimental rotating-disk data at a rotation speed of 1600 rpm are presented. The polarization curves are analyzed to determine the transfer coefficients and rate constants for the anodic zinc-dissolution and cathodic hydrogen-evolution reactions. The set of parameters that may be used to fit best the experimental data was compared to those reported in the literature, and significant differences are apparent for the corrosion of zinc. Electrolyte and electrode impurities are possible causes for the differences.

It is of interest to use the experimentally determined kinetic parameters in a mathematical model to predict corrosion rates. A modified Butler-Volmer equation is used to describe the kinetics of the zinc and hydrogen charge-transfer reactions accounting for the forward and back terms of each reaction. Mass transfer of the electroactive and complexed zinc species is accounted for with the assumption that the homogeneous reactions are in equilibrium.

The experimental polarization curve shows good agreement with that predicted theoretically provided the back reactions are neglected. However, when the modified Butler-Volmer equation is used, the cathodic polarization sweep away from the open-circuit potential is significantly different from what was expected owing to the effect of the cathodic zinc reaction. The results of the model are compared to conventional polarization techniques that underestimate the corrosion-current density. This comparison indicates the importance of the model.

2. A General Energy Balance for Battery Systems (Publication 10)

Dawn Bernardi, Ellen Pawlikowski, and John Newman

A general energy balance for battery systems has been developed. This equation is useful for estimating cell thermal characteristics. Reliable predictions of cell temperature and heat-generation rate are required for the design and thermal management of battery systems. The temperature of a cell changes as a result of electrochemical reactions, phase changes, mixing effects, and joule heating. The equation developed incorporates these effects in a complete and general manner. Simplifications and special cases are discussed. The results of applying the energy balance to a mathematical model of the LiAl/FeS cell discharged through two different reaction mechanisms are given as examples. The examples illustrate how the energy equation may be applied to a specific system to examine the relative contributions corresponding to the terms in the equation. The examples show that the processes involved in cell-heat generation may be complex and that the application of a sufficiently general energy equation is advantageous.

*This work was supported by the Assistant Secretary of Conservation and Renewable Energy, Office of Energy Systems Research, Energy Storage Division of the U.S. Department of Energy under Contract No. DE-AC03-76SF00098.

3. Work in Progress

A mathematical model incorporating concentrated-solution theory has been developed to analyze experimental data from the corrosion of a zinc rotating-disk electrode in one-molar hydrochloric acid. This model will be used to predict the electrochemical impedance of the rotating-disk electrode. An experimental alternating-current impedance investigation will accompany the mathematical-modeling effort.

The method of restricted diffusion is being used to determine differential diffusion coefficients in sodium polysulfide melts. The experimental apparatus that will perform the measurements has been designed and tested. The diffusion coefficient will be measured as a function of melt composition and temperature. Comparisons will be made to the predictions of a microscopic melt model and to the scant published data.

A mathematical model has been developed to calculate the concentration, potential, and current distribution in a thin-gap channel flow cell. The model is being used to show the effects of interacting diffusion boundary layers on current distribution. Preliminary experimental work is being done to test the model. In future work, the model will be used to assess the effects of multiple reactions and to compare channel flow cells to flow-by porous electrodes.

A model is being developed to predict the isothermal/galvanostatic discharge behavior of the Li-Al/FeS_2 battery. The model does not yet simulate the entire discharge, but it confirms experimental data that show that the low conductivity of the product of the first reaction limits the utilization of the electrode. The modeling effort will continue to allow the simulation to proceed to greater depths of discharge and to predict the behavior of the Li(Si)/FeS_2 battery.

In the preparation of porous nickel electrodes, nickel hydroxide is precipitated from acidified nickel nitrate solutions. This electrochemical system is being studied by observing the current response to slow potential sweeps and potential steps. A mechanism has been proposed to explain the observed behavior. The experimental studies will continue, and theoretical work will be done to propose quantitatively the reaction sequence.

A computer model has been developed to predict the response to alternating-current signals of a redox reaction with soluble reactants and products in a flow-through porous electrode. A glassy carbon rotating-disk electrode will be used in preliminary experiments designed to find a suitable redox couple for use in the flow-through-porous-electrode experiments. The transport and kinetic parameters needed for the model will be measured by linear-sweep voltammetry. Finally, the model will be verified by comparing its predictions to experimental measurements of the frequency response of the flow system.

Sustained current oscillations in the iron-sulfuric acid system have been reported by several investigators, and models have been proposed to explain them. However, the observed oscillatory behavior is not yet completely understood, and more experimental information is needed. Potentiostatic experiments using iron rotating hemispherical electrodes will be performed to determine the effect of geometry on the electrochemical oscillations. In addition, the ac impedance behavior of the iron corrosion system will be studied experimentally, using a frequency response analyzer.

1984 PUBLICATIONS AND REPORTS

Refereed Journals

1. Tim Risch and John Newman, "A Theoretical Comparison of Flow-Through and Flow-By Porous Electrodes at the Limiting Current," J. Electrochem. Soc. **131**, 2569–2574 (1984); LBL-16143.
2. Philip Lessner and John Newman, "Hydrodynamics and Mass Transfer in a Porous-Wall Channel," J. Electrochem. Soc. **131**, 1828–1831 (1984); LBL-16568.
3. Bernard Tribollet and John Newman, "Impedance Model for a Concentrated Solution," J. Electrochem. Soc. **131**, 2780–2785 (1984).†

Other Publications

4. John Van Zee, Greg Klein, Ralph E. White, and John Newman, "Extension of Newman's Numerical Technique to Pentadiagonal Systems of Equations," in *Electrochemical Cell Design,* Ralph E. White, Ed., New York, Plenum Press, 1984, pp. 377–389.
5. John Newman, "Transport Properties of Concentrated Solutions," in *Proc. EPRI/LBL Workshop on the Electrochemistry of Zinc/Halogen Batteries,* Nov. 30–Dec. 1, 1983, Philip C. Symons, Electrochemical Engineering Consultants Inc., Northville, Michigan, 1984, pp. 5–5 to 5–21.

LBL Reports

6. Alan Hauser (M.S. Thesis), "The Corrosion of a Zinc Rotating Disk in One Molar Hydrochloric Acid," LBL-17461.

Invited Talks

7. John Newman, "Transport Studies," Sixth DOE Battery and Electrochemical Contractor's Conference, Washington, D.C., June 25, 1984.
8. William Tiedemann (speaker) and John Newman, "Mathematical Modeling of Phenomena Contributing to Thermal Rise in Lead-Acid Batteries Used in Electric Vehicles," Symposium on Advances in Lead-Acid Batteries, New Orleans meeting, The Electrochemical Society, October 7–14, 1984.
9. Bryan McKinney, William Tiedemann (speaker), and John Newman, "Short Circuit Currents in UPS Batteries," Symposium on Advances in Lead-Acid Batteries, New Orleans meeting, The Electrochemical Society, October 7–14, 1984.
10. Dawn Bernardi (speaker), Ellen Pawlikowski, and John Newman, "A General Energy Balance for Battery Systems," New Orleans meeting, The Electrochemical Society, October 7–14, 1984; LBL-17776.
11. Richard Pollard (speaker) and John Newman, "The Juxtaposition of Discharging Solid Phases," invited address, Berkeley meeting, International Society of Electrochemistry, August 5–10, 1984.
12. William Tiedemann (speaker) and John Newman, "Relaxation of Potential in Battery Electrodes," invited address, Berkeley meeting, International Society of Electrochemistry, August 5–10, 1984.

---

†Supported by the National Science Foundation through the United States-France Exchange of Scientists Program with le Centre National de la Recherche Scientifique No. G050252.

Magnetic Fusion Energy

MAGNETIC FUSION ENERGY

Structural Materials and Weldments for High-Field Superconducting Magnets*

J.W. Morris, Jr., Investigator

INTRODUCTION

The purpose of this work is the design and laboratory development of improved structural materials for the cases and support structures of high-field superconducting magnets. The research is motivated by the structural-material needs for future generations of high-field superconducting magnets, which call for alloys that have exceptional strength and toughness in welded structures in high magnetic fields at 4.2 K. The research is divided into three tasks. The first is the development of high-strength ferritic steels and weldments for the magnet structure. The second is the development of austenitic Fe-Mn steels and weldments. The third is the identification of those mechanical phenomena that may influence structural reliability in high magnetic fields at 4 K. The third task now concentrates on low-temperature fatigue and on the influence of high magnetic fields on the mechanical properties of metastable austenitic steels.

1. Cryogenic Materials for High-Field Superconducting Magnets (Publication 2)

J.W. Morris, Jr., and E.N.C. Dalder†

This paper reviews needs and current research on materials for high-field superconducting magnets. The review is written from an American perspective but recognizes that much of the most important current research is done interactively in parallel programs in the United States and Japan. High-field superconducting magnets are used principally for magnetic-fusion-energy devices and accelerators for research in particle physics. The advance of both technologies has increased the field, size, and performance requirements of such magnets. More stringent requirements are expected in the future. The needed materials include both structural materials for the magnet case and support structure and high-field superconducting wire for magnet winding. Current research on both classes of materials is briefly described and discussed.

*This work was supported by the Director, Office of Energy Research, Office of Development and Technology, Magnetic Systems Division of the U.S. Department of Energy under Contract No. DE-AC03-76SF00098.

†Permanent address: Superconducting Magnet Development Group, Lawrence Livermore National Laboratory, Livermore, California.

2. Temperature and Mn Content Dependences of Tensile Deformation in Fe/High-Mn Binary Alloys (Publication 4)

Y. Tomota and J.W. Morris, Jr.

The microstructure and mechanical properties of Fe-Mn binary alloys depend strongly on the Mn content. However, despite extensive research this dependence is poorly understood. This research used 16 to 35 wt% Mn binary alloys to identify the microstructure dependence on the tensile properties. As the Mn content is decreased from 36 to 25% Mn, the work hardening is increased rapidly. This work hardening is due to the intrusion of ϵ-martensite. Although appropriate ϵ formation during deformation enhances the uniform elongation as transformation-induced plasticity (TRIP), large amounts of ϵ deteriorate the ductility drastically. From 20 to 16% Mn, α' is also induced by deformation and is effective in lowering the work hardening and increasing the ductility. Martensite transformations also depend on temperature, and tensile tests were conducted at various temperatures between 77 and 573 K. In the 25Mn alloy a reverse transformation occurs from $\epsilon \rightarrow \gamma$ above 473 K. Through these elevated-temperature experiments, the plastically deformed γ was found to be stabilized against the $\gamma \rightarrow \epsilon$ transformation.

3. Mechanical Stabilization of Austenite Against ϵ-Martensite and its Effect on Deformation Behavior in High-Mn Steels (Publication 5)

Y. Tomota and J.W. Morris, Jr.

The ϵ-martensite phase is induced by deformation in several commercially developed high-Mn steels; however, the role of ϵ formation during deformation has not been clarified. Although the influence of grain size on the amount of ϵ at room temperature (RT) is small in 17 and 25% Mn binary alloys, ausforming is found very effective in stabilizing austenite. Austenite was stable at 473 K in the 25Mn alloy, and the strength was increased by ausforming but the elongation dropped. At RT or 77 K about 50% ϵ generation increases elongation (TRIP) but decreases the yield strength of the ausformed material. This means that the stress for the onset of ϵ-martensite formation becomes smaller than that for conventional plastic flow (slip), causing a decreased yield strength as the temperature is lowered. In the 17Mn alloy α' martensite is also induced with ϵ, and the flow curves are characteristic of α' formation. A very low work-hardening region exists at the early stage of plastic flow, followed by high work hardening.

4. Strength vs. Toughness Relation in Fe/High-Mn Alloys (Publication 6)

Y. Tomota and J.W. Morris, Jr.

The effect of Mn content on the ductile-brittle transition (DBT) behavior was investigated in 16 to 36 wt% Mn steels using Charpy impact tests and the previously determined tensile properties. The hcp ϵ-martensite existing in the as-quenched condition and/or formed during deformation deteriorates the toughness, although the fractured surfaces consist of dimples. The deformation-induced α-martensite in 16 to 20% Mn alloys enhances the toughness but leads to the DBT associated with intergranular fracture at low temperatures. The alloys with more than 36% Mn also show intergranular fracture at 77 K, although the impact energy remains quite high. Auger spectroscopy of the fracture surfaces has not shown clear evidence of impurity segregation, and the reasons for intergranular fracture in these alloys are under investigation.

5. Weldability of 2BT-Treated 9Ni Steel with Ferritic Filler Metal (Publication 3)

H.J. Kim and J.W. Morris, Jr.

Fracture-toughness tests show that the weldment of 9% Ni steel has very high toughness values (300 MPa $\sqrt{m}$) at 77 K but becomes brittle at 4.2 K. Values of 110, 90, and 145 MPa $\sqrt{m}$ were obtained for the base metal, heat-affected zone (HAZ), and weld metal, respectively. It has also been determined that the microstructural source of HAZ toughness differs from that of the base metal.

6. The Influence of Processing on the Cryogenic Mechanical Properties of High-Strength, High-Manganese Stainless Steel (Publication 1)

R. Ogawa and J.W. Morris, Jr.

New high-strength structural steels have been required for the large superconducting magnets that will be used for the next-step test facility for fusion-reactor research. The new materials must have high yield strength accompanied with better toughness and better fatigue resistance compared with the conventional nitrogen-strengthened stainless steels such as AISI 304LN and 316LN that were used for the cases of the toroidal field coils for the Large Coil Project. A number of new high-manganese austenitic steels have been proposed for new cryogenic structural alloys since they can offer low costs, stable austenite, and high strength.

The influence of the hot-rolling condition and cold rolling on the mechanical properties of a nitrogen-strengthened high-manganese steel of nominal composition 18Mn-5Ni-16Cr-0.02C-0.22N was investigated. The results include: (1) grain refinement by low-temperature hot rolling raises the strength of the alloy but decreases the toughness rapidly; (2) cold rolling at room temperature is an effective way to raise the strength without rapid deterioration of the toughness; and (3) changing the hot-rolling condition did not affect the fatigue-crack growth rates, but a decrease in the fatigue-crack growth rates was observed for cold-rolled plates. This improvement of the fatigue resistance might be attributed to the improvement of the ductility through the suppression of the formation of the phase.

1984 PUBLICATIONS AND REPORTS

Refereed Journals

1. R. Ogawa and J.W. Morris, Jr., "The Influence of Processing on the Cryogenic Mechanical Properties of High Strength High Manganese Stainless Steel," Adv. Cryogenic Eng. **30**, 177 (1984); LBL-16528.
2. J.W. Morris, Jr., and E.N.C. Dalder, "Cryogenic Materials for High Field Superconducting Magnets," Kobe Steel Works Eng. Rep. **34**, 1 (1984); LBL-17921.

LBL Reports

3. H.J. Kim and J.W. Morris, Jr., "Weldability of 2BT-Treated 9Ni Steel with Ferritic Filler Metal," LBL-16531.
4. Y. Tomota and J.W. Morris, Jr., "Temperature and Mn Content Dependences of Tensile Deformation in Fe-High Mn Binary Alloys," LBL-18890.
5. Y. Tomota and J.W. Morris, Jr., "Mechanical Stabilization of Austenite Against ϵ Martensite and Its Effect on Deformation Behavior in High Mn Steels," LBL-18891.
6. Y. Tomota and J.W. Morris, Jr., "Strength vs. Toughness Relation in Fe-High Mn Alloys," LBL-18892.

Health and Environmental Sciences

Semiconductor Materials and Devices*

Eugene E. Haller, Investigator

INTRODUCTION

The recently achieved ultrahigh purity and crystalline perfection of large germanium single crystals and, to a lesser degree, silicon single crystals have led to the discovery of a large number of novel impurity and defect complexes that exhibit energy levels in the band gap of these semiconductors. Understanding the composition and electronic structure of these novel acceptors and donors through the use of a sensitive far-infrared spectroscopy technique and novel radioactive-tracer schemes represents one component of this research effort. Another closely coupled component focuses on the formation of these centers during crystal growth.

Two factors have helped greatly in identifying the composition of these novel acceptors and donors: (1) correlations between concentration and electronic-structure effects of a given center, and (2) control of the materials involved in the crystal growth and purification, such as the crucible material (typically synthetic silica or graphite) and the ambient (typically H_2, N_2, or vacuum). One of the major findings is that atomic hydrogen plays an important role in the formation and composition of many of the new impurity complexes. The information gained through this research is of immediate use to LBL's semiconductor radiation-detector program, which originated this research.

The use of ultrapure crystals as starting material for specially doped crystals is studied in connection with the development of sensitive far-infrared photoconductors for low-photon-flux applications in outer space and neutron-transmutation-doped germanium bolometers. The high ratio of intentional-dopant concentrations and residual-impurity concentrations has led to photoconductors with very high responsivity working at close to the photon noise limit.

The close coupling between crystal synthesis and analysis has enabled us to effectively study and use these extremely pure and structurally perfect materials.

*This work was supported in part by the Director, Office of Energy Research, Office of Health and Environmental Research, U.S. Department of Energy under Contract No. DE-AC03-76SF00098, and in part by NASA Contract No. W-14,606, under interagency agreement with the Department of Energy.

1. Positively Charged Acceptors with $(1s)^3$ and $(1s)^4$ Configurations (Publication 26)

E.E. Haller, R.E. McMurray, Jr., N.M. Haegel, and L.M. Falicov

We show that multiple acceptors in Ge can readily bind an extra hole. Experimental values for the binding energies of the extra hole for the multiple acceptors Be, Mg, Mn, Zn, Hg, and Cu in Ge are compared to model calculations. One such center (Zn^+) has been used for the first time as a long-wavelength ($\lambda < 500$ μm) photoconductor at T = 1.2 K. Using the Zn^+ photoconductor in high-resolution spectroscopy, we have discovered that the linear absorption coefficients for shallow acceptor and donor transitions are substantially larger than previously reported, making possible absorption spectroscopy of lightly doped ($<10^{12}$ cm^{-3}) samples (see Figure 1-1).

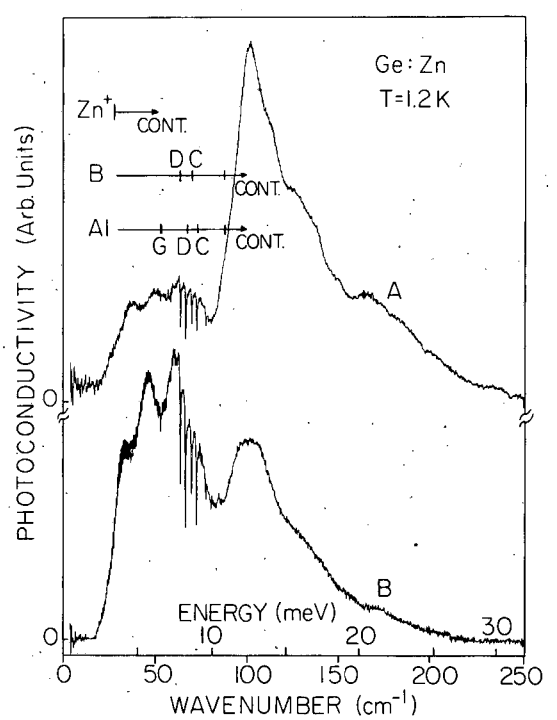

Figure 1-1. Far-infrared photoconductivity spectra of a Ge:Zn crystal recorded at T = 1.2 K. Trace A is obtained with a cold (1.2 K) black polyethylene filter, and trace B is obtained with a warm (300 K) black polyethylene filter. The spectra have not been normalized with the instrument response. (XBL 846-7092)

2. Deuterium in Germanium: Interaction with Point Defects (Publication 9)

S.J. Pearton, J.M. Kahn, W.L. Hansen, and E.E. Haller

Electrical measurements on deuterium plasma-treated germanium samples containing deep-level recombination centers show significant neutralization of these defects to depth of ~80 μm (see Figure 2-1). Chemical measurement of the deuterium profile after similar plasma treatment shows apparent incorporation depths of ~0.2 μm. We discuss experiments that resolve this discrepancy and show that hydrogen diffusion into the bulk of the germanium is responsible for the observed neutralization.

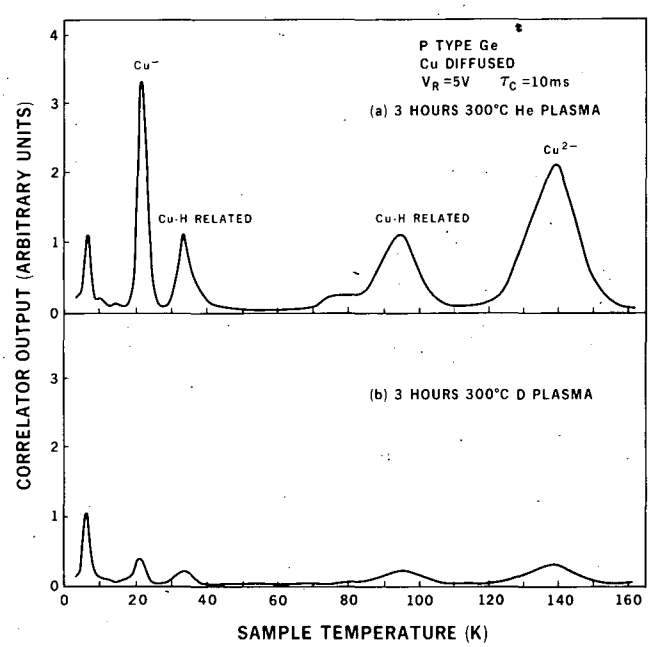

Figure 2-1. Deep-level transient-spectroscopy (DLTS) spectra taken at the same spectral conditions from copper-diffused germanium samples after (a) exposure to a 300-W, 0.1-Torr helium plasma for 32 hr at 300°C (this spectrum is identical to that of an unheated sample); and (b) exposure to a 300-W, 0.1-Torr deuterium plasma for 3 hr at 300°C, showing neutralization of the deep copper-related defects. The reverse bias V_R is 5 V and the correlator time constant T_c is 10 ms for both spectra. (XBL 838-11107)

3. The Nature of the Dominant γ-Induced Defects in High-Purity Germanium (Publication 8)

S.J. Pearton, A.J. Tavendale, J.M. Kahn, and E.E. Haller

For relatively low Co-60 γ-irradiation doses (3×10^{15} γcm^{-2}) and dose rates (2.0×10^{10} γcm^{-2} sec^{-1}), two hole traps (E_v + 0.23 eV, E_v + 0.38 eV) are the dominant defects introduced in high-purity germanium (see Figure 3-1). A comprehensive study involving crystals grown under a wide variety of conditions supports the hypothesis that these centers are most likely due to complexes between oxygen and lattice vacancies. Injection-enhanced annealing was observed for both these hole-trapping states, and a discussion is given of the seemingly dose-dependent nature of the defects produced in γ-irradiated high-purity p-type germanium.

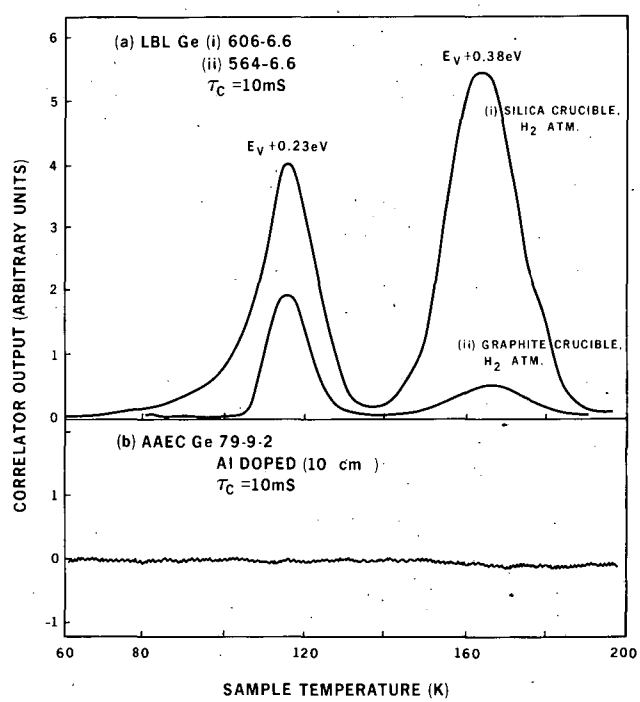

Figure 3-1. (a)(i) DLTS spectrum from γ-irradiated (dose = 3.4×10^{15} cm^{-2}) p-type sample ($N_A - N_D = 2 \times 10^{10}$ cm^{-3} prior to irradiation) grown from a silica crucible under H_2. (ii) DLTS spectrum from γ-irradiated (dose = 3.4×10^{15} γ cm^{-2}) p-type sample ($N_A - N_D = 2 \times 10^{10}$ cm^{-3} prior to irradiation) grown from a graphite crucible under H_2. Note the reduced defect density in this material of lower oxygen content. (b) DLTS spectrum from γ-irradiated (dose = 5×10^{16} cm^{-2}) aluminum-doped (p = 8×10^{14} cm^{-3}) p-type sample grown from a graphite crucible under H_2. No evidence of the two defect states is found in this low-oxygen-content material. (XBL 838-11099)

4. Development of High Responsivity Ge:Ga Photoconductors (Publication 17)

N.M. Haegel, M.R. Hueschen, and E.E. Haller

Czochralski-grown gallium-doped germanium (Ge:Ga) single-crystal samples with a compensation of 10^{-4} have been modified by the indiffusion of Cu to produce photoconductors that provide noise-equivalent powers (NEPs) comparable to current optimum Ge:Ga detectors but that exhibit responsivities a factor of 5–6 times higher when tested at a background photon flux of 10^8 photons/sec at $\lambda = 93$ μm (see Figure 4-1). The introduction of Cu, a triple acceptor in Ge that acts as a neutral scattering center, reduces carrier mobility and extends the breakdown field significantly in this ultralow-compensation material.

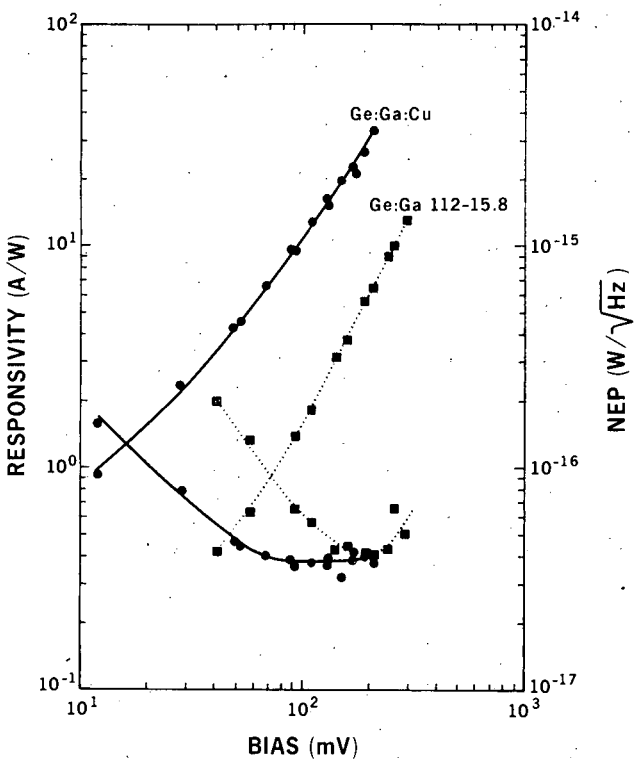

Figure 4-1. Responsivity (ascending lines) and NEP (descending lines) as a function of bias for the Cu-diffused detector (solid lines) and a standard Ge:Ga detector (dotted lines) ($N_{Ga} = 2 \times 10^{14}\,cm^{-3}$, $N_D \simeq 1 \times 10^{12}\,cm^{-3}$) at 3.0 K and 20 Hz. The higher responsivity at comparable NEP values shows the superior behavior of Ge:Ga:Cu photoconductors. (XBL 837-10633)

5. Work in Progress

The interaction of hydrogen with numerous defects and impurities in pure semiconductors is being studied. Hydrogenation can drastically reduce the concentration of deep levels, and hydrogen changes the electronic structure of shallow centers. We are working towards a comprehensive understanding of the role of hydrogen.

Far-infrared photoconductors exhibit a number of time-dependent phenomena in the signal formation that are not understood. Through experiments at low photon flux we are determining the dependencies of the various time constants on temperature, photon flux, electric field, detector geometry, and electrical-contact parameters.

1984 PUBLICATIONS AND REPORTS

Refereed Journals

1. E.E. Haller, N.P. Palaio, M. Rodder, W.L. Hansen, and E. Kreysa, "NTD Germanium: A Novel Material for Low Temperature Bolometers," in *Proc. Fourth Int. Conf. on Neutron Transmutation Doping of Semiconductor Materials,* National Bureau of Standards, June 1–3, 1982, Gaithersburg, Maryland, R.D. Larrabee, Ed., Plenum Press, 1984 p. 21; LBL-14649.
2. J.T. Walton and E.E. Haller, "Silicon Radiation Detectors—Materials and Applications," in *Proc. Materials Research Soc. 1982 Annual Meeting, Symposium F,* Vol. 16, Elsevier Science Publishing Co., Inc., New York, 1983, p. 141; LBL-14909.
3. W.L. Hansen and E.E. Haller, "High-Purity Germanium Crystal Growing," in *Proc. Materials Research Soc. 1982 Annual Meeting, Symposium F,* Vol. 16, Elsevier Science Publishing Co., Inc., New York, 1983, p. 1; LBL-14916.
4. C.W. Clawson, S.S. Rosenblum, K.M. Crowe, E.E. Haller, and J.H. Brewer, "Effects of Electronically Neutral Impurities on Muonium in Silicon and Germanium," in *Proc. Yamada Conference on Muon Spin Rotation,* April 18–22, 1983, Shimoda, Japan; Hyperfine Interactions **17–19**, 603 (1984); LBL-16944.
5. K.P. Doring, K.P. Arnold, M. Gladisch, N. Haas, E.E. Haller, D. Herlach, W. Jacobs, M. Krause, M. Krauth, H. Orth, and A. Seeger, "Muonium in

Ultra-Pure and Si-Doped Germanium," in *Proc. Yamada Conference on Muon Spin Rotation*, April 18–22, 1983, Shimoda, Japan; Hyperfine Interactions **17–19**, 629 (1984).

6. S.R. Amendolia, F. Bedeschi, E. Bertolucci, D. Bettoni, L. Bosisio, C. Bradaschia, M. Budinich, M. Dell'Orso, F. Fidecaro, L. Foa, E. Focardi, P. Giannetti, A. Giazotto, M.A. Giorgi, P.S. Marrocchesi, A. Manzione, L. Ristori, A. Scribano, A. Stefanini, G. Tonelli, G. Triggiani, E.E. Haller, W.L. Hansen, and P.N. Luke, "A Monolithic Germanium Target with 100 Microns Granularity for Life-Time Measurement of Charmed Particles," IEEE Trans. Nucl. Sci. **NS-30** (1), 98 (1983).
7. S.J. Pearton, J.M. Kahn, and E.E. Haller, "Deep Level Effects in Silicon and Germanium after Plasma Hydrogenation," J. Electron. Mater. **12** (6), 1003 (1983); LBL-15920.
8. S.J. Pearton, A.J. Tavendale, J.M. Kahn, and E.E. Haller, "The Nature of the Dominant γ-Induced Defects in High-Purity Germanium," Radiat. Eff. **81**, 293 (1984); LBL-15921.
9. S.J. Pearton, J.M. Kahn, W.L. Hansen, and E.E. Haller, "Deuterium in Germanium: Interaction with Point Defects," J. Appl. Phys. **55** (6), 1464 (1984); LBL-15944.
10. S.J. Pearton, E.E. Haller, and J.M. Kahn, "Quenched-In Deep Acceptors in Germanium," J. Phys. C **17**, 2375 (1984); LBL-16198.
11. S.J. Pearton, A.J. Tavendale, J.M. Kahn, and E.E. Haller, "Deep Level Impurities in Germanium and Silicon: Low Temperature Passivation or Removal Techniques," IEEE Trans. Nucl. Sci. **NS-31** (1), 326 (1984); LBL-15943.
12. W.L. Hansen, S.J. Pearton, and E.E. Haller, "Bulk Acceptor Compensation Produced in P-Type Silicon at Near Ambient Temperatures by an H_2O Plasma," Appl. Phys. Lett. **44** (6), 606 (1984); LBL-16688.
13. W.L. Hansen, S.J. Pearton, and E.E. Haller, "Low-Temperature Oxygen Diffusion in Silicon," Appl. Phys. Lett. **44**, 889 (1984); LBL-16961.
14. S.R. Amendolia, F. Bedeschi, E. Bertolucci, D. Bettoni, L. Bosisio, U. Bottigli, C. Bradaschia, M. Dell'Orso, F. Fidecaro, L. Foa, E. Focardi, P. Giannetti, M.A. Giorgi, P.S. Marrocchesi, A. Menzione, G. Raso, L. Ristori, A. Scribano, A. Stefanini, R. Tenchini, G. Tonelli, G. Triggiani, E.E. Haller, W.L. Hansen, and P.N. Luke, "A 50 Microns Granularity Monolithic Ge Target," IEEE Trans. Nucl. Sci. **NS-31** (2), 945 (1984).
15. N.M. Amer, E.E. Haller, and E.R. Weber, "Photothermal Spectroscopy and Imaging of GaAs," in *Semi-Insulating III-V Materials*, D.C. Look and J.S. Blakemore, eds., Shiva Publishing, Ltd., 1984, p. 460; LBL-17802.

Other Publications

16. S.R. Amendolia, F. Bedeschi, E. Bertolucci, D. Bettoni, L. Bosisio, U. Bottigli, C. Bradaschia, M. Dell'Orso, F. Fidecaro, L. Foa, E. Focardi, P. Giannetti, M.A. Giorgi, P.S. Marrocchesi, A. Menzione, G. Raso, L. Ristori, A. Scribano, A. Stefanini, R. Tenchini, G. Tonelli, G. Triggiani, E.E. Haller, W.L. Hansen, and P.N. Luke, "Germanium Microstrip Detectors with 50 and 100 μm Pitch," in *Proc. III European Symp. on Semiconductor Detectors*, September 14–15, 1983, Munich, Germany, 1984.
17. N.M. Haegel, M.R. Hueschen, and E.E. Haller, "Development of High Responsivity Ge:Ga Photoconductors," in *Proc. Third Int. Conf. on Infrared Physics*, July 23–27, 1984, Zurich, Switzerland.
18. N.M. Amer, E.R. Weber, and E.E. Haller, "Photothermal Spectroscopy of GaAs," Abstract, 3rd Int. Conf. on Semi-Insulating III-V Materials, Warm Springs, Georgia, April 24–26, 1984; LBL-17139.
19. E.E. Haller, "Physics and Design of Advanced Infrared Bolometers and Photoconductors," in *Proc. Third Int. Conf. on Infrared Physics*, Zurich, Switzerland, July 23–27, 1984.
20. J.C. Culbertson, J.E. Furneaux, and E.E. Haller, "A Study of the Dynamics of the Electron-Hole-Liquid Free Exciton System in Ge Using No-Phonon Luminescence," in *Proc. 17th Int. Conf. on the Physics of Semiconductors*, San Francisco, California, August 6–10, 1984.
21. J.C. Culbertson, J.E. Furneaux, and E.E. Haller, "A Study of the Dynamics of the Electron-Hole-Liquid Free-Exciton System in Ge Using No-Phonon Luminescence Mediated by Shallow Impurities," in *Proc. First Int. Conf. on the Spectroscopy of Shallow Centers in Semiconductors* SSCS '84, Berkeley, California, August 2–3, 1984, E.E. Haller, K.K. Bajaj, and A.K. Ramdas, eds.
22. J.C. Culbertson, J.E. Furneaux, and E.E. Haller, "A New Probe of the Electron-Hole-Liquid Free-Exciton System in Ge: No-Phonon Luminescence," submitted to Phys. Rev. Lett.
23. G.S. Hubbard, E.E. Haller, and S. J. Pearton, "Novel Deep Donors in As-Grown Ultra-Pure Germanium," in *Proc. 13th Int. Conf. on Defects in Semiconductors*, San Diego, California, August 13–17, 1984, L.C. Kimberly and J.M. Dorsey, eds., The Metallurgical Society of AIME, Vol. 14a, p. 903.
24. N.A. Stolwijk, W. Frank, J. Holzl, S.J. Pearton, and E.E. Haller, "Diffusion and Solubility of Copper in Germanium," submitted to J. Appl. Phys.
25. S. Komiyama, N. Iizuka, H. Sukeda, and E.E. Haller, "Sample-Purity Dependence of Far-Infrared Emission from Accumulated Holes in p-Ge," submitted to Int. J. Infrared and Millimeter Waves.

26. E.E. Haller, R.E. McMurray, Jr., N.M. Haegel, and L.M. Falicov, "Positively Charged Acceptors with $(1s)^3$ and $(1s)^4$ Configuration," in *Proc. 17th Int. Conf. on the Physics of Semiconductors,* San Francisco, California, August 6–10, 1984; LBL-18052.
27. R.E. McMurray, Jr., N.M. Haegel, J.M. Kahn, and E.E. Haller, "Shallow Zinc-Hydrogen and Beryllium-Hydrogen Complexes in Germanium," in *Proc. First Int. Conf. on the Spectroscopy of Shallow Centers in Semiconductors* SSCS '84, Berkeley, California, August 2–3, 1984, E.E. Haller, K.K. Bajaj, and A.K. Ramdas, eds.
28. G.A. Held, C.D. Jeffries, and E.E. Haller, "Turbulence in Electron-Hole Plasma in Ge," in *Proc. 17th Int. Conf. on the Physics of Semiconductors,* San Francisco, California, August 6–10, 1984; LBL-18071.
29. K.M. Yu, J.M. Jaklevic, and E.E. Haller, "Applications of Heavy-Ion Rutherford Backscattering Spectrometry (HIRBS) to the Analysis of Contact Structures on GaAs and Ge," in *Proc. 8th Conf. on the Application of Accelerators in Research and Industry,* North Texas University, November 12–14, 1984; Nucl. Instr. and Methods (in press); LBL-18466.
30. L.M. Falicov and E.E. Haller, "Dynamic Impurities in Ultra-Pure Semiconductors," in *Proc. First Int. Conf. on the Spectroscopy of Shallow Centers in Semiconductors* SSCS '84, Berkeley, California, August 2–3, 1984; E.E. Haller, K.K. Bajaj, and A.K. Ramdas, eds; LBL-17659.

LBL Reports

31. N.M. Haegel, M.R. Hueschen, and E.E. Haller, "Development of High-Responsivity Ge:Ga Photoconductors," submitted to Infrared Physics; LBL-17032.
32. E.E. Haller, "Physics and Design of Advanced Infrared Bolometers and Photoconductors," submitted to Infrared Physics; LBL-17483.
33. R.E. McMurray, Jr. (Ph.D. Thesis), "Impurity Complexes in Pure Elemental Semiconductors," LBL-18554.
34. K.M. Yu, (M.S. Thesis), "Heavy Ion Rutherford Backscattering Spectrometry (HIRBS) for Near Surface Characterization of Electronic Materials," LBL-18897.

Invited Talks

35. H.G. Spieler and E.E. Haller, "Assessment of Present and Future Large-Scale Semiconductor Detector Systems," 1984 IEEE Nuclear Science Symposium, Orlando, Florida, October 31–November 2, 1984; IEEE Trans. Nucl. Sci. (in press); LBL-18684.
36. E.E. Haller, "GaAs Research at the Center for Advanced Materials," Physics Department, Sonoma State University, Rohnert Park, California, April 30, 1984.
37. E.E. Haller, "Physics and Design of Advanced Infrared Bolometers and Photoconductors," 3rd International Conference on Infrared Physics, Zurich, Switzerland, July 23–27, 1984.
38. E.E. Haller, "Far Infrared Photoconductors: Materials and Device Considerations," Department of Materials Science, University of California, Berkeley, September 13, 1984.
39. R.E. McMurray, Jr., "Spectroscopy of Positively Charged Multiple Acceptors," First International Conference on the Spectroscopy of Shallow Centers in Semiconductors, University of California, Berkeley, August 2–3, 1984.

Work for
Others

OFFICE OF NAVAL RESEARCH

Quantum Monte Carlo for Molecular Studies*

William A. Lester, Jr., Investigator

INTRODUCTION

We are pursuing the use of the quantum Monte Carlo (QMC) method for the computation of molecular properties. This approach, borrowed from statistical mechanics, allows one to calculate essentially exact quantum-mechanical expectation values. Thus it provides an alternative to traditional *ab initio* quantum-chemical approaches. The method takes advantage of the formal similarity of the Schrödinger equation in imaginary time to a diffusion equation.

1. Quantum Monte Carlo Study of the Classical Barrier Height for the $H + H_2$ Exchange Reaction: Restricted Versus Unrestricted Trial Functions (Publications 1 and 2)

Peter J. Reynolds, Robert N. Barnett, and William A. Lester, Jr.

The fixed-node quantum Monte Carlo (FNQMC) method is used to obtain the classical barrier height of the $H + H_2$ exchange reaction. Using a spin-restricted single-determinant trial function Ψ_T, we find that the reaction barrier E_b is less than 9.69 ± 0.25 kcal/mole. This mean value is below the calculated energy barrier obtained by Liu[1] in the most extensive configuration-interaction (CI) calculations on this system. Furthermore, the QMC saddle-point energy of -1.65903 ± 0.00040 hartrees at the CI-determined geometry lies 0.00027 a.u. (0.17 kcal/mole) below Liu's best CI values. Although the variational energy $\langle\Psi_T |H| \Psi_T\rangle$ for a self-consistent-field (SCF) Ψ_T must be lower for the unrestricted case, this proves not to be true generally for QMC. In fact, we show that if the unrestricted SCF Ψ_T has the lower QMC energy, then there exists another spin-restricted, single-determinant Ψ_T whose QMC energy is lower than the QMC energy of the spin-restricted SCF Ψ_T.

1. B. Liu, J. Chem. Phys. **80**, 581 (1984).

2. Work in Progress

We are writing a new program that will enable us to calculate properties whose operators do not commute with the Hamiltonian, such as the dipole moment. Other directions we are exploring are: (1) guiding functions that might help reduce variance, (2) better Green's functions, which may enable us to sample configuration space more efficiently, and (3) algorithms for calculating energy derivatives directly.

1984 PUBLICATIONS AND REPORTS

LBL Reports

1. R.N. Barnett, P.J. Reynolds, and W.A. Lester, Jr., "Fixed-Node Quantum Monte Carlo Study of the Classical Barrier Height for the $H + H_2$ Exchange Reaction," accepted by J. Chem. Phys.; LBL-17610.†
2. P.J. Reynolds, R.N. Barnett, and W.A. Lester, Jr., "Quantum Monte Carlo Study of the Classical Barrier Height for the $H + H_2$ Exchange Reaction: Restricted versus Unrestricted Trial Function," accepted by Int. J. Quan. Chem.; LBL-17611.†
3. P.J. Reynolds, M. Dupuis, and W.A. Lester, Jr., "Quantum Monte Carlo Calculation of the Singlet-Triplet Splitting in Methylene," accepted by J. Chem. Phys.; LBL-17823.‡

*This work was supported by the U.S. Office of Naval Research.

†W.A. Lester was supported by the Director, Office of Energy Research, Office of Basic Energy Sciences, Chemical Sciences Division of the U.S. Department of Energy under Contract No. DE-AC03-76SF00098.

‡M. Dupuis and W.A. Lester were supported by the Director, Office of Energy Research, Office of Basic Energy Sciences, Chemical Sciences Division of the U.S. Department of Energy under Contract No. DE-AC03-76SF00098.

Electron-Phonon Coupling and the Properties of Thin Films and Inhomogeneous Superconductors*

Vladimir Z. Kresin, Investigator

INTRODUCTION

Research efforts have focused on the induced superconductivity (proximity effect), the search for new mechanisms of superconductivity, and the effect of the interface region on the properties of superconducting films.

1. Proximity Effect. Properties of Thin Films (Publications 3 and 5)

Vladimir Z. Kresin

Both screening in proximity systems and critical temperature (T_c) have been evaluated. In the low-temperature region nonlocality plays an important role. The obtained temperature and thickness dependences of the penetration depth are in good agreement with the experimental data. An expression for T_c for different systems has been obtained. This expression describes the decrease of T_c in Nb and NbN films.

A special type of low-temperature structural transition occurs in thin, size-quantized films (e.g., in Bi films). The instability of the lattice results in a structural transition, which is accompanied by the appearance of charge-density waves and is characterized by peculiar temperature and thickness dependence of the electron concentration.

2. Critical-Temperature Strong Coupling (Publication 2)

Vladimir Z. Kresin

The behavior of the critical temperature in the limit of strong electron-phonon coupling has been considered. The effect of Coulomb interaction, the contribution of low phonon modes, and the relative contribution of phonon and nonphonon interactions have been considered.

A method that allows separation of different mechanisms of superconductivity is proposed. It is based on the analysis of tunneling data and the temperature dependence of heat capacity.

3. Interface States (Publications 4 and 7)

Vladimir Z. Kresin

Localized states hybridize yielding interface states. Such states show a strong electron-phonon coupling and enhanced tunneling. One can introduce a Hamiltonian describing resonant tunneling to study, for example, inelastic processes.

4. Work in Progress

The general expression describing the critical temperature of the S_α-S_β system will be evaluated. The strong coupling effect should be taken into consideration. We are in the process of analyzing the properties of multilayers. Their thermodynamic and electromagnetic properties will be analyzed.

1984 PUBLICATIONS AND REPORTS

Refereed Journals

1. V.Z. Kresin, "Coexistence of Phonon and Nonphonon Mechanisms of Superconductivity and a Method of Their Separation," Phys. Rev. **13**, 450 (1984); LBL-16816.
2. V.Z. Kresin, H. Gutfreund, and W.A. Little, "Superconducting State in Strong Coupling," Solid State Commun. **51**, 339 (1984); LBL-16581.
3. V.Z. Kresin, "Structural Transition and Charge Density Waves in Thin Film," J. Low Temp. Phys. **57**, 547 (1984); LBL-17175.

Other Publications

4. V.Z. Kresin and J. Halbritter, "On the Interaction and Transport Properties of Interface States," in *Proc. 17th Int. Conf. on Low-Temp. Phys.*, Karlsruhe, West Germany, August 15–22, 1984, U. Eckern, A. Schmid, W. Weber, and H. Wuhl, eds., North-Holland, Amsterdam, 1984, p. 1061.
5. V.Z. Kresin, "Critical Temperature and Electromagnetic Properties of Proximity Systems," in *Proc. 17th*

*This work was supported by the U.S. Office of Naval Research under Contract No. N00014-84-F-0095.

Int. Conf. on Low-Temp. Phys., Karlsruhe, West Germany August 15–22, 1984, U. Eckern, A. Schmid, W. Weber, and H. Wuhl, eds., North-Holland, Amsterdam, 1984, p. 1030.

LBL Reports

6. V.Z. Kresin, "Behavior of T_c of High Temperature Superconducting Films and a Determination of Their Parameters," submitted to IEEE Proc. Magn.; LBL-17747.
7. V.Z. Kresin and J. Halbritter, "Superconducting Junction with Resonant Tunneling," submitted to IEEE Proc. Magn.; LBL-17748.
8. V.Z. Kresin, "Inducted Superconducting State in Semiconductors and Semimetals," submitted to *Proc. 17th Int. Conf. Phys. Semiconductors;* LBL-17746.

Invited Talks

9. V.Z. Kresin, "Superconducting Properties of a Proximity System," special seminar series "Distinguished Lecturer on Superconductivity," sponsored by the Office of Naval Research, the Naval Research Laboratory, and the National Bureau of Standards, March 14, 1984.
10. V.Z. Kresin, "Induced Superconducting State in Semiconductors and Semimetals," 17th International Conference on the Physics of Semiconductors, San Francisco, California, August 5–12, 1984.
11. V.Z. Kresin, "Critical Temperature and Electromagnetic Properties of Proximity Systems," 17th International Conference on Low-Temperature Physics, Karlsruhe, West Germany, August 15–22, 1984.
12. V.Z. Kresin and J. Halbritter, "On the Interaction and Transport Properties of Interface States," 17th International Conference on Low-Temperature Physics, Karlsruhe, West Germany, August 15–22, 1984.
13. V.Z. Kresin, "Behavior of T_c of High Temperature Superconducting Films and a Determination of Their Parameters," 1984 Applied Superconductivity Conference, San Diego, California, September 9–13, 1984.
14. V.Z. Kresin and J. Halbritter, "Superconducting Junction with Resonant Tunneling," 1984 Applied Superconductivity Conference, San Diego, California, September 9–13, 1984.

DEPARTMENT OF TRANSPORTATION

Enhanced Fuel Capability of Marine Diesels*

Alan V. Levy, Investigator

1. Protective Coatings for Diesel Engine Components (Publication 1)

Jeff Jones, Stewart McAdam, and Alan Levy

Protective ceramic and metal coatings were selected for application on 135 diesel engine components that were to be evaluated in towboat engine service. Several versions of partially stabilized zirconia and MCrAlY plasma spray coatings were applied to engine valves, piston crowns, and cylinder heads by five different suppliers. Test parts of each configuration were also coated for microscopic analysis. All of the coatings have been applied to the parts, characterized, and inspected; they are currently in two operating diesel engines propelling two boats on midwestern rivers.

The range of coating morphologies that were accepted for engine service evaluation was quite large, particularly regarding porosity and thickness. The bonds between the coating layers were much more closely controlled than the porosity, with essentially no unbondedness permitted on any parts. Outer surface textures and coating colors were permitted to vary over a significant range. To date there have been no reported failures of coatings in the engines. The first parts to be analyzed after towboat engine service are scheduled to be removed after 750 hours of operation.

1984 PUBLICATIONS AND REPORTS

Other Publications

1. J. Jones, S. McAdam, and A. Levy, "Protective Coatings for Diesel Engine Components," MARAD Status Report, 1984.

*Supported by the U.S. Department of Transportation, Maritime Administration, P.O. No. 400-49002.

LOS ALAMOS NATIONAL LABORATORY

Determination of the Solubilities and Complexation of Waste Radionuclides Pertinent to Geologic Disposal at the Nevada Tuff Site*

Heino Nitsche and Norman Edelstein, Investigators

1. Solubilities and Speciation of Actinide Ions in Near-Neutral Solution (Publication 1)

H. Nitsche and N.M. Edelstein

The permanent disposal of nuclear waste in repositories excavated in deep geologic formations appears to be technically feasible. The Yucca Mountain, a tuff formation located on the Nevada Test Site, is one of several potential disposal sites. The objective of this study was to determine the solubilities and speciation of neptunium, plutonium, and americium in a groundwater (J-13) from the proposed repository at Yucca Mountain and in aqueous perchlorate solution of similar pH. In noncomplexing perchlorate solution, hydroxide formation and hydrolysis are the sole controlling factors of actinide solubility. In groundwater, additional anions can influence the actinide solubility by forming new solids, new solution complexes, or both.

In this study steady-state solution concentrations were determined in batch experiments for each of the following ions under supersaturated conditions (listed by initial oxidation state) at 25°C and at a pH value of 7.0: Pu^{4+}, PuO_2^+, PuO_2^{2+}, NpO_2^+, NpO_2^{2+}, and Am^{3+}. The oxidation-state distributions at equilibrium were investigated by spectrophotometry or by an extraction-coprecipitation method. The precipitates were characterized by x-ray powder diffraction measurements.

Comparison of the results showed that some groundwater anions (i.e., CO_3^{2-}) exert an important influence on the actinide solubility, and that hydroxide formation is not the principal factor controlling solubility. The results in perchlorate solution were compared with existing literature data on the solubilities of actinide hydroxides.

Detailed results are published in quarterly reports[1] and a topical report on the subject.

1. H. Nitsche, N.M. Edelstein, and A.E. Ogard, "Research and Development Related to the Nevada Nuclear Waste Storage Investigations," Progress Report LA-10032-PR (last quarter 1983) and progress reports for the first three quarters of 1984 (in print), Los Alamos National Laboratory.

1984 PUBLICATIONS AND REPORTS

LBL Reports

1. H. Nitsche and N.M. Edelstein, "Solubilities and Speciation of Actinide Ions in Near-Neutral Solution," Topical Report, LBL-18900.

*This work was supported by the Los Alamos National Laboratory under Contract W-7405-ENG-36 as part of the Nevada Nuclear Waste Storage Investigations (NNWSI) managed by the Nevada Operations Office of the U.S. Department of Energy.

OAK RIDGE NATIONAL LABORATORY

Tribology of Cylinder Wall-Piston Ring Pairs*

Alan V. Levy, Investigator

1. Sliding Wear of Hard Metal and Ceramic Pairs

Nancy Jee and Alan Levy

Six experimental coating systems were studied for sliding wear service at elevated temperatures in the cylinder wall-piston ring couple of heat insulated diesel engines. The coatings were tested at both room temperature and elevated temperatures to 730°C in a washer on disk, unlubricated wear test at contact pressures to 2000 PSI. At pressures above 1000 PSI and temperatures $\geqslant$ 425°C, most of the coating pairs failed in 1–2 minutes. When the pairs were first tested at 25°C at low contact pressures (100 PSI) for 5 minutes, a polishing action occurred on the already honed surfaces that permitted subsequent successful testing at higher pressures or temperatures.

All pairs tested experienced an initial large, incremental wear rate, after which a much lower steady state wear rate was achieved within 5–10 minutes of test initiation. Thus, it was determined that sliding wear tests on the hard metal and ceramic coatings being investigated could be conducted for short times (10–15 minutes) and achieve a steady state wear rate that should be able to be extrapolated to much longer service periods. Test results indicated that wear debris has some promise as a solid film lubricant for this type of sliding wear.

1984 PUBLICATIONS AND REPORTS

Invited Talks

1. A. Levy, "Sliding Wear Behavior of Ceramic Coating Systems," seminar at Cummins Engine Co., Columbus, Indiana, December 1984.
2. A. Levy, "Sliding Wear Behavior of Ceramic Coating Systems," seminar at Oak Ridge National Laboratory, Oak Ridge, Tennessee, December 1984.

*This work was supported by Martin Marietta Corp., Oak Ridge National Laboratory, Work Order No. 347667-5225 (AC423GA1).

ELECTRIC POWER RESEARCH INSTITUTE

Reaction Mechanism of the Oxidation of Bisulfite Ion by Oxygen*

Robert E. Connick, Investigator

INTRODUCTION

Bisulfite ion in aqueous solution is oxidized by oxygen according to the reaction

$$2\ HSO_3^- + O_2 \rightarrow 2\ SO_4^{2-} + 2\ H^+ .$$

This reaction is of importance in flue-gas desulfurization schemes making use of aqueous scrubbers and in the atmospheric oxidation of sulfur dioxide on suspended particles coated with an aqueous film. The understanding and control of the rate of reaction is an important objective. Although the kinetics of the reaction has been studied for more than 80 years, there is no agreement on the rate law or the mechanism. Because the reaction is a chain reaction, it is very sensitive to small amounts of a great variety of chemicals. The present research is aimed at elucidating the mechanism of the reaction and the catalytic and inhibitory effect on the rate of a variety of chemicals.

Funding for the project was exhausted in mid-year.

1. Work in Progress

Robert E. Connick and Paul Chieng

The reaction is catalyzed by ceric ion. Because the ceric ion is reduced immediately but acceleration lasts for a finite time, the interpretation given is that the ceric ion increases the concentration of chain carriers, which then return to their steady-state concentration over a period of minutes. Using this model it is possible in principle to separate the rate law into the three components of initiation, propagation, and termination. As yet satisfactory results have not been obtained, and it may be that the model is flawed.

*This work was supported by the Electric Power Research Institute, Palo Alto, California.

Selective Catalytic Hydrogenation of Polynuclear Heteroaromatic Nitrogen Compounds*

Heinz Heinemann and Richard H. Fish, Investigators

INTRODUCTION

Recently, we found that a wide variety of transition-metal compounds catalyzed the regiospecific reduction of polynuclear heteroaromatic nitrogen and sulfur compounds. These findings may, in fact, have important effects on the various synthetic-fuel processes. Hydrogen-gas consumption is known to be an economically limiting factor in the upgrading of synthetic fuels and in the removal of nitrogen and sulfur from these complex matrices. Hydrogen-gas consumption by selective hydrogenation will be lower than hydrogen-gas consumption using conventional catalytic methods; furthermore, the reactions described in our previous homogeneous studies were carried out at lower temperatures and pressures than are used in conventional industrial processing.

Homogeneous catalysts have their own limitations in that catalyst recovery is often difficult or impossible. In addition, thermal stability and solubility may also present problems in practical applications. The use of polymer supports, such as cross-linked polystyrene-divinylbenzene (PS-DVB), as well as silica and alumina, to anchor homogeneous transition-metal catalysts and overcome some of the difficulties mentioned above, has been the subject of intensive research over the last fifteen years.

1. A Comparison of Polymer-Supported Chloro(tristriphenylphosphine)rhodium (I) to its Homogeneous Analogue in the Selective Reduction of Polynuclear Heteroaromatic Compounds (Publication 1)

R.H. Fish, A.D. Thormodsen, and H. Heinemann

The reduction of polynuclear heteroaromatic compounds of nitrogen and sulfur with 2% cross-linked phosphinated PS-DVB beads modified with chloro(tristriphenylphosphine)rhodium (I) was compared to the reduction rate using the homogeneous analogue of PS-DVB. The polymer-supported catalyst $\boxed{P} - P\theta_2Rh(\theta_3P)_2Cl$ had initial hydrogenation rates 10 to 20 times faster than the homogeneous equivalent. The reduction mechanism of the nitrogen heterocyclic ring was investigated by substituting deuterium gas for hydrogen gas. The lack of aromatic hydrogen exchange in the polymer-supported chloro(tristriphenylphosphine)rhodium (I) is evidence for the importance of steric effects. Regioselectivity for the nitrogen heterocyclic ring in the presence of other model-coal-liquid constituents verifies the potential of anchored catalysts in various synthetic-fuel applications.

1984 PUBLICATIONS AND REPORTS

LBL Reports

1. Richard H. Fish, Arne D. Thormodsen, and Heinz Heinemann, "A Comparison of Polymer-Supported Chloro(tristriphenylphosphine)rhodium (I) to its Homogeneous Analogue in the Selective Reduction of Polynuclear Heteroaromatic Compounds," J. Molec. Catal. (in press); LBL-16918.

*This work was supported by a grant from the Electric Power Research Institute under Project RP 2147-7.

Appendices

APPENDIX A

DIVISION PERSONNEL

1984 Scientific Staff

Investigators	Postdoctoral and Other Scientists	Graduate Students
Neil Bartlett	G. Feng J. Huston R. Kaner M. Motoyama F. Okino T. Richardson G. Rosenthal H. Takenaka	K. Guerrero K. Kourtakis J. Kouvetakis F. Okino G. Rosenthal
Alexis Bell		W. Cannella R. Dictor D. Jordan M. Reichmann J. Rieck D. Stern R. Underwood P. Winslow G. Yokomizo
Robert Bergman		J. Buchanan E. Burkhardt J. Chang J. Doney T. Gilbert K. Goldberg E. Jacobsen M. Krause W. McGhee L. Newman R. Periana-Pillai M. Seidler P. Seidler P. Stoutland M. Trost G. Yang

Investigators	Postdoctoral and Other Scientists	Graduate Students
Robert Bragg	A. Lachter B. Mehrotra	B. Mehrotra M. Tidjani
Leo Brewer	C. Myers G. Rosenblatt	J. Bularzik M. Cima K. Krushwitz
John Clarke	M. Devoret D. Esteve	N. Fan M. Heaney C. Hilbert J. Martinis R. Miracky J. Pelz F. Wellstood
Marvin Cohen	W. Maysenholder D. Vanderbilt	K. Chang M. Chou A. Cleland J. Northrup S. Zhang
Robert Connick	C. Chieng D. Horner	M. Wagner
Didier de Fontaine	A. Finel O. Lyon T. Mohri S. Takeda	J. Hoyt J. Kulik M. Lafon R. Pro
Lutgard De Jonghe	M. Armand D. Hitchcock C. Mailhe M. Rahaman J. Sasaki S. Shinde S. Visco	Y. Boiteux D. Hitchcock M. Liu C. Mailhe N. Naito D. Olson I. Reimanis E. Reiner M. Weiser S. Wu

Investigators	Postdoctoral and Other Scientists	Graduate Students
Norman Edelstein Richard Andersen John Conway Kenneth Raymond Glenn Seaborg Andrew Streitwieser, Jr. David Templeton Allan Zalkin	H. Amberger J. Boncella J. Bucher S. Kinsley J. Koningstein C. Ng H. Nitsche N. Rosch G. Shalimoff A. Stuart D. White K. Yunlu D. Zhang D. Zhu	N. Abraham P. Becker D. Berg J. Brennan S. Fletcher G. Freeman S. Kinsley W. Kot R. Moore J. Rigsbee R. Rosen P. Sasse R. Shinomoto P. Smith S. Stults G. Williams
Anthony Evans	R. Brook B. Dalgleish W. Kriven R. Loh P. Ruegg	G. Campbell G. Crumley M. Drory S. Inoue R. Loh M. Lu J. Maasberg J. Marion C. Ostertag C. Rossington M. Thouless
James Evans	T. Huh M. Rau D. Rieck	H. Choi M. Hall T. Huh H. Lee M. Rau O. Rego-Monteiro N. Tuffrey
Leo Falicov	L. de Oliveira	R. Victora Y. Wu
Iain Finnie	J. Dydo S. Soemantri R. Wilkes	D. Melton P. Riedl S. Soemantri R. Wilkes
Andreas Glaeser		W. Carter J. Chen L. Edelson

Investigators	Postdoctoral and Other Scientists	Graduate Students
Ronald Gronsky	J. Howe E. Kamenetzky M. Kawazoe L. Kihlborg R. Kilaas E. Lodge M. O'Keefe J. Rose G. van Tendeloo	J. Bierach J. Howe E. Kamenetzky R. Kilaas M. Kundmann J. Rose T. Sands M. Takahashi
Eugene Haller*		
Charles Harris		M. Arndt M. Berg J. Brown G. Goncher A. Harris
Heinz Heinemann	E. Petersen P. Zollinger	
Dennis Hess		C. Blair
Joseph Humphrey		Y. Choi S. Dosanjh W. To
Carson Jeffries		P. Bryant G. Held J. Testa
Harold Johnston	R. Carlson A. Young	L. Humphreys D. Kinnison B. Oh W. Sisk D. Swanson
William Jolly	C. Li	D. Beach

*Also affiliated with the
Engineering and Technical Services Division

Investigators	Postdoctoral and Other Scientists	Graduate Students
Yuan Lee	P. Felder J. Mestdagh D. Normand H. Schmidt	B. Balko R. Brudzynski K. Busarow L. Butler R. Continetti M. Covinsky J. Frey E. Hintsa M. Kramer T. Minton D. Neumark M. Okumura J. Reutt G. Robinson A. Schmoltner T. Turner P. Weiss A. Wodtke L. Yeh
William Lester, Jr.	M. Dupuis V. Kresin S. Rothstein P. Reynolds	R. Barnett C. Dateo R. Grimes B. Hammond S. Huang R. Owen S. Roman
Alan Levy	D. Boone H. Frank I. Kliafas A. Ninham	M. Aghazadeh M. Arnal J. Azzola E. Ettehadieh
Steven Louie		C. Chan S. Fahy M. Hybertsen
Richard Marrus	E. Commins P. Drell H. Gould M. Prior H. Shugart	C. Munger C. Tanner

Investigators	Postdoctoral and Other Scientists	Graduate Students
William Miller	M. Hermann R. Jaquet E. Pollack K. Yamashita	T. Carrington P. Dardi B. Ruf S. Schwartz S. Shi J. Tromp K. White
C. Bradley Moore	S. Filseth C. Kahler D. Nesbitt	D. Bamford T. Butenhoff D. Darwin M. Foltz J. Frisoli W. Green Y. Guo
John Morris, Jr.	B. Fultz D. Grivas K. Katagiri H. Kim Y. Kim K. Xue	J. Chan G. Chang K. Davis D. Dietderich T. Edgecumbe R. Emigh G. Fior D. Frear J. Glazer Y. Im P. Johnson-Walls Y. Kim T. Lindsey D. Marinaro M. McCormack S. Shaffer M. Strum L. Summers D. Tribula K. Xue
Earl Muetterties*	B. Marchon	T. Gentle V. Grassian R. Lum K. Shanahan
Rolf Muller	G. Nazri	M. Armstrong D. Barkey J. Gyory S. Mayer

*Deceased

Investigators	Postdoctoral and Other Scientists	Graduate Students
John Newman		D. Bernardi V. Edwards C. Haili A. Hauser M. Matlosz P. Russell P. Shain S. Thompson
Donald Olander	M. Balooch	J. Abrefah M. Berg M. Derzon L. Hansson K. Kim M. Moalem K. Park W. Sailor D. Sherman
Joseph Pask	X. Zhang	
Norman Phillips	M. Mayberry J. Van Curen	C. Lisse J. Van Curen
Alexander Pines	A. Garroway M. Munowitz D. Weitekamp	J. Baum A. Bielecki H. Cho C. Connor G. Davenport M. Gochin T. Jarvie B. Kim C. Lee J. Millar E. Schneider D. Shykind R. Tycko D. Zax
Kenneth Pitzer	D. Schreiber S. Wang	R. Neisler

Investigators	Postdoctoral and Other Scientists	Graduate Students
John Prausnitz		F. Anderson R. Cotterman A. Harvey J. Wong A. Wu
Paul Richards	W. McGrath	G. Bernstein M. Fischer A. Kogut A. Lange W. McGrath R. Tobin
Robert Ritchie	A. Brass	V. Dutta T. George T. Lin T. Oh R. Pendse J. Shang J. Tzou
Philip Ross	P. Andricacos B. Beard A. D'Agostino D. Dahlgren K. Gaugler N. Staud J. Willsau	
Richard Saykally		M. Grübele D. Gwo D. Hovde K. Laughlin D. Ray R. Robinson S. Strahan

Investigators	Postdoctoral and Other Scientists	Graduate Students
Henry Schaefer III	J. George M. Hoffmann W. Meyer G. Raine R. Remington Y. Yamaguchi	W. Allen D. Clabo M. Colvin G. Fitzgerald J. Gaw R. Grev M. Hoffmann T. Lee R. Remington A. Scheiner
Alan Searcy	H. Akuezue D. Beruto R. Fischer D. Meschi T. Reis F. Yang	A. Hegedus M. Kim
Y. Ron Shen	G. Boyd R. Ma T. Rasing E. Santamoto	G. Boyd A. Karn R. Page H. Tom X. Zhu
David Shirley	J. Barton Z. Hussain G. Kalkowski D. Lindle G. Liu M. Piancastelli	A. Baca C. Bahr J. Barton T. Ferrett P. Heimann A. Johnson L. Klebanoff S. Robey A. Schach von Wittenau M. Schulz L. Terminello L. Wang

Investigators	Postdoctoral and Other Scientists	Graduate Students
Gabor Somorjai	M. Asscher	B. Bent
	S. Bare	G. Blackman
	M. Khan	M. Bussell
	M. Kudo	J. Carrazza
	J. Naegele	A. Gellman
	H. Nakanishi	D. Godbey
	C. Sanchez	M. Hendewerk
	K. Sieber	D. Kelly
	J. Turner	M. Levin
	W. Tysoe	K. Lewis
	M. Van Hove	M. Logan
	F. Zaera	C. Mate
	C. Zhang	B. Naasz
	K. Zhen	D. Ogletree
		T. Rucker
		R. Yeates
		F. Zaera
Angelica Stacy		J. Badding
		W. Ham
		D. Klarup
		R. Patterson
		J. Platenak
		J. Womack
		H. zur Loye
John Stringer		S. Choi
		P. Hou
		J. Lee
Gareth Thomas	H. de Klerk	J. Ahn
	E. Goo	M. Dass
	N. Kim	B. Demczyk
	K. Krishnan	H. Ho
	R. Mishra	K. Krishnan
	R. Rai	C. Kwok
	J. Rincon	M. Ohmura
	M. Sarikaya	R. Ramesh
		J. Wasynczuk
		Y. Yoon

Investigator	Postdoctoral and Other Scientists	Graduate Students
Charles Tobias		P. Andersen R. Anderson J. Dukovic S. Elliott S. Galante K. Hanson R. McIntosh L. McVay D. Sutija M. Verbrugge G. Whitney B. Wines
K. Peter Vollhardt	H. Mestdagh	J. Drage M. Huffman M. Madigan D. Newman M. Tilset W. Tolman T. Weidman
Jack Washburn	C. Lampert Z. Liliental J. Mazur T. Sands Y. Shih	J. Ding C. Jou H. Ling D. Lopes J. Mazur Y. Shih
Kenneth Westmacott	U. Dahmen P. Ferguson M. Madden J. Posthill A. Singh P. Veyssiere	S. Puranikmath
Peter Yu	D. Erskine	Y. Huang J. Weiner

Support Staff

Division Administrative Staff

C. Peterson — Assistant Dvision Head, Administration
K. McArthur — Assistant Division Administrator

Administration

M. Janzen
L. Irvin
S. Jones
J. Leonard
F. Livingston

Personnel

M. Montogomery
M. Bowman
P. Paladini

Purchasing

S. Stewart
C. Sterling
P. Ogden

Technical Editing

R. Albert

Special Projects

E. Skrydlinski

Travel

S. Quarello

Administrative/Secretarial Staff

R. Arcol
M. Atkinson
K. Bean
C. Becker
H. Benson
G. Brazil
D. Carmichael
C. Coolahan
N. Corwin
J. Denney
L. Donahue
K. Dukes
E. Edelson
S. Ewing
S. Gangwer
M. Gill
C. Gliebe
M. Hammond
D. Horne
R. Jones
A. Kahn
A. Kameoka
R. King
M. Knight
S. Mikesell
N. Miller
K. Mishita
M. Momii
M. Moore
B. Moriguchi
V. Narasimhan
M. Noyd
M. Olbrich
A. Ozturkmen
M. Penton
P. Ray
W. Rodeen
R. Rodriguez
S. Ruth
J. Shull
J. Smith
A. Stringfellow
C. Stutz
N. Su
E. Weightman
S. Wilde
K. Wilkinson
J. Wortendyke
L. Wroth
C. Yoder
B. Zambrano
J. Zissler

Technical Staff

D. Krieger — Technical Coordinator

D. Ackland
R. Anders
T. Bakker
G. Baum
J. Bierach
E. Boden
R. Castillo
J. Chen
H. Choy
B. Clark
C. Clark
P. Dahlberg
R. Dick
G. Dieckmann
T. DiMagno
D. Dittman
C. Echer
L. Edelson
T. Edgecumbe
M. Flach-Aznar
K. Franck
G. Gager
S. Gensler
M. Gifford
J. Glazer
R. Gray
A. Gronsky
M. Gruebele
S. Hahn
B. Hammond
S. Hardesty
W. Heppler
G. Hickey
J. Holthuis
L. Hsiao
R. Huntley
H. Huynh
Y. Ikezi
J. Jacobsen
E. January
N. Jee
L. Johnson
P. Johnson
K. Johnston
J. Jones
L. Junta
D. Jurica
R. Kennedy
G. King
J. Kouvetakis
R. Kulawiec
M. Kujala
S. Lecker
T. Lo
W. Lynn
S. Macadam
D. MacDonald
E. Mah
G. Maloney
D. Marinaro
S. McCabe
J. Miwa
S. Miyasato
P. Monardo
B. Morrison
D. Neiman
E. Nelson
R. Owen
L. Purvis
H. Qayum
J. Quintana
S. Shane
T. Shoemaker
W. Sisk
H. Sokol
D. Solvin
M. Sorbi
S. Spier
I. Tepermeister
K. Tomasu
G. Tong
J. Turner
C. Tzou
S. Verzasconi
A. Whitehead
R. Wilmer
W. Wong
J. Wu
J. Yan

APPENDIX B

DIVISION COMMITTEES

DIVISIONAL COUNCIL

A. Bell
M. Cohen
N. Edelstein
L. Falicov
H. Heinemann
H. Johnston*
C. Bradley Moore
J. Morris, Jr.

DIVISIONAL RESEARCH STAFF COMMITTEE

N. Edelstein
L. Falicov
R. Muller*
K. Westmacott

ELECTRON MICROSCOPE USERS COMMITTEE

R. Gronsky
J. Morris, Jr.
P. Ross*
K. Westmacott

EQUIPMENT REVIEW COMMITTEE

J. Clarke
A. Glaeser
R. Ritchie
R. Saykally
R. Muller*

TECHNICAL STAFF AND SHARED FACILITIES COMMITTEE

L. De Jonghe*
R. Gronsky
J. Morris, Jr.
P. Ross
G. Somorjai

ADMINISTRATIVE STAFF COMMITTEE

K. McArthur*
R. Muller
C. Peterson
M. Van Hove
P. Yu

SAFETY AND LABORATORY STANDARDS COMMITTEE

D. Ackland
M. Cima
D. Colomb
B. Fultz
K. Gaugler
J. Holthuis
L. Irvin
J. Jacobsen
L. Johnson
D. Krieger
M. Kujala
E. (Fong) Mah
K. McArthur
K. Medlock
D. Meschi*
R. Muller
E. Perez
C. Peterson
H. Riebe
J. Severns
C. Sterling
S. Stewart
W. Wong
J. Wu

MMRD Building 62 Building
Manager: D. Meschi
(Deputy: C. Peterson)

MMRD Building 72 Building
Manager: K. Westmacott
(Deputy: D. Ackland)

*Chairman

APPENDIX C

LIST OF DIVISIONAL SEMINARS

Surface Science and Catalysis Seminars

Date	Speaker and Affiliation	Seminar Title
1-19-84	Prof. P. Kumar, University of Florida, Gainesville	Low-temperture physics: liquid-helium surfaces
1-26-84	Prof. P.M. Marcus, IBM, Yorktown Heights, New York	Recent methods and results in surface structure determination by LEED
1-27-84	Dr. A. Bewick, University of Southampton, England	Spectroscopy and the renaissance in electrochemistry
2-2-84	Prof. K.P. Vollhardt, LBL	Homogeneous models of potential surface reactions
2-9-84	Dr. Robert Lane, ARCO Corporation, Los Angeles, California	Layered metal (IV) phosphonates as catalyst supports and selective sorbants
2-16-84	Dr. D.G. Castner, Chevron Research Corporation	*In situ* x-ray spectroscopy studies of cobalt catalysts
3-1-84	Dr. R. Graselli, SOHIO Research Laboratories	Selective heterogeneous oxidation catalysis
3-5-84	Prof. J. Livage, Université Pierre et Marie Curie, Paris, France	Transition metal oxide gels: structure and electronic properties
3-8-84	Dr. D. Rollman, Mobil Research and Development Laboratories	Zeolites and their synthesis
3-14-84	Dr. R.L. Schwoebel, Sandia National Laboratory, Albuquerque, New Mexico	Surface modifications: technology of science

Date	Speaker and Affiliation	Seminar Title
3-22-84	Prof. H. Metiu, University of California, Santa Barbara	Use of metastable atomic beams to probe the additive effects on adsorbed CO
3-29-84	Prof. A. Hubbard, University of California, Santa Barbara	Electrochemical processes at well-defined surfaces
3-30-84	Prof. S.L. Bernasek, Princeton University, Princeton, New Jersey	The vibrational state distribution of product CO_2 in the oxidation of CO on platinum
4-5-84	Prof. G. Haller, Yale University, New Haven, Connecticut	Description dynamics of scattering and reaction on Pt foils investigated by transient infrared emission spectroscopy
4-12-84	Prof. K. Klier, Lehigh University, Bethlehem, Pennsylvania	Methanol and low alcohol synthesis
4-26-84	Prof. W. Ho, Cornell University, Ithica, New York	Dynamical processes on surfaces
5-3-84	Dr. H. Wise, Stanford Research Institute, Menlo Park, California	Defect structure and methanation activity of molybdenum sulfide catalysts
5-4-84	Dr. C.J. Machiels, Dupont	Selective oxidation over molybdate catalysts
5-10-84	Dr. L.B. Ebert, Exxon Research and Engineering Co.	
7-26-84	Prof. F.H. Read, Manchester University, England	Optimization of electrostatic lenses for focussing charged particles with application to Auger and x-ray photoelectron spectroscopies
8-9-84	Prof. J. Fraissard, Université Pierre et and Marie Curie, Paris, France	Studies of Zeolites by NMR spectroscopy using xenon as a probe
8-17-84	Prof. J. Schulz, University of Karlsruhe, Germany	Catalyzed hydrodenitrogenation
8-24-84	Prof. J.T. Yates, University of Pittsburgh, Pennsylvania	Reaction channels for decomposition of organic molecules on surfaces

Date	Speaker and Affiliation	Seminar Title
9-6-84	Dr. R.J. Koestner, Exxon Research and Engineering Company	The observation of novel intermediates from H_2S, CH_3SH, and C_4H_4S decomposition on the Pt(111) surface
9-13-84	Dr. J.A. Labinger, Atlantic Richfield Company, Los Angeles, California	Approaches to homogeneous carbon monoxide hydrogenation using amphoteric ligands
9-20-84	Dr. M.S. Daw, Sandia National Laboratory, Albuquerque, New Mexico	Applications of the embedded-atom method to hydrogen on metal surfaces
9-27-84	Dr. W.L. Callender, Shell Development Company	Mechanisms of ring closures
10-4-84	Dr. E. Derouane, University of Namur, Belgium	Factors affecting the synthesis of pentasil Zeolites
10-11-84	Mr. S.B. Alpert, Electric Power Research Institute, Palo Alto, California	Clean advanced technology for generating electric power in California
10-15-84	Dr. L.B. Ebert, Exxon Research and Engineering Company	The interaction of potassium with graphite and other benzenoid species
10-17-84	Prof. W.M.H. Sachtler, Northwestern University, Evanston, Illinois	Bimetallic catalysis
10-25-84	Dr. R. Steiger, Ciba-Geigy, Freiburg, Switzerland	Energy transfer and light conduction for the spectral sensitation of silver halides and semiconductors
11-1-84	Dr. S. Tauster, Exxon Research and Engineering Company	Strong metal-support interactions
11-15-84	Prof. C.M. Friend, Harvard University, Cambridge, Massachusetts	Surface chemistry of nitrogen oxides on clean and oxidized W(100)
11-16-84	Dr. J. Weimer, Technical University, Munich, West Germany	The properties of K and coadsorbed CO + K on Ru(100)

Date	Speaker and Affiliation	Seminar Title
11-29-84	Prof. P.C. Stair, Northwestern University, Evanston, Illinois	Studies of desorption and surface diffusion by pulsed laser techniques
12-3-84	Dr. L.H. Dubois, AT&T Bell Laboratories, Murray Hill, New Jersey	Novel chemistry and physics at the metal-semiconductor interface
12-6-84	Prof. W. Maier, Department of Chemistry, University of California Berkeley	Mechanistic studies in heterogeneous catalysis
12-10-84	Prof. L.L. Kesmodel, Indiana University	Surface vibrational spectroscopy with low-energy electrons
12-14-84	Prof. P. Stenius, Institute for Surface Chemistry, Stockholm, Sweden	Adsorption of polyethylene oxide and polyethylene oxide-based surfactants on solid polymer surfaces

Reaction Dynamics Seminars

1-11-84	Prof. Dr. J. Troe, Institut für Physikalische Chemie der Universität Göttingen, West Germany	Photolysis quantum yields and atom recombination rates of halogens in highly compressed gases
1-12-84	Prof. Jan Kommandeur, Laboratory of Physical Chemistry, University of Groningen, The Netherlands	Radiationless transitions
1-13-84	Dr. D.A. Ramsay, National Research Council of Canada, Herzberg Institute of Astrophysics, Ottawa, Ontario	High-resolution studies of the electronic spectra of simple polyatomic molecules and free radicals
3-13-84	Prof. Earl Evleth, University of Paris, Orsay, Paris, France	Theoretical speculation on the photochemistry of ammonia clusters

Date	Speaker and Affiliation	Seminar Title
3-14-84	Prof. J.O. Hirschfelder, Department of Chemistry, University of California, Santa Barbara, and University of Wisconsin, Madison	The effect of natural lifetimes and permanent dipole moments on resonance spectra of atoms and molecules
3-16-84	Dr. William G. Harter, Theoretical Division, Los Alamos National Laboratory, and School of Physics, Georgia Institute of Technology	Rotational energy surfaces and high-J spectra of polyatomic molecules
3-23-84	Dr. Erik Deumens, Dienst Theoretische Natuurkunde, University of Antwerp, Belgium	The generator coordinate approximation for H_2^+: a nonadiabatic approach
3-30-84	Dr. Moshe Shapiro, Weizmann Institute of Science, Rehovot, Israel	Theory of laser photodissociation and photodissociation lasers
4-2-84	Dr. J. Römelt, Lehrstuhl für Theoretische Chemie der Universität Bonn, West Germany	DIVAH theory — predicting and interpreting reactive scattering resonances
4-25-84	Prof. Wendell Forst, Department of Chemistry, Laval University, Quebec	Theory of thermal decomposition of formaldehyde
5-21-84	Prof. Joel M. Bowman, Department of Chemistry, Illinois Institute of Technology, Chicago	Reduced dimensionality theories of quantum reactive scattering
5-20-84	Dr. Robert G. Gilbert, School of Chemistry, University of Sydney, New South Wales, Australia	Theory of collisional energy transfer in highly vibrational excited molecules
8-6-84	Prof. Donald L. Thompson, Department of Chemistry, Oklahoma State University, Stillwater	Statistical and dynamical studies of unimolecular reactions
9-6-84	Dr. Mark G. Sceats, School of Chemistry, University of Sydney, New South Wales, Australia	The dynamics of iodine recombination in dense gases and liquids

Date	Speaker and Affiliation	Seminar Title

Electron Microscopy Seminars

8-6-84	Dr. M.A. O'Keefe, LBL	Simulation of high-resolution electron micrographs
9-10-84	Dr. M. Sarikaya, University of Washington, Seattle	Basics of convergent-beam electron diffraction and its use in materials science
11-12-84	Dr. T. Sands, Bell Laboratories and LBL	Identification of microscopic interfacial phases: the first step toward understanding the structure-property relationships of electronic interfaces
12-10-84	J.M. Howe, LBL	A TEM study of the atomic mechanisms of γ' precipitate plate growth in the Al-Ag system

Other Seminars Hosted

1-15-84	Dr. Josef Bicerano, Energy Conservation Devices, Troy, Michigan	
2-22-84	Dr. Ken Easterling, University of Lulea, Sweden	Laser hardening and the determination of weldability diagrams for steel
2-23-84	Prof. Ilhan Aksay, University of Washington	Colloidal forming of ceramics
2-28-84	Dr. Hans-Joachim Werner, Department of Chemistry, Kaiserslautern University, West Germany	
3-13-84	Dr. Bowen Liu, IBM Research Laboratory, San Jose, California	
3-25-84	Dr. Fredrick Lange, Rockwell Science Center	Multiparticle effects and particle packing in sintering
4-84	Dr. Jose Moya, Instituto de Ceramica y Vidrio, Madrid, Spain	Processing and properties of mullite/zirconia ceramics

Date	Speaker and Affiliation	Seminar Title
4-18-84	Prof. Notker Rosch, Technical University, Munich, West Germany	Group theory of quaterions
5-84	Dr. Anil K. Sachder, General Motors	Fe-Ni steels
5-84	Dr. Eric Navara, Lulea University, Sweden	Dual phase steels
5-15-84	Prof. Mihaly T. Beck, Kossuth Lojos University, Debrecen, Hungary	Kinetics, mechanism, and design of oligo-oscillatory reactions
6-22-84	Dr. Zahid Hussain, University of Petroleum and Minerals, Dhahran, Saudi Arabia	Electron spectroscopy for petroleum processing studies
6-26-84	Dr. Nicholas C. Handy, Department of Theoretical Chemistry, Cambridge University, England	
6-26-84	Dr. J. Ma. Rincon, Instituto de Ceramica y Vidrio, Madrid, Spain	TEM study of high-toughness zirconia/mullite composite ceramic materials
8-7-84	Dr. Francois Auzel, Centre National d'Etudes des Telecommunications, Paris, France	Optical spectroscopy of rare earth ions and U^{4+} in solids
8-10-84	Prof. D. van der Marel, University of Groningen, The Netherlands	Inverse photoemission and Auger spectroscopy of dilute transition metal impurities
8-22-84	Prof. Michel Genet, Institute de Physique Nucleaire, Université de Paris-Sud, Orsay, France	Optical spectroscopy of actinide ions and $ThBr_4$
8-31-84	Dr. Combet Farnoux, University of Paris-South, Orsay, France	Atomic aspects of the resonant photoemission
9-26-84	Dr. R.A. Street, Xerox Palo Alto Research Center, Palo Alto, California	Doping effects in hydrogenated amorphous Si

Date	Speaker and Affiliation	Seminar Title
10-10-84	Dr. Jeff Bokor, AT&T Bell Laboratories, Holmdel, New Jersey	Time-resolved and angle-resolved photoemission in Si
10-11-84	Dr. J.W. Cahn, National Bureau of Standards	Elastic effects in coherent phase changes
10-19-84	Dr. Roland Bougon, Centre d'Etudes Nucleaires de Saclay, France	Recent results in fluorine chemistry: elements in their higher oxidation states
10-23-84	Dr. D. Gratias, Institue for Theoretical Physics, University of California, Santa Barbara	Pair interactions calculated from short-range intensity data
10-30-84	Dr. Jack L. White, Aerospace Corporation	New directions in carbon science and technology
11-1-84	Prof. E. Matievic, Clarkson College	Colloid shape and stability
11-6-84	Dr. Malcolm Howells, Lawrence Berkeley Laboratory	Science and technology relating to the LBL beam line
11-13-84	K. Keefer, Sandia National Laboratory	Application of fractals to ceramic powder morphology
11-15-84	Dr. John Greenstadt, IBM Scientific Center, Palo Alto, California	
11-17-84	Prof. Russell M. Pitzer, Department of Chemistry, Ohio State University, Columbus, Ohio	
11-20-84	Prof. K.H. Jack, Newcastle-upon-Tyne, England	Recent work on the Si Al ON system of novel ceramic materials
12-3-84	Dr. M. Hetherington, Oxford University, England	Magnetization processes in alnico-type materials
12-3-84	Dr. J. Gau, Kodak, Rochester, New York	Research opportunities in thin films for magnetic recording

Date	Speaker and Affiliation	Seminar Title
12-4-84	Prof. Wilfried Meyer, Department of Chemistry, Kaiserslautern University, West Germany	
12-7-84	Prof. Dr. Konrad Seppelt, Freie Universität Berlin	Carbon-sulfur double and triple bonds
12-13-84	Dr. Werner Muller, European Institute for Transuranium Elements, Karlsruhe, West Germany	Actinide chemistry at the European Institute for Transuranium Elements

APPENDIX D

INDEX OF INVESTIGATORS*

Andersen, Richard A. **237**

Bartlett, Neil **224**, 237
Bell, Alexis T. 37, **210**, **222**, **260**
Bergman, Robert G. **228**
Bragg, Robert H. **70**
Brewer, Leo **118**

Clarke, John **94**
Cohen, Marvin L. **102**, 108, 109
Connick, Robert E. **208**, **303**
Conway, John G. **237**

de Fontaine, Didier **34**
De Jonghe, Lutgard C. **67**, **265**, **282**

Edelstein, Norman M. **237**, **301**
Evans, Anthony G. **46**, 50, 77
Evans, James W. **32**, **265**, **278**

Falicov, Leo M. 58, **99**, 292
Finnie, Iain **75**
Fish, Richard H. **222**, **260**, **304**

Glaeser, Andreas M. **73**
Gronsky, Ronald **1**, **18**, 62, 63, 64

Haller, Eugene E. 89, 100, **292**
Harris, Charles B. **161**
Heinemann, Heinz **222**, **260**, **304**
Hess, Dennis W. **123**
Humphrey, Joseph A.C. **253**

Jeffries, Carson D. **89**
Johnston, Harold S. **158**
Jolly, William L. **219**

Kresin, Vladimir Z. 173, **298**

Lee, Yuan T. 86, **191**
Lester, William A., Jr. **172**, **297**
Levy, Alan V. **258**, **300**, **302**
Louie, Steven G. 103, 104, 105, **107**

Marrus, Richard **203**
Miller, William H. **178**, 199
Moore, C. Bradley **165**
Morris, John W., Jr. **38**, **289**
Muller, Rolf H. 114, **124**, **265**, **272**

Newman, John **223**, **265**, **285**
Nitsche, Heino **301**

Olander, Donald R. **120**

Pask, Joseph A. **56**
Phillips, Norman E. **37**, **111**
Pines, Alexander **138**
Pitzer, Kenneth S. **168**
Prausnitz, John M. **232**

Raymond, Kenneth N. **237**
Richards, Paul L. **80**, 162
Ritchie, Robert O. 6, **50**
Ross, Philip N. 127, **255**, **265**, **275**

Saykally, Richard J. **175**
Schaefer, Henry F., III **198**
Seaborg, Glenn T. **237**
Searcy, Alan W. **58**
Shen, Yuen-Ron **84**, 127, 191
Shirley, David A. **182**, 194, 195
Somorjai, Gabor A. 84, **127**, **155**
210, **222**, **260**, 261
Streitwieser, Andrew, Jr. **237**

Templeton, David H. **237**
Thomas, Gareth **5**, **18**
Tobias, Charles W. **114**, 126, **265**, **267**
269

Vollhardt, K. Peter C. **216**

Washburn, Jack 1, 2, **62**
Westmacott, Kenneth H. **14**, **18**

Yu, Peter Y. **92**

Zalkin, Allan **237**

*Boldface numbers indicate investigators' main programs.

This report was done with support from the Department of Energy. Any conclusions or opinions expressed in this report represent solely those of the author(s) and not necessarily those of The Regents of the University of California, the Lawrence Berkeley Laboratory or the Department of Energy.

Reference to a company or product name does not imply approval or recommendation of the product by the University of California or the U.S. Department of Energy to the exclusion of others that may be suitable.

LAWRENCE BERKELEY LABORATORY
TECHNICAL INFORMATION DEPARTMENT
UNIVERSITY OF CALIFORNIA
BERKELEY, CALIFORNIA 94720